UMTRI-86-30

EVALUATION OF EXPERIMENTAL TECHNIQUES IN HEAD INJURY RESEARCH

Guy S. Nusholtz
Patricia S. Kaiker
Richard J. Lehman
Wendy S. Gould

FINAL TECHNICAL REPORT

July 1986

Prepared under Contract No. DTNH-22-83-C-07095

UMTRI The University of Michigan
Transportation Research Institute

Technical Report Documentation Page

1. Report No.	2. Government Accession No.	3. Recipient's Catalog No.

4. Title and Subtitle

Evaluation of Experimental Techniques in Head Injury Research
(1 Volume)

5. Report Date
July 1, 1986

6. Performing Organization Code

7. Author(s) Guy S. Nusholtz, Patricia S. Kaiker, Richard J. Lehman, and Wendy S. Gould

8. Performing Organization Report No.
UMTRI-86-30

9. Performing Organization Name and Address
Biosciences Division, Transportation Research Institute, The University of Michigan, 2901 Baxter Road, Ann Arbor, MI 48109

10. Work Unit No.

11. Contract or Grant No.
DTNH22-83-C-07095

12. Sponsoring Agency Name and Address
National Highway Traffic Safety Administration
Department of Transportation, Seventh and E Streets, S.W., Washington, DC 2059

13. Type of Report and Period Covered
Final
11-12-82 to 7-31-86

14. Sponsoring Agency Code

15. Supplementary Notes

Experimental Data

16. Abstract

Modeling of head trauma impact biodynamics cannot be validated without descriptive experimental data. The purpose of the dynamic biomechanic blunt head impact project being reported here was to qualify, in a limited sense, the differences among the anesthetized-, the unrepressurized-postmortem, and the repressurized-postmortem Rhesus models. Five anesthetized and five postmortem subjects were tested. In addition, these data were compared to earlier Rhesus study data on five anesthetized subjects and five postmortem subjects plus previous studies on twenty-six unembalmed repressurized human cadaver subjects. It is hoped this comparative information will assist the evaluation of the unembalmed repressurized human cadaver model as a dynamic biomechanics surrogate for the injurious blunt head impact response of the live human. Jeffrey Marcus was the Contact Technical Monitor at the National Highway Traffic Safety Administration.

17. Key Words	18. Distribution Statement
Lower primate experimental data, Impact response, Impact biomechanics, Head trauma, Anesthetized versus postmortem	

19. Security Classif. (of this report)	20. Security Classif. (of this page)	21. No. of Pages	22. Price
		468	

CONTENTS

LIST OF TABLES

LIST OF FIGURES

1.0 OVERVIEW OF RESEARCH PROGRAM

In the United States roughly half of the head injuries can be attributed to motor vehicle accidents (1-3)[1]. Investigations of trauma to the head and of mechanisms of injury become invaluable for allocating resources and for formulating policy to reduce its incidence, morbidity, and mortality.

A major difficulty in the investigation of head trauma is designing kinematic experiments which minimally interfere with the biological and physical systems being observed, yet produce results that correspond well with clinically observed trauma. Some understanding of head injury mechanisms as a result of blunt impact has resulted from relating kinematic parameters to injury modes. However, with the possibility of several injury mechanisms, correlations of this type do not always imply causation. The parameters commonly used for describing head mechanical response during impact have been angular and translational accelerations, velocities, displacements of the head as a rigid body, skull bone deformations, and internal pressures in the brain. Many investigations have chosen to study but a single parameter, and later employ it as an index of severity or tolerance threshold (e.g., resultant head acceleration used to calculate the Head Injury Criterion).

The dynamic-biomechanics literature concerning mechanisms of injury is a rich one (4-60). However, despite conscientious speculation as to the mechanics which produce head trauma and theoretical and experimental scrutiny of various hypotheses about it, considerable controversy still exists. The hypotheses usually cannot wholly fit

---

[1]Numbers in parentheses refer to references found at the end of the text.

clinical or pathological observations, assessment of biomaterial properties, or predictions of mathematical models.

Several of these controversies involve angular and linear accelerations and skull deformation (5-8,12,16-17,21-22,35,39,41). The debates are confounded by the complex mechanical structure of the head and brain. A number of mathematical analyses (e.g., finite element analyses, in particular) have attempted to model the brain with reasonable geometric precision. However, the calculations involve over-simplifying the characteristics of the biomaterials (e.g., by assuming simple elasticity or homogeneity) as well as of the dynamics (12-13,23,24,39,42-45). A number of investigators have attempted to define the pressure-volume response of the skull-brain system to impact using dynamic-biomechanics experiments (19,25-26,28-30,32,37,44-45). However, the skull-brain interface as well as the effects of skull deformation on the impact response of the brain and its cerebrospinal system are still not well understood.

Mechanisms of blunt-impact head trauma must be investigated with human surrogate models because the human volunteer and accident investigation data do not provide the information needed to determine head injury mechanisms. A dynamic-biomechanics trauma model, the laboratory animal, is chosen in order to monitor the physiological response associated with the neuropathology (46-60). Although the subhuman primate geometry is the most similar to man's of the available animal surrogates, the laboratory Rhesus' geometry, in particular, is significantly different in soft-tissue distribution and skull morphology. Translating and scaling laboratory Rhesus' dynamic-biomechanics data are constrained not only by statistical, mathematical, and experimental techniques but also by what is still unknown about quantifying the

differences among Rhesus subjects and between the Rhesus model and the expected response in the live human.

An alternative model, the unembalmed cadaver, is often chosen as a dynamic-biomechanics experimental model because its geometry and soft-tissue distribution is similar to that of the live human. In addition, the gross soft-tissue damage can be directly related to the injury patterns observed in clinical settings. However, postmortem changes of brain tissues may lead to the misinterpretation of the damage and kinematic responses in the cadaver model.

Some laboratory evidence has indicated that the repressurized human cadaver model provides a better estimate of the expected response in the live human than that of the unrepressurized human cadaver model (28-30). However, to date few dynamic-biomechanics experiments have compared the available human surrogates (69). Of the anesthetized laboratory animal surrogates which have been selected to investigate trauma, the lower subhuman primates have not been adequately characterized in terms of response between the anesthetized versus the postmortem and/or the unrepressurized postmortem versus the repressurized postmortem. One purpose of the dynamic-biomechanics blunt head impact project being reported here was to qualify, in a limited sense, the differences among the anesthetized-, the unrepressurized-postmortem, and the repressurized-postmortem Rhesus models. It was hoped that this information would assist the evaluation of the unembalmed repressurized human cadaver model as a dynamic-biomechanics surrogate for the injurious blunt head impact response of the live human.

This final report discusses techniques developed and used by the University of Michigan Transportation Research Institute (UMTRI) for measuring three-dimensional

head motion and epidural pressure. Live anesthetized and repressurized/unrepressurized postmortem Rhesus were subjected to a posterior-to-anterior direction occipital head impact. The results are compared to those previously presented (30-32,34) so that they cover the data from related research programs conducted over the last nine years.

1.1 Brief Summary of Project - The response of the head to blunt impact was investigated using anesthetized- and repressurized/unrepressurized postmortem Rhesus. The stationary test subject was struck by a 10 kg guided moving impactor on the occipital. The impactor striking surface was fitted with padding to vary the contact force-time characteristics. A nine-accelerometer system, rigidly affixed to the skull, measured head motion. Transducers placed at specific points below the skull recorded epidural pressure. For the repressurized postmortem subjects, both the vascular and cerebrospinal systems were repressurized. The results of the tests demonstrate that:

1) In terms of peak pressure, the repressurized postmortem and the anesthetized Rhesus responses were significantly different from that of the unrepressurized postmortem Rhesus;

2) Although the repressurized Rhesus was more similar in response to the anesthetized Rhesus (in terms of transfer functions of tangential acceleration divided by epidural pressure), the differences detected between them may be important kinematic differences;

3) In terms of subarachnoid hemorrhage in the medulla pons area associated with skull fracture, the repressurized-postmortem and anesthetized Rhesus were similar in injury response;

4) The initial position of the head-neck system was a critical factor associated with the cerebrospinal system's response to head impact;

5) The thermodynamic response of the cerebrospinal system was an important consideration when the impact produced significant tension; and

6) No relationships could be found between injury and negative pressures equal to one atmosphere.

2.0 RESEARCH APPROACH AND METHODOLOGY

The goal of the dynamic biomechanics blunt head impact project was to qualify, in a limited sense, the differences among the anesthetized, the repressurized-postmortem, and the unrepressurized-postmortem Rhesus models. The purpose was to gather experimental data which would add to the existing knowledge of head trauma.

The methods and procedures that were used in this dynamic-biomechanics trauma research are outlined below. Additional information can be found elsewhere (30-34). Appendix H is the impact testing protocol.

2.1 Impact Testing - Using the pneumatic impacting device with a 10 kg impactor, five anesthetized and five postmortem Rhesus were subjected to a single head impact to the occipital region. The ten adult laboratory animal subjects used in these experiments were obtained by UMTRI from the University of Michigan Unit for Laboratory Animal Medicine. The final analysis included a comparison with 5 anesthetized Rhesus and 6 postmortem Rhesus from a previous project (30) plus a comparison with 26 unembalmed repressurized human cadavers from previous/concurrent projects (33). The Rhesus were instrumented using procedures similar to those used to instrument human cadaver subjects (31). A nine-accelerometer array was rigidly affixed to the skull and epidural pressure transducers were used to document pressure changes. The cerebrospinal and vascular systems of four of the postmortem Rhesus were repressurized.

2.11 UMTRI Pneumatic Impact Device. The pneumatic impact device consists of an air reservoir, a ground and honed cylinder, and two carefully fitted pistons (See Figure 1). The driver piston was secured at the reservoir end of the cylinder by an electronically controlled locking mechanism. At the opposite end of the cylinder, the striker piston was rigidly connected to the impact force head. Both steel pistons have interchangeable elastic bumpers. Compressed air from the building's air compression system was introduced into the reservoir. When the air reservoir was pressurized and the locking mechanism released, the driver piston was propelled by the compressed air through the cylinder until its bumper impacted the bumper on the striker piston, which was allowed to travel up to 25.4 cm.

The impactor surface was a 10.2 cm rigid metal plate padded with 2.5 cm Ensolite. The impactor force transducer assembly consisted of a Kistler 904A piezoelectric load washer with a Kistler 804A piezoelectric accelerometer mounted internally for inertial compensation.

A specially designed timer box was used to synchronize the impact events during each test, such as the release of the striker and activation and de-activation of the high-speed photographic equipment. The impact conditions between tests were controlled by varying the impact velocity and the initial positioning of the test subject. The piston velocity was measured by timing the pulses from a magnetic probe which sensed the motion of targets in the piston.

2.12 Cineradiograph - High speed cineradiographs were taken of the impact events at 400 or 1000 frames per second. The UMTRI high-speed cineradiographic system (61) consists of a Milliken high-speed 16 mm motion-picture camera which views a 5 cm diameter output phosphor of a high-gain, four-stage, magnetically focused image

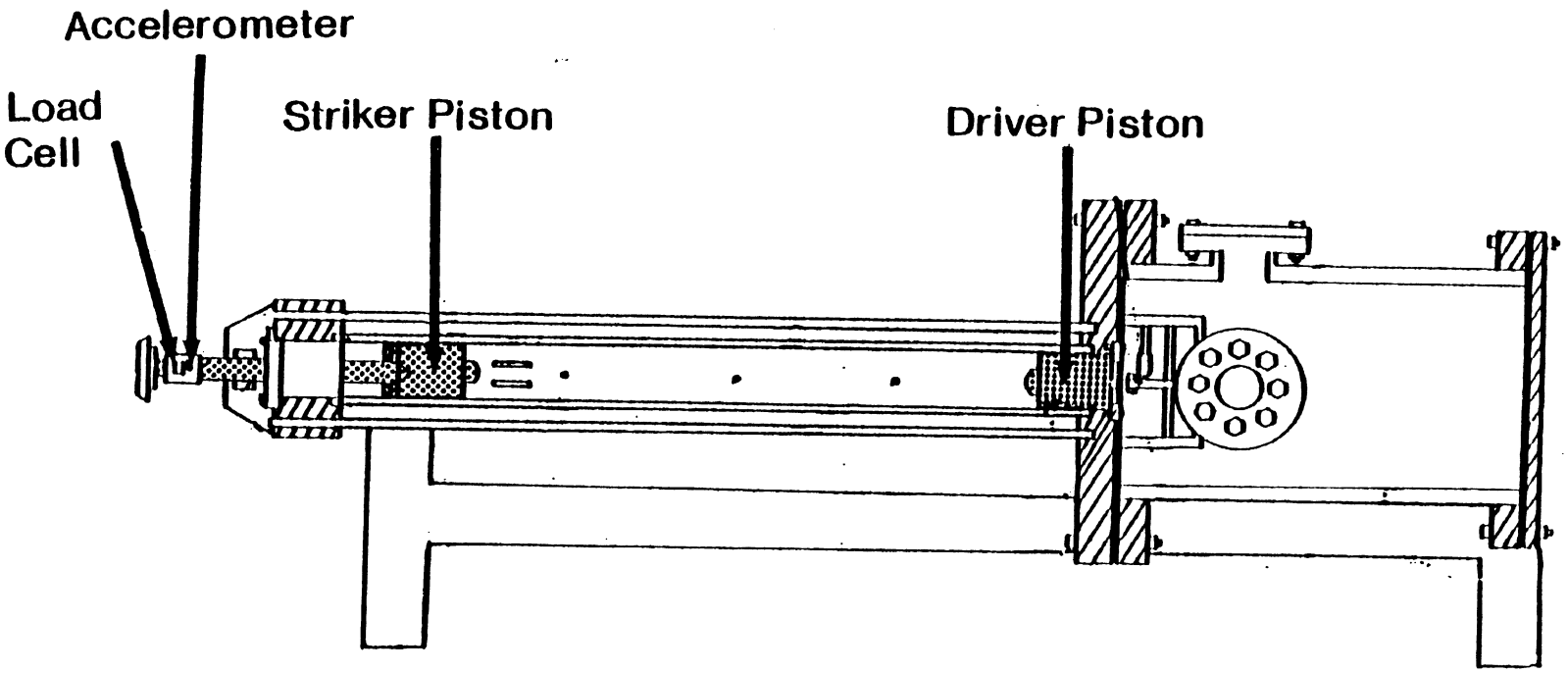

Figure 1

UMTRI Pneumatic Impact Device

intensifier tube, gated on and off synchronously with shutter pulses from the motion-picture camera. A lens optically couples the input photocathode of the image intensifier tube to x-ray images produced on a fluorescent screen by a smoothed direct-current x-ray generator. Smoothing of the full-wave rectified x-ray output is accomplished by placing a pair of high-voltage capacitors in parallel with the x-ray tube. The viewing field for these experiments was between 20-by-40 cm

2.13 Acceleration Measurement - An interrelated set of three triaxial accelerometers (the nine-accelerometer array) recorded head accelerations. The accelerometers were either Endevco 2264-2000 piezoresistive ones or Kistler Model 8694 piezoelectric ones.

2.14 Epidural Pressure Measurement - Epidural pressures were measured with Kulite model MCP-055-5F catheter tip pressure transducers or with Endevco 8507-50 pressure transducers.

2.15 Data Handling - All transducer time-histories (i.e., impact force, impact acceleration, epidural pressures, nine head-accelerations) were recorded unfiltered on a Honeywell 96 FM Tape Recorder with an EMI multiplex unit or a Honeywell 7600 FM Tape Recorder. A synchronizing gate was recorded on all tapes. The analog data on the FM tapes were played back for digitizing through proper anti-aliasing analog filters. The analog-to-digital process for all data resulted in a digital signal sampled at 6400 Hz equivalent sampling rate.

2.16 Test Synopsis

Test Subject Preparation - Five head impacts were conducted on postmortem Rhesus. Upon termination, they were stored in a cooler at 4°C for 5 days (85R005-86R015)/3 weeks (85R002) prior to testing. Anesthetized Rhesus were used in the other

five experiments. Six additional head impacts were conducted in a previous project on postmortem Rhesus (30). Upon termination, those subjects had been stored in a cooler at 4°C for 72 hours (78A232-79A260). That previous study also included five additional anesthetized Rhesus (78A239-78A253). The protocol for postmortem animals presented in detail elsewhere (32) was less complex than that for the anesthetized laboratory animals, which is outlined below.

The animal was first anesthetized with an injection of ketamine and then maintained with ketamine and sodium pentobarbital by means of a catheter with a three-way valve which had been inserted into the *long saphenous* vein of the leg. An airway was established to aid breathing when necessary. Then the subject was weighed and measured. Next, using a cauterizing scalpel, the scalp and muscle mass were removed from the frontal bone and the screws used to secure the epidural pressure transducer coupling devices were screwed into place. Then the nine-accelerometer plate was installed. The subject was then taken to the impact laboratory and placed in an erect sitting position with its posterior side towards the impactor, so that the line of impact was in the mid-sagittal plane in the posterior-anterior direction.

Subject Positioning - The subject was held in place with paper tape which secured the body under the armpits, suspending the head and torso from an overhead hoist. For tests 85R002-86R015, the subjects were positioned such that the eyes were raised above the horizontal line through the impact site; thus, the estimated center of mass was above the line of impact. In the previous study, in tests 78A232 and 78A234 the eyes were on a horizontal line through the impact site, thus the estimated center of mass was below the line of impact. In tests 78A236 and 78A239 the eyes were raised to a point slightly above a horizontal line through the impact site, thus the line of impact was through the

estimated center of mass. In tests 78A238 and 78A241 the eyes were raised higher than the previous two tests, thus the center of mass was above the line of impact (See Figure 2). Tests 79A249-79A260 were similar to those just described except that higher impact energy levels were used and the subjects were positioned so that impact occurred through the estimated center of mass.

The initial positioning of the subject also included placing the subject in either the neck-stretched (86R011-86R013) or neck-unstretched position (85R002-8 and 86R014-15). See Figure 3 for illustration of the initial positioning of the head-neck. To achieve the neck-stretched configuration, strings were placed in the ears and the subject was suspended by an overhead hoist so that approximately one-half of its entire body weight was supported by the neck. To achieve the neck-unstretched configuration, paper tape was used to support the head via the overhead hoist so that only one-half the weight of the head and none of the remaining body weight was supported by the neck.

After the positioning, three triaxial accelerometer clusters were fastened to the nine-accelerometer plate. Silicon fluid was injected into the pressure couplings, removing all air, and the pressure transducers were inserted. The subject was positioned in front of the impactor and stabilized with paper tape. All of the transducer wires were then connected and cabled, and the transducers checked for continuity and function. Then the subject was impacted at the occiput.

Figure 4 shows the basic dynamic-biomechanics impact test setup. One and a half hours after impact for Tests 85R002-86R015, a 5 ml dose of Uthol (concentrated, unpure sodium pentobarbital) was injected via the hind leg intravenous catheter to euthanize the anesthetized laboratory animal subjects. A bilateral pneumothorax was performed to insure termination. A necropsy was performed.

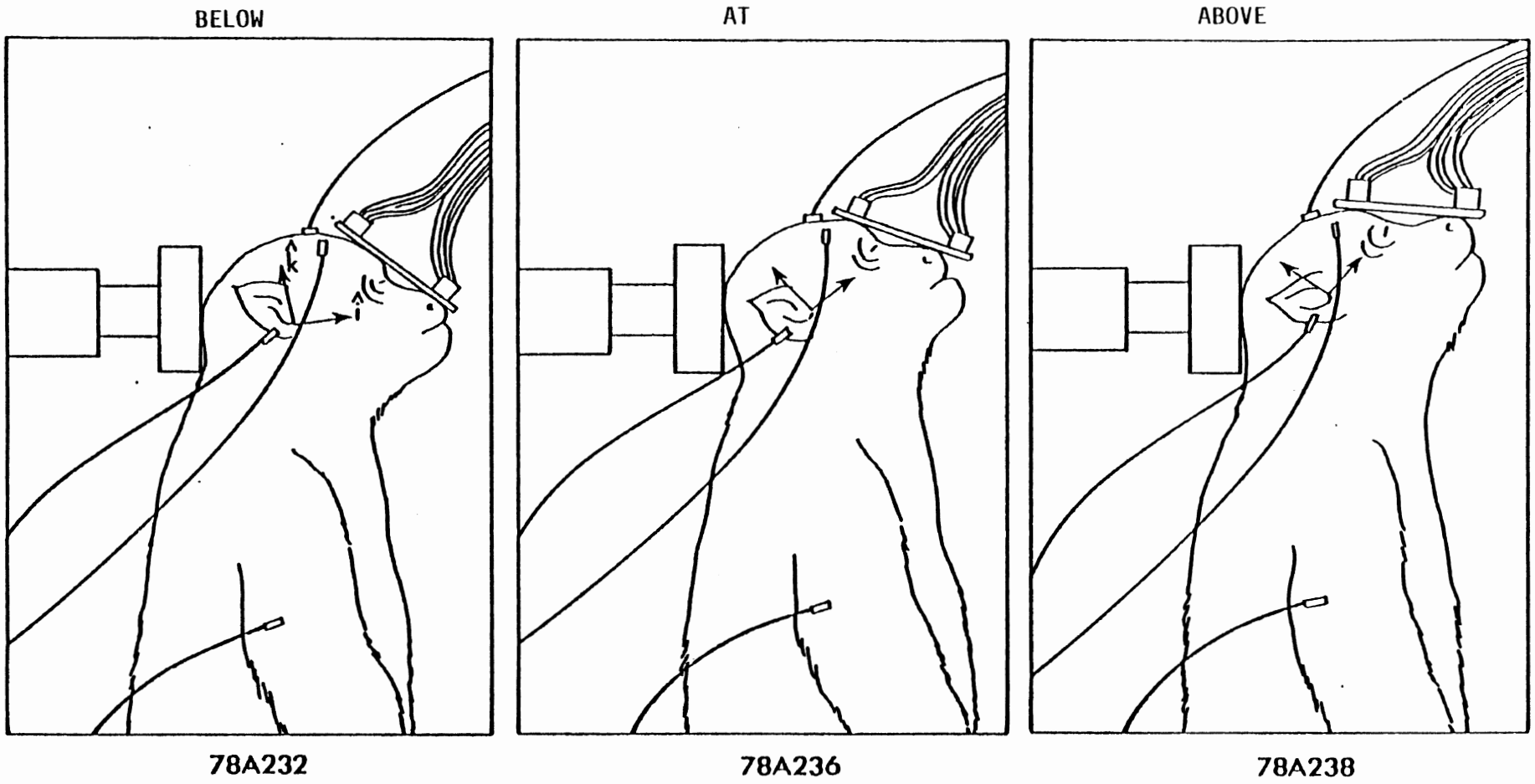

Figure 2

Subject Postitioning
Center of Gravity Relative to Line of Impact

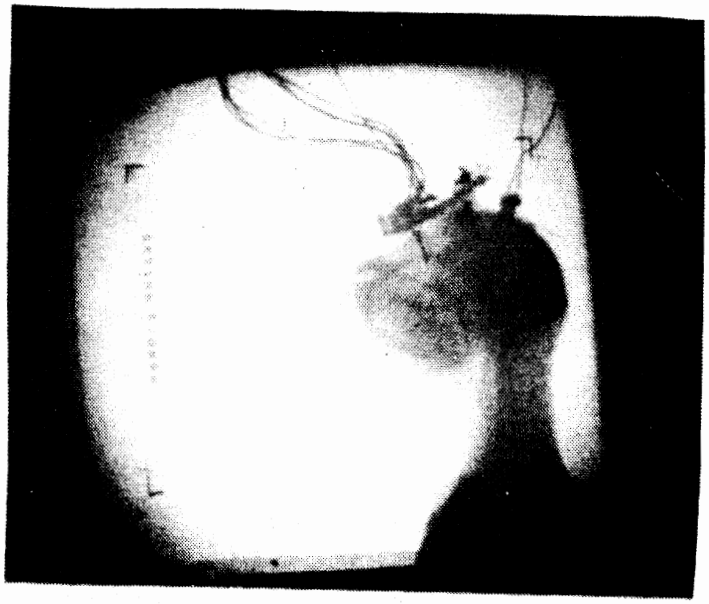

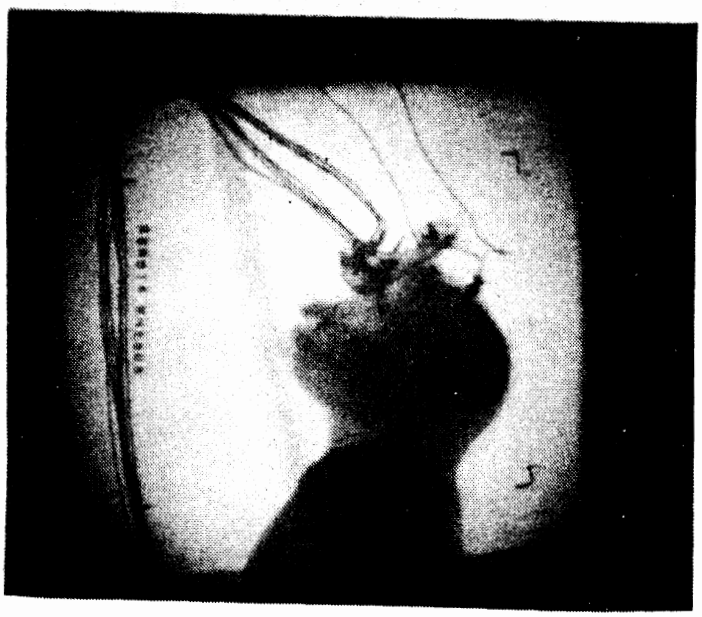

Figure 3

Initial Positioning
Neck-stretched (top) vs. Neck-unstretched (bottom)

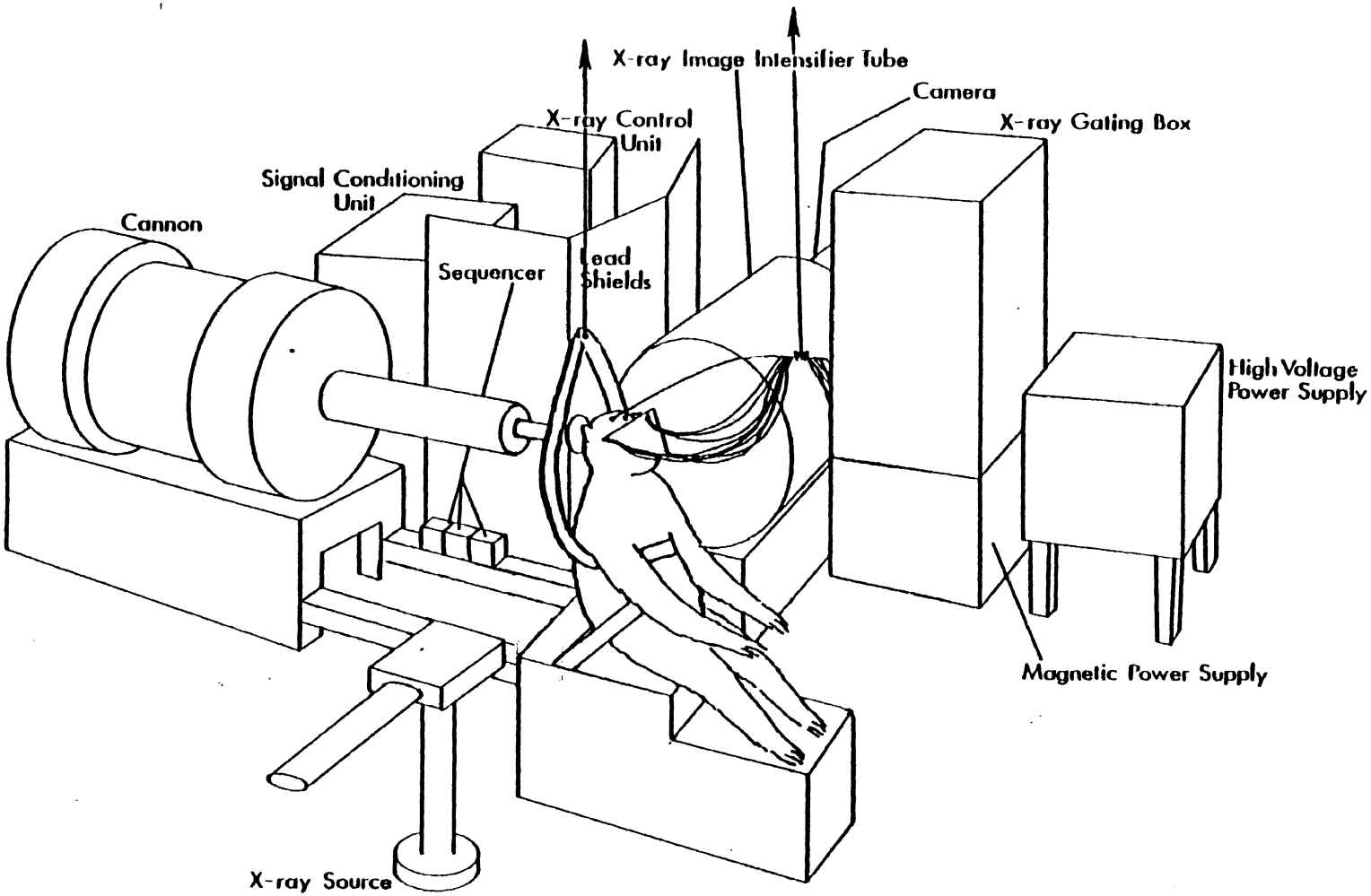

Figure 4

Test Setup for Dynamic Biomechanic Impact Test

2.17 Surgical Instrumentation

Nine-Accelerometer Head Plate - To install the nine-accelerometer plate, the scalp was removed from the frontal bone over the orbital ridges. Five metal self-tapping screws were attached firmly to the skull through small pilot holes drilled into the orbital ridges and into the dental palate above the canine teeth. Quick-setting acrylic plastic was molded around each of the screws and the nine-accelerometer plate mount, embedding the mount in the plastic. After the acrylic set, the plate was rigidly attached to the skull. The orientation of the plate in this position is shown in Figure 5.

Since it was necessary to determine the instrumentation frame's exact location and orientation in relation to the anatomical frame, a three-dimensional x-ray technique was developed. Two orthogonal radiographs of the instrumented head were taken as part of the necropsy examination. The procedure required the identification of four anatomical landmarks (i.e. two superior edges of the auditory meati and two infraorbital notches) with four distinguishable lead pellets, plus the identification of four lead pellets inlaid in the plate which defined the instrumentation frame. The targets were digitized and related using a mathematical algorithm which resolved the instrumentation center of gravity into the translations and rotations of the anatomical center of gravity.

Epidural Pressure Couplings - After the scalp was removed from a small area over the right and left side of the frontal bone, the surface was sanded. Next, two 0.3 cm diameter holes were drilled using a Stryker bone coring tool, the bone was tapped, and the *dura mater* was punctured under each hole. Aluminum couplings for the pressure transducers were screwed into the tapped holes (See Figure 6). Dental acrylic was applied around the base of the couplings to secure them.

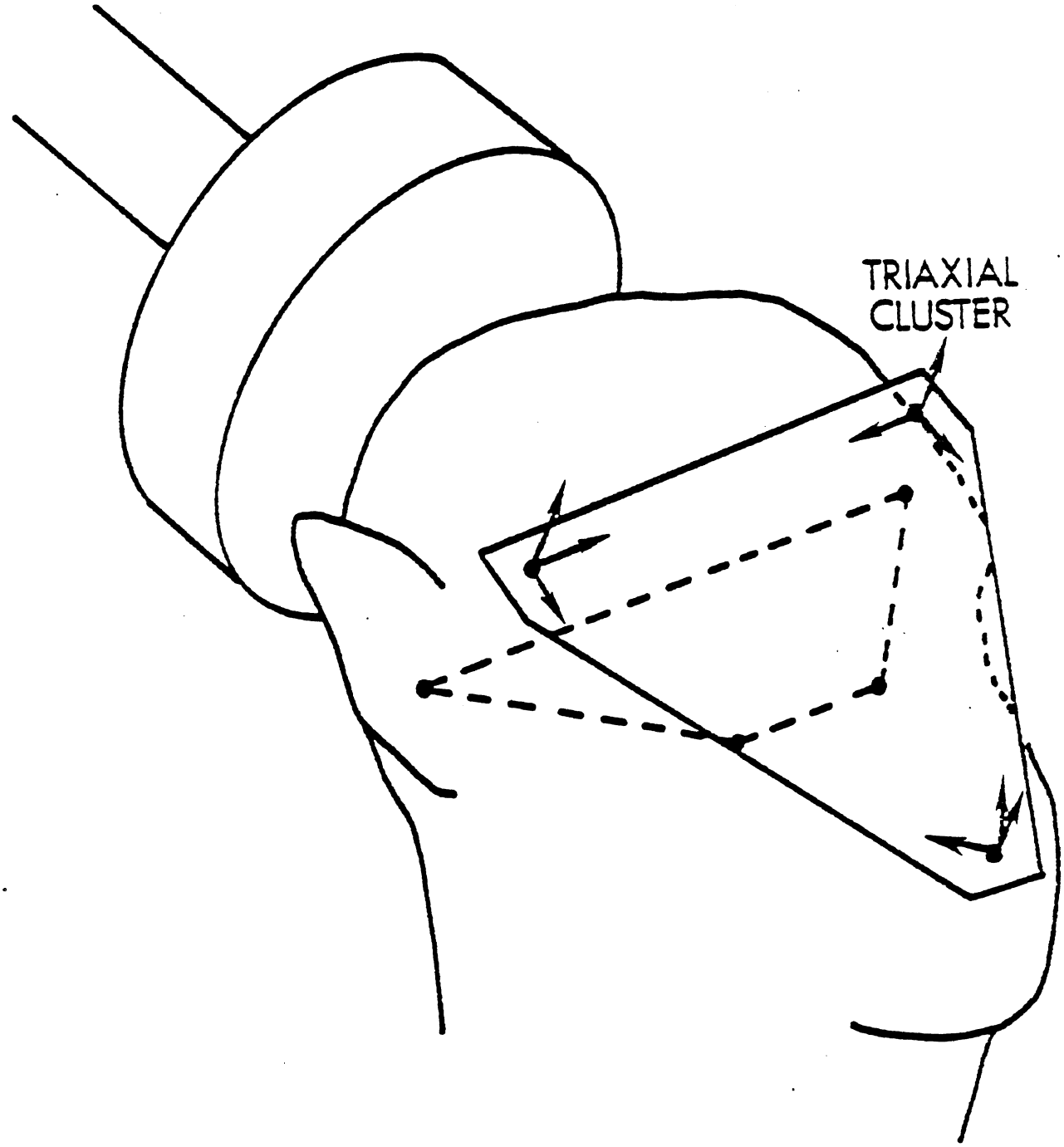

Figure 5

Orientation of Nine-Accelerometer Plate

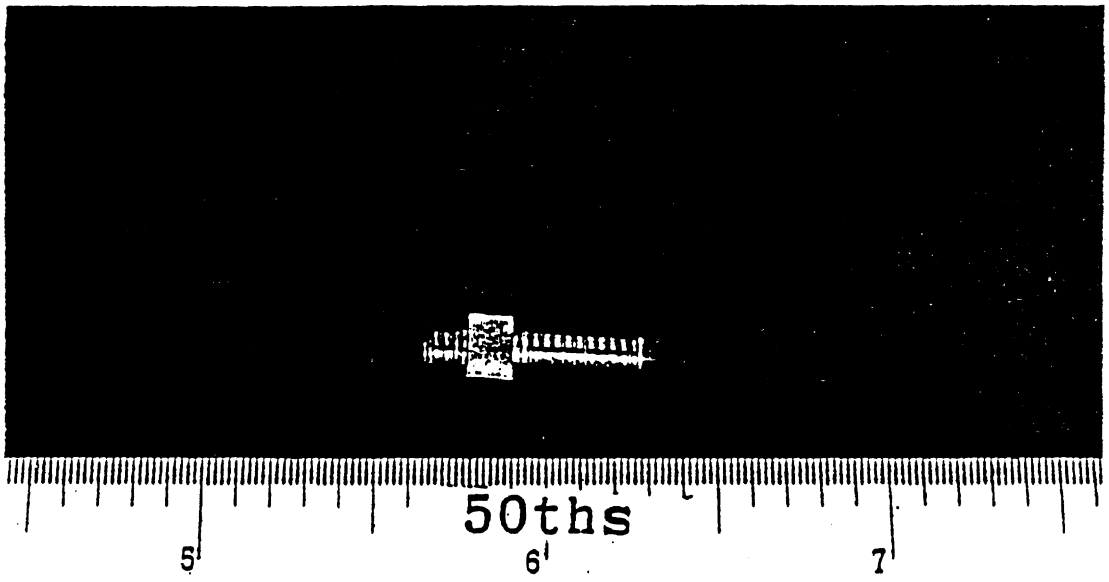

Figure 6

Epidural Pressure Coupler

Cerebrospinal Repressurization - A small hole was cored in the L2 lumbar vertebra and a Foley catheter was inserted under the dura of the spinal cord such that the balloon of the catheter reached mid-thorax level (See Figure 7). The point at which the catheter passed through the lamina of the second lumbar vertebra was sealed with plastic acrylic. To check fluid flow through the ventricles, saline was injected through the Foley catheter until it rose to the top of the couplings. The couplings were capped until the pressure transducers (either Kulite Model MCP-055-5F catheter tip or Endevco series 8510 piezoelectric transducers) were attached in the impact laboratory. Dow Corning dielectric gel (silicon fluid) was injected into each coupling device to act as a securing medium. The pressure transducer was then inserted and secured at the proper depth. Then a setup radiograph was made of the head.

Vascular Repressurization - The common carotid artery was located at a point in the neck and an incision was made. String was looped around the common carotid and it was cut lengthwise. A polyethylene tube was inserted into the ascending common carotid, and the descending common carotid was ligated. The opposite common carotid was located and similarly cut. Vascular flow was checked. Then a Millar catheter tip pressure transducer was inserted into the ascending common carotid to the point of its branching with the external carotid, secured with tape and sewn in place. (See Figure 8).

2.2 Method of Analysis

The techniques used to analyze the results are outlined below. Additional information can be found elsewhere (30-34,61-66).

2.21 Reference Frames - The impact response of the human body and its surrogates may be described as kinematic quantities derived from experimental measurements and expressed as vectors in reference frames which vary from one

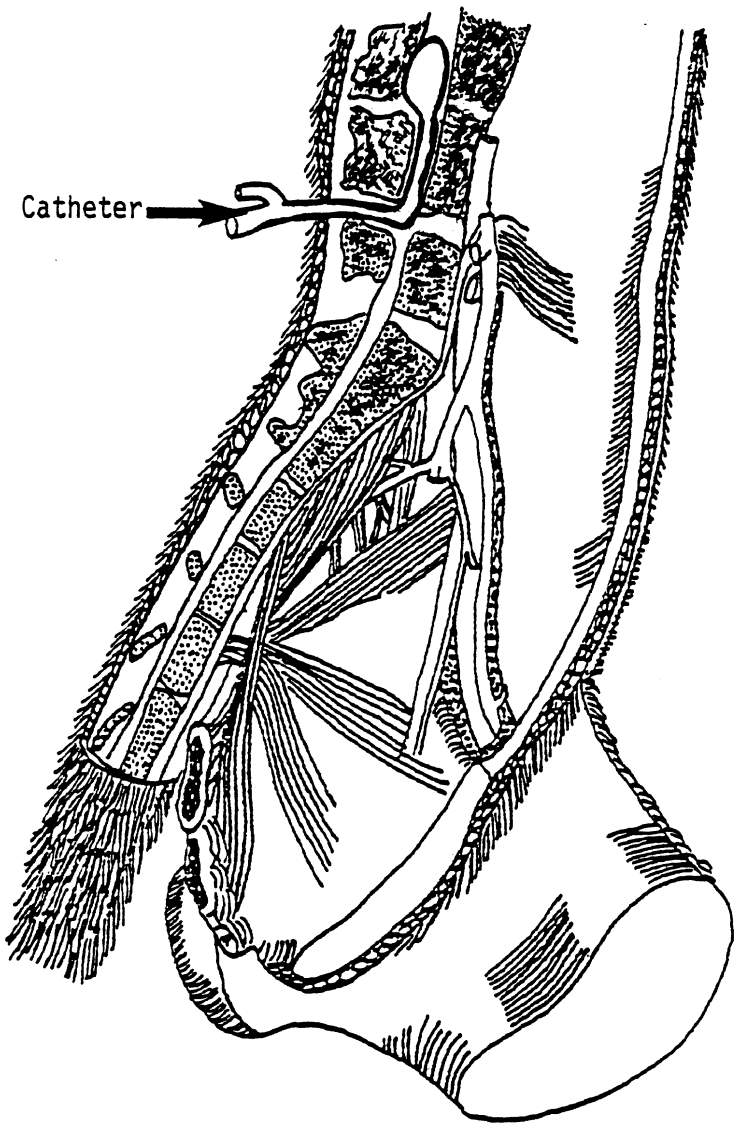

Figure 7

Cerebrospinal Repressurization of Rhesus Subject

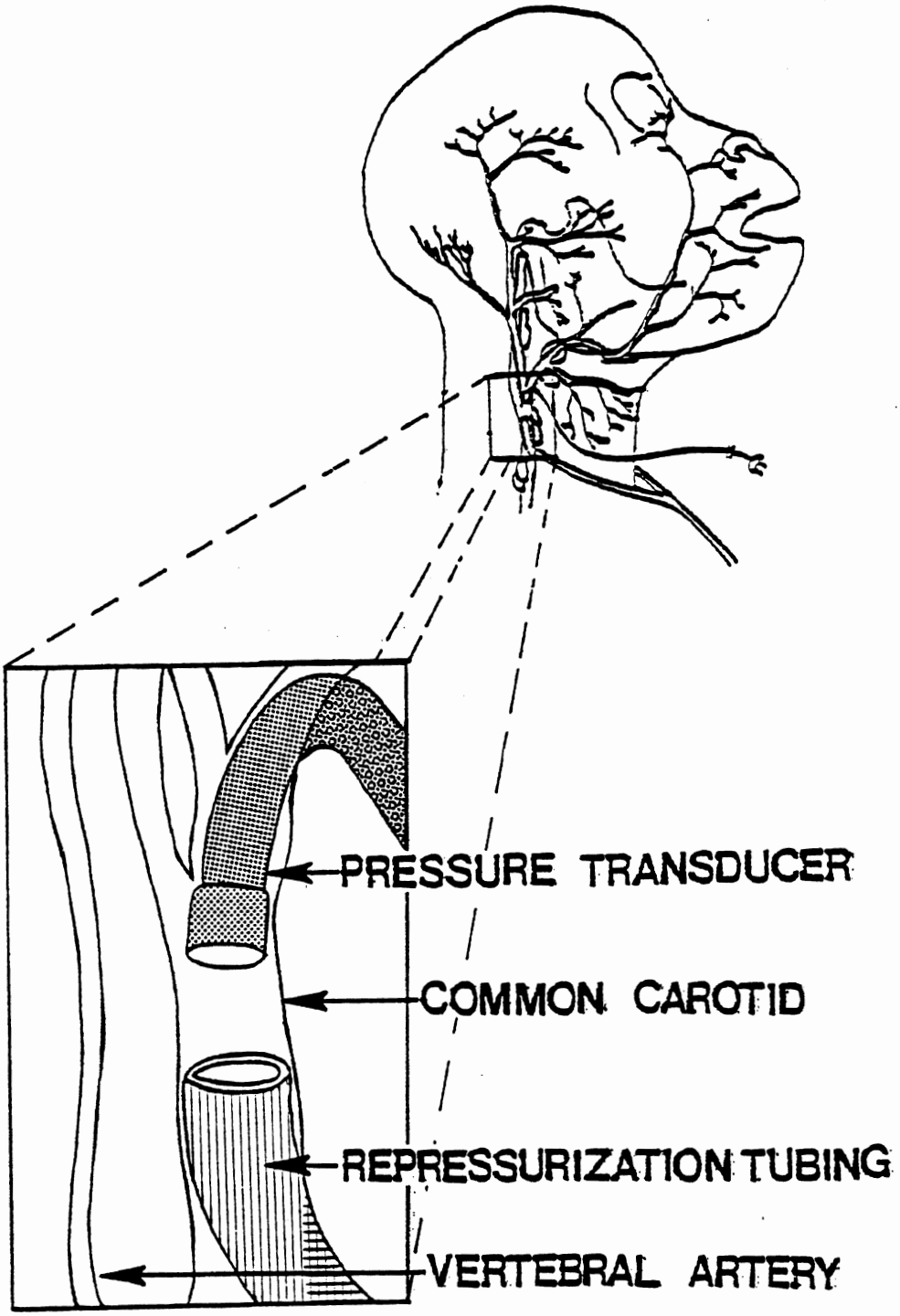

Figure 8

Vascular Repressurization Technique for Rhesus Subject

instrumentation method to another. In general, comparison of mechanical responses between subjects is achieved by referring results to a "standard" anatomical frame which may be easily identified. However, it is impractical to require that transducers be aligned with this anatomical frame, since this may create unnecessary problems. Our alternative is to mount transducers in an arbitrary and convenient reference frame, then describe the transformation necessary to convert the data from this frame to the desired anatomical frame (4).

The three basic reference frames which were used to describe the kinematic quantities are: the instrumentation frame, the anatomical frame, and the inertial (or laboratory) frame. An additional method used to describe the motion in space are the concepts of vectors and frame fields.

Anatomical Reference Frame ($\hat{i},\hat{j},\hat{k}$). The $\hat{i}$-axis and the $\hat{j}$-axis of this reference frame lie in the Frankfort plane. The Frankfort plane is defined as passing through the superior edges of the two auditory meati and the two infraorbital notches. The $\hat{i}$-axis is defined along the intersection of the Frankfort and mid-sagittal planes in the posterior-to-anterior (P-A) direction. The $\hat{j}$-axis is defined along the line joining the two superior edges of the auditory meati, in the right-to-left (R-L) direction. The $\hat{j}$-axis is perpendicular to the mid-sagittal plane at the "anatomical center," which is taken as the origin of the anatomical frame (Figure 9). Finally, the $\hat{k}$-axis is defined as the cross-product of the unit vectors of the $\hat{i}$- and $\hat{j}$-axes, and therefore, will lie in the mid-sagittal plane perpendicular to the Frankfort plane, and will be in the inferior-to-superior (I-S) direction. Thus, the anatomical reference frame ($\hat{i},\hat{j},\hat{k}$), can be completely defined once the four anatomical landmarks are specified.

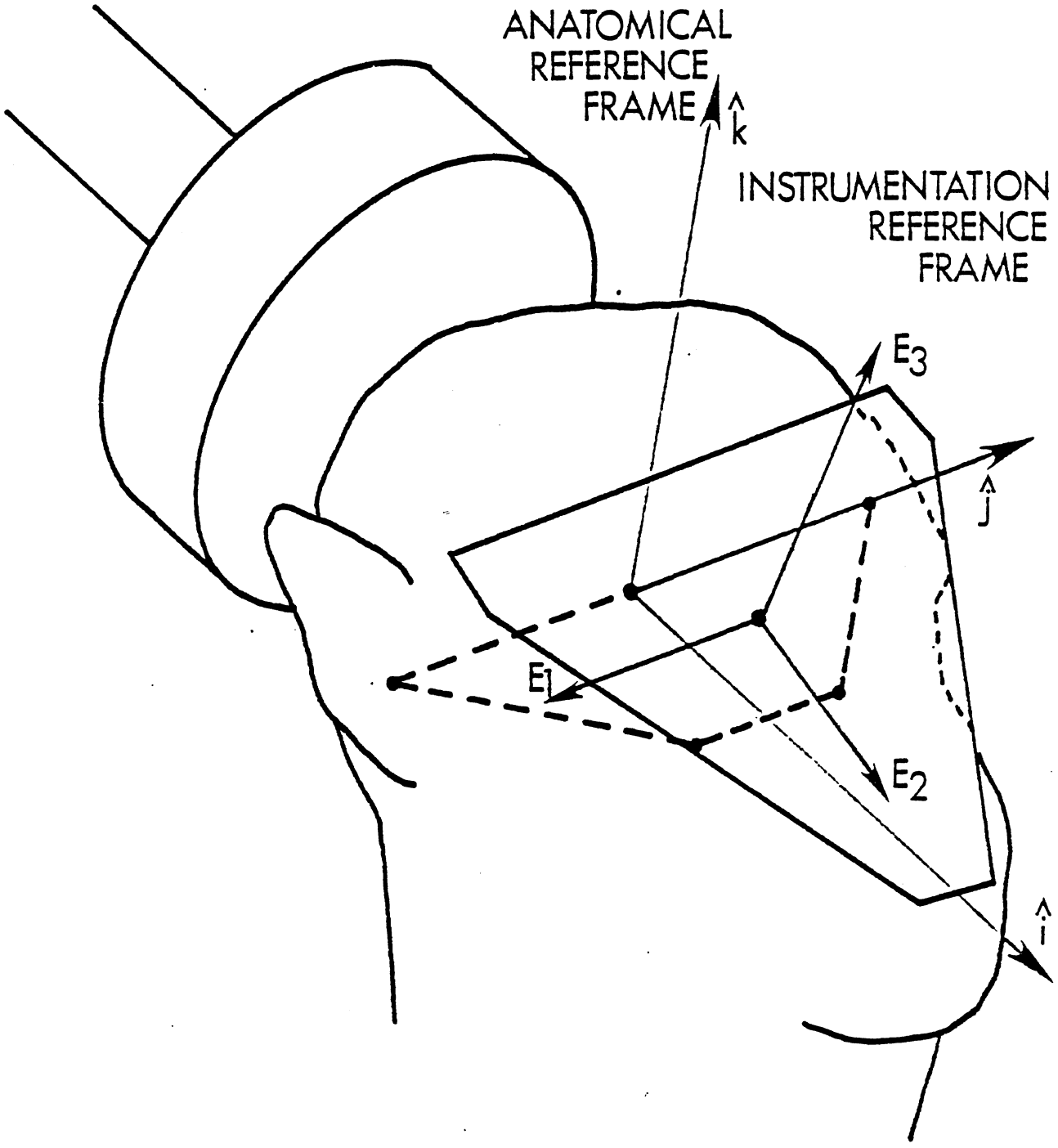

Figure 9

Reference Frames

Instrumentation Reference Frame ($\hat{E}1, \hat{E}2, \hat{E}3$). This orthogonal frame is embedded in the rigid magnesium plate which carries the nine-accelerometers and is defined by its origin and the plane of ($\hat{E}1, \hat{E}2$) which is parallel to the plate (Figure 9). The $\hat{E}3$ axis is defined as the cross-product $\hat{E}1 \times \hat{E}2$. During 3-D radiographic reconstruction this reference plane is identified by the coordinates of four lead pellets permanently installed in the plate to serve as instrumentation landmarks.

The nine-accelerometers are arranged in three clusters, each forming an orthogonal triad, and are designed to be installed on the plate at precise locations and orientations. Thus, once instrumentation reference frame ($E\hat{1},E\hat{2},E\hat{3}$) has been determined, the location and direction of all nine acceleration readings may be accurately determined. These readings are immediately transformed to the anatomical reference frame before any 3-D motion computations are carried out.

Laboratory Reference Frame ($\hat{I},\hat{J},\hat{K}$). It is desired to describe the instrumentation reference frame ($\hat{E}1, \hat{E}2,\hat{E}3$) in terms of the anatomical reference frame ($\hat{i},\hat{j},\hat{k}$) unit vectors:

$$\begin{matrix} \hat{E}1 \\ \hat{E}2 = [E] \\ \hat{E}3 \end{matrix} \qquad \begin{matrix} \hat{i} \\ \hat{j} \\ \hat{k} \end{matrix}$$

where [E] is an orthogonal transformation matrix consisting of the nine unknown direction cosines. This matrix may be determined by first expressing each of the ($\hat{E}1,\hat{E}2,\hat{E}3$) and ($\hat{i},\hat{j},\hat{k}$) in terms of an arbitrary frame ($\hat{I},\hat{J},\hat{K}$):

$$\begin{matrix} \hat{E}1 \\ \hat{E}2 = [U] \\ \hat{E}3 \end{matrix} \qquad \begin{matrix} \hat{I} \\ \hat{J} \\ \hat{K} \end{matrix} \qquad \begin{matrix} \hat{i} \\ \hat{j} = (V) \\ \hat{k} \end{matrix} \qquad \begin{matrix} \hat{I} \\ \hat{J} \\ \hat{K} \end{matrix}$$

then eliminating the $(\hat{I},\hat{J},\hat{K})$ between the two expressions to obtain the matrix [E]:

$$[E] = [U]\,[V]^{-1}$$

Since [U] and [V] are determined from coordinates of several points, the arbitrary frame $(\hat{I},\hat{J},\hat{K})$ will simply be the laboratory frame in which these coordinates are measured. The x-ray method used at UMTRI to measure the points automatically defines the laboratory reference frame.

2.22 Frame Fields - As the head moves through space, any point on the head generates a path in space. In head injury research we are interested in the description of the path of the anatomical center and in events which occur as it moves. A very effective tool for analyzing the motion of the anatomical center as it moves along a curved path (a one-dimensional manifold) in space is the concept of a moving frame (62-65). The path generated as the anatomical center travels through space is a function of time and velocity. A vector field is a function which assigns a uniquely defined vector to each point (such as the anatomical center) along a path. Thus, any collection of three mutually orthogonal unit vectors defined on a path is a frame field. Therefore, any vector defined on such a path (for example, acceleration) may be resolved into three orthogonal components of any well-defined frame field, such as the laboratory or anatomical reference frames. Changes in a frame field over time (e.g. the angular velocity of the frame field) can also be resolved into three components and are then expressed in the dual frame field for the analysis.

In dynamic-biomechanics trauma research, frame fields are defined based on anatomical reference frames. Other frame fields, such as the Frenet-Serret frame (62-64), which contain information about the motion embedded in the frame field, are also useful for describing the motion caused by blunt impact.

The curvilinear distance traveled along the path of the anatomical center is a function of time and can be denoted by s(t) as shown in Figure 10. For a point moving along the path, the absolute vector $(\vec{R}(t))$ is then defined relative to the initial starting position at t=0. The first and second derivatives of the position vector with respect to time yield the velocity and acceleration vectors of the point (the anatomical center), respectively. The time derivative of the path distance, denoted V(t), is called the speed of the curve. At any instant of time, a unit vector $(\hat{T})$ which is tangent to the path at that point on the curve is defined as the derivative $(d\vec{R}/ds)$ of the position vector with respect to the curvilinear distances. Since the velocity vector of the point $(d\vec{R}/dt)$ can be written as $d\vec{R}/ds \cdot ds/dt$, it is possible to substitute the tangent vector $(\hat{T})$ for $d\vec{R}/ds$ and the speed of the curve (V(t)) for ds/dt resulting in the expression $d\vec{R}/dt = T \cdot V(t)$ or $\hat{T} = dR/dt/V(t)$. Thus, $\hat{T}$ can be considered a normalized velocity vector. A second unit vector which is perpendicular to $\hat{T}$, called the principal normal unit vector, $\hat{N}$, can be defined as co-directional with the vector $d\hat{T}/ds$ (since the derivative of a vector is normal to the vector). A third unit vector, the binormal unit $(\hat{B}=\hat{T}x\hat{N})$, completes the orthongal frame and is defined as the cross product of $\hat{T}$ and $\hat{N}$. It can be shown that $\hat{N}$ lies in the plane that contains both the acceleration vector $(\vec{A})$ and velocity vector $(\vec{V})$ of the moving point. Since $\hat{B}$ is perpendicular to both $\hat{T}$ and $\hat{N}$, it is computed as a normalized cross product $\vec{V} \times \vec{A}$ and then $\hat{N}$ is obtained by forming the cross product $\hat{B} \times \hat{T}$.

The three orthogonal unit vectors $(\hat{T},\hat{N},\hat{B})$ shown in Figure 10 form a right-handed triad, called the Frenet-Serret triad at each point along the space curve. The collection of these triads along a given curve is shown as a Frenet-Serret frame field, which is stationary in three-dimensional space. The turning and twisting of a space curve

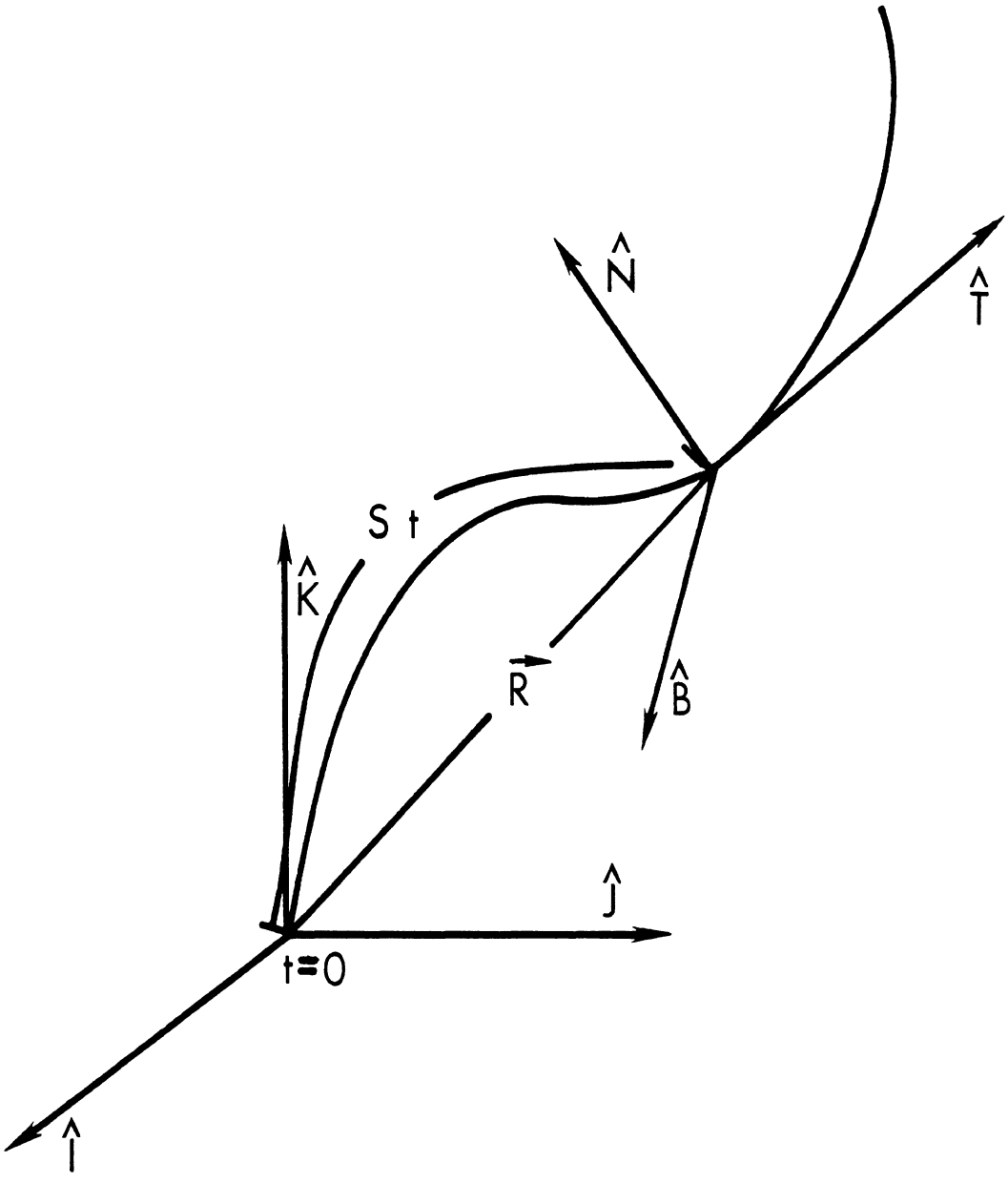

Figure 10

Representation of the Frenet-Serret Frame
for Idealized Motion

generated by a moving point can be described in terms of curvature, κ, and torsion, τ. Curvature, in terms of the Frenet-Serret triad, is defined as $N = d\hat{T}/ds$, while the torsion is given by $N\tau = - d\hat{B}/ds$. The rates of change of $(\hat{T},\hat{N},\hat{B})$ with respect to time may be obtained from the following relations: (T-rate) $d\hat{T}/sr = -\kappa VN, dN/dt = -\kappa VT+\kappa V\hat{B}$, and (B-rate) $d\hat{B}/dt = - \kappa V\hat{N}$. Thus, the turning and twisting of a space curve and the rates of turning and twisting are described by the Frenet-Serret triad $(\hat{T},\hat{N},\hat{B})$.

In many instances, the motion of a point along a path in space can be usefully reparameterized to describe the motion in terms of distance along the path rather than in terms of time. Such a procedure can simplify the formulas associated with the description of the curves and clarifies the similarities and differences in the events that occur as the curve is transversed. Transfer Function Analysis works in this manner.

2.23 Transfer Function Analysis - With blunt impacts, the relationship between a transducer time history at a given point and the transducer time history of another given point of a system can be expressed in the frequency domain through the use of a transfer function. A Fast Fourier Transformation of simultaneously monitored transducer time-histories can be used to obtain the frequency response functions of the impact force and the accelerations of remote points. Once obtained, a transfer function of the form:

$$(Z)(i\omega) = (\omega)\ \mathbf{F}[F(t)/\mathbf{F}[A(t)]$$

can be calculated from the transformed quantities where ω is the given frequency, and $\mathbf{F}[F(t)]$ and $\mathbf{F}[A(t)]$ are the Fourier transforms of the impact force and acceleration of the point of interest, at the given frequency. This particular transfer function is closely related to a mechanical transfer impedance (66) which can be defined as the ratio between the harmonic driving force and the corresponding velocity of the point of interest. Mechanical transfer impedance is a complex valued function which will be discussed

simply in terms of its magnitude and its phase angle. In addition to a transfer function relating force to velocity, a transfer function can be generated which relates the response of one point in the system to another point in the system, the response being expressed in the frequency domain. Analogous to mechanical impedance, a Fast Fourier Transformation of simultaneously monitored transducer time-histories from any two points in the system can be used to obtain the frequency response functions relating those two points. In the case of a force and a pressure, such as impact force and epidural pressure, a transformation of the form:

$$(X)(i\omega) = \mathbf{F}[F(t)]/\mathbf{F}[p(t)]$$

can be calculated from the transformed quantities, where ω is the given frequency, and $\mathbf{F}[F(t)]$ and $\mathbf{F}[p(t)]$ are the Fourier transforms of the impact force time-history and the pressure time-history.

2.24 Spectral Coherence - The coherence function $Cxy^2(\omega)$ is not strictly speaking a transfer function, but instead is a measure of the quality of a given transfer function at a given frequency.

$$Cxy^2(\omega) = |Gxy(\omega)|^2/(Gxx(\omega)Gyy(\omega))$$

where $Gxx(\omega)$ and $Gyy(\omega)$ are the power spectral densities of the two signals, respectively. Power Spectral Density is a Fourier Transform of each signal's auto-correlation. $|Gxy(\omega)|^2$ is the Cross-Spectral Density function squared. Cross-Spectral Density is the Fourier Transform of the cross-correlation of the two signals and ω at the given frequency. By definition, $0 \leq Gxy^2(\omega) \leq 1$. Values of $Cxy^2(\omega)$ near 1 indicate that the two signals may be considered causally connected at that frequency. Values significantly below 1 at a given frequency indicate that the transfer function at that frequency cannot accurately be determined. In the case of an input-output relationship,

values of $Cxy^2(\omega)$ less than 1 indicate that the output is not attributable to the input and is perhaps due to extraneous noise. The coherence function in the frequency domain is analogous to the correlation coefficient in the time domain. The coherence function can be used to determine the useful ranges of the data in the frequency domain.

2.25 Pulse Duration - In order to define the pulse duration, a standard procedure was adopted which determined the beginning and end of the pulse. The procedure was to determine first the peak and the time at which it occurred. Next, the left half of the pulse, defined from the point where the pulse started to rise to the time of peak, was least-squares fitted with a straight line. The rise line intersected the time-axis at a point which was taken as the formal beginning of the pulse. A similar procedure was followed for the right half of the pulse, i.e., a least squares straight line was fitted to the fall section of the pulse which was defined from the peak to the point where the first pulse minimum occurred. The formal end of the pulse was defined then as the point where the fall line intersected the time axis.

2.26 Correlation Functions - Correlation functions will also be used in the analysis of the data. To describe some of the fundamental properties of a time-history, such as acceleration or force, two types of statistical measures may be used:

Auto-correlation Function. This measure is the correlation between two points on a time-history and is a measure of the dependence of the amplitude at time t_1 on the amplitude at t_2.

Cross-correlation Function. This is a measure of how predictable, on the average, a signal (transducer time-history) at any particular moment in time is from a second signal at any other particular moment in time.

The auto-correlation function is formally defined as the average over the ensemble of the product of two amplitudes.

$$R_x(t_1,t_2)=\int\int x_1 \cdot x_2 \cdot p(x_1,x_2,t_1,t_2)dx_1,dx_2$$

where x_1,x_2 are the amplitudes of the time-history and $p(x_1,x_2,t_1,t_2)$ is the joint probability density. Normally, the above definition cannot be used to generate an auto-correlation function directly. However, it can be shown that for a discrete time-history of a finite duration, a close approximation of the auto-correlation function can be obtained through the use of a Fourier transform.

In addition to auto-correlation, cross-correlation can be used to obtain useful information about the relationship between two different time-histories. For example, the cross-correlation between the acceleration measurements at two different points of a material body may be determined for the purpose of studying the propagation of differential motion through the material body. Cross-correlation functions are not restricted to correlations of parameters with the same physical units; for example, one might determine the cross-correlation between the applied force and the acceleration response to that force. Similar to the auto-correlation function, the calculation of the cross-correlation of two signals begins by taking the Fourier transform of both time-histories (Y_1,Y_2). The cross-spectral density is the complex valued function ($Y_1 \cdot Y_2^*$). The cross-correlation is then the Fourier transform of the cross-spectral density.

3.0 RESULTS

Table 1 lists the initial test conditions. Table 2 lists the Rhesus biometric measurements. Table 3 summarizes the head impacts. Table 4 reports the injuries/damages for which the preliminary analysis of the kinematic response was

reported earlier (30) and Table 5 reports the injuries/damages for which the kinematic response is being reported here.

A gross pathological inspection was carried out for each test subject. The observed injuries included linear and basilar skull fractures as well as subdural/ subarachnoid hemorrhaging. These have been coded in DOT format and are illustrated in Appendix A. All of the injuries reported are focal injuries. No attempt was made to analyze diffuse injuries.

The general kinematic relationships associated with injury were that when skull fracture occurs, a rapid increase in angular velocity, acceleration, and the normal components of the translational acceleration results. These are illustrated in the data included in Appendix B. Particularly significant mechanisms are presented in the discussion section.

Appendix C is the ECG information from selected subjects (30). Appendix D is the preliminary data reported at the 23rd Stapp Car Crash Conference. Appendix E is the preliminary data reported at the 28th Stapp Car Crash Conference. Appendix F is a paper on the finite element modeling analysis reported in the Journal of Space, Aviation and Environmental Medicine. Appendix G is the preliminary analysis submitted to the 30th Stapp Car Crash Conference. Appendix H is the testing protocol.

Table 1. Rhesus Head Impact
Initial Test Conditions

Test No.	Subject Condition	Repressurization Condition	Subject Positioning Center of Gravity With Respect to Occipital Impact	Neck Condition	Velocity (m/s)
78A232	postmortem	unrepressurized	below	unstretched	11.5
78A234	postmortem	unrepressurized	below	unstretched	13.5
78A236	postmortem	unrepressurized	at	unstretched	12.5
78A238	postmortem	unrepressurized	above	unstretched	12.5
78A239	anesthetized	--	at	unstretched	12.5
78A241	anesthetized	--	above	unstretched	12.5
79A249	anesthetized	--	at	unstretched	15.4
79A251	anesthetized	--	at	unstretched	13.0
79A253	anesthetized	--	at	unstretched	14.8
79A256	postmortem	unrepressurized	at	unstretched	15.4
79A258	postmortem	unrepressurized	at	unstretched	14.5
79A260	postmortem	unrepressurized	at	unstretched	16.0
85R002	postmortem	repressurized	above	unstretched	11.0
85R005	postmortem	repressurized	above	unstretched	12.2
85R006	postmortem	repressurized	above	unstretched	11.9
85R008	postmortem	repressurized	above	unstretched	11.0
86R010	postmortem	unrepressurized	above	unstretched	11.0
86R011	anesthetized	--	above	stretched	10.0
86R012	anesthetized	--	above	stretched	12.2
86R013	anesthetized	--	above	stretched	11.9
86R014	anesthetized	--	above	unstretched	11.9
86R015	anesthetized	--	above	unstretched	12.1

Table 2. Rhesus Biometric Measurements*

Test No.	Height (Sitting) (cm)	Mass (kg)	Max. Skull Length (cm)	Max. Skull Breadth (cm)	Ave. Skull Thickness (cm)	Head Muscle Mass (g)	Head Mass (g)	Brain Mass (g)	Brain Volume (ml)
78A232	49.1	6.9	7.4	6.1	0.47	94	276	70	N/A
78A234	53.6	9.5	7.4	5.6	0.28	135	907	105	95
78A236	53.4	8.2	6.6	5.6	0.24	149	510	100	100
78A238	53.9	8.2	6.9	5.6	0.23	130	540	115	90
78A239	48.8	8.2	6.4	5.3	0.22	80	510	85	75
78A241	47.0	10.6	8.4	6.4	0.43	190	750	125	115
79A249	55.0	5.8	6.5	5.5	0.40	128	454	85	80
79A251	66.1	7.7	8.0	6.0	0.45	113	726	113	105
79A253	58.5	5.0	6.8	5.5	0.25	99	610	92	85
79A256	61.3	6.9	7.0	6.0	0.10	106	823	99	80
79A258	62.0	7.6	7.0	5.5	0.26	85	595	110	90
79A260	61.8	7.1	7.3	6.0	0.41	113	957	85	90
85R002	71.0	5.0	6.2	5.8	0.38	116	475	71	75
85R005	72.3	9.1	7.5	6.0	0.38	287	N/A	99	100
85R006	67.3	8.4	7.2	6.0	0.31	191	481	99	90
85R008	65.0	6.8	N/A	N/A	0.25	156	511	N/A	70
86R010	70.0	7.3	7.2	5.5	0.25	198	595	99	80
86R011	66.0	4.9	6.5	5.0	0.41	142	425	99	80
86R012	68.5	6.9	6.5	5.5	0.35	170	479	99	70
86R013	86.5	8.7	6.8	5.6	0.30	225	709	113	100
86R014	71.0	8.6	6.5	5.5	0.35	298	759	113	95
86R015	69.0	8.0	7.0	6.0	0.25	255	730	113	90

*All test subjects were Macaca mulatta except 78A232 which was Macaca assamenis.

Table 3. Rhesus Impact Test Summary

Test No.	Linear Acceleration Tangent m/s/s/	Resultant Acceleration m/s/s/	Resultant Angular Acceleration r/s/s	Resultant Angular Velocity r/s	Linear Velocity m/s	Epidural Pressure Kpa	Force N	Force Duration ms
78A232	7000	7000	22000	40	12	117	5800	3
78A234	8000	6400	38000	40	14	N/A	5700	4
78A236	7000	7000	28000	30	13	-9	5600	4
78A238	7100	8000	40000	60	13	-100,55	6600	4
78A239	8000	8000	41000	60	13	260	5000	5
78A241	8400	8000	54000	70	13	490	8700	3
79A249	14000	15000	70000	63	16	-70	7200	4
79A251	13000	14000	64000	75	13	200,-110	7500	4
79A253	10000	10000	40000	75	15	-101	5400	5
79A256	11000	11000	70000	84	16	N/A	6000	10
79A258	10000	12000	70000	75	15	-35,40	5700	5
79A260	13000	13000	60000	80	16	140,-100	7100	4
85R002	5300	5300	7900	30	12	270	4000	4
85R005	20000	18000	28000	45	15	-100,-105	N/A	N/A
85R006	11000	10000	65000	75	13	375	7500	5
85R008	11000	11000	60000	70	16	-98,-100	5800	5
86R010	7900	7900	16000	33	11	-375	7000	4
86R011	6000	5300	33000	24	13	11	N/A	N/A
86R012	18000	18000	110000	130	16	45	7000	4
86R013	9000	8800	80000	105	13	75	4900	5
86R014	12000	11000	120000	105	15	250	7000	4
86R015	13000	11000	120000	90	16	140,190	6500	4

Table 4. Rhesus Injuries/Damage Summary

Test No.	Gross Skull	Gross Brain	Gross Other
78A232	No injury	No injury	Epidural hematoma at C1, dura lacerated at C1
78A234	No injury	No injury	Epidural hematoma at C1, torn muscle at base of occiput
78A236	No injury	No injury	No abnormality or injury
78A238	No injury	No injury	Epidural hematoma at C1 disk
78A239	No injury	No injury	1/4 cc blood in occiput from epidural hematoma at C1
78A241	No injury	No injury	Epidural hematoma at C1
79A249	Basilar fracture (ring)	3/4 cc subdural hematoma right frontal lobe (cerebrum) subarachnoid hemorrhage base of cerebellum, pons, and medulla	Epidural hematoma at C1, occipital muscles damaged
79251	Linear basilar fracture from foramen magnum to occipital contact point	No injury	Epidural hematoma at C1 and C2
79A253	Basilar fracture (quasi-ring), temporal fracture	Petechial lesion left frontal lobe (cerebrum) subarachnoid hemorrhage base, pons, medulla and vermis of cerebellum	Damaged neck ligaments
79A256	Basilar fracture (petrous to petrous). Connected linear fracture to parietal bone*	Dura torn along sagittal sinus, emaciated tissue cerebellum, medulla	Lacerated spinal cord
79A258	Basilar fracture (quasi-ring)	Lacerated medulla	Epidural hematoma at C1
79A260	Basilar fracture (right petrous)	Subdural hematoma along sagittal sinus	Epidural hematoma at C1

*Abnormality - Test subject had very thin skull.

Table 5. Rhesus Injuries/Damage Summary

Test No.	Gross Skull	Gross Brain	Gross Other
85R002	No injury	No injury	No injury
85R005	Basilar skull fracture	Subarachnoid hemorrhage at medulla and brain stem	No injury
85R006	No injury	No injury	No injury
85R008	Basilar ring fracture*	Subarachnoid hemorrhage at medulla and brain stem	No injury
86R010	Basilar ring fracture	No injury	No injury
86R011	No injury	No injury	Subdural hemorrhage of spinal cord at base of brain
86R012	No injury	Subdural hemorrhage left frontal lobe	No injury
86R013	No injury	Subdural hemorrhage left frontal lobe	No injury
86R014	No injury	No injury	Subdural hemorrhage of spinal cord at base of brain
86R015	Linear fracture of superior right petrous Linear fracture of left occipital, Linear fracture of right temporal	No injury	Bilateral hemorrhage to side of spinal cord at base of medulla

*Abnormality - Test subject had a thin skull

4.0 DISCUSSION

The results of a series of head impact experiments conducted over the past nine years at the University of Michigan Transportation Research Institute (UMTRI) using anesthetized and postmortem Rhesus are presented. The tests entail different initial conditions and are compared to tests of another human surrogate (i.e., the repressurized human cadaver) reported previously (30-34). Frame-independent variables and vectors were used to compare these different tests. The frame-independent vectors used included tangential and normal acceleration. The significant frame-independent vector, tangential acceleration, will be presented in detail throughout the discussion.

It would be preferable to be able to run a limited set of experiments and to generalize the results. However, because of the geometry of the skull-brain-spinal cord, the possible different initial conditions, the complex interaction of the skull with the brain, and the different injury modes that can result from blunt impact, the results presented here apply only to the test conditions in which the experiments were run and may not apply to all situations. The features of the data, discussed in this section in abbreviated form, represent trends that are felt to be important factors in head injury research.

Head impact response is a complicated phenomenon; however, the results from these experiments indicated that, in a limited sense, the injury and kinematic response of a repressurized-postmortem subject is probably closer to that of the live subject than is that of the unrepressurized-postmortem subject. In all cases, negative pressure peaks occurring during an impact event equal to or greater than one atmosphere did not appear to produce injury in Rhesus subjects. The cervical cord and foramen magnum seemed to be important structural features in head impact response, and their interaction with the

rest of the head (e.g., the skull, brain, cerebrospinal fluid) was an important aspect of the injury mechanisms.

The experiments can be broken into three significant classes: repressurized-postmortem subjects, unrepressurized-postmortem subjects and live anesthetized subjects. Each class can be divided into two groups, skull fracture and no skull fracture. In addition, the anesthetized test subjects can be divided into two groups, neck-stretched and neck-unstretched. In general, there were two-four subjects in each grouping. Therefore, when comparing between groupings, it is necessary to use only the most robust aspects of the data.

4.1 Overview of Previous Studies - A previous study indicated that frame fields, such as the Frenet-Serret Frame, would be useful in describing head impact motion (30). The study also showed that the response of the head in blunt impact is affected by the geometry of the skull in the region of contact during the time of contact, that is, during the interval between the initiation of head impact response (Q_1) and the positive maximum (Q_2) of the tangential acceleration time-history. During the Q_1-Q_2 interval, the angular acceleration of the head was found to be principally in the binormal direction (although lesser components in the normal and tangential directions also were found). This implies that the skull may have been rotating about a point of closest approach of the skull to the impactor (soft tissue prevented the actual contact of the skull and impactor surface). Figure 11, a reconstruction of subject x-rays, shows that the shape of the human skull in the posterior region is considerably different from the non-human macaques[2].

---

[2]The study consisted of a sample of macaques. All of the macaques were Macaca mulatta (Rhesus), except one which was Macaca assamenis.

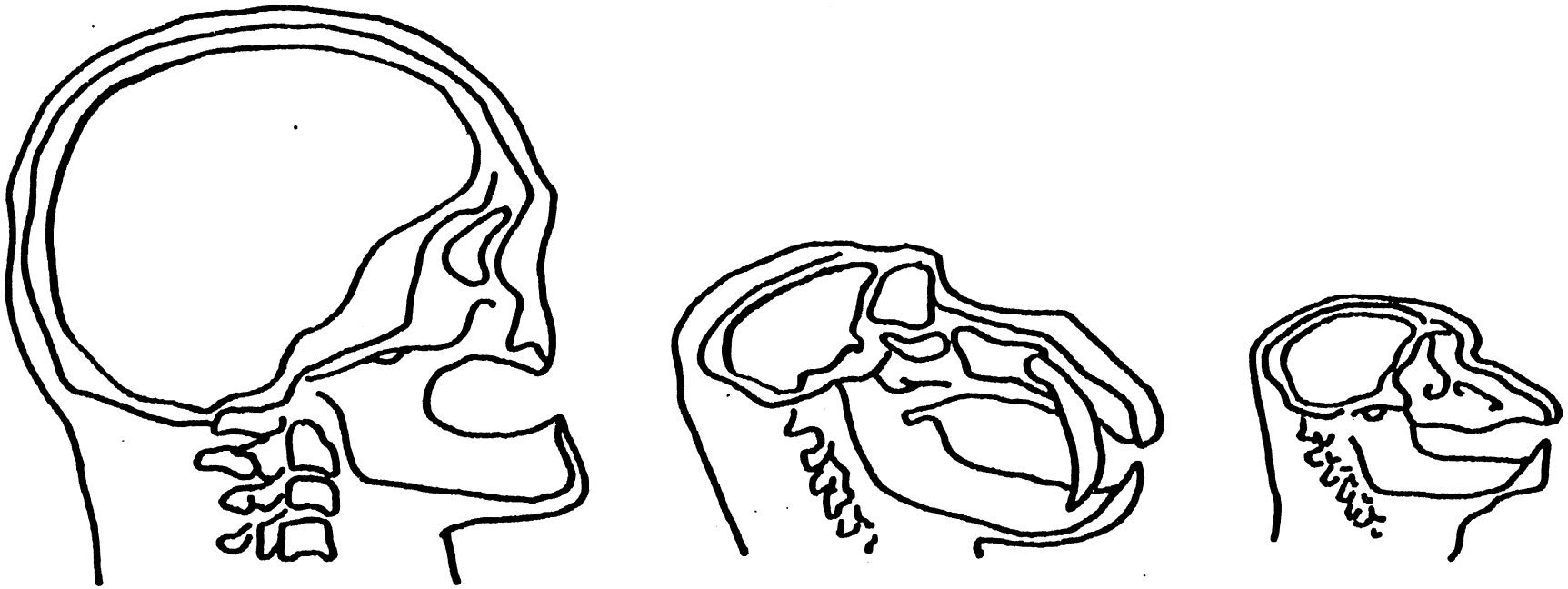

X-RAY RECONSTRUCTION

Figure 11

By varying the center of mass of the macaque subjects in relation to the applied impact force axis to adjust the applied torque, this study demonstrated that head motions dynamically similar to cadaver impacts can be generated only if the macaque subjects are placed in an initial position which compensates for the difference in skull geometry between the lower primate and cadaver.

Similarly, this study showed that the differences between the macaque and the cadaver in soft tissue distribution and mass of the head-neck also significantly affected the response of the head during blunt impact. Physically, head impact response is interpreted as the response of a material body (the skull) which is in contact with other material bodies (e.g., the neck, the impactor, the brain and soft tissues). In the cadaver, the brain is the primary source of soft tissue, while in the macaque, the external head and neck muscle masses constitute the majority of the soft tissue. These differences in the mass and distribution of the soft tissues of the cadaver and macaque may create problems in determining which of the material bodies contribute more to the impact motion of the skull. For example, the motion of the external muscle masses in the macaques can mask the effects of the motion of the brain on skull response.

This study also indicated that differences in impact response exist between anesthetized and postmortem macaque subjects. In addition, the values for peak epidural pressures in anesthetized macaques were found to be two to five times the values of those in the postmortem macaques. A comparison between the power spectra of the two conditions implied that the brain of the anesthetized subject was "stiffer" than that of unrepressurized postmortem subject.

The differences between the live anesthetized and postmortem macaque brains were further substantiated in a study conducted in which the results from five Rhesus

head impacts were integrated by simulating the tests using a three-dimensional mathematical model of the macaque brain (34). The results of the modeling showed that to simulate the live, anesthetized response, the mathematical model (a finite element model) must have a Poisson's ratio of .4999 and a 20 cm cervical cord. In order to simulate a postmortem response, the mathematical model must have a lower Poisson's rato of .499 and no cervical cord. These results implied that the response of the postmortem brain is slower and more damped than that of the live brain. Also, the postmortem brain was, in effect, more compressible than the anesthetized brain and, as a result, pressure (stress) in the postmortem brain was lower than what would have occurred in the live brain under similar conditions. In addition, the unpressurized cervical cord and flaccid neck in the postmortem subject may uncouple the cervical cord from brain response. Thus, it appeared that one effect of the spinal cord was to increase the intracranial pressure of the impact response for the live, anesthetized macaque subjects.

In another previous study, it was concluded that the three-dimensional rigid body motion of the head is not well defined during a "severe head impact" when the motion is measured by accelerometers affixed to the skull (31). In such impacts, local skull deformation near the accelerometers was interpreted by the nine-accelerometer array as an angular acceleration. Therefore, when the skull deformations were significant, the three-dimensional motion recorded by the nine-accelerometer array and the interpreted motion of the skull local to the instrumentation mount could only be used to estimate the motion of the rest of the skull. This study also showed that skull deformation correlated well with injury. Subarachnoid hemorrhage, especially, did not occur without significant skull deformation being present. In addition, it was shown that two skull-brain interactions seem to operate in head impacts. Initially, during impact, energy is

transferred from the skull to the brain with a pressure gradient, positive pressures near the frontal bone to negative pressures near the occipital bones, resulting. Secondly, the energy stored in the brain is transmitted during or after impact back to the skull, with positive pressures occurring at the frontal, parietal, and occipital bones.

When observed injuries were correlated with epidural pressure changes, this study also implied that cavitation might not be a mechanism of injury. For some anesthetized Rhesus subjects, for example, the epidural pressure transducers measured negative pressure peaks of -1 atmosphere or slightly greater during an impact event, yet no injuries were observed near the pressure transducer sites.

The preliminary analysis of the data being reported here (33) compared the results of two Rhesus head impact studies and qualified, in a limited sense, the differences among the anesthetized, the unrepressurized-postmortem, and the repressurized-postmortem Rhesus models. It was anticipated that the information would assist the evaluation of the unembalmed repressurized human cadaver model as a dynamic-biomechanics surrogate for the injurious blunt head impact response of the live human.

That analysis generated conclusions which may prove significant for modeling head impact response. First, in terms of peak pressure, the repressurized-postmortem and the anesthetized Rhesus were significantly different from the unrepressurized-postmortem Rhesus. The peak pressures of the unrepressurized-postmortem Rhesus were between 95 and 150 kpa and the peak pressures for the anesthetized and repressurized-postmortem Rhesus were between 250 and 500 kpa. In addition, for some tests, the peak pressures for unrepressurized-postmortem Rhesus were opposite in sign to those of the anesthetized and repressurized-postmortem Rhesus. Second, the repressurized-postmortem Rhesus, when compared to the unrepressurized-postmortem Rhesus, was more similar in response

to that of the anesthetized Rhesus, as determined by the similarities in the transfer functions between tangential acceleration divided by epidural pressure for the two classes. However, the differences detected between the repressurized-postmortem and anesthetized Rhesus may be important in terms of kinematic response. When a cross-correlation function was done between tangential acceleration and epidural pressure, analysis showed that the anesthetized and repressurized-postmortem subjects had very similar phase lags. However, it seemed that the postmortem brain, whether repressurized or unrepressurized, was not as "stiff" as that of an anesthetized subject, either due to postmortem degradation of brain tissues or incomplete repressurization. Third, in terms of subarachnoid hemorrhage in the medulla-pons area associated with skull fracture, the repressurized-postmortem and anesthetized Rhesus were similar in focal injury response. Therefore, for the above reasons, it appears that the repressurized-postmortem Rhesus subjects may most closely approximate the anesthetized subject. This result may have important implications on the use and effectiveness of unembalmed repressurized human cadavers as surrogates for live humans in dynamic-biomechanics studies.

The final analysis of the data being reported here reconfirmed the preliminary analysis reported earlier (33). The most recent Rhesus impacts clearly indicate that: 1) The initial positioning of the head-neck system is a critical factor associated with the brain-cerebrospinal fluid system's response to head impact; 2) The thermodynamic response of the cerebrospinal system is an important consideration when the impact produced significant tension; 3) No relationship could be found between focal injury and negative pressures equal to one atmosphere; and 4) The stress in the brain, as well as the interaction of the brain with the skull, are significantly affected by: the tension in the brain, limited by vaporization in "severe impact"; the interial properties of the cervical

cord as well as the flow of material through the foramen magnum; the initial position of the head-neck system; and the repressurization of postmortem surrogates.

4.2 Impact Response Definition - Using the UMTRI nine-accelerometer array, it is possible to record three-dimensional six-degrees-of-freedom motion of an area of the skull in which the accelerometers are located. Thus, head impact response can be defined as a continuum of "events" characterized by the path traced by the motion of the "estimated anatomical center," by all the vectors defined on that path, and by the changes of the accelerated frame fields. Physically, head impact response is interpreted as the response of a material body (i.e. the nine-accelerometer array and the area of the skull local to it) in contact with other material bodies. The curve and the vectors generated as the "estimated anatomical center" moves in time are, therefore, a result of the interactions of the skull-mount area with other material bodies.

The motion of a rigid body in space is the result of generalized forces: the total force and the total torque about an axis. The dynamic problem of the motion of the area of the skull local to the nine-accelerometer array can be interpreted similarly. However, because of the complex interactions of the area of the skull local to the nine-accelerometer array with the other material bodies involved (i.e. the muscle soft tissues of the neck, the rest of the skull, the brain, or the impactor), serious problems can arise in determining which of the bodies contributes more to these generalized forces.

Specifically, when the head receives an impact, several events occur: 1) stress waves are propagated from the impact site, 2) the skull starts to deform, and 3) the skull begins to move due to the impact, transmitting energy to the brain via the dura mater. Eventually, the stress waves are dissipated, the deformation of the skull recovers partially or fully on removal of the impact loads, and the acceleration of the skull continues

primarily from forces generated by the brain and neck. If the differential skull motion is severe, essentially due to the high frequency components of the force time-history or to injurious peak force, the stresses at some point in the skull may exceed the failure strength of the bone, thereby producing fracture. Dynamic human cadaver impact experiments have shown that the motion of the entire skull as a rigid body as estimated by the nine-accelerometer array depends on the degree of skull deformation as well as on the degree of precision being used in the investigation (31). If the skull deformations are small during and after impact and the accelerometers are sufficiently far from the impact contact point, then valid rigid body motion can be assumed. However, if skull deformations are significant, then the three-dimensional motion of the nine-accelerometer array and of the skull local to its instrumentation mount can only be used to approximate the motion of the rest of the skull through the use of an "estimated anatomical center." Interpretation of the data from the nine-accelerometer array, therefore, must take into account the non-rigid body motion taking place during "significant skull deformation" impacts. Using translations obtained from x-rays, the three-dimensional approximate motion of an "estimated anatomical center" can be determined. For the Rhesus model, however, the accelerometers are located on the orbital ridges and dental palate, sufficiently far from the impact site so that the local perturbations are small even when the skull fractures (30-31). If the skull near the nine-accelerometer array had been significantly perturbed by skull fracture, then the mechanical impedance of the skull fracture tests should have been different from that of the no-skull-fracture tests. This, in general, was not the case. The mechanical impedance transfer functions in the appendix show that the Rhesus mechanical impedance for both skull-fracture and no-skull-fracture tests were the same. Based upon human cadaver data, that result is different from what

would be expected for the live human. It is believed that the mechanical impedance observed for the Rhesus tests was a result of the different skull geometry and soft-tissue distribution between the Rhesus and human cadaver models. The observation implies that the effect of skull deformation on the nine-accelerometer recording is different for the Rhesus as compared to the human cadaver models.

4.3 Repressurization Technique - The results presented here regarding the repressurized-postmortem Rhesus are potentially a function of the repressurization technique used. Different repressurization techniques may give different results. The repessurization techniques developed for Rhesus subjects are similar to those used for repressurized human cadavers (30-34). However, because of the smaller size of the vessels of the vascular system of the Rhesus as compared to that of the human cadaver, somewhat different procedures had to be used (See Figure 12). The Rhesus vertebral arteries were not ligated. The pressure transducer used to monitor the carotid pressures, and, therefore, used to determine the vascular pressure in the brain, was placed in different locations in the two species. In the cadaver model the transducer was in the internal carotid close to the entrance of the carotid into the brain. In the Rhesus model the transducer was in the external carotid distal to the brain. In the Rhesus model the pressure transducer in the external carotid artery restricts the flow of the internal carotid artery at the measurement site. The precise differences this makes between the results is unknown. The initial repressurization levels may not be comparable. In addition, it was more difficult to remove the air in the Rhesus skull-brain area than in the cadaver model; thus, a greater proportion of the Rhesus brain cavity may have contained air than that of the cadaver brain cavity.

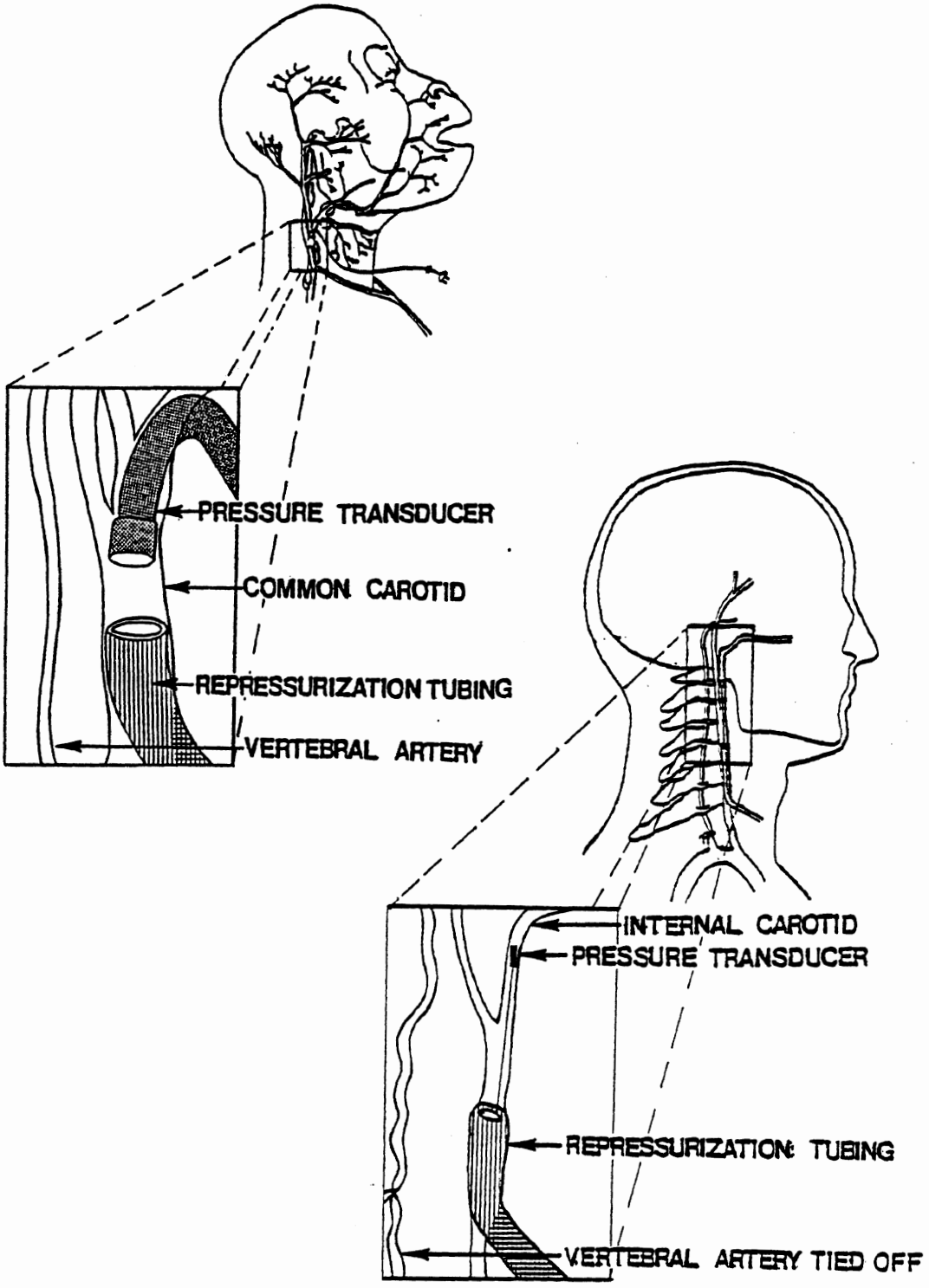

Figure 12

Vascular Repressurixation of the Rhesus and Human Cadaver

Transfer functions are useful tools in characterizing the impact response of a material body (e.g., a biological subsystem). In the case of the head, energy is transferred from the impactor to the skull and from the skull to the brain. Therefore, to assist in characterizing this energy flow, transfer functions, such as ones for tangential acceleration divided by epidural pressure, are useful. Successful understanding of the performance of a given system depends on being able to predict accurately the output response for a given input. In the case of a time invariant linear system, a transfer function can be generated that characterizes the system and is independent of the input to the system, i.e., it is an invariant of the system. Comparisons of outputs for different inputs will show some variations, but transfer functions that characterize the system will not. In general, systems in the real world are inherently non-linear and that is probably also true for the head when struck by a blunt impactor. We can, however, assert that a linear system is a valid approximation of a non-linear one over a limited range such as the range seen in these experiments. For example, if a transfer function generated for a tangential acceleration divided by epidural pressure for an impact to an unrepressurized Rhesus subject is compared to another transfer function of the same parameters for an anesthetized Rhesus subject and is found to be similar, then the transfer functions correlated well and represent the same biological system, when they are found to be different, then the transfer functions do not correlate well and are said to be representing different biological systems. For the tests being reported here the force time-histories are similar enough so that a valid linear range can be assumed.

4.4 The No-Skull-Fracture-Impacts - Comparison of the three classes of no-fracture head impacts in which the initial conditions were impact velocity of 11.5-12.5 m/s, neck-unstretched positioning, line of impact below the head center of mass,

2.5 cm Ensolite padding and the pressure transducer located at the front of the skull imply that:

1. The unrepressurized-postmortem Rhesus is significantly different than the anesthetized Rhesus as shown by the transfer function relationships of - tangential acceleration divided by epidural pressure.
2. In terms of peak pressure (largest absolute value), the repressurized postmortem Rhesus' response is more similar to the anesthetized Rhesus' than the unrepressurized-postmortem Rhesus'.
3. The impact responses of the anesthetized and unrepressurized/repressurized postmortem Rhesus were all different as shown by the transfer function relationships of tangential acceleration divided by epidural pressure.

Inspection of the peak pressures presented in Table 3 shows that the peak pressures of the unrepressurized-postmortem Rhesus were between 95 and 150 kpa and that the peak pressures for the anesthetized and repressurized-postmortem Rhesus were between 250 and 500 kpa. Although there was a limited number of tests in each category, the results were consistent enough to show that in terms of peak pressures, the anesthetized and the repressurized-postmortem subjects were similar. In addition, for some of the tests, the peak pressures for the unrepressurized postmortem Rhesus were opposite in sign to those of the anesthetized- and repressurized-postmortem Rhesus. See Test 78A236 in the appendix.

Figure 13 represents the transfer function corridors for the tangential acceleration divided by the epidural pressure for the no-fracture class of Rhesus subjects. The key defines the corridors for the anesthetized, the unrepressurized-postmortem, and the repressurized-postmortem Rheus subjects. It is clear from this figure that the analysis of

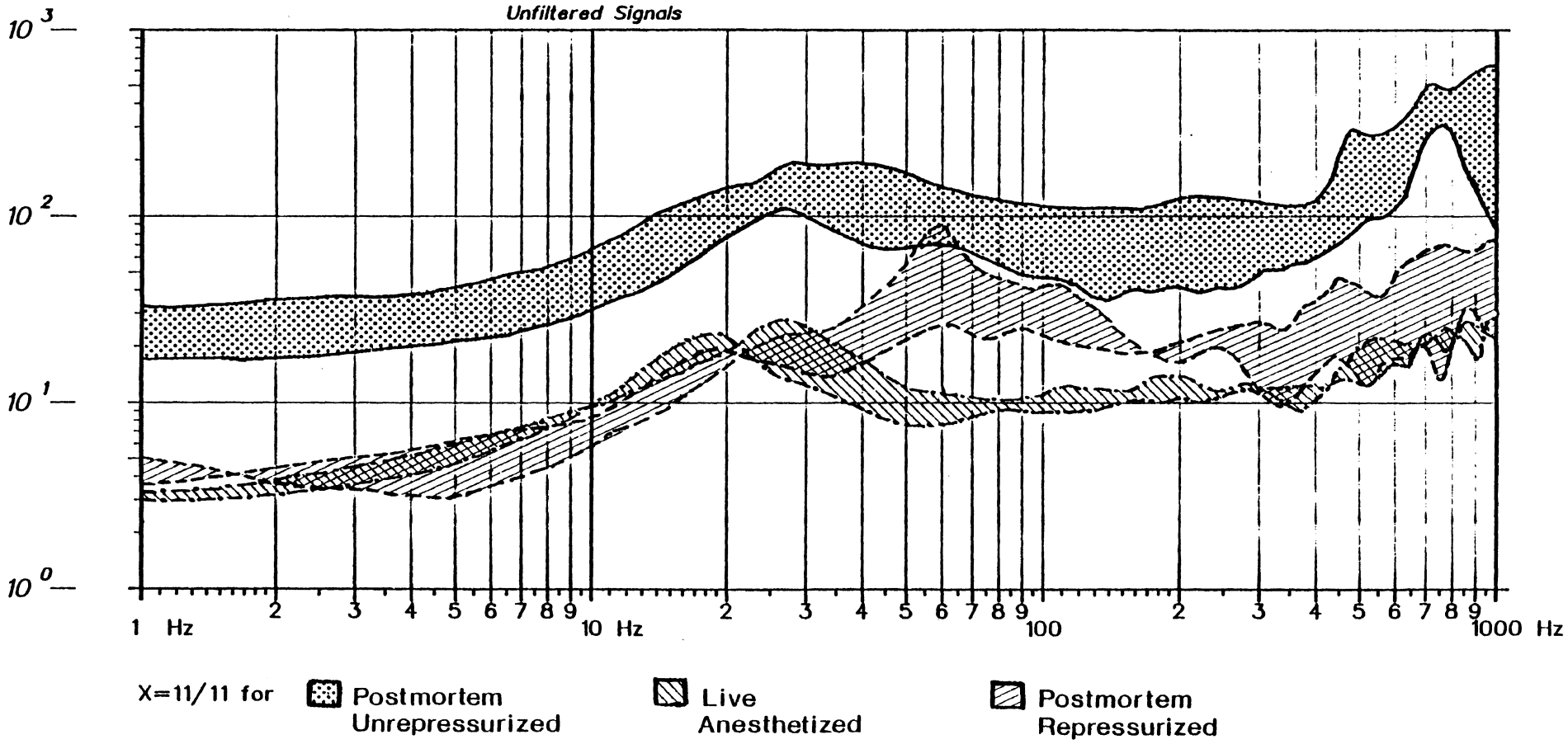

FIGURE 13: TRANSFER FUNCTION CORRIDORS TANGENTIAL ACCELERATION/EPIDURAL PRESSURE NO-FRACTURE RHESUS

the relative magnitudes of the signals agrees with that associated with the comparison of the peak pressures. However, it is also evident that the waveforms of the epidural pressures with respect to the tangential acceleration have some detectable differences. Therefore, it can be concluded that even though the repressurized-postmortem Rhesus was more similar than the unrepressurized-postmortem Rhesus to the anesthetized Rhesus in response, there were still detectable differences between them.

Transfer functions are complex-valued, including both magnitude and phase. The phase relationship was evaluated with the cross-correlation function. The analysis obtained from the cross-correlation function between the tangential acceleration and the epidural pressures shows that: 1) Effectively there was no phase lag between the tangential acceleration and the epidural pressure for the anesthetized subjects (See Figure 14 which illustrates the maximum positive cross-correlation at zero lag; 2) An effective phase lag between the tangential acceleration and the epidural pressure of one or two milliseconds for repressurized postmortem Rhesus was observed (See Figure 15 which illustrates the maximum positive cross-correlation at one to two milliseconds); and 3) the greatest phase lags between tangential acceleration and the epidural pressure were observed for unrepressurized subjects (See Figure 16 which illustrates the maximum negative cross-correlation for some of the tests). The anesthetized and the repressurized-postmortem subjects had very similar phase lags between tangential acceleration and epidural pressure. Therefore, repressurization seemed to make the postmortem subject a better model of the anesthetized subject. However, it seems that the postmortem brain, whether repressurized or unrepressurized, was not as "stiff" as that of an anesthetized subject. This may have been due to the postmortem degradation of the brain tissues, incomplete repressurization, or to the repressurization process not removing all of the air

FIGURE 14: ANESTHETIZED RHESUS, NO SKULL FRACTURE, NECK UNSTRETCHED

Cross- and Auto- Correlations

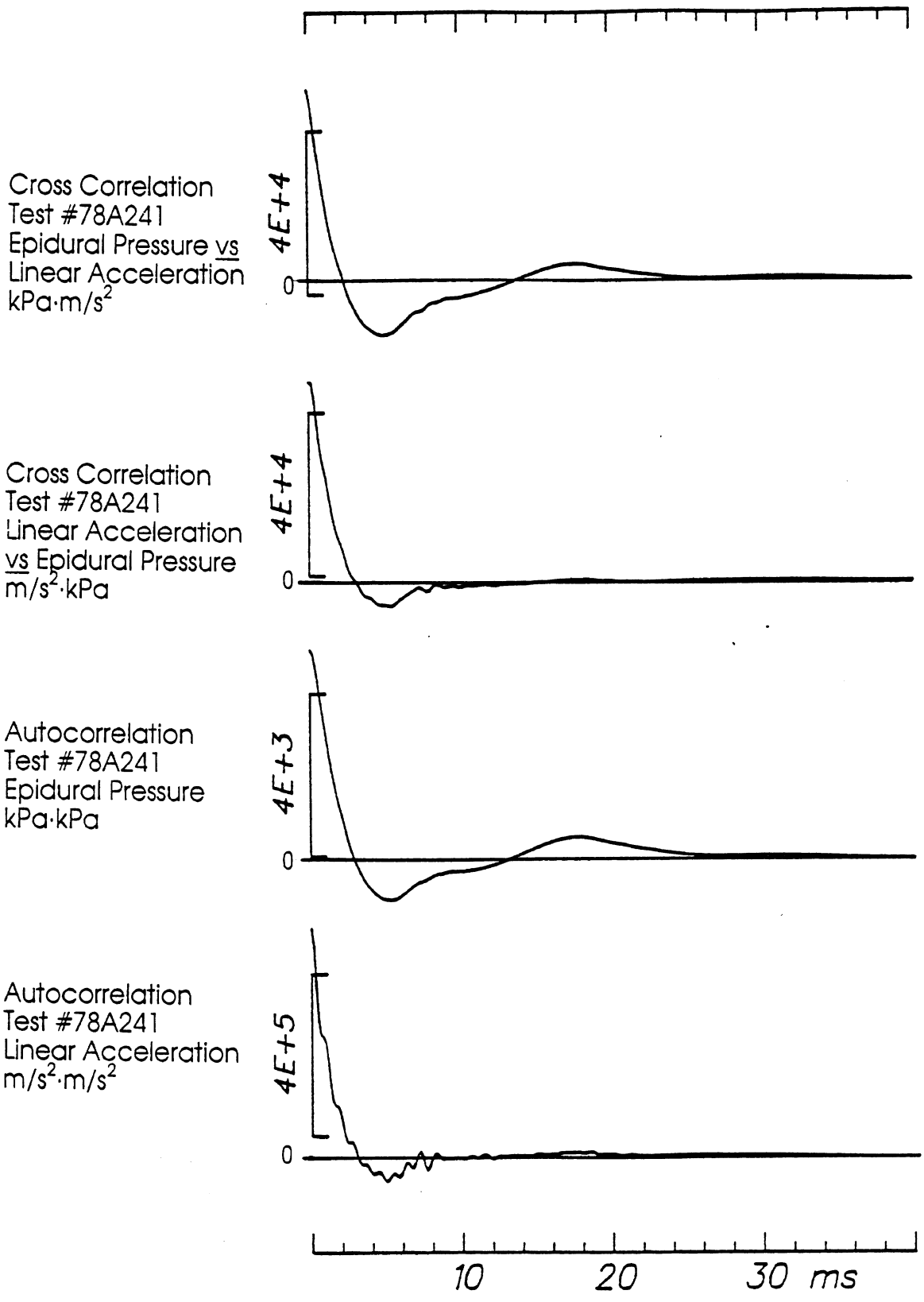

HEAD CENTER OF GRAVITY WITH RESPECT TO LINE OF IMPACT = ABOVE

FIGURE 15: REPRESSURIZED POSTMORTEM RHESUS, NO SKULL FRACTURE, NECK UNSTRETCHED

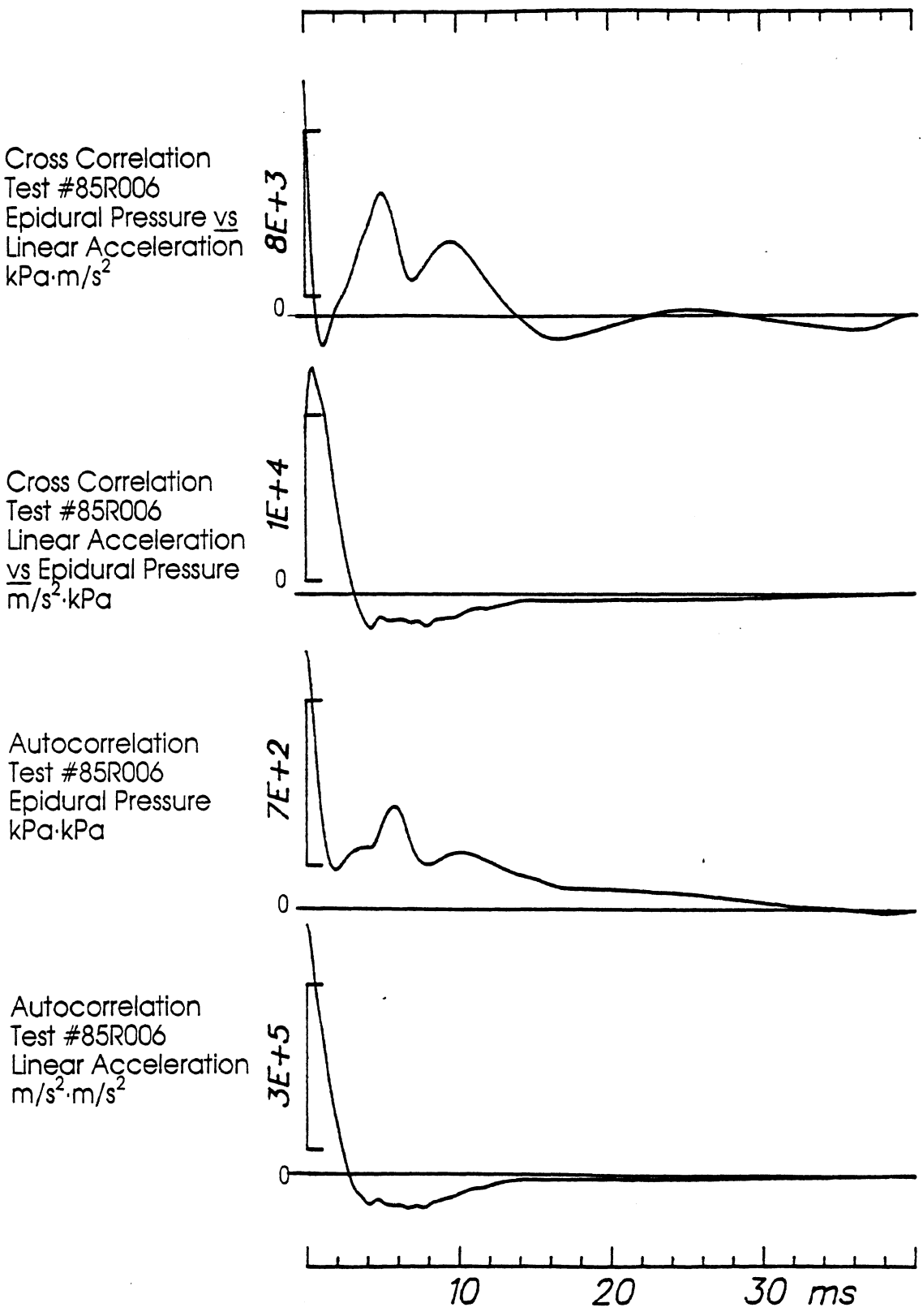

HEAD CENTER OF GRAVITY WITH RESPECT TO LINE OF IMPACT = ABOVE

FIGURE 16: UNREPRESSURIZED POSTMORTEM RHESUS, NO SKULL FRACTURE, NECK UNSTRETCHED

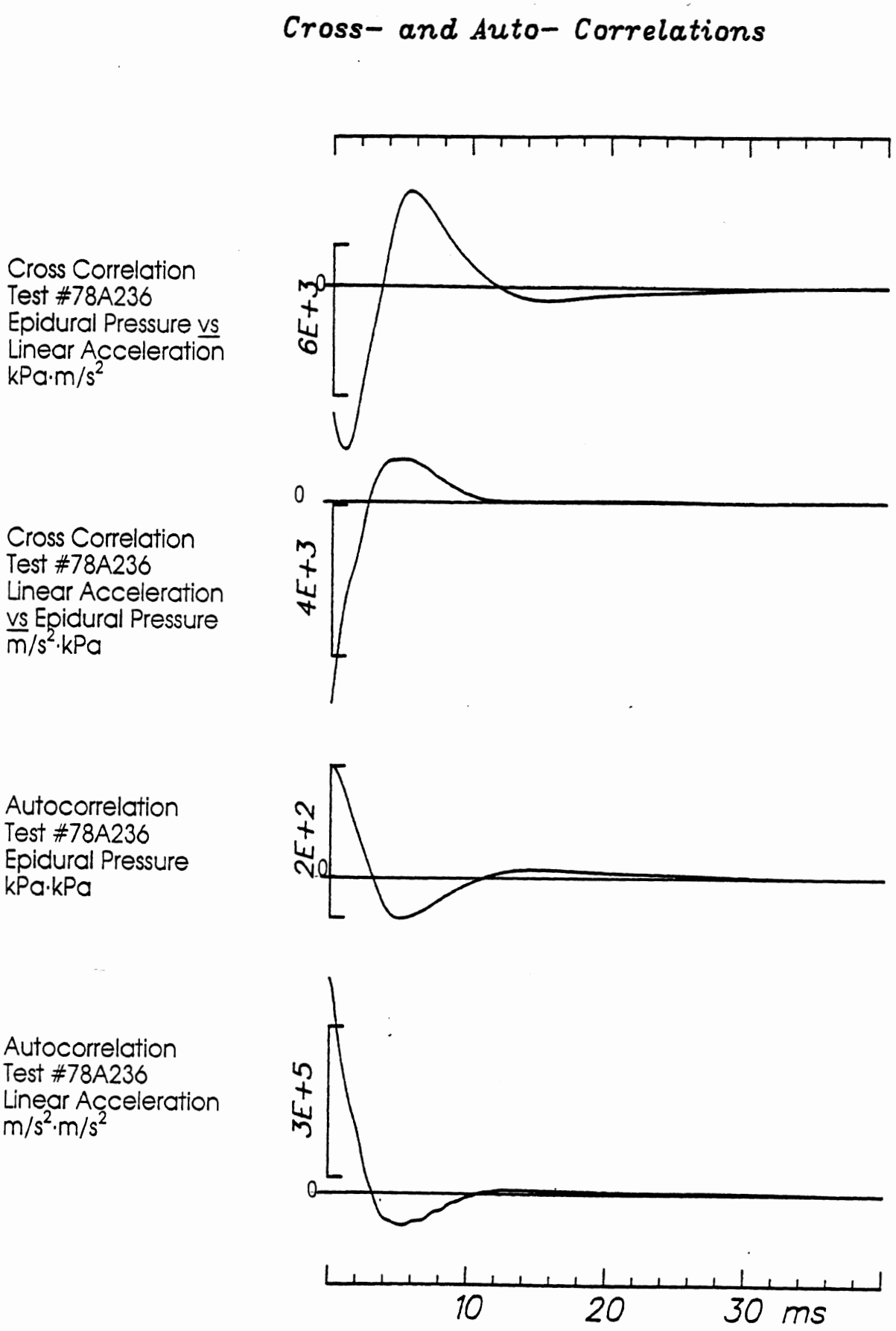

HEAD CENTER OF GRAVITY WITH RESPECT TO LINE OF IMPACT = AT

from the skull-brain area.

The results reported elsewhere (31) indicated that when basal skull fracture occurred in Rhesus subjects, subarachnoid hemorrhaging was common in the medulla pons area. In addition, this focal injury did not occur in the unrepressurized-postmortem Rhesus. For the repressurized-postmortem Rhesus, injuries similar to those of the anesthetized subject were observed. The implications were that in terms of focal injury response for this type of injury mode, the repressurized-postmortem subject was similar to the anesthetized subject. Caution must be exercised in interpreting these results because one injury mode for a very particular type of impact was involved and the sample size was small. The results may not occur for other injury modes or impact conditions.

The results reported elsewhere (34) indicated that the interaction of the cervical cord and the foramen magnum with the rest of the brain-cerebrospinal fluid system was a critical factor in certain types of head impact response. In an attempt to determine the effect of the interaction of the head with the cervical spine, a series of impacts were run with the neck stretched. (Figure 3 is an x-ray of the two types of initial neck conditions: the neck-stretched configuration, and the neck-unstretched configuration). Although the impedance values between force and tangential acceleration as well as the time-histories of the linear and angular accelerations for the two neck conditions were similar (See appendix), the transfer functions for the tangential acceleration divided by epidural pressure were not (Figure 17). This implies that the flow of material through the foramen magnum as well as the inertial properties of the cord may have been critical factors in determining the type of pressure and stress that developed in the brain during impact. In addition, the neck-stretched tests were the only ones in which subdural hemorrhaging was observed in the frontal lobes of the brain. Therefore, not only was the impact response in

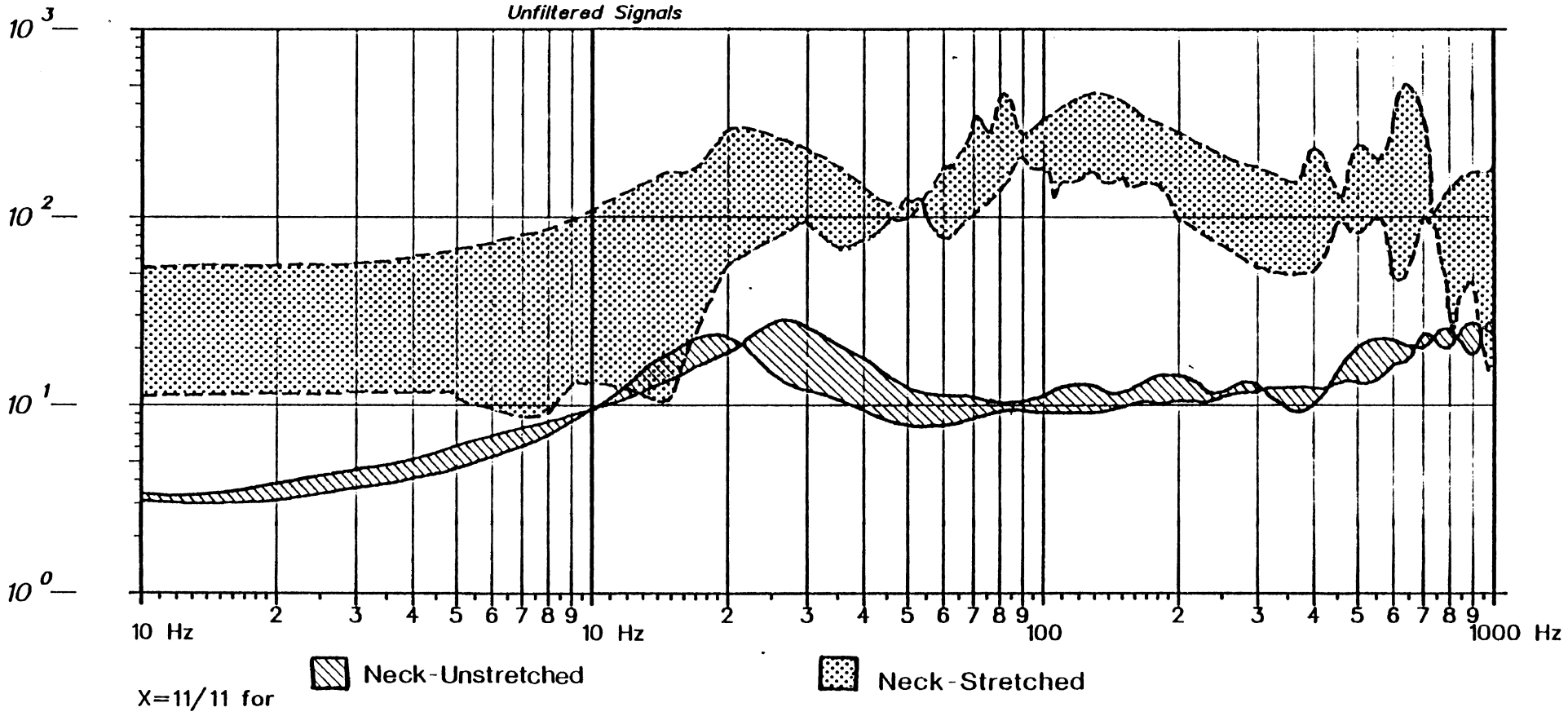

FIGURE 17: TRANSFER FUNCTION CORRIDORS TANGENTIAL ACCELERATION/EPIDURAL PRESSURE NECK-STRETCHED VS. NECK UNSTRETCHED RHESUS

terms of transfer functions for tangential acceleration divided by epidural pressure different, but the focal injury response also changed. Potentially, the difference in initial positioning may have changed the hydrodynamic lubrication and the mechanical restriction associated with the skull-brain interface. In addition, the large pressures that developed during impact in the neck-unstretched anesthetized Rhesus subject and the inertial properties of the restricted flow of the spinal cord - cerebrospinal fluid through the foramen magnum may have helped to reduce the differential motion between the brain and the skull during impact. The observed focal injuries (subdural hematomas in the frontal lobes) in the neck-stretched case with angular acceleration similar to the neck-unstretched case imply that the interaction of the cervical cord and the head and material flow through the foramen magnum may be critical for these types of focal injury, and perhaps are more important than the angular or linear velocity/accelerations for determining head-impact tolerance levels.

4.5 The Skull-Deformation Impacts - In a manner similar to that of the repressurized cadaver, skull deformation played a small part in the pressure response of the anesthetized Rhesus brain up to the level where the skull fractured. The features of the data that indicated this are: 1) The auto-correlations of the tangential acceleration and epidural pressure were similar to those of the cross-correlation between the two signals (Figure 14 illustrates this); and 2) The greatest absolute maximum value for severe skull-fracture subjects was generally a negative quantity (i.e. a negative cross-correlation near zero lag as shown in Figure 18), whereas for simple skull fracture subjects the tangential acceleration correlated better with epidural pressure than for severe skull fracture subjects.

FIGURE 18: ANESTHETIZED RHESUS, SKULL FRACTURE, NECK UNSTRETCHED

Cross- and Auto- Correlations

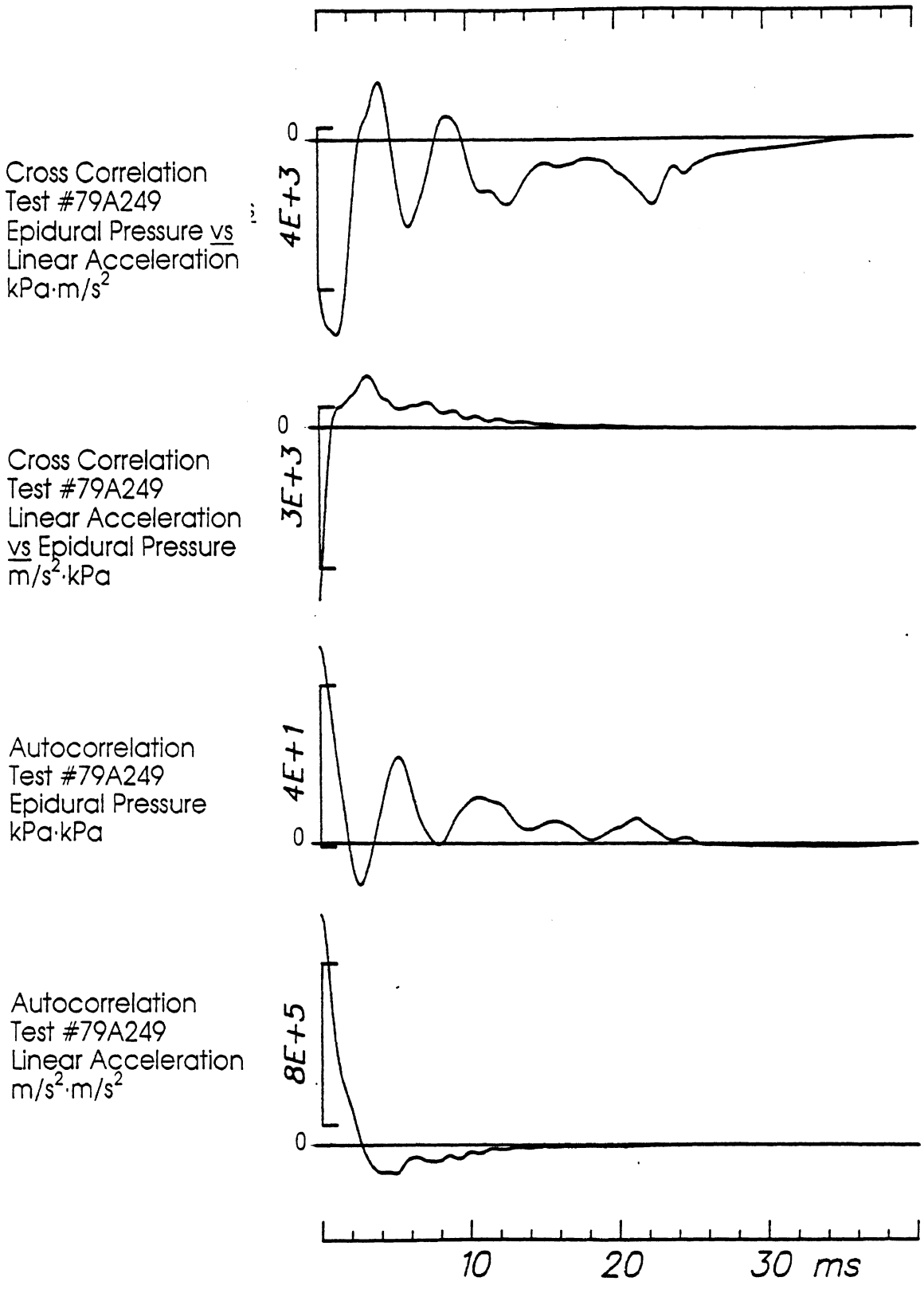

HEAD CENTER OF GRAVITY WITH RESPECT TO LINE OF IMPACT = ABOVE

This result that skull deformation played a small part in the epidural pressure response of the anesthetized Rhesus brain up to the level where the skull fractured has important implications in terms of head trauma modeling. If the head is viewed as a closed shell and the brain and its surrounding tissues and fluids as an incompressible, or nearly incompressible, viscoelastic material (i.e. as having a bulk modulus near that of water), then small changes in volume would be expected to produce larger pressure changes than those observed in the response of the anesthetized test subjects. In addition, one would expect negative pressures and a negative cross-correlation between tangential acceleration and epidural pressure for the no-skull fracture subjects, because the pressure volume change mechanism would dominate any of the inertial phenomena. The results imply three possibilities for head trauma modelers: 1) the foramen magnum was significantly large enough so that it needs to be included in modeling of blunt head impact response; 2) the effective bulk modulus of the brain may need to be viewed as significantly less than that of water or an equivalent system should be used; and 3) or both.

In addition, during skull-fracture Rhesus tests, pressures only slightly below one negative atmosphere were observed. These were the only tests in which negative pressures of that magnitude were produced. Therefore, it seems that vaporization of the fluid near the pressure transducer was rapid enough to effectively act as a pressure limiting function. This thermodynamic phenomenon would have affected significantly the stresses that were being produced in other parts of the brain during the severe impacts. It seems that injury prediction based on stress or the differential motion between the skull and the brain should address this phenomenon. Therefore, it may be essential to include this phenomenon in any modeling effort of head impact response.

4.6 Summary Conclusions - However, the following conclusions result from the comparisons of the head trauma research data from Rheus and human cadaver model experiments conducted by UMTRI over the last nine years (30-34). This has been a limited study of a few important kinematic factors and injury modes associated with blunt impact to the head. Because of the complex nature of the head during impact, more work is necessary before these kinematic factors can be generalized to describe the responses of the skull, brain, cerebrospinal fluid, and the neck to blunt head impact.

1. In terms of peak pressure, the repressurized-postmortem and the anesthetized Rhesus responses were significantly different from that of the unrepressurized-postmortem Rhesus.

2. Although the repressurized-postmortem Rhesus, when compared to the unrepressurized-postmortem Rhesus, was more similar in response to that of the anesthetized Rhesus (as shown by transfer functions of tangential acceleration divided by epidural pressure), the differences detected between the repressurized-postmortem and the anesthetized Rhesus may be important in terms of kinematic response.

3. In terms of subarachnoid hemorrhage in the medulla-pons area associated with skull fracture, the repressurized-postmortem and the anesthetized Rhesus were similar in injury response.

4. The initial positioning of the head-neck system is a critical factor associated with the cerebrospinal system's response to head impact. For given linear and angular acceleration time-histories, the initial positioning of the head-neck system was, in general, successful in predicting the pressure and focal injury response. Unless the initial position of the head-neck system is included in the head tolerance criteria functions

(unlike those currently popular functions solely based on linear and angular accelerations, intracranial pressure, and skull strain), they may prove less useful.

5. The thermodynamic response (fluid vaporization) of the cerebrospinal system is an important consideration when the impact produces significant tension.

6. In the results presented here for anesthetized Rhesus and in the results presented elsewhere (31,34), no relationships could be found between focal injury and negative pressures equal to one atmosphere. This implies that cavitation does not seem to be a mechanism of injury in head impact response.

7. The above conclusions are important for both the mathematical modeling of head trauma and the determination of the injury tolerance of the head. The following factors significantly affect the stress in the brain as well as the interaction of the brain with the skull.

- The tension in the brain, limited by vaporization in "severe impacts";
- The inertial properties of the cervical cord as well as the flow of material through the foramen magnum;
- The initial positioning of the head-neck system; and
- The repressurization of postmortem surrogates.

5.0 RECOMMENDATIONS FOR FUTURE RESEARCH

The analysis of these related head injury research programs (30-34) implies that further dynamic experimental work in a controlled laboratory setting is justified and necessary to enable meaningful modeling of head trauma. The following research programs are suggested to answer questions presented from the analysis being reported in this document:

1. An unembalmed repressurized cadaver dynamic-biomechanics experiment that contrasts neck-stretched vs. neck-unstretched positioning while measuring intracranial pressure at the foramen magnum, as well as flow through the foramen magnum.
2. An unembalmed repressurized cadaver dynamic-biomechanics experiment using high-speed x-ray cineradiography to evaluate whether increased intracranial pressure and the initial positioning of the cervical spine can effect the differential motion of the brain cortex with the skull.
3. Mathematical modeling efforts which address the interaction of the skull with the brain.
4. An additional dynamic-biomechanics research program that evaluates repressurization techniques for postmortem subjects by contrasting the repressurized postmortem and anesthetized response of a laboratory animal surrogate.

6.0 RESOURCE PERSONNEL

The research program was directed by Guy S. Nusholtz. The key resource personnel who performed the research included Patricia S. Kaiker, Richard J. Lehman, and Wendy S. Gould. The pertinent vitae are attached.

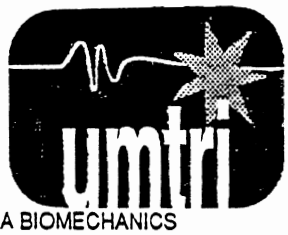

TRAUMA BIOMECHANICS

NAME: Guy S. Nusholtz

TITLE: Assistant Research Scientist

EDUCATION: B.S., Physics, Antioch College, 1972
M.S., Bioengineering, University of Michigan, 1974

RESEARCH INTERESTS: Impact Trauma Research, Biomechanical Instrumentation, and Mathematical Modeling of Mechanisms of Injury

EXPERIENCE:
1981 to present: Assistant Research Scientist, UMTRI
1978-1981: Senior Research Associate, UMTRI
1977-1978: Research Associate II, UMTRI
1975-1976: Research Associate I, UMTRI
1973-1974: Research Assistant, Chemical Engineering, University of Michigan
1971-1970: Fire Chief, Antioch College Fire Department
1969-1970: Research Assistant, Scripps Institute
1968-1969: Research Assistant, Harvard University, Solar Satellite Project
1967-1968: Research Assistant, Massachusetts Institute of Technology

Mr. Nusholtz has been the project director of many of the dynamic biomechanics of impact injury programs at UMTRI. Currently, he directs the scientific investigation and management of the Biosciences Division's Trauma Biomechanics Laboratory. Mr. Nusholtz has been responsible for overseeing all aspects of completing a dynamic biomechanics program and has directed for each given project: the experimental design, protocol development, and improvement of techniques in instrumentation, data analysis and synthesis. His areas of expertise include trauma to the head, neck, thorax, abdomen, pelvis and femur.

PUBLICATIONS:

Nusholtz, G.S., Stalnaker, R.L., and Melvin, J.W. "Vascular System Pressurization Techniques." International Workshop on Human Subjects for Biomechanical Research, 4th Annual Meeting, October 22, 1976, pp. 80-83.

Stalnaker, R.L., Nusholtz, G.S., and Melvin, J.W. Femur Impact Study. HSRI, May 1977. Report No. UM-HSRI-77-25. Sponsored by General Motors Research Laboratories.

Stalnaker, R.L., Melvin, J.M., Nusholtz, G.S., Alem, N.M., and Benson, J.B. "Head Impact Response." Proceedings of the Twenty-First Stapp Car Crash Conference. Society of Automotive Engineers, 1977, pp. 303-335.

Nusholtz G.S., "Vascular and Respiratory Pressurization of the Thorax." International Workshop on Human Subjects for Biomechanical Research, Fifth Annual Meeting, Committee Reports and Technical Discussions, October 18, 1977, New Orleans. N.p., 1978, pp. 81-95.

Nusholtz, G.S., Alem, N.M., Stalnaker, R.L. and Melvin, J.W. "Reference Frames and Direct Head Impacts." International Workshop on Human Subjects for Biomechanical Research, Fifth Annual Meeting, Committee Reports and Technical Discussions, October 18, 1977, New Orleans. N.p., 1978, pp. 96-110.

Nusholtz, G.S., Melvin, J.W., and Alem, N.M. "Head Impact Response Comparisons of Human Surrogates," Proceedings of the Twenty-Third Stapp Car Crash Conference. October 17-19, 1979, San Diego. Warrendale, Pa., Society of Automotive Engineers, 1979, pp. 497-541. SAE Paper No. 791020. Sponsored by the Motor Vehicle Manufacturers Association.

Nusholtz, G.S., Axelrod, J.B., Melvin, J.W., and Ward, C. Comparison of Epidural Pressure in Live Anesthetized and Post-Mortem Primates, HSRI and Naval Civil Engineering Laboratory, Nov. 1979. 25 p. Report No. UM-HSRI-79-90. Sponsored by the Motor Vehicle Manufacturers Association.

Melvin, J.W. and Nusholtz, G.S. Tolerance and Response of the Knee-Femur-Pelvis Complex to Avoid Impacts - Impact Sleds, Final Report. HSRI, June 1980. 29 p. Report No.UM-HSRI-80-27. Sponsored by the Motor Vehicle Manufacturers Association.

Nusholtz, G.S., Melvin, J.W., Mueller, G., MacKenzie, J.R., and Burney, R. "Thoraco Abdominal Response and Injury." Proceedings of the Twenty-Fourth Stapp Car Crash Conference. October 15-17, 1980, Troy, Michigan. Warrendale, Society of Automotive Engineers, 1980, pp. 189-228. SAE Paper No. 801305. Sponsored by the Motor Vehicle Manufacturers Association.

Bender, M., Alem, N., Nusholtz, G., Melvin, J., and Rogers, W. "High-Speed Cineradiographic System for Biomechanics Impact Research." In: Proceedings of the 1st European Conference on Cineradiography with Photons or Particles, May 18-21, 1981. Paris, France.

Nusholtz, G.S., Melvin, J.W., Huelke, D.F., Alem, N.M., and Blank, J.G. "Response of the Cervical Spine to Superior-Inferior Head Impact." Proceedings of the Twenty-Fifth Stapp Car Crash Conference. Warrendale, Pa., Society of Automotive Engineers, 1981, pp. 197-237. AWARDED publication in SAE Transactions. 1981.

Nusholtz, G.S., Alem, N.M., and Melvin, J.W. "Impact Response and Injury of the Pelvis." Proceedings of the Twenty-Sixth Stapp Car Crash Conference. Society of Automotive Engineers, Warrendale, PA. 1982, pp. 3564-3605. AWARDED publication in SAE Transactions. 1983.

Nusholtz, G.S., Huelke, D.F., Lux, P., Alem, N.M., and Montalvo, F. "Cervical Spine Injury Mechanisms." Proceedings of the Twenty-Seventh Stapp Car Crash Conference, October 17-19, 1983. San Diego. Warrendale, Society of Automotive Engineers, 1983, pp. 179-197. SAE 831616.

Nusholtz, G.S., Janicki, M.A., Huelke, D.F., and Lux, P. Strength and Response of the Human Cadaver Cervical Spine Under Impact Loading, Interim Report. UMTRI, August 1983. 160 p. Report No. UMTRI-83-32. Sponsored by the General Motors Corporation, Technical Center.

Nusholtz, G.S., Melvin, J.W., and Lux, P. "The Influence of Impact Energy and Direction on Thoracic Response." Proceedings of the Twenty-Seventh Stapp Car Crash Conference, October 17-19, 1983. San Diego. Warrendale, Society of Automotive Engineers, 1983, pp. 69-94. SAE 831606. Sponsored by the National Highway Traffic Safety Administration. Contract No. DOT-HS-7-01636. AWARDED publication in SAE Transactions. 1983.

Nusholtz, G.S., Lux, P., Kaiker, P.S., and Janicki, M.A. "Head Impact Response--Skull Deformation and Angular Accelerations." Proceedings of the 28th Stapp Car Crash Conference, November 5-7, 1984. Chicago, IL. SAE Paper No. 841657. Society of Automotive Engineers, Warrendale, PA. AWARDED publication in SAE Transactions. 1984.

Alem, N.M., Nusholtz, G.S., and Melvin, J.W. "Head and Neck Response to Axial Impacts." Proceedings of the 28th Stapp Car Crash Conference, November 5-7, 1984. Chicago, IL. SAE Paper No. 841667. Society of Automotive Engineers, Warrendale, PA.

Culver, C.C., Haut, R.C., and Nusholtz, G.S. "Significance of Head-to-Knee Impacts-A Comparison of Dummy and Cadaver Responses." Proceedings of the 28th Stapp Car Crash Conference, November 6-7, 1984. Chicago, IL. SAE Paper No. 841662. Society of Automotive Engineers, Warrendale, PA.

Nusholtz, G.S., Kaiker, P.S., Muscott, G.J. and Suggitt, B.R. "UMTRI Experimental Techniques in Head Injury Research." Proceedings SAE Government/Industry Meeting and Exposition. Washington, D.C. May 20-23, 1985. AWARDED publication in SAE Transactions. 1985.

Nusholtz, G.S., Bender, M., Suggitt, B.R., Kaiker, P.S. and Muscott, G.J. "Photogrammetric Techniques Using High-Speed Cineradiography." 29th Annual International Technical Symposium of the Society of Photo-Optical Instrumentation Engineers Proceedings.

Nusholtz, G.S., Kaiker, P.S., Kirsh, M.M., and Bosio, A.C. "Thoraco-Abdominal Response to Frontal Impact." Proceedings from the Twenty-Ninth Stapp Car Crash Conference, October 10-11, 1985. Washington, D.C. SAE Paper No. 851721. Society of Automotive Engineers, Warrendale, PA.

Nusholtz, G.S., Kaiker, P.S., Huelke, D.F. and Suggitt, B.R. Thoraco-Abdominal Response to Steering Wheel Impacts." Proceedings from the Twenty-Ninth Stapp Car Crash Conference, October 10-11, 1985. Washington, D.C. SAE Paper No. 851737. Society of Automotive Engineers, Warrendale, PA.

Nusholtz, G.S. and Ward, C.C. "Comparison of Epidural Pressure in Live Anesthetized and Post-Mortem Primates," Journal of Aviation, Space and Environmental Medicine. 1986. In press.

Huelke, D.F. and Nusholtz, G.S. "Cervical Spine Biomechanics: A Review of the Literature." Journal of Orthopaedic Research. 1986. In press.

Nusholtz, G.S., Bender, M. and Kaiker, P.S. "Photogrammetric Techniques Using High-Speed Cineradiography." Optical Engineering 25:791-798. 1986.

Nusholtz, G.S. and Kaiker, P.S. "Pelvic Stress." Journal of Biomechanics. 1986. In press.

Huelke, D.F., Nusholtz, G.S. and Kaiker, P.S. "Use of Quadruped Models in Thoraco-Abdominal Biomechanics Research." Journal of Biomechanics. 1986. In press.

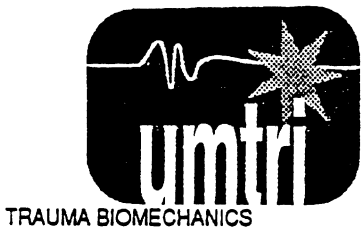

NAME: Patricia S. Kaiker

TITLE: Engineer Research Associate II
Biosciences Division

EDUCATION: B.A., Spanish-English, Ohio State University, 1967
M.A.-Ph.D. Program Studies (89+ credit-hours), Physical/Medical Anthropology, Michigan State University, 1976-1981

RESEARCH INTERESTS: Dynamic Measurement, Properties of Biomaterials, Mechanisms of Injury, and Biomechanics Modeling

EXPERIENCE: 1986 to present: Engineer Research Associate II, UMTRI

1983-1985: Engineer Research Associate I, UMTRI

1979-1980: Technical Assistant, Anatomical Pathology
E.W. Sparrow Hospital, Lansing, MI

1978-1979: Graduate Research Assistant,
Family Medicine (Pediatrics)
Michigan State University

1977-1979: Medical Biographer, Libraries,
Michigan State University

Ms. Kaiker has been involved at UMTRI with the development, performance and funding of research into the dynamic biomechanics of impact injury. She is the assistant manager of the Biosciences Division's Trauma Biomechanics Laboratory. Ms. Kaiker has assisted in the development of improved techniques in photogrammetry, cineradiography, photography, compression testing of biomaterials, and repressurization of human surrogate pulmonary and vascular systems. She has been responsible for the development of anthropometry protocols, injury assessment reporting, and partially responsible for experimental designs in impact trauma biomechanics.

SOCIETIES: Society of Automotive Engineers
American Association of Physical Anthropologists
American Society of Biomechanics
Society of Photo-Optical Instrumentation Engineers

PUBLICATIONS:

Nusholtz, G.S., Lux, P., Kaiker, P.S. and Janicki, M.A. "Head Impact Response--Skull Deformation and Angular Acceleration." Proceedings of the 28th Stapp Car Crash Conference, November 6-7, 1984. Chicago, IL. SAE Paper No. 841662. Society of Automotive Engineers, Warrendale, PA. AWARDED publication in 1984 SAE Transactions.

Nusholtz, G.S. and Kaiker, P.S. "UMTRI Thoraco-Abdominal Impact Experiments." 12th International Workshop on Human Subjects for Biomechanical Research Proceedings. 1984.

Nusholtz, G.S., Kaiker, P.S., Muscott, J. and Suggitt, B.R. "UMTRI Experimental Techniques in Head Injury Research." Society of Automotive Engineers Government/Industry Meeting and Exposition Proceedings. AWARDED publication in 1985 SAE Transactions.

Nusholtz, G.S., Bender, M., Suggitt, B.R., Kaiker, P.S. and Muscott, G.J. "Photogrammetric Techniques Using High-Speed Cineradiography." 29th Annual International Technical Symposium of the Society of Photo-Optical Instrumentation Engineers Proceedings. 1985.

Nusholtz, G.S., Kaiker, P.S., Kirsh, M.M. and Bosio, A.C. "Thoracic Response to Frontal Impact." Proceedings of the 29th Stapp Car Crash Conference. SAE Paper No. 851721. Society of Automotive Engineers, Warrendale, PA. 1985.

Nusholtz, G.S., Kaiker, P.S., Huelke, D.F. and Suggitt, B.R. "Thoraco-Abdominal Response to Steering Wheel Impacts." Proceedings of the 29th Stapp Car Crash Conference. SAE Paper No. 851737. Society of Automotive Engineers, Warrendale, PA. 1985.

Kaiker, P.S. and Nusholtz, G.S. "Pedestrian Impacts with a Pendulum Impactor." 13th International Workshop on Human Subjects for Biomechanical Research Proceedings. 1985.

Nusholtz, G.S. and Kaiker, P.S. Experimental Data for Development of Finite Element Models: Head/Thoraco-Abdomen/Pelvis. Final Report in three volumes. University of Michigan Transportation Research Institute. Department of Transportation, National Highway Traffic Safety Administration. Contract Number: DOT-C-HS-7-01636. December, 1985.

Nusholtz, G.S., Bender, M. and Kaiker, P.S. "Photogrammetric Techniques Using High-Speed Cineradiography." Optical Engineering. 1986. In press.

Nusholtz, G.S. and Kaiker, P.S. "Pelvic Stress." Journal of Biomechanics. 1986. In press.

Huelke, D.F., Nusholtz, G.S. and Kaiker, P.S. "Use of Quadruped Models in Thoraco-Abdominal Biomechanics Research." Journal of Biomechanics. 1986. In press.

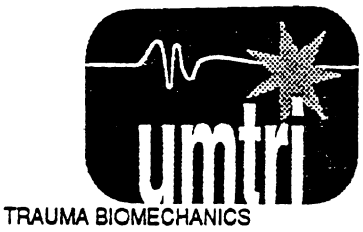

NAME: Richard J. Lehman

TITLE: Program Analyst II
Biosciences Division

EDUCATION: B.A., Psychology (Honors), University of Texas/Austin, 1970

RESEARCH INTERESTS: Dynamic Biomechanics and Biomathematics Databases

EXPERIENCE:

1974 to present: Computer Programmer data analyst; microcomputer specialist; laboratory equipment operator, UMTRI

1973 - 1974: Field Interviewer, laboratory equipment operation and maintenance, data structure design and implementation, computer programming, Alcohol Systems, UMTRI

1971 - 1973: Experimental design and implementation, computer programming, subject management, finances, supplies, logistics. Engineering Psychology, UMTRI.

1970 - 1971: Research Assistant in Psycho-linguistics, University of Texas.

1965 - 1968: Primary Instructor in advanced Clinical Toxicology, Instructor in General and Clinical Chemistry, U. S. Army (Fort Sam Houston, San Antonio, Texas).

1964 - 1965: General duties in all major areas of the clinical laboratory: Chemistry, Hematology, Immunohematology, Urinalysis, Bacteriology, Bridgeport Hospital, Bridgeport, Connecticut.

At UMTRI Mr. Lehman, as a scientific programmer, has had experience in the management and manipulation of large databases, display/interactive graphics, and numerical problem solving. He has been working with microcomputers since 1976, and has the ability to effectively integrate on- and off-line computer resources, including mainframe and post-processor linkages.

PUBLICATIONS:

Edwards, W., Lathrop, J., Seaver, D., Seghers, R., and Lehman, R. Development and Evaluation for Behavioral Tests for Driver Impairment. Final Report. HSRI. August 1973. 48 p. Sponsored by the General Motors Coporation.

Lehman, R.J., Wolfe, A.C., and Kay, R.D. A Compuer Archive of ASAP Roadside Breathtesting Surveys, 1970-1974, Interim Report. HSRI, January 1975. 168 p. Report No. UM-HSRI-AL-75-1. Sponsored by the National Highway Traffic Safety Administration, Contract No. DOT-HS-031-3-722.

Robbins, D.H. and Lehman, R.J. Data from lateral Impact Sled Tests. Final Report. HSRI, August 22, 1978. 305 p. Report No. UM-HSRI-78-34. Sponsored by the National Highway Traffic Safety Administration.

Robbins, D.H., Lehman, R.J., and Augustyn, K. "Prediction of Thoracic Injuries as a Function of Occupant Kinematics." Presented at the Seventh International Technical Conference on Experimental Safety Vehicles, June 7, 1979. Paris, France. 24 p.

Bennett, R.O., Lehman, R.J., and Robbins, D.H. Validation Command Language: Supplement to 1979 Version, Final Report. UMTRI, June 15, 1983. 40 p. Report No. UMTRI-83-28. Sponsored by the National Highway Traffic Safety Administration, Contract No. DTNH22-82-A-07046.

Lehman, R.J., Bennett, R.O., and Robbins, D.H. Ellipsoidal Man Plotting Package for MVMA 2-D and CVS(HSRI Version) Occupant Motion Models, Final Report. UMTRI, June 15, 1983. 56 p. Report No. UMTRI-83-27. Sponsored by the National Highway Traffic Safety Administration, Contract No. DTNH22-82-A-07045.

Robbins, D.H., Melvin, J.W., Lehman, R.J., and Benson, J.B. "Thoracic Injury Prediction Using Anthromorphic Test Devices as Subjects", International Workshop on Human Subjects for Biomechanical Research, Seventh Annual Proceedings), 1979, pp. 71-114.

Robbins, D.H., Lehman, R.J., Nusholtz, G.S., and Melvin, J.W. Quantification of Thoracic Response and Injury: The Gathering of Data. Final Report. UM-HSRI-82-33-1. Sponsored by the National Highway Traffic Safety Administration, Contract No. DOT-HS-4-00921.

Robbins, D.H., Lehman, R.J., Nusholtz, G.S., and Melvin, J.W. Quantification of Thoracic Response and Injury: The Gathering of Data. Ap. A: Individual Test Reports. Volume I, Report No. UM-HSRI-82-33-2-1.

Robbins, D.H., Lehman, R.J., Nusholtz, G.S., and Melvin, J.W. Quantification of Thoracic Response and Injury: The Gathering of Data. Volume II, Report No. UM-HSRI-82-33-2-2.

Robbins, D.H., Lehman, R.J., Nusholtz, G.S., and Melvin, J.W. Quantification of Thoracic Response and Injury: The Gathering of Data. Ap. B: Rib Test Data. Final Report. Report No. UM-HSRI-82-33-3. Volume 3.

Robbins, D.H., Lehman, R.J., Nusholtz, G.S., and Melvin, J.W. Quantification of Thoracic Response and Injury: Tests Using Human Surrogate Subjects. Final Report. May 2, 1983. Report No. UMTRI-83-26. 211 pages.

Weber, K., Lehman, R.J., and Schneider, L.W. Child Anthropometry for Restraint System Design. UMTRI-85-23. 34 p.

Schneider, L.W., Lehman, R.J., Pflug, M.A. Owings, C.L. Size and Shape of the Head and Neck from Birth to Four Years. January 1986, 490 pp. Report No. UMTRI-86-2. Consumer Products Safety Commission, Contract No. CPSC-C-83-1250.

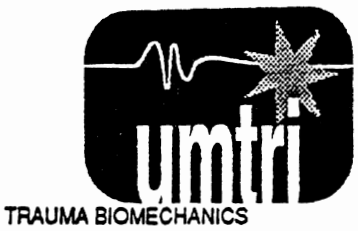

NAME: Wendy S. Gould

TITLE: Student Research Assistant

EDUCATION: Fall 1986 enters Baylor Medical College, Houston, Texas
B.A. 1986 English Honors, University of Michigan

RESEARCH INTERESTS: Mechanisms of Trauma

Ms. Gould served as a research technician on this project, assisting to some degree in all aspects of the work. Her impact biomechanics work at UMTRI complemented her pre-medical school training program.

7.0 ACKNOWLEDGEMENTS

The results in this final report were obtained through a series of independently funded research programs conducted during the past nine years. The funding agencies were: The Motor Vehicle Manufacturers Association and the United States Department of Transportation. The assistance in injury evaluation provided by C. J. D'Amato, P. W. Gikas, D. F. Huelke, and J. Hoff is gratefully acknowledged. The authors are indebted to Nabih Alem, Joseph Benson, Miles Janicki, John Melvin, Richard Stalnaker, Paula Lux, Carley Ward, Marvin Dunlap, Steven Richter, Valerie Karime, and Jennifer Mallock for their technical assistance. A special thanks is given to Jeff Marcus for his encouragement.

In conducting the research on the laboratory Rhesus subjects described in this study, the investigators adhered to the "Guide for the Care and Use of Laboratory Animals of the Institute of Laboratory Animal Resources, National Research Council.

To date DOT-NHTSA Contract No. DTNH22-83-C-07095 has produced this final report and the manuscript to be presented at the 30th Stapp Car Crash Conference (33).

8.0 REFERENCES

1. Anderson, D.F.; Miller, J.D.; and Kalsbeek, W.D. 1983. Findings from a Major Survey of Persons Hospitalized with Head Injuries. Public Health Reports, 98(5):475-478.

2. Insurance Institute for Highway Safety, 1982. The Year's Work 1981-1982. Washington, D.C.

3. Kraus, J.F., et al. 1984. The Incidence of Acute Brain Injury and Serious Impairment in a Defined Population. American Journal of Epidemiology. 19(2):186-201.

4. Thomas, D.J.; Robbins, D.H.; Eppinger, R.H.; King, A.I.; and Hubbard, R.P. 1974. Guidelines for the Comparison Human and Human Analogue Biomechanical Data. A report of an ad hoc committee, Ann Arbor, Michigan, December 6.

5. Abel, J.M.; Gennarelli, T.A.; and Segawa, H. 19778. Incidence and Severity of Cerebral Concussion in the Rhesus Monkey Following Sagittal Plane Angular Acceleration. Proc. 22nd Stapp Car Crazsh Conf. 24-26 October 1978, Ann Arbor, MI, Warrendale, PA: SAE Paper No. 780886, pp. 35-53.

6. Adams, J.H.; Graham, D.I.; and Gennarelli, T.A. 1981. Acceleration Induced Head Injury in the Monkey. II Neuropathology. In: K. Jellinger, F. Gullotta, M. Mosakowski, eds., Experimental Clinical Neuropathology. Acta Neuropathol. (Berl.) Suppl. vii, pp. 26-28.

7. Aldman, B.; Thorngren, L.; and ljung, C. 1981. Patterns of Deformation in Brain Models Under Rotational Motion. In: DOT, NHTSA, Head and Neck Injury Criteria, Washington, D.C.

8. Alem, N.M. 1974. Simulation of Head Injury Due to Combined Rotation and Translation of the Brain. Proc. 18th Stapp Car Crash Conf., pp. 579.

9. Chan, M. and Ward, C. 1981. Relative Importance of Skull Deformation. Proceedings ASME. Biomechanics Symposium, June 22-24.

10. Engin, A.E. 1969. Axisymmetric Response of a Fluid-filled Spherical Shell to a Local Radial Impulse--A Model for Head Injury. Journal of Biomechanics 2(3):395-341.

11. Engin, A.E. and Akkas, N. 1978. Application of a Fluid-filled Spherical Sandwich Shell as a Biodynamic Head Injury Model for Primates. Aviation, Space and Environemntal Medicine, pp. 120-124.

12. Evans, F.G.; Lissner, H.R.; and Lebow, M. 1958. The Relation of Energy, Velocity and Acceleration to Skull Deformation and Fracture. Surgery, Gynecology and Obstetrics, 107:593-601.

13. Ewing, C.L. and Thomas, D.J. 1972. Human Head and Neck Response to Impact Acceleration. Naval Aerospace Medical Research Laboratory Detachment, New Orleans, Monograph 21, August.

14. Ewing, C.L. and Thomas, D.J. 1973. Torque Versus Angular Displacement Response of Human Head to -Gx Impact Acceleration. Proc. 17th Stapp Car Crash Conf., Paper No. 730976.

15. Ewing, C.L., et al. 1975. The Effect of the Initial Position of the Head and Neck on the Dynamic Response of the Human Head and Neck to -Gx Impact Acceleration. Proc. 19th Stapp Car Crash Conf., Paper No. 751157.

16. Gennarelli, T.A., et al. 1979. Differential Tolerance of Frontal and Temporal Lobes to Contusion Induced by Angular Accleration. Proc. 23rd Stapp Car Crash Conf.,

17-19 October, San Diego, pp. 563-586. SAE Paper No. 791022.

17. Gennarelli, T.A.; Adams, J.H.; and Graham, D.I. 1981. Acceleration Induced Head Injury in the Monkey. 1. The Model Its Mechanical and Physiological Correlates. In: K. Jellinger, F. Gullotta, M. Mossakowski, edts. Experimental Clinical Neuropathology. Acta Neuropathol. (Berl.) Suppl. vii, pp. 23-25.

18. Gennarelli, T.A., et al. 1982. Diffuse Axonal Injury and Trauma Coma in the Primate. Ann. Neurol. 12:564-74.

19. Gurdjian, E.S., et al. 1961. Intracranial Pressure and Acceleration Accompanying Head Impacts in Human Cadavers. Surgery, Gynecology and Obstetrics, 113:185-190.

20. Gurdjian, E.S., et al. 1968. Significance of Relative Movements of Scalp, Skull and Intracranial Contents During Impact Injury of the Head. Journal of Neurosurgery, 29(1):70-72.

21. Higgins, L.S. and Schmall, R.A. 1967. A Device for the Investigation of Head Injury Efected by Non-Deforming Head Accelerations. Proc. 11th Stapp Car Crash Conf., pp. 35-46.

22. Hodgson, V.R. and Thomas, L.M. 1979. Acceleration Induced Shear Strains on a Monkey Brain Hemisection. Proc. 23rd Stapp Car Crash Conf., 17-19 October, San Diego, CA., pp. 589-611. SAE Paper No. 791023.

23. Hosey, R.R. and Liu, Y.K. 1982. A Homeomorphic Finite Element Model of the Human Head and Neck. In: R. H. Gallagher, et al., Finite Elements in Biomechanics, New York: John Wiley and Sons, Ltd., pp. 379-401.

24. Khalil, T.B. and Hubbard, R.P. 1977. Parametric Study of Head Response by Finite Element Modeling. Journal of Biomechanics, 10(2):119-132.

25. Lissner, H.R.; Lebow, M.; and Evans, F.G. 1960. Experimental Studies on the Relation between Acceleration and Intracranial Pressure Changes in Man. Surgery, Gynecology, and Obstetrics, 111:329-338.

26. Lowenhielm, P. 1974. Strain Tolerance of the W. Cerebri Sup. (bridging veins) Calculated from Head-on Collision Tests with Cadavers. Z. Rechtsmedizin, 75:131-144.

27. McElhaney, J.H.; Stalnaker, R.L.; and Roberts, V.L. 1972. Biomechanical Aspects of Head Injury. In: W. F. King and H. J. Mertz, eds., Human Impact Response: Mesurement and Simulation, New York: Plenum Press.

28. Nahum, A.M. and Smith, R.W. 1976. An Experimental Model for Closed Head Injury. Proc. 20th Stapp Car Crash Conf., Paper No. 760825.

29. Nahum, A.M.; Smith, R.W.; and Ward, C.C. 1977. Intracranial Pressure Dynamics During Head Impact. In: Proc. 21st Stapp Car Crash Conf., pp. 337-366.

30. Nusholtz, G.S.; Melvin, J.W.; and Alem, N.M. 1979. Head Impact Response Comparisons of Human Surrogates. Proc. 23rd Stapp Car Crash Conf., 17-19 October, San Diego, CA, pp. 499-541. SAE Paper No. 791020.

31. Nusholtz, G.S., et al. 1984. Head Impact Response - Skull Deformation and Angular Accelerations. Proc. 28th Stapp Car Crash Conf., pp. 41-74.

32. Nusholtz, G.S., et al. 1979. Comparison of Epidural Pressure in Live Anesthetized and Postmortem Primates. In: 7th International Workshop on Human Subjects for Biomechanical Research Proceedings, 16 October 1979, Coronado, CA., pp. 175-200. Washington, D.C.: Distributed by National Highway Traffic Safety Administration.

33. Nusholtz, G.S., et al. 1986. Critical Limitations on Significant Factors in Head Injury Research. Submitted to Proc. 30th Stapp Car Crash Conf.

34. Nusholtz, G.S. and Ward, C.C. 1986. Comparison of Epidural Pressure in Live Aneshetized and Postmortem Primates. Journal of Aviation, Space and Environmental Medicine. In press.

35. Ommaya, A.K.; Hirsch, A.E.; Flammin, E.S.; and Mahone, R.H. 1966. Cerebral Concussion in the Monkey: An Experimental Model. Science, 153:211-212.

36. Ono, K.; Kikuchi, K.; and Nakamura, M. 1980. Human Head Tolerance to Sagittal Impact Reliable Estimation Deduced from Experimental Head Injury Using Subhuman Primates and Human Cadaver Skulls. Proc. 24th Stapp Car Crash Conf., 15-17 October, Troy, MI, pp. 104-160. SAE Paper No. 801300.

37. Padgaonkar, A.J.; Krieger, K.W.; and King, A.J. 1975. Measurement of Angular Acceleration of a Rigid Body Using Linear Accelerations. ASME Preprint-75-APM3, June.

38. Roberts, V.L.; Hodgson, V.R.; and Thomas, L.M. 1967. Fluid Pressure Gradients Caused by Impact to the Human Skull. In: Biomechanics Monograph, pp. 223-235. New York: American Society of Mechanical Engineers.

39. Sances, A., et al. 1984. Biodynamics of Vehicular Injuries. In: G. A. Peters and B. J. Peters, Eds., Automotive Engineering and Litigation, New York: Garland Law Publishing, pp. 449-550.

40. Shugar, T.A. 1975. Transient Structural Response of the Linear Skull-Brain System. Proc. 19th Stapp Car Crash Conf., pp. 581-614.

41. Stalnaker, R.L., et al. Door Crashworthiness Criteria. Final Report. 1971. Contract No. FH-11-7288. U. S. Department of Transportation, National Highway

Traffic Safety Administration, Washington, D.C.

42. Stalnaker, R.L., et al. 1977. Head Impact Response. Proc. 21st Stapp Car Crash Conf., 19-21 October, New Orleans, pp. 303-335. SAE Paper No. 770921.

43. Thomas, L.M., et al. 1968. Static Deformation and Volume Changes in the Human Skull. Proc. 12th Stapp Car Crash Conf., pp. 260-270.

44. Unterharnscheidt, F. 1983. Neuropathology of Rhesus Monkeys Undergoing - Gx impact acceleration. In: C. L. Ewing, et al., eds., Impact Injury of the Head and Spine, Springfield, IL: Thomas, pp. 94-176.

45. Ward, C.C.; Chan, M.; and Nahum, A. 1980. Intracranial Pressure - A Brain Injury Criterion. Proc. 24th Stapp Car Crash Conf., SAE Paper No. 801304.

46. Ward, C.C.; Nikravesch, P.E.; and Thompson, R.B. 1978. Biodynamic Finite Element Models Used in Brain Injury Research. Journal of Aviation, Space and Environemntal Medicine, 49(1).

47. Abel, J.M., et al. 1978. Incidence and Severity of Cerebral Concussion in the Rhesus Monkey Follwoing Sagittal Plane Angular Acceleration. Proc. 22nd Stapp Car Crash Conf., pp. 33-53.

48. Atluri, S.; Kobayashi, A.S.; Cheng, J.S. 1975. Brain Tissue Fragility - A Finite Strain Analysis by Hybrid Finite - Element Method. Journal of Applied Mechanics:269-273. June.

49. Brinn, J.; Staffield, S.E. 1970. Evaluation of Impact Test Accelerations. Proc. 14th Stapp Car Crash Conf., pp. 188-207.

50. Brown, G.W.; Brown, M.L. 1954. Cardiovascular Response to Experimental Cerebral Concussion in the Rhesus Monkey: Discussion of Similarity of Responses to

Electroconvulsive Shock and Cerebral Concussion in Dogs, Monkeys, and Man. A.M.A. Arch. Neuro. Psychia. 71:707-713.

51. Douglass, J.M., et al. 1968. Applications of Experimental Head Injury Research. Proc. 12th Stapp Car Crash Conf., pp. 317-337.

52. Flexner, L.B.; Weed, L.H. 1983. Note on Cerebrospinal Elasticity in a Chimpanzee. Am. J. Physiol. 105:571-573.

53. Hashizume, K. 1972. A Study of the Experimental Brain Injury. Brain and Nerve, 14:991-1002.

54. Miller, J.D.; Becker, D.P.; Ward, J.D., et al. 1977. Significance of Intracranial Hypertension in Severe Head Injury. Journal of Neurosurgery, 47:503-516.

55. Ommaya, A.K. et al. 1967. Scaling of Experimental Data on Cerebral Concussion Threshold for Man. Proc. 11th Stapp Car Crash Conf., pp. 45-52.

56. Portnoy, H.D., et al. 1970. Intracranial Pressure and Head Acceleration During Whiplash. Proc. 14th Stapp Car Crash Conf., pp. 152-168. SAE Paper No. 700900.

57. Saczalski, K.J. 1976. A Critical Assessment of the Use of Non-Human Surrogates for Safety System Evaluation. Proc. 20th Stapp Car Crash Conf., pp. 159-187.

58. Symon, L. 1967. A Comparative Study of Middle Cerebral Pressure in Dogs and Macaques. Journal of Physiol. 191:449-465.

59. Unterharnschedit, F.; Higgins, L.S. 1969. Traumatic Lesions of Brain and Spinal Cord Due to Nondeforming Angular Accelerations of the Head. Texas Report on Biol. and Med. 27:127-166.

60. Weed, L.H., Flexner, L.B. 1932. Cerebrospinal Elasticity in the Cat and Macaques. American Journal of Physiol. 101:667-668.

61. Nusholtz, G.S.; Bender, M.; and Kaiker, P.S. 1986. Photogrammetric Techniques Using High-Speed Cineradiography. Optical Engineering. 25: 791-798.

62. Bishop, R.L. and Goldberg, S.I. 1968. Tensor Analysis on Manifolds, New York: MacMillan.

63. Cartan, E. 1946. Lecons dur la Geometrie des Espaces de Rieman, Second Edition, Paris: Gautheir Villars.

64. O'Neill, B. 1967. Elementary Differential Geometry, New York: Academic Press.

65. Stoker, J.J. 1969. Differential Geometry, New York: Wiley Intersciences.

66. Harris, C.M. and Crede, C.E. Shock and Vibration Handbook. New York: McGraw-Hill Book Company.

67. Hartman, C.G. and Straus, Jr., W.L., eds. The Anatomy of the Rhesus Monkey (Macaca mulatta), New York: Hafner Publishing Co., 1965 edition.

68. Heimer, L. 1983. The Human Brain and Spinal Cord Functional Neuroanatomy and Dissection Guide, New York: Springer-Verlag.

69. Ommaya, A.K. 1973. Head Injury Mechanisms. Final Report Contract No. DOT-HS-081-1-1061A, U. S. Department of Transportation, National Highway Traffic Sfety Administration.

70. Smith, R.W. 1979. The Response of Unembalmed Cadaveric and Living Cerebral Vessels to Graded Injury - A Pilot Study. Proc. 23rd Stapp Car Crash Conf., pp. 543-560. SAE Paper No. 791021.

9.0 APPENDIX A: INJURY/DAMAGE REPORT

DOT GENERAL TEST INJURY INFORMATION
EVALUATION OF EXPERIMENTAL TECHNIQUES IN
HEAD INJURY RESEARCH

				TITLE
CONTRACT NO:	ADTNH22-83-C-07095			CONNO
LABORATORY:		TRI		TSTPRF
TEST OBJECTIVE:	OCCIPITAL HEAD P-A			TSTOBJ
TEST NO:	85R002			TSTREF
TEST DATE:	08/NOV/85			TSTDAT
TOTAL NUMBER TESTS THIS SUBJECT		1		NOTEST
SUBJECT NO:	85R1			CADREF
(F/M/N)		F		OCCSEX
(AN/CD)	POSTMORTEM	AN		OCCTYP
AGE		99		OCCAGE
WEIGHT		5.0		OCCWT(Kg)
STATURE		71.0		STATUR(cm)
TEST TYPE:	HEAD	BIO		TSTTYP
(DRP/PED/PEN/OTH)		OTH	CANNON	TSTCFN
		0		VEHNO
		OT		OCCLOC
RESTRAINT SYSTEM 1:		NON		RESTR1
RESTRAINT SYSTEM 2:		NON		RESTR2

CANNON VELOCITY (m/s): 11 IMPACTOR MASS (Kg): 10
PADDING: 2.5 cm Ensolite. STRIKER: 10 cm round flat
OCCUPANT INJURY GROUP IDENTIFIER 8

NUMBER OF FRACTURED RIBS:	0	FRCTRB
NUMBER OF RIB FRACTURES:	0	RBFRCT

	BODYRG	ASPECT	LESION	SYSORG	AIS
1					
2					
3					
4					
5					
6					
7					
8					
9					
10					

INJTXT: TEXT OF INJURY Note: Up to 80 characters of text.

1 NO INJURY OBSERVED.
2
3
4
5
6
7
8
9
10

ANOMALY NOTES:

DOT GENERAL TEST ANTHROPOMETRIC INFORMATION

EVALUATION OF EXPERIMENTAL TECHNIQUES IN HEAD INJURY RESEARCH				TITLE
CONTRACT NO:	ADTNH22-83-C-07095			CONNO
LABORATORY:		TRI		TSTPRF
TEST NO:		85R002		TSTREF
TEST DATE:		08/NOV/85		TSTDAT
TOTAL NUMBER TESTS THIS SUBJECT		1		NOTEST
ANTHROPOMETRIC GROUP IDENTIFIER 7				
SUBJECT NO:		85R1		CADREF
(F/M/N)		F		OCCSEX
(AN/CD)	POSTMORTEM	AN		OCCTYP
AGE		99		OCCAGE
WEIGHT		5.0		OCCTWT(Kg)
		cm	in	
STATURE		71.0	28.0	STATUR
BUTTOCK-CROWN		53.0	20.9	SEATHT
TOP HEAD TOP SHOULDER		62.8	24.7	SHLDHT
SHOULDER ELBOW		15.6	06.1	SHLDEL
HEEL-TOE (foot)		14.5	05.7	FOOTLN
FOREARM-HAND		23.7	09.3	FARMHD
NECK CIR.		23.0	09.1	NECKCR
CHEST CIR.		31.5	12.4	CHESTCR
THIGH CIR.		22.0	08.7	THGHCR
CALF CIR.		13.0	05.1	CALFCR
ANKLE CIR.		10.5	04.1	ANKLCR
POPLITEAL HEIGHT		18.0	07.1	
TRUNK LENGTH		40.2	15.7	
BUTTOCK-KNEE		18.6	07.3	
TOTAL ARM REACH		31.5	12.4	
HAND		10.1	04.0	
HEAD CIR.		28.0	11.0	
SHOULDER CIR.		33.5	13.2	
			999	BEDCON
			07/OCT/85	DTEDTD
EUTHANIZED AT ULAM FOR SICKNESS				CSEDTH
POSTMORTEM ADULT RHESUS				CADAPP
UNREMARKABLE				CADAN

DOT GENERAL TEST INJURY INFORMATION
EVALUATION OF EXPERIMENTAL TECHNIQUES IN
HEAD INJURY RESEARCH

TITLE				
CONNO			ADTNH22-83-C-07095	CONTRACT NO:
TSTPRF			TRI	LABORATORY:
TSTOBJ			OCCIPITAL HEAD P-A	TEST OBJECTIVE:
TSTREF			85R005	TEST NO:
TSTDAT			25/NOV/85	TEST DATE:
NOTEST			1	TOTAL NUMBER TESTS THIS SUBJECT
CADREF			85R2	SUBJECT NO:
OCCSEX			M	(F/M/N)
OCCTYP			AN	(AN/CD) POSTMORTEM
OCCAGE			99	AGE
OCCWT(Kg)			9.0	WEIGHT
STATUR(cm)			72.3	STATURE
TSTTYP			BIO	TEST TYPE: HEAD
TSTCFN	CANNON		OTH	(DRP/PED/PEN/OTH)
VEHNO			0	
OCCLOC			OT	
RESTR1			NON	RESTRAINT SYSTEM 1:
RESTR2			NON	RESTRAINT SYSTEM 2:

CANNON VELOCITY (m/s): 12.2 IMPACTOR MASS (Kg): 10
PADDING: 2.5 cm Ensolite. STRIKER: 10 cm round flat
OCCUPANT INJURY GROUP IDENTIFIER 8

FRCTRB	0	NUMBER OF FRACTURED RIBS:
RBFRCT	0	NUMBER OF RIB FRACTURES:

	BODYRG	ASPECT	LESION	SYSORG	AIS
1	H	I	L	B	6
2	H	I	F	S	4
3					
4					
5					
6					
7					
8					
9					
10					

INJTXT: TEXT OF INJURY Note: Up to 80 characters of text.

1 Subarachnoid hemorrhage at medulla and brain stem
2 Two basilar skull fractures
3
4
5
6
7
8
9
10

ANOMALY NOTES:

Test No: 85R005 Laboratory: TRI

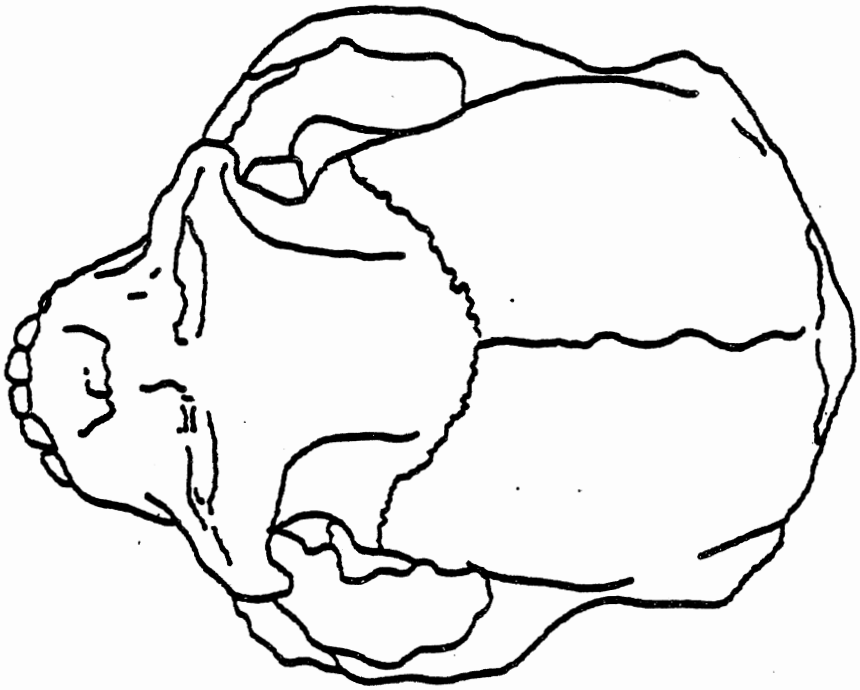

2 Basilar skull fractures

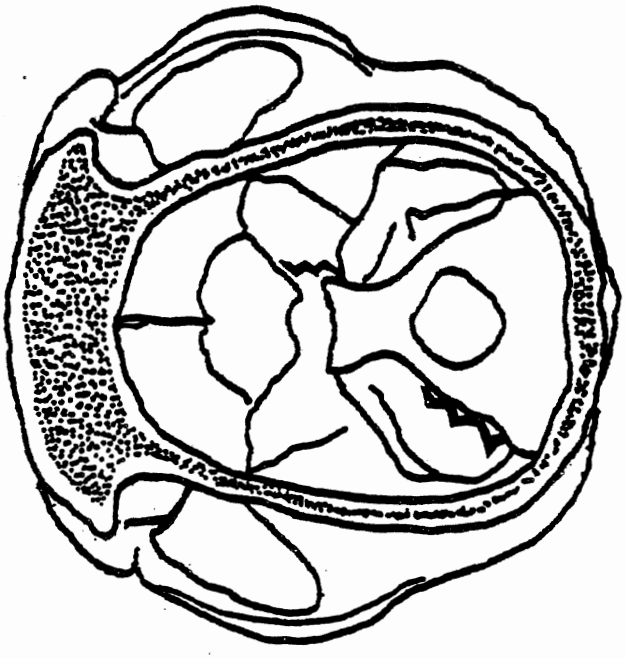

Test No: 85R005

Laboratory: TRI

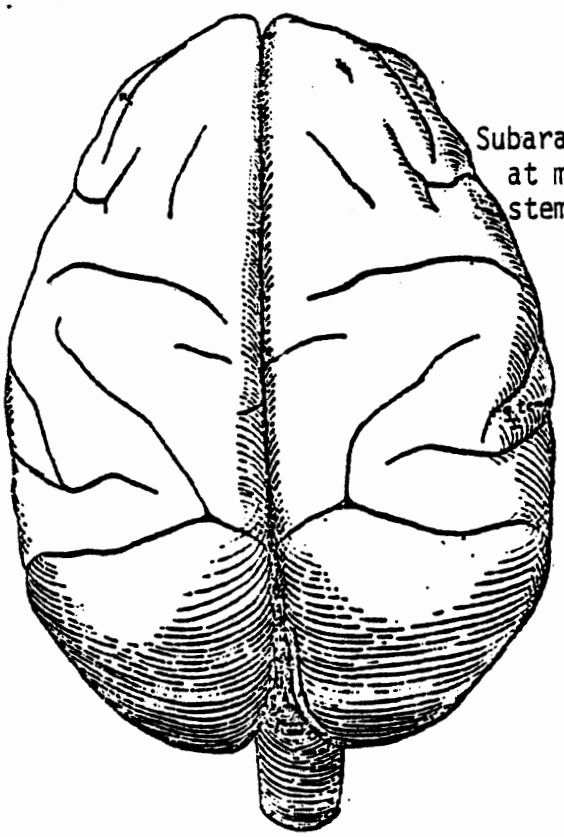

The brain from above

Subarachnoid hemorrhage at medulla and brain stem indicates lesion

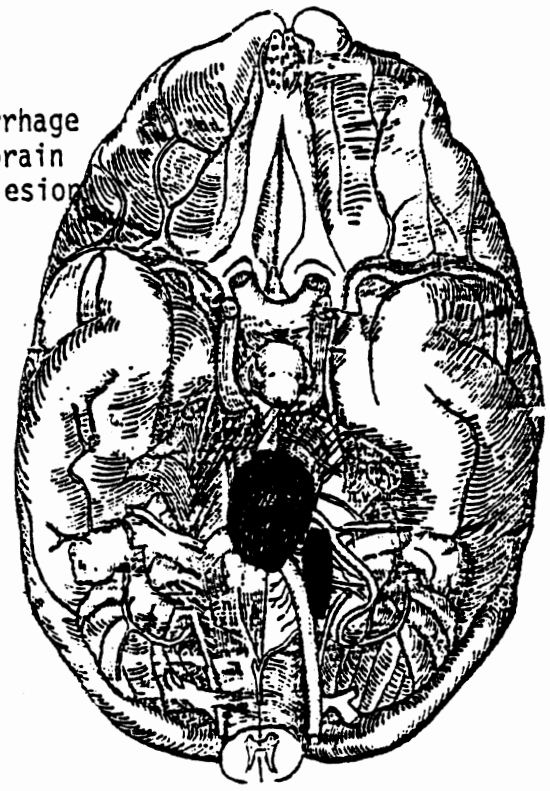

Base of the brain

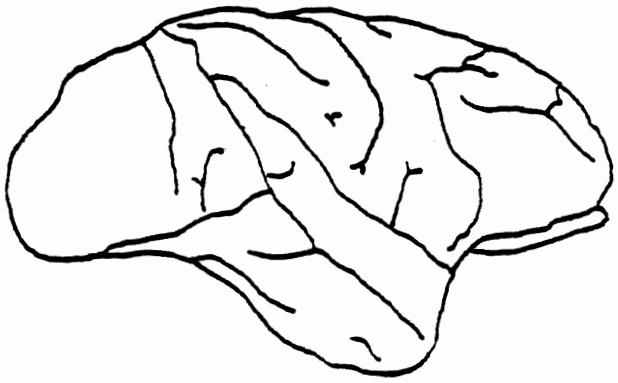

Right cerebral hemisphere
(Lateral view)

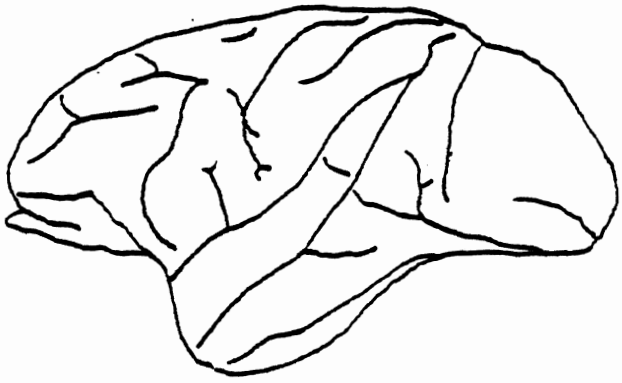

Left cerebral hemisphere
(Lateral view)

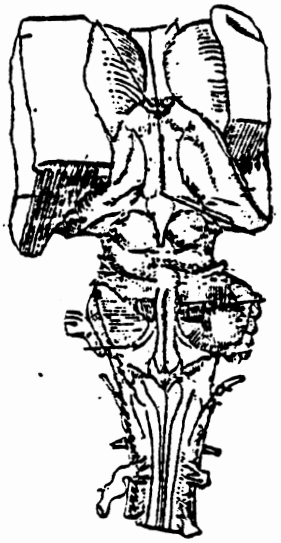

Dissection of brain stem
(Dorsal view)

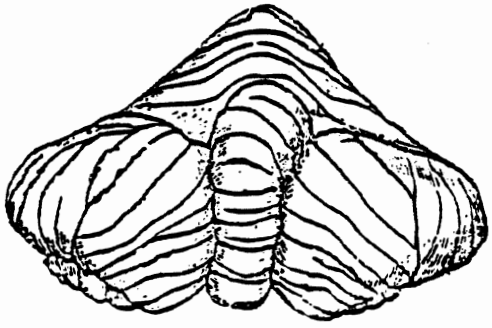

Cerebellum
(Posterior view)

DOT GENERAL TEST ANTHROPOMETRIC INFORMATION
EVALUATION OF EXPERIMENTAL TECHNIQUES IN
HEAD INJURY RESEARCH

TITLE				
CONNO		ADTNH22-83-C-07095		
TSTPRF		TRI		
TSTREF		85R005		
TSTDAT		25/NOV/85		
NOTEST		1		
		ANTHROPOMETRIC GROUP IDENTIFIER 7		
CADREF		85R2		
OCCSEX		M		
OCCTYP	POSTMORTEM	AN		
OCCAGE		99		
OCCTWT(Kg)		9.0		
		cm	in	
STATUR		72.3	28.5	
SEATHT		59.5	23.4	
SHLDHT		58.1	22.9	
SHLDEL		15.3	06.0	
FOOTLN		14.0	05.5	
FARMHD		24.6	09.7	
NECKCR		999	999	
CHESTCR		42.0	16.5	
THGHCR		23.0	09.0	
CALFCR		15.0	05.9	
ANKLCR		10.0	03.9	
		13.0	05.1	
		45.0	17.7	
		18.6	07.3	
		38.6	15.2	
		09.0	03.5	
		33.0	13.0	
		49.0	19.3	
BEDCON			999	
DTEDTD			20/NOV/85	
CSEDTH		UTHOL AND BILATERAL PNEUMOTHORAX		
CADAPP		POSTMORTEM ADULT RHESUS		
CADAN		UNREMARKABLE		

DOT GENERAL TEST INJURY INFORMATION
EVALUATION OF EXPERIMENTAL TECHNIQUES IN
HEAD INJURY RESEARCH

TITLE				
CONNO			ADTNH22-83-C-07095	CONTRACT NO:
TSTPRF		TRI		LABORATORY:
TSTOBJ		OCCIPITAL HEAD P-A		TEST OBJECTIVE:
TSTREF		85R006		TEST NO:
TSTDAT		26/NOV/85		TEST DATE:
NOTEST		1		TOTAL NUMBER TESTS THIS SUBJECT
CADREF		85R3		SUBJECT NO:
OCCSEX		M		(F/M/N)
OCCTYP		AN	POSTMORTEM	(AN/CD)
OCCAGE		99		AGE
OCCWT(Kg)		8.4		WEIGHT
STATUR(cm)		67.3		STATURE
TSTTYP		BIO	HEAD	TEST TYPE:
TSTCFN	CANNON	OTH		(DRP/PED/PEN/OTH)
VEHNO		0		
OCCLOC		OT		
RESTR1		NON		RESTRAINT SYSTEM 1:
RESTR2		NON		RESTRAINT SYSTEM 2:

CANNON VELOCITY (m/s): 11.9 IMPACTOR MASS (Kg): 10
PADDING: 2.5 cm Ensolite. STRIKER: 10 cm round flat
OCCUPANT INJURY GROUP IDENTIFIER 8

FRCTRB	0	NUMBER OF FRACTURED RIBS:
RBFRCT	0	NUMBER OF RIB FRACTURES:

	BODYRG	ASPECT	LESION	SYSORG	AIS
1					
2					
3					
4					
5					
6					
7					
8					
9					
10					

INJTXT: TEXT OF INJURY Note: Up to 80 characters of text.

1 NO INJURY OBSERVED.
2
3
4
5
6
7
8
9
10

ANOMALY NOTES:

DOT GENERAL TEST ANTHROPOMETRIC INFORMATION

EVALUATION OF EXPERIMENTAL TECHNIQUES IN HEAD INJURY RESEARCH				TITLE
CONTRACT NO:	ADTNH22-83-C-07095			CONNO
LABORATORY:		TRI		TSTPRF
TEST NO:		85R006		TSTREF
TEST DATE:		26/NOV/85		TSTDAT
TOTAL NUMBER TESTS THIS SUBJECT		1		NOTEST
ANTHROPOMETRIC GROUP IDENTIFIER 7				
SUBJECT NO:		85R3		CADREF
(F/M/N)		M		OCCSEX
(AN/CD)	POSTMORTEM	AN		OCCTYP
AGE		99		OCCAGE
WEIGHT		8.4		OCCTWT(Kg)
		cm	in	
STATURE		67.3	26.5	STATUR
BUTTOCK-CROWN		54.2	21.3	SEATHT
TOP HEAD TOP SHOULDER		55.3	21.7	SHLDHT
SHOULDER ELBOW		18.3	07.2	SHLDEL
HEEL-TOE (foot)		15.5	06.1	FOOTLN
FOREARM-HAND		25.5	10.0	FARMHD
NECK CIR.		25.5	10.0	NECKCR
CHEST CIR.		38.0	15.0	CHESTCR
THIGH CIR.		24.0	09.4	THGHCR
CALF CIR.		15.0	05.9	CALFCR
ANKLE CIR.		10.0	03.9	ANKLCR
POPLITEAL HEIGHT		13.0	05.1	
TRUNK LENGTH		42.2	16.6	
BUTTOCK-KNEE		19.6	07.7	
TOTAL ARM REACH		42.5	16.7	
HAND		07.0	02.8	
HEAD CIR.		36.0	14.2	
SHOULDER CIR.		43.0	16.9	
			999	BEDCON
			22/NOV/85	DTEDTD
UTHOL AND BILATERAL PNEUMOTHORAX				CSEDTH
POSTMORTEM ADULT RHESUS				CADAPP
UNREMARKABLE				CADAN

DOT GENERAL TEST INJURY INFORMATION
EVALUATION OF EXPERIMENTAL TECHNIQUES IN
HEAD INJURY RESEARCH

TITLE				
CONTRACT NO:	ADTNH22-83-C-07095			CONNO
LABORATORY:		TRI		TSTPRF
TEST OBJECTIVE:	OCCIPITAL HEAD P-A			TSTOBJ
TEST NO:	85R008			TSTREF
TEST DATE:	04/DEC/85			TSTDAT
TOTAL NUMBER TESTS THIS SUBJECT		1		NOTEST
SUBJECT NO:	85R4			CADREF
(F/M/N)		F		OCCSEX
(AN/CD)	POSTMORTEM	AN		OCCTYP
AGE		99		OCCAGE
WEIGHT		6.8		OCCWT(Kg)
STATURE		65.0		STATUR(cm)
TEST TYPE:	HEAD	BIO		TSTTYP
(DRP/PED/PEN/OTH)		OTH	CANNON	TSTCFN
		0		VEHNO
		OT		OCCLOC
RESTRAINT SYSTEM 1:		NON		RESTR1
RESTRAINT SYSTEM 2:		NON		RESTR2

CANNON VELOCITY (m/s): 11 IMPACTOR MASS (Kg): 10
PADDING: 2.5 cm Ensolite. STRIKER: 10 cm round flat
OCCUPANT INJURY GROUP IDENTIFIER 8

NUMBER OF FRACTURED RIBS:	0	FRCTRB
NUMBER OF RIB FRACTURES:	0	RBFRCT

	BODYRG	ASPECT	LESION	SYSORG	AIS
1	H	I	F	S	6
2	H	I	L	B	6
3					
4					
5					
6					
7					
8					
9					
10					

INJTXT: TEXT OF INJURY Note: Up to 80 characters of text.

1 Basilar ring skull fracture
2 Subarachnoid hemorrhage at medulla and brain stem
3
4
5
6
7
8
9
10

ANOMALY NOTES:
Parietal thickness was 1 mm, indicating thin skull

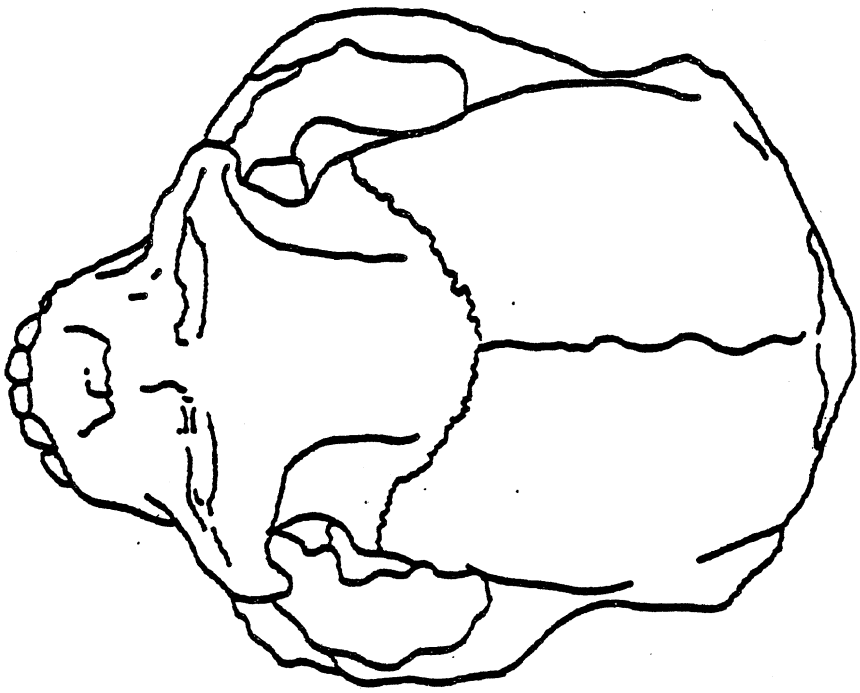

Basilar ring skull fracture

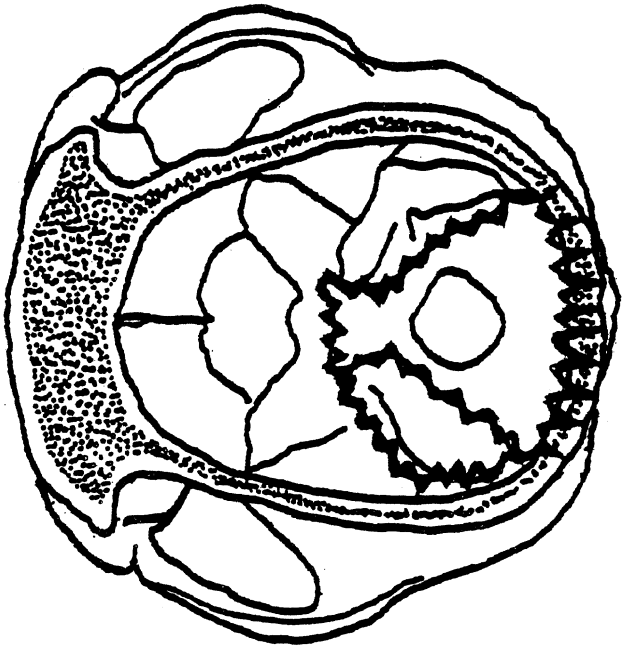

Test No: 86R008

Laboratory: TRI

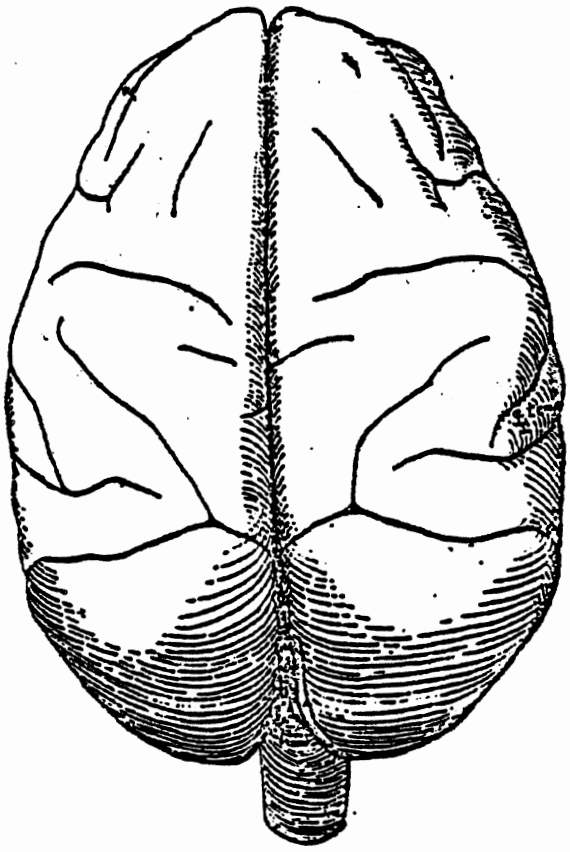

The brain from above

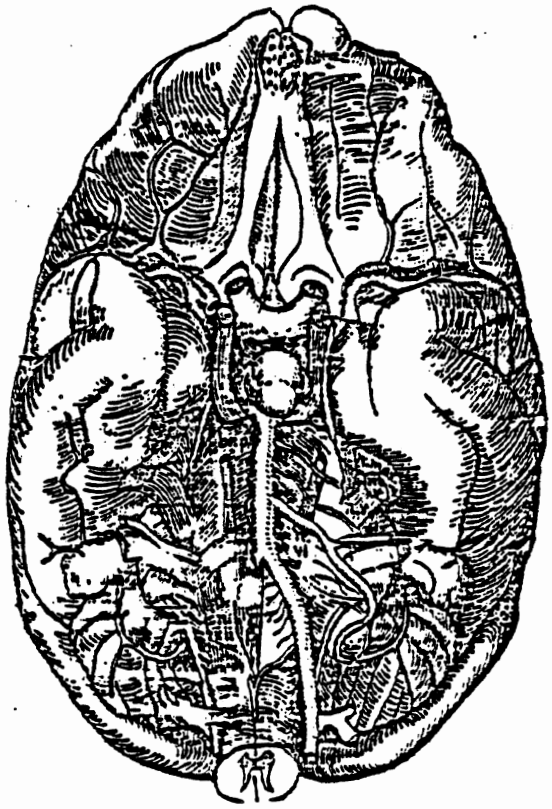

Base of the brain

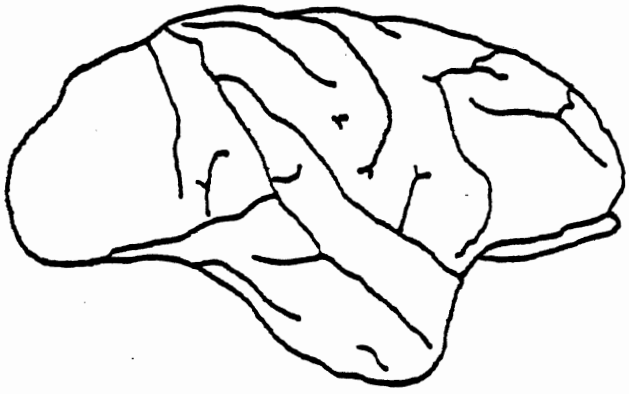

Right cerebral hemisphere
(Lateral view)

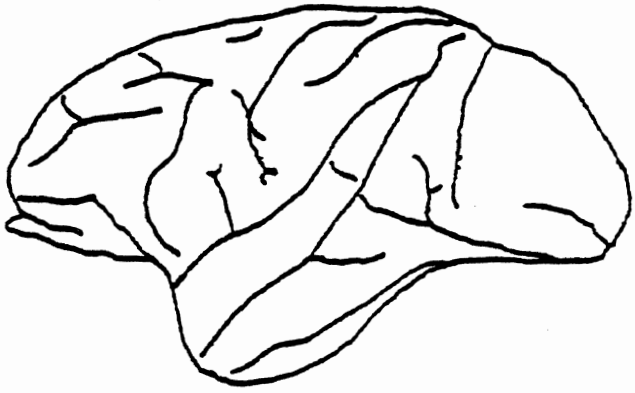

Left cerebral hemisphere
(Lateral view)

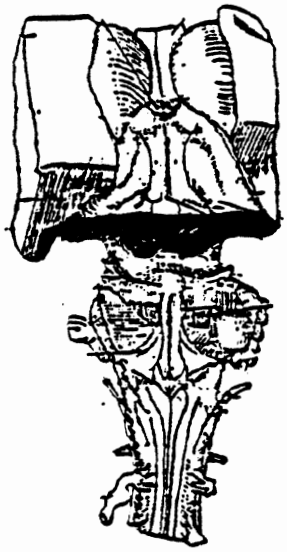

Subarachnoid hemorrhage
at medulla and brain stem

Dissection of brain stem
(Dorsal view)

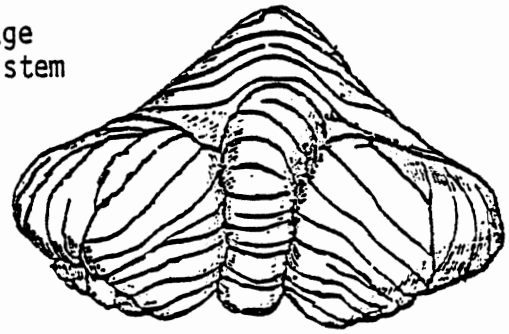

Cerebellum
(Posterior view)

DOT GENERAL TEST ANTHROPOMETRIC INFORMATION

EVALUATION OF EXPERIMENTAL TECHNIQUES IN HEAD INJURY RESEARCH				TITLE
CONTRACT NO:	ADTNH22-83-C-07095			CONNO
LABORATORY:		TRI		TSTPRF
TEST NO:		85R008		TSTREF
TEST DATE:		04/DEC/85		TSTDAT
TOTAL NUMBER TESTS THIS SUBJECT		1		NOTEST
ANTHROPOMETRIC GROUP IDENTIFIER 7				
SUBJECT NO:		85R4		CADREF
(F/M/N)		F		OCCSEX
(AN/CD)	POSTMORTEM	AN		OCCTYP
AGE		99		OCCAGE
WEIGHT		6.8		OCCTWT(Kg)
		cm	in	
STATURE		65.0	25.6	STATUR
BUTTOCK-CROWN		52.0	20.5	SEATHT
TOP HEAD TOP SHOULDER		51.0	20.1	SHLDHT
SHOULDER ELBOW		15.0	05.9	SHLDEL
HEEL-TOE (foot)		13.0	05.1	FOOTLN
FOREARM-HAND		24.0	09.4	FARMHD
NECK CIR.		29.0	11.4	NECKCR
CHEST CIR.		37.0	14.6	CHESTCR
THIGH CIR.		21.0	08.3	THGHCR
CALF CIR.		14.0	05.5	CALFCR
ANKLE CIR.		09.0	03.5	ANKLCR
POPLITEAL HEIGHT		13.0	05.1	
TRUNK LENGTH		38.0	15.0	
BUTTOCK-KNEE		22.0	08.7	
TOTAL ARM REACH		36.0	14.2	
HAND		12.0	04.7	
HEAD CIR.		29.0	11.4	
SHOULDER CIR.		39.0	15.4	
			999	BEDCON
			3/DEC/85	DTEDTD
UTHOL AND BILATERAL PNEUMOTHORAX				CSEDTH
POSTMORTEM ADULT RHESUS				CADAPP
UNREMARKABLE				CADAN

DOT GENERAL TEST INJURY INFORMATION
EVALUATION OF EXPERIMENTAL TECHNIQUES IN
HEAD INJURY RESEARCH

TITLE				
CONTRACT NO:	ADTNH22-83-C-07095			CONNO
LABORATORY:		TRI		TSTPRF
TEST OBJECTIVE:	OCCIPITAL HEAD P-A			TSTOBJ
TEST NO:	86R010			TSTREF
TEST DATE:	10/JAN/86			TSTDAT
TOTAL NUMBER TESTS THIS SUBJECT		1		NOTEST
SUBJECT NO:	85R5			CADREF
(F/M/N)		M		OCCSEX
(AN/CD)	POSTMORTEM	AN		OCCTYP
AGE		99		OCCAGE
WEIGHT		7.4		OCCWT(Kg)
STATURE		70.0		STATUR(cm)
TEST TYPE:	HEAD	BIO		TSTTYP
(DRP/PED/PEN/OTH)		OTH	CANNON	TSTCFN
		0		VEHNO
		OT		OCCLOC
RESTRAINT SYSTEM 1:		NON		RESTR1
RESTRAINT SYSTEM 2:		NON		RESTR2

CANNON VELOCITY (m/s): 11 IMPACTOR MASS (Kg): 10
PADDING: 2.5 cm Ensolite. STRIKER: 10 cm round flat
OCCUPANT INJURY GROUP IDENTIFIER 8

NUMBER OF FRACTURED RIBS:	0	FRCTRB
NUMBER OF RIB FRACTURES:	0	RBFRCT

	BODYRG	ASPECT	LESION	SYSORG	AIS
1	H	I	F	S	6
2					
3					
4					
5					
6					
7					
8					
9					
10					

INJTXT: TEXT OF INJURY Note: Up to 80 characters of text.

1 Basilar ring skull fracture
2
3
4
5
6
7
8
9
10

ANOMALY NOTES:

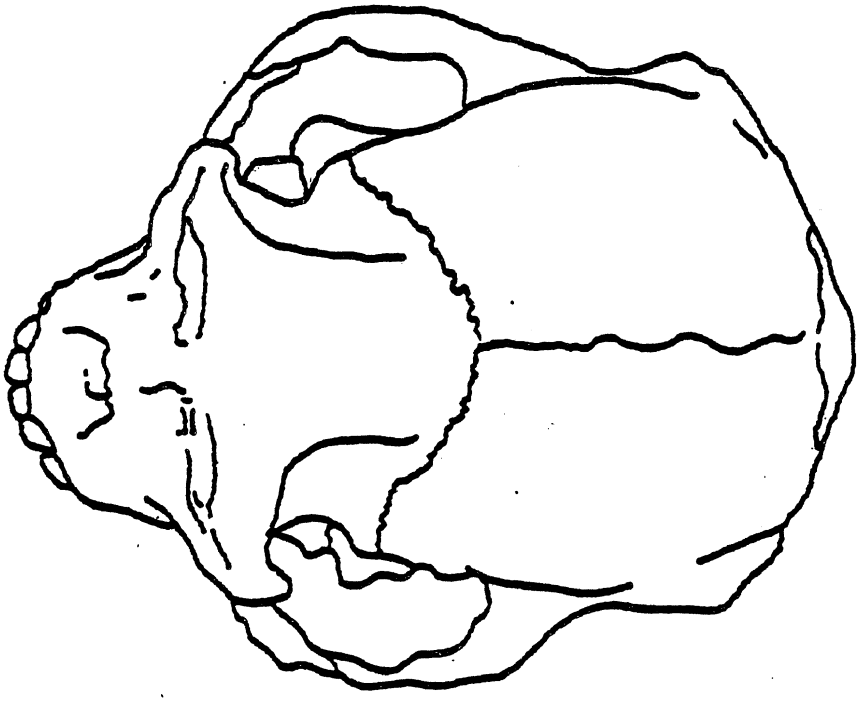

Basilar ring skull fracture

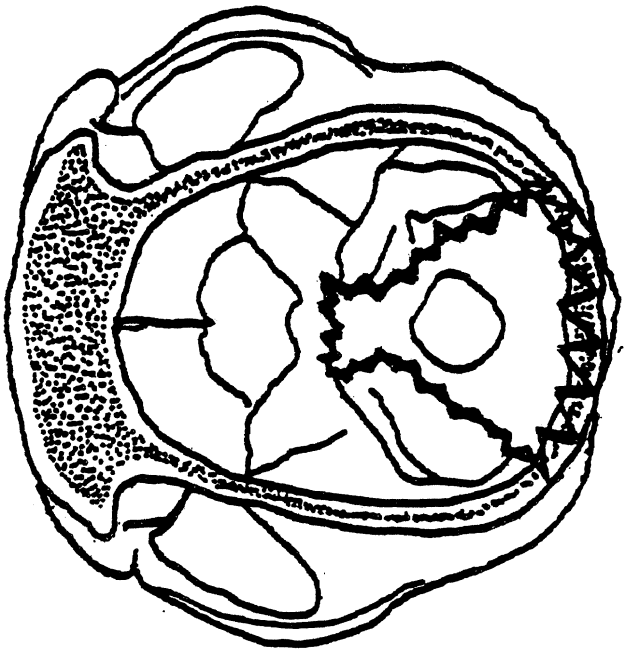

DOT GENERAL TEST ANTHROPOMETRIC INFORMATION

EVALUATION OF EXPERIMENTAL TECHNIQUES IN HEAD INJURY RESEARCH				TITLE
CONTRACT NO:	ADTNH22-83-C-07095			CONNO
LABORATORY:		TRI		TSTPRF
TEST NO:		85R010		TSTREF
TEST DATE:		10/JAN/86		TSTDAT
TOTAL NUMBER TESTS THIS SUBJECT		1		NOTEST
ANTHROPOMETRIC GROUP IDENTIFIER 7				
SUBJECT NO:		86R5		CADREF
(F/M/N)		M		OCCSEX
(AN/CD)	POSTMORTEM	AN		OCCTYP
AGE		99		OCCAGE
WEIGHT		7.4		OCCTWT(Kg)
		cm	in	
STATURE		70.0	27.6	STATUR
BUTTOCK-CROWN		53.0	20.9	SEATHT
TOP HEAD TOP SHOULDER		58.0	22.8	SHLDHT
SHOULDER ELBOW		18.0	07.1	SHLDEL
HEEL-TOE (foot)		16.0	06.3	FOOTLN
FOREARM-HAND		27.0	10.6	FARMHD
NECK CIR.		22.0	08.7	NECKCR
CHEST CIR.		35.0	13.8	CHESTCR
THIGH CIR.		20.0	07.9	THGHCR
CALF CIR.		13.5	05.3	CALFCR
ANKLE CIR.		11.0	04.3	ANKLCR
POPLITEAL HEIGHT		17.0	06.7	
TRUNK LENGTH		43.0	16.9	
BUTTOCK-KNEE		18.0	07.1	
TOTAL ARM REACH		40.0	15.7	
HAND		10.0	03.9	
HEAD CIR.		30.0	11.8	
SHOULDER CIR.		40.0	15.7	
			999	BEDCON
			8/JAN/86	DTEDTD
UTHOL AND BILATERAL PNEUMOTHORAX				CSEDTH
POSTMORTEM ADULT RHESUS				CADAPP
UNREMARKABLE				CADAN

DOT GENERAL TEST INJURY INFORMATION
EVALUATION OF EXPERIMENTAL TECHNIQUES IN
HEAD INJURY RESEARCH TITLE

CONTRACT NO:	ADTNH22-83-C-07095			CONNO
LABORATORY:		TRI		TSTPRF
TEST OBJECTIVE:	OCCIPITAL HEAD P-A			TSTOBJ
TEST NO:	86R011			TSTREF
TEST DATE:	15/JAN/86			TSTDAT
TOTAL NUMBER TESTS THIS SUBJECT		1		NOTEST
SUBJECT NO:	86R6			CADREF
(F/M/N)		F		OCCSEX
(AN/CD)	ANESTHETIZED	AN		OCCTYP
AGE		99		OCCAGE
WEIGHT		4.9		OCCWT(Kg)
STATURE		66.0		STATUR(cm)
TEST TYPE:	HEAD	BIO		TSTTYP
(DRP/PED/PEN/OTH)		OTH	CANNON	TSTCFN
		0		VEHNO
		OT		OCCLOC
RESTRAINT SYSTEM 1:		NON		RESTR1
RESTRAINT SYSTEM 2:		NON		RESTR2

CANNON VELOCITY (m/s): 10 IMPACTOR MASS (Kg): 10
PADDING: 2.5 cm Ensolite. STRIKER: 10 cm round flat
OCCUPANT INJURY GROUP IDENTIFIER 8

NUMBER OF FRACTURED RIBS:	0	FRCTRB
NUMBER OF RIB FRACTURES:	0	RBFRCT

	BODYRG	ASPECT	LESION	SYSORG	AIS
1	H	R	F	V	3
2	N	S	L	C	4
3					
4					
5					
6					
7					
8					
9					
10					

INJTXT: TEXT OF INJURY Note: Up to 80 characters of text.

1 Closed fracture C1 vertebra
2 Subdural hemorrhage of spinal cord at base of brain
3
4
5
6
7
8
9
10

ANOMALY NOTES:
Epidural hematoma under EPI 1

Test No: 86R011

Laboratory: TRI

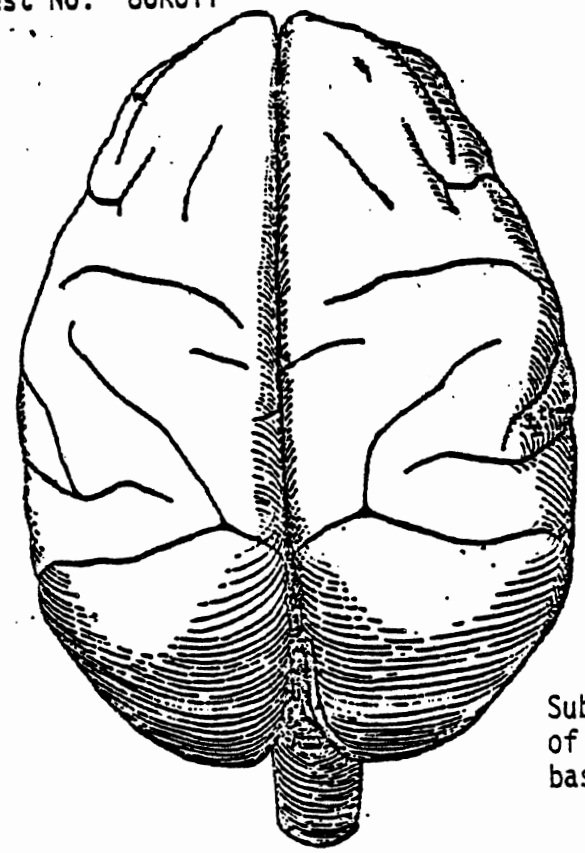

The brain from above

Subdural hemorrhage of spinal cord at base of brain

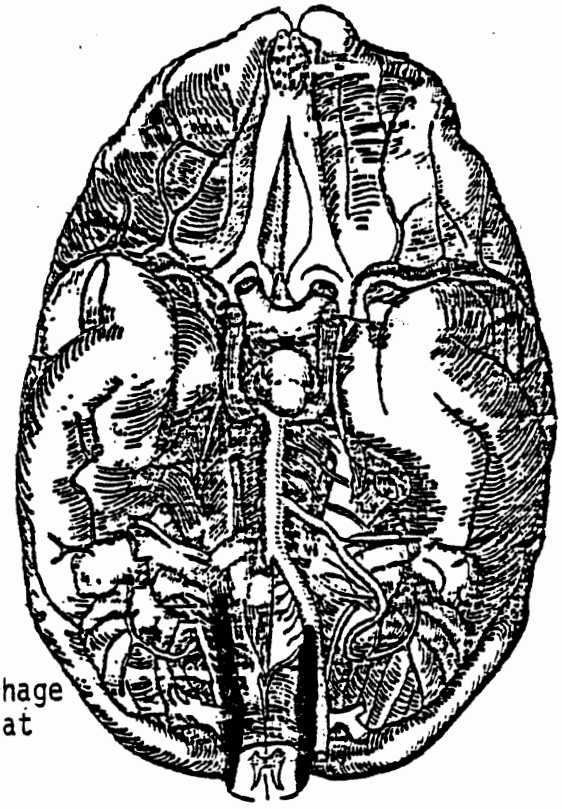

Base of the brain

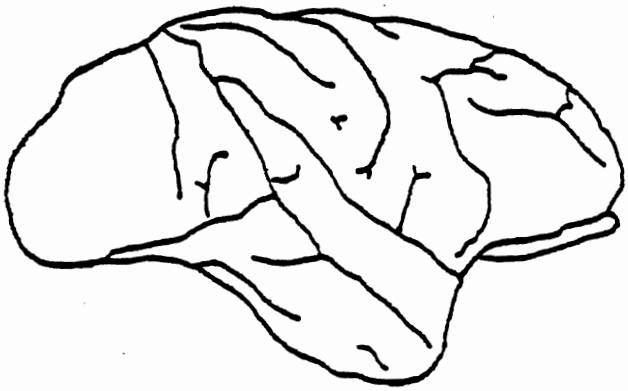

Right cerebral hemisphere
(Lateral view)

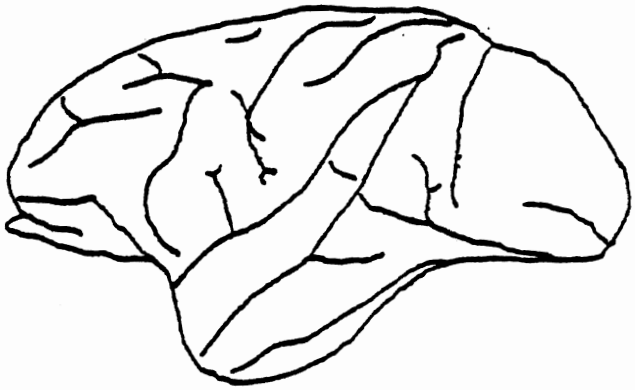

Left cerebral hemisphere
(Lateral view)

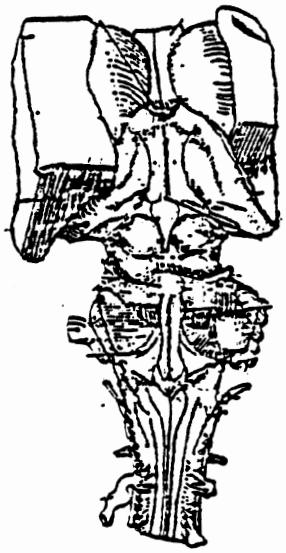

Dissection of brain stem
(Dorsal view)

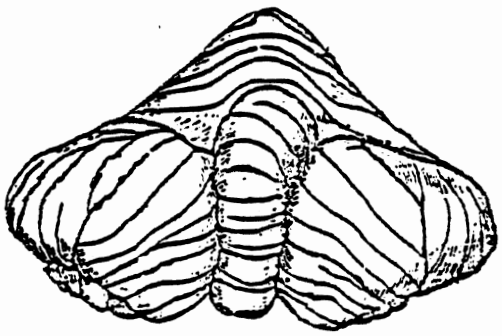

Cerebellum
(Posterior view)

DOT GENERAL TEST ANTHROPOMETRIC INFORMATION

EVALUATION OF EXPERIMENTAL TECHNIQUES IN HEAD INJURY RESEARCH				TITLE
CONTRACT NO:	ADTNH22-83-C-07095			CONNO
LABORATORY:		TRI		TSTPRF
TEST NO:		86R011		TSTREF
TEST DATE:		15/JAN/86		TSTDAT
TOTAL NUMBER TESTS THIS SUBJECT		1		NOTEST
ANTHROPOMETRIC GROUP IDENTIFIER 7				
SUBJECT NO:		86R6		CADREF
(F/M/N)		F		OCCSEX
(AN/CD)	ANESTHETIZED	AN		OCCTYP
AGE		99		OCCAGE
WEIGHT		4.9		OCCTWT(Kg)
		cm	in	
STATURE		66.0	26.0	STATUR
BUTTOCK-CROWN		50.0	19.7	SEATHT
TOP HEAD TOP SHOULDER		54.0	21.3	SHLDHT
SHOULDER ELBOW		14.0	05.5	SHLDEL
HEEL-TOE (foot)		15.0	05.9	FOOTLN
FOREARM-HAND		24.0	09.4	FARMHD
NECK CIR.		18.0	07.1	NECKCR
CHEST CIR.		31.0	12.2	CHESTCR
THIGH CIR.		15.5	06.1	THGHCR
CALF CIR.		10.0	03.9	CALFCR
ANKLE CIR.		07.5	03.0	ANKLCR
POPLITEAL HEIGHT		19.0	07.5	
TRUNK LENGTH		40.0	15.7	
BUTTOCK-KNEE		17.0	06.7	
TOTAL ARM REACH		36.0	14.2	
HAND		08.5	03.3	
HEAD CIR.		31.0	12.2	
SHOULDER CIR.		30.5	12.0	
			999	BEDCON
			999	DTEDTD
NOT APPLICABLE				CSEDTH
ANESTHETIZED ADULT RHESUS				CADAPP
POOR HEALTH, WEAK SECTION OF SKULL				CADAN

DOT GENERAL TEST INJURY INFORMATION
EVALUATION OF EXPERIMENTAL TECHNIQUES IN
HEAD INJURY RESEARCH

				TITLE
CONTRACT NO:	ADTNH22-83-C-07095			CONNO
LABORATORY:		TRI		TSTPRF
TEST OBJECTIVE:	OCCIPITAL HEAD P-A			TSTOBJ
TEST NO:	86R012			TSTREF
TEST DATE:	17/JAN/86			TSTDAT
TOTAL NUMBER TESTS THIS SUBJECT		1		NOTEST
SUBJECT NO:	86R7			CADREF
(F/M/N)		F		OCCSEX
(AN/CD)	ANESTHETIZED	AN		OCCTYP
AGE		99		OCCAGE
WEIGHT		6.9		OCCWT(Kg)
STATURE		68.5		STATUR(cm)
TEST TYPE:	HEAD	BIO		TSTTYP
(DRP/PED/PEN/OTH)		OTH	CANNON	TSTCFN
		0		VEHNO
		OT		OCCLOC
RESTRAINT SYSTEM 1:		NON		RESTR1
RESTRAINT SYSTEM 2:		NON		RESTR2

CANNON VELOCITY (m/s): 12.2 IMPACTOR MASS (Kg): 10
PADDING: 2.5 cm Ensolite. STRIKER: 10 cm round flat
OCCUPANT INJURY GROUP IDENTIFIER 8

NUMBER OF FRACTURED RIBS:	0	FRCTRB
NUMBER OF RIB FRACTURES:	0	RBFRCT

	BODYRG	ASPECT	LESION	SYSORG	AIS
1	H	S	L	B	3
2					
3					
4					
5					
6					
7					
8					
9					
10					

INJTXT: TEXT OF INJURY Note: Up to 80 characters of text.

1 Subdural hemorrhage left frontal lobe
2
3
4
5
6
7
8
9
10

ANOMALY NOTES:

Test No: 86R012

Laboratory: TRI

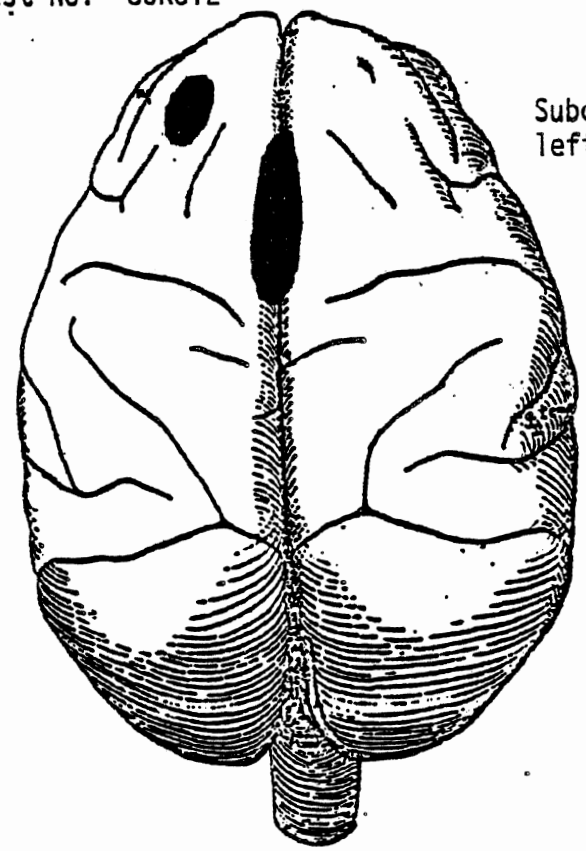

Subdural hemorrhage
left frontal lobe

The brain from above

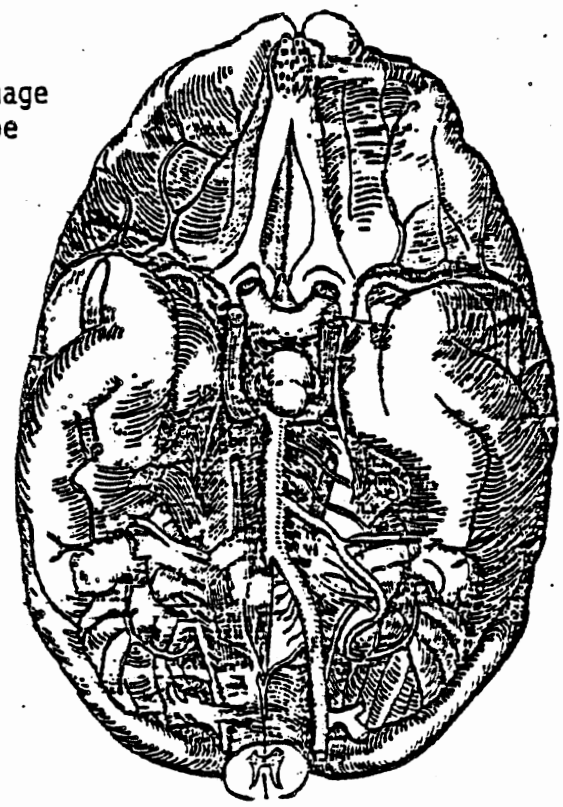

Base of the brain

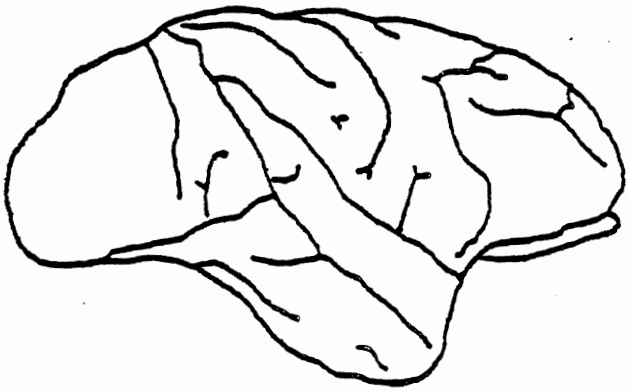

Right cerebral hemisphere
(Lateral view)

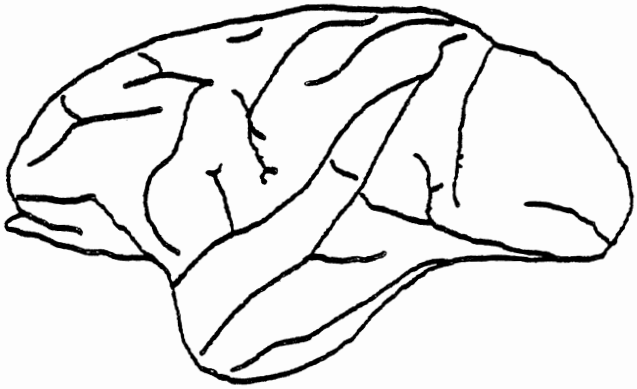

Left cerebral hemisphere
(Lateral view)

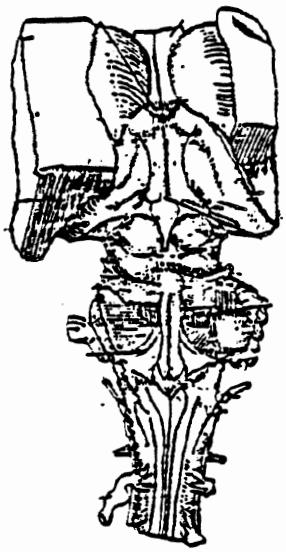

Dissection of brain stem
(Dorsal view)

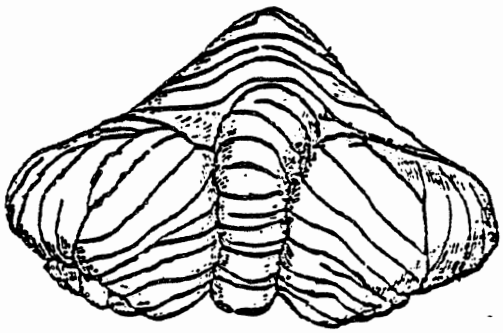

Cerebellum
(Posterior view)

DOT GENERAL TEST ANTHROPOMETRIC INFORMATION
EVALUATION OF EXPERIMENTAL TECHNIQUES IN
HEAD INJURY RESEARCH

				TITLE
CONTRACT NO:	ADTNH22-83-C-07095			CONNO
LABORATORY:	TRI			TSTPRF
TEST NO:	86R012			TSTREF
TEST DATE:	17/JAN/86			TSTDAT
TOTAL NUMBER TESTS THIS SUBJECT	1			NOTEST
ANTHROPOMETRIC GROUP IDENTIFIER	7			
SUBJECT NO:	86R7			CADREF
(F/M/N)	F			OCCSEX
(AN/CD) ANESTHETIZED	AN			OCCTYP
AGE	99			OCCAGE
WEIGHT	6.9			OCCTWT(Kg)
	cm	in		
STATURE	68.5	27.0		STATUR
BUTTOCK-CROWN	49.5	19.5		SEATHT
TOP HEAD TOP SHOULDER	59.0	23.2		SHLDHT
SHOULDER ELBOW	14.0	05.5		SHLDEL
HEEL-TOE (foot)	15.0	05.9		FOOTLN
FOREARM-HAND	24.0	09.4		FARMHD
NECK CIR.	21.0	08.3		NECKCR
CHEST CIR.	36.0	14.2		CHESTCR
THIGH CIR.	24.0	09.4		THGHCR
CALF CIR.	13.0	05.1		CALFCR
ANKLE CIR.	11.0	04.3		ANKLCR
POPLITEAL HEIGHT	19.0	07.5		
TRUNK LENGTH	41.0	16.1		
BUTTOCK-KNEE	18.0	07.1		
TOTAL ARM REACH	34.5	13.6		
HAND	08.5	03.3		
HEAD CIR.	29.5	11.6		
SHOULDER CIR.	41.0	16.1		
			999	BEDCON
			999	DTEDTD
NOT APPLICABLE				CSEDTH
ANESTHETIZED ADULT RHESUS				CADAPP
FAT, THICK SKULL AT EPI1,2				CADAN

DOT GENERAL TEST INJURY INFORMATION
EVALUATION OF EXPERIMENTAL TECHNIQUES IN
HEAD INJURY RESEARCH

				TITLE
CONTRACT NO:	ADTNH22-83-C-07095			CONNO
LABORATORY:		TRI		TSTPRF
TEST OBJECTIVE:	OCCIPITAL HEAD P-A			TSTOBJ
TEST NO:	86R013			TSTREF
TEST DATE:	20/JAN/86			TSTDAT
TOTAL NUMBER TESTS THIS SUBJECT		1		NOTEST
SUBJECT NO:	86R8			CADREF
(F/M/N)		M		OCCSEX
(AN/CD)	ANESTHETIZED	AN		OCCTYP
AGE		99		OCCAGE
WEIGHT		8.7		OCCWT(Kg)
STATURE		86.5		STATUR(cm)
TEST TYPE:	HEAD	BIO		TSTTYP
(DRP/PED/PEN/OTH)		OTH	CANNON	TSTCFN
		0		VEHNO
		OT		OCCLOC
RESTRAINT SYSTEM 1:		NON		RESTR1
RESTRAINT SYSTEM 2:		NON		RESTR2

CANNON VELOCITY (m/s): 11.9 IMPACTOR MASS (Kg): 10
PADDING: 2.5 cm Ensolite. STRIKER: 10 cm round flat
OCCUPANT INJURY GROUP IDENTIFIER 8

NUMBER OF FRACTURED RIBS:	0	FRCTRB
NUMBER OF RIB FRACTURES:	0	RBFRCT

	BODYRG	ASPECT	LESION	SYSORG	AIS
1	H	S	L	B	4
2	H	I	L	B	3
3					
4					
5					
6					
7					
8					
9					
10					

INJTXT: TEXT OF INJURY Note: Up to 80 characters of text.

1 Subdural hemorrhage superior left frontal lobe
2 Subdural hemorrhage inferior left frontal lobe
3
4
5
6
7
8
9
10

ANOMALY NOTES:

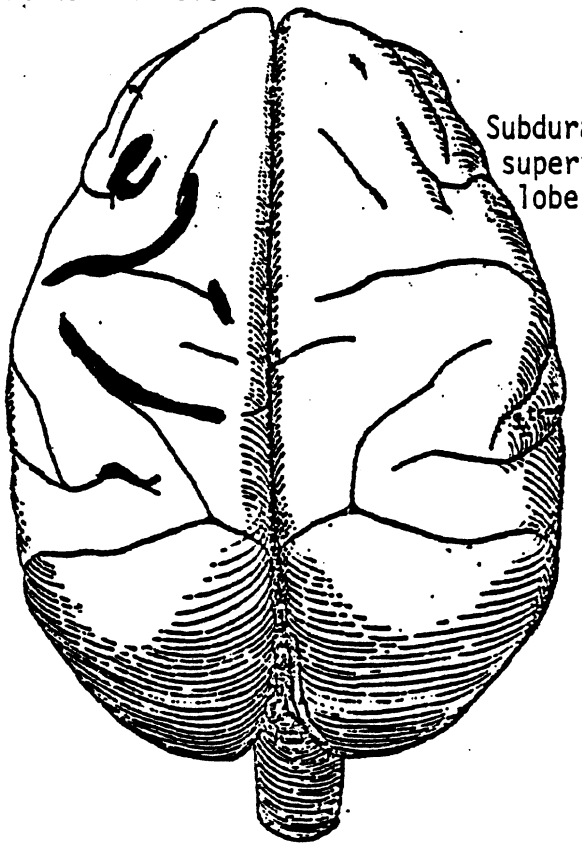

Subdural hemorrhage superior left frontal lobe

The brain from above

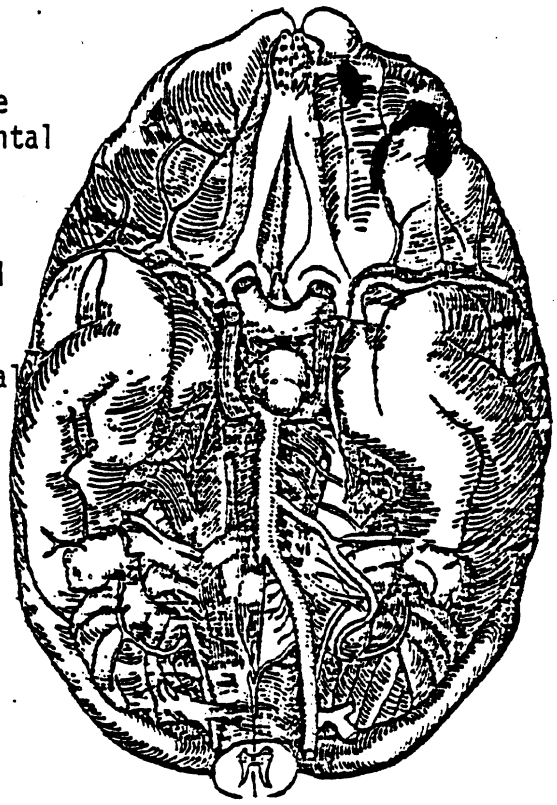

Subdural hemorrhage inferior left frontal lobe

Base of the brain

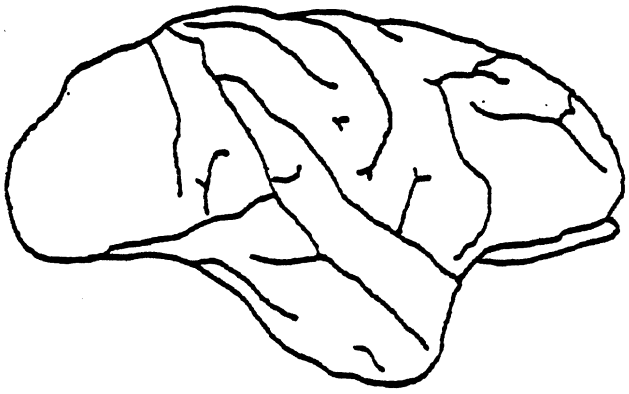

Right cerebral hemisphere
(Lateral view)

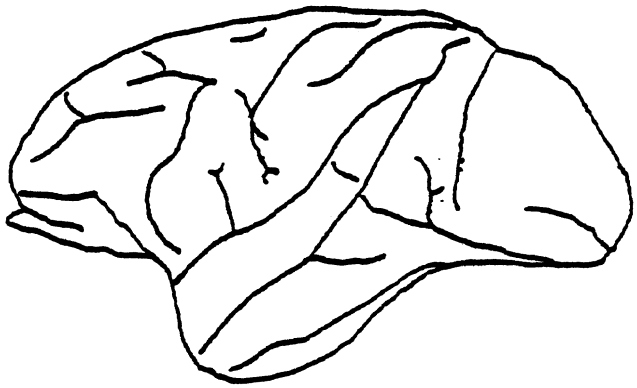

Left cerebral hemisphere
(Lateral view)

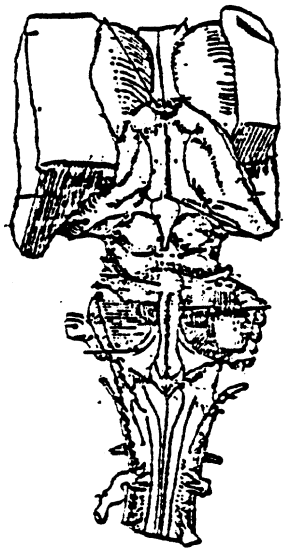

Dissection of brain stem
(Dorsal view)

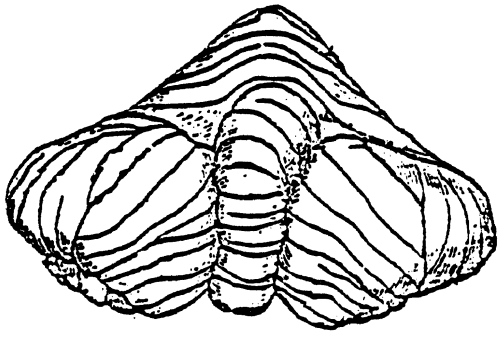

Cerebellum
(Posterior view)

DOT GENERAL TEST ANTHROPOMETRIC INFORMATION

EVALUATION OF EXPERIMENTAL TECHNIQUES IN HEAD INJURY RESEARCH				TITLE
CONTRACT NO:	ADTNH22-83-C-07095			CONNO
LABORATORY:		TRI		TSTPRF
TEST NO:		86R013		TSTREF
TEST DATE:		20/JAN/86		TSTDAT
TOTAL NUMBER TESTS THIS SUBJECT		1		NOTEST
ANTHROPOMETRIC GROUP IDENTIFIER 7				
SUBJECT NO:		86R8		CADREF
(F/M/N)		M		OCCSEX
(AN/CD)	ANESTHETIZED	AN		OCCTYP
AGE		99		OCCAGE
WEIGHT		8.7		OCCTWT(Kg)
		cm	in	
STATURE		86.5	34.1	STATUR
BUTTOCK-CROWN		60.0	23.6	SEATHT
TOP HEAD TOP SHOULDER		75.5	29.7	SHLDHT
SHOULDER ELBOW		18.5	07.3	SHLDEL
HEEL-TOE (foot)		18.0	07.1	FOOTLN
FOREARM-HAND		29.0	11.4	FARMHD
NECK CIR.		20.0	07.9	NECKCR
CHEST CIR.		35.0	13.8	CHESTCR
THIGH CIR.		21.0	08.3	THGHCR
CALF CIR.		12.0	04.7	CALFCR
ANKLE CIR.		09.0	03.6	ANKLCR
POPLITEAL HEIGHT		26.5	10.4	
TRUNK LENGTH		46.0	18.1	
BUTTOCK-KNEE		24.5	09.6	
TOTAL ARM REACH		41.0	16.1	
HAND		12.0	04.7	
HEAD CIR.		30.0	11.8	
SHOULDER CIR.		43.0	16.9	
			999	BEDCON
			999	DTEDTD
NOT APPLICABLE				CSEDTH
ANESTHETIZED ADULT RHESUS				CADAPP
UNREMARKABLE				CADAN

DOT GENERAL TEST INJURY INFORMATION
EVALUATION OF EXPERIMENTAL TECHNIQUES IN
HEAD INJURY RESEARCH

				TITLE
CONTRACT NO:	ADTNH22-83-C-07095			CONNO
LABORATORY:		TRI		TSTPRF
TEST OBJECTIVE:	OCCIPITAL HEAD P-A			TSTOBJ
TEST NO:	86R014			TSTREF
TEST DATE:	22/JAN/86			TSTDAT
TOTAL NUMBER TESTS THIS SUBJECT		1		NOTEST
SUBJECT NO:	86R9			CADREF
(F/M/N)		M		OCCSEX
(AN/CD)	ANESTHETIZED	AN		OCCTYP
AGE		99		OCCAGE
WEIGHT		8.6		OCCWT(Kg)
STATURE		71.0		STATUR(cm)
TEST TYPE:	HEAD	BIO		TSTTYP
(DRP/PED/PEN/OTH)		OTH	CANNON	TSTCFN
		0		VEHNO
		OT		OCCLOC
RESTRAINT SYSTEM 1:		NON		RESTR1
RESTRAINT SYSTEM 2:		NON		RESTR2

CANNON VELOCITY (m/s): 11.9 IMPACTOR MASS (Kg): 10
PADDING: 2.5 cm Ensolite. STRIKER: 10 cm round flat
OCCUPANT INJURY GROUP IDENTIFIER 8

NUMBER OF FRACTURED RIBS:	0	FRCTRB
NUMBER OF RIB FRACTURES:	0	RBFRCT

	BODYRG	ASPECT	LESION	SYSORG	AIS
1	H	I	L	B	5
2					
3					
4					
5					
6					
7					
8					
9					
10					

INJTXT: TEXT OF INJURY Note: Up to 80 characters of text.

1 Subdural hemorrhage of spinal cord at base of brain
2
3
4
5
6
7
8
9
10

ANOMALY NOTES:

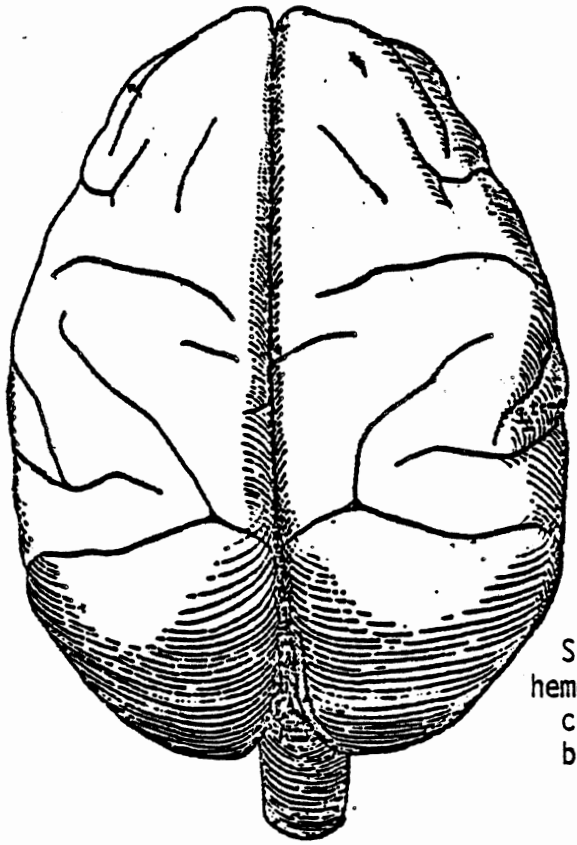

The brain from above

Subdural hemorrhage of spinal cord at base of brain

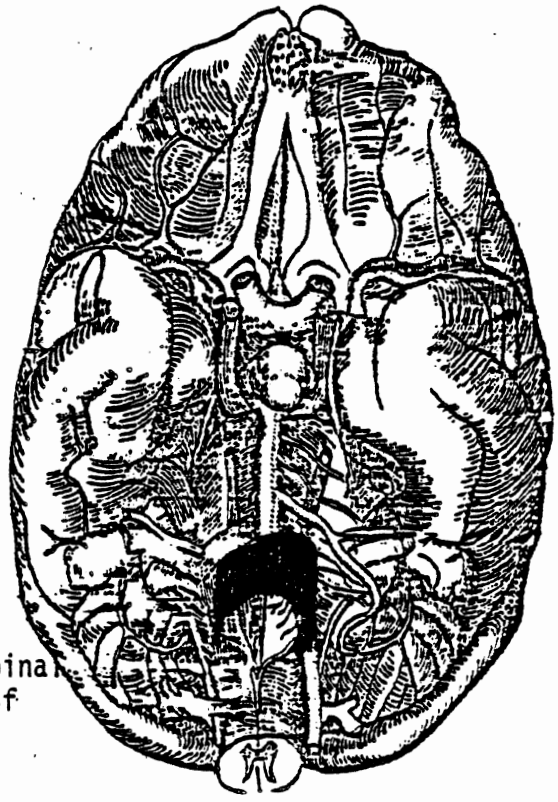

Base of the brain

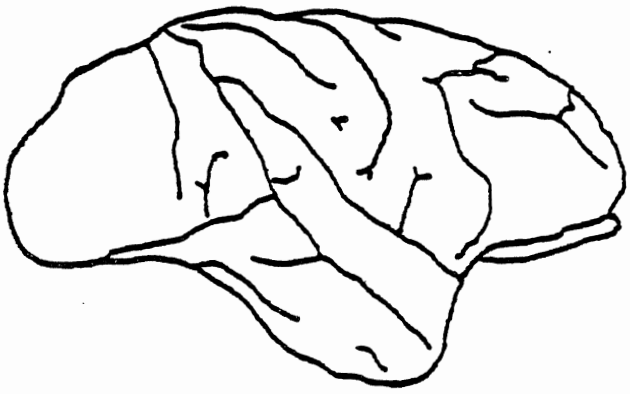

Right cerebral hemisphere
(Lateral view)

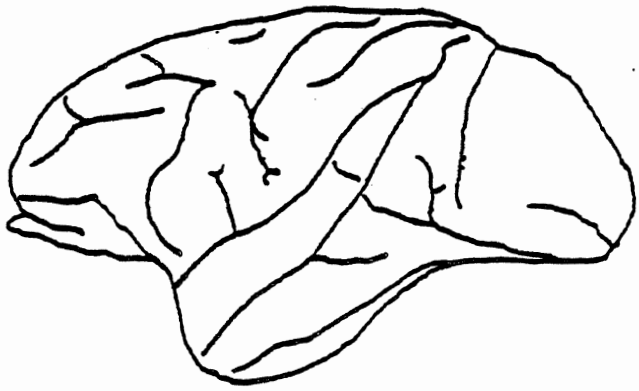

Left cerebral hemisphere
(Lateral view)

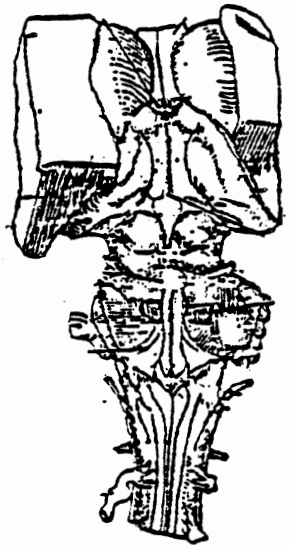

Dissection of brain stem
(Dorsal view)

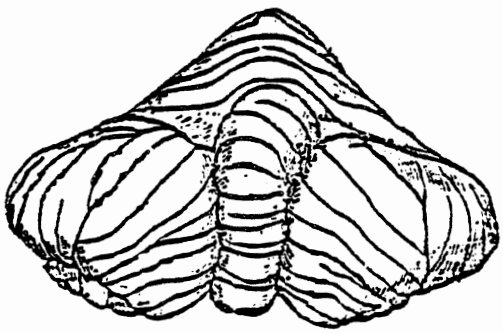

Cerebellum
(Posterior view)

DOT GENERAL TEST ANTHROPOMETRIC INFORMATION

EVALUATION OF EXPERIMENTAL TECHNIQUES IN HEAD INJURY RESEARCH				TITLE
CONTRACT NO:	ADTNH22-83-C-07095			CONNO
LABORATORY:	TRI			TSTPRF
TEST NO:	86R014			TSTREF
TEST DATE:	22/JAN/86			TSTDAT
TOTAL NUMBER TESTS THIS SUBJECT	1			NOTEST
ANTHROPOMETRIC GROUP IDENTIFIER 7				
SUBJECT NO:	86R9			CADREF
(F/M/N)	M			OCCSEX
(AN/CD) ANESTHETIZED	AN			OCCTYP
AGE	99			OCCAGE
WEIGHT	8.6			OCCTWT(Kg)
	cm	in		
STATURE	71.0	28.0		STATUR
BUTTOCK-CROWN	56.0	22.0		SEATHT
TOP HEAD TOP SHOULDER	999	999		SHLDHT
SHOULDER ELBOW	19.0	07.5		SHLDEL
HEEL-TOE (foot)	17.0	06.7		FOOTLN
FOREARM-HAND	28.0	11.0		FARMHD
NECK CIR.	25.0	09.8		NECKCR
CHEST CIR.	38.0	15.0		CHESTCR
THIGH CIR.	24.0	09.4		THGHCR
CALF CIR.	14.5	05.7		CALFCR
ANKLE CIR.	11.0	04.3		ANKLCR
POPLITEAL HEIGHT	15.0	05.9		
TRUNK LENGTH	45.5	17.9		
BUTTOCK-KNEE	22.5	08.9		
TOTAL ARM REACH	40.0	15.7		
HAND	11.0	04.3		
HEAD CIR.	32.0	12.6		
SHOULDER CIR.	42.0	16.5		
			999	BEDCON
			999	DTEDTD
NOT APPLICABLE				CSEDTH
ANESTHETIZED ADULT RHESUS				CADAPP
UNREMARKABLE				CADAN

DOT GENERAL TEST INJURY INFORMATION
EVALUATION OF EXPERIMENTAL TECHNIQUES IN
HEAD INJURY RESEARCH

				TITLE
CONTRACT NO:	ADTNH22-83-C-07095			CONNO
LABORATORY:		TRI		TSTPRF
TEST OBJECTIVE:	OCCIPITAL HEAD P-A			TSTOBJ
TEST NO:	86R015			TSTREF
TEST DATE:	24/JAN/86			TSTDAT
TOTAL NUMBER TESTS THIS SUBJECT		1		NOTEST
SUBJECT NO:	86R10			CADREF
(F/M/N)		M		OCCSEX
(AN/CD)	ANESTHETIZED	AN		OCCTYP
AGE		99		OCCAGE
WEIGHT		7.9		OCCWT(Kg)
STATURE		69.0		STATUR(cm)
TEST TYPE:	HEAD	BIO		TSTTYP
(DRP/PED/PEN/OTH)		OTH	CANNON	TSTCFN
		0		VEHNO
		OT		OCCLOC
RESTRAINT SYSTEM 1:		NON		RESTR1
RESTRAINT SYSTEM 2:		NON		RESTR2

CANNON VELOCITY (m/s): 12.1 IMPACTOR MASS (Kg): 10
PADDING: 2.5 cm Ensolite. STRIKER: 10 cm round flat
OCCUPANT INJURY GROUP IDENTIFIER 8

NUMBER OF FRACTURED RIBS:	0		FRCTRB
NUMBER OF RIB FRACTURES:	0		RBFRCT

	BODYRG	ASPECT	LESION	SYSORG	AIS
1	H	R	F	S	2
2	H	I	F	S	2
3	H	R	F	S	2
4	H	B	L	B	5
5					
6					
7					
8					
9					
10					

INJTXT: TEXT OF INJURY Note: Up to 80 characters of text.

1 Linear fracture superior portion of right petrous
2 Linear fracture left occipital
3 Linear fracture right temporal
4 Bilateral hemorrhage to side of spinal cord at base of medulla
5
6
7
8
9
10

ANOMALY NOTES:

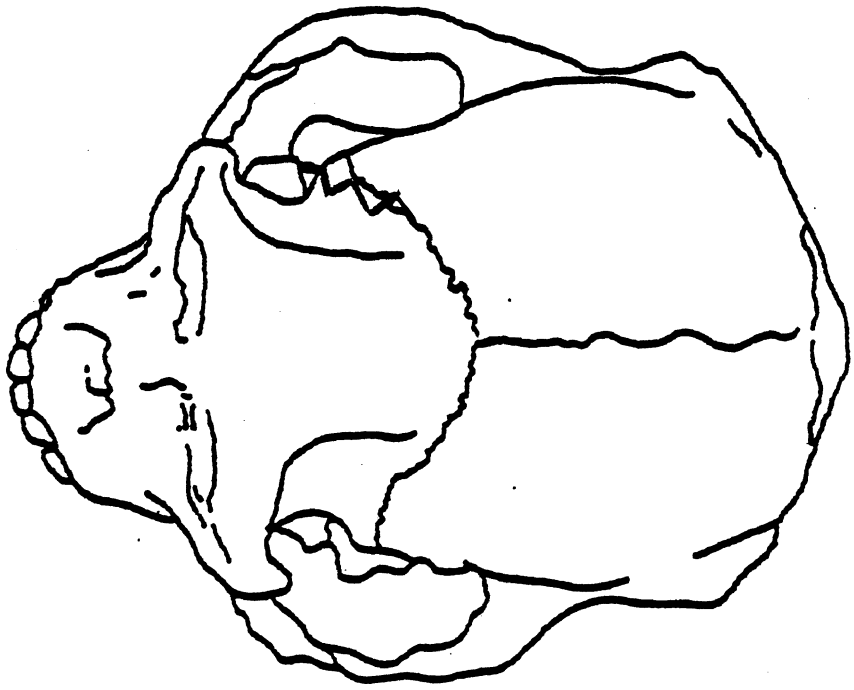

Linear fracture superior portion of right petrous
Linear fracture left occipital
Linear fracture right temporal

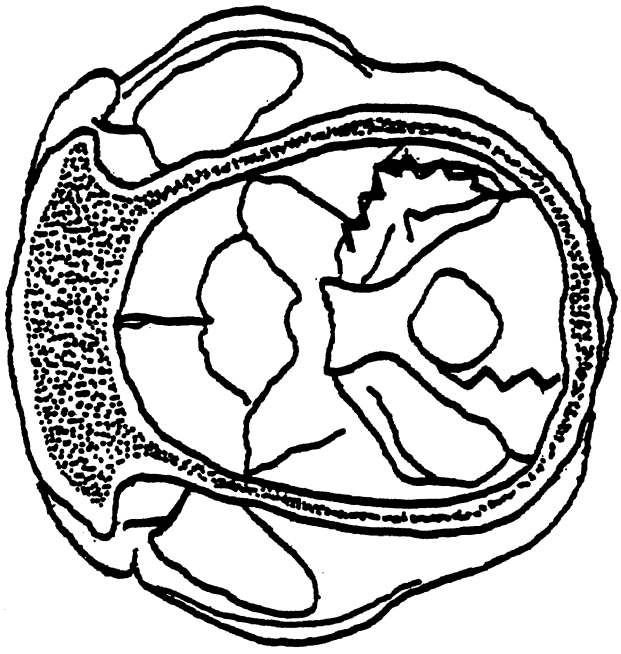

Test No: 86R015

Laboratory: TRI

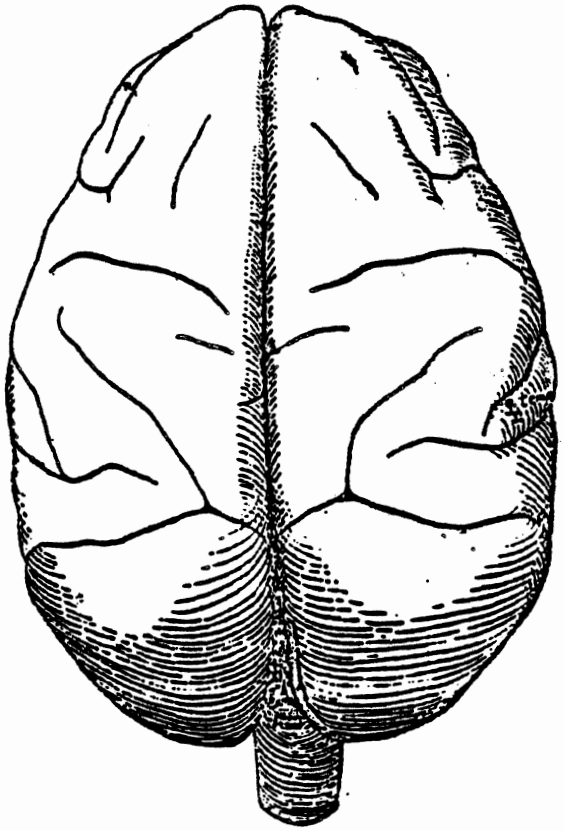

The brain from above

Basilar hematomas indicate lesions

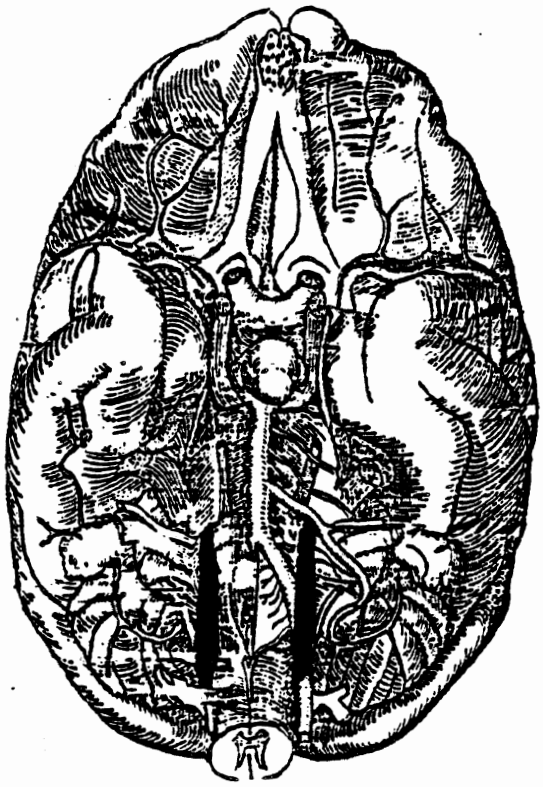

Base of the brain

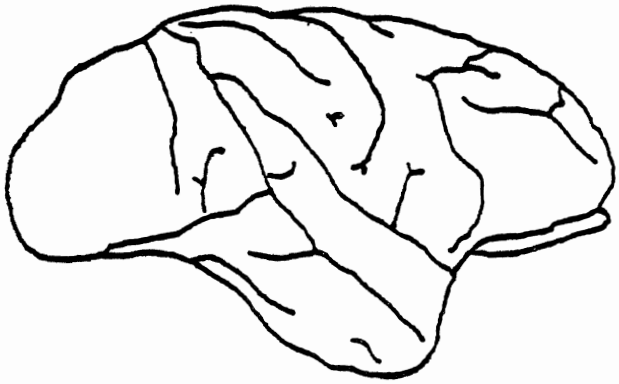

Right cerebral hemisphere
(Lateral view)

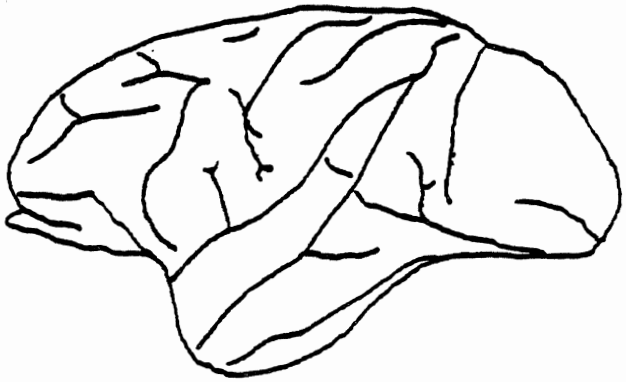

Left cerebral hemisphere
(Lateral view)

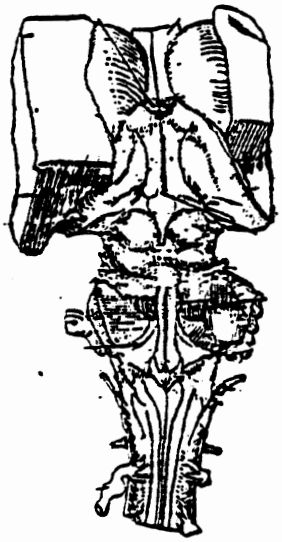

Dissection of brain stem
(Dorsal view)

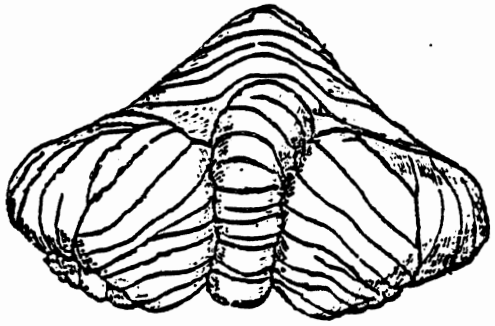

Cerebellum
(Posterior view)

DOT GENERAL TEST ANTHROPOMETRIC INFORMATION
EVALUATION OF EXPERIMENTAL TECHNIQUES IN
HEAD INJURY RESEARCH

TITLE				
CONNO		ADTNH22-83-C-07095		
TSTPRF		TRI		
TSTREF		86R015		
TSTDAT		24/JAN/86		
NOTEST		1		
	ANTHROPOMETRIC GROUP IDENTIFIER 7			
CADREF		86R10		
OCCSEX	(F/M/N)	M		
OCCTYP	(AN/CD)	ANESTHETIZED AN		
OCCAGE		99		
OCCTWT(Kg)		7.9		
		cm	in	
STATUR	STATURE	69.0	27.2	
SEATHT	BUTTOCK-CROWN	56.0	22.0	
SHLDHT	TOP HEAD TOP SHOULDER	54.0	21.0	
SHLDEL	SHOULDER ELBOW	20.0	07.9	
FOOTLN	HEEL-TOE (foot)	18.0	07.1	
FARMHD	FOREARM-HAND	30.0	11.8	
NECKCR	NECK CIR.	20.0	07.9	
CHESTCR	CHEST CIR.	34.0	13.4	
THGHCR	THIGH CIR.	21.0	08.3	
CALFCR	CALF CIR.	14.0	05.5	
ANKLCR	ANKLE CIR.	09.0	03.5	
	POPLITEAL HEIGHT	13.0	05.1	
	TRUNK LENGTH	48.0	18.9	
	BUTTOCK-KNEE	23.0	09.1	
	TOTAL ARM REACH	40.0	15.7	
	HAND	12.0	04.7	
	HEAD CIR.	30.0	11.8	
	SHOULDER CIR.	42.0	16.5	
BEDCON			999	
DTEDTD			999	
CSEDTH	NOT APPLICABLE			
CADAPP	ANESTHETIZED ADULT RHESUS			
CADAN	UNREMARKABLE			

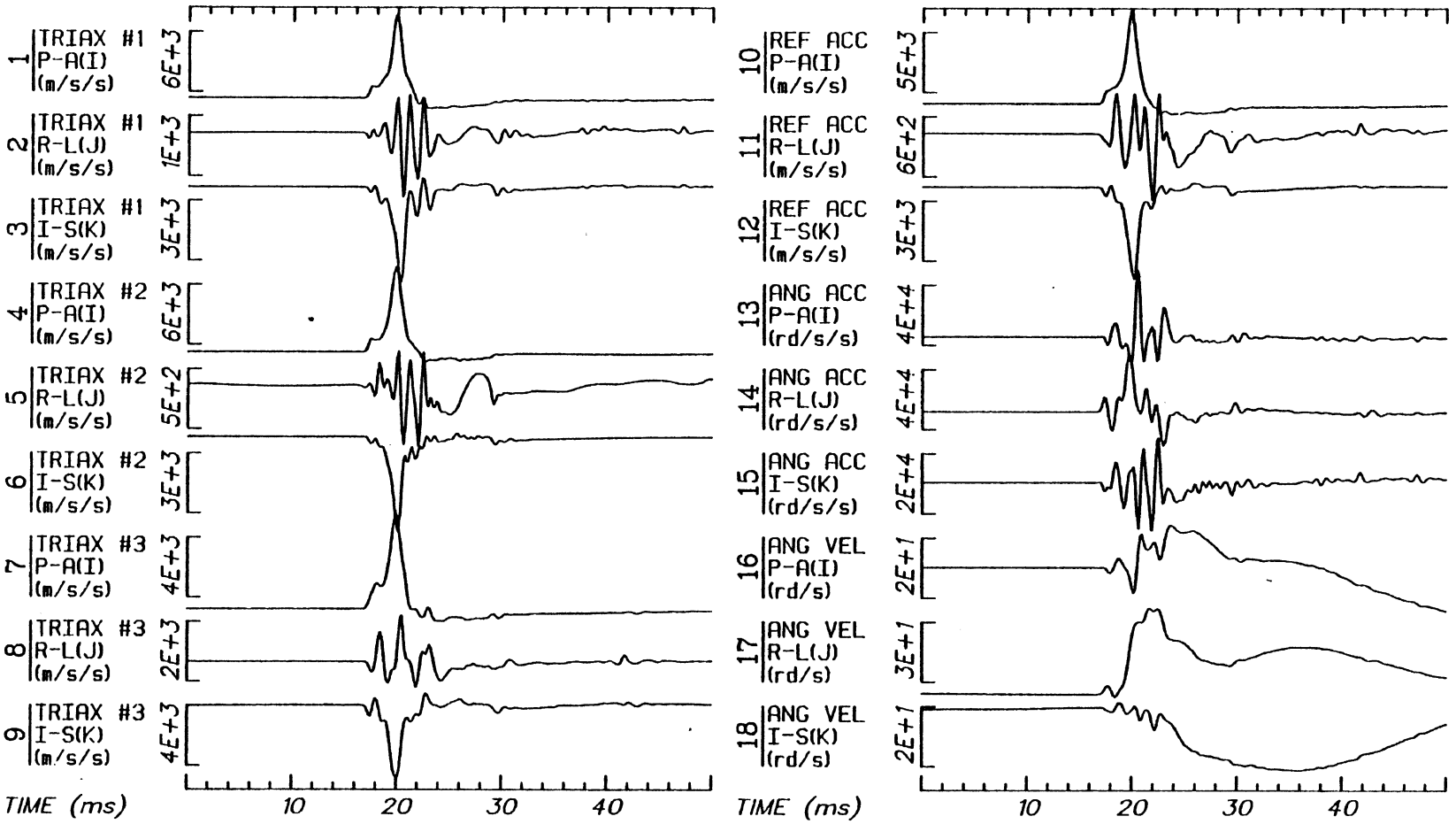

Run ID: 78A232 Disk: 78A232.3 File: 1 Date: JUN 23, 1985 Sheet: 1

Filter:1600*4C Smooth: 3SD

APPENDIX B: KINEMATIC DATA

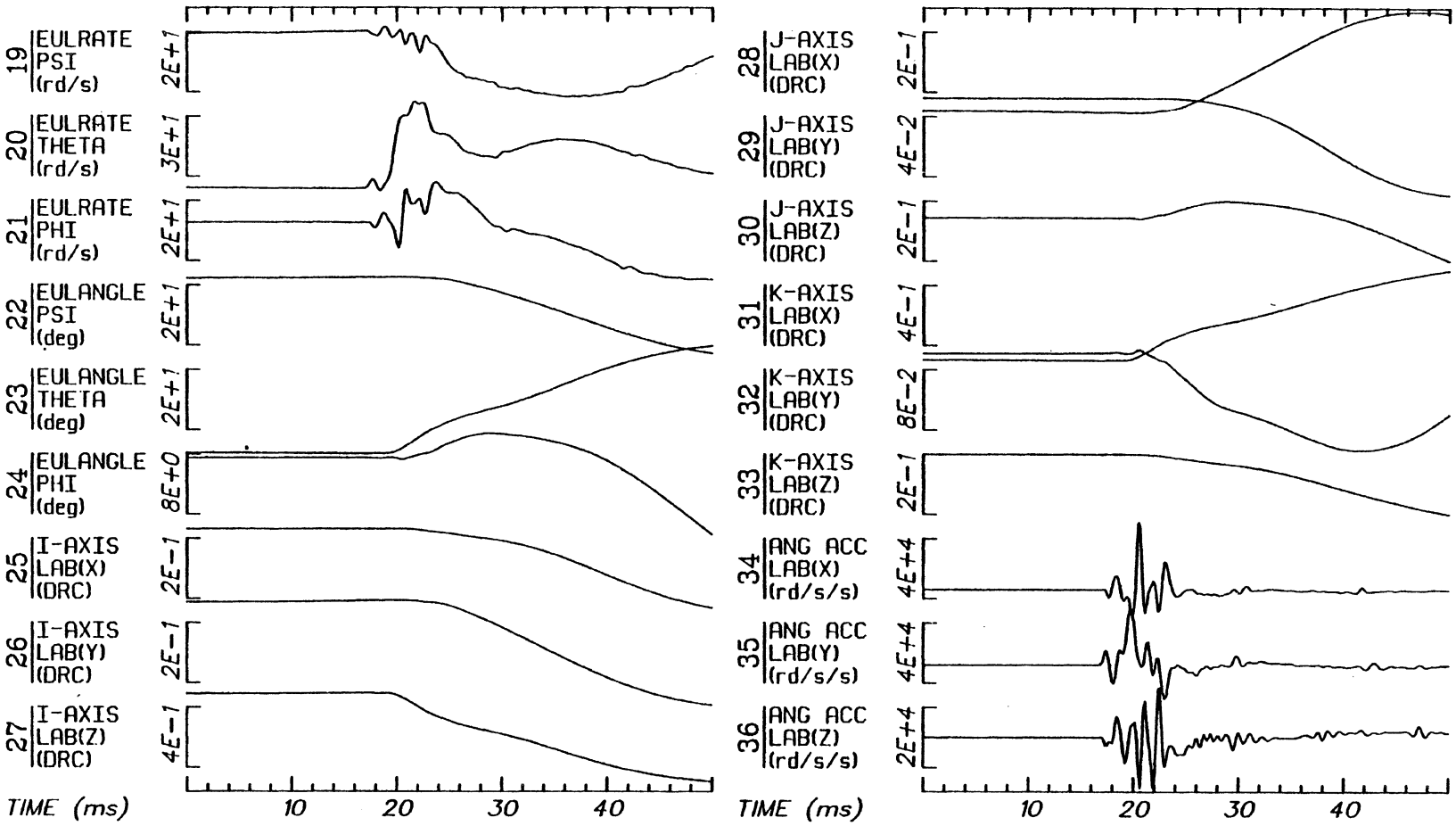

Run ID: 78A232 Disk: 78A232.3 File: 1 Date: JUN 23, 1985 Sheet: 2

Filter:1600*4C Smooth: 3SD

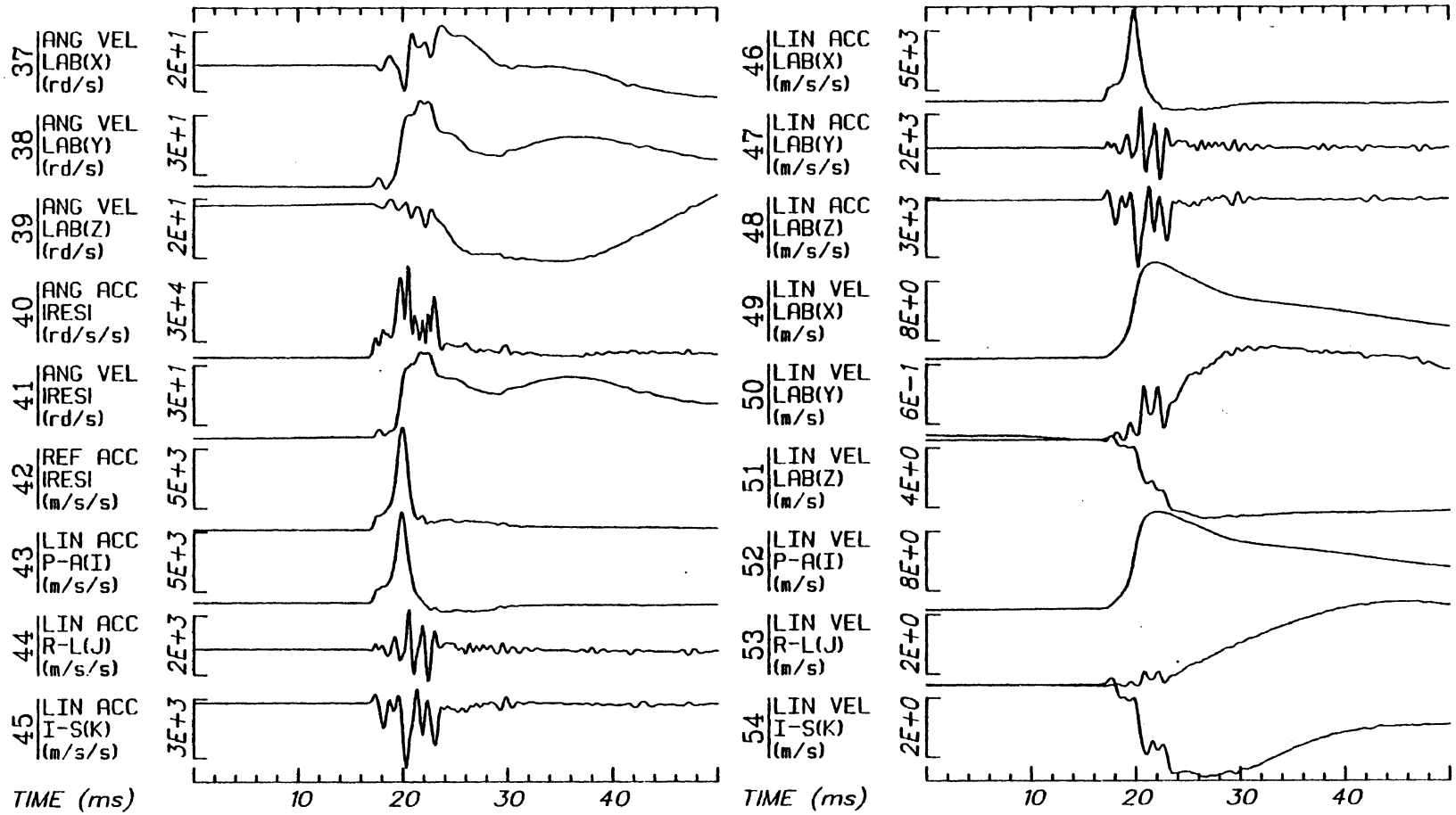

Run ID: 78A232 Disk: 78A232.3 File: 1 Date: JUN 23, 1985 Sheet: 3

Filter:1600*4C Smooth: 3SD

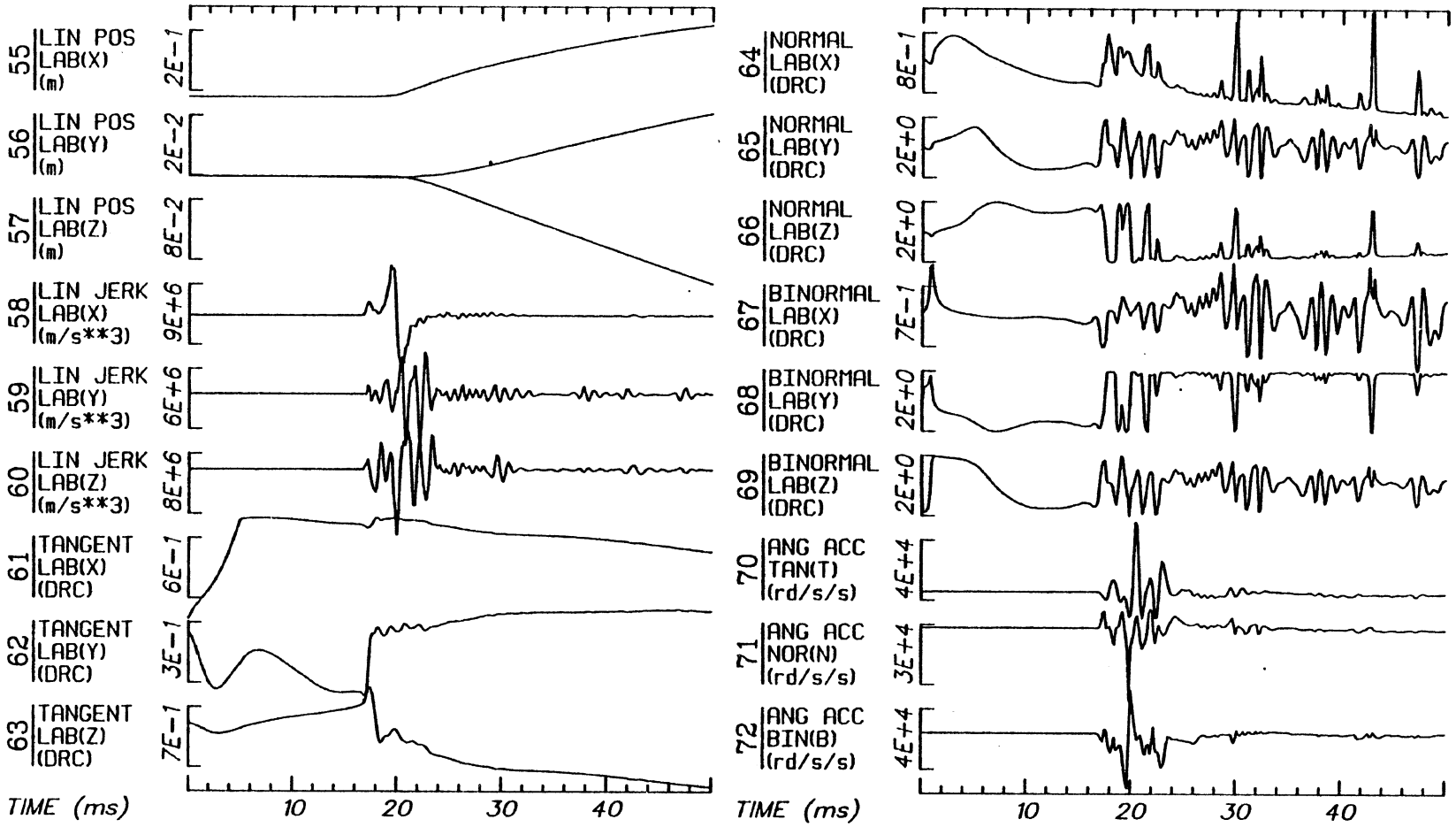

Run ID: 78A232 Disk: 78A232.3 File: 1 Date: JUN 23, 1985 Sheet: 4

Filter:1600*4C Smooth: 3SD

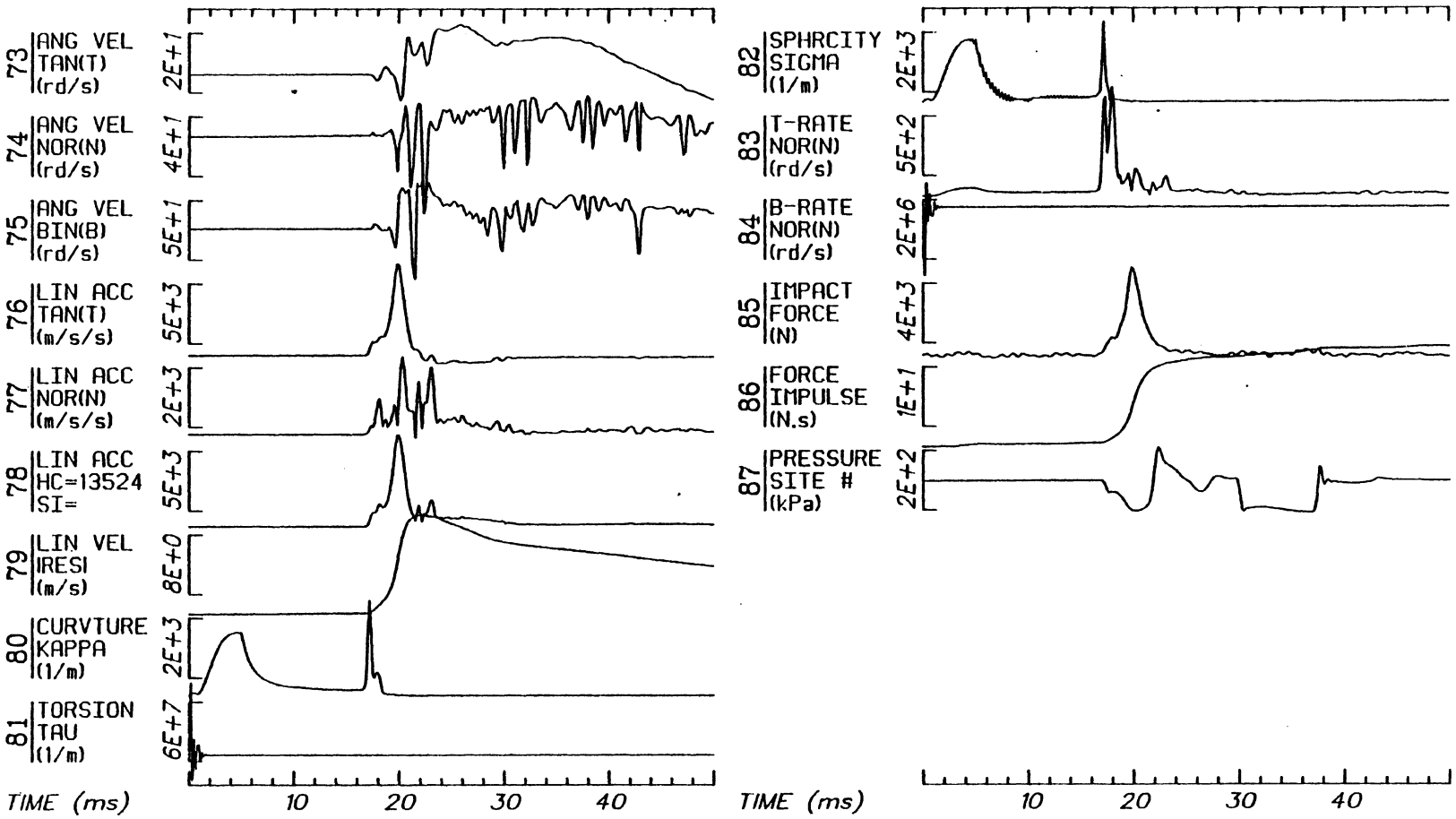

Run ID: 78A232 Disk: 78A232.3 File: 1 Date: JUN 23, 1985 Sheet: 5

Filter:1600*4C Smooth: 3SD

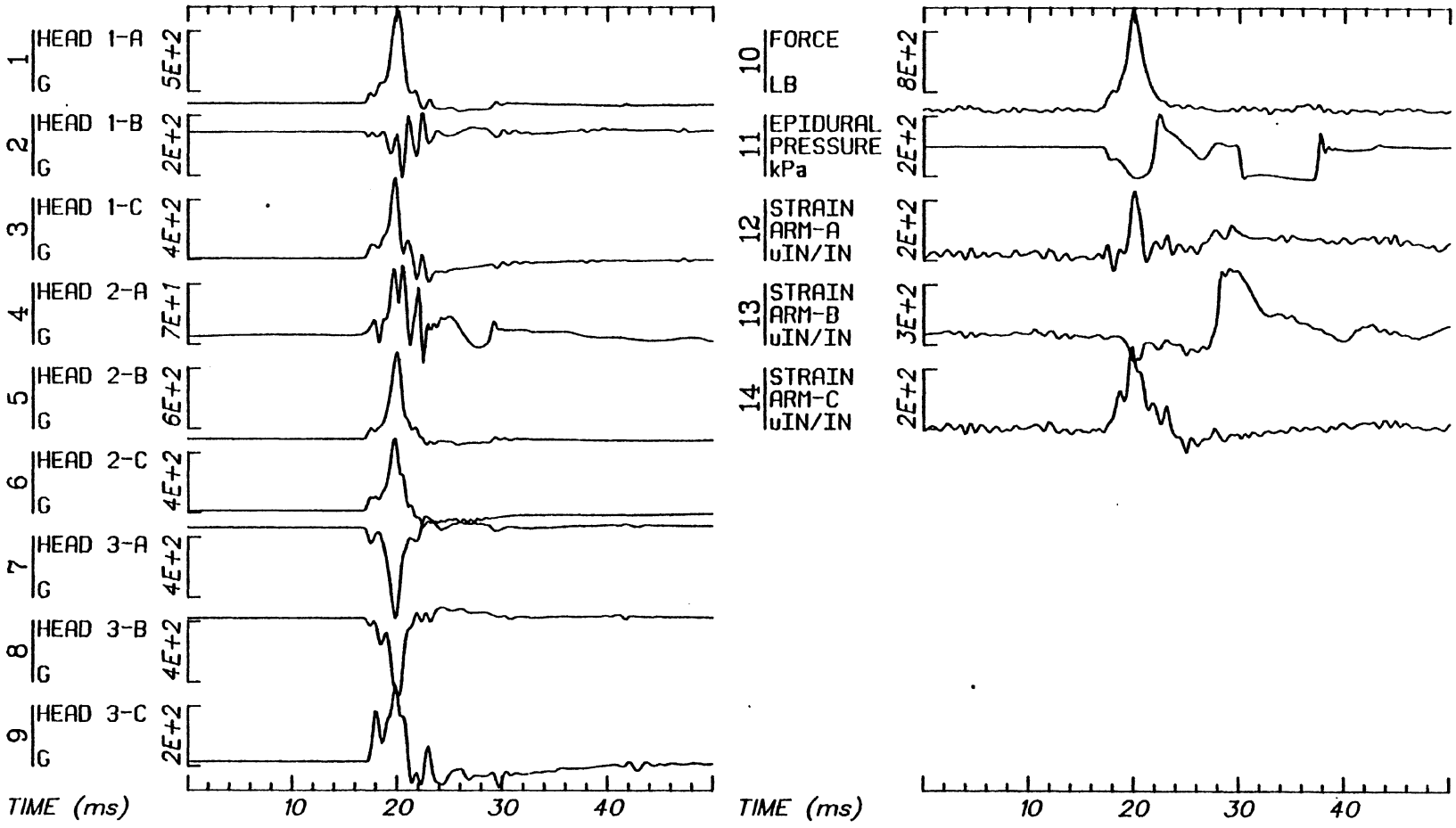

Run ID: 78A232 Disk: 78A232.S File: 1 Date: JUN 16, 1985 Sheet: 1

*Filter:1600*4C Smooth: 3SD SIDFA DATA: Filter – 1600*4c, Smooth – 3SD*

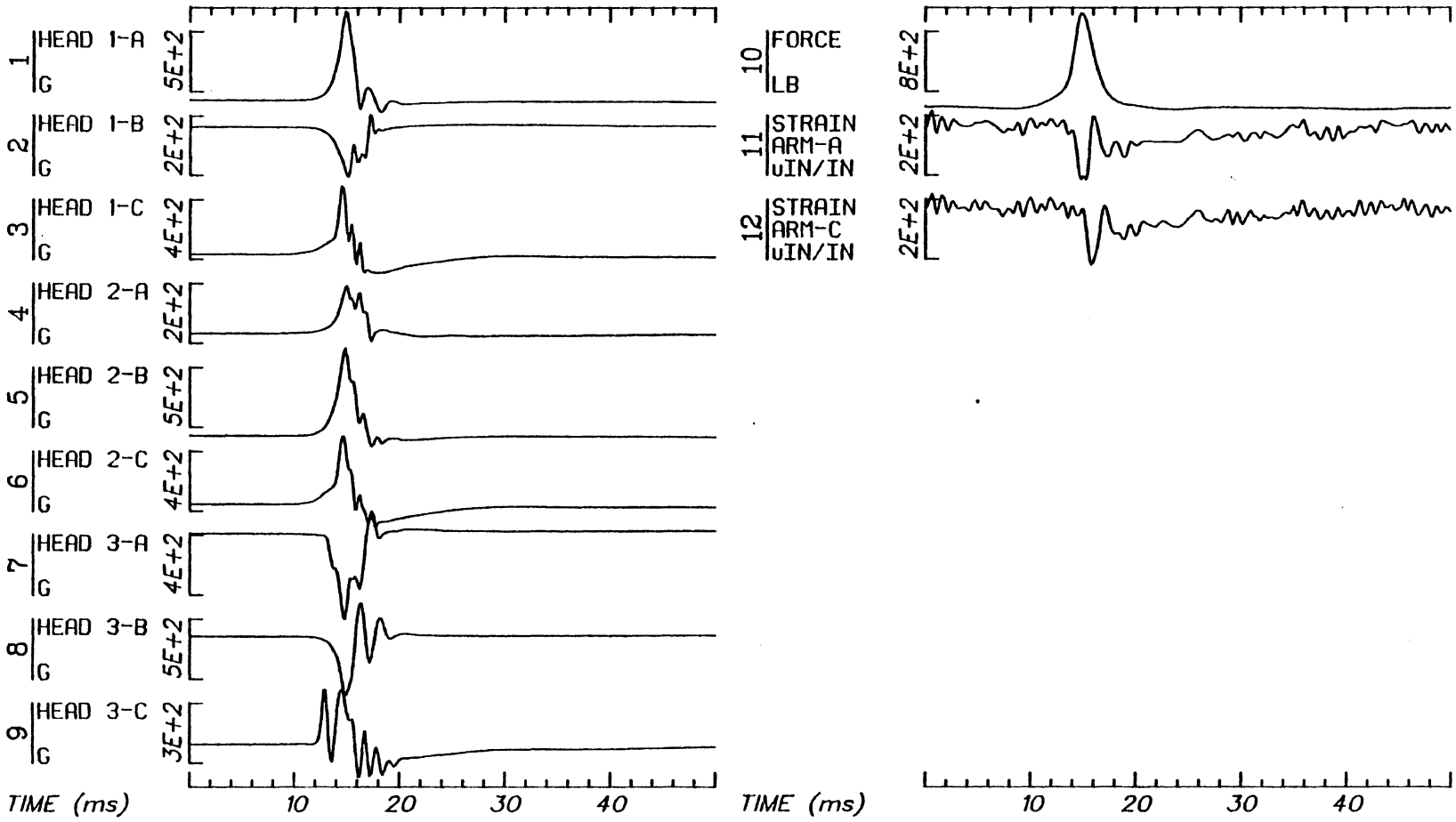

Run ID: 78A234 Disk: 78A234.S File: 1 Date: JUN 16, 1985 Sheet: 1

Filter:1600*4C Smooth: 3SD SIDFA DATA: Filter - 1600*4c, Smooth - 3SD

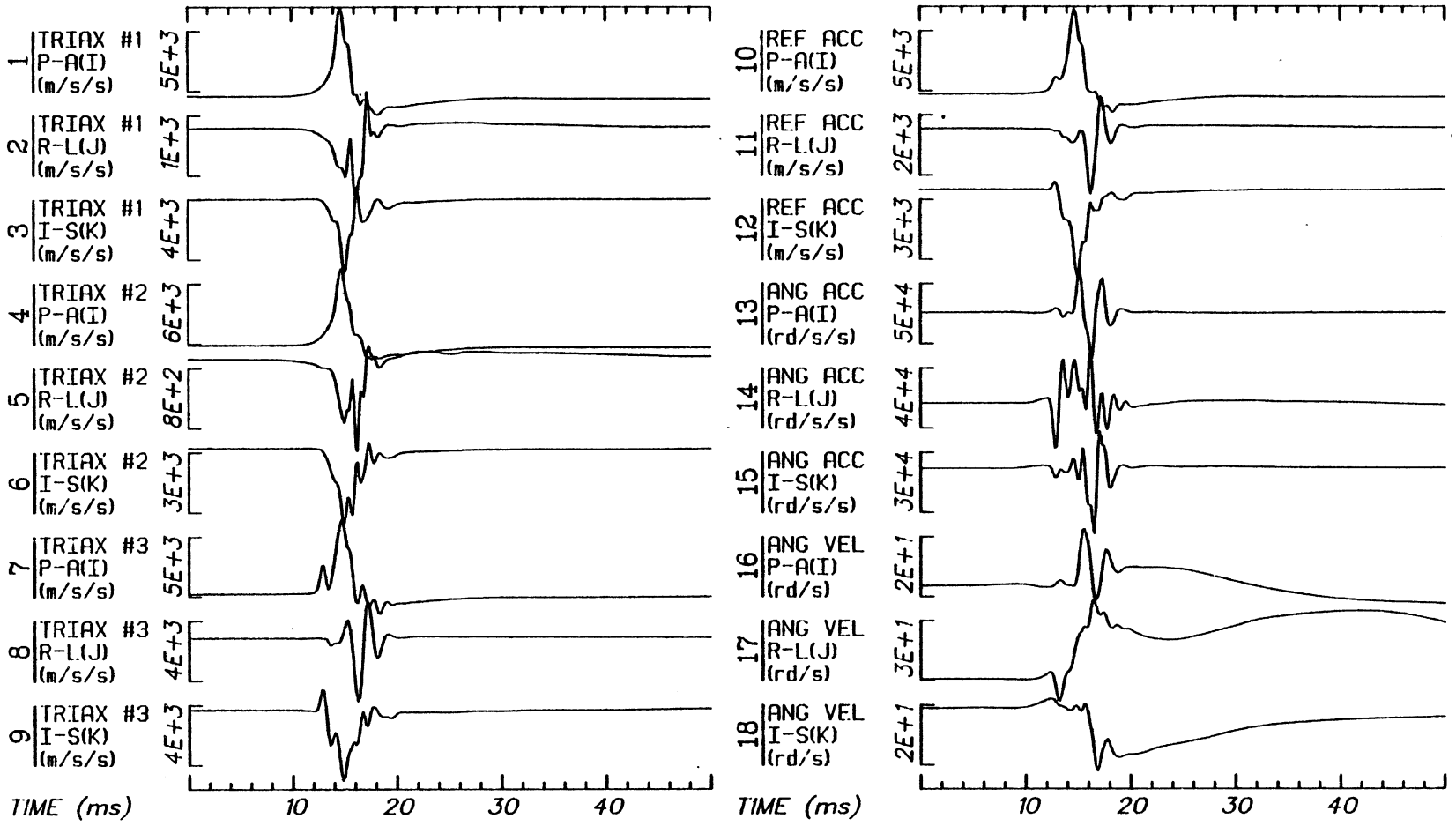

Run ID: 78A234 Disk: 78A234.3 File: 1 Date: JUN 23, 1985 Sheet: 1

No Filtering

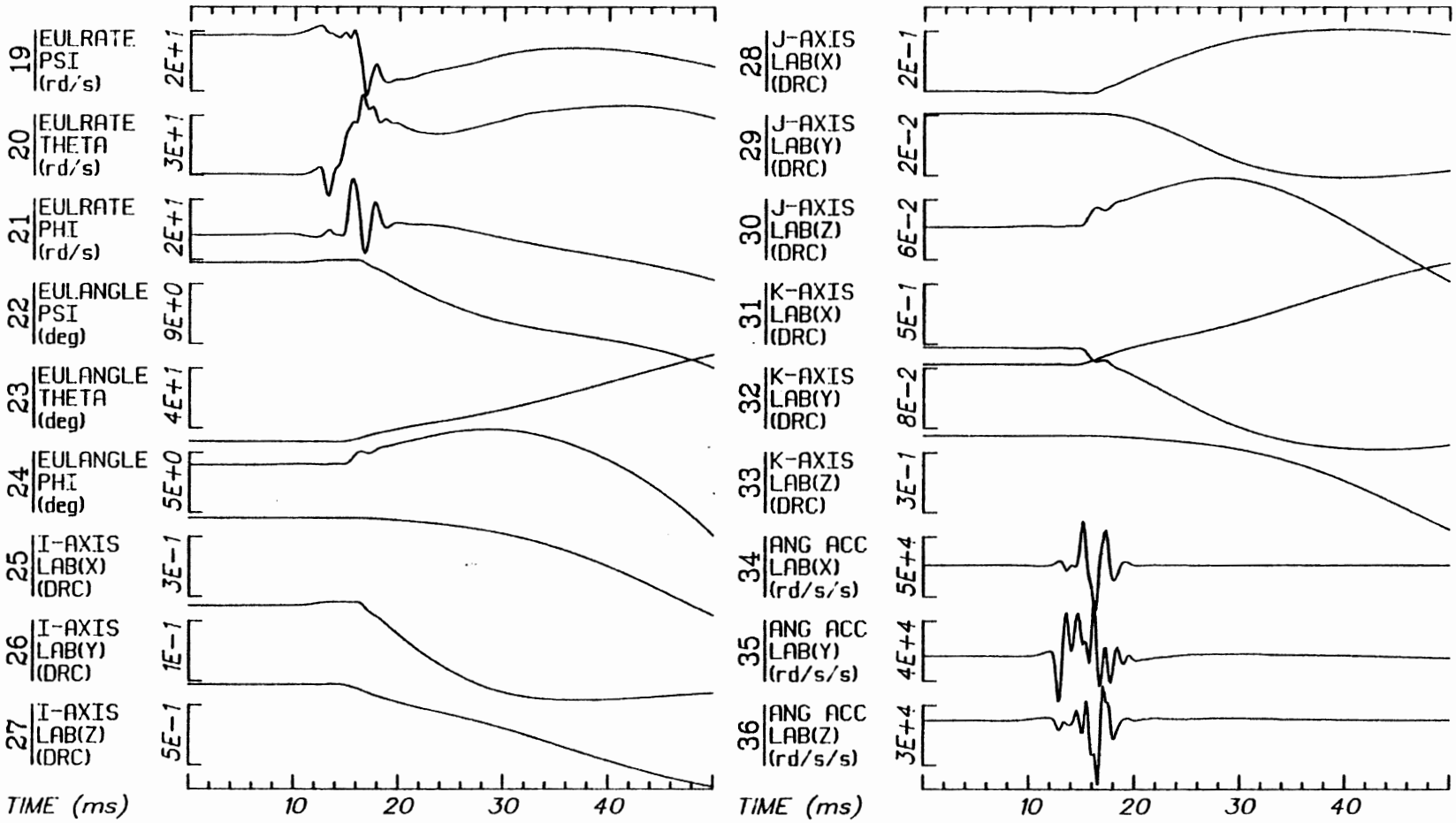

Run ID: 78A234 Disk: 78A234.3 File: 1 Date: JUN 23, 1985 Sheet: 2

No Filtering

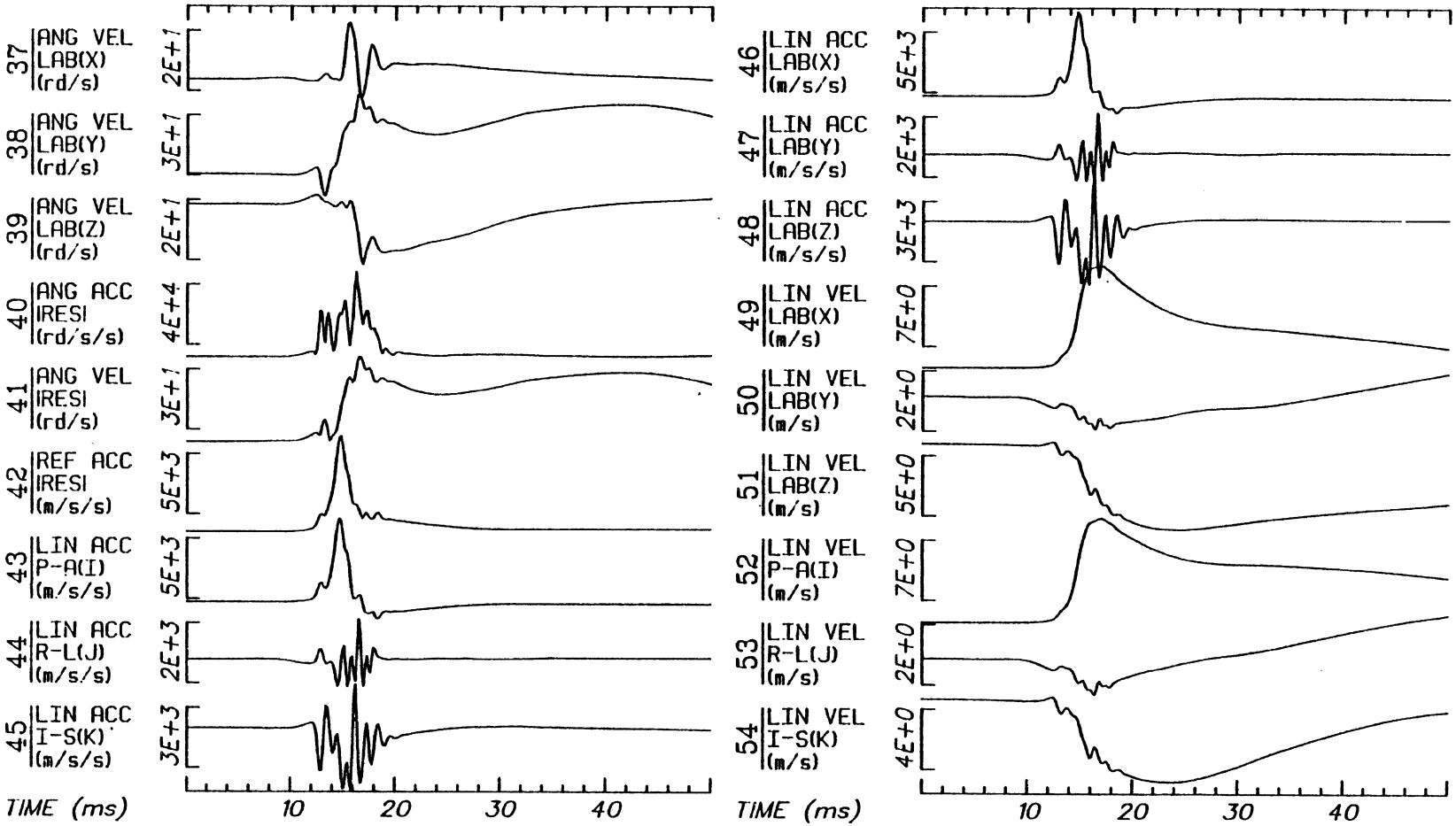

Run ID: 78A234 Disk: 78A234.3 File: 1 Date: JUN 23, 1985 Sheet: 3

No Filtering

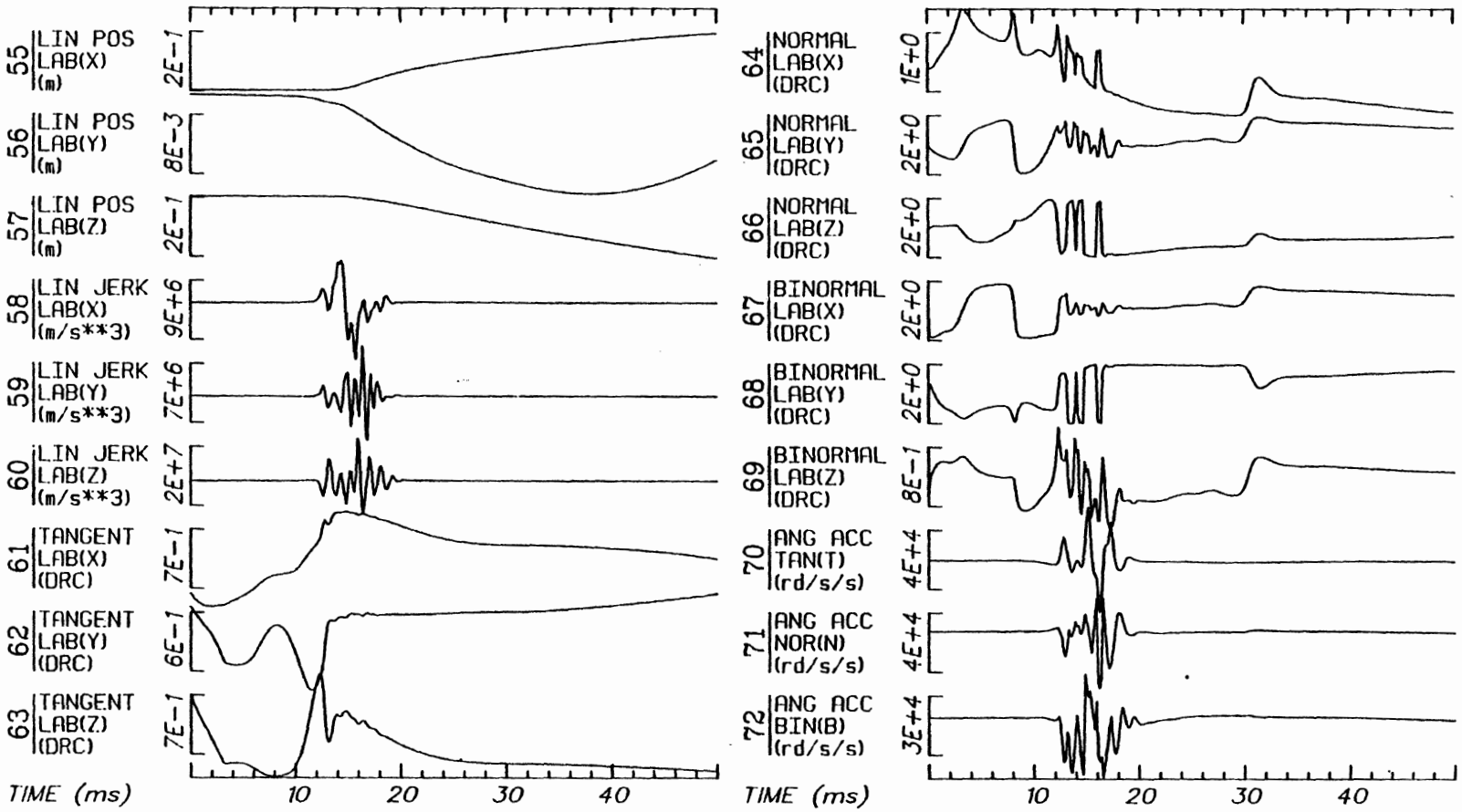

Run ID: 78A234 Disk: 78A234.3 File: 1 Date: JUN 23, 1985 Sheet: 4

No Filtering

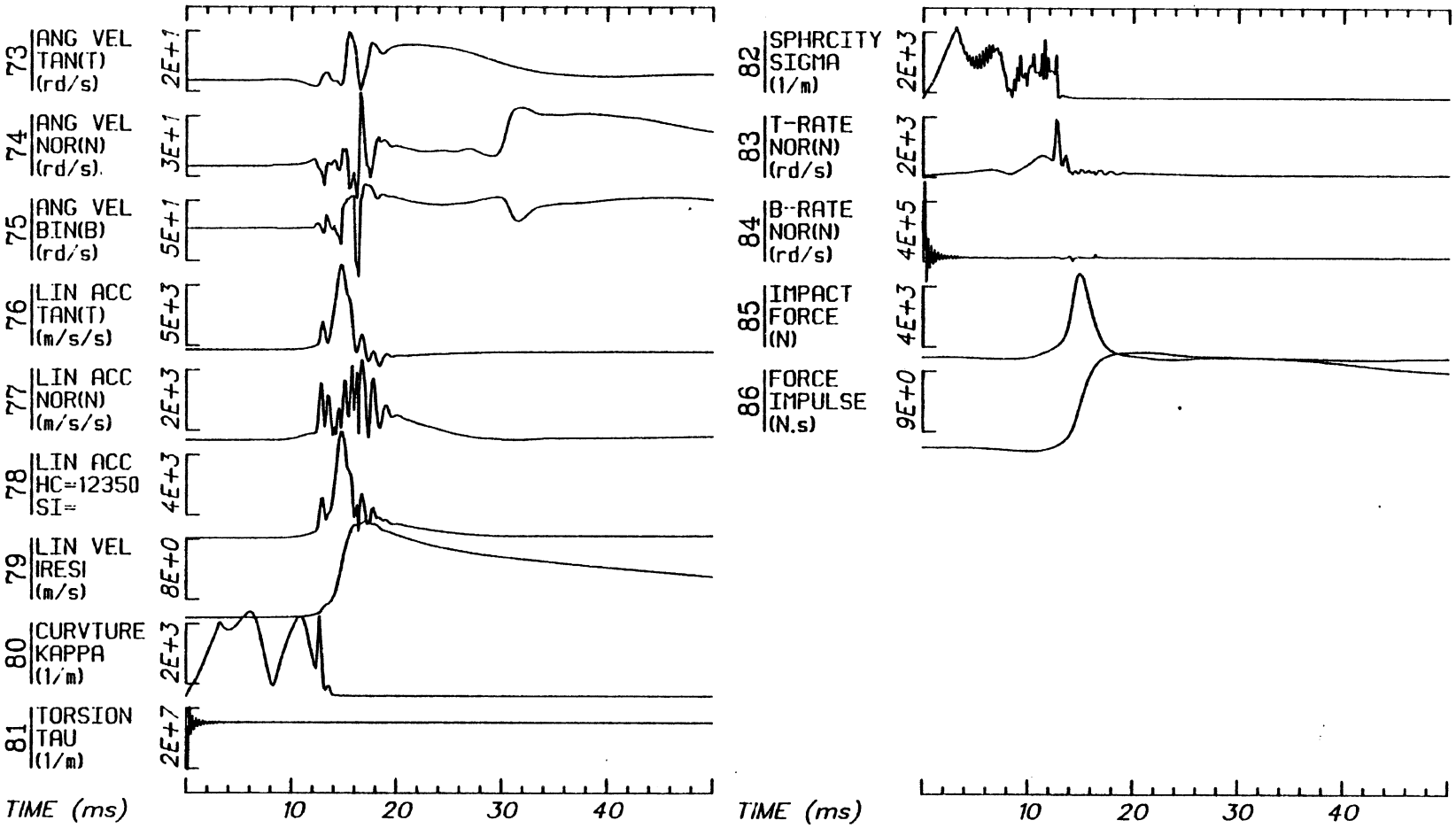

Run ID: 78A234 Disk: 78A234.3 File: 1 Date: JUN 23, 1985 Sheet: 5

No Filtering

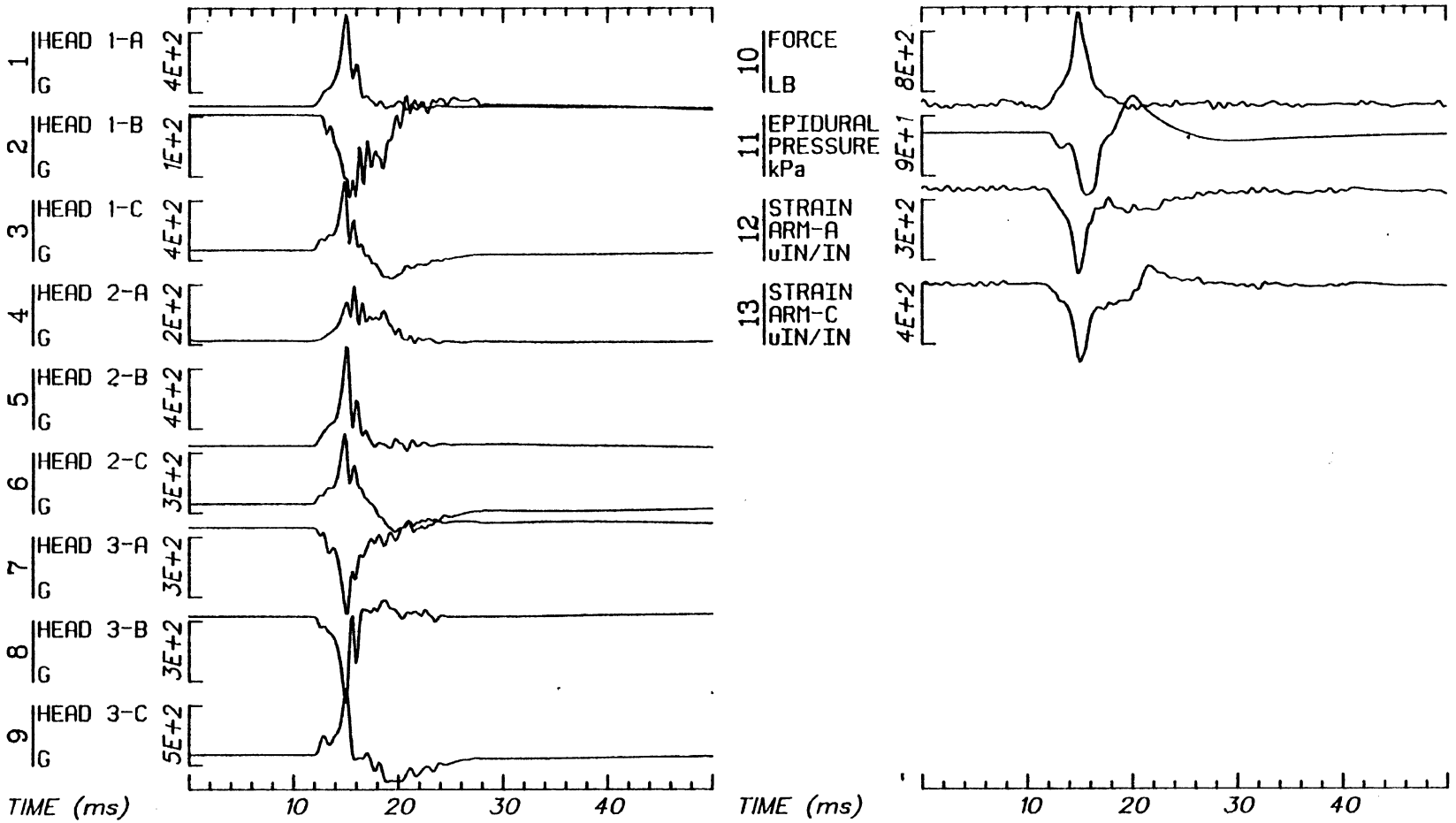

Run ID: 78A236 Disk: 78A236.S File: 1 Date: JUN 16, 1985 Sheet: 1

Filter:1600*4C Smooth: 3SD SIDFA DATA: Filter – 1600*4C, Smooth – 3SD

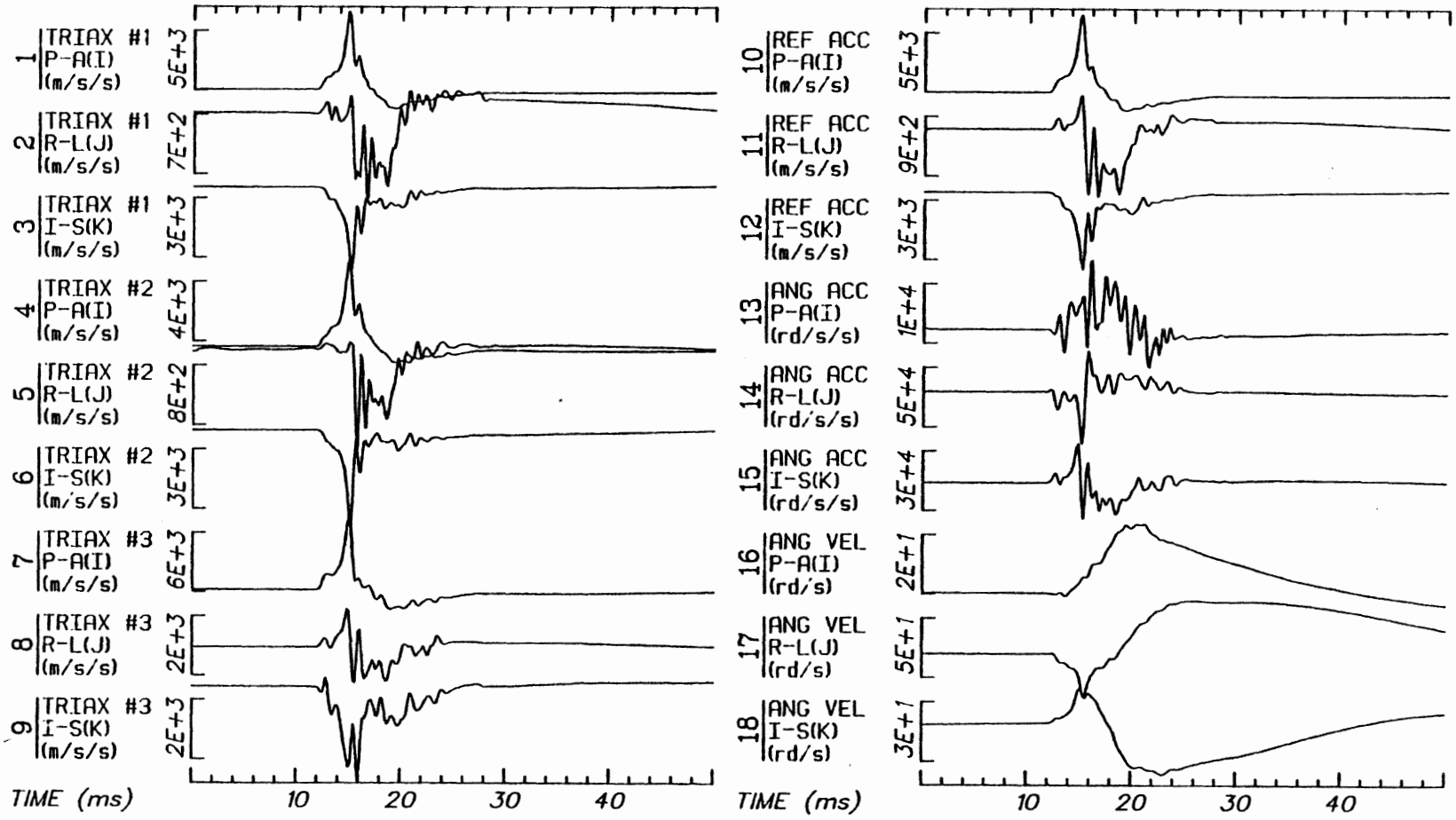

Run ID: 78A236 Disk: 78A236.3 File: 1 Date: JUN 23, 1985 Sheet: 1

No Filtering

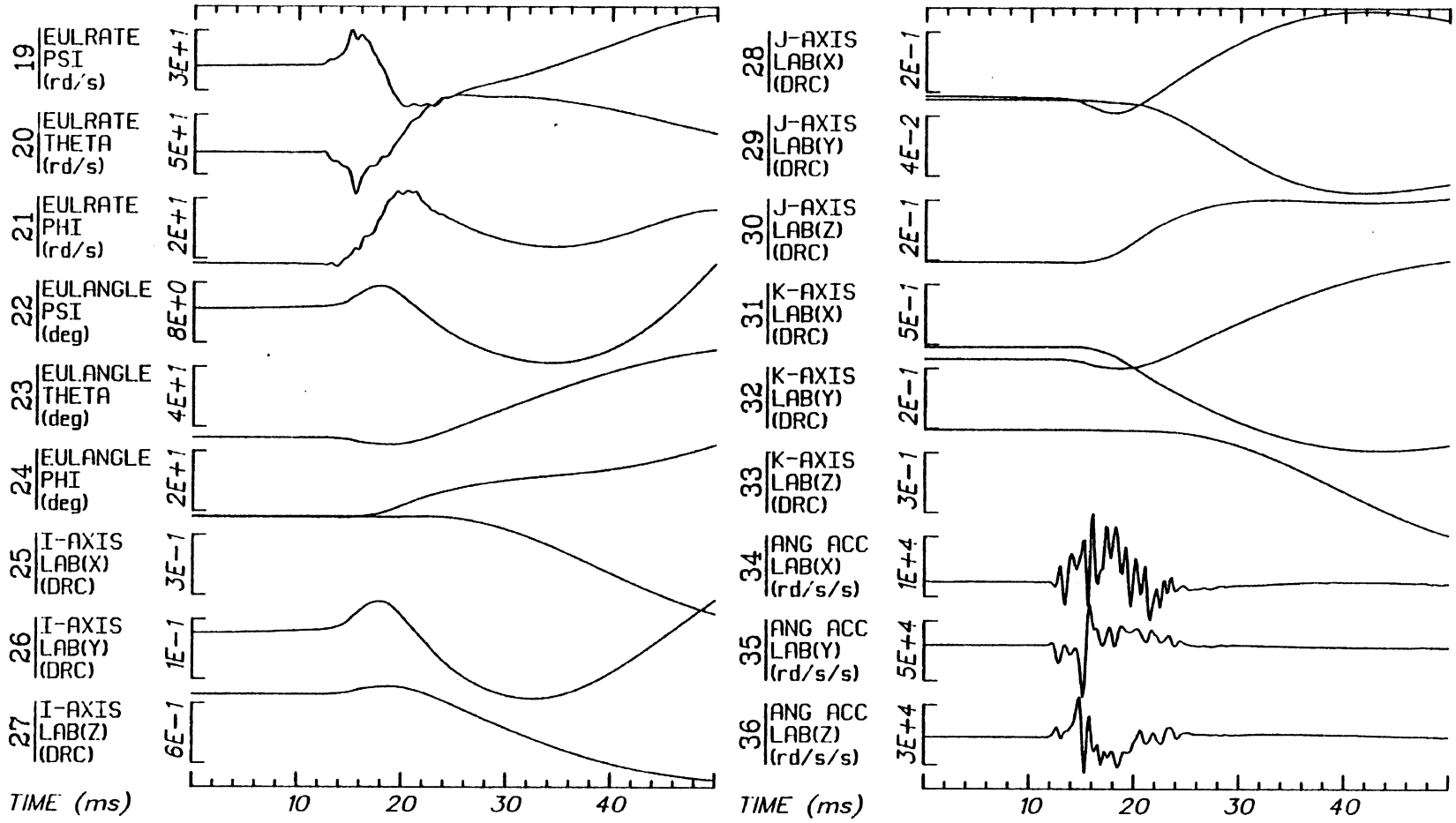

Run ID: 78A236 Disk: 78A236.3 File: 1 Date: JUN 23, 1985 Sheet: 2

No Filtering

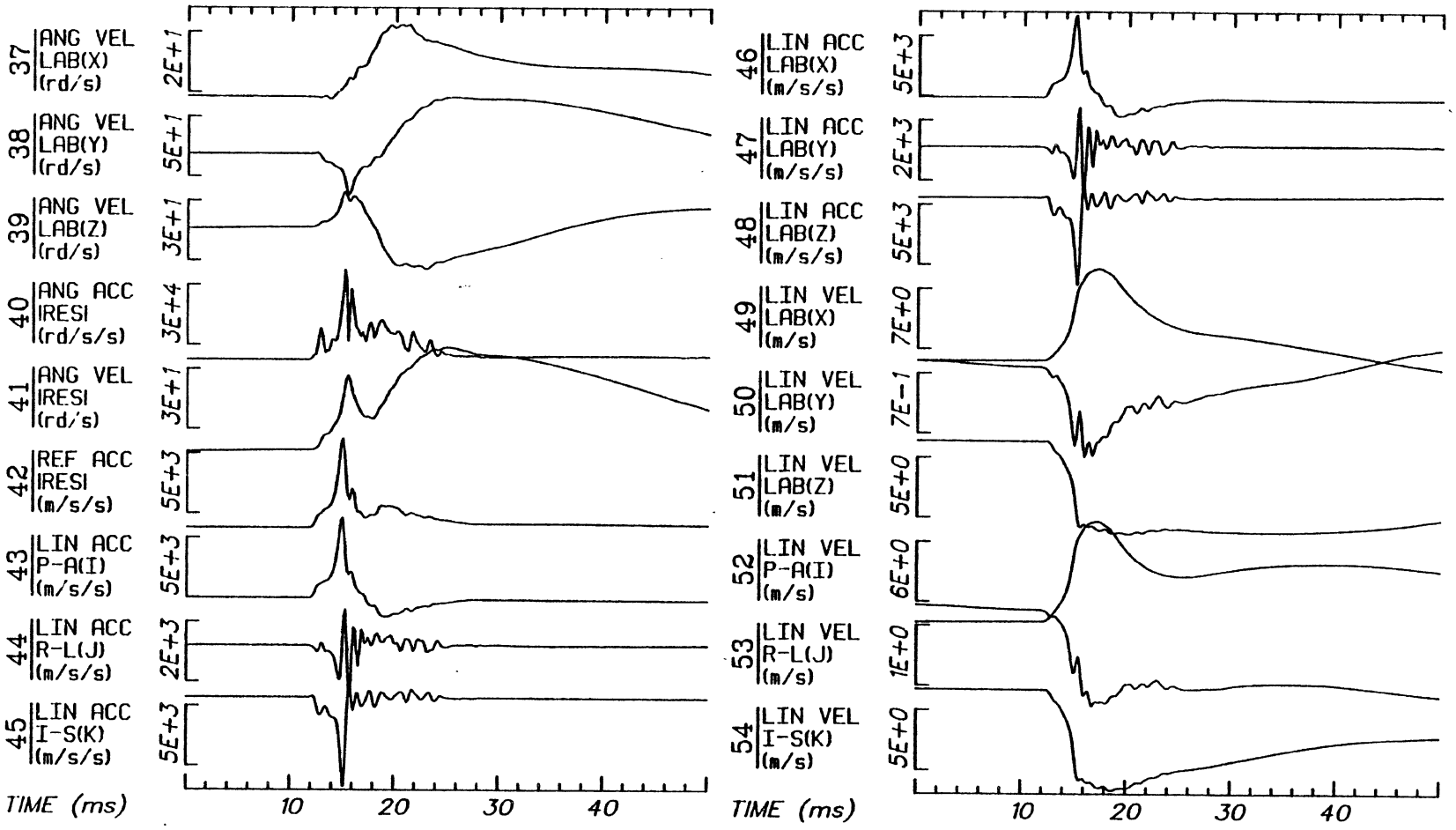

Run ID: 78A236 Disk: 78A236.3 File: 1 Date: JUN 23, 1985 Sheet: 3

No Filtering

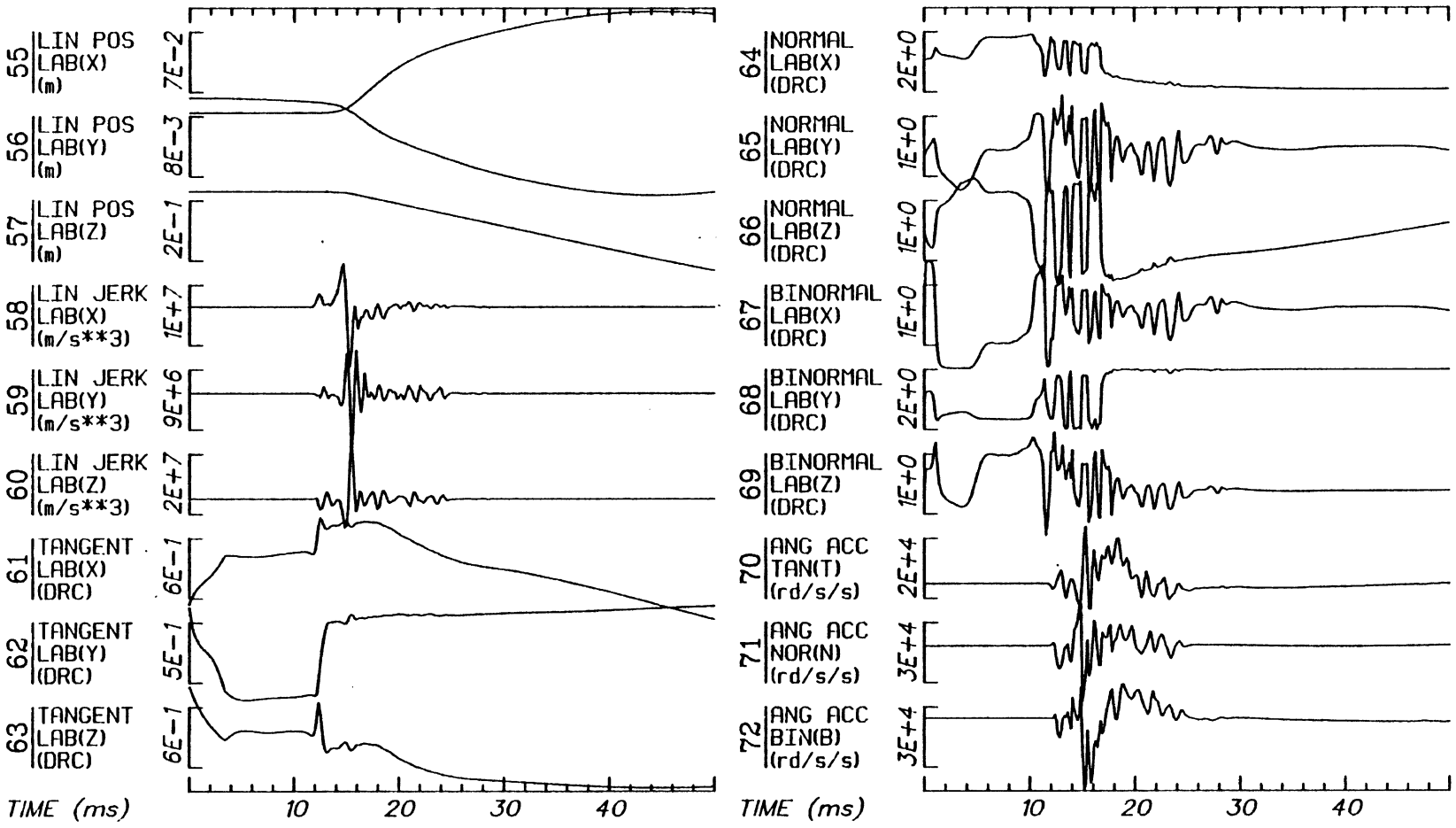

Run ID: 78A236 Disk: 78A236.3 File: 1 Date: JUN 23, 1985 Sheet: 4

No Filtering

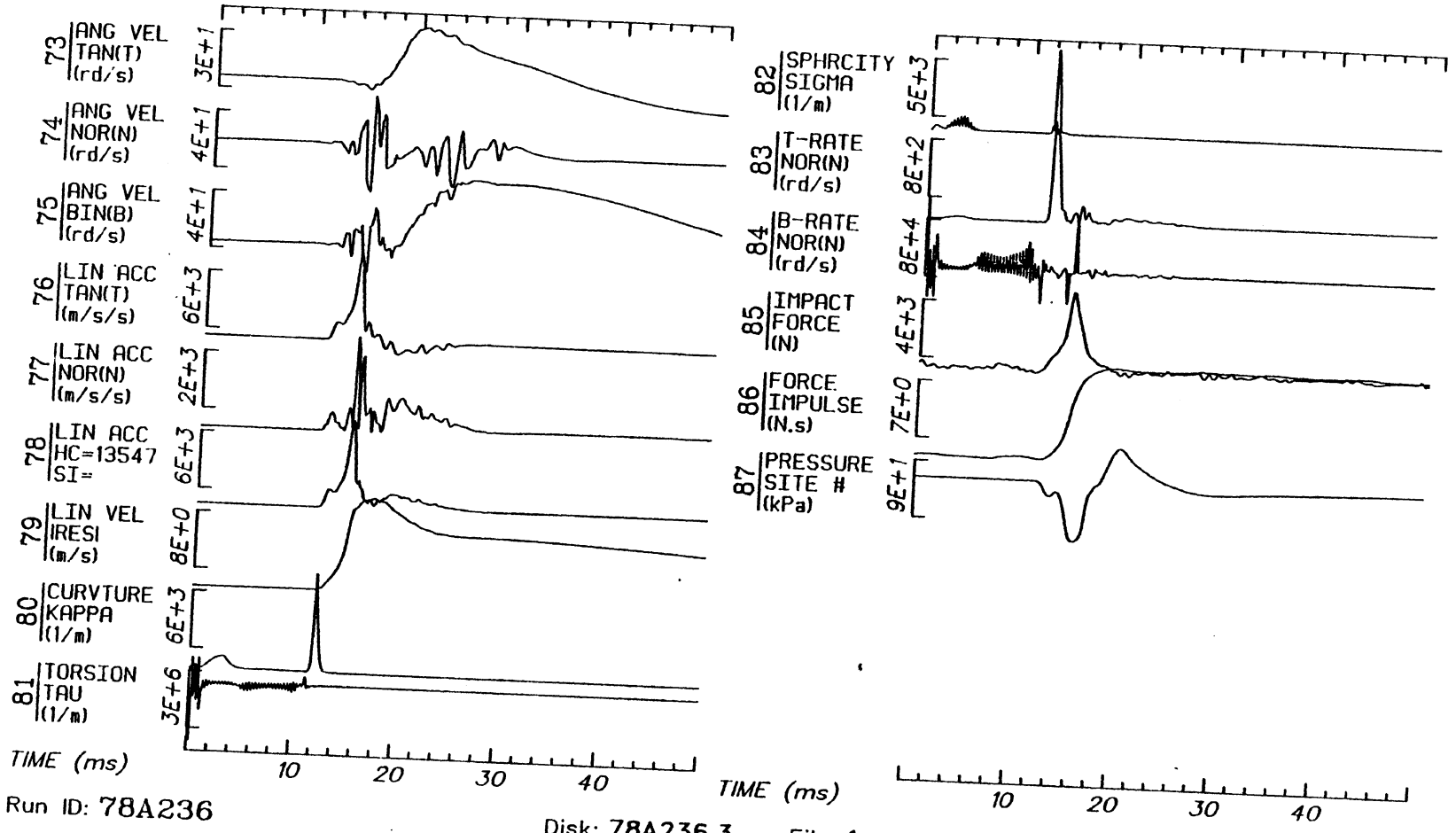

Run ID: 78A236

No Filtering

Disk: 78A236.3 File: 1

Date: JUN 23, 1985 Sheet: 5

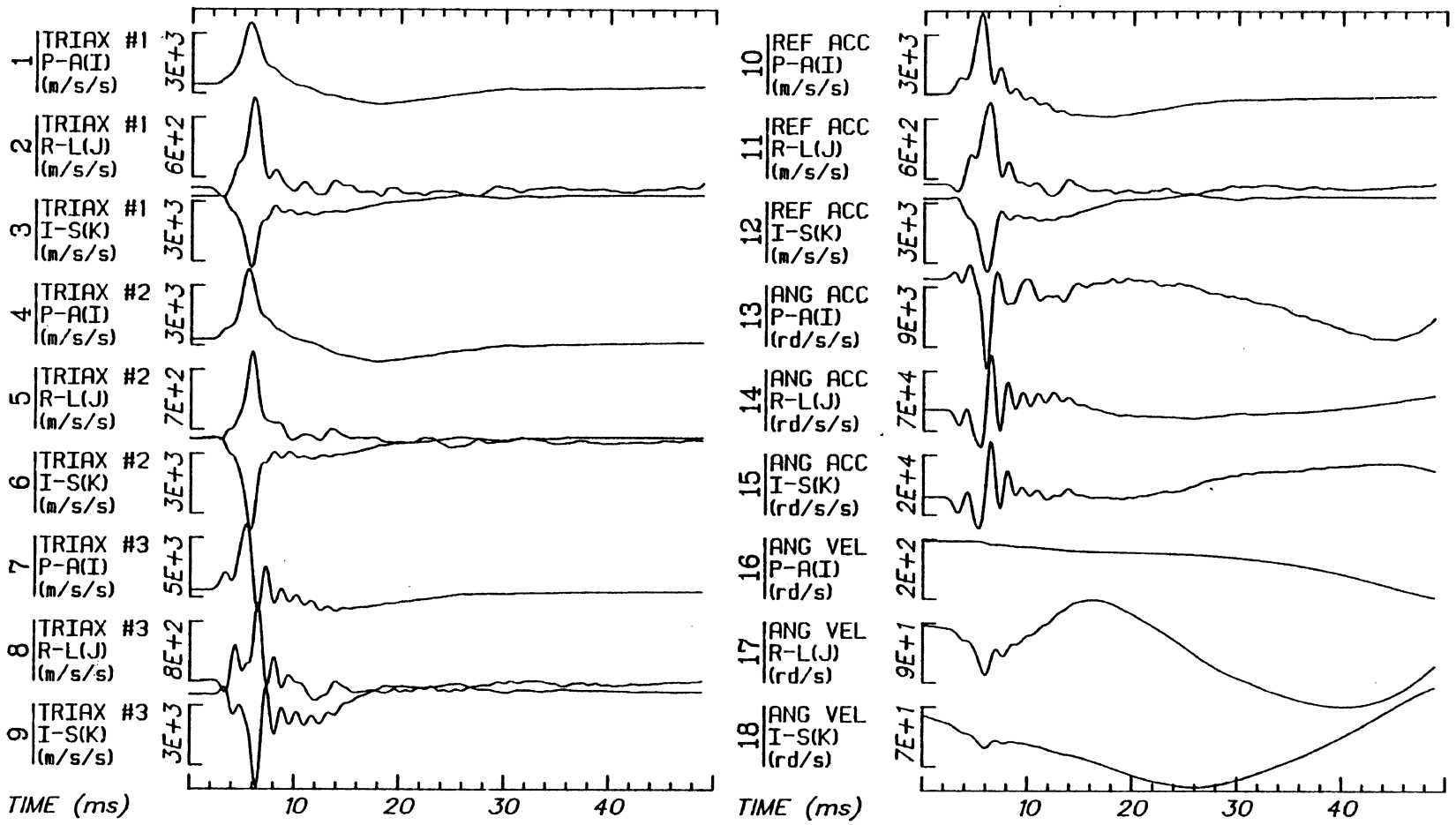

Run ID: 78A238 Disk: 78A238 File: 1 Date: MAY 14, 1984 Sheet: 1

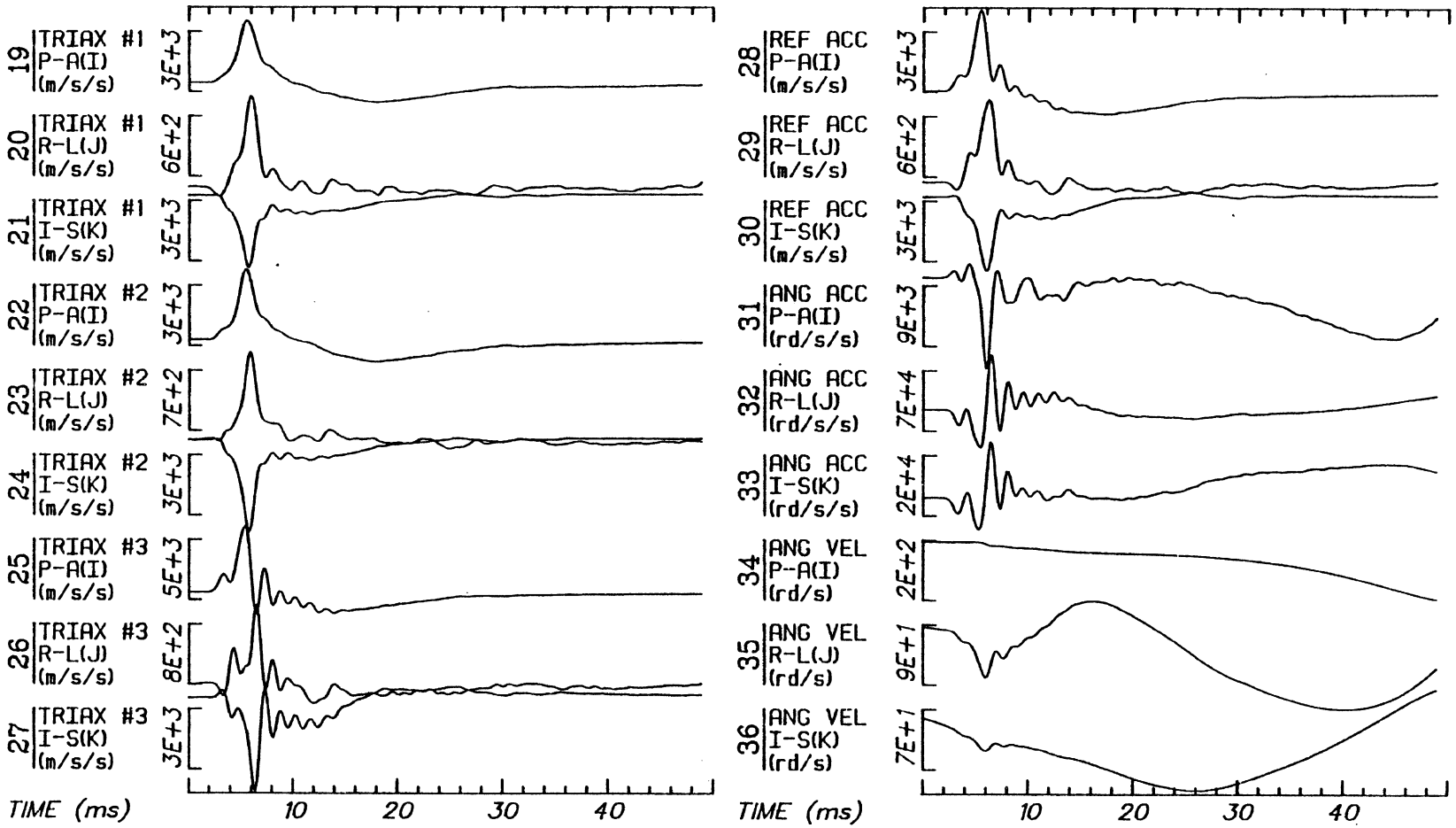

Run ID: 78A238 Disk: 78A238 File: 1 Date: MAY 14, 1984 Sheet: 2

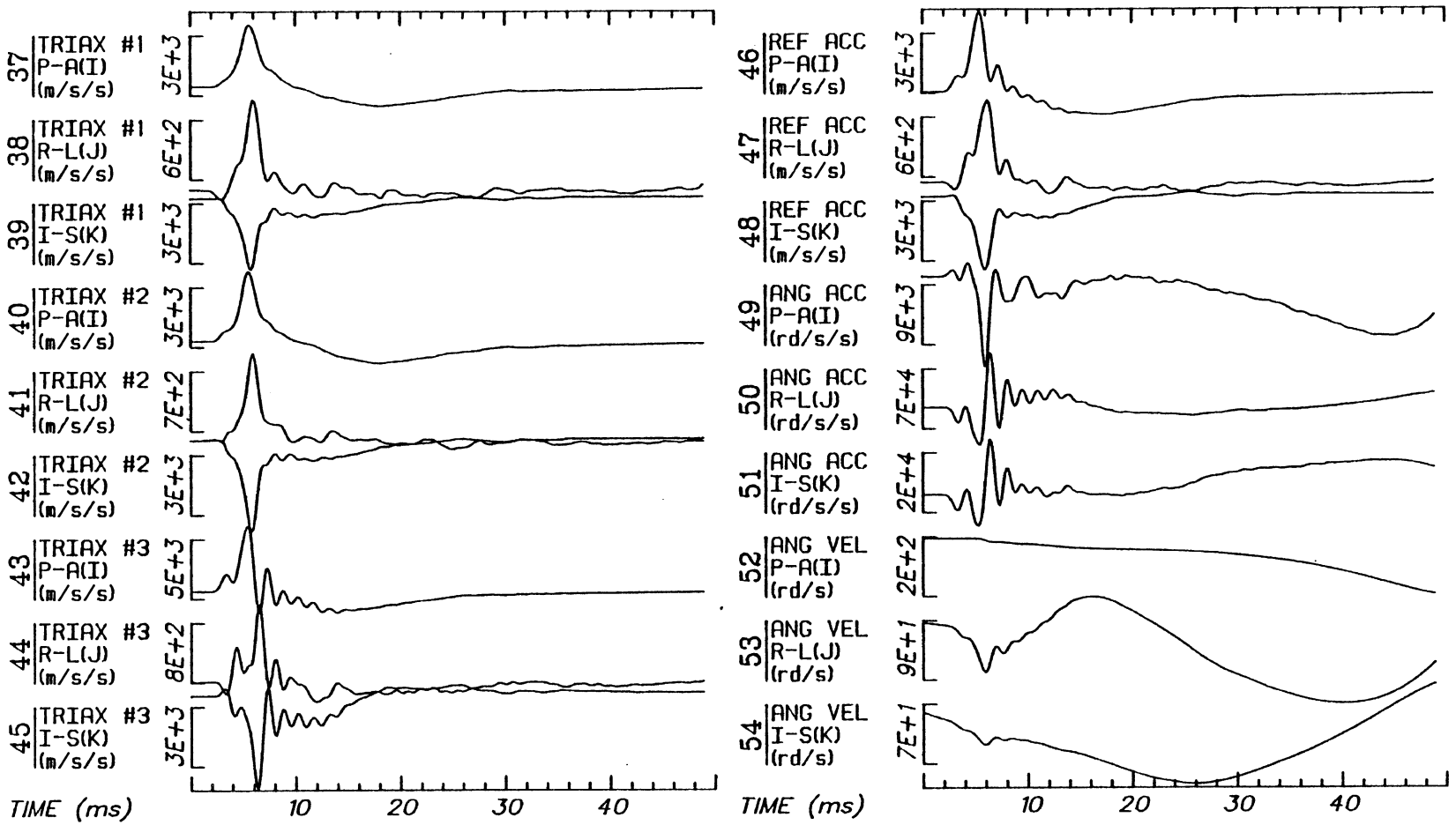

Run ID: 78A238 Disk: 78A238 File: 1 Date: MAY 14, 1984 Sheet: 3

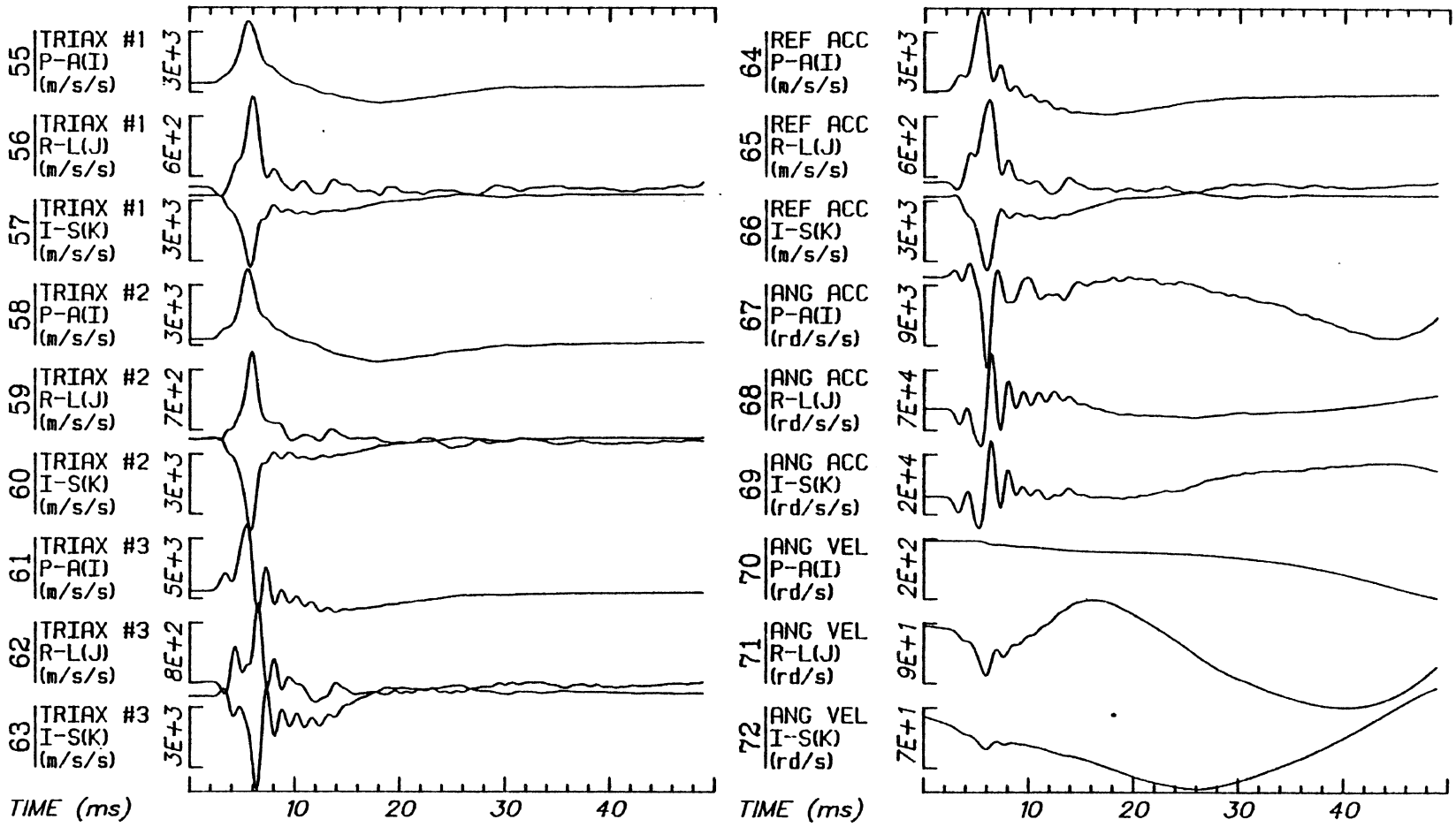

Run ID: 78A238 Disk: 78A238 File: 1 Date: MAY 14, 1984 Sheet: 4

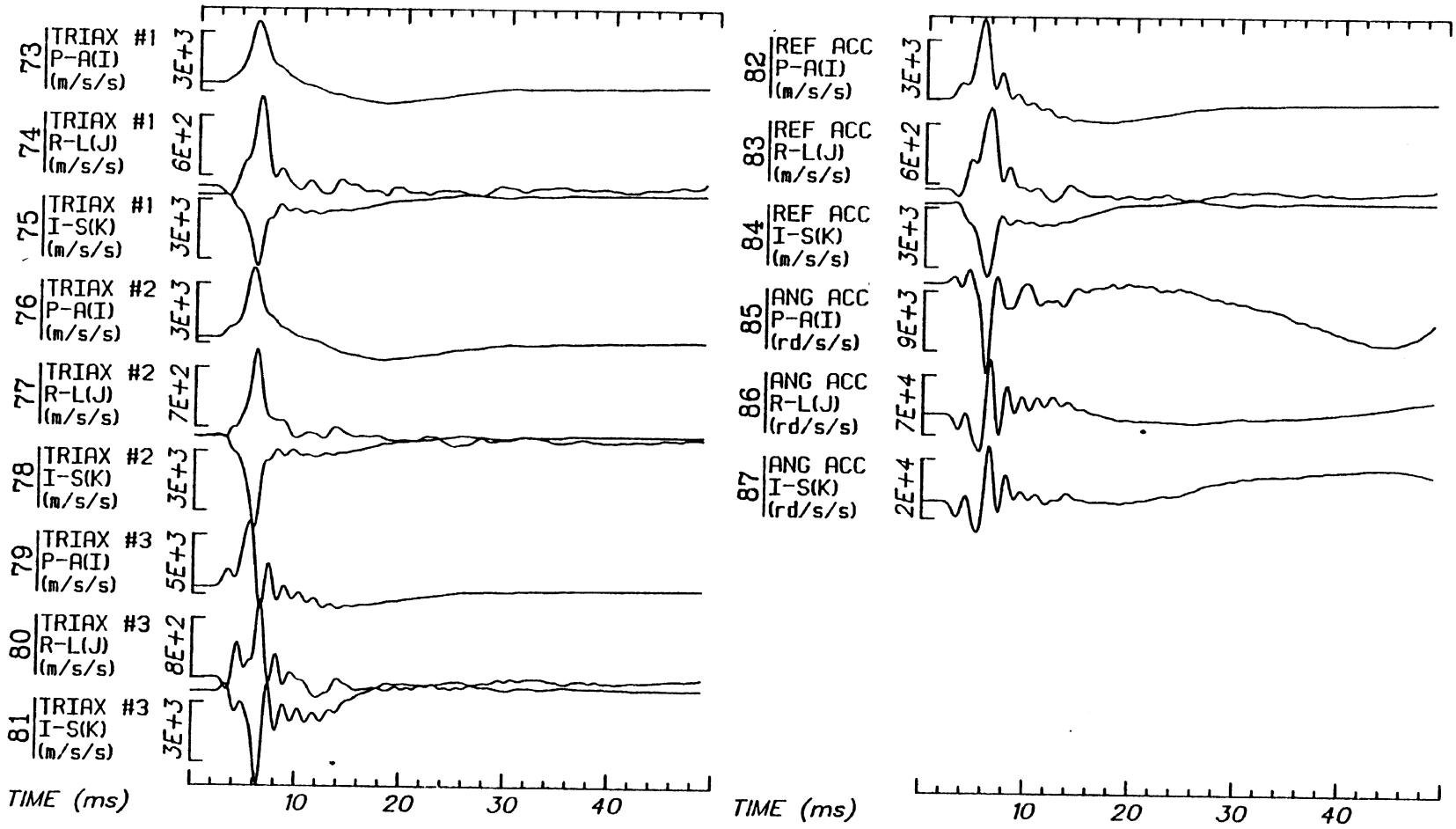

Run ID: 78A238 Disk: 78A238 File: 1 Date: MAY 14, 1984 Sheet: 5

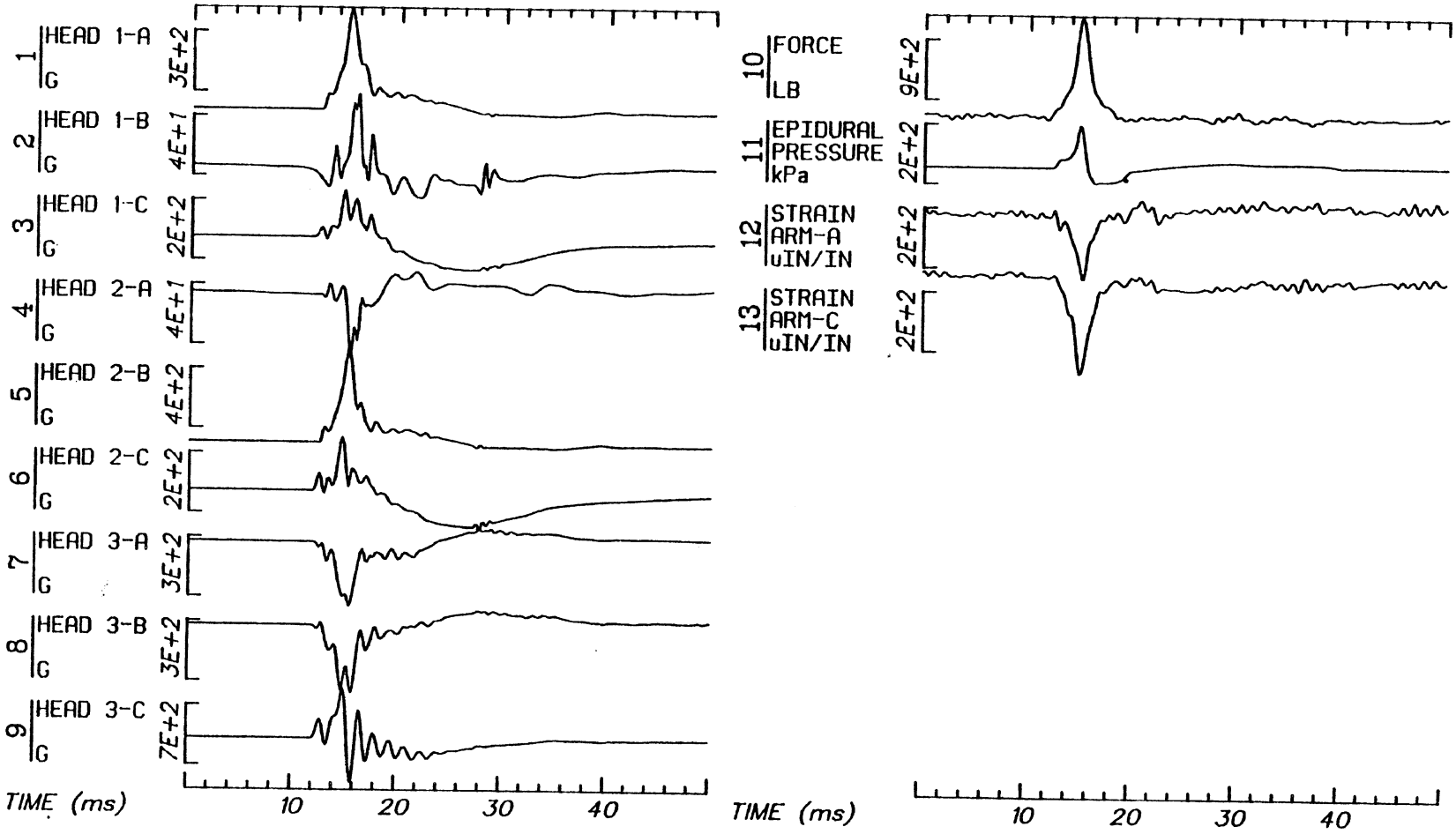

Run ID: 78A238 Disk: 78A238.S File: 1 Date: JUN 16, 1985 Sheet: 1

Filter:1600*4C Smooth: 3SD SIDFA DATA: Filter - 1600*4C, Smooth - 3SD

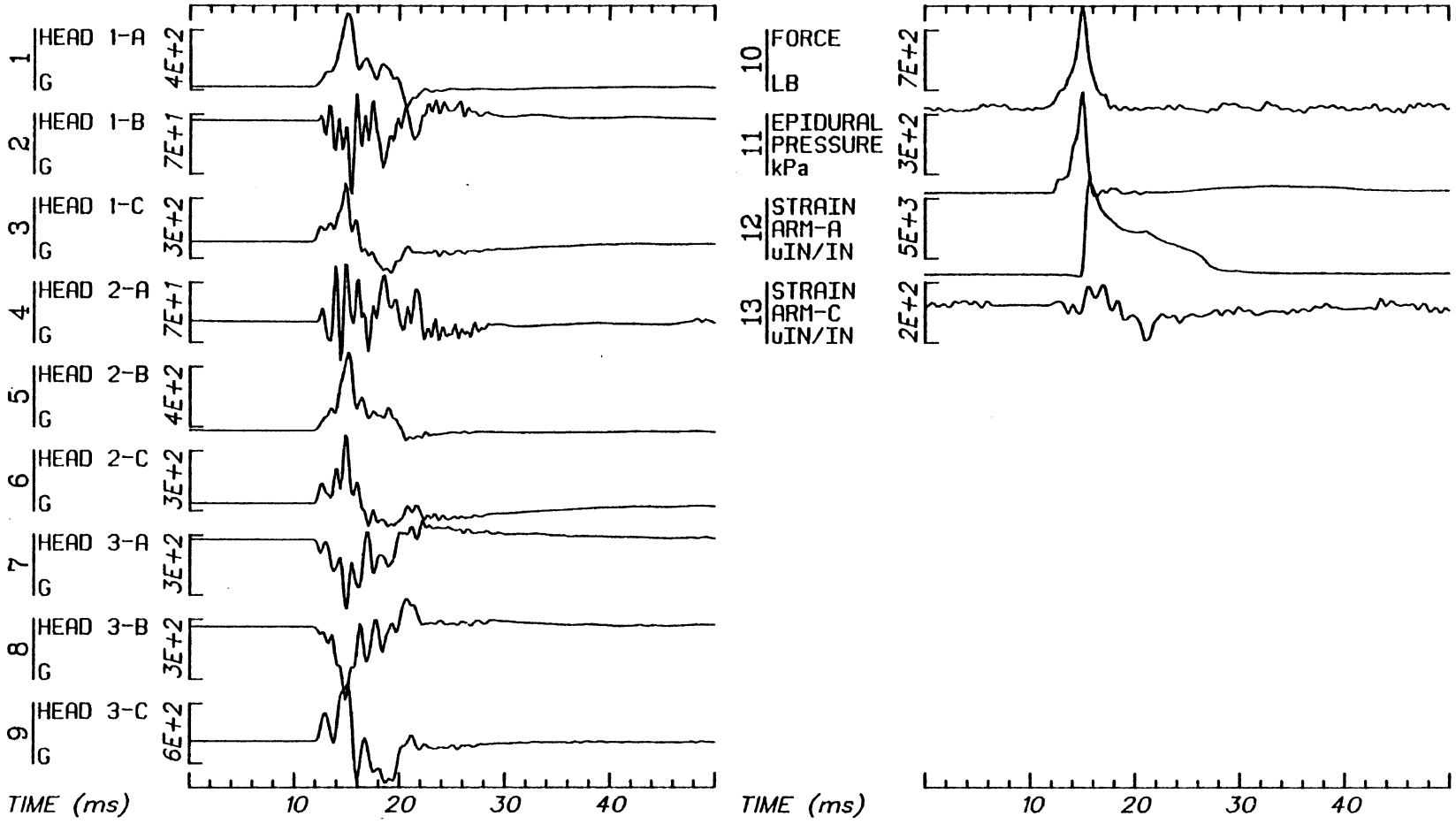

Run ID: 78A239 Disk: 78A239.S File: 1 Date: JUN 16, 1985 Sheet: 1

Filter:1600*4C Smooth: 3SD SIDFA DATA: Filter – 1600*4C, Smooth – 3SD

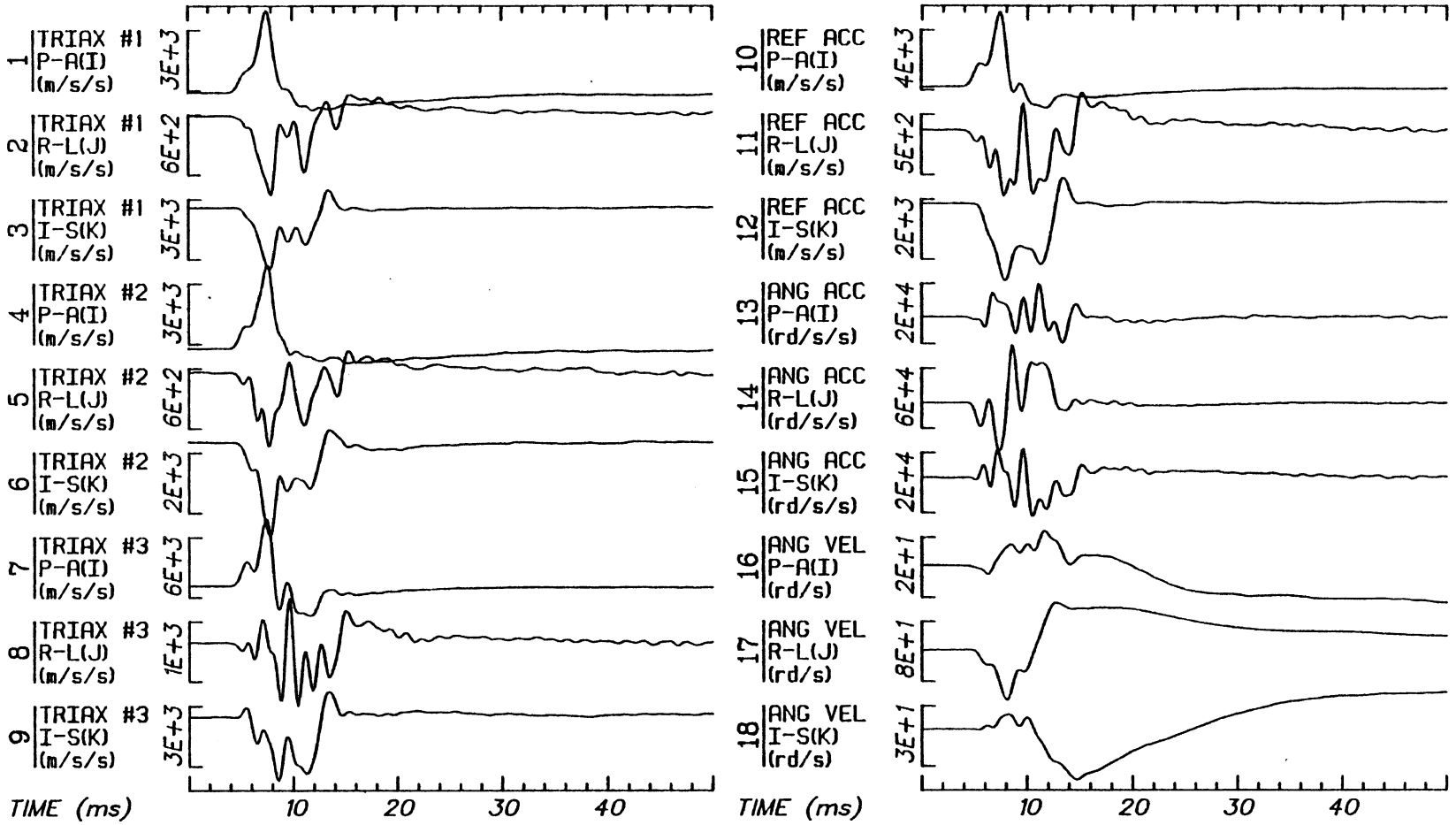

Run ID: 78A239 Disk: 78A239 File: 1 Date: MAY 14, 1984 Sheet: 1

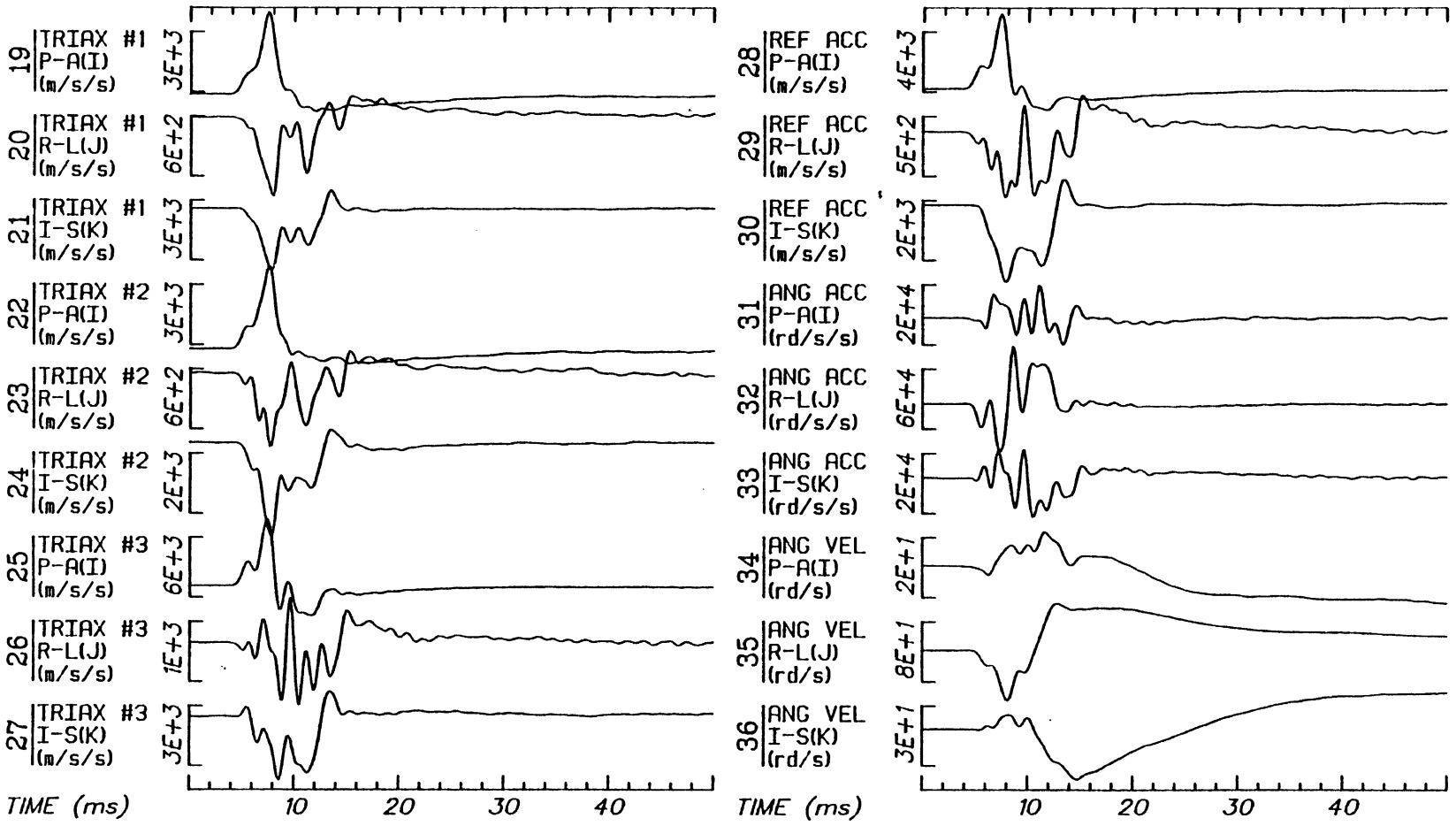

Run ID: 78A239 Disk: 78A239 File: 1 Date: MAY 14, 1984 Sheet: 2

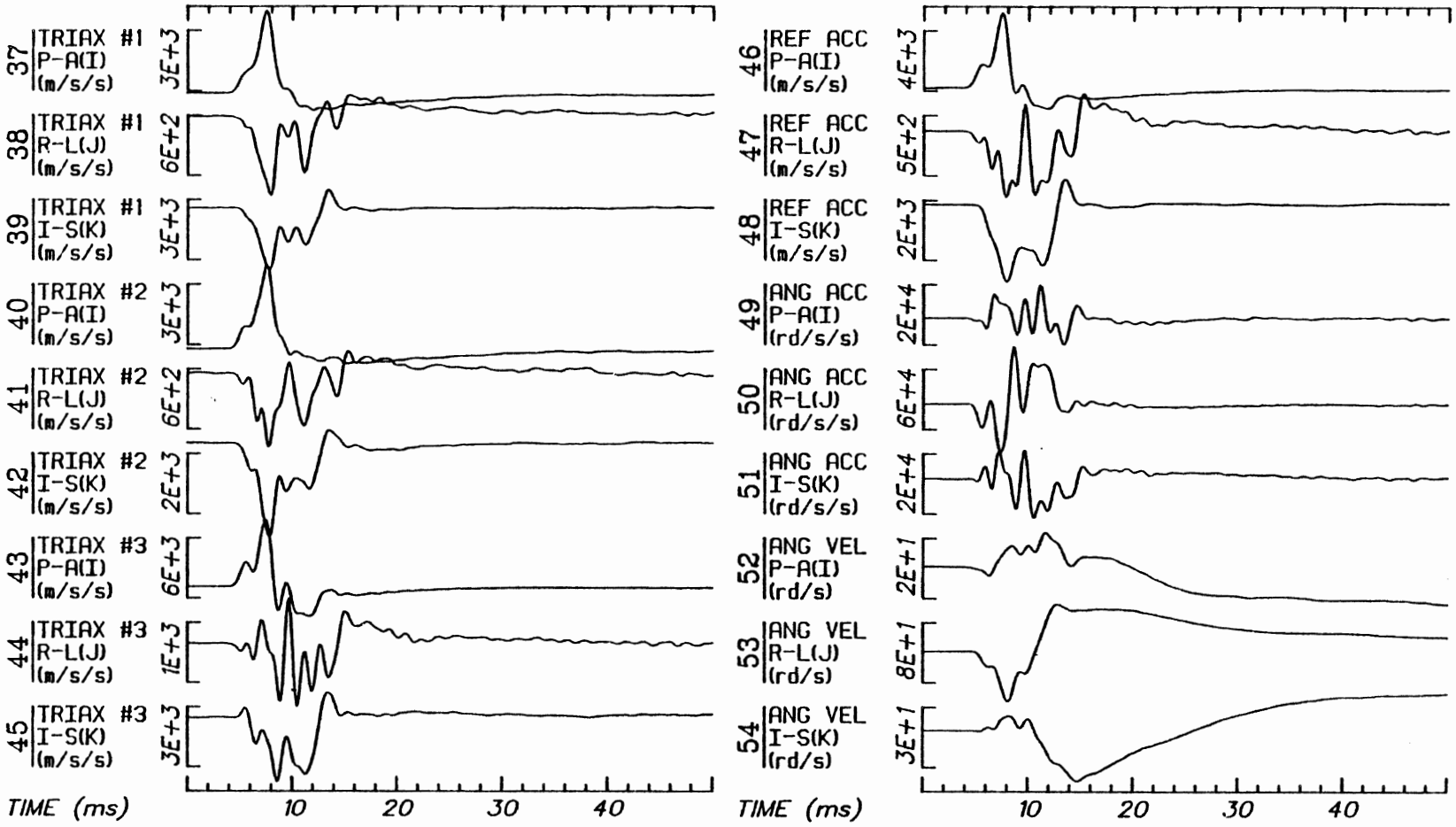

Run ID: 78A239 Disk: 78A239 File: 1 Date: MAY 14, 1984 Sheet: 3

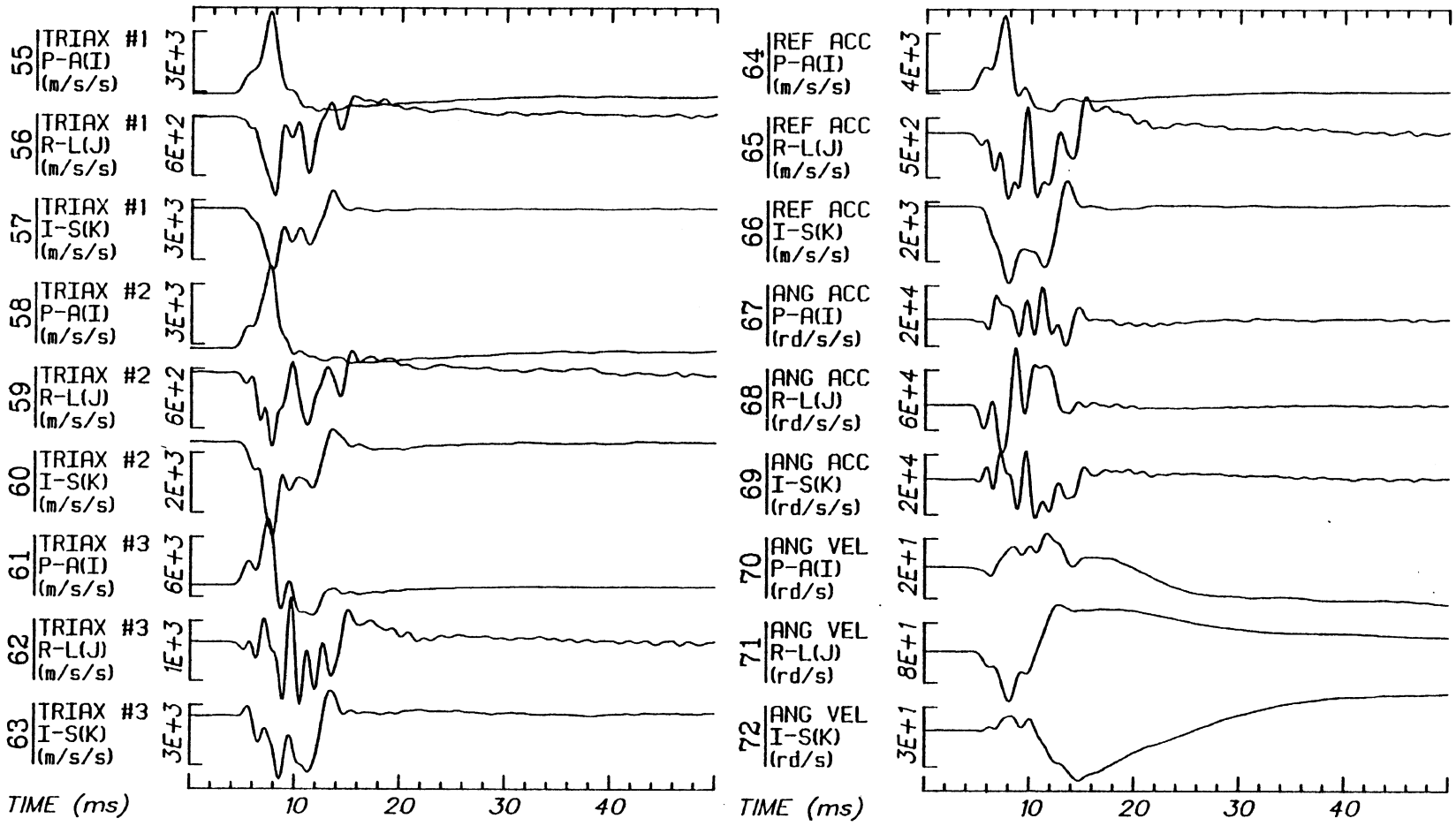

Run ID: 78A239 Disk: 78A239 File: 1 Date: MAY 14, 1984 Sheet: 4

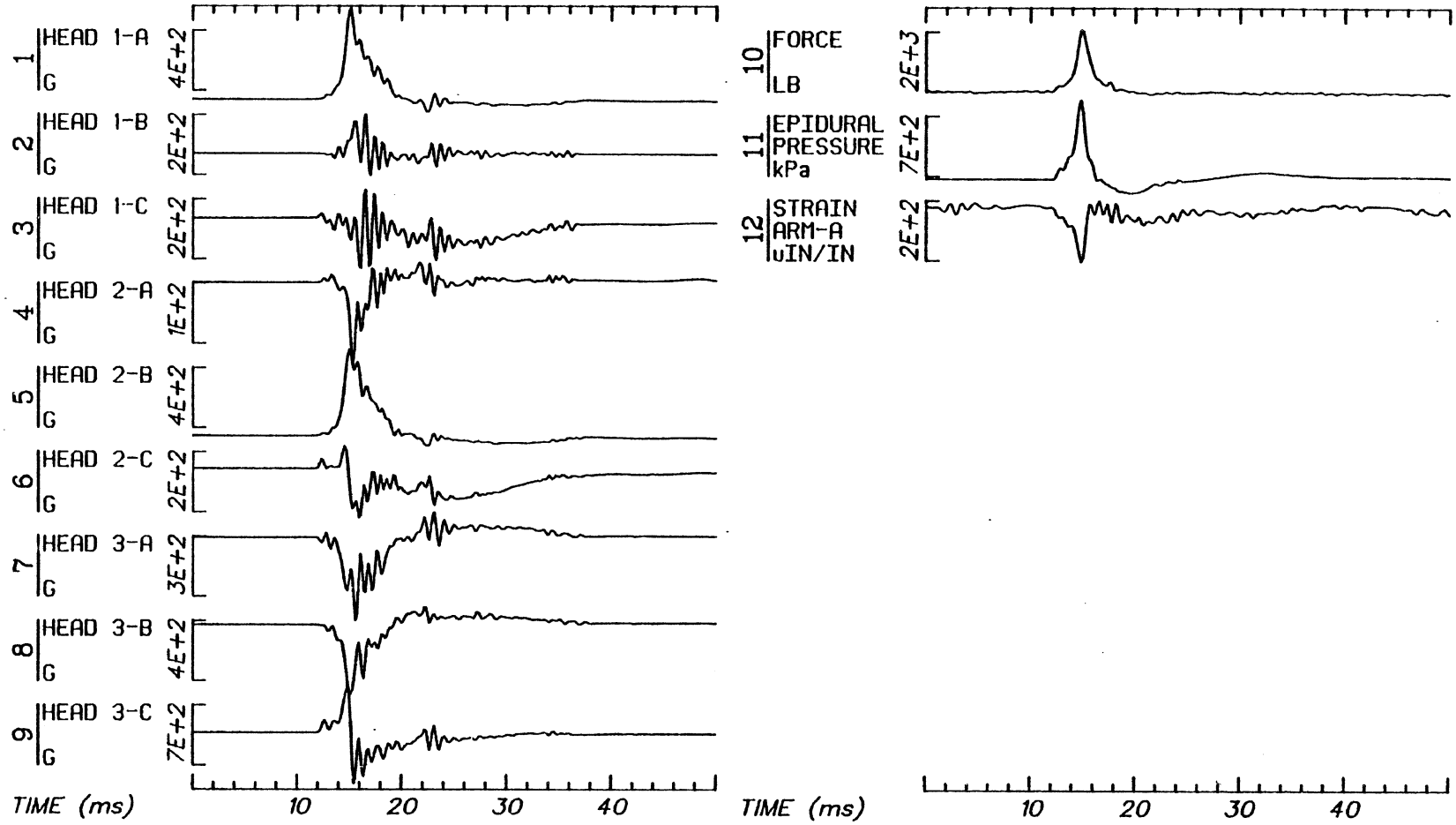

Run ID: 78A241 Disk: 78A241.S File: 1 Date: JUN 16, 1985 Sheet: 1

Filter:1600*4C Smooth: 3SD SIDFA DATA: Filter – 1600*4C, Smooth – 3SD

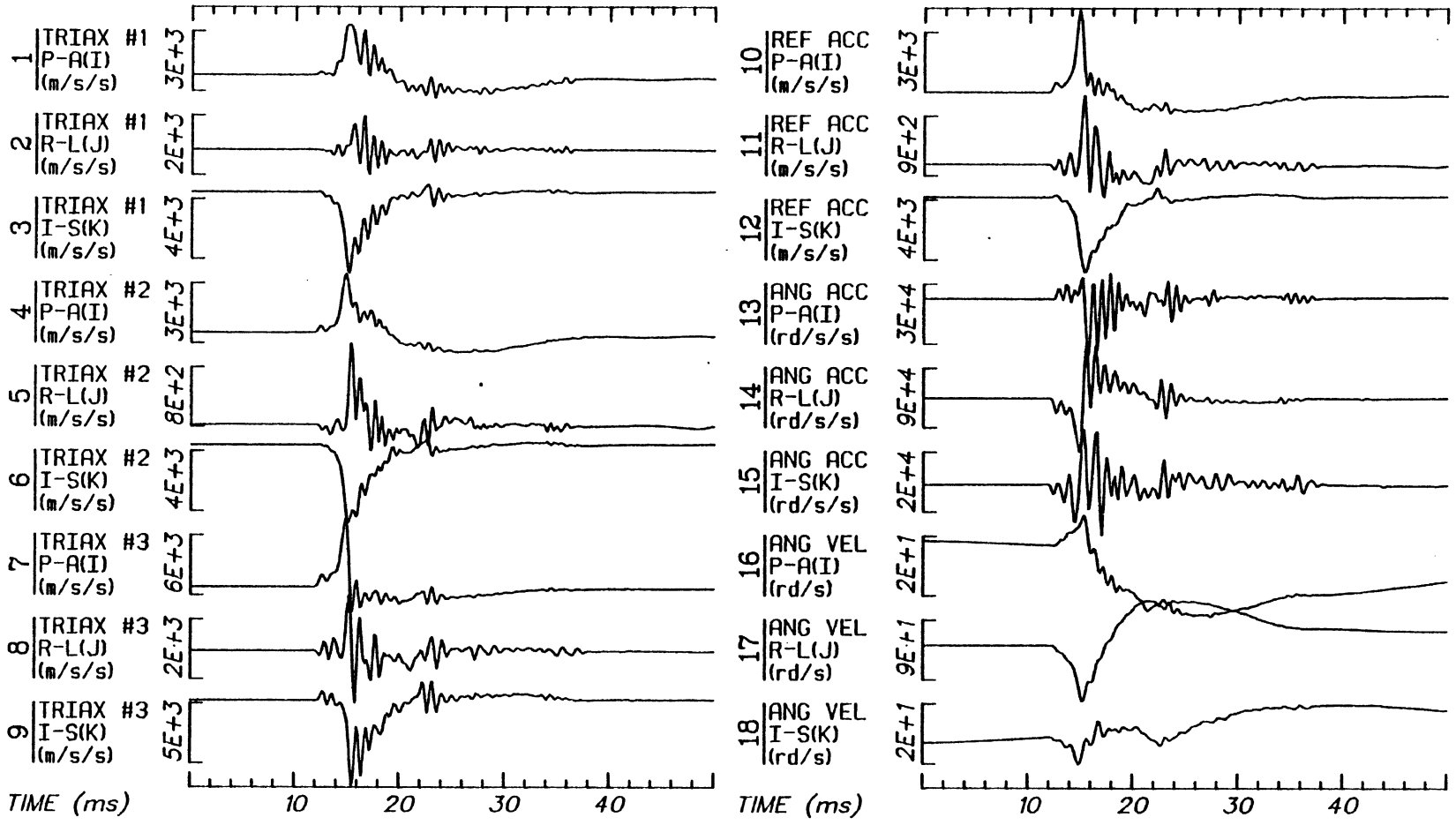

Run ID: 78A241 Disk: 78A241.3 File: 1 Date: JUN 23, 1985 Sheet: 1

No Filtering

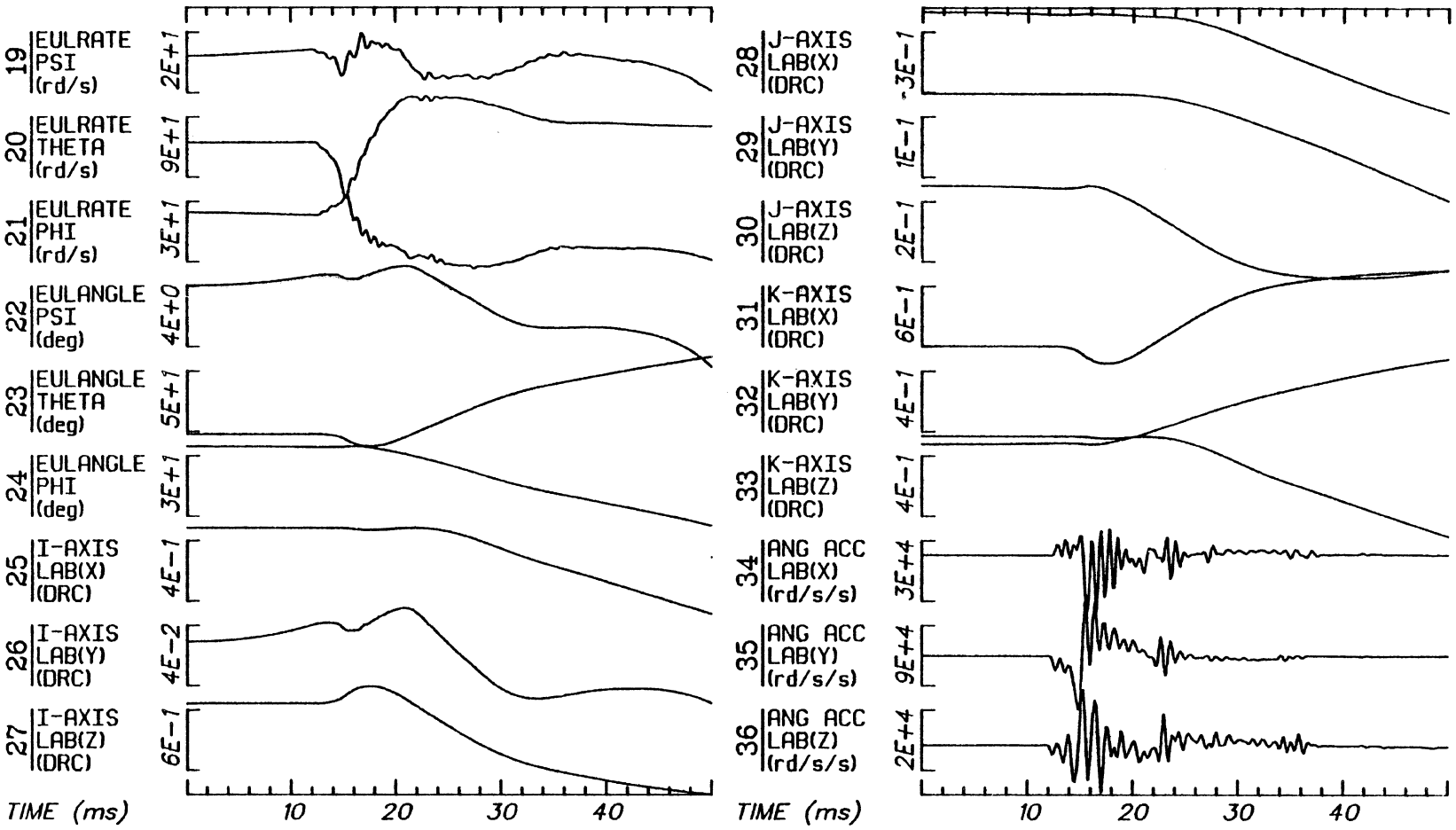

Run ID: 78A241 Disk: 78A241.3 File: 1 Date: JUN 23, 1985 Sheet: 2

No Filtering

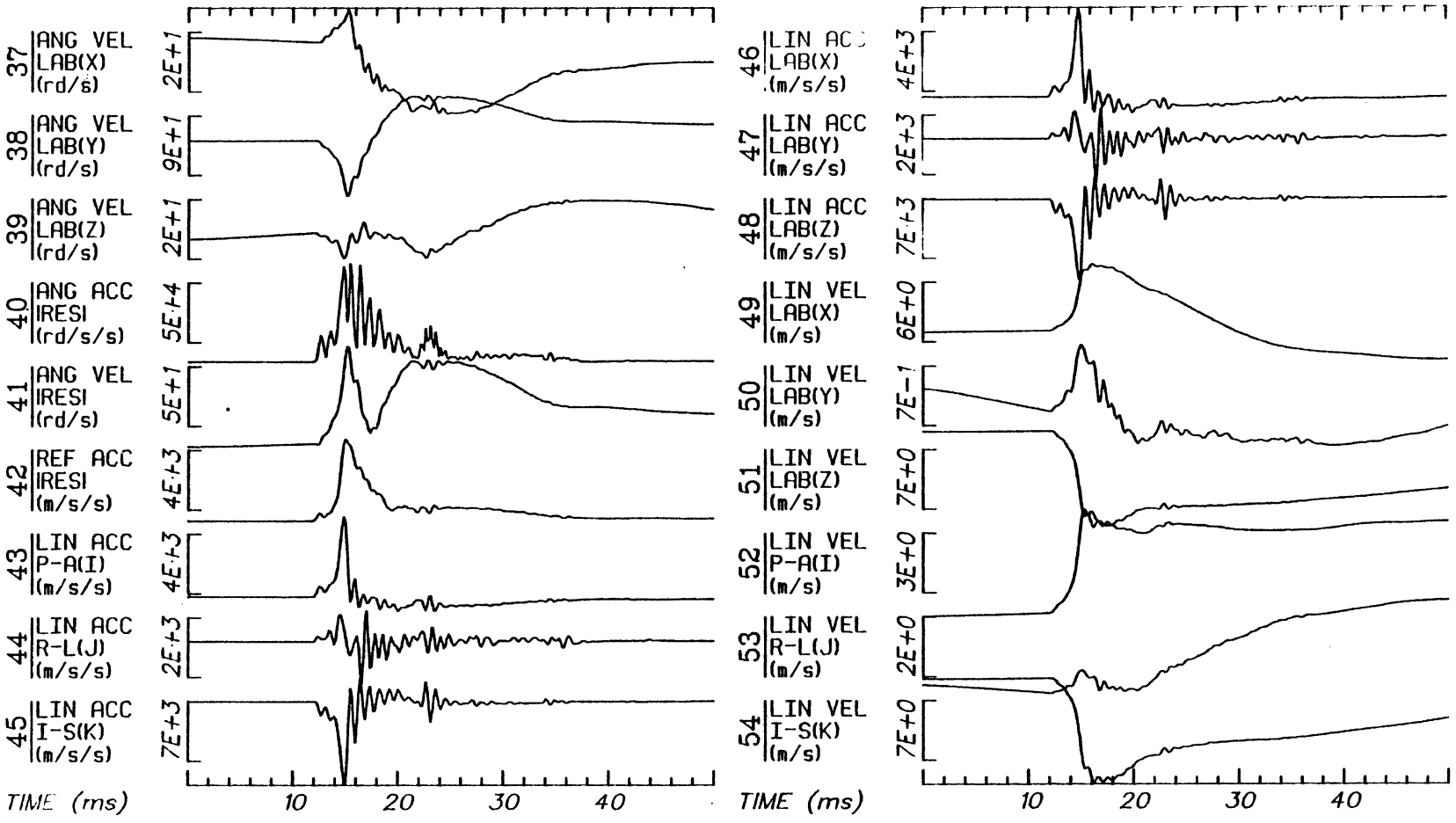

Run ID: 78A241 Disk: 78A241.3 File: 1 Date: JUN 23, 1985 Sheet: 3

No Filtering

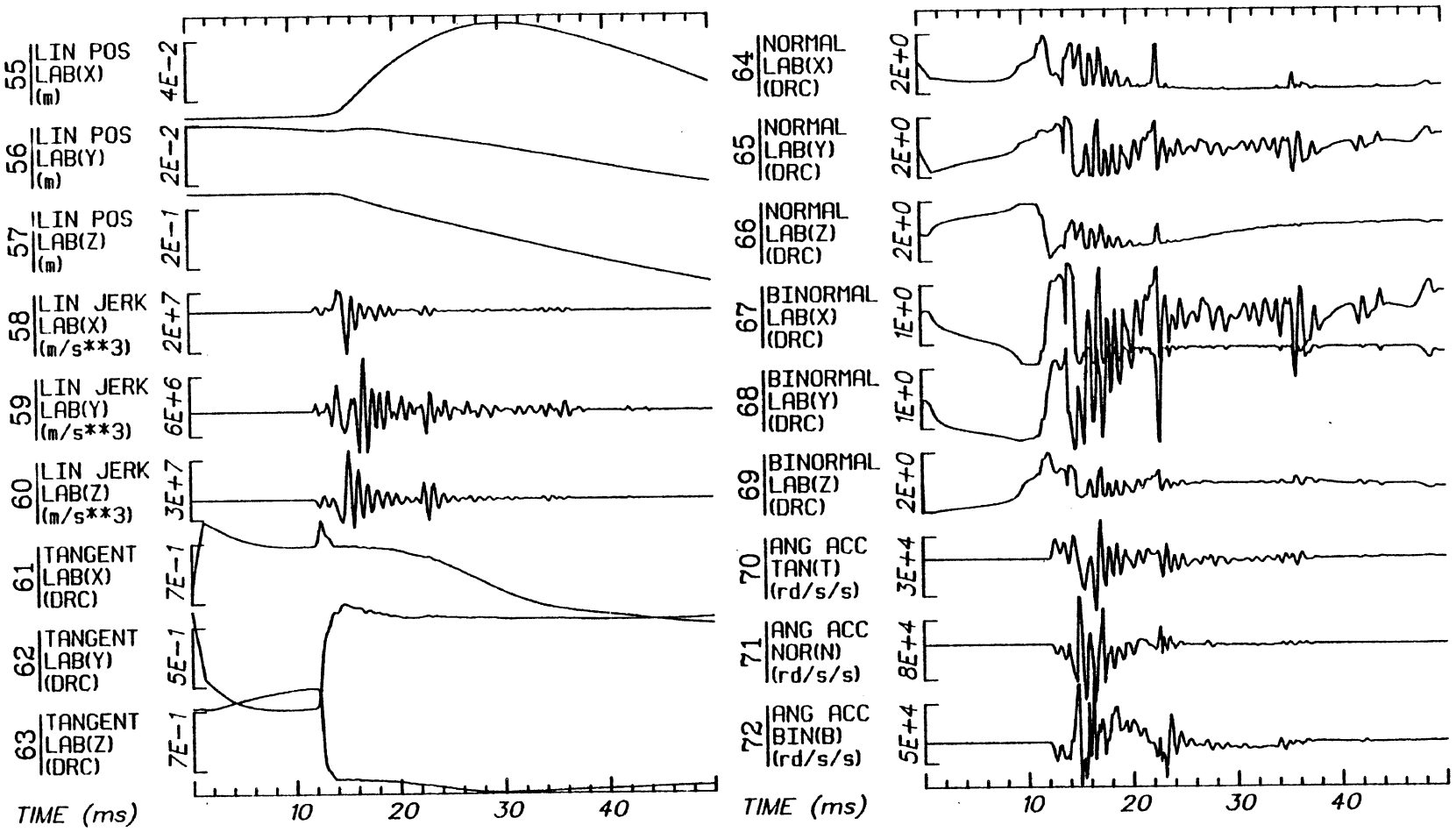

Run ID: 78A241 Disk: 78A241.3 File: 1 Date: JUN 23, 1985 Sheet: 4

No Filtering

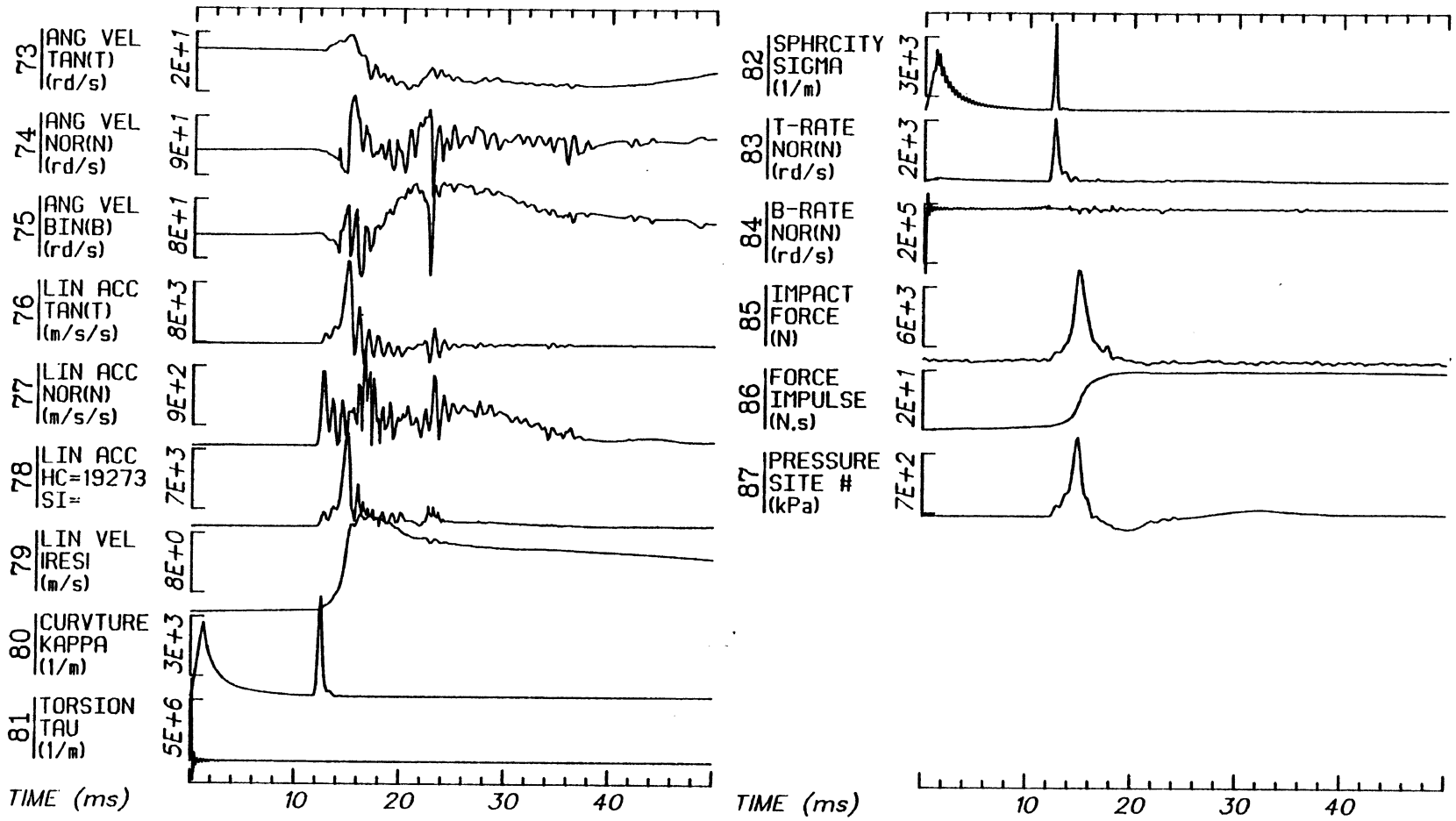

Run ID: 78A241 Disk: 78A241.3 File: 1 Date: JUN 23, 1985 Sheet: 5

No Filtering

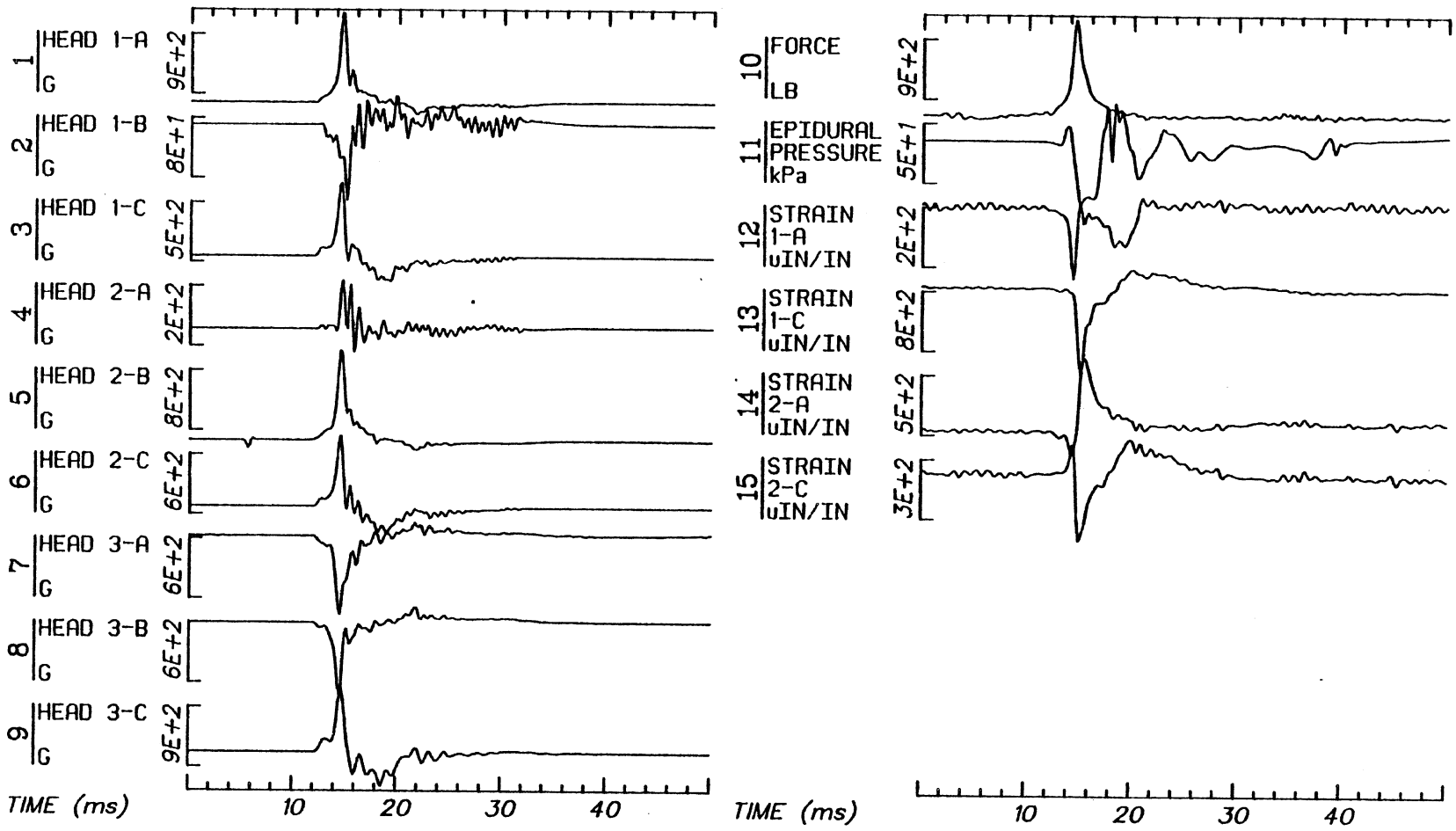

Run ID: 79A249 Disk: 79A249.S File: 1 Date: JUN 16, 1985 Sheet: 1

Filter:1600*4C Smooth: 3SD SIDFA DATA: Filter – 1600*4C, Smooth – 3SD

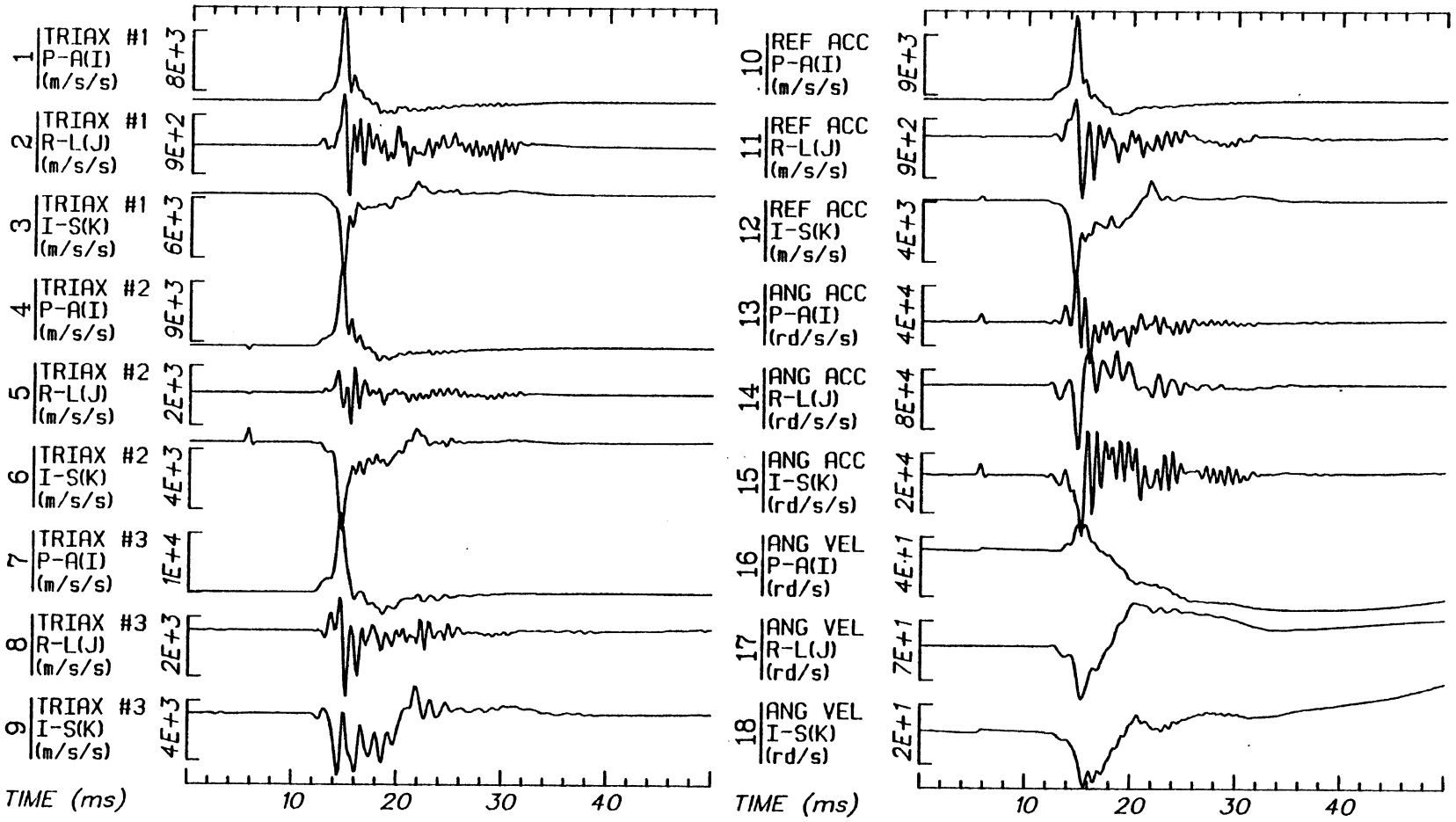

Run ID: 79A249 Disk: 79A249.3 File: 1 Date: JUN 23, 1985 Sheet: 1

No Filtering

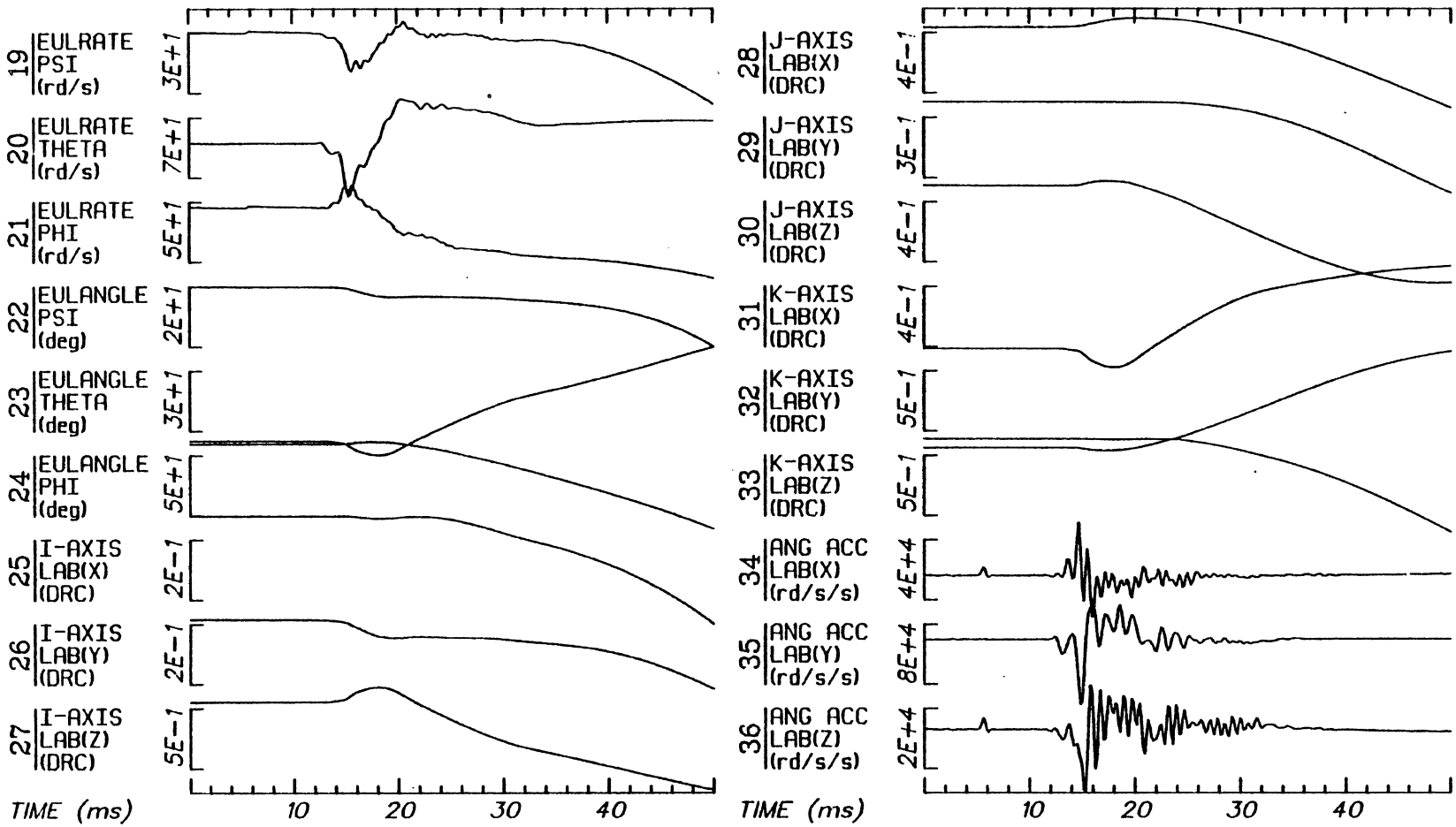

Run ID: 79A249 Disk: 79A249.3 File: 1 Date: JUN 23, 1985 Sheet: 2

No Filtering

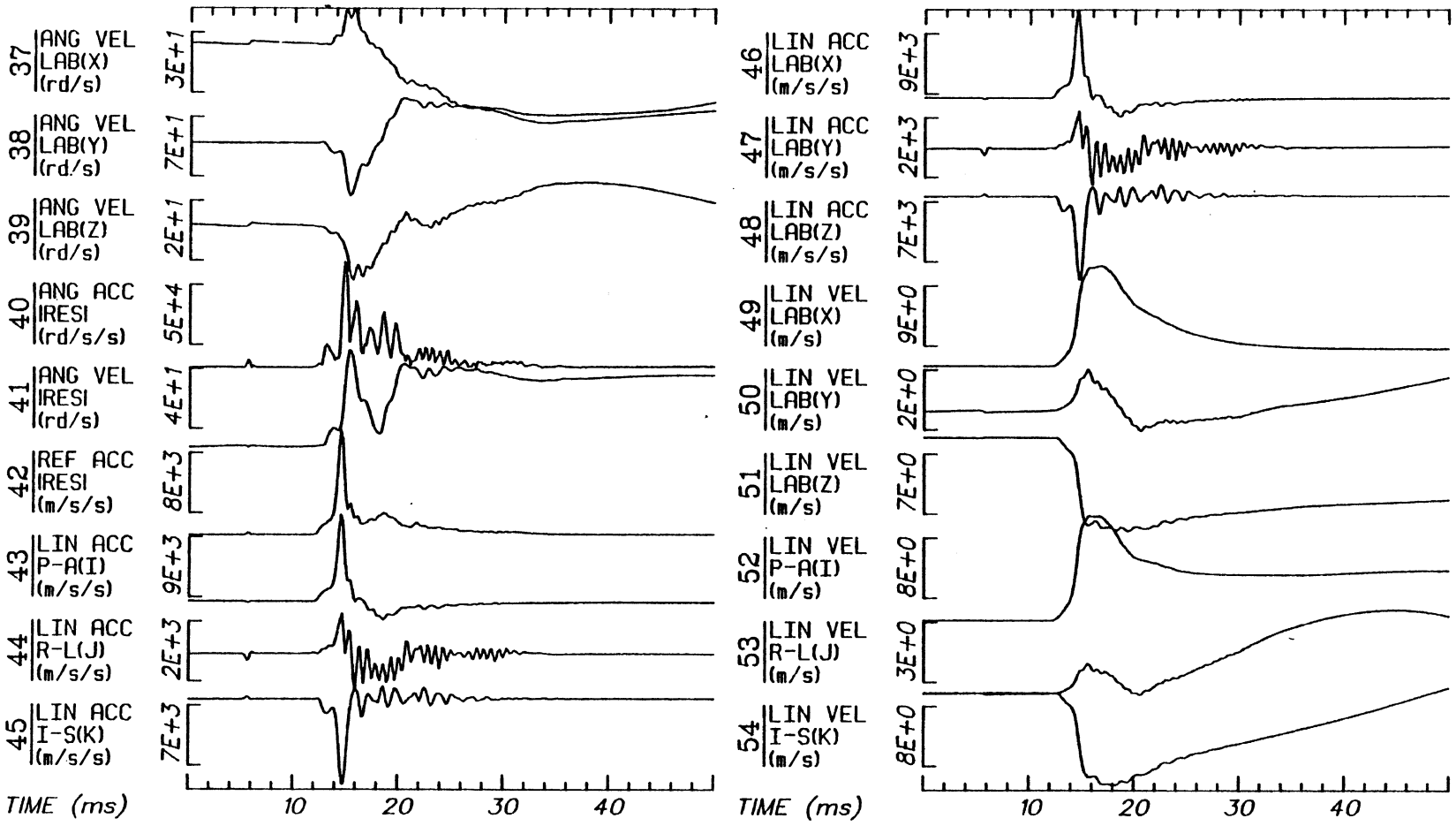

Run ID: 79A249 Disk: 79A249.3 File: 1 Date: JUN 23, 1985 Sheet: 3

No Filtering

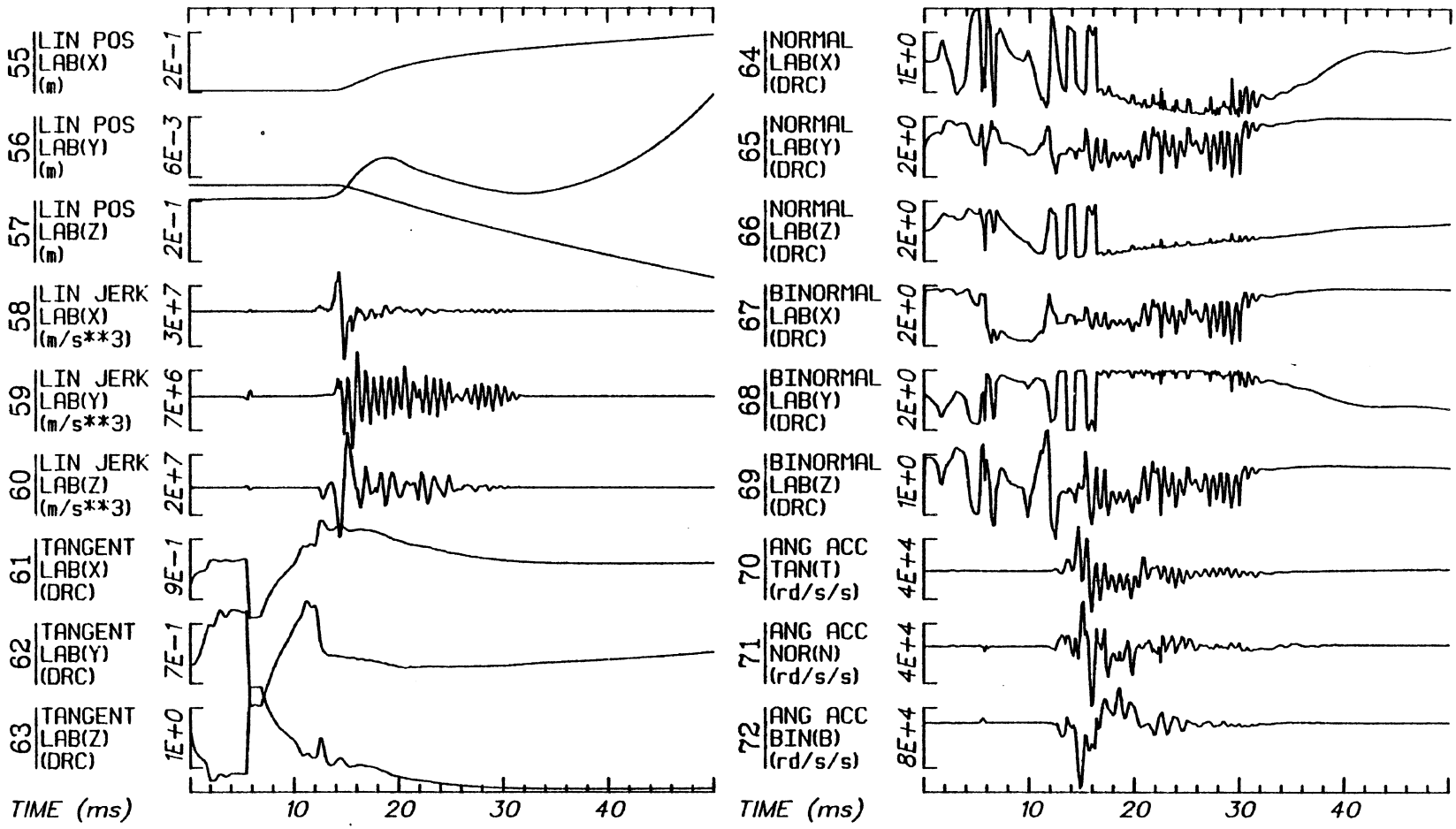

Run ID: 79A249 Disk: 79A249.3 File: 1 Date: JUN 23, 1985 Sheet: 4

No Filtering

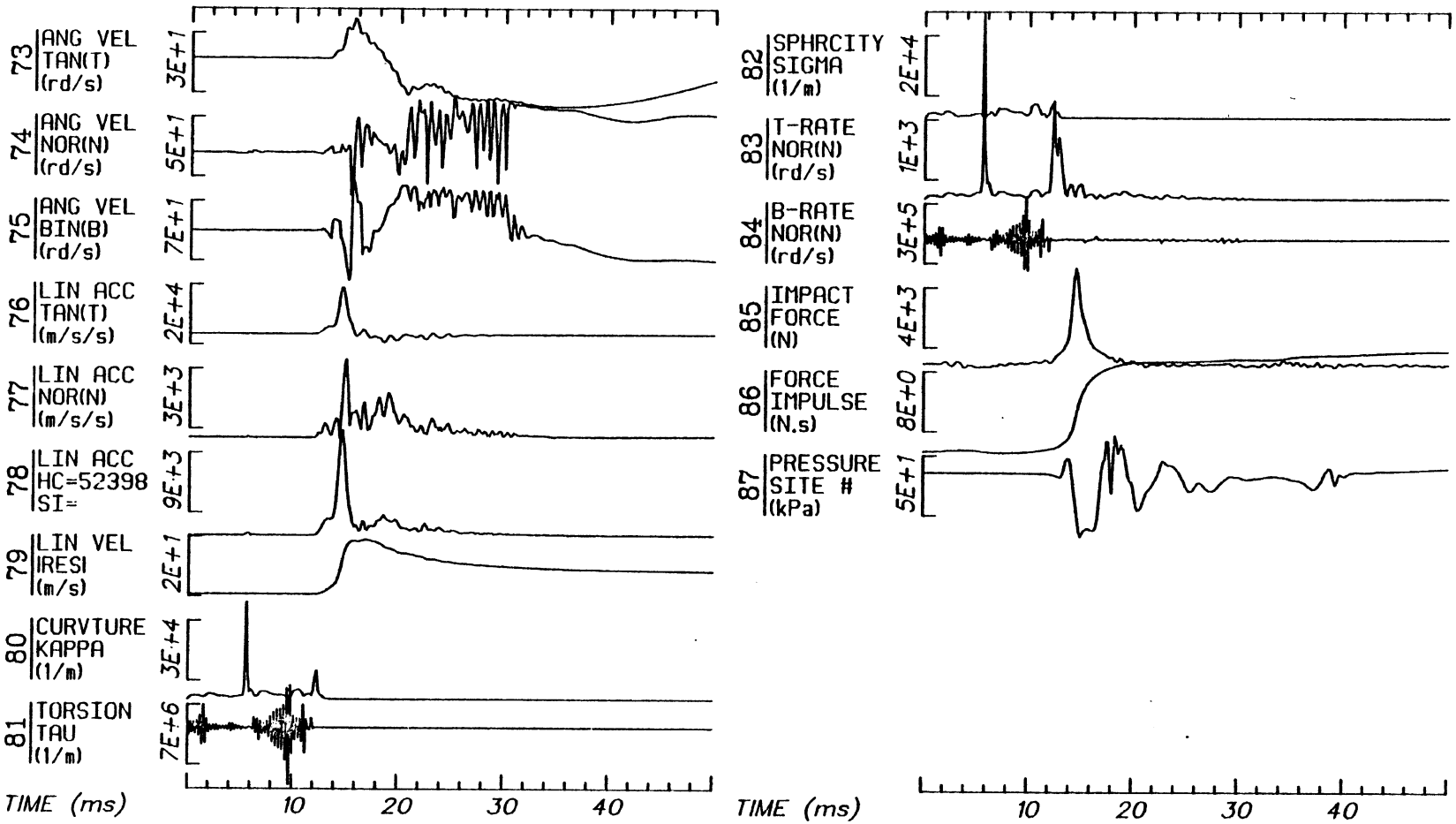

Run ID: 79A249 Disk: 79A249.3 File: 1 Date: JUN 23, 1985 Sheet: 5

No Filtering

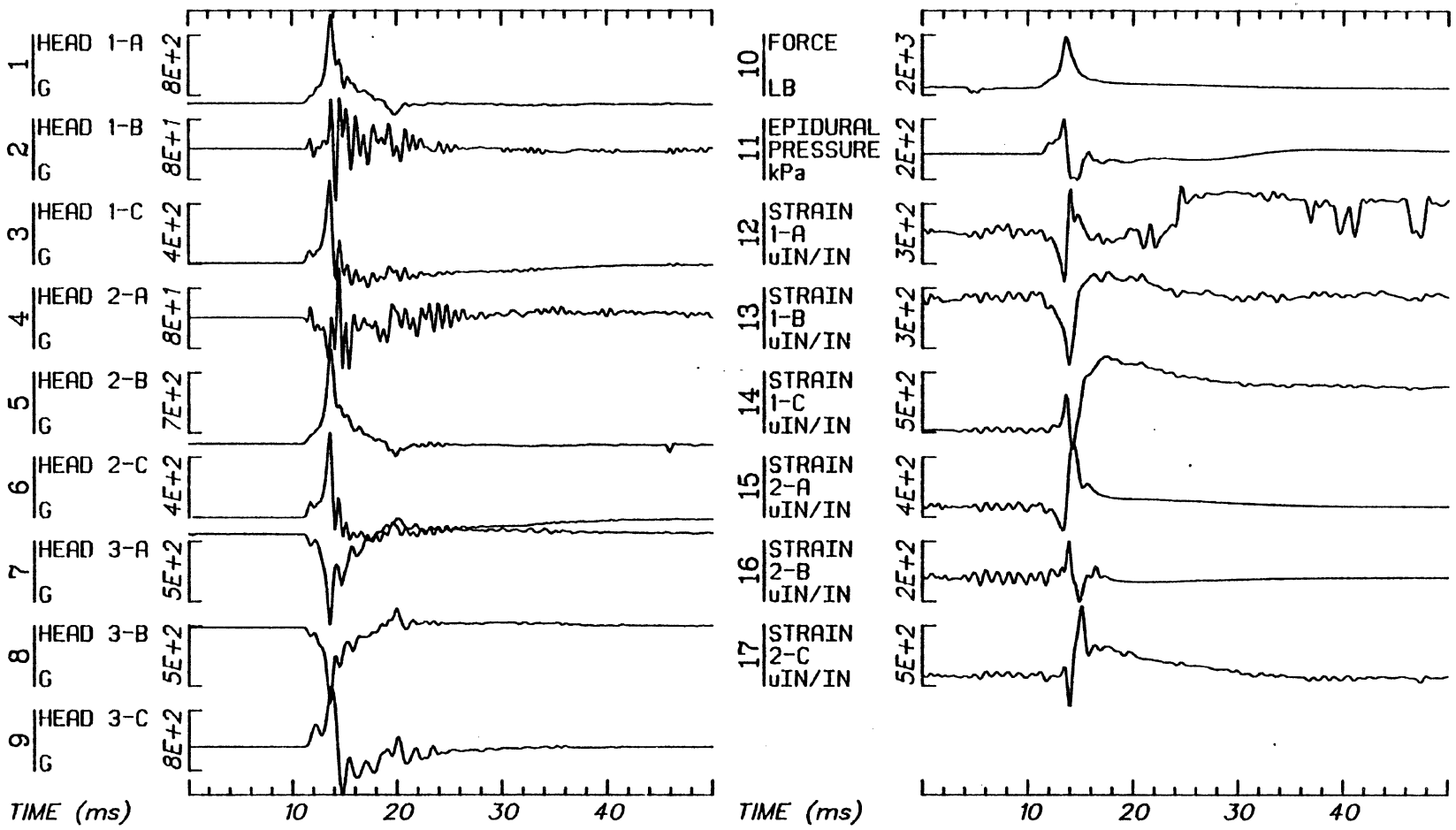

Run ID: 79A251 Disk: 79A251.S File: 1 Date: JUN 16, 1985 Sheet: 1

Filter:1600*4C Smooth: 3SD SIDFA DATA: Filter – 1600*4C, Smooth – 3SD

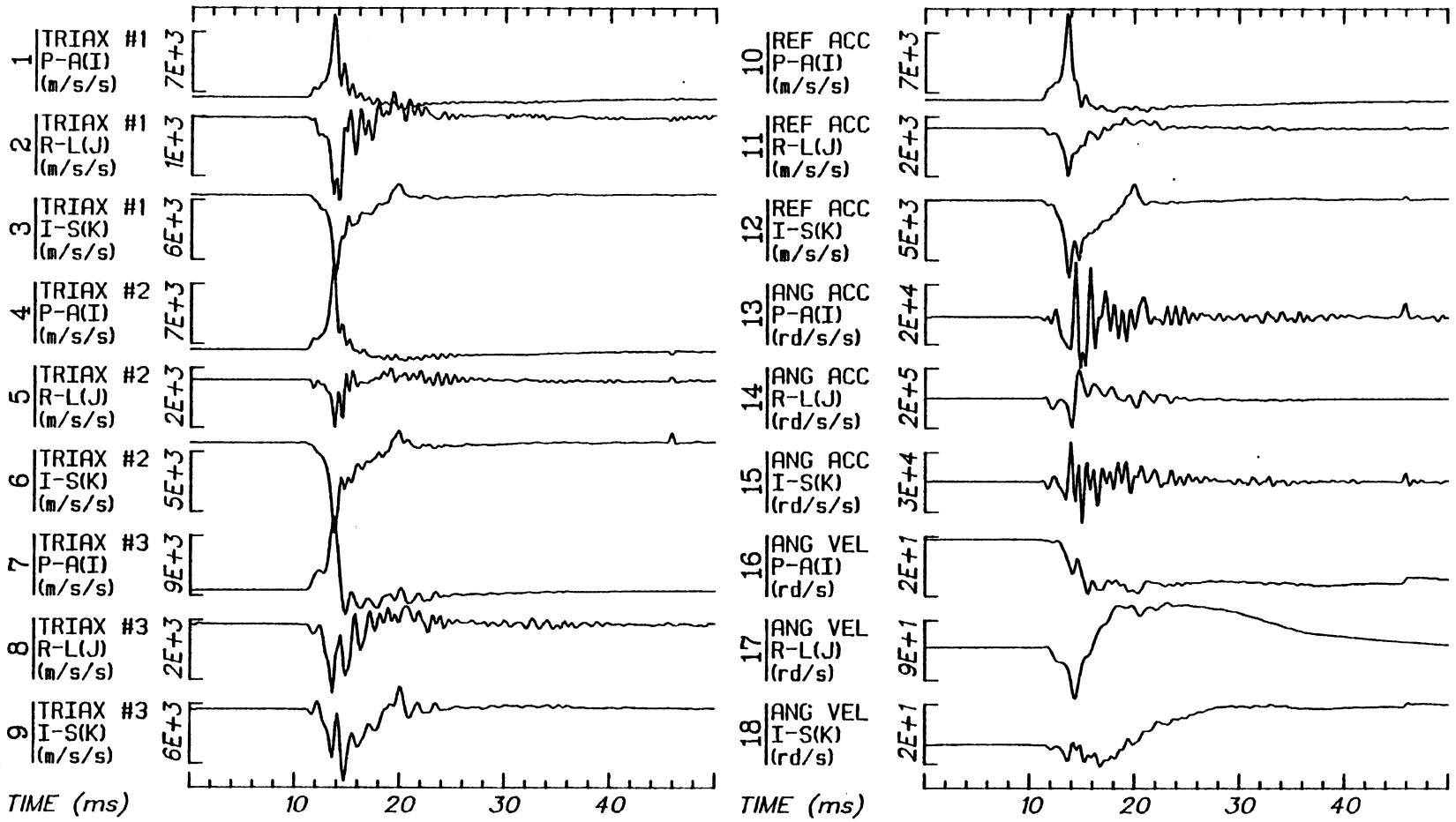

Run ID: 79A251 Disk: 79A251.3 File: 1 Date: JUN 23, 1985 Sheet: 1

No Filtering

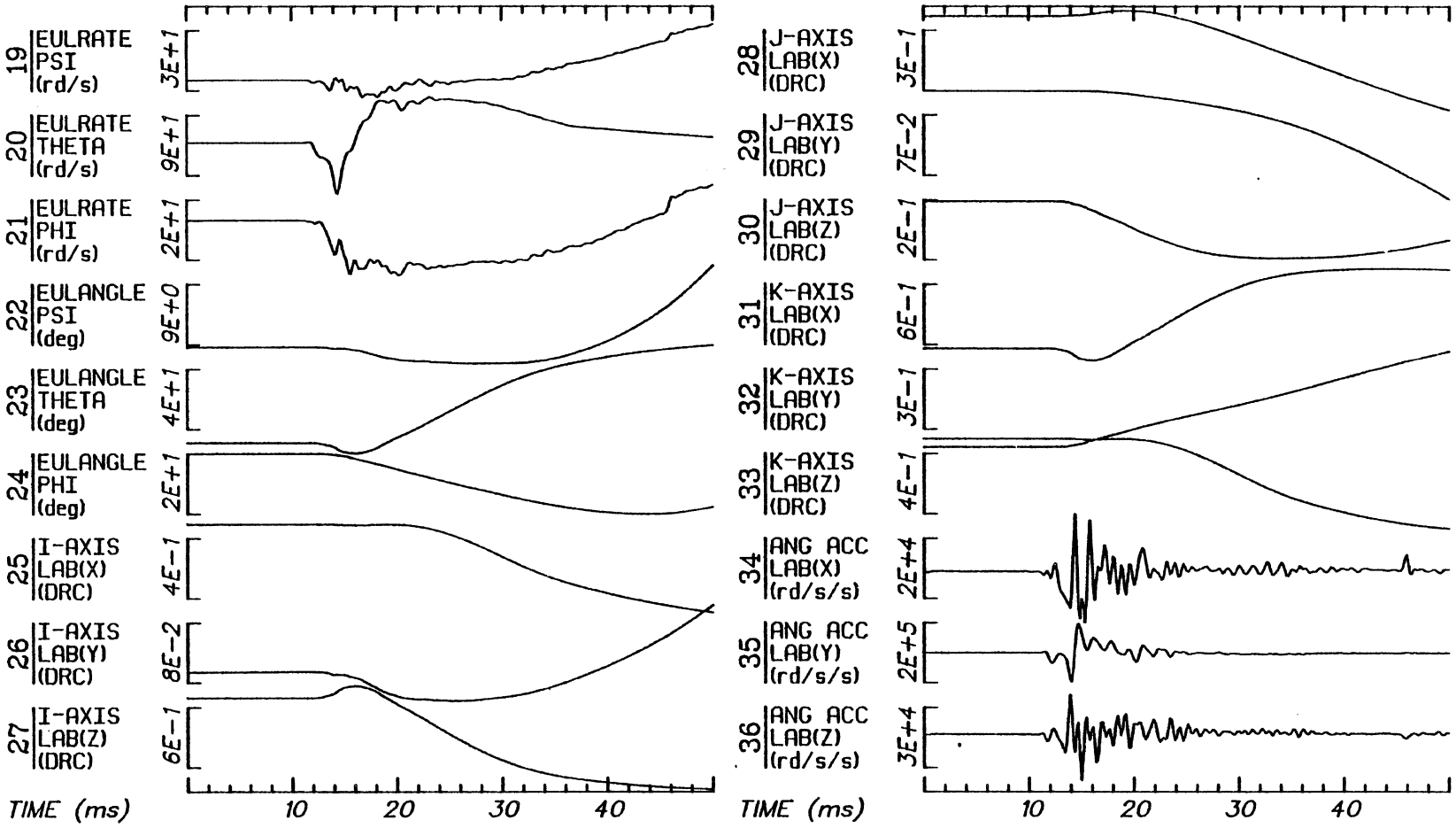

Run ID: 79A251 Disk: 79A251.3 File: 1 Date: JUN 23, 1985 Sheet: 2

No Filtering

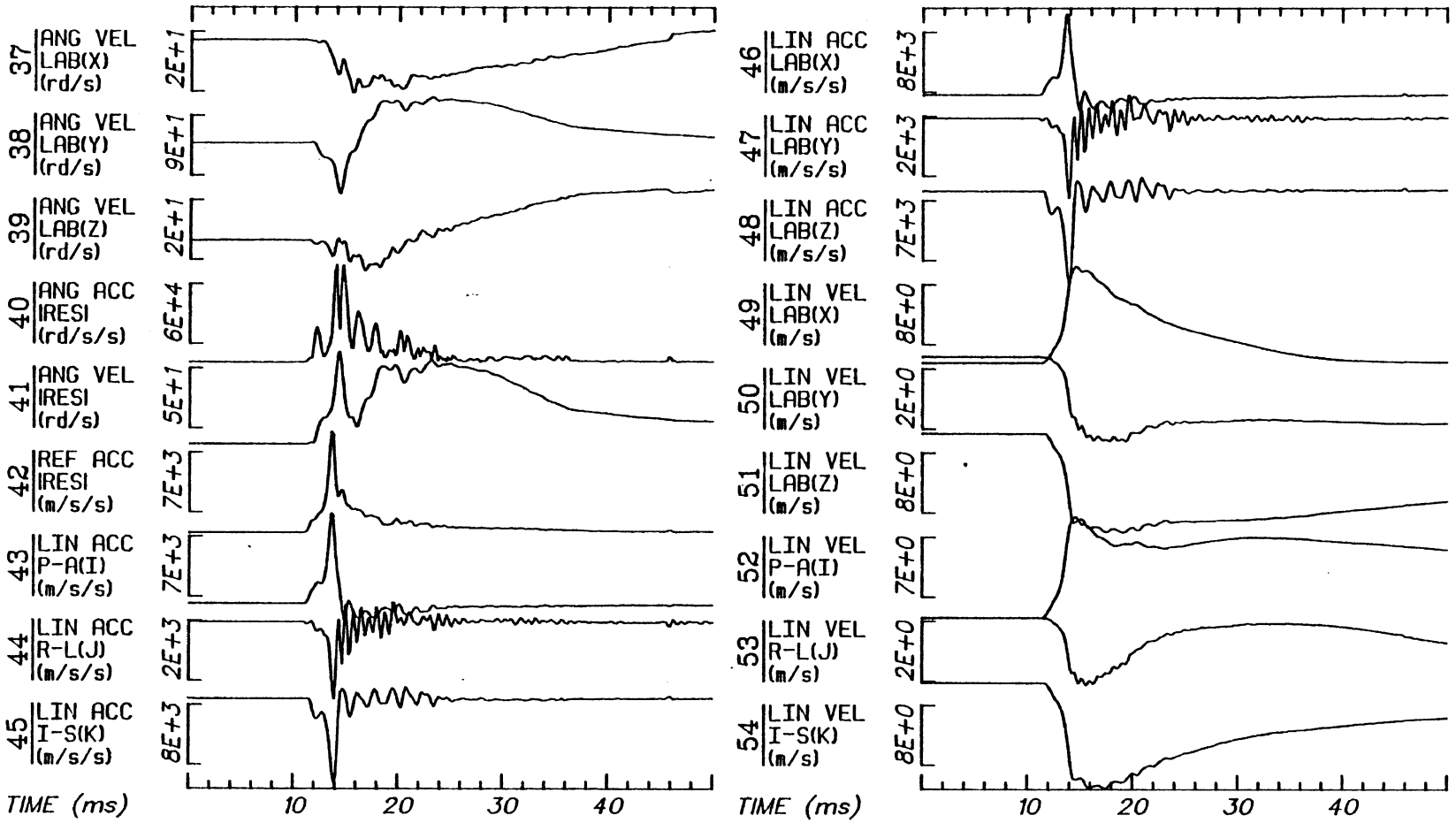

Run ID: 79A251 Disk: 79A251.3 File: 1 Date: JUN 23, 1985 Sheet: 3

No Filtering

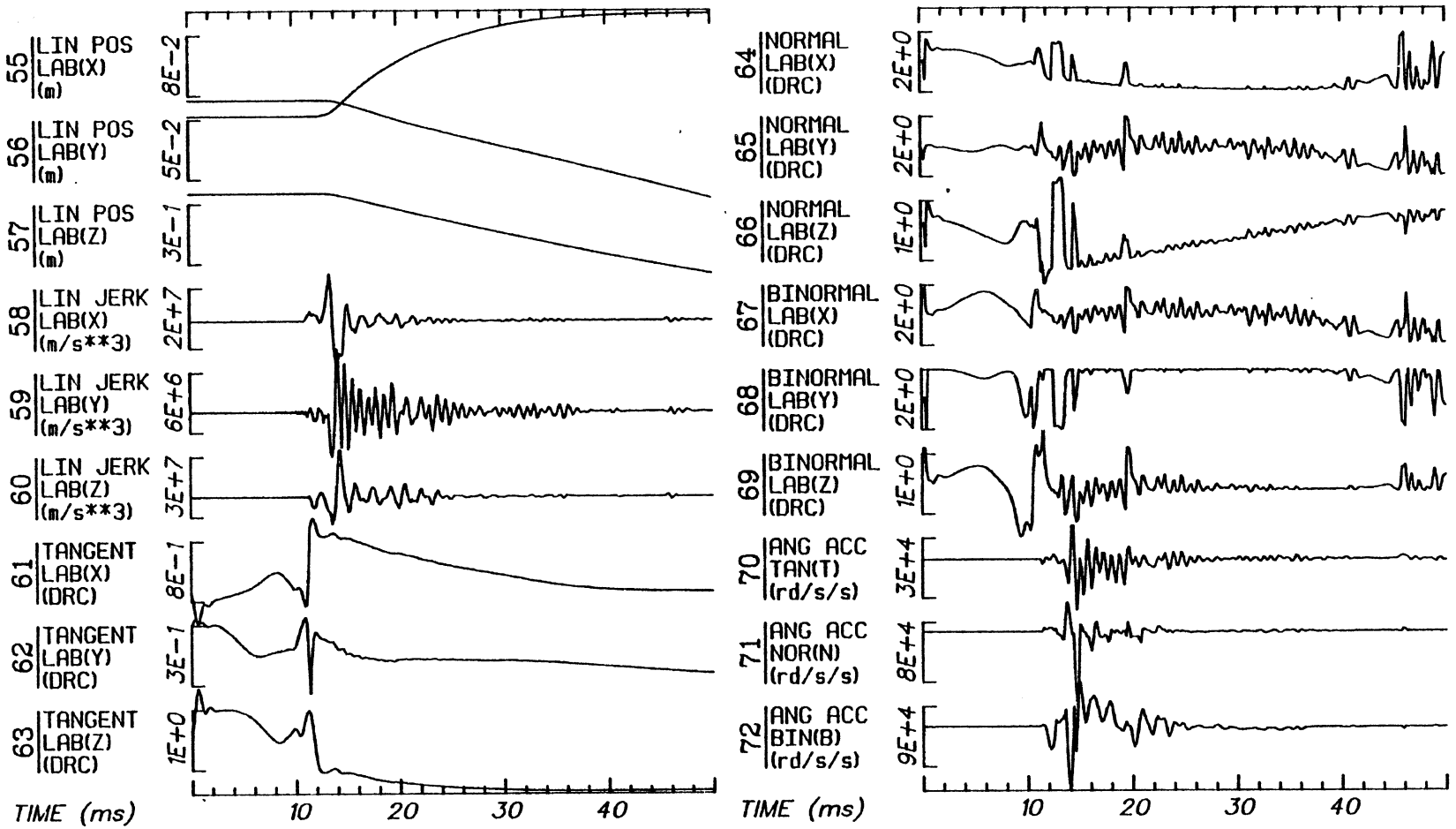

Run ID: 79A251 Disk: 79A251.3 File: 1 Date: JUN 23, 1985 Sheet: 4

No Filtering

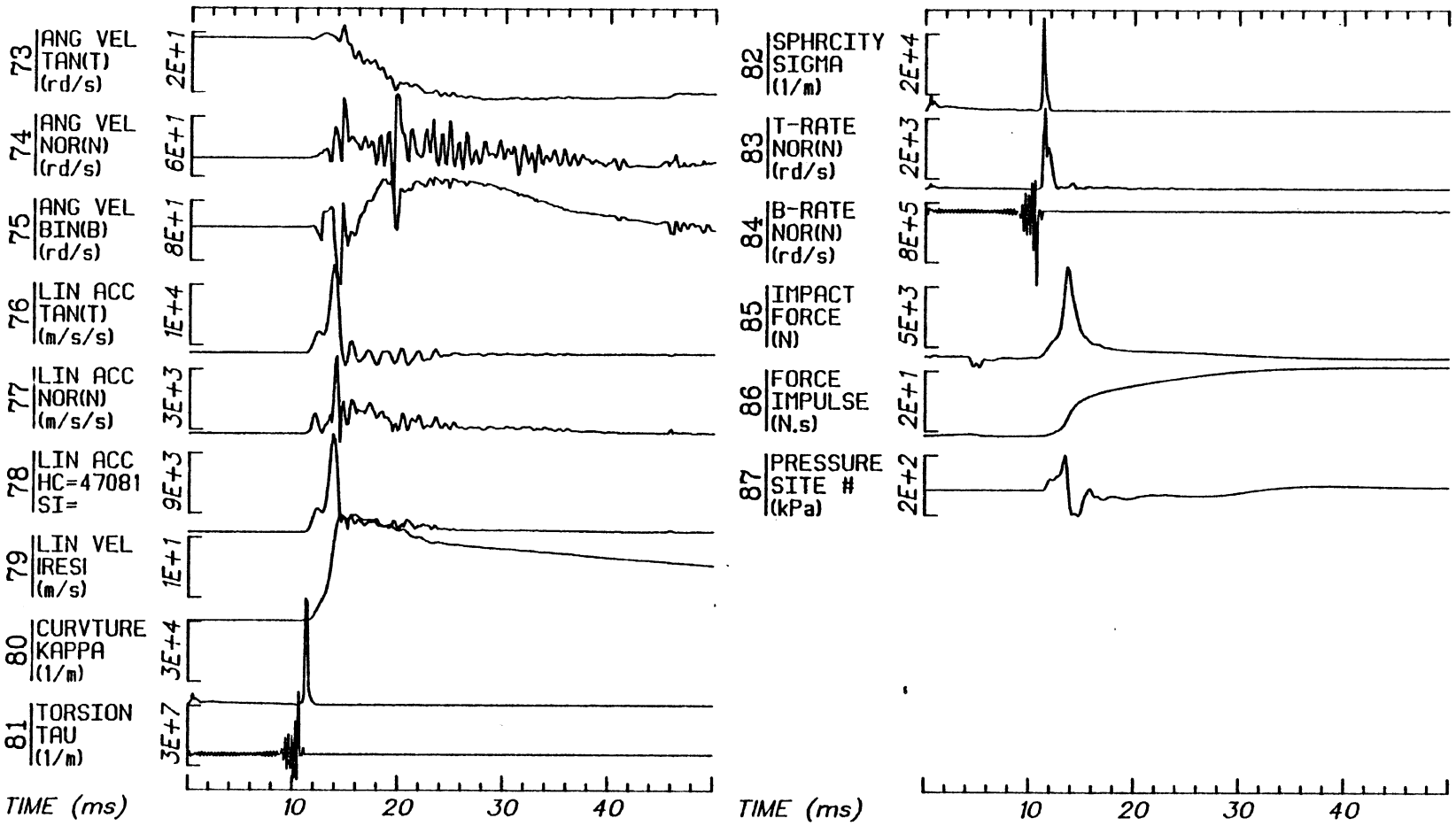

Run ID: 79A251 Disk: 79A251.3 File: 1 Date: JUN 23, 1985 Sheet: 5

No Filtering

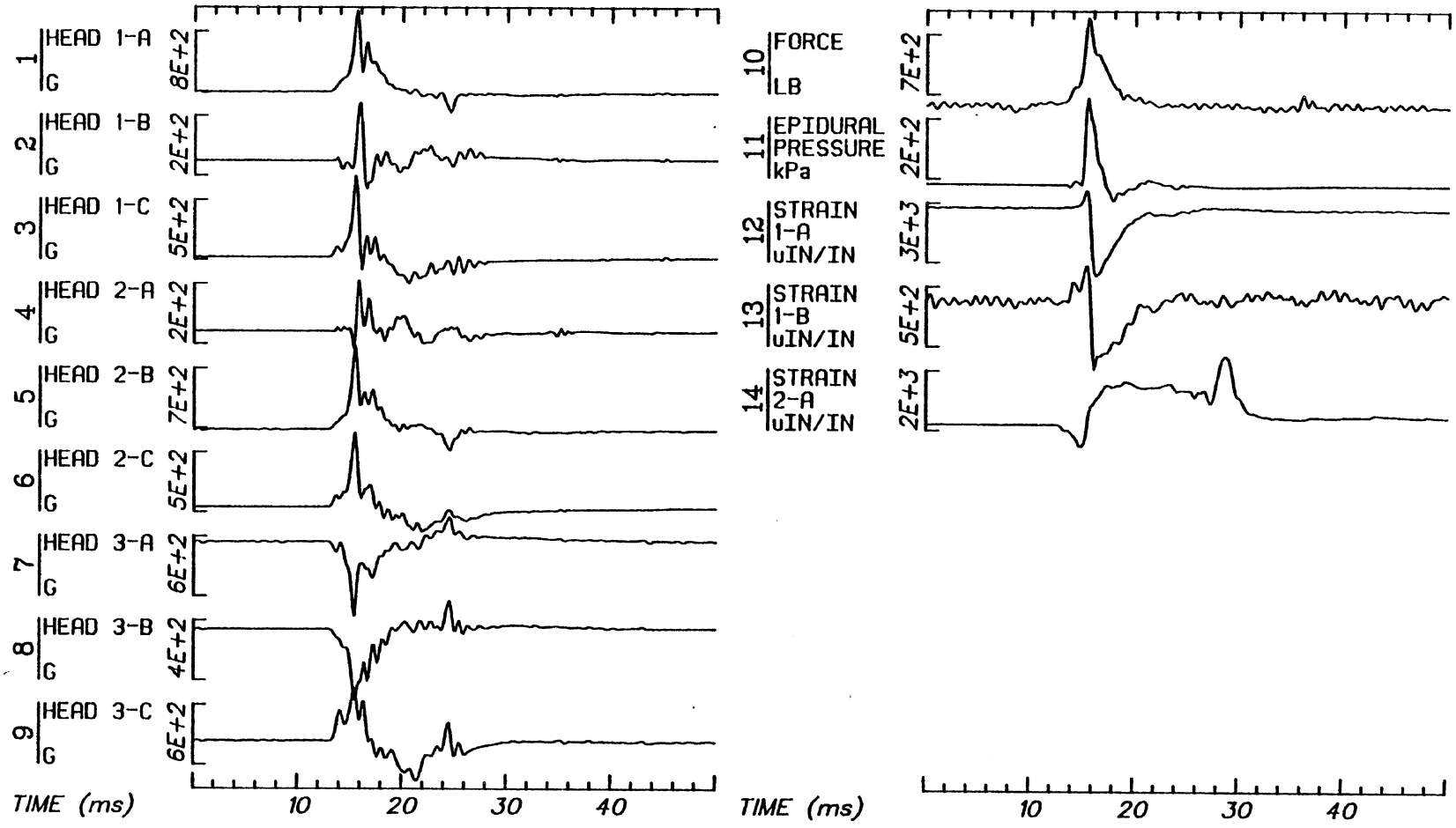

Run ID: 79A253 Disk: 79A253.S File: 1 Date: JUN 16, 1985 Sheet: 1

Filter:1600*4C Smooth: 3SD SIDFA DATA: Filter – 1600*4C, Smooth – 3SD

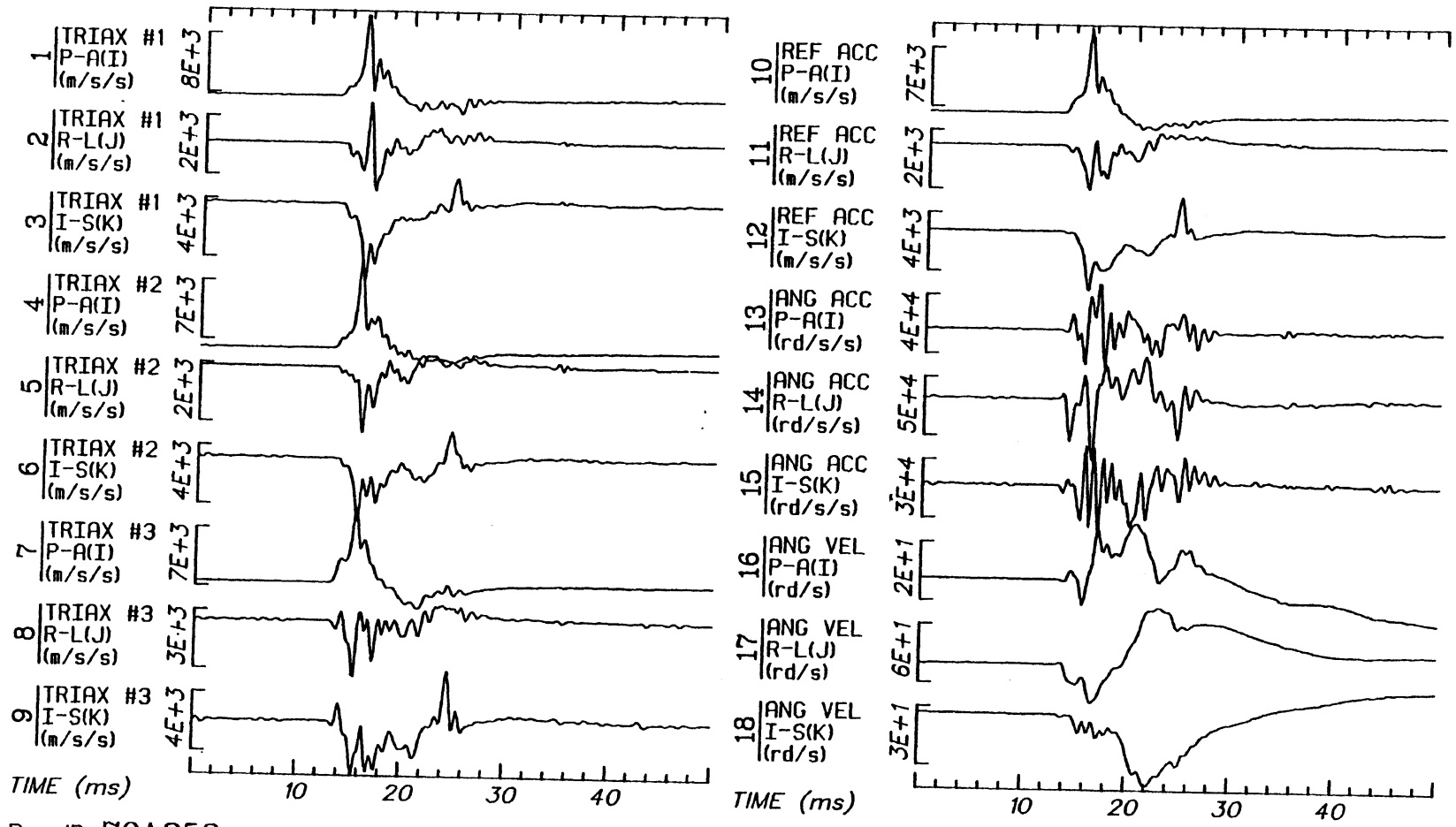

Run ID: 79A253 Disk: 79A253.3 File: 1 Date: JUN 23, 1985 Sheet: 1

No Filtering

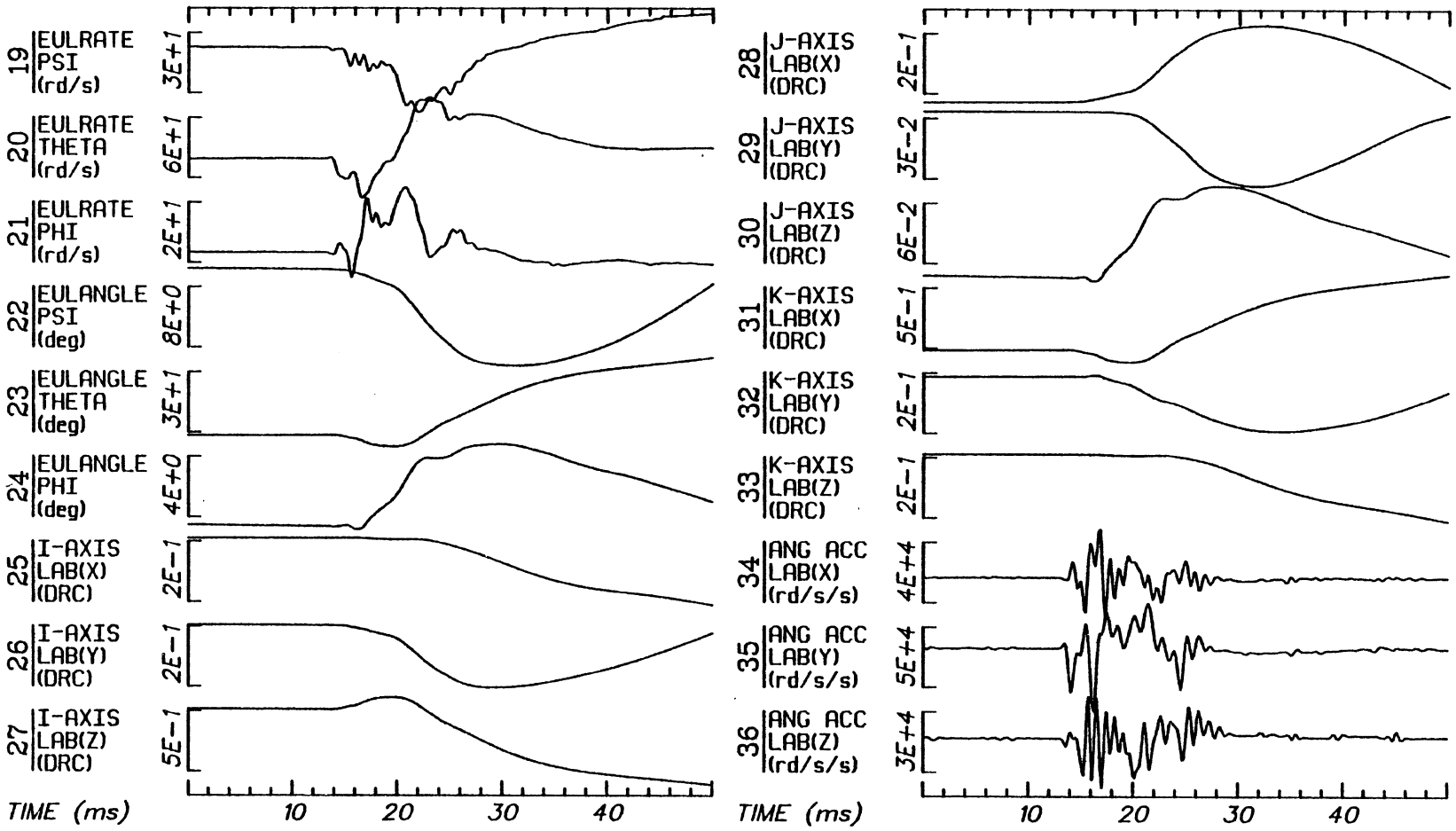

Run ID: 79A253 Disk: 79A253.3 File: 1 Date: JUN 23, 1985 Sheet: 2

No Filtering

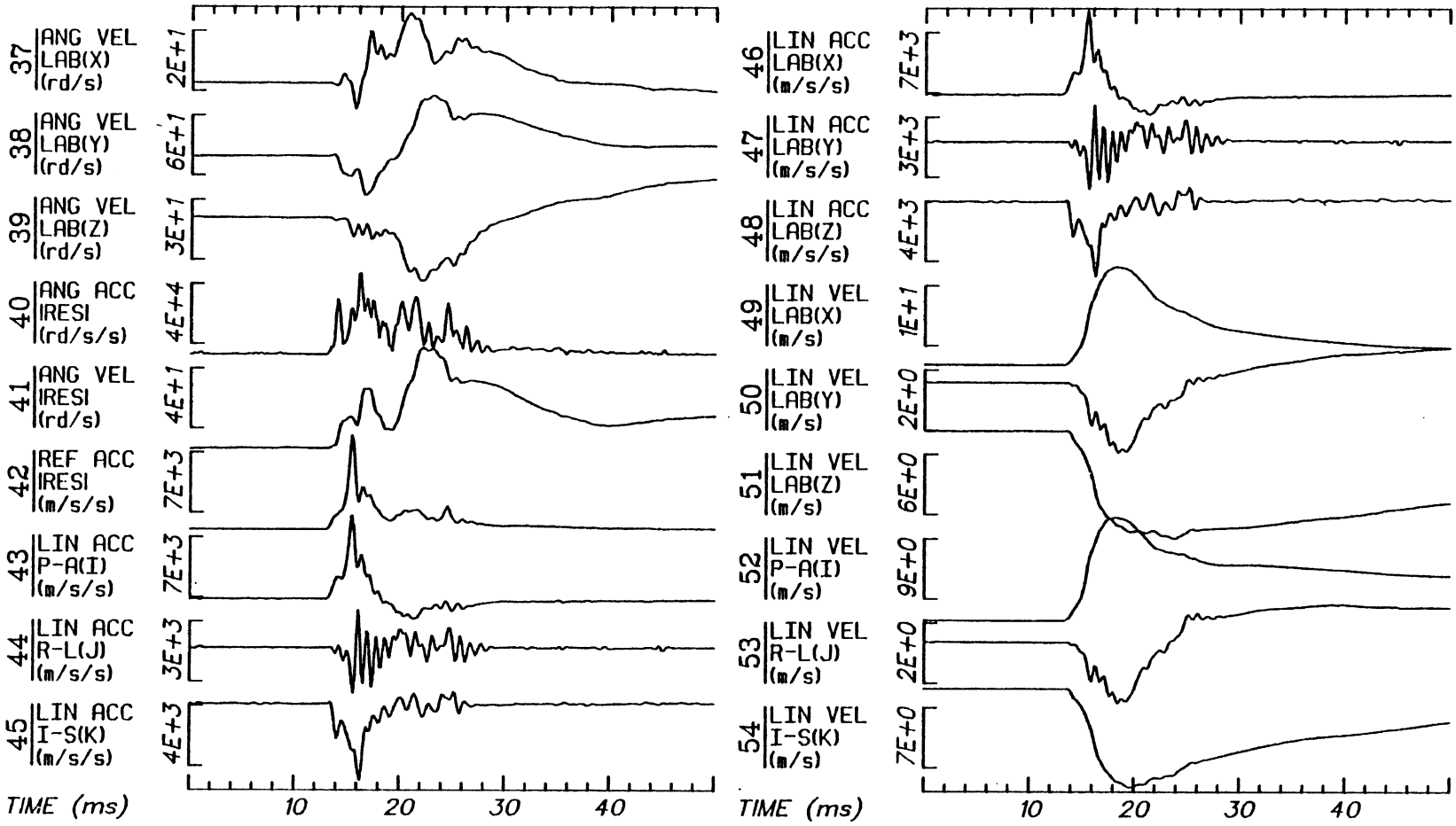

Run ID: 79A253 Disk: 79A253.3 File: 1 Date: JUN 23, 1985 Sheet: 3

No Filtering

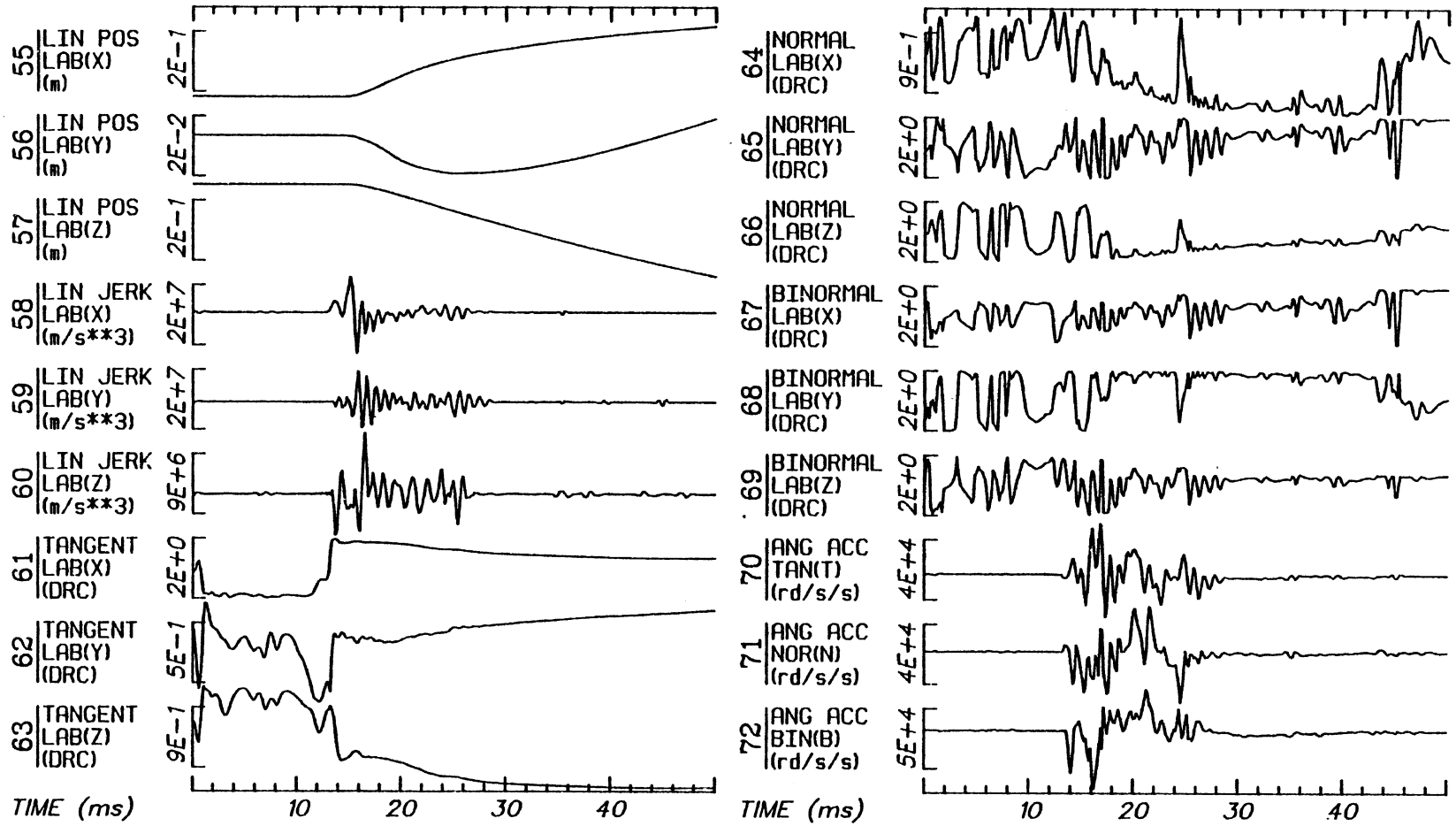

Run ID: 79A253 Disk: 79A253.3 File: 1 Date: JUN 23, 1985 Sheet: 4

No Filtering

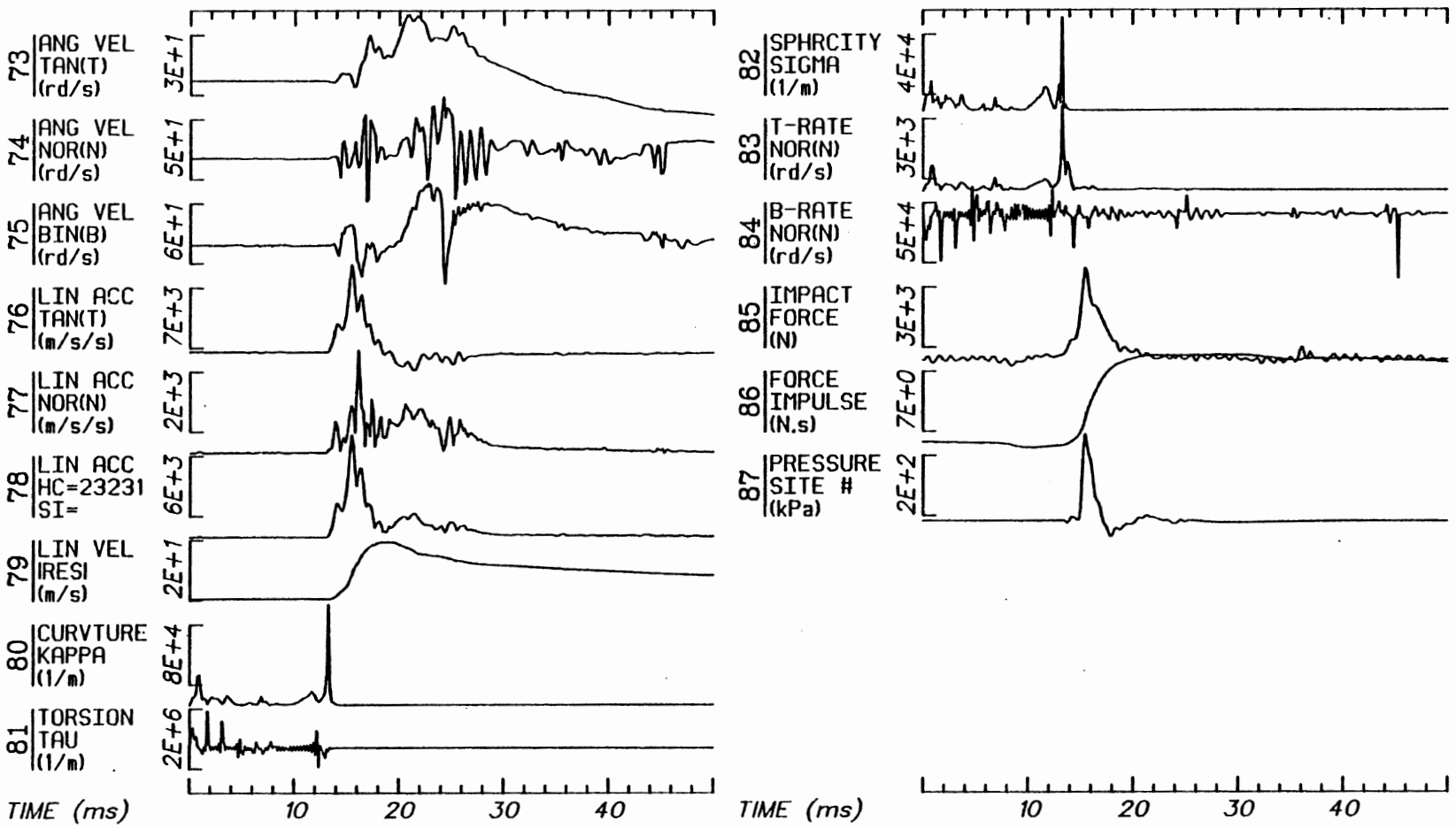

Run ID: 79A253 Disk: 79A253.3 File: 1 Date: JUN 23, 1985 Sheet: 5

No Filtering

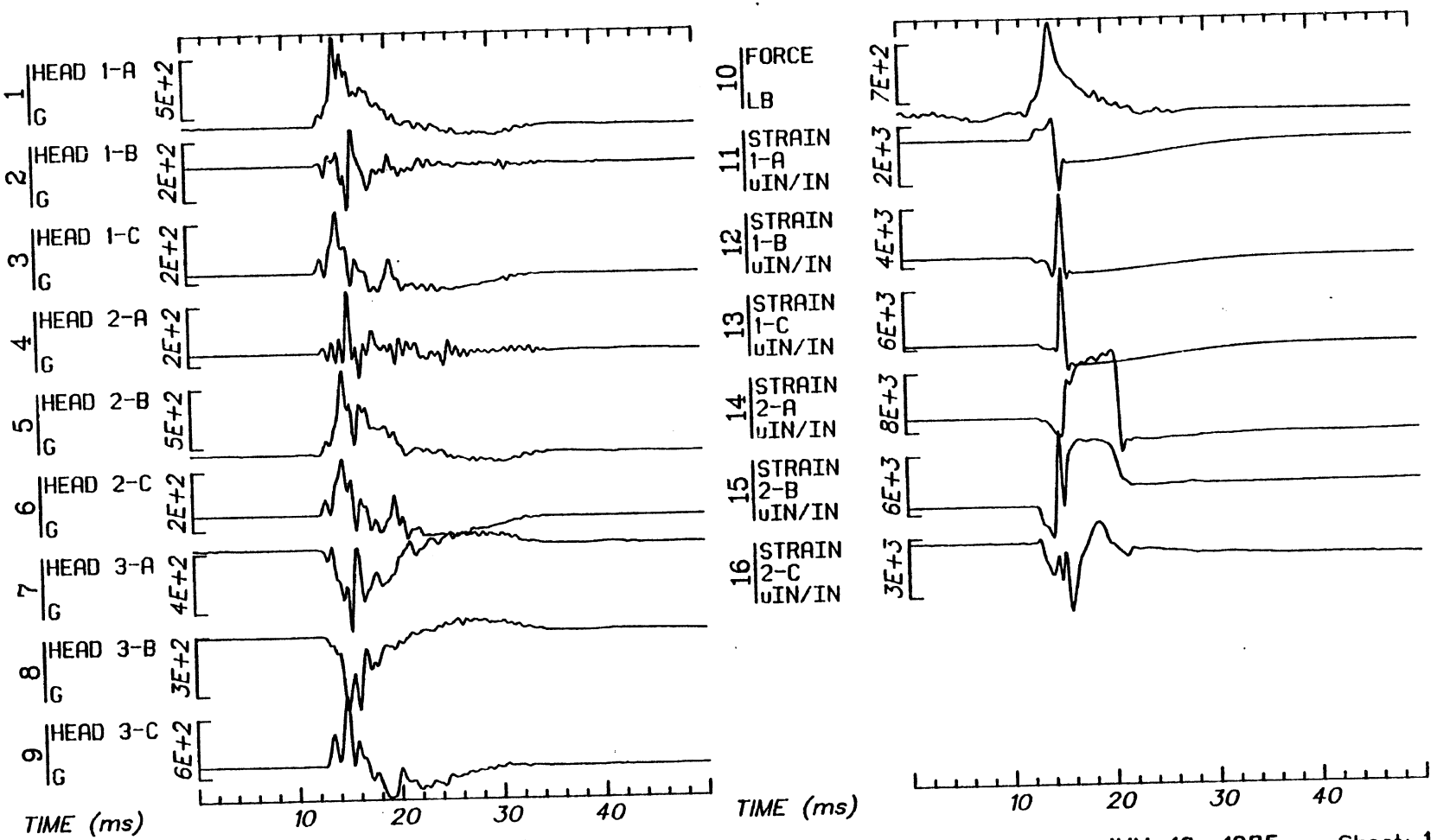

Run ID: 79A256 Disk: 79A256.S File: 1 Date: JUN 16, 1985 Sheet: 1

Filter:1600*4C Smooth: 3SD SIDFA DATA: Filter - 1600*4C, Smooth - 3SD

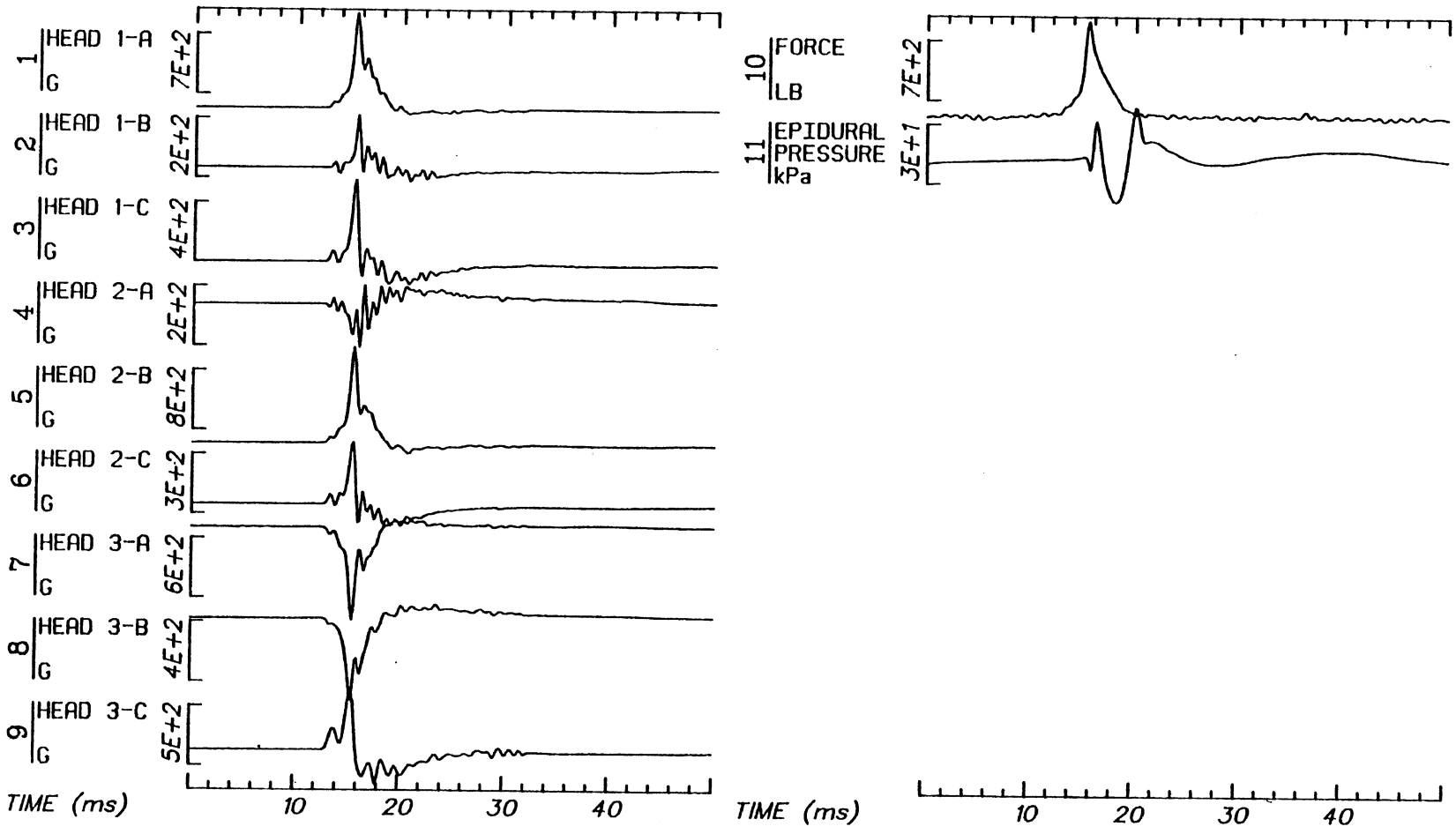

Run ID: 79A258 Disk: 79A258.S File: 1 Date: JUN 16, 1985 Sheet: 1

Filter:1600*4C Smooth: 3SD SIDFA DATA: Filter – 1600*4C, Smooth – 3SD

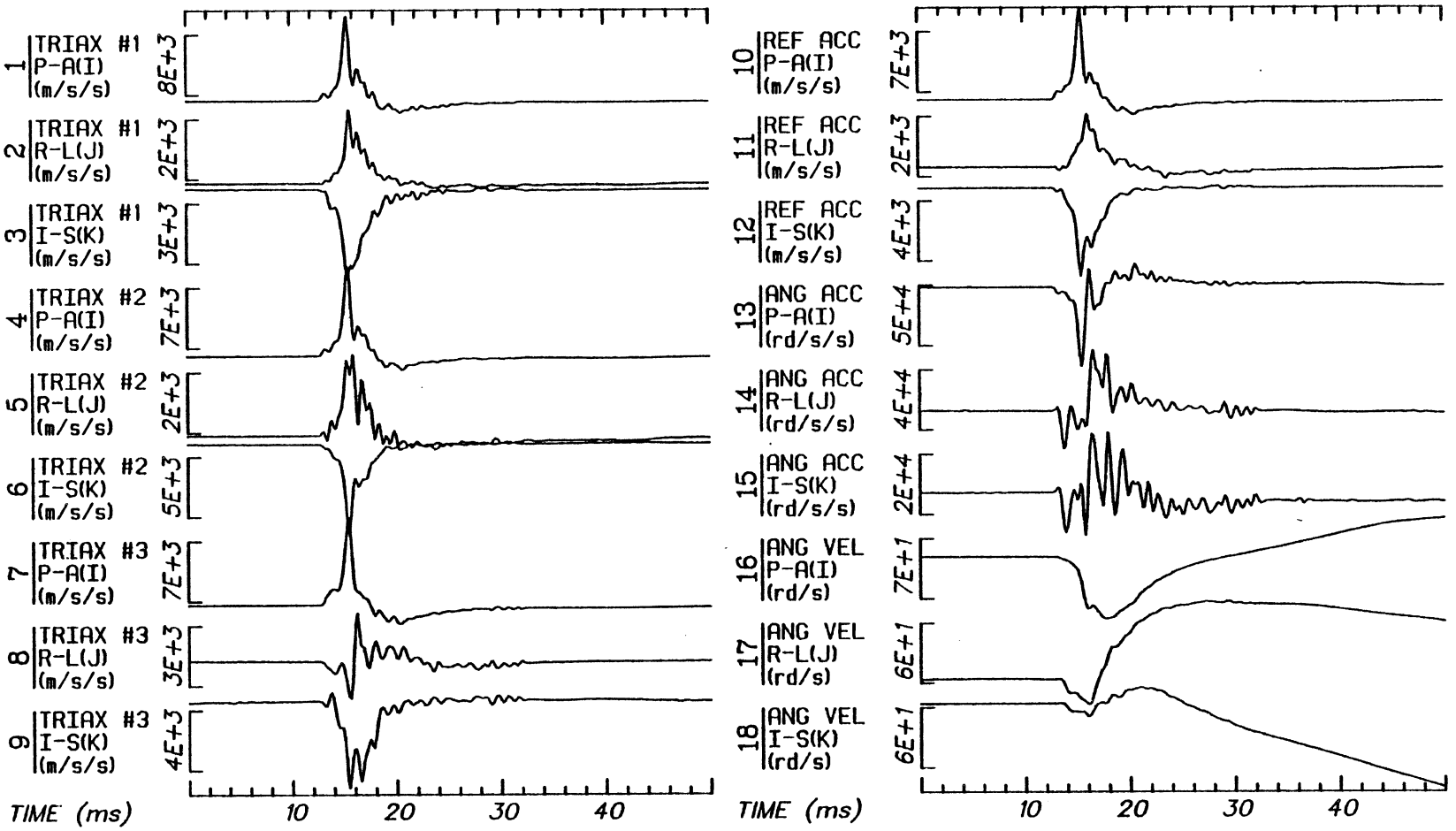

Run ID: 79A258 Disk: 79A258.3 File: 1 Date: JUN 23, 1985 Sheet: 1

No Filtering

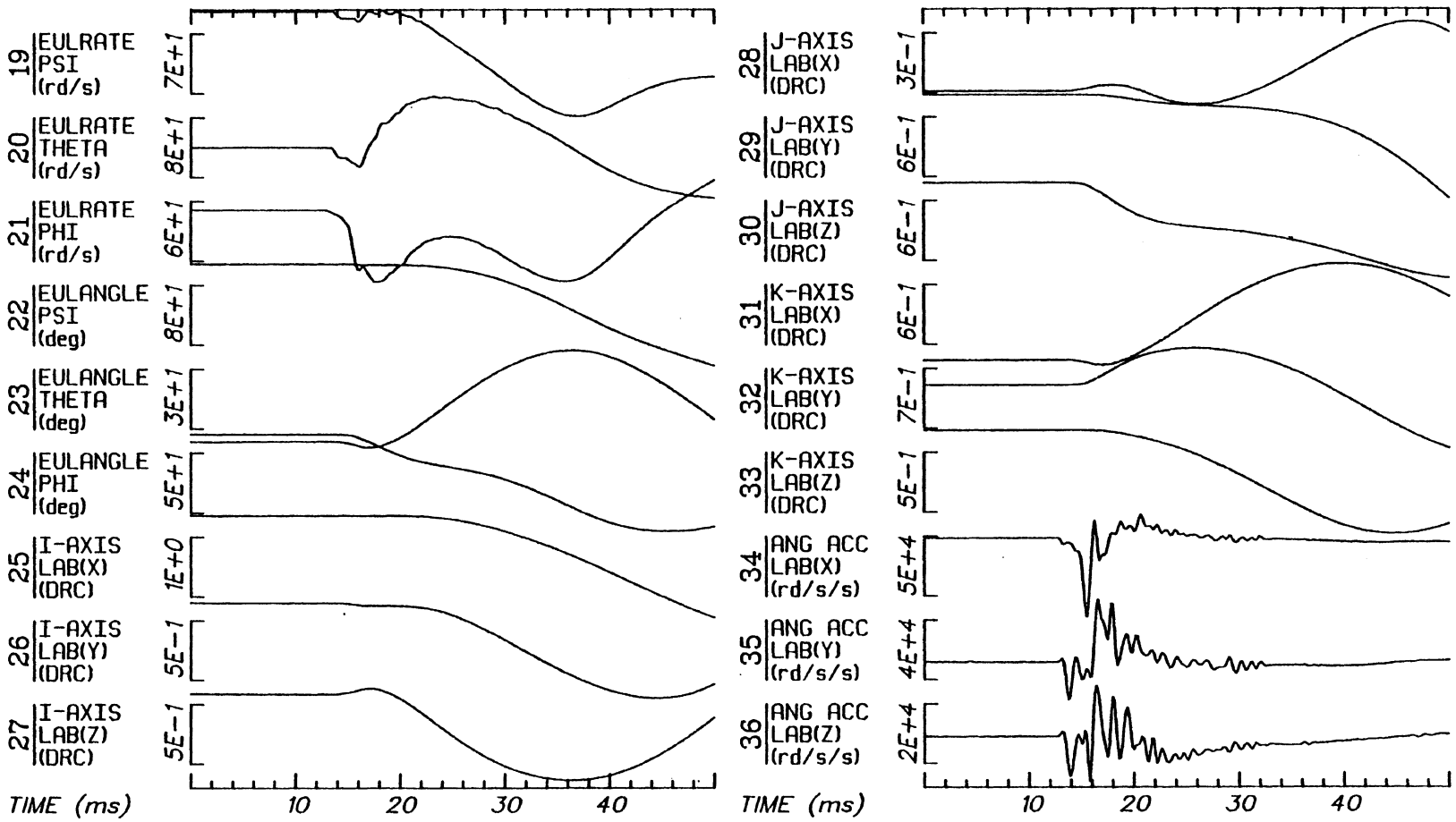

Run ID: 79A258 Disk: 79A258.3 File: 1 Date: JUN 23, 1985 Sheet: 2

No Filtering

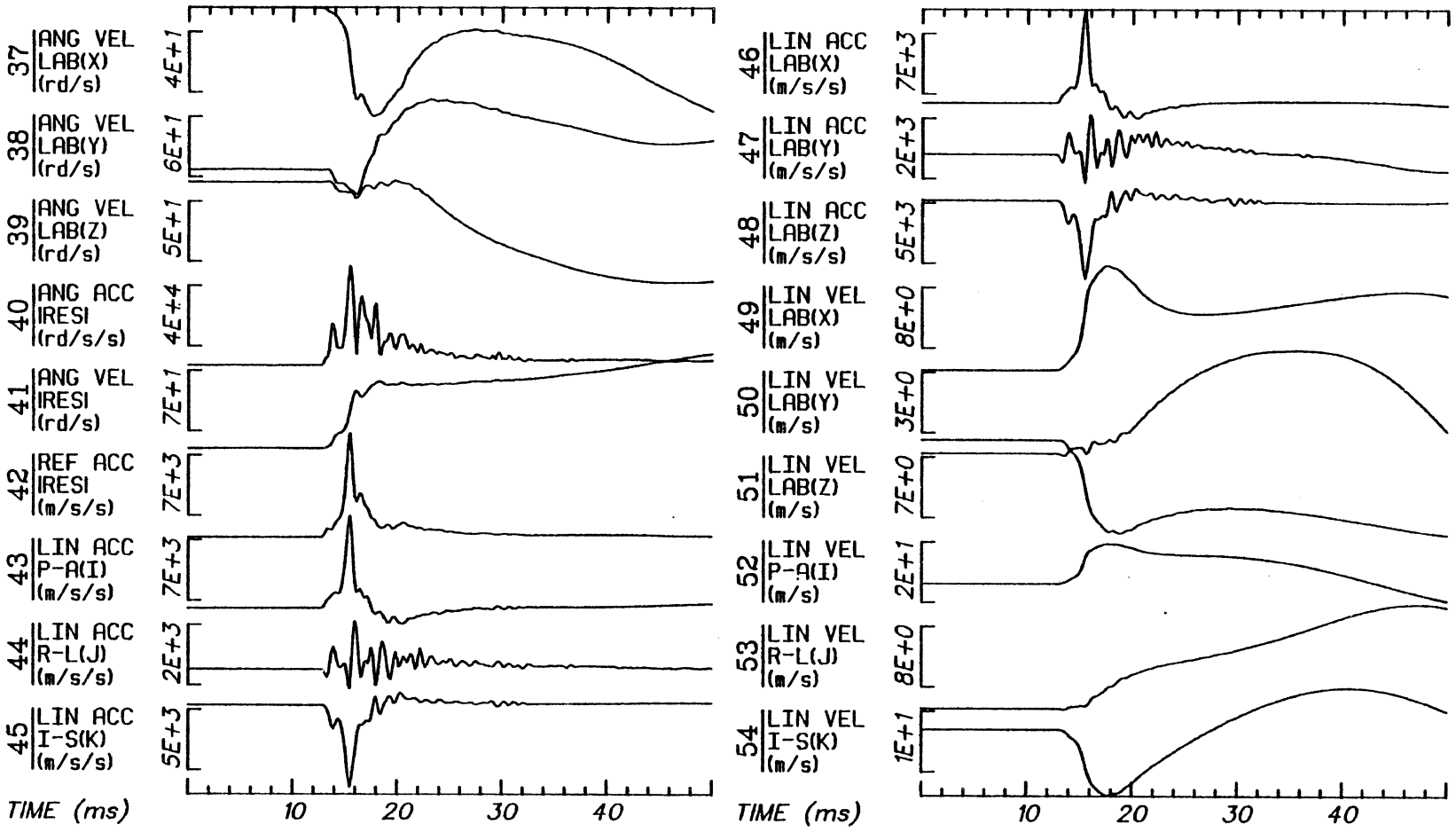

Run ID: 79A258 Disk: 79A258.3 File: 1 Date: JUN 23, 1985 Sheet: 3

No Filtering

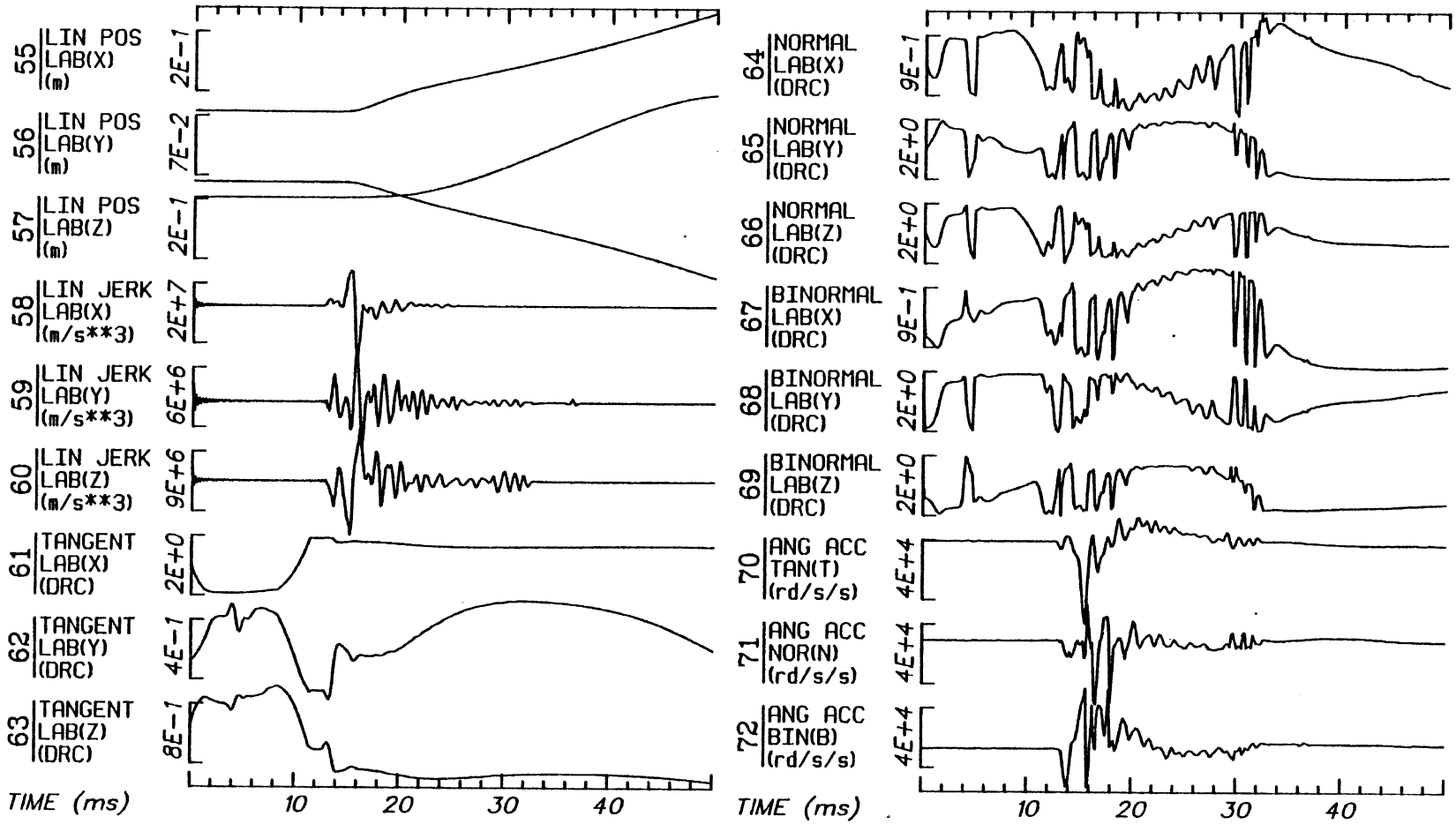

Run ID: 79A258 Disk: 79A258.3 File: 1 Date: JUN 23, 1985 Sheet: 4

No Filtering

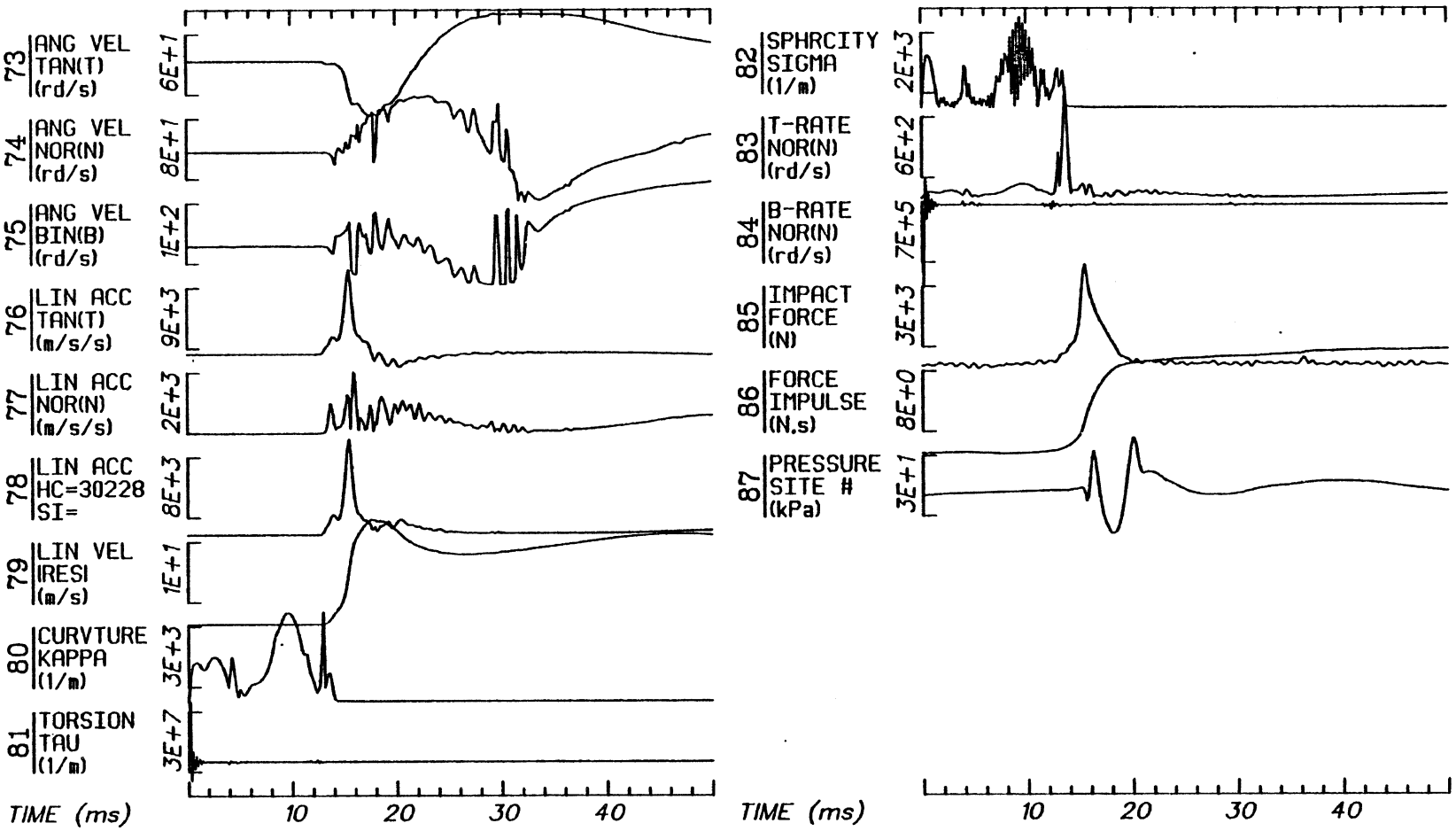

Run ID: 79A258 Disk: 79A258.3 File: 1 Date: JUN 23, 1985 Sheet: 5

No Filtering

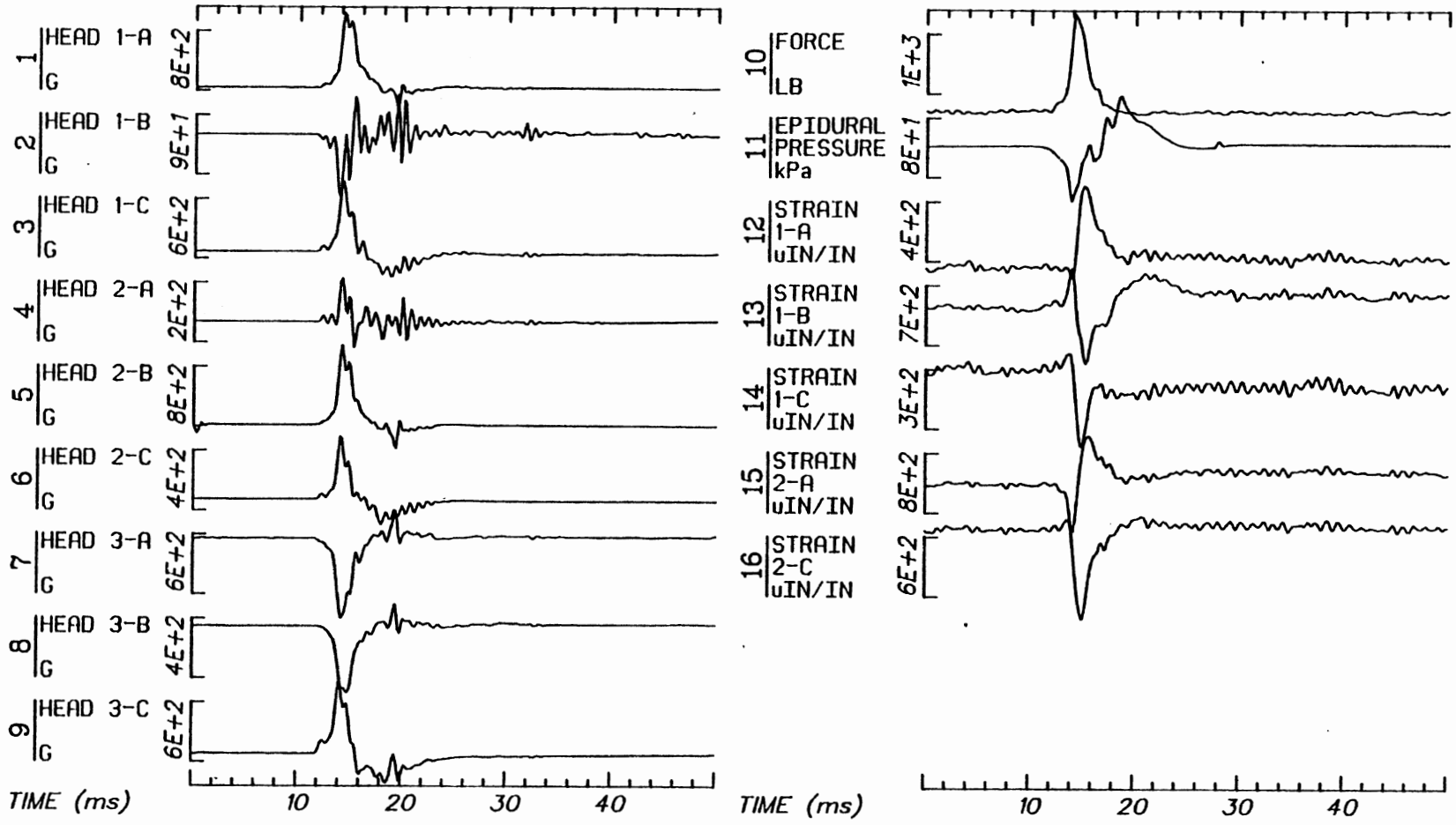

Run ID: 79A260 Disk: 79A260.S File: 1 Date: JUN 16, 1985 Sheet: 1

Filter:1600*4C Smooth: 3SD SIDFA DATA: Filter – 1600*4C, Smooth – 3SD

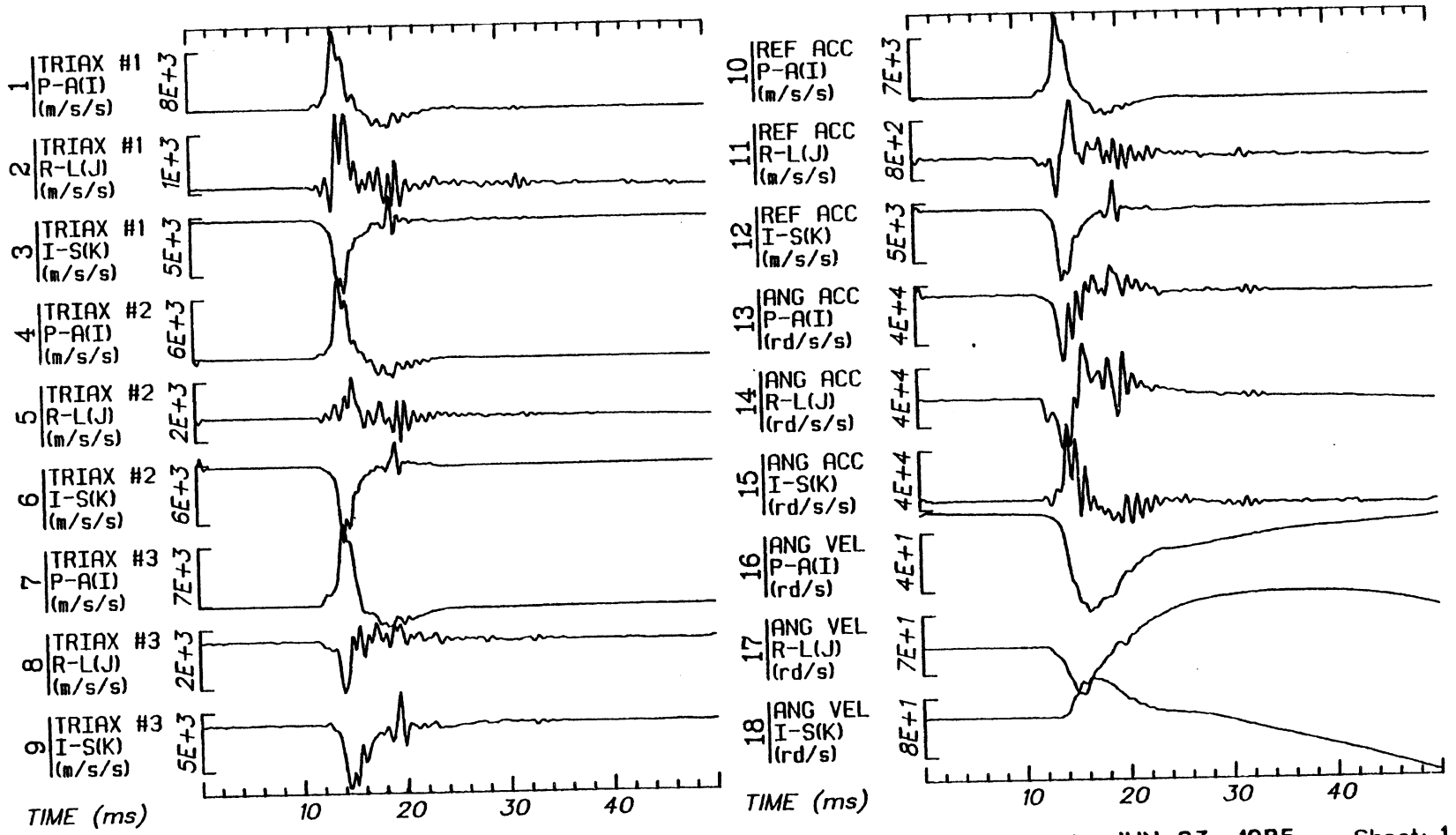

Run ID: 79A260 Disk: 79A260.3 File: 1 Date: JUN 23, 1985 Sheet: 1

No Filtering

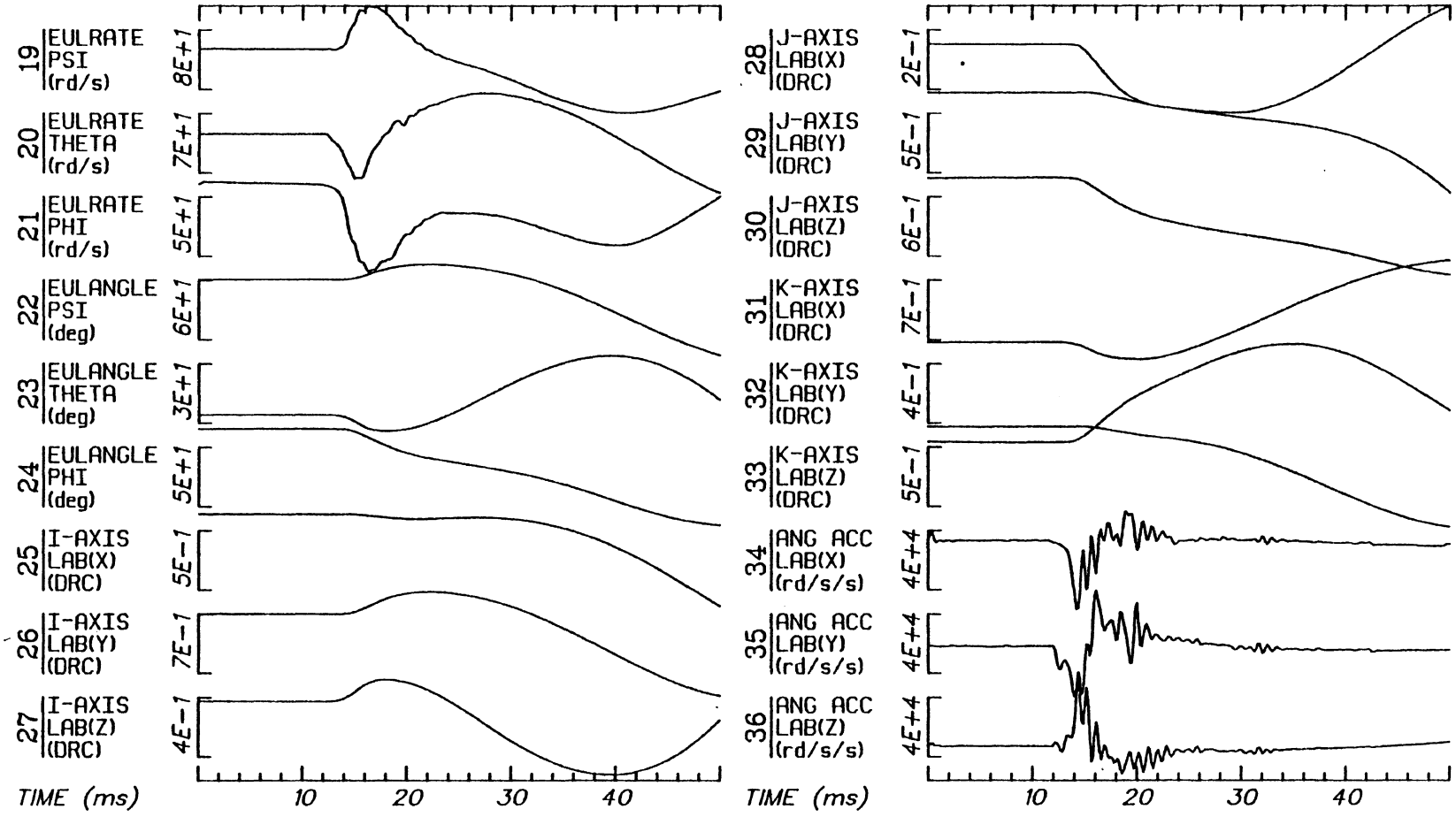

Run ID: 79A260 Disk: 79A260.3 File: 1 Date: JUN 23, 1985 Sheet: 2

No Filtering

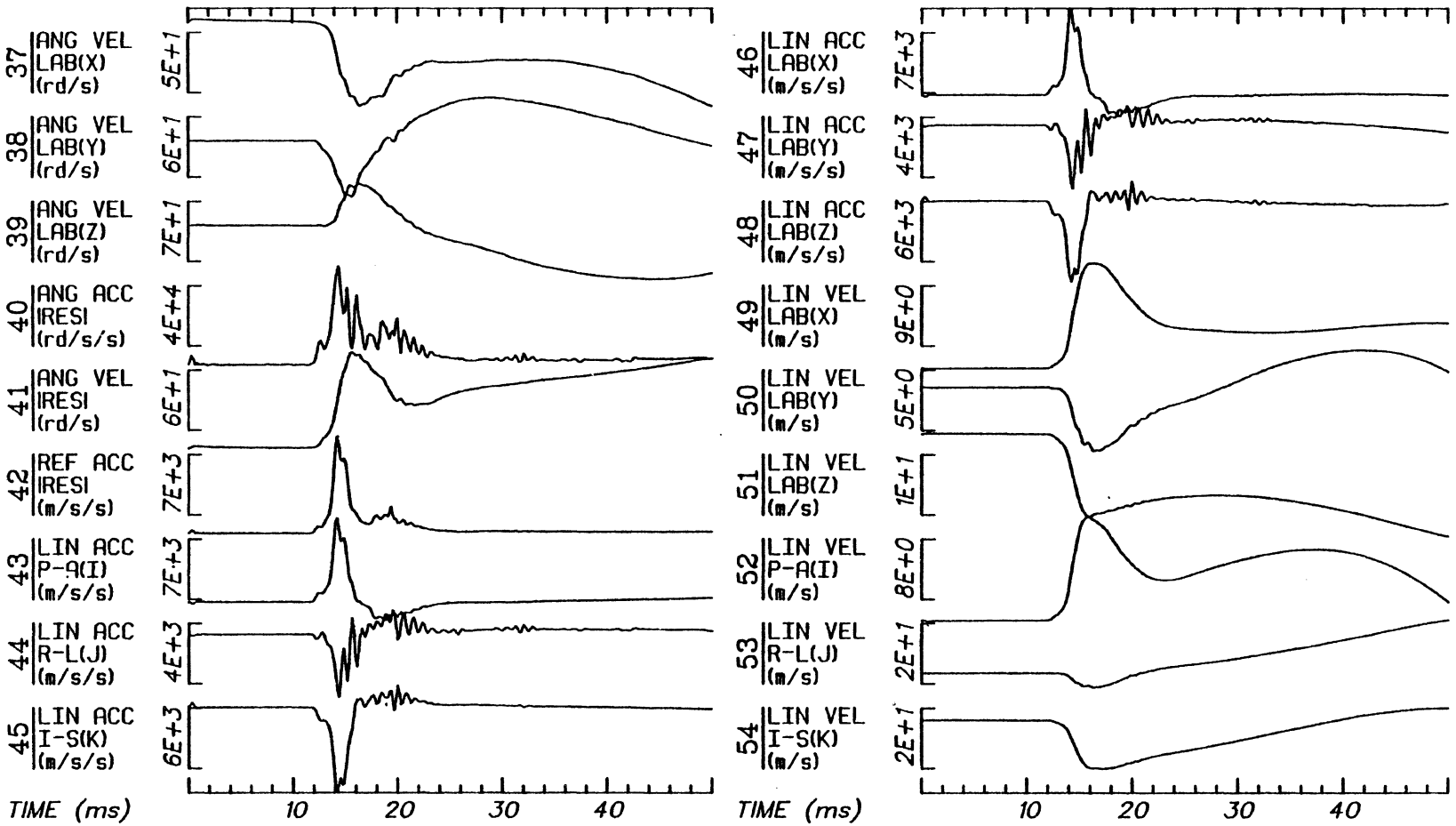

Run ID: 79A260 Disk: 79A260.3 File: 1 Date: JUN 23, 1985 Sheet: 3

No Filtering

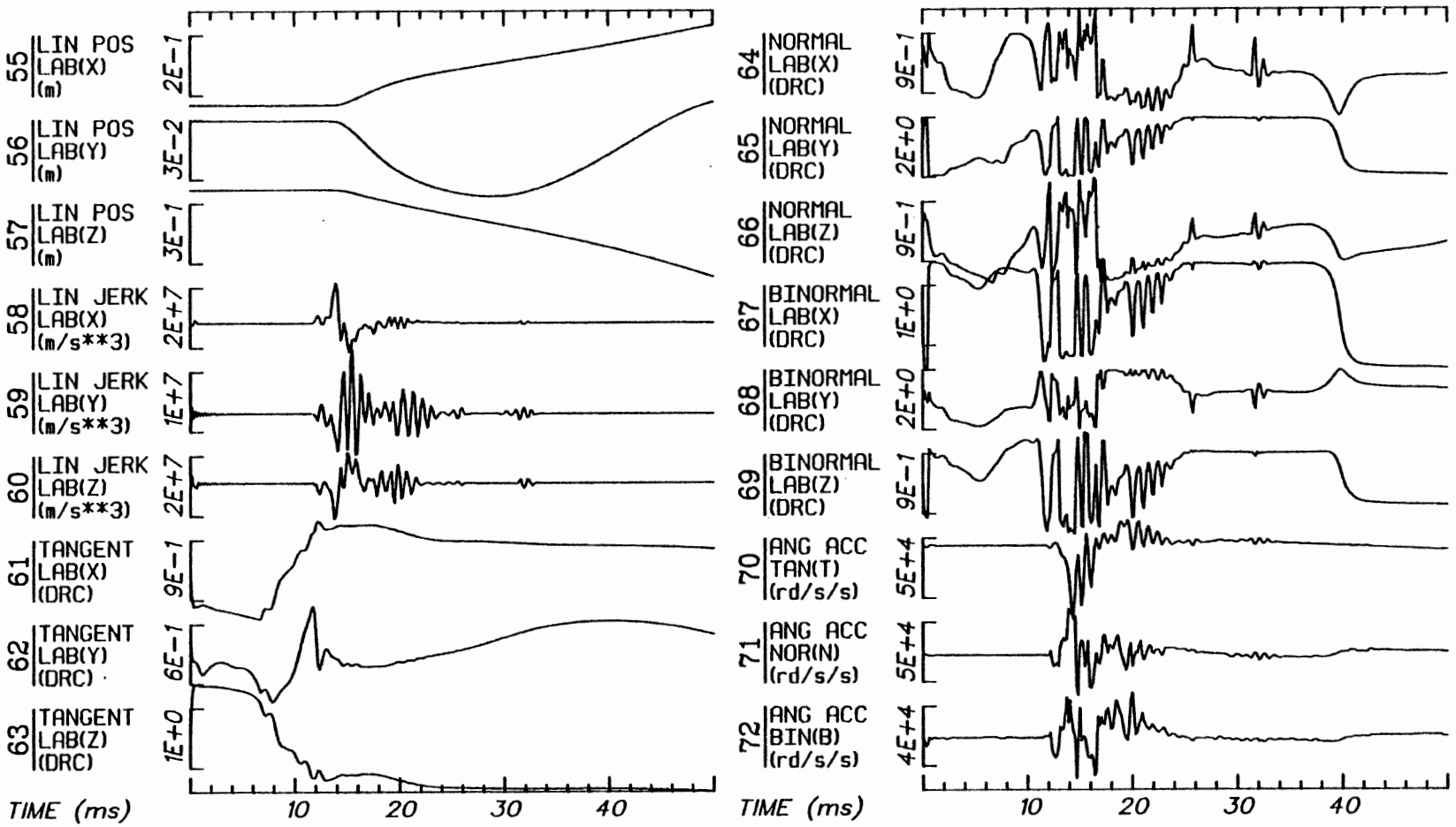

Run ID: 79A260 Disk: 79A260.3 File: 1 Date: JUN 23, 1985 Sheet: 4

No Filtering

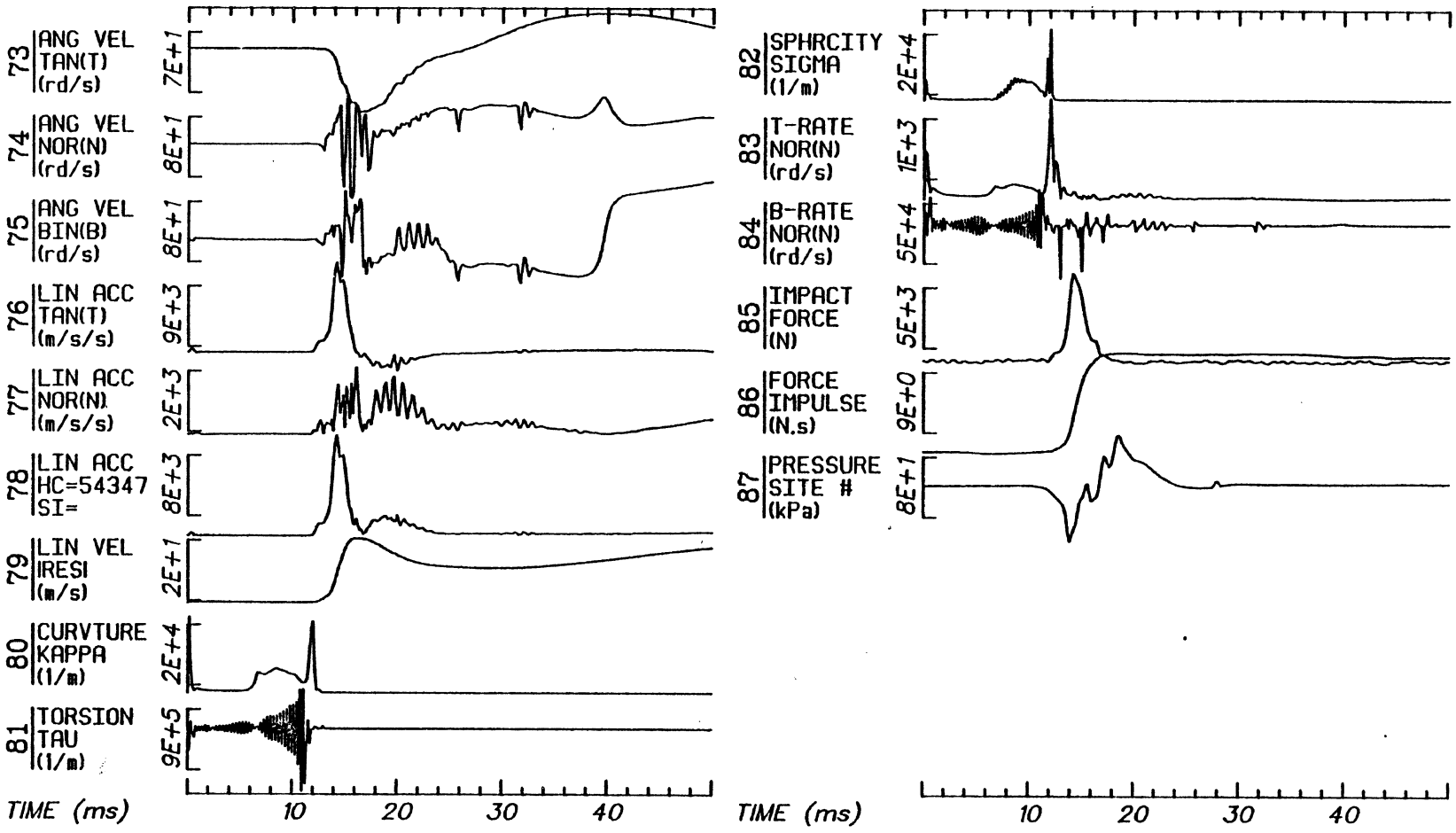

Run ID: 79A260 Disk: 79A260.3 File: 1 Date: JUN 23, 1985 Sheet: 5

No Filtering

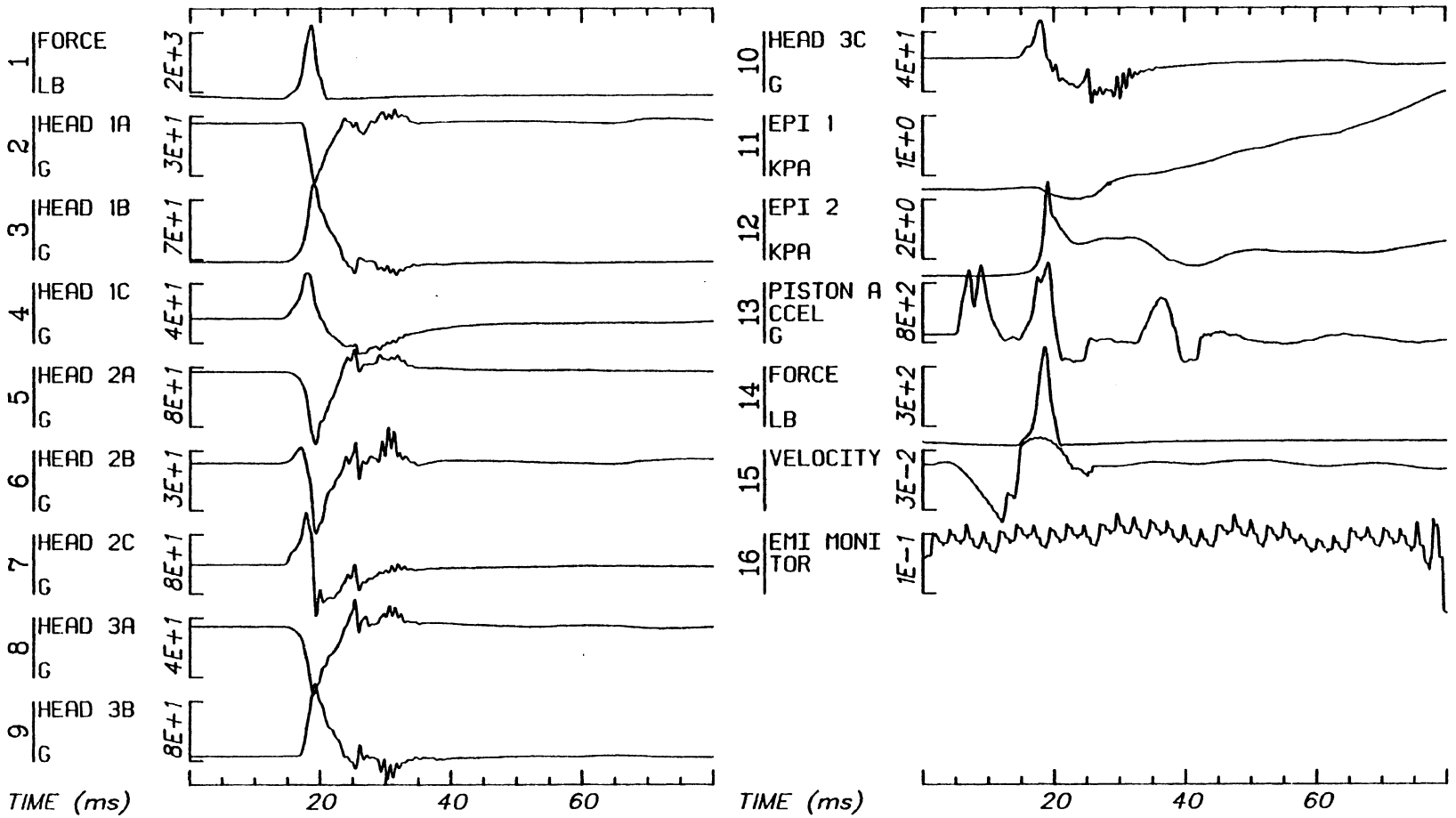

Run ID: 85R002 H9 Disk: R002.SD File: 1 Date: MAR 27, 1986 Sheet: 1

*Filter:1000*4C Smooth: 3SD*

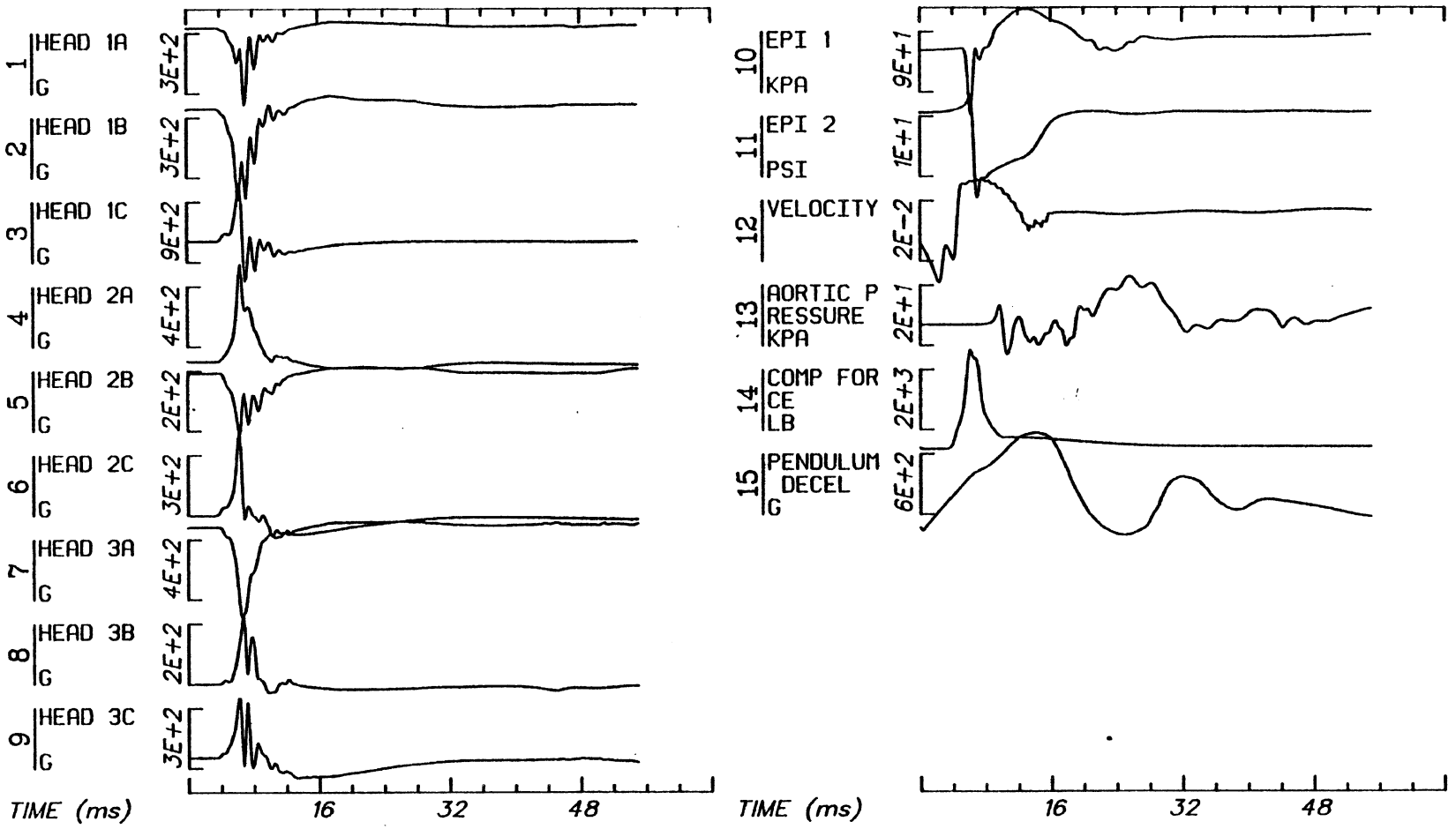

Run ID: 85R005 H9 Disk: R005.SD File: 1 Date: MAR 28, 1986 Sheet: 1

Filter:1000*4C Smooth: 3SD

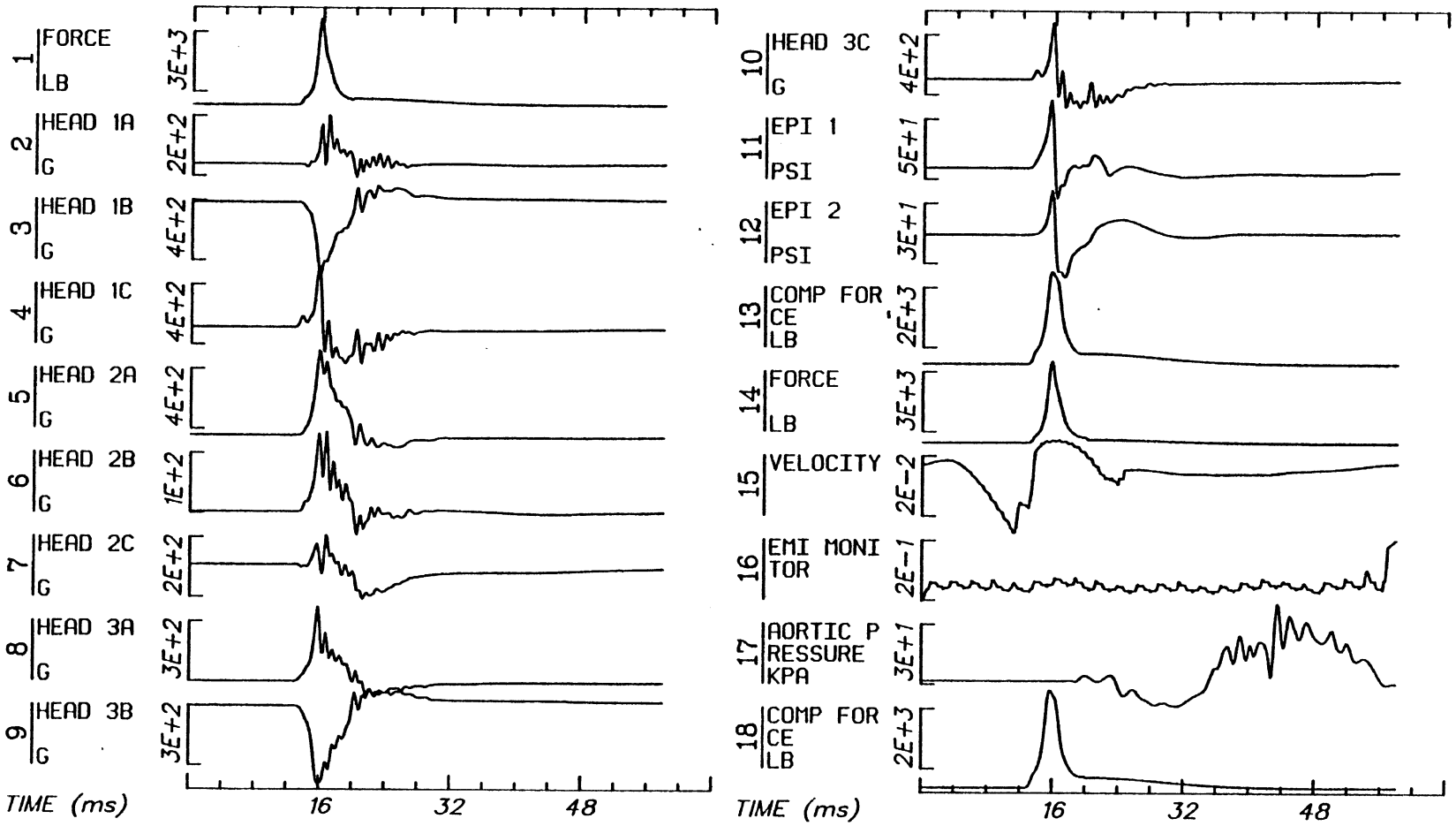

Run ID: 85R006 H9 Disk: R006.SD File: 1 Date: MAR 30, 1986 Sheet: 1

Filter:1000*4C Smooth: 3SD

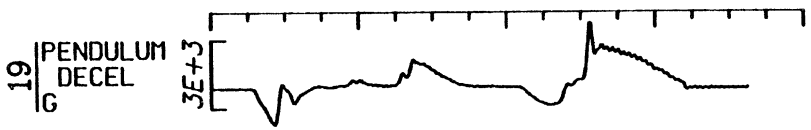

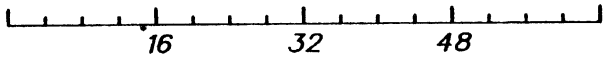

Run ID: 85R006 H9 Disk: R006.SD File: 1 Date: MAR 30, 1986 Sheet: 2

Filter:1000*4C Smooth: 3SD

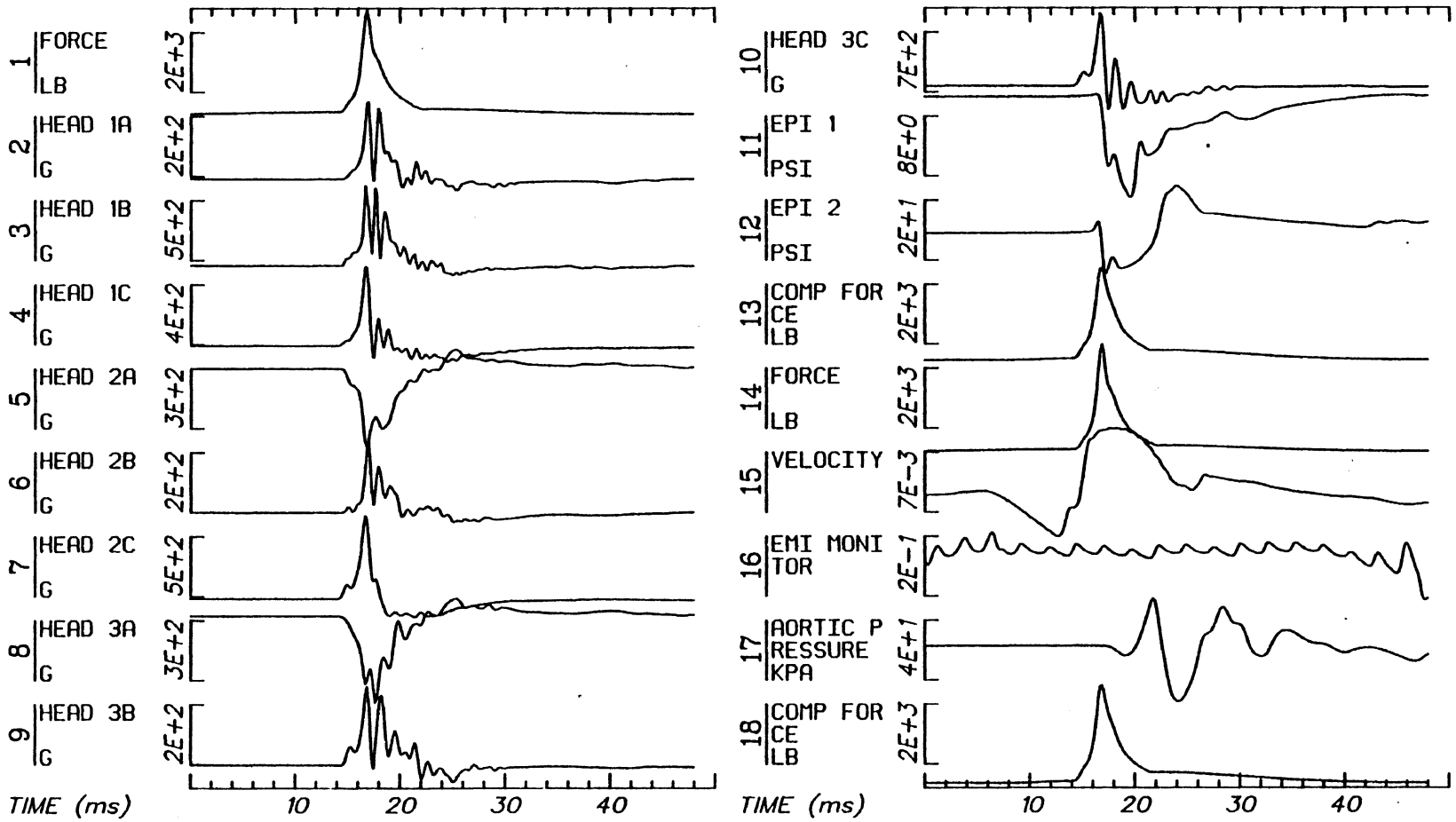

Run ID: 85R008 H9 Disk: R008.SD File: 1 Date: MAR 30, 1986 Sheet: 1

Filter:1000*4C Smooth: 3SD

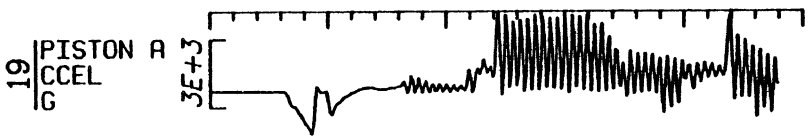

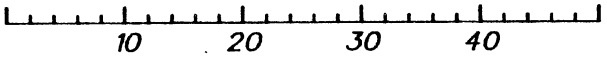

Run ID: 85R008 H9 Disk: R008.SD File: 1 Date: MAR 30, 1986 Sheet: 2

*Filter:1000*4C Smooth: 3SD*

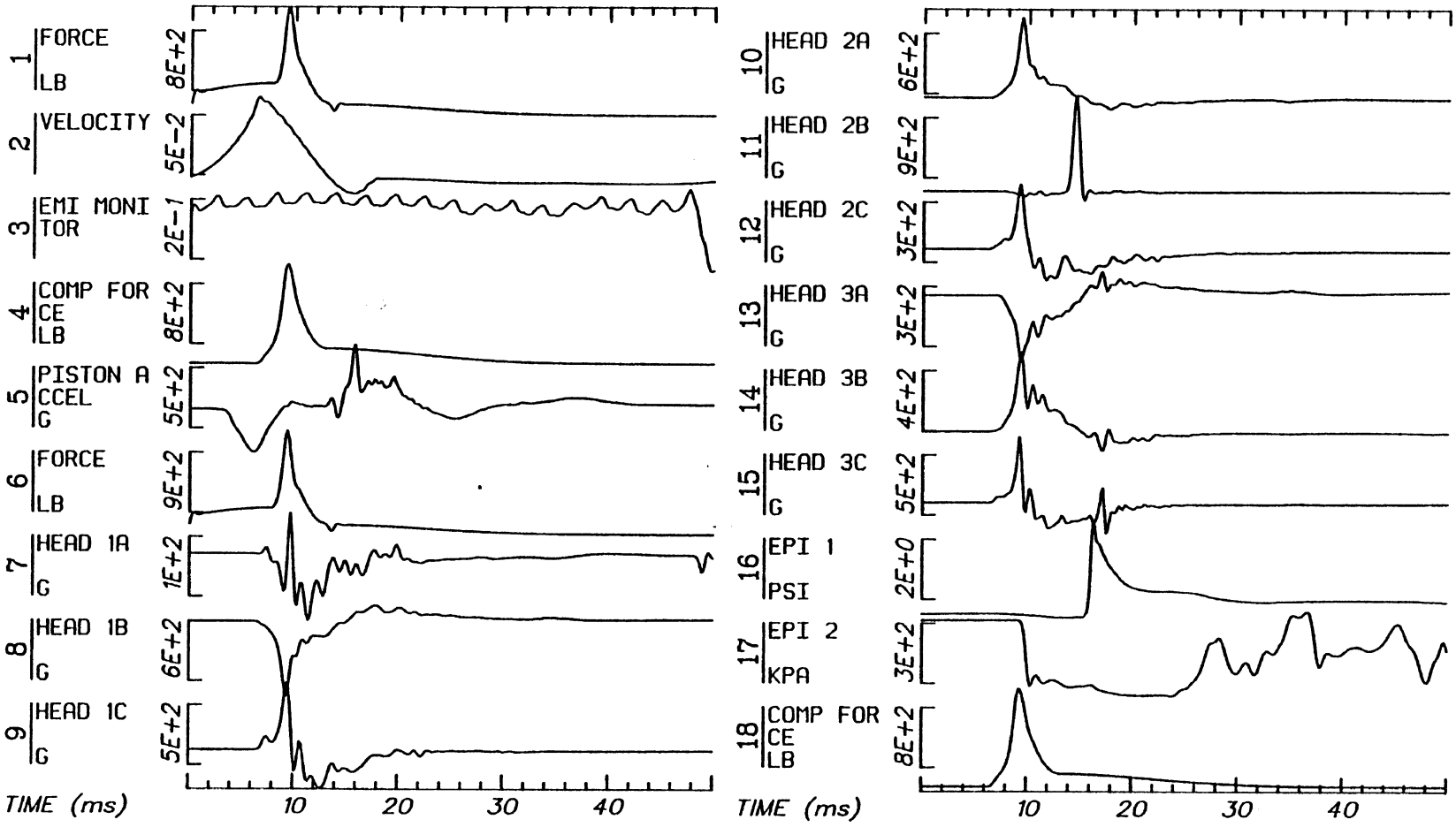

Run ID: 86R010 H7 Disk: R010.SD File: 1 Date: MAR 30, 1986 Sheet: 1

Filter:1000*4C Smooth: 3SD

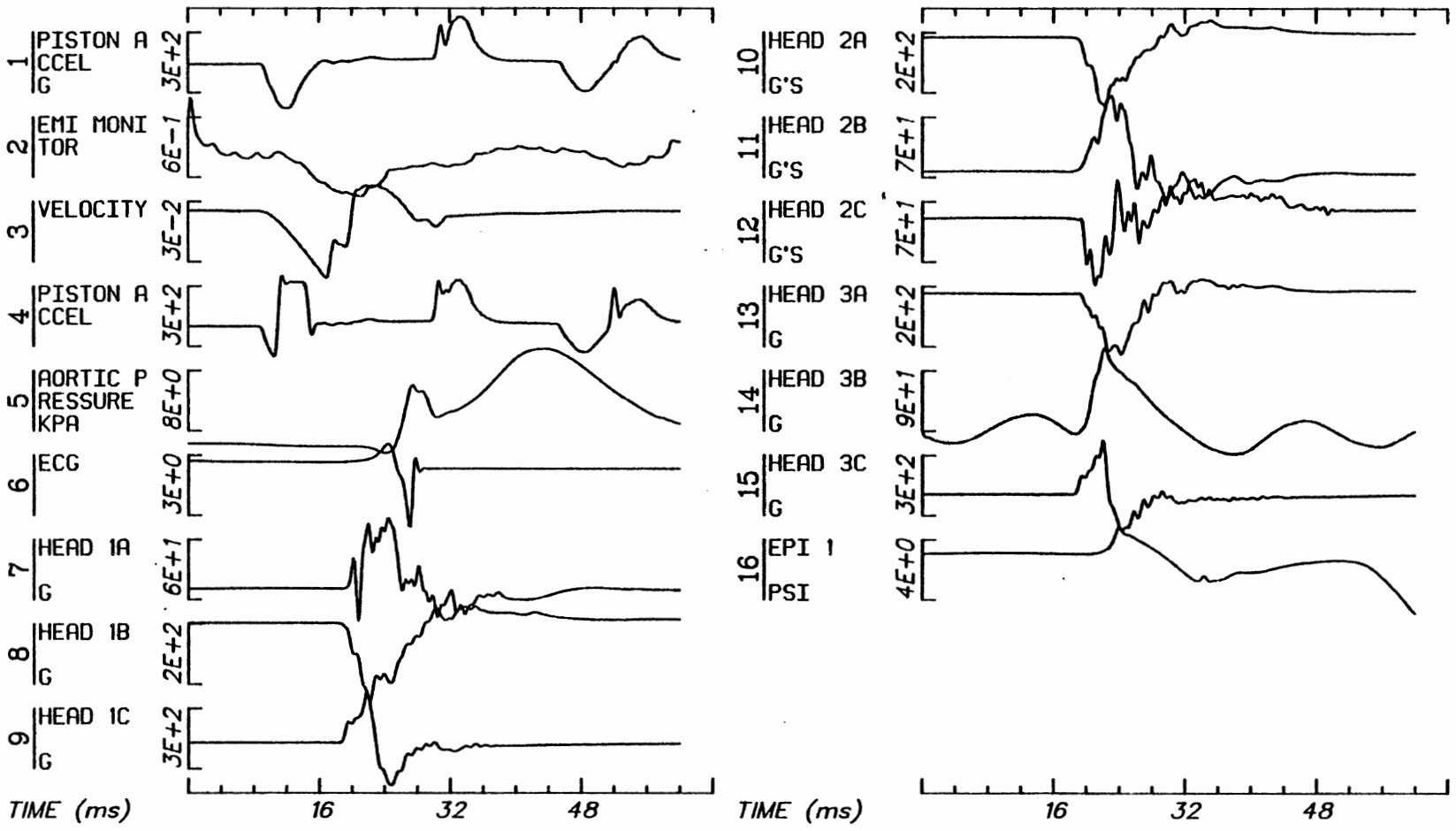

Run ID: 86R011 H7 Disk: R011.SD File: 1 Date: MAR 30, 1986 Sheet: 1

Filter:1000*4C Smooth: 3SD

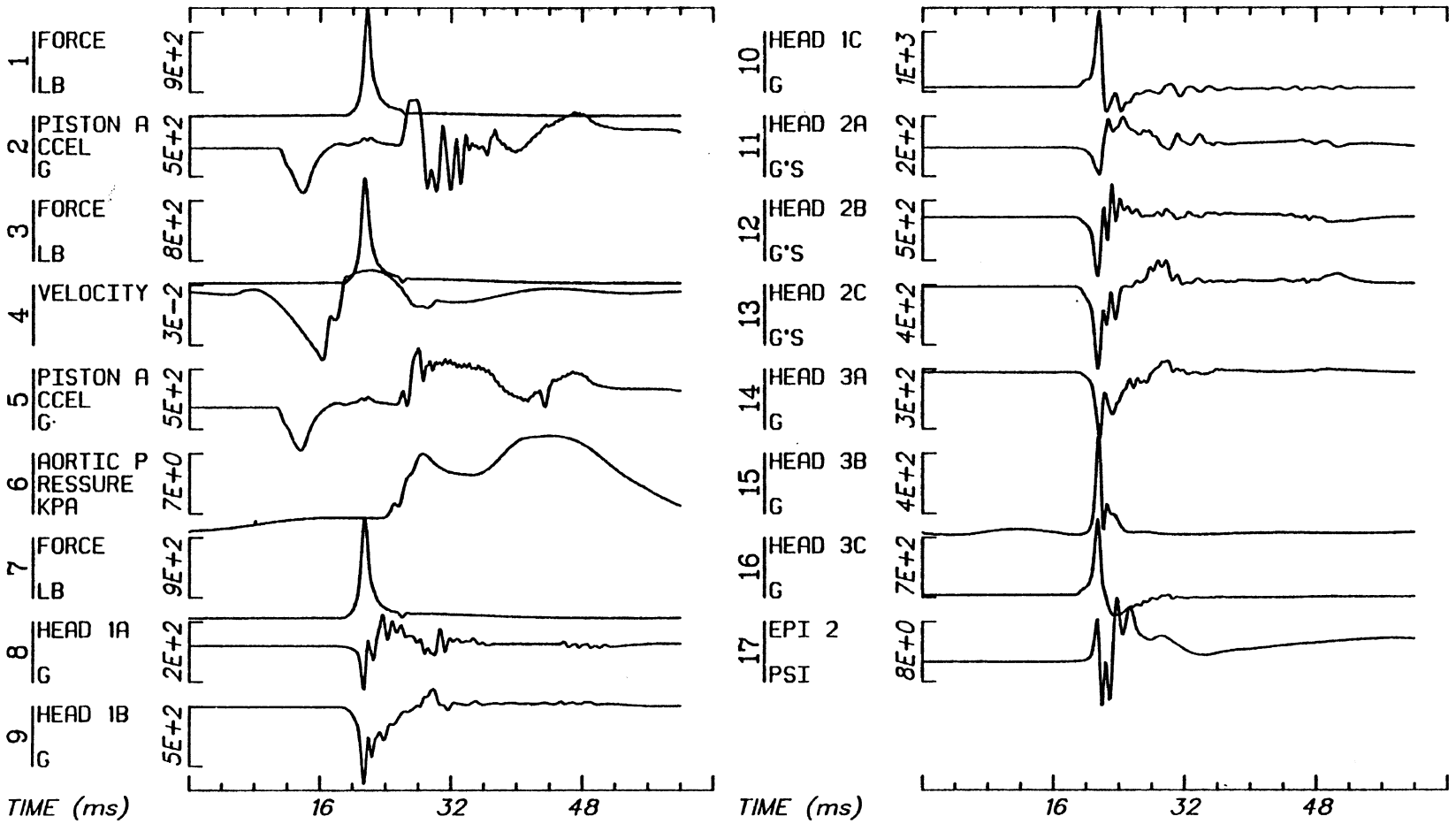

Run ID: 86R012 H7 Disk: R012.SD File: 1 Date: MAR 30, 1986 Sheet: 1

Filter:1000*4C Smooth: 3SD

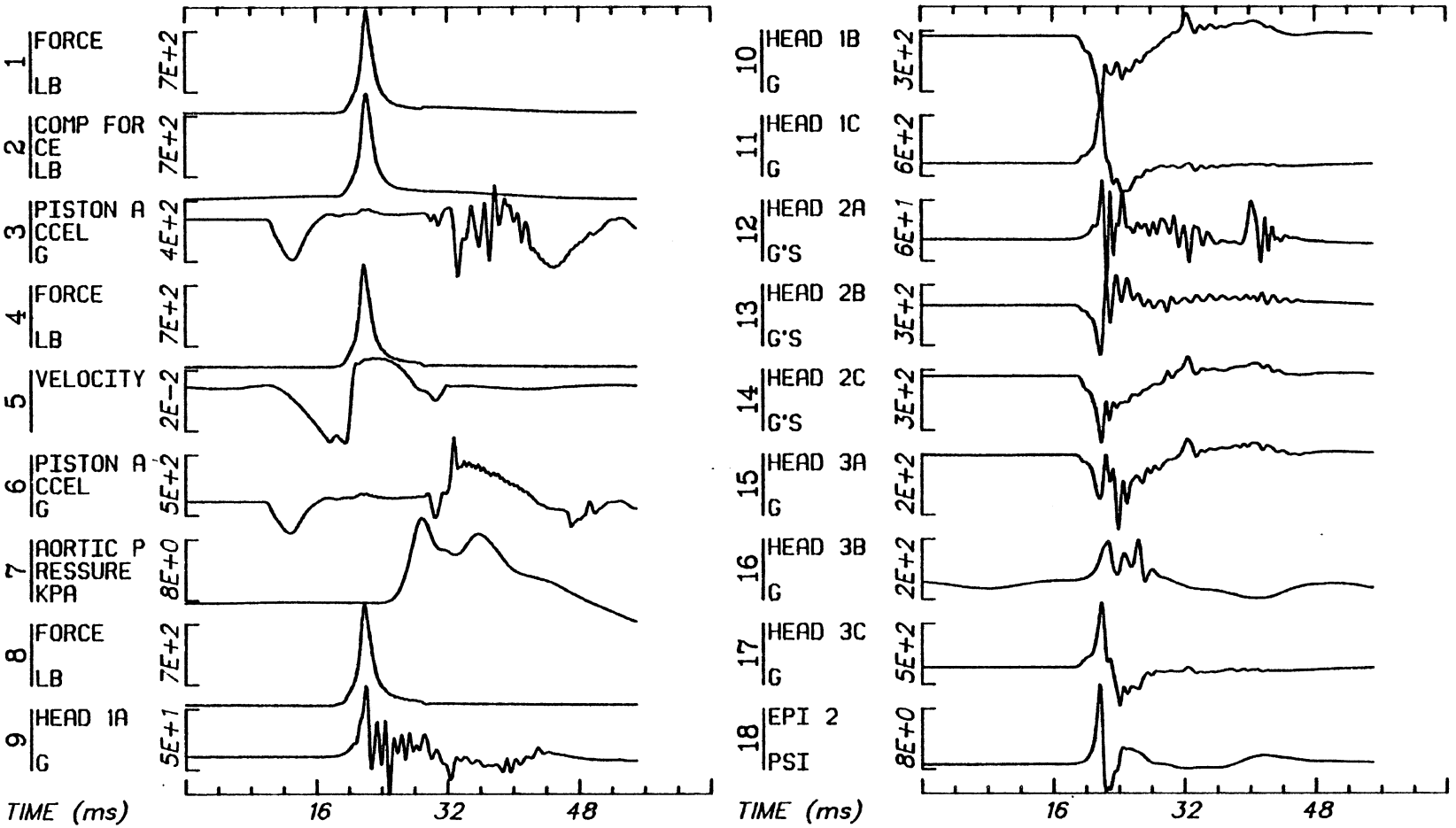

Run ID: 86R013 H7 Disk: r013.sd File: 1 Date: JUN 9, 1986 Sheet: 1

*Filter:1000*4C Smooth: 3SD*

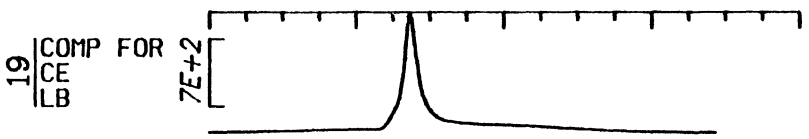

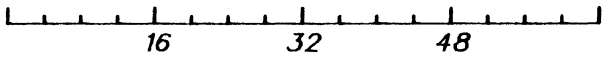

Run ID: 86R013 H7 Disk: r013.sd File: 1 Date: JUN 9, 1986 Sheet: 2

Filter:1000*4C Smooth: 3SD

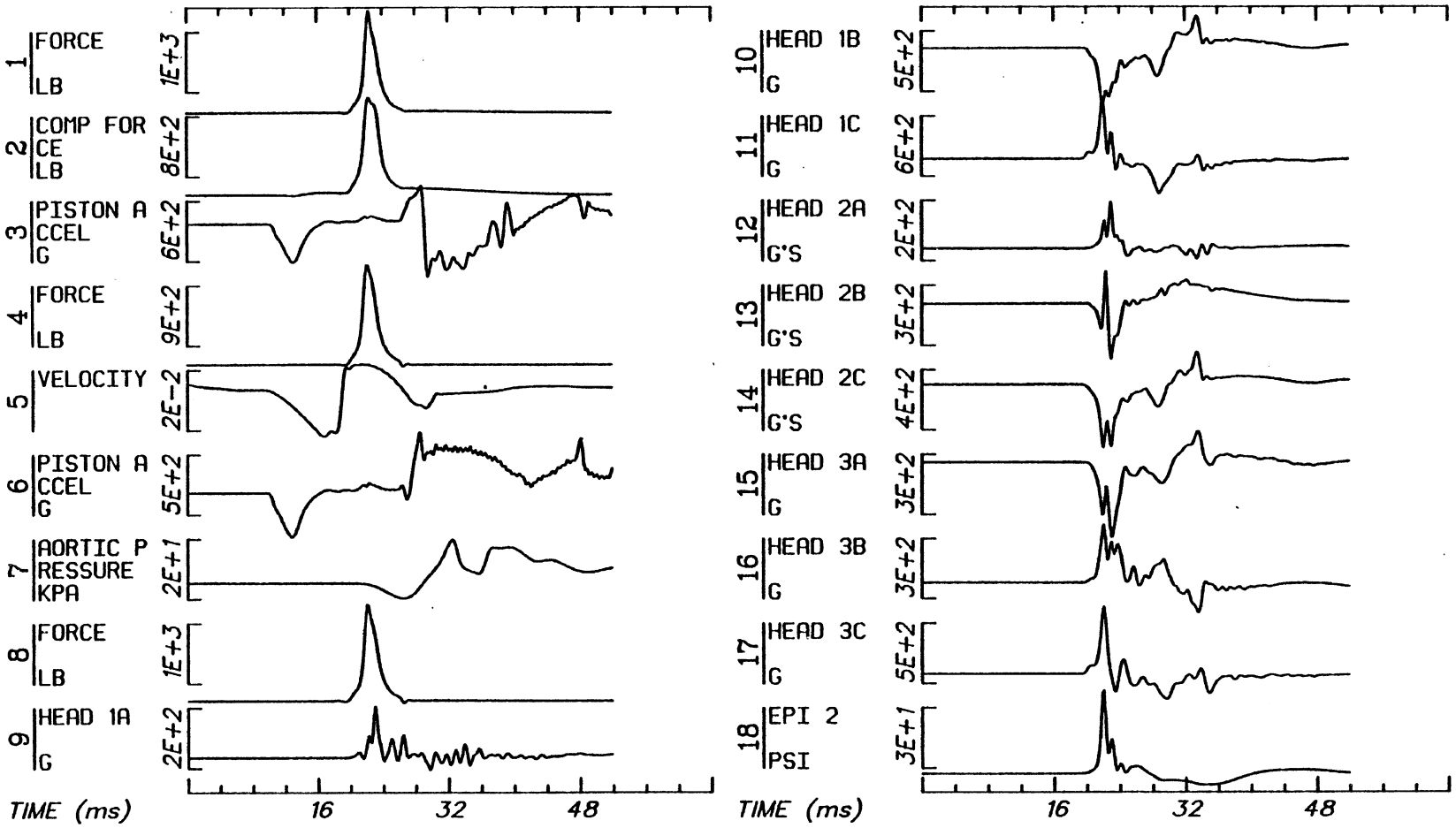

Run ID: 86R014 H7 Disk: R014.SD File: 1 Date: MAR 30, 1986 Sheet: 1

*Filter:1000*4C Smooth: 3SD*

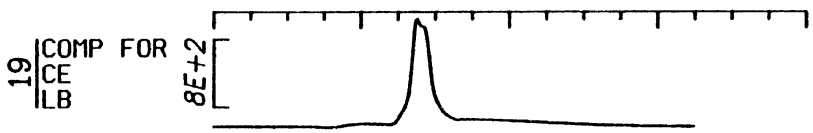

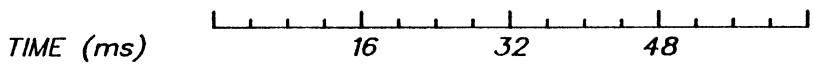

Run ID: 86R014 H7 Disk: R014.SD File: 1 Date: MAR 30, 1986 Sheet: 2

Filter:1000*4C Smooth: 3SD

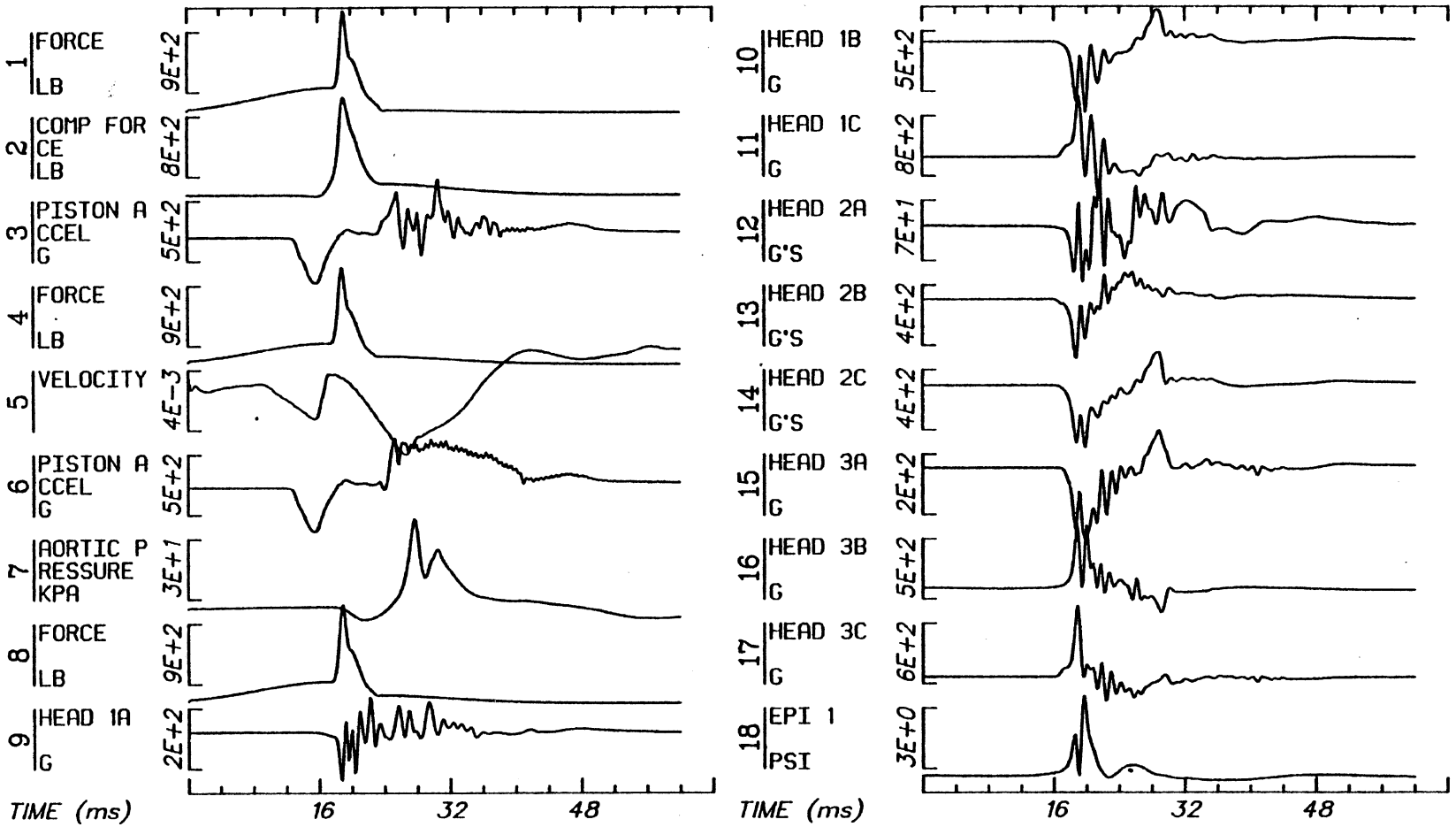

Run ID: 86R015 H7 Disk: R015.SD File: 1 Date: MAR 30, 1986 Sheet: 1

Filter:1000*4C Smooth: 3SD

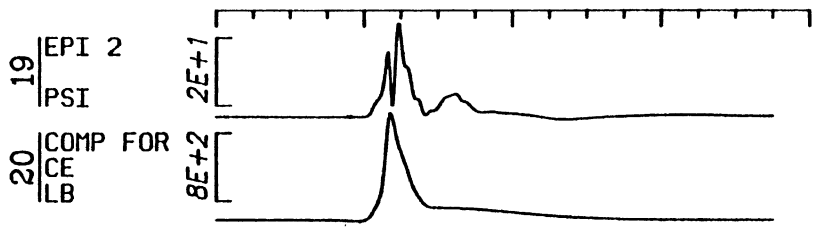

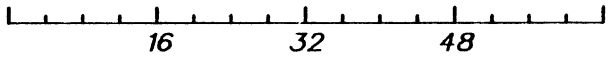

Run ID: 86R015 H7 Disk: R015.SD File: 1 Date: MAR 30, 1986 Sheet: 2

Filter:1000*4C Smooth: 3SD

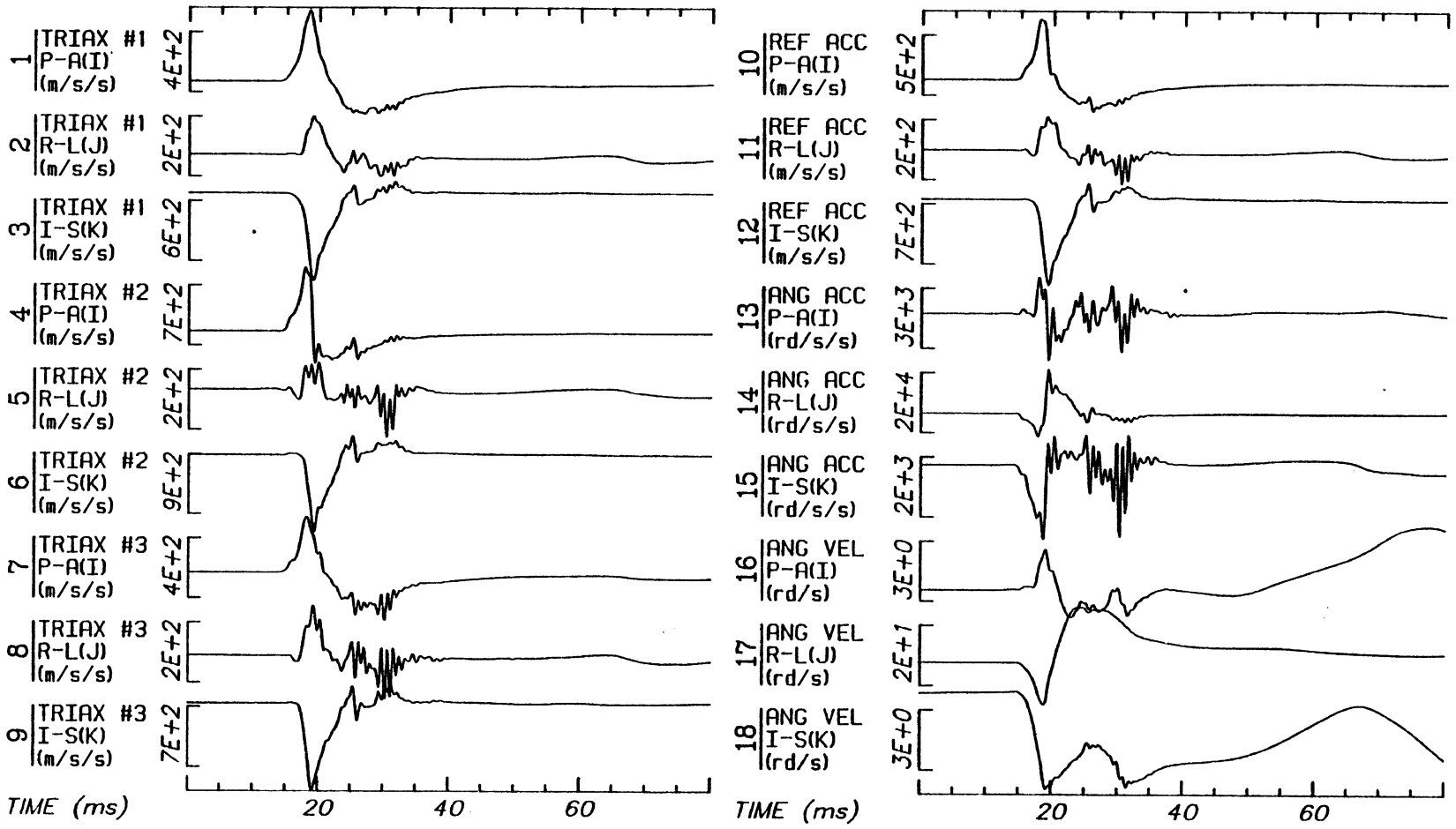

Run ID: 85R002 H9 Disk: R002.3D File: 1 Date: APR 8, 1986 Sheet: 1

No Filtering

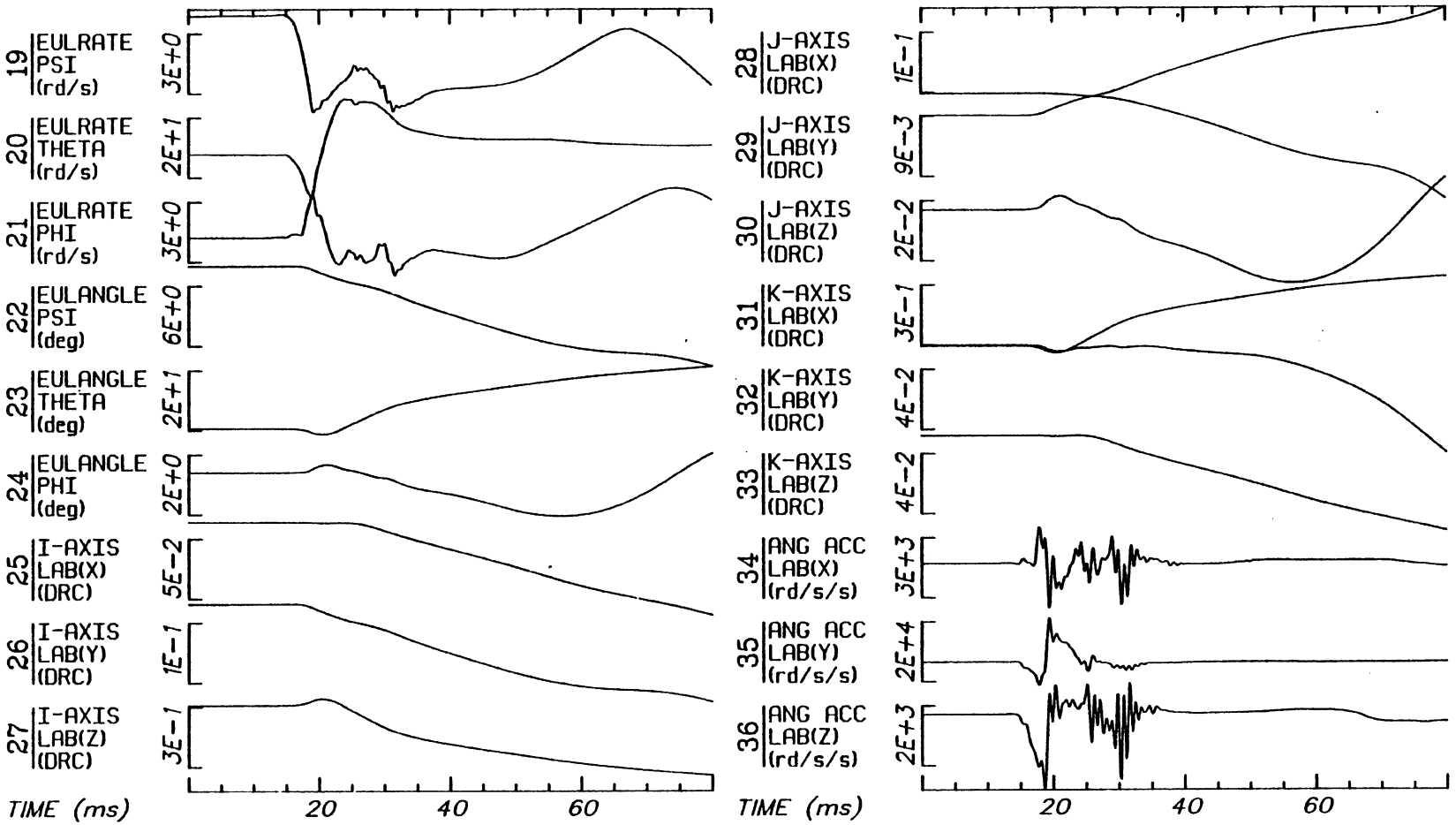

Run ID: 85R002 H9 Disk: R002.3D File: 1 Date: APR 8, 1986 Sheet: 2

No Filtering

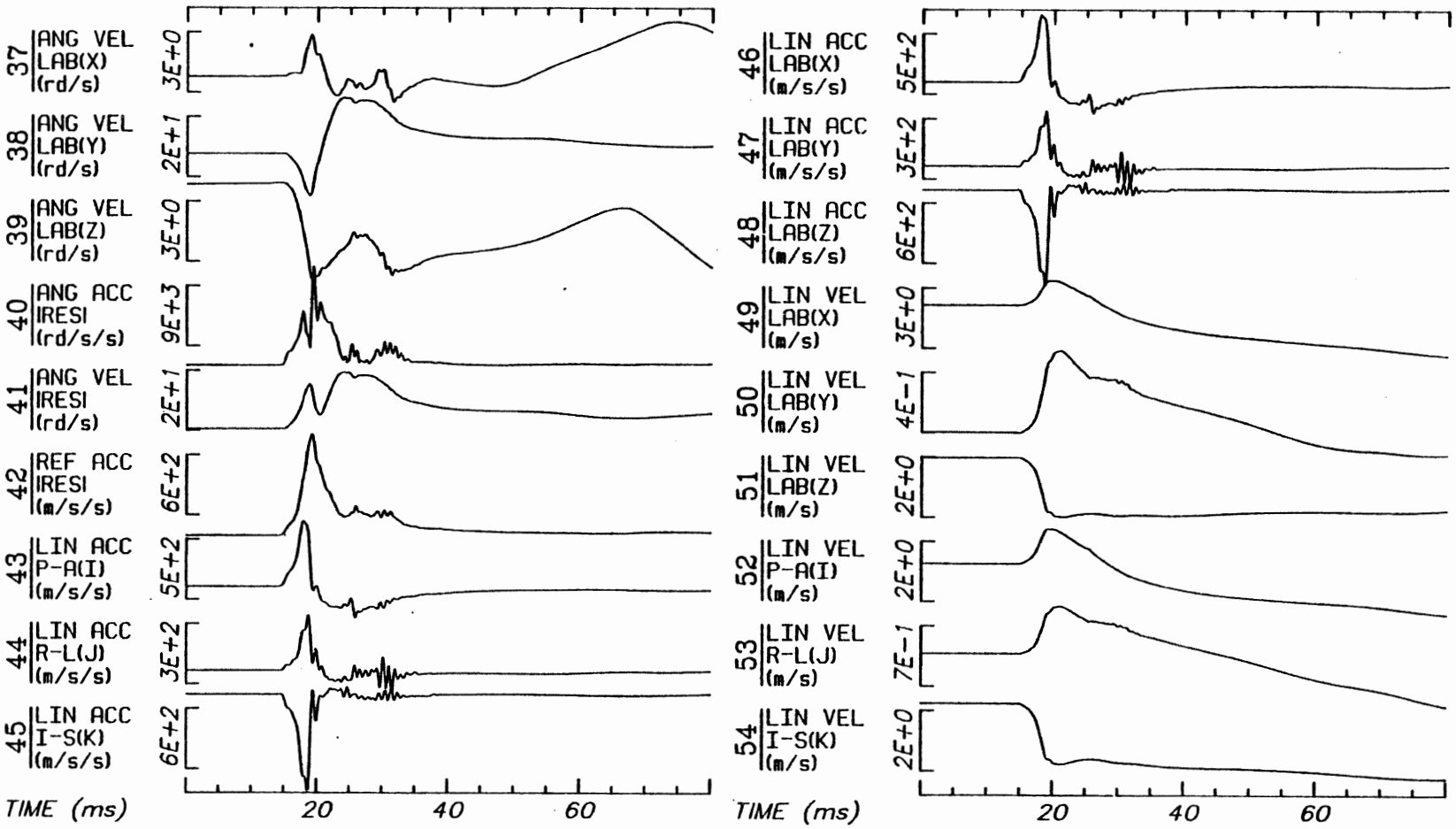

Run ID: 85R002 H9 Disk: R002.3D File: 1 Date: APR 8, 1986 Sheet: 3

No Filtering

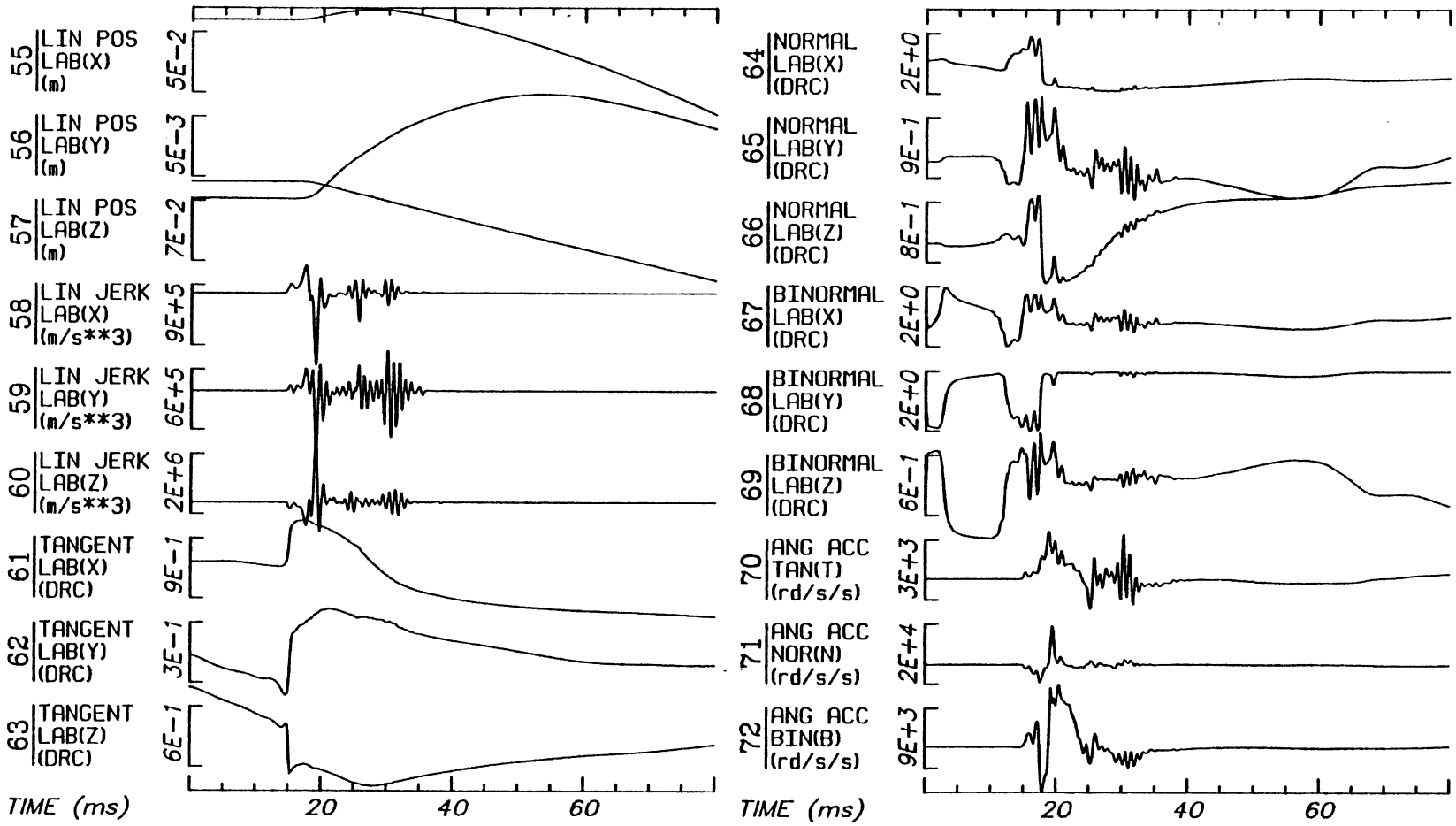

Run ID: 85R002 H9 Disk: R002.3D File: 1 Date: APR 8, 1986 Sheet: 4

No Filtering

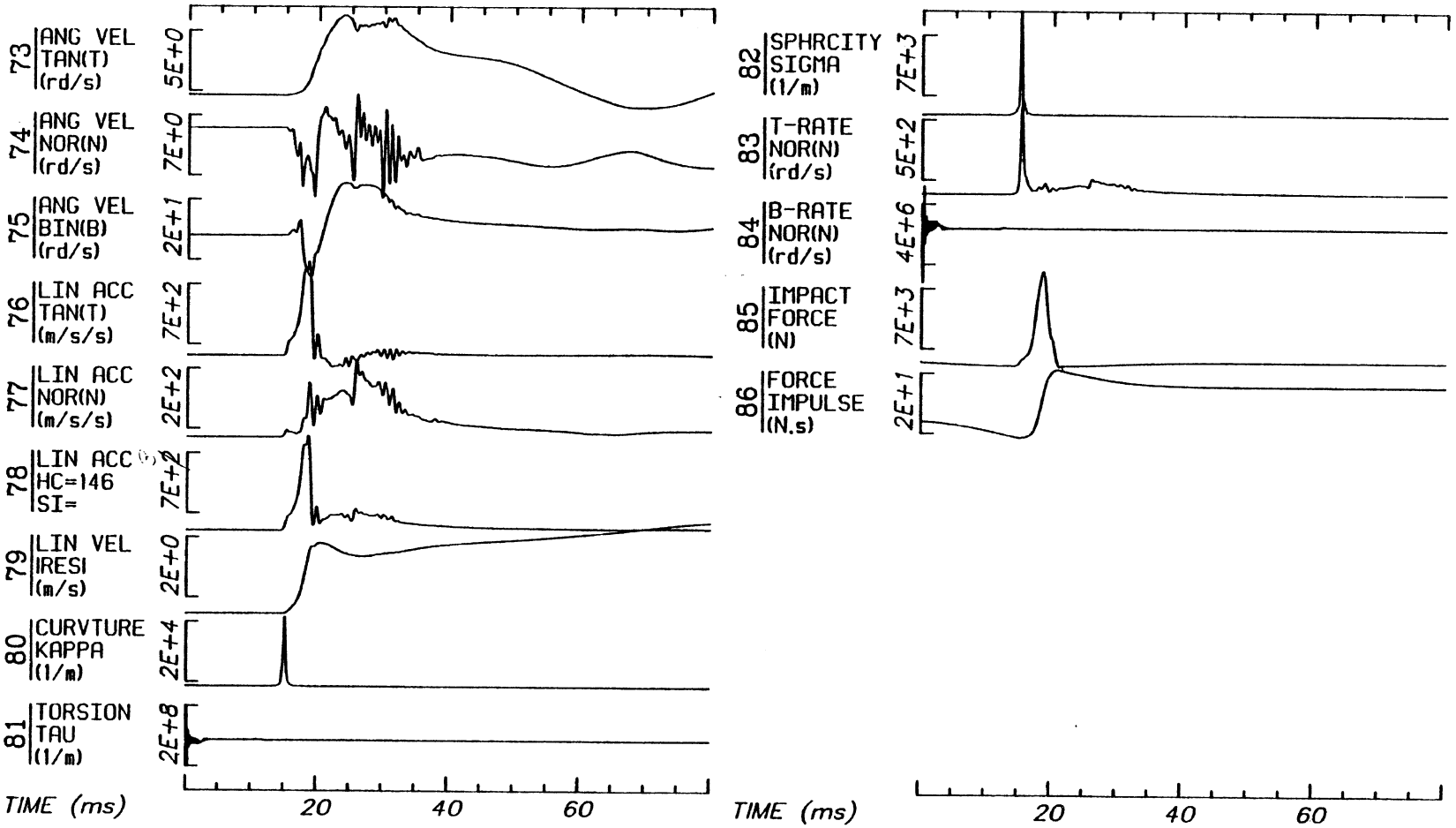

Run ID: 85R002 H9 Disk: R002.3D File: 1 Date: APR 8, 1986 Sheet: 5

No Filtering

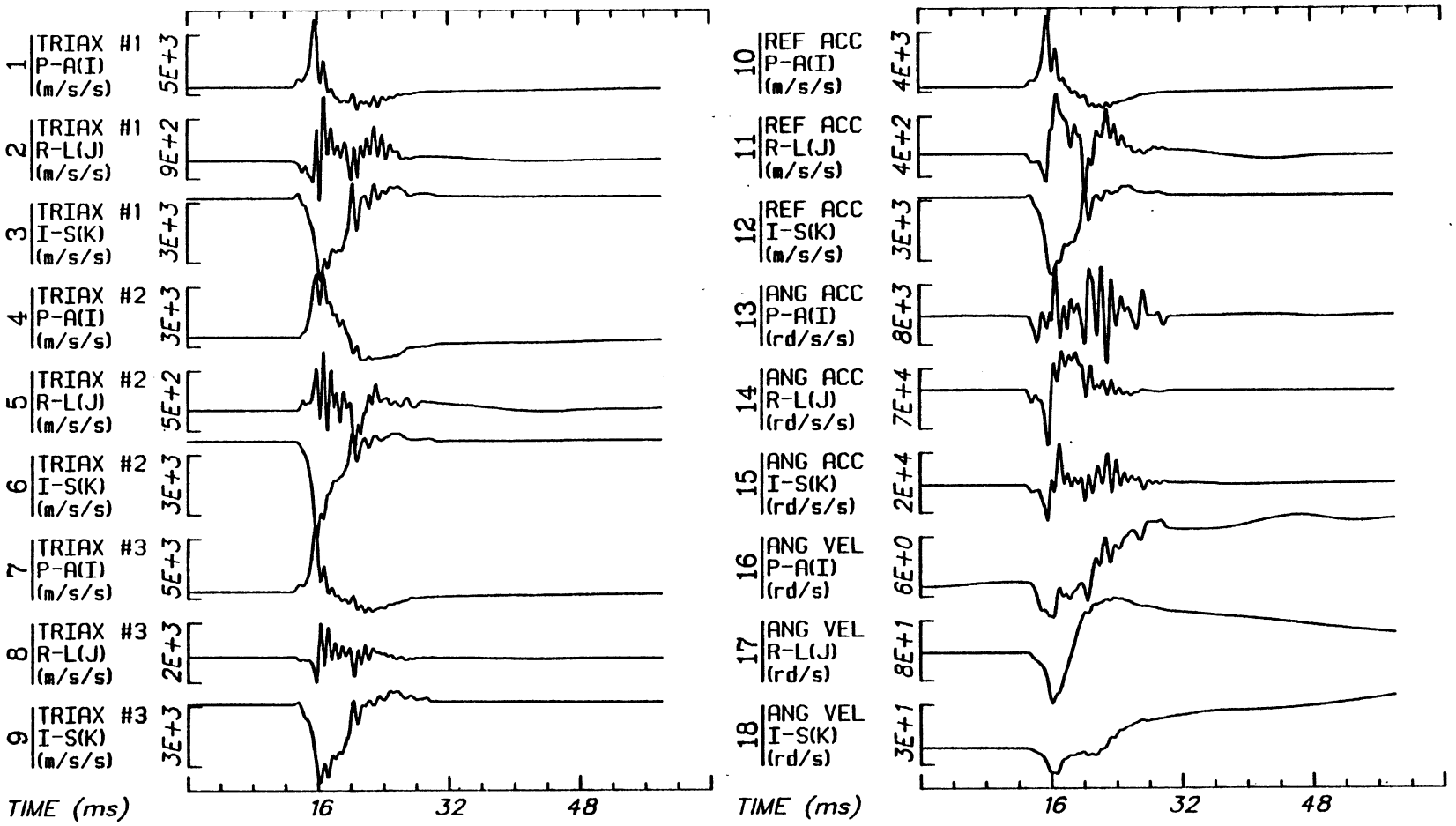

Run ID: 85R006 H9 Disk: R006.3D File: 1 Date: APR 8, 1986 Sheet: 1

No Filtering

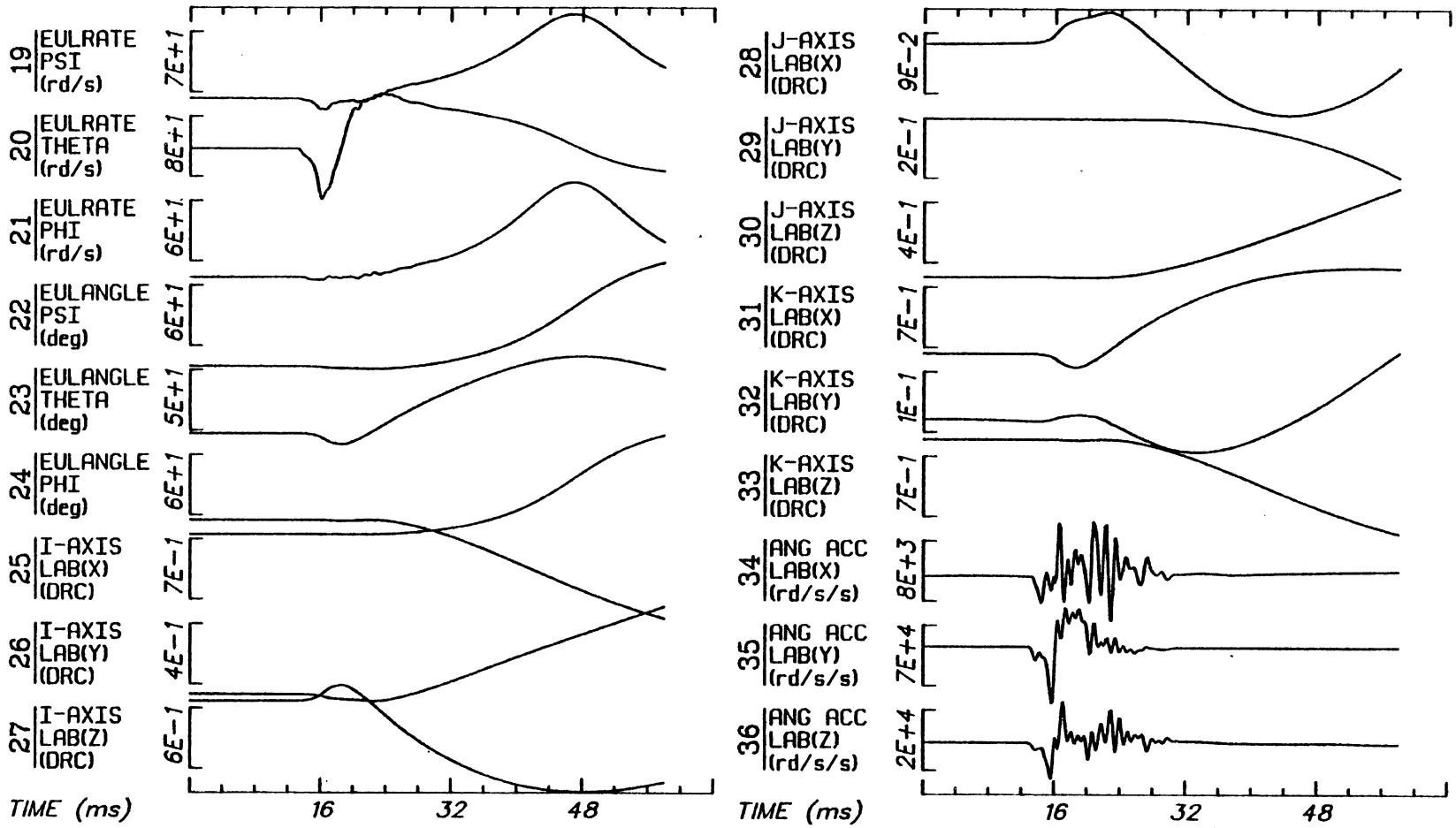

Run ID: 85R006 H9 Disk: R006.3D File: 1 Date: APR 8, 1986 Sheet: 2

No Filtering

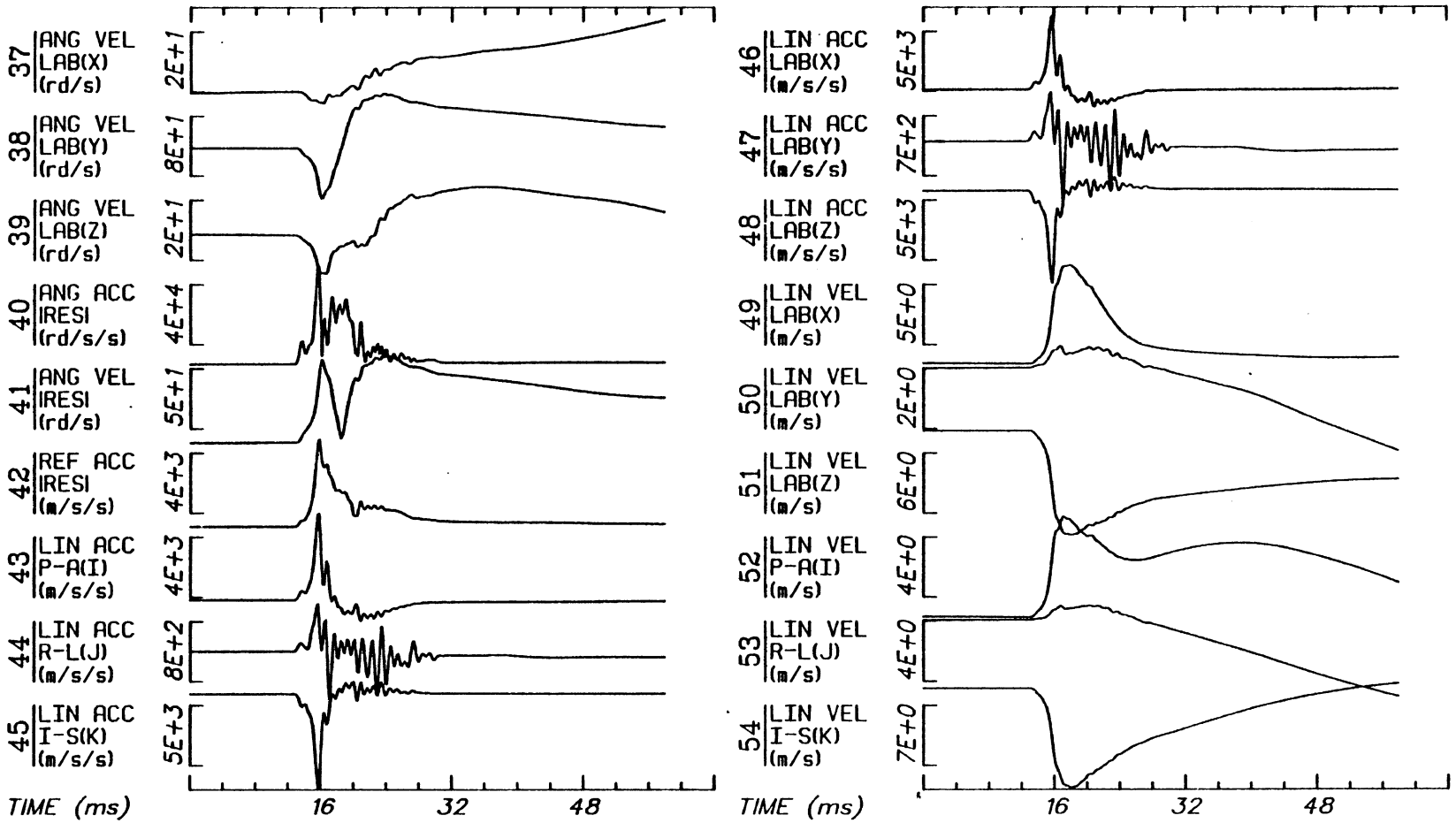

Run ID: 85R006 H9 Disk: R006.3D File: 1 Date: APR 8, 1986 Sheet: 3

No Filtering

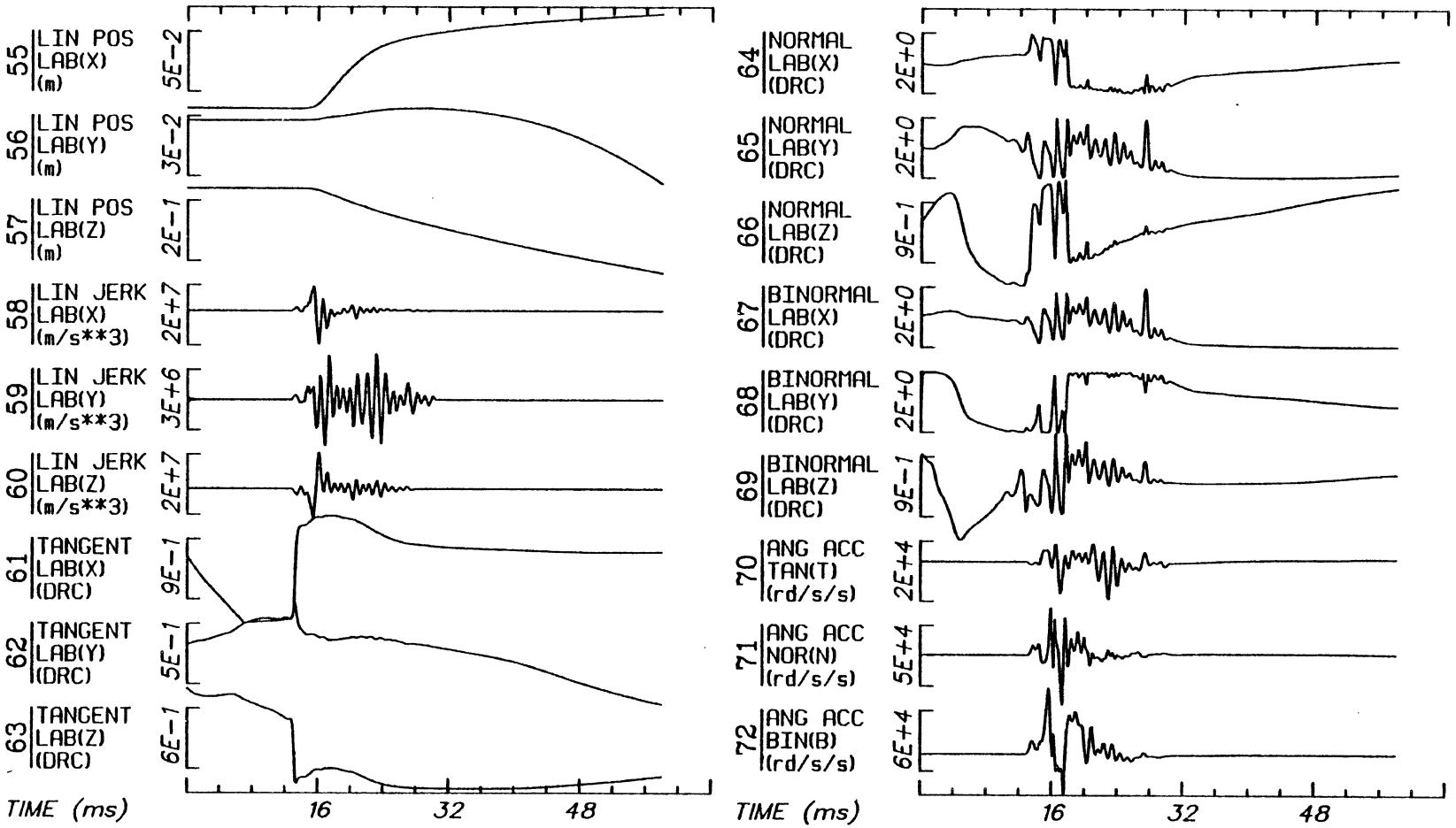

Run ID: 85R006 H9 Disk: R006.3D File: 1 Date: APR 8, 1986 Sheet: 4

No Filtering

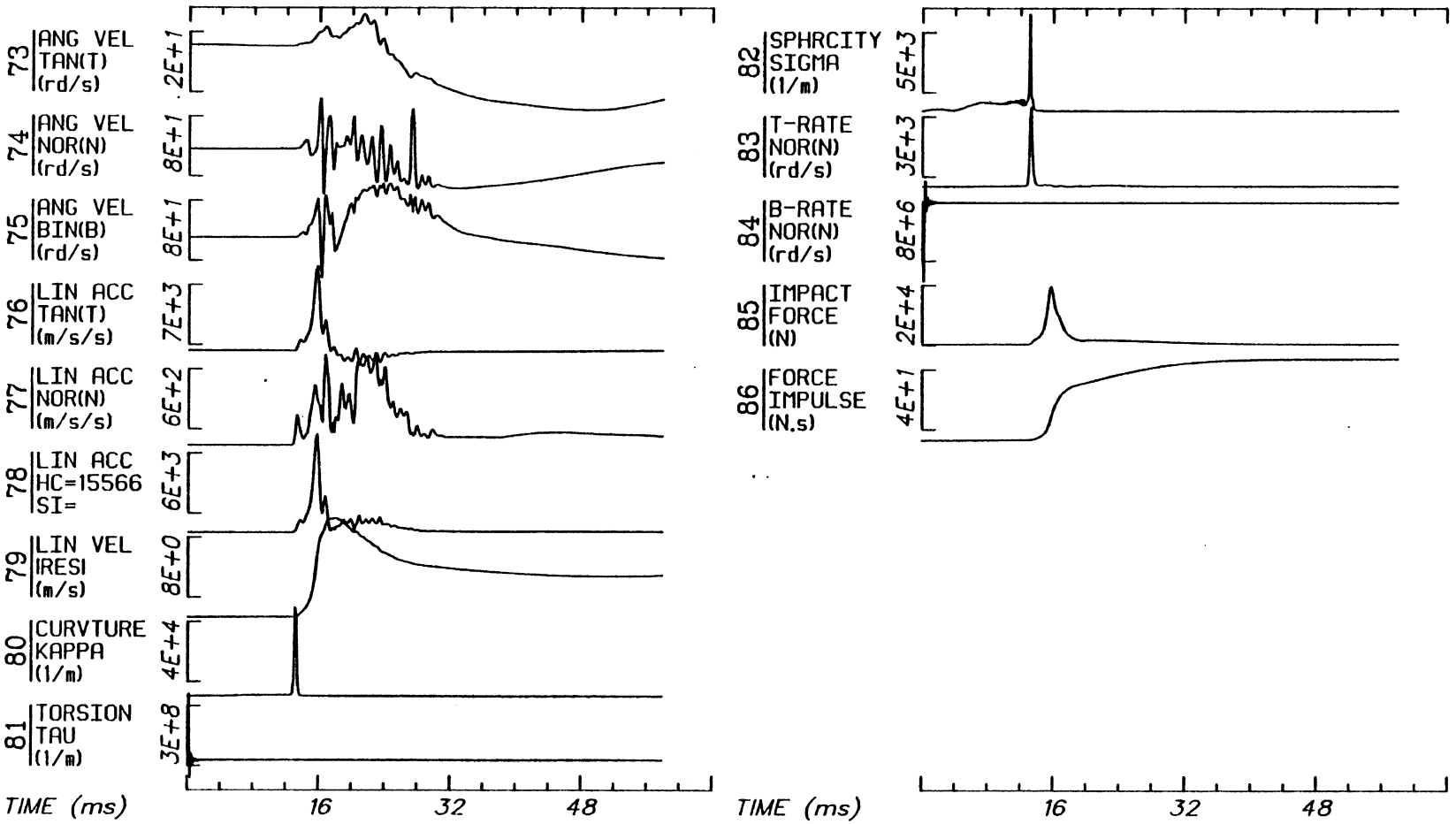

Run ID: 85R006 H9 Disk: R006.3D File: 1 Date: APR 8, 1986 Sheet: 5

No Filtering

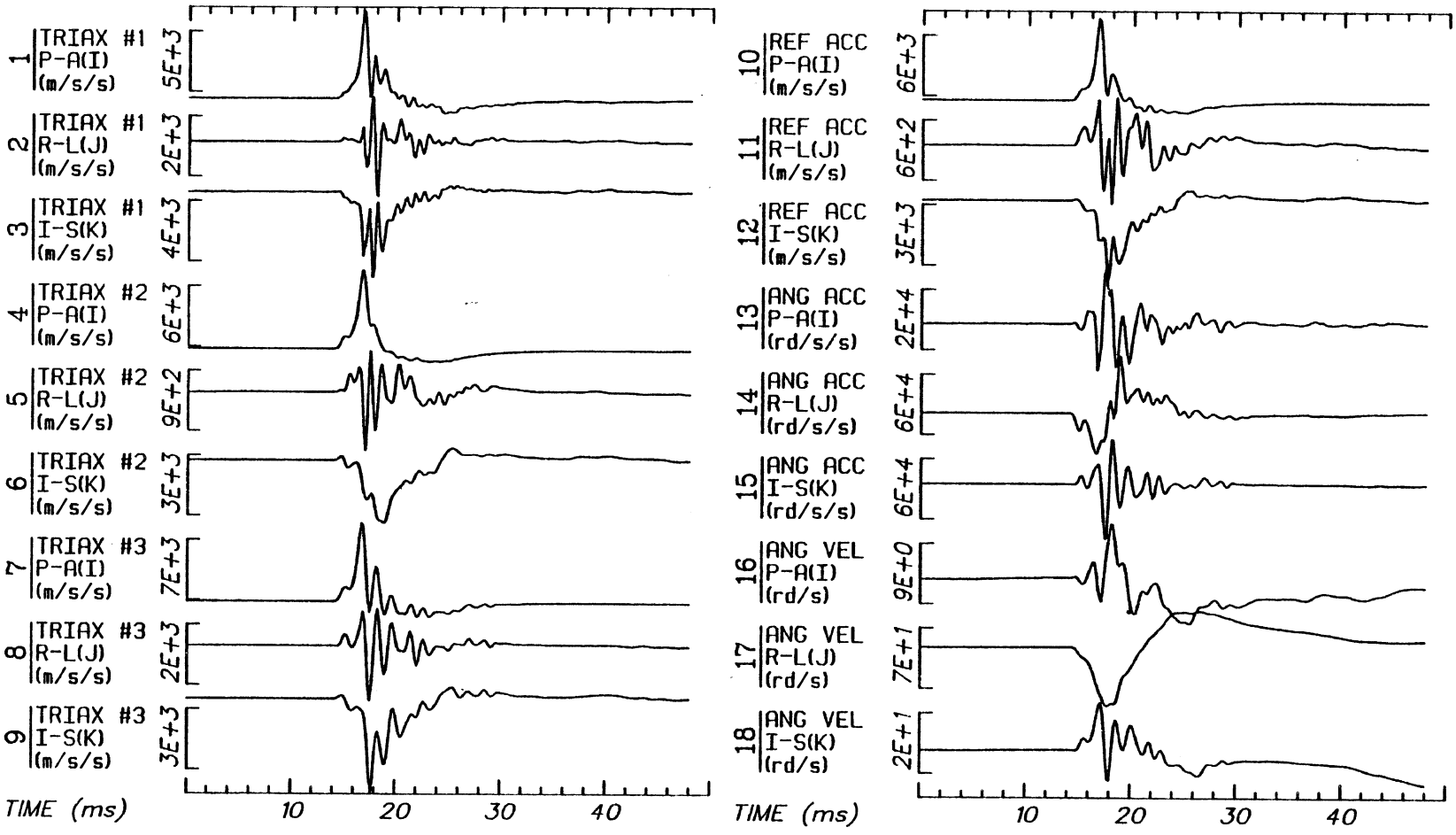

Run ID: 85R008 H9 Disk: R008.3D File: 1 Date: APR 8, 1986 Sheet: 1

No Filtering

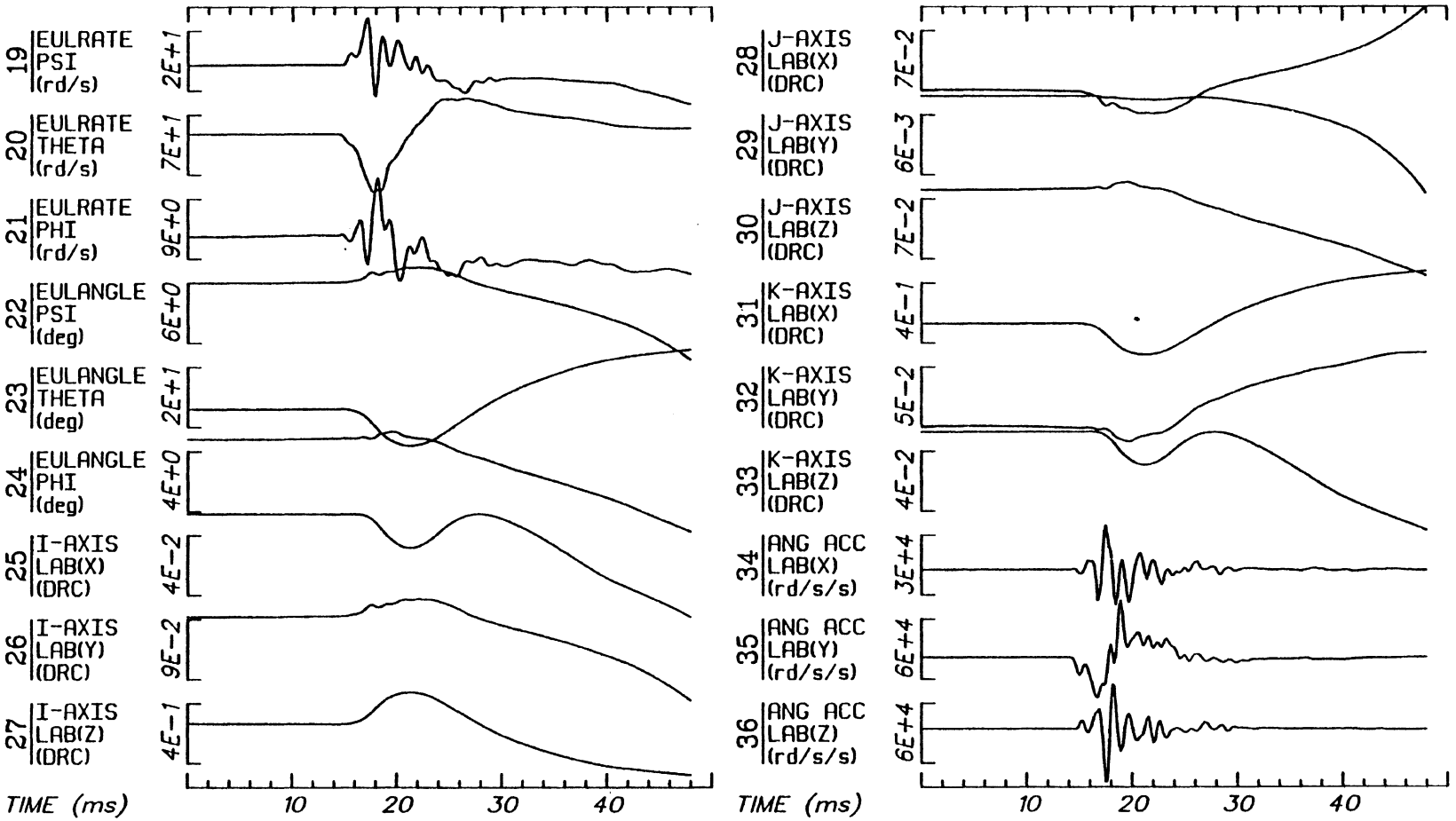

Run ID: 85R008 H9 Disk: R008.3D File: 1 Date: APR 8, 1986 Sheet: 2

No Filtering

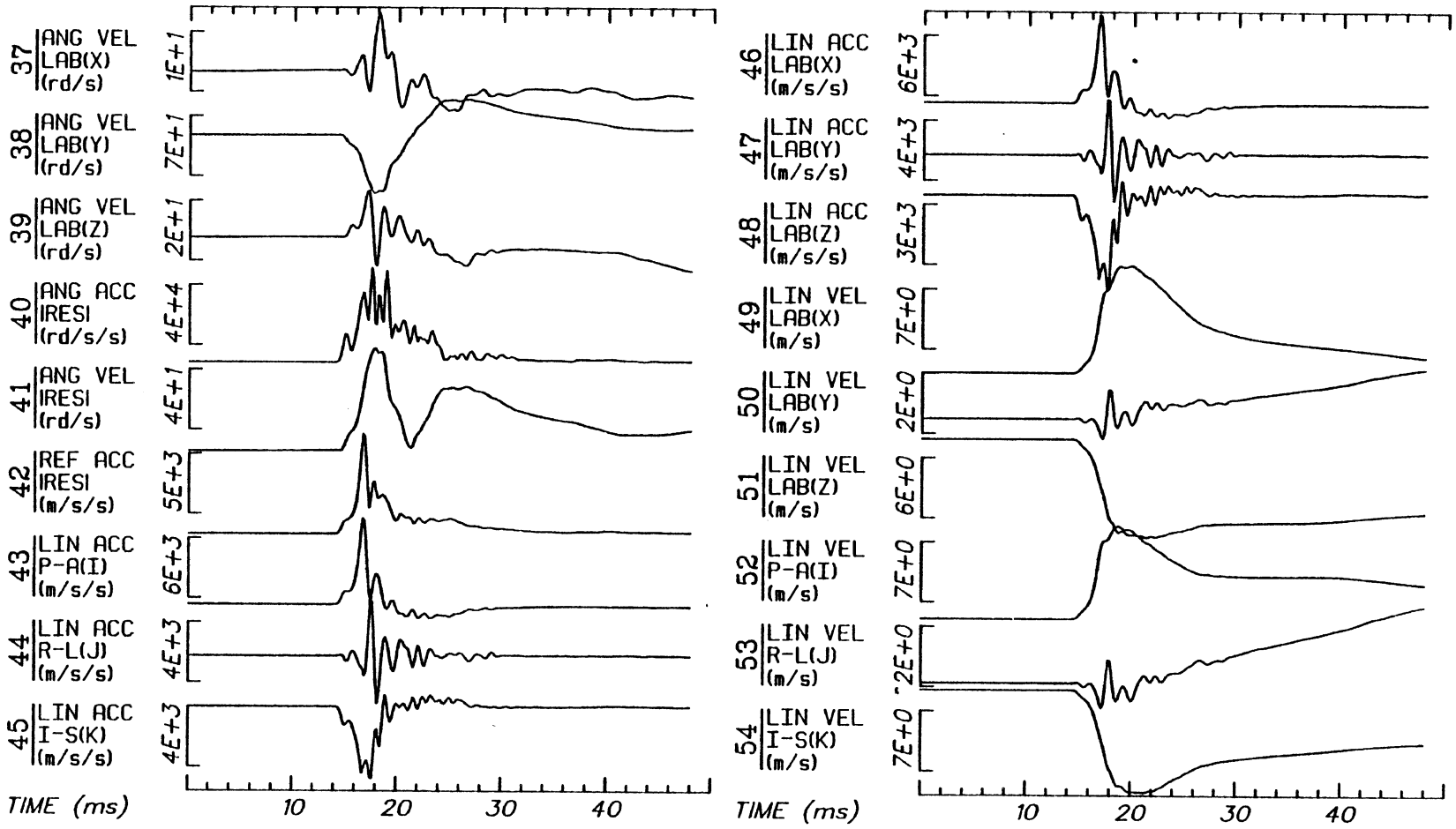

Run ID: 85R008 H9 Disk: R008.3D File: 1 Date: APR 8, 1986 Sheet: 3

No Filtering

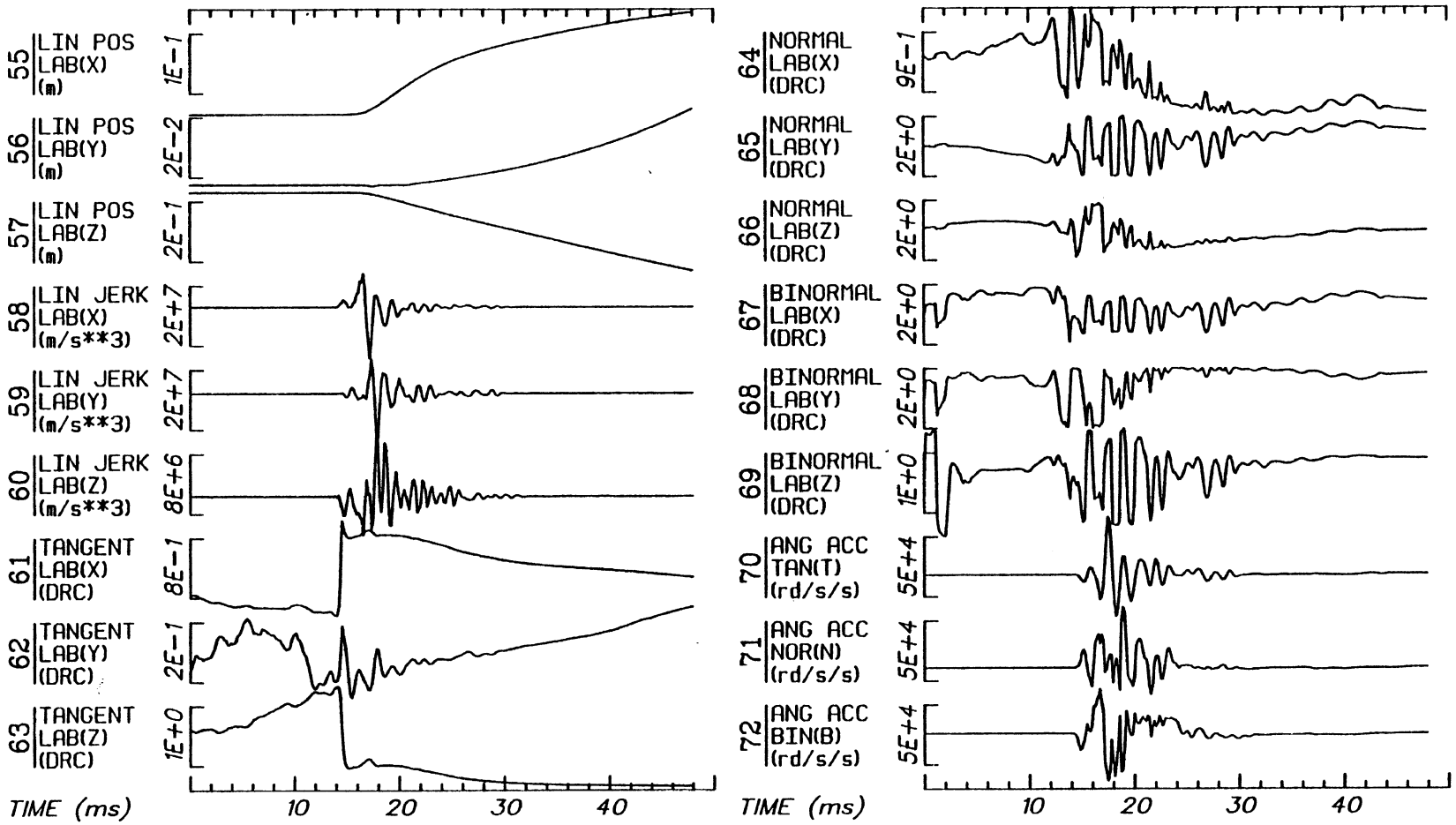

Run ID: 85R008 H9 Disk: R008.3D File: 1 Date: APR 8, 1986 Sheet: 4

No Filtering

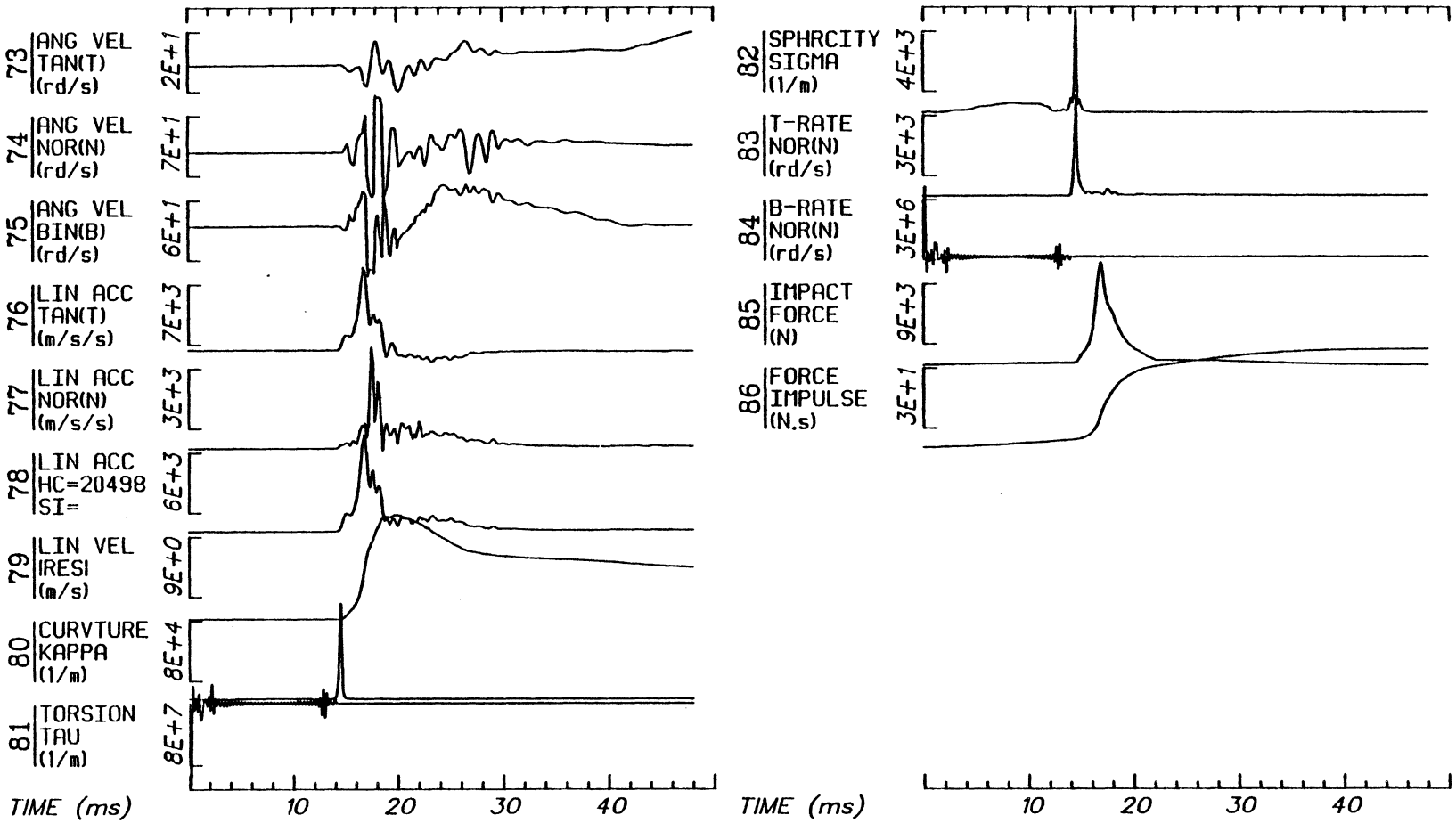

Run ID: 85R008 H9 Disk: R008.3D File: 1 Date: APR 8, 1986 Sheet: 5

No Filtering

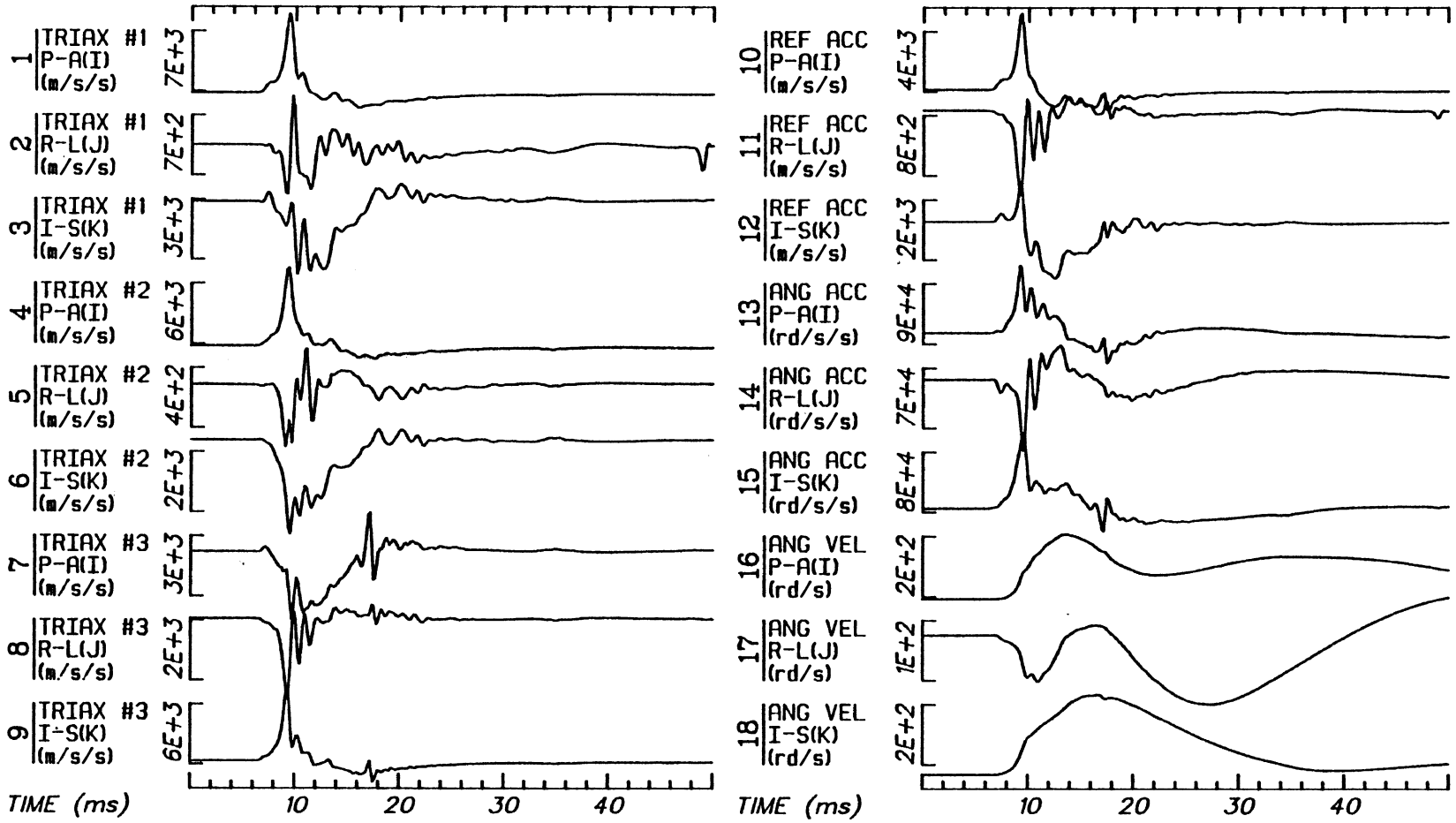

Run ID: 86R010 H7 Disk: R010.3D File: 1 Date: APR 15, 1986 Sheet: 1

No Filtering

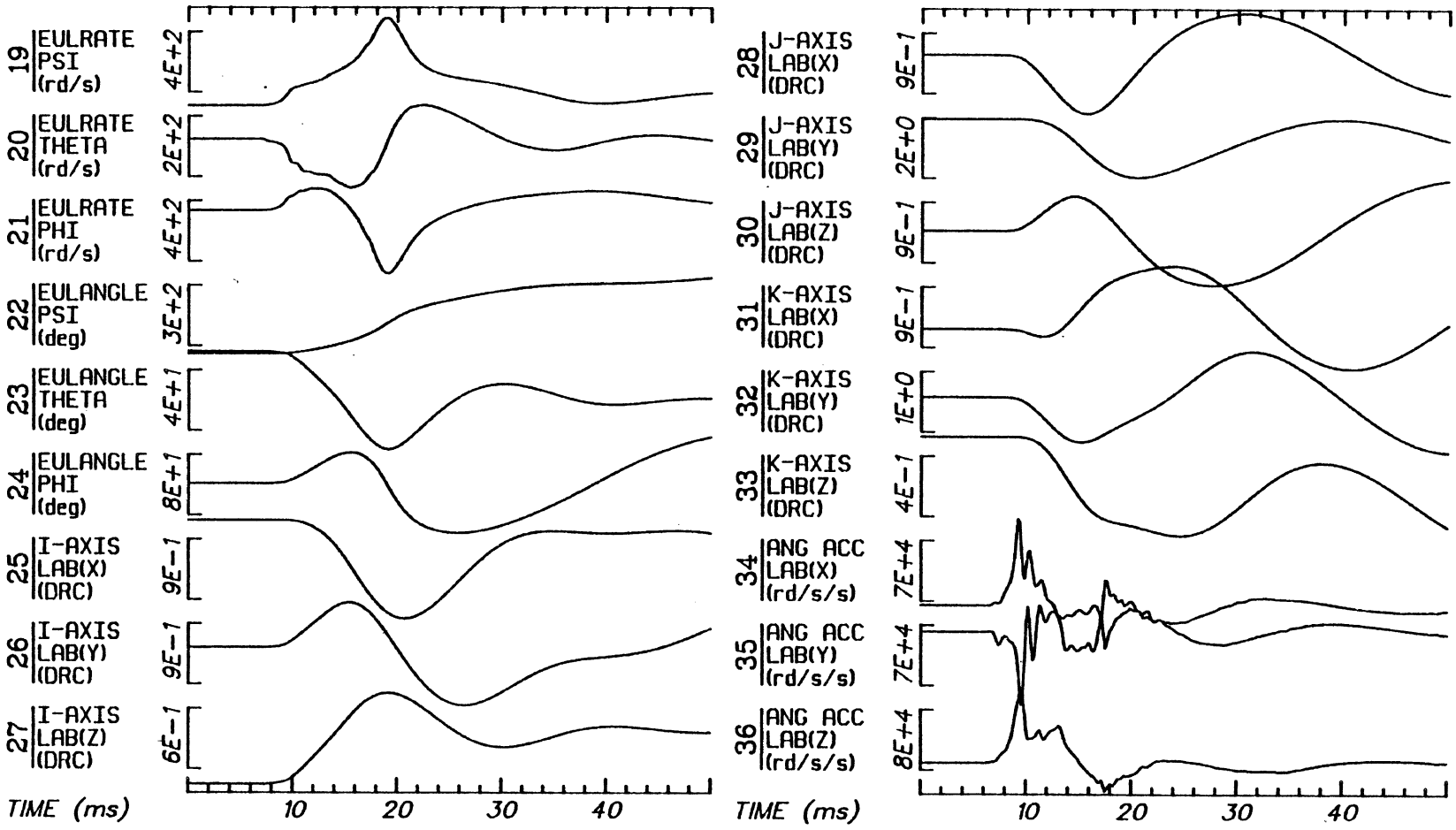

Run ID: 86R010 H7 Disk: R010.3D File: 1 Date: APR 15, 1986 Sheet: 2

No Filtering

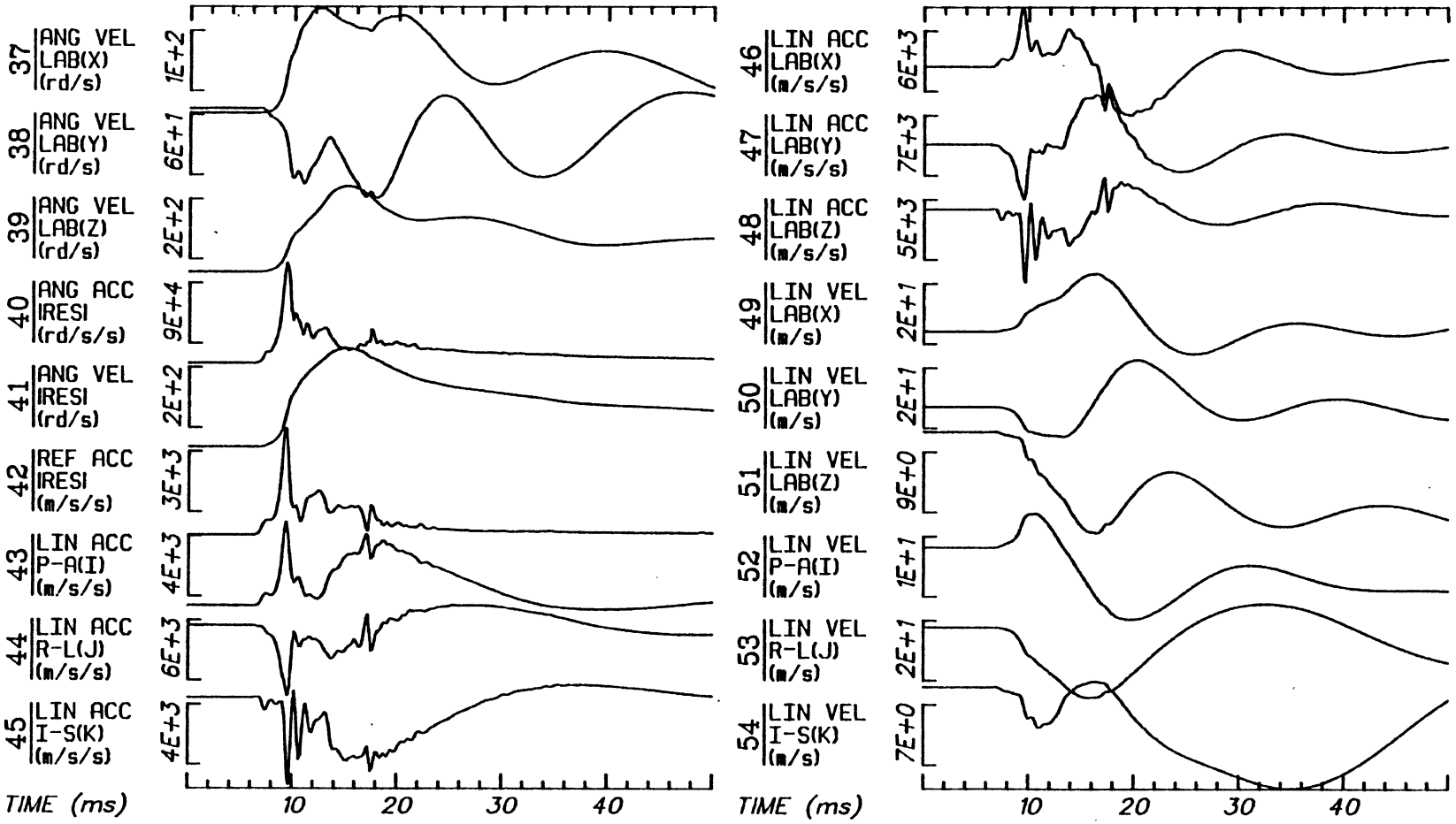

Run ID: 86R010 H7 Disk: R010.3D File: 1 Date: APR 15, 1986 Sheet: 3

No Filtering

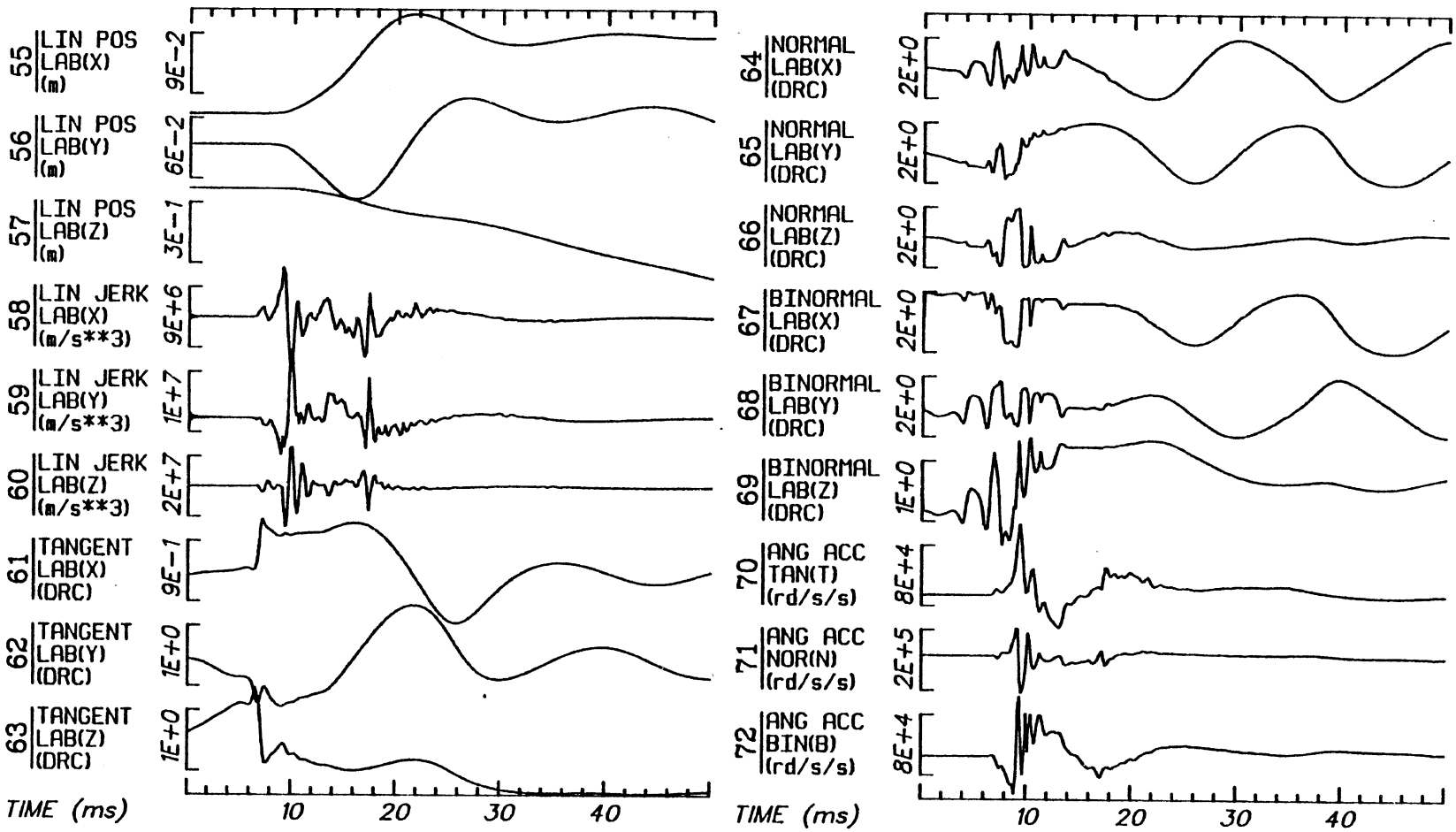

Run ID: 86R010 H7 Disk: R010.3D File: 1 Date: APR 15, 1986 Sheet: 4

No Filtering

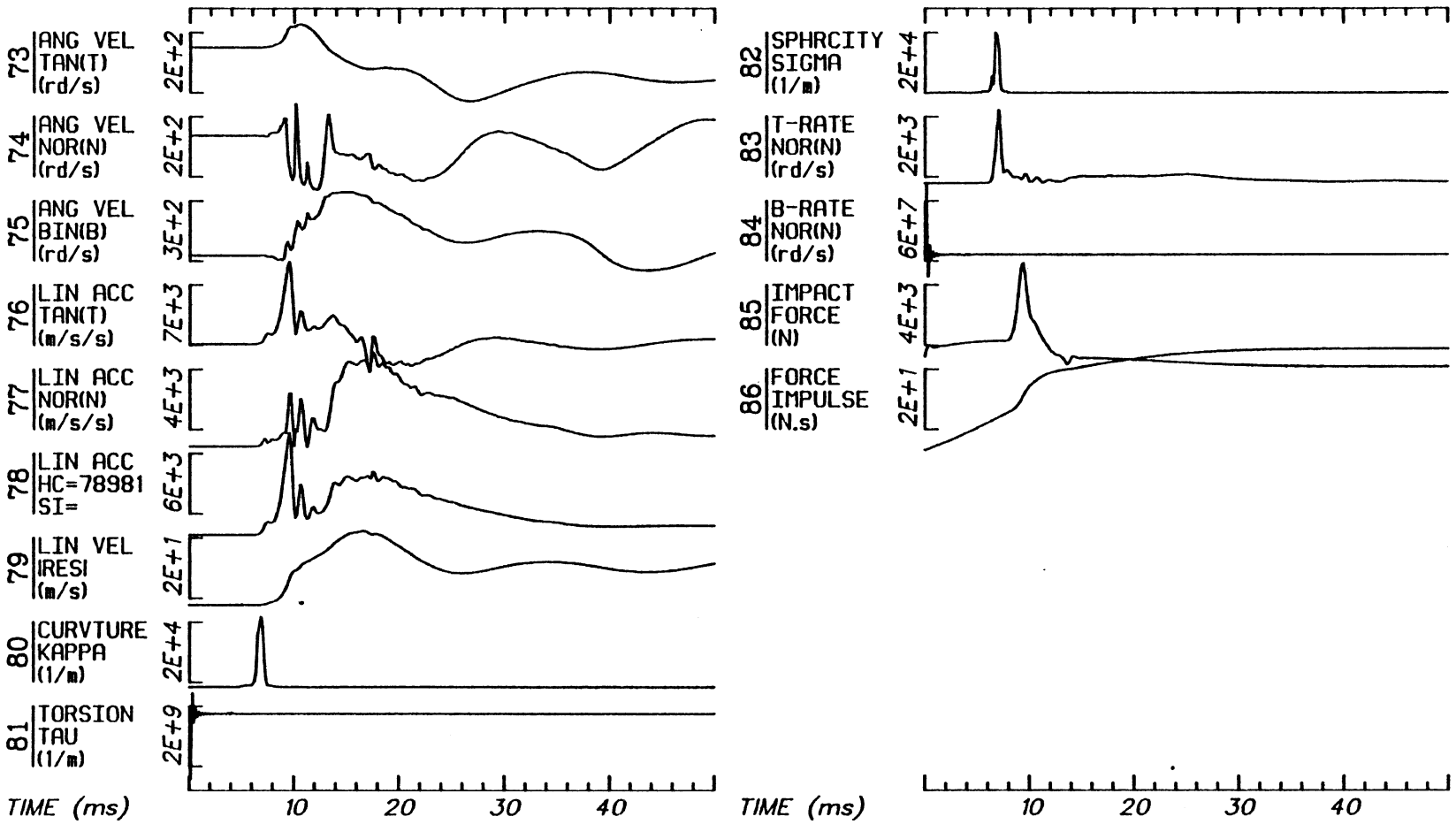

Run ID: 86R010 H7 Disk: R010.3D File: 1 Date: APR 15, 1986 Sheet: 5

No Filtering

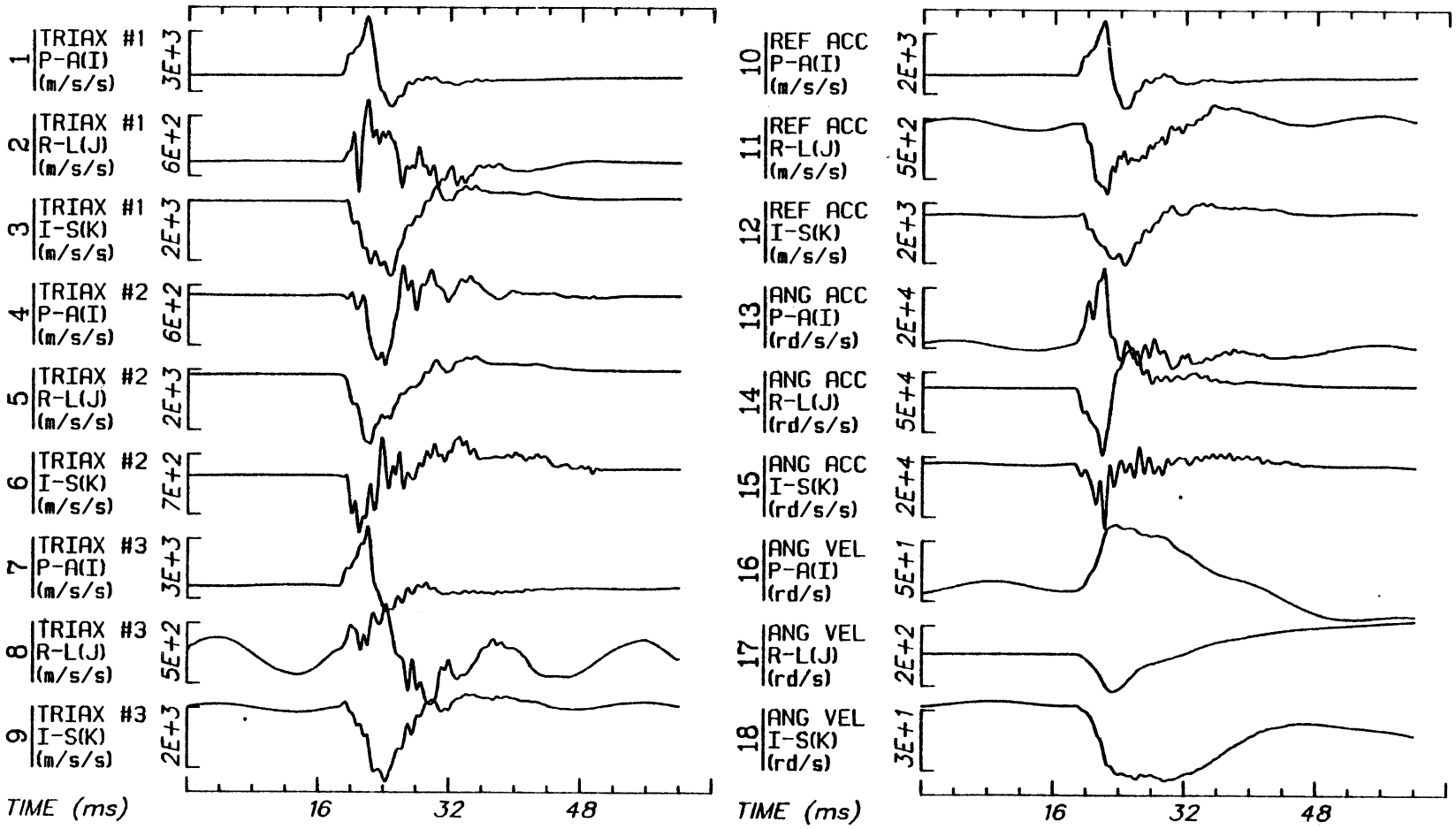

Run ID: 86R011 H7 Disk: R011.3D File: 1 Date: APR 8, 1986 Sheet: 1

No Filtering

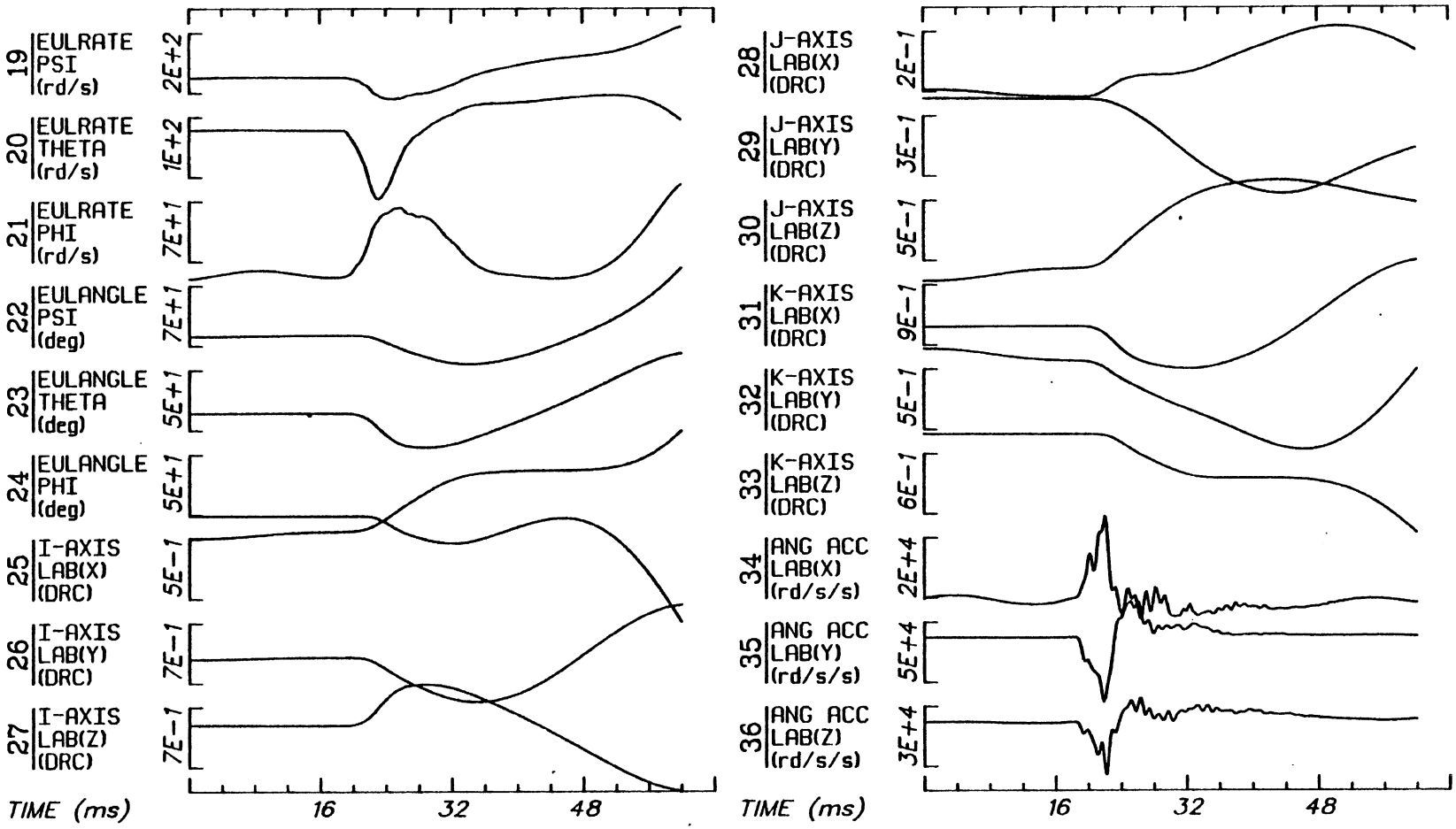

Run ID: 86R011 H7 Disk: R011.3D File: 1 Date: APR 8, 1986 Sheet: 2

No Filtering

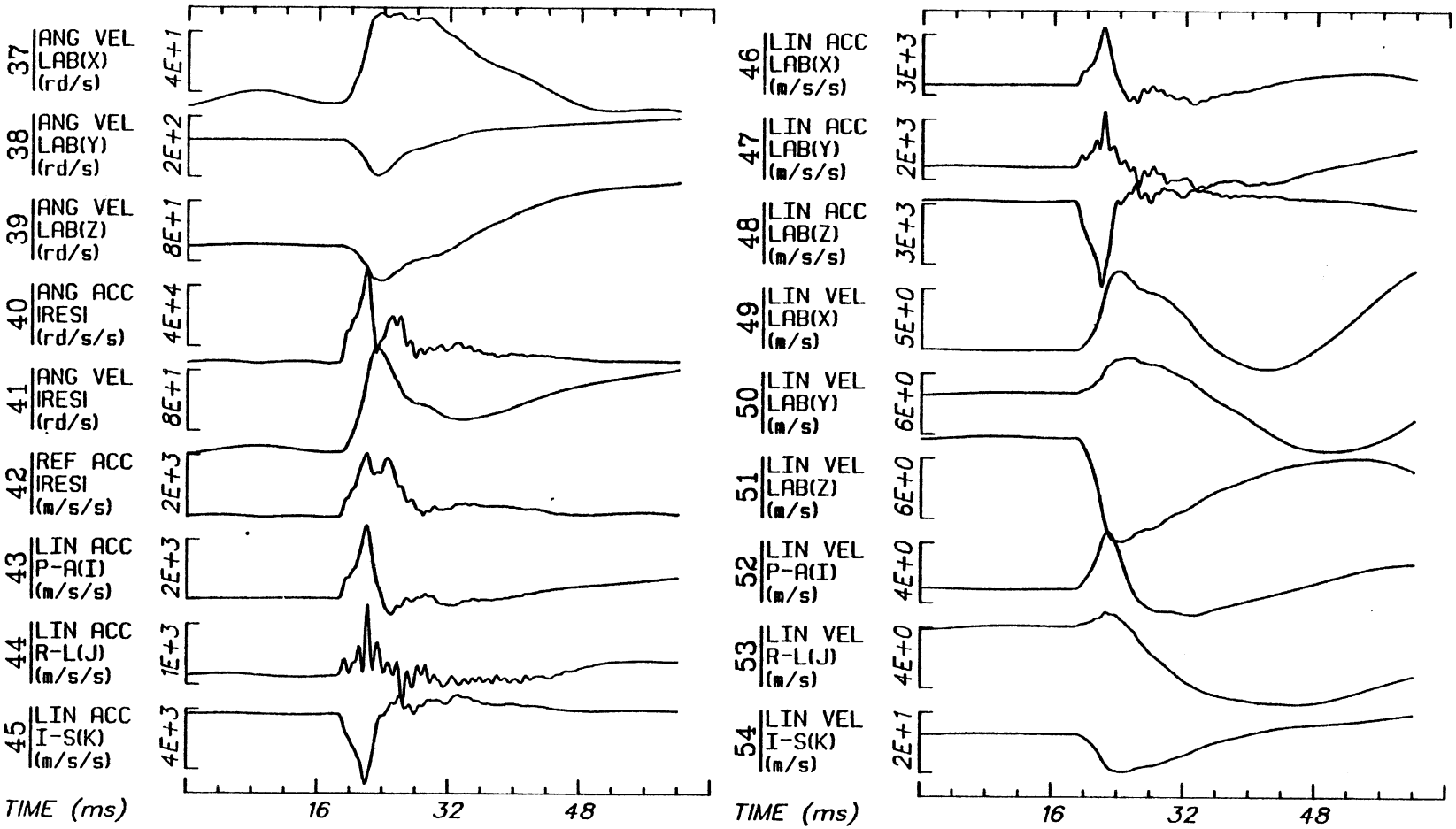

Run ID: 86R011 H7 Disk: R011.3D File: 1 Date: APR 8, 1986 Sheet: 3

No Filtering

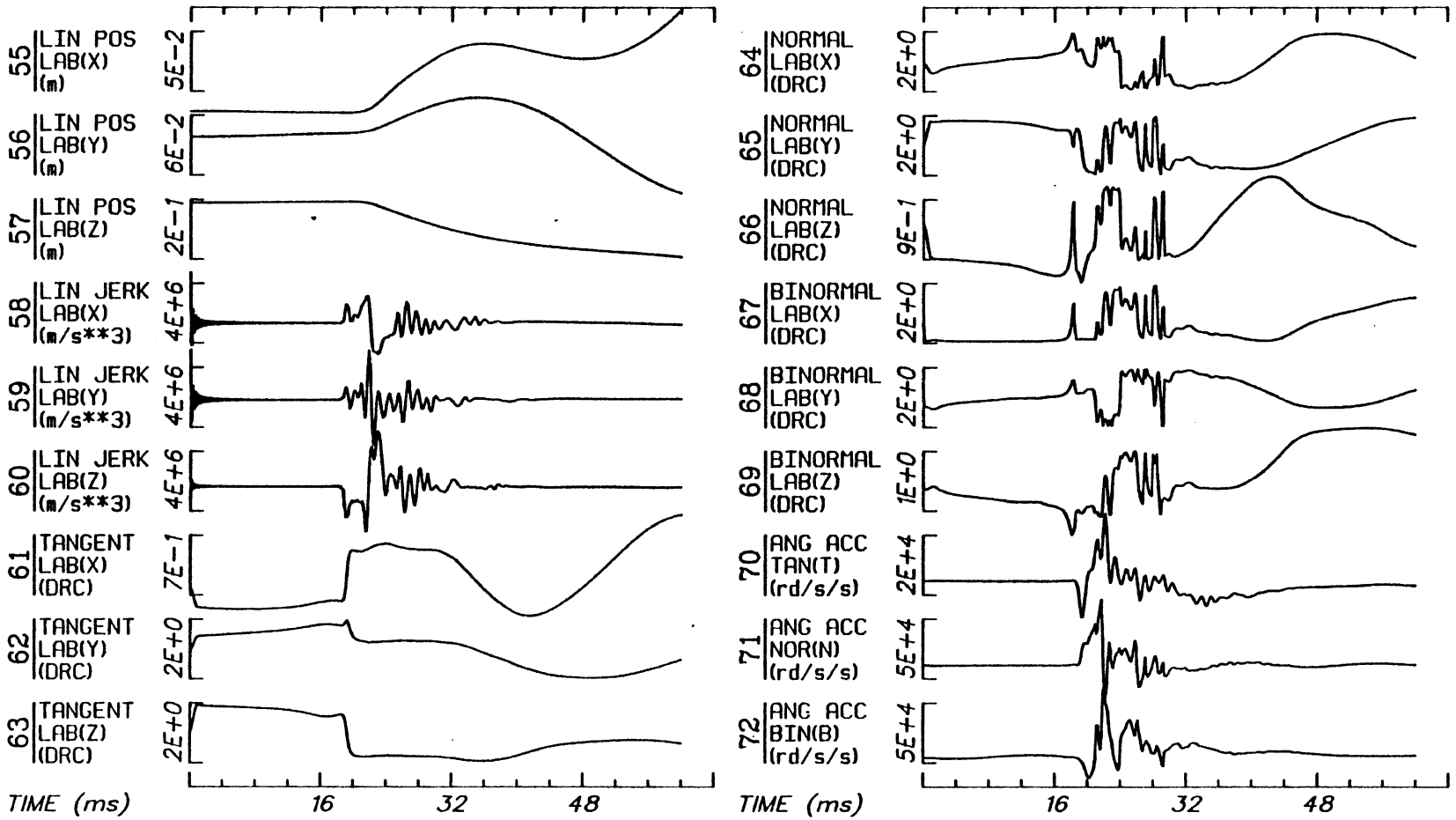

Run ID: 86R011 H7 Disk: R011.3D File: 1 Date: APR 8, 1986 Sheet: 4

No Filtering

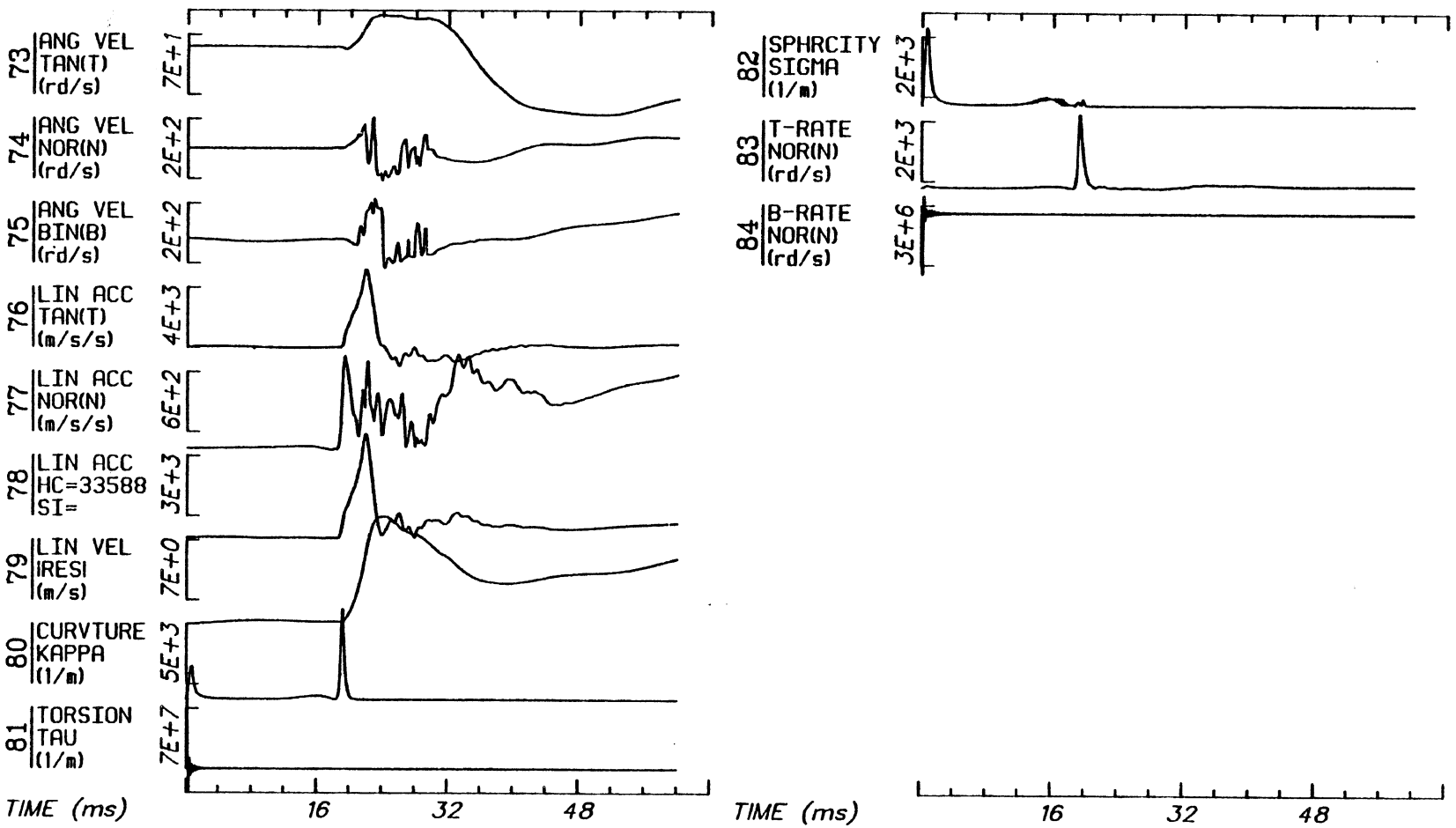

Run ID: 86R011 H7 Disk: R011.3D File: 1 Date: APR 8, 1986 Sheet: 5

No Filtering

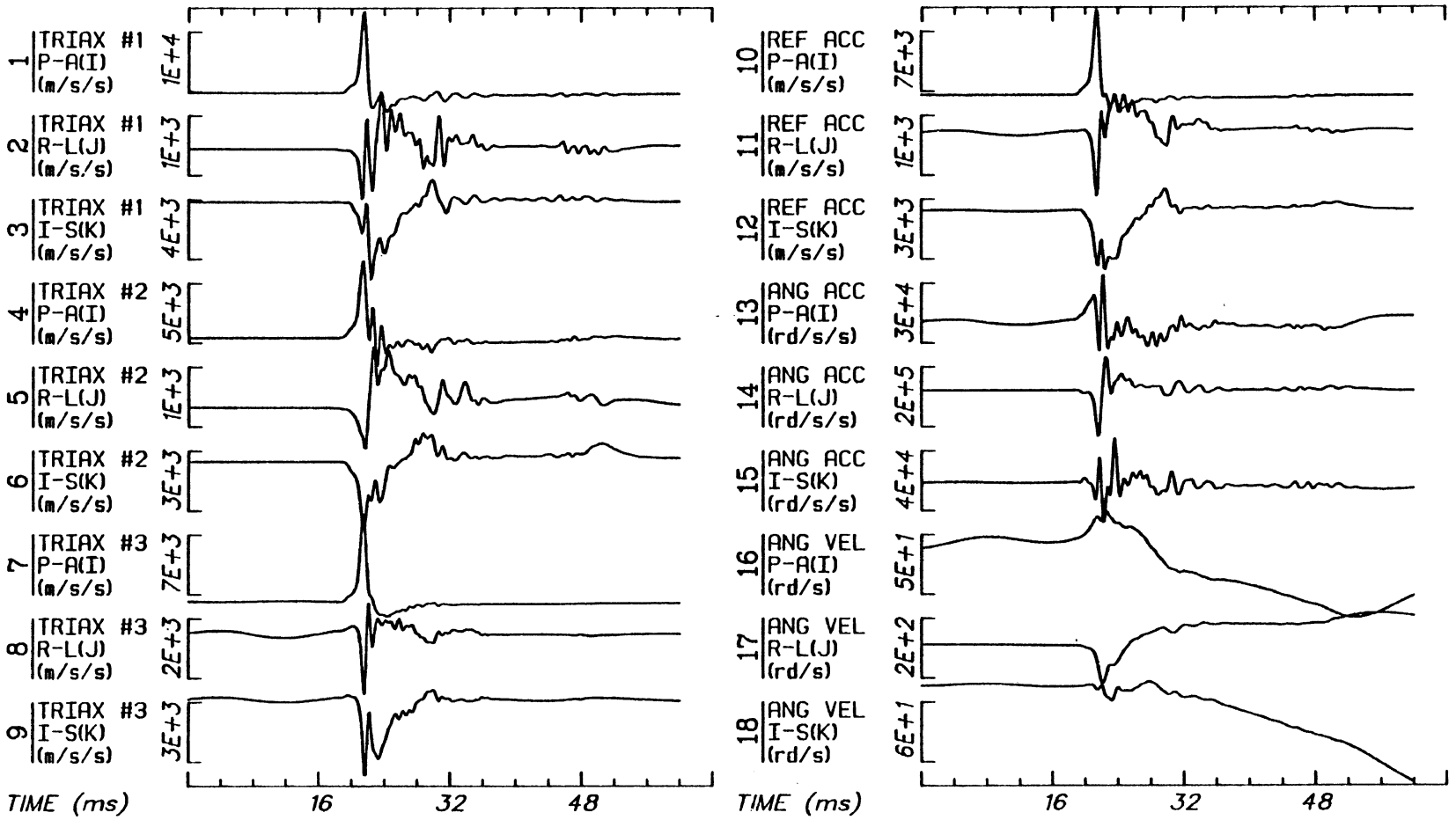

Run ID: 86R012 H7 Disk: R012.3D File: 1 Date: APR 8, 1986 Sheet: 1

No Filtering

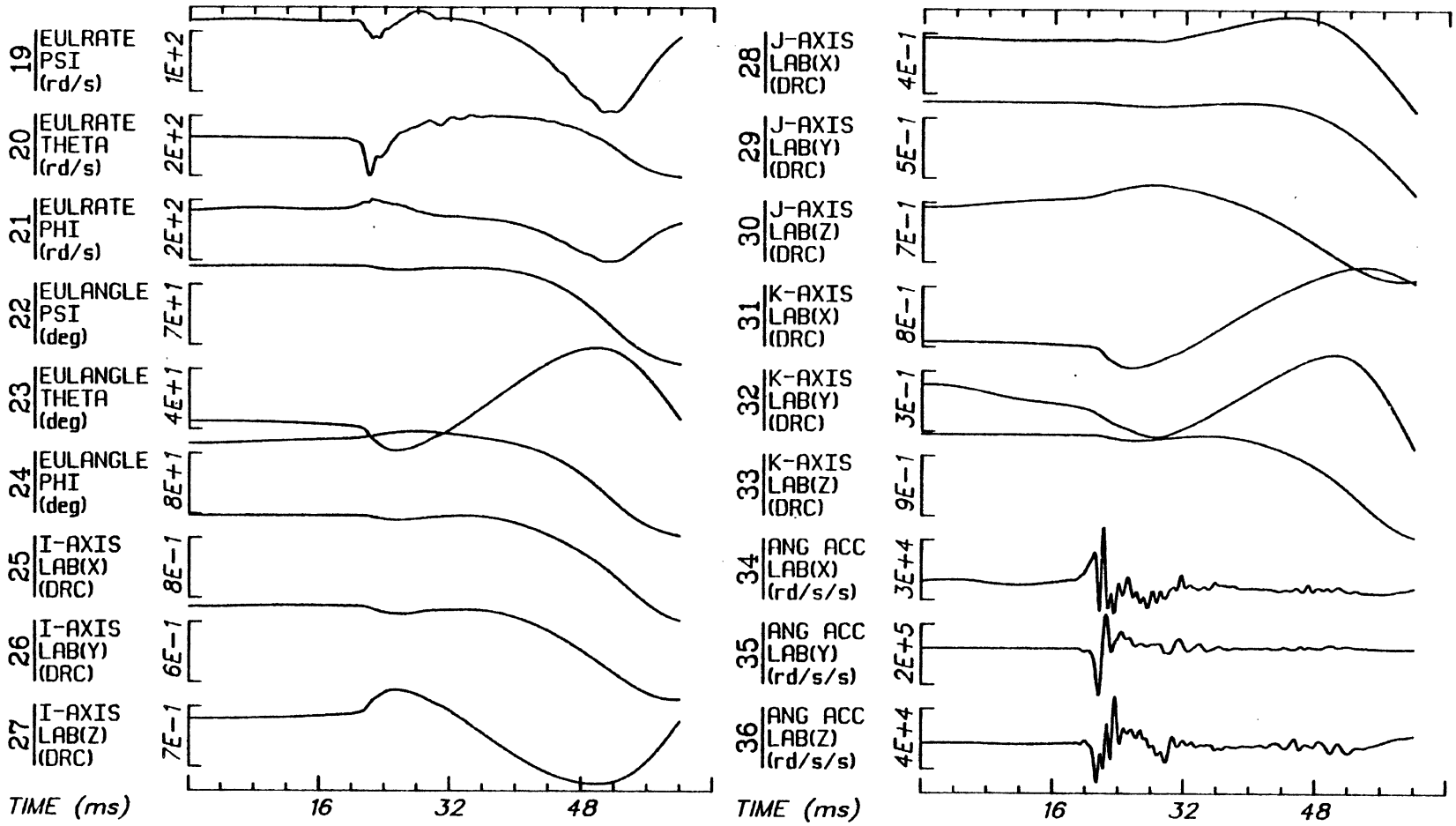

Run ID: 86R012 H7 Disk: R012.3D File: 1 Date: APR 8, 1986 Sheet: 2

No Filtering

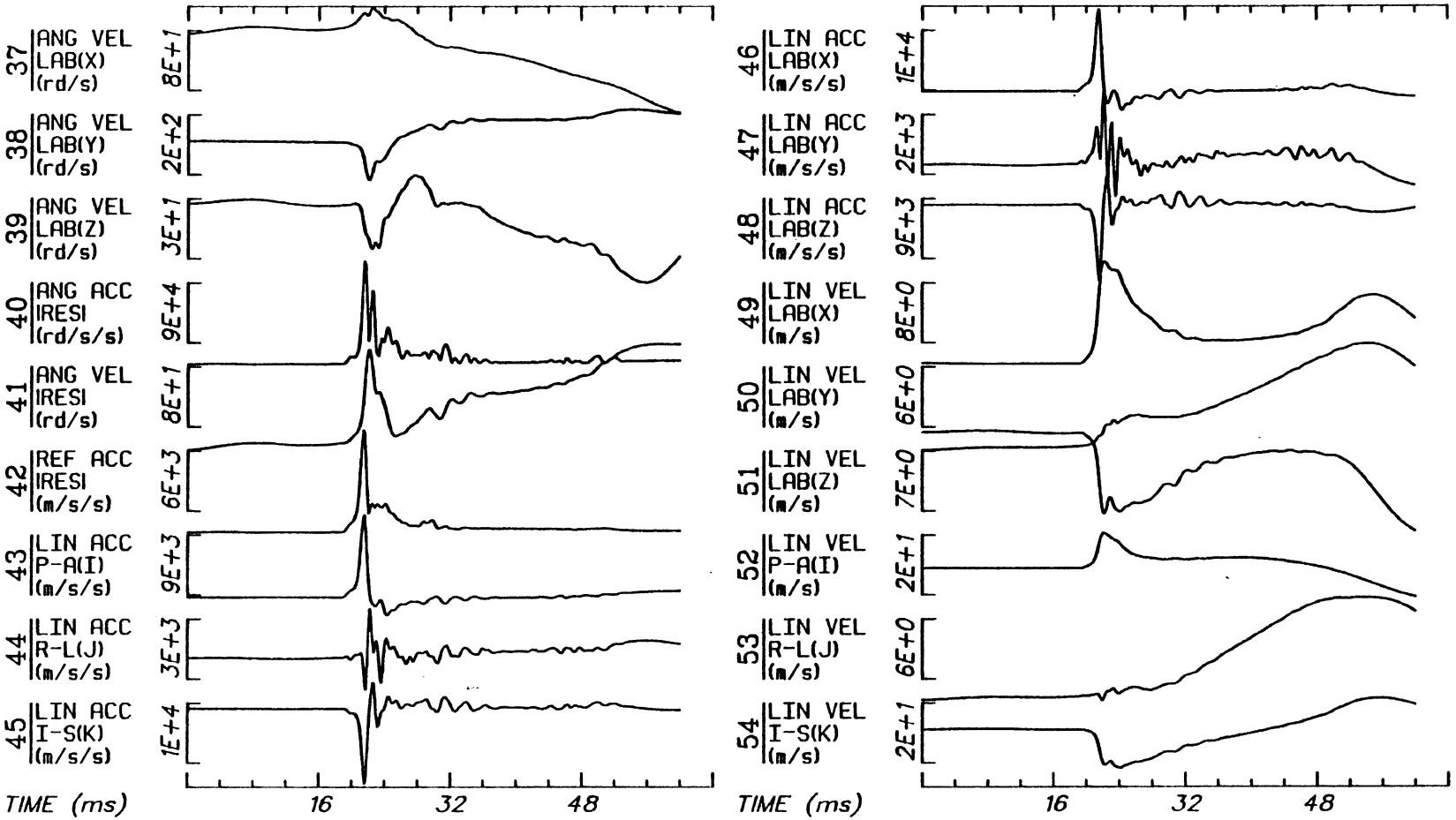

Run ID: 86R012 H7 Disk: R012.3D File: 1 Date: APR 8, 1986 Sheet: 3

No Filtering

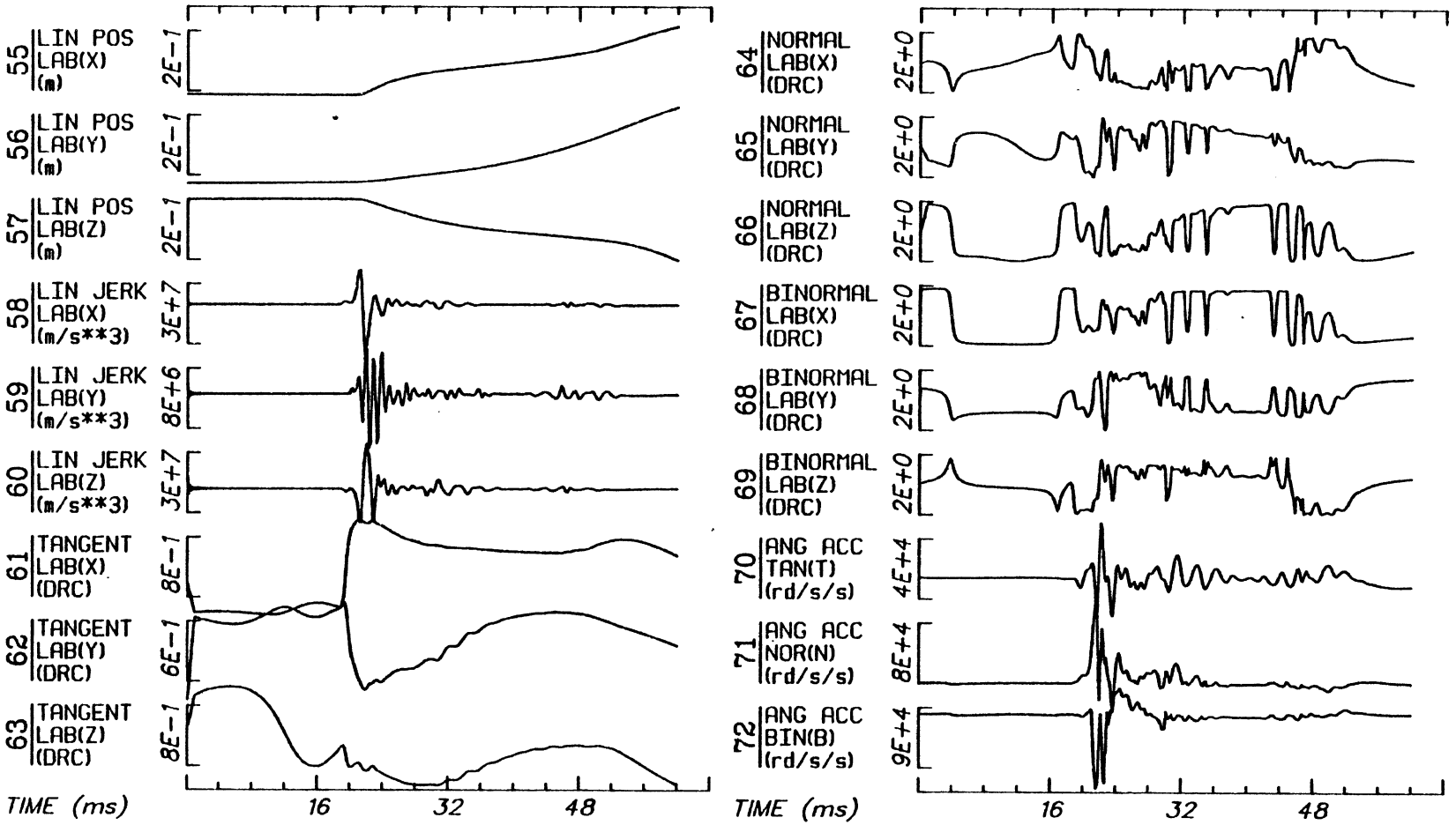

Run ID: 86R012 H7 Disk: R012.3D File: 1 Date: APR 8, 1986 Sheet: 4

No Filtering

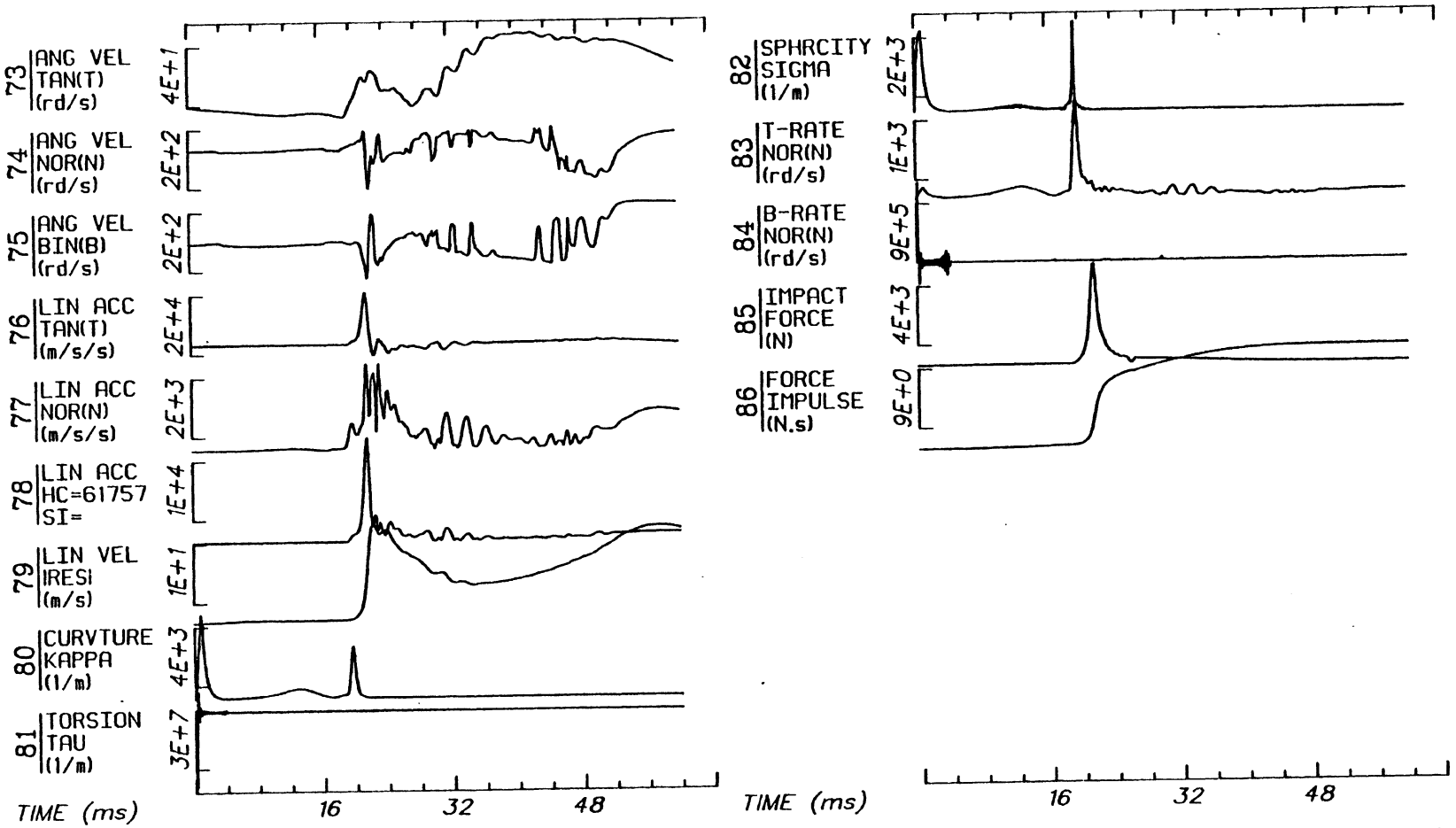

Run ID: 86R012 H7 Disk: R012.3D File: 1 Date: APR 8, 1986 Sheet: 5

No Filtering

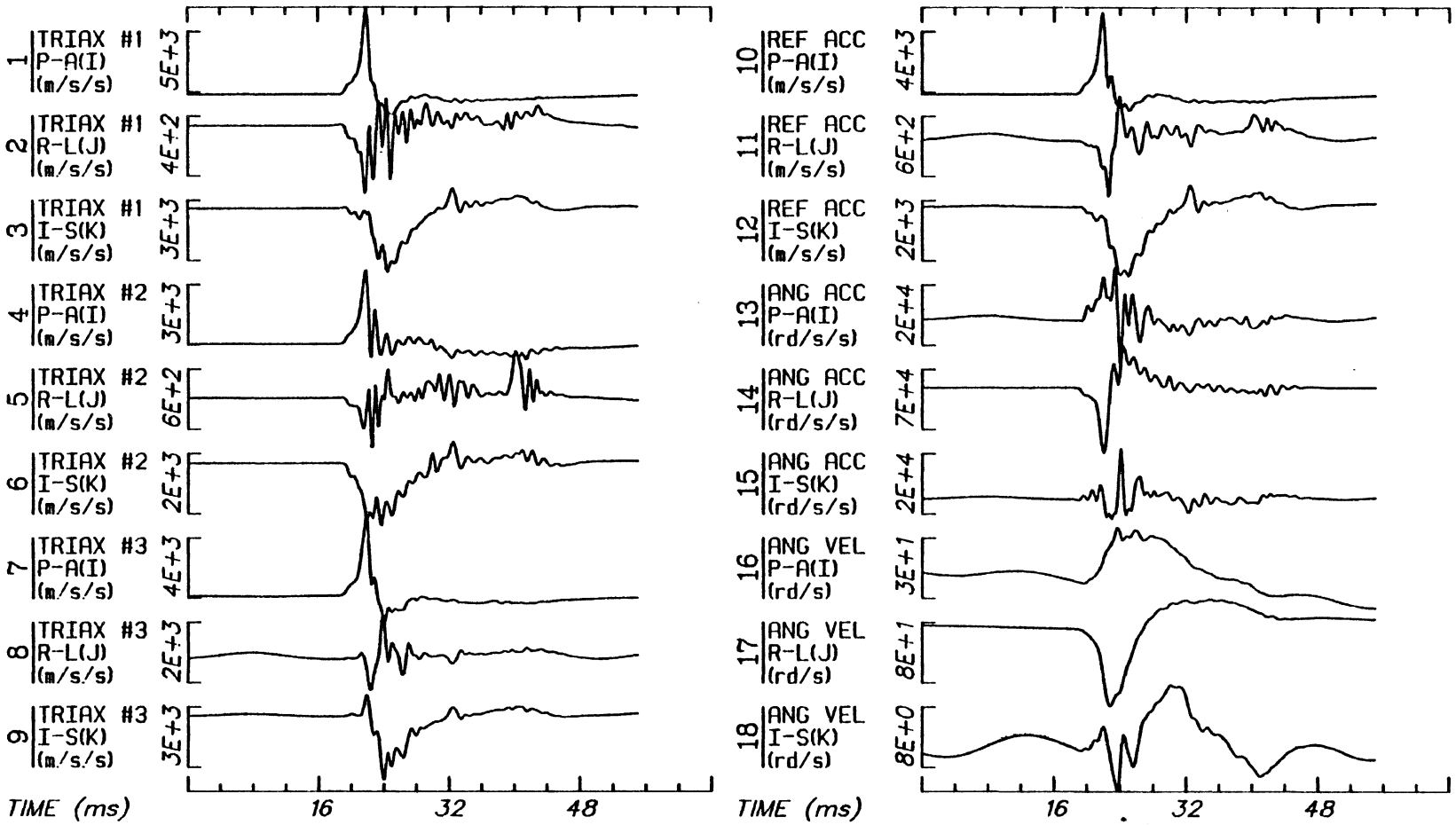

Run ID: 86R013 H7 Disk: R013.3D File: 1 Date: APR 8, 1986 Sheet: 1

No Filtering

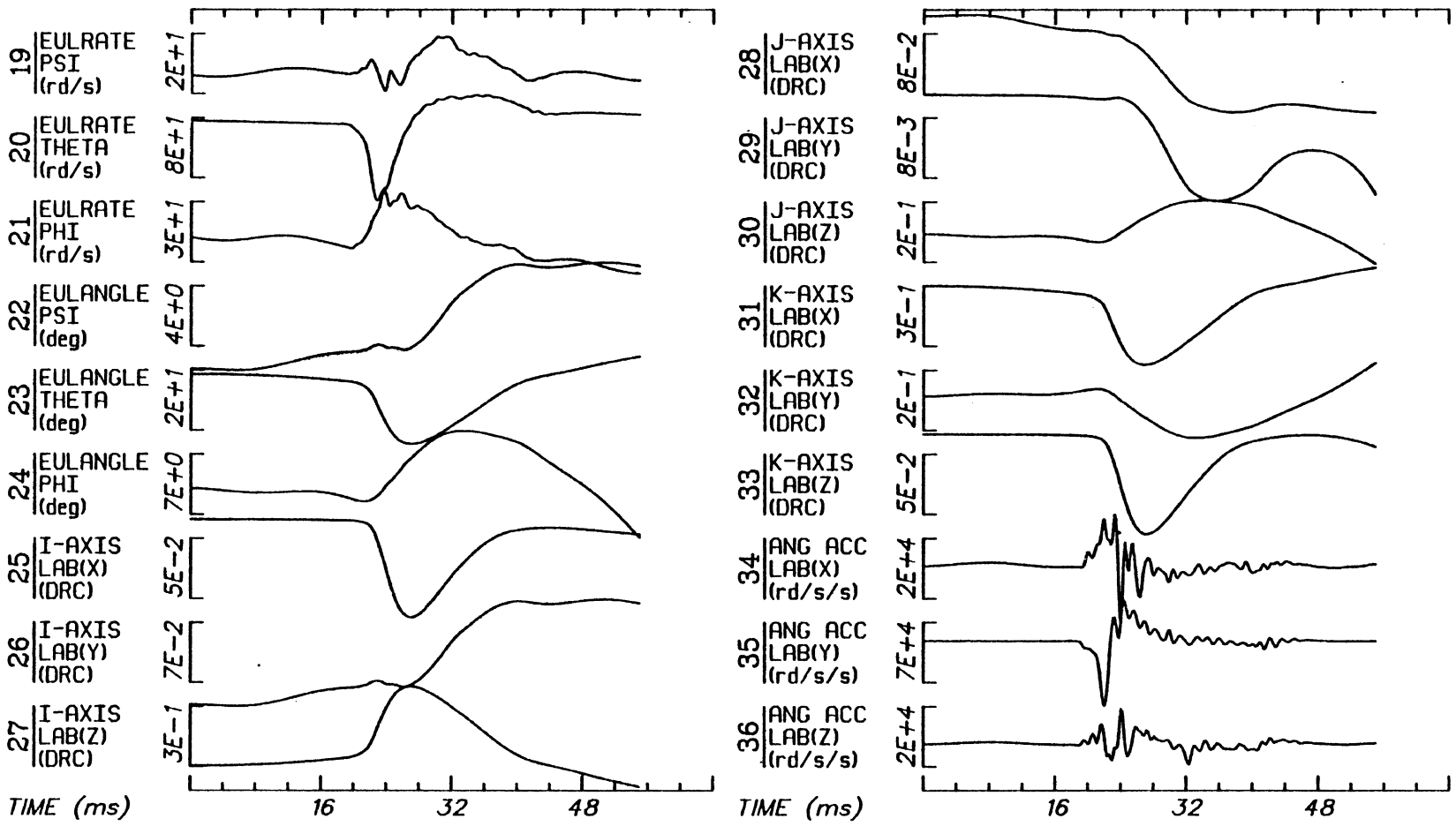

Run ID: 86R013 H7 Disk: R013.3D File: 1 Date: APR 8, 1986 Sheet: 2

No Filtering

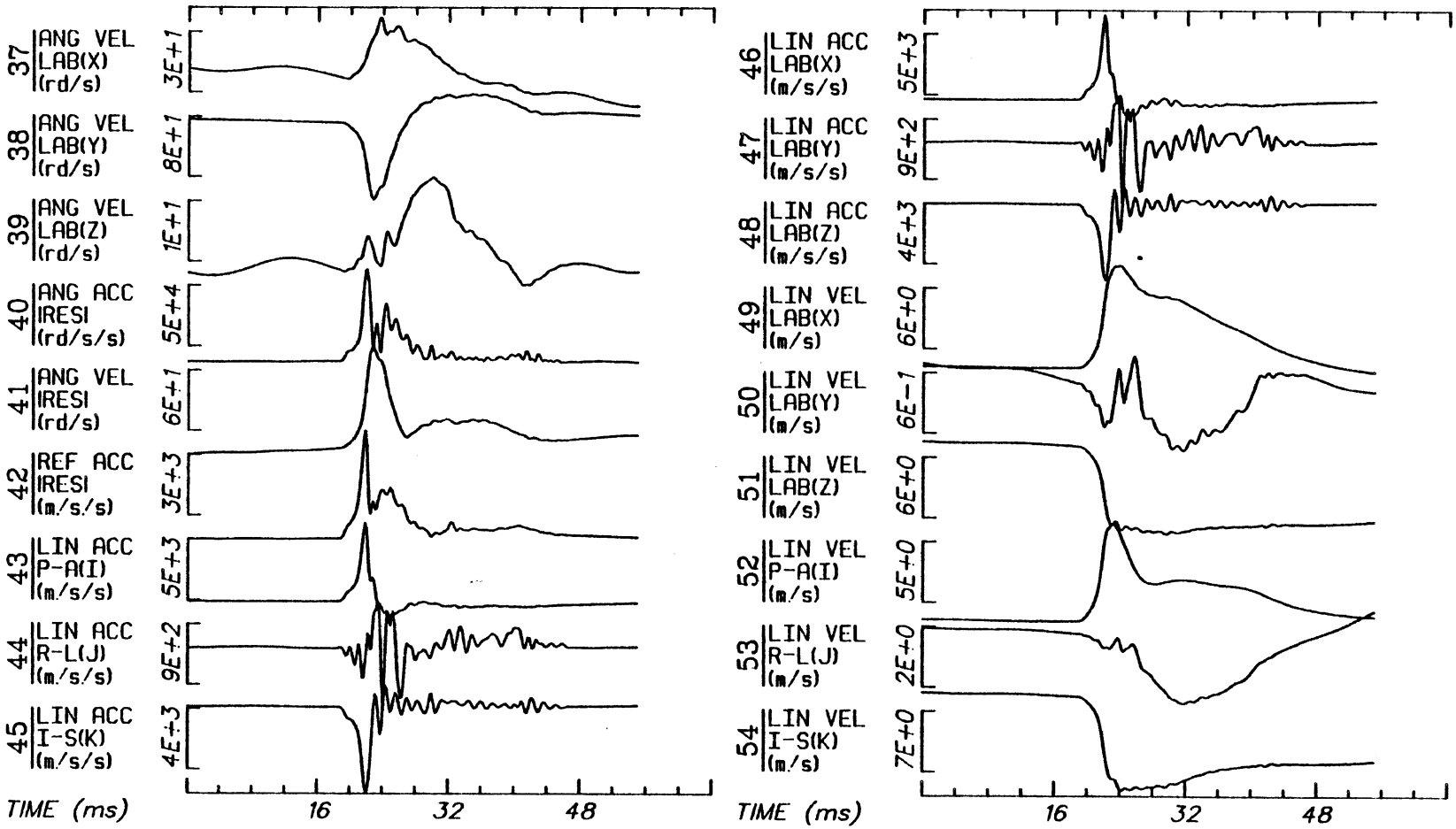

Run ID: 86R013 H7 Disk: R013.3D File: 1 Date: APR 8, 1986 Sheet: 3

No Filtering

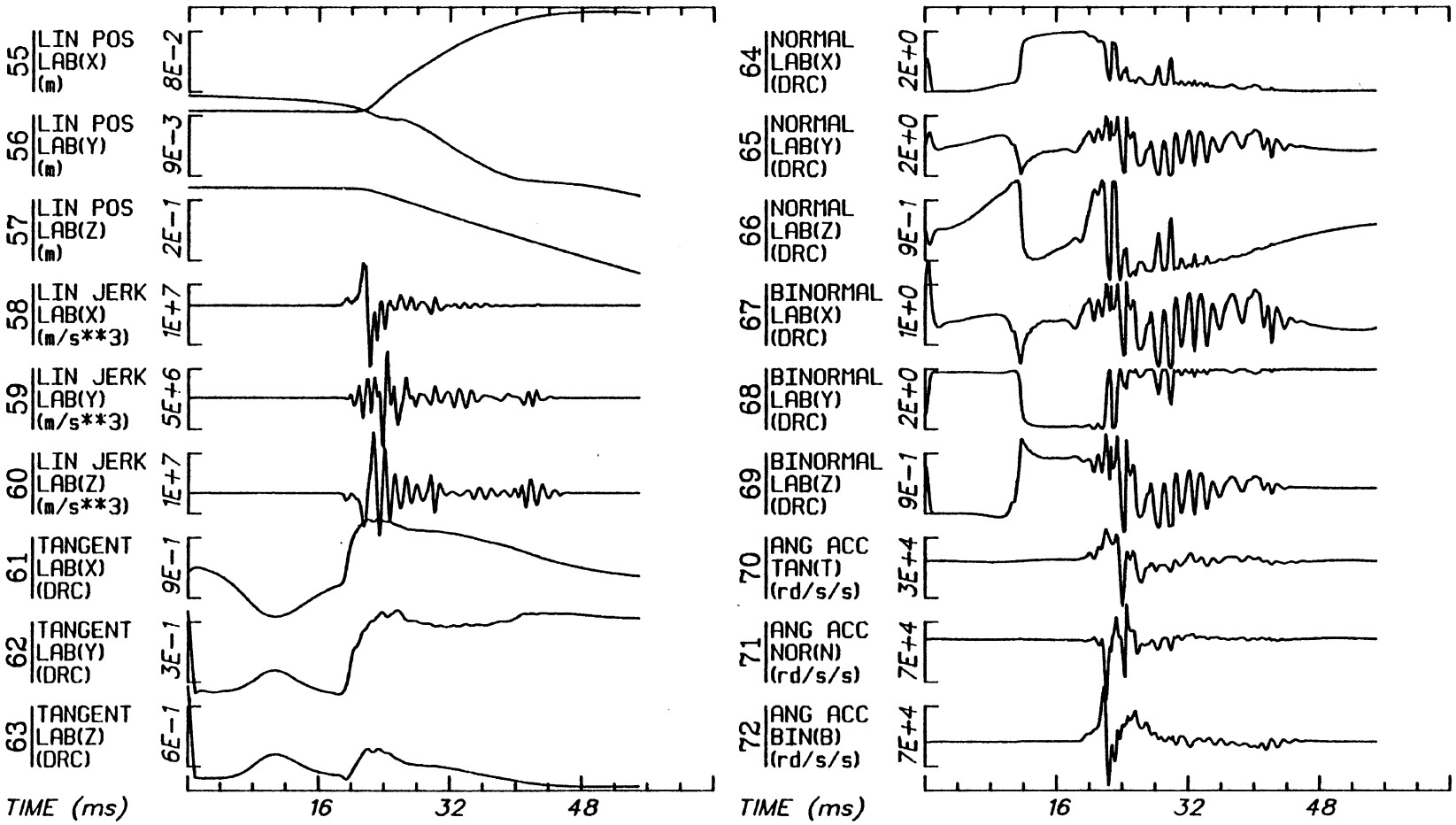

Run ID: 86R013 H7 Disk: R013.3D File: 1 Date: APR 8, 1986 Sheet: 4

No Filtering

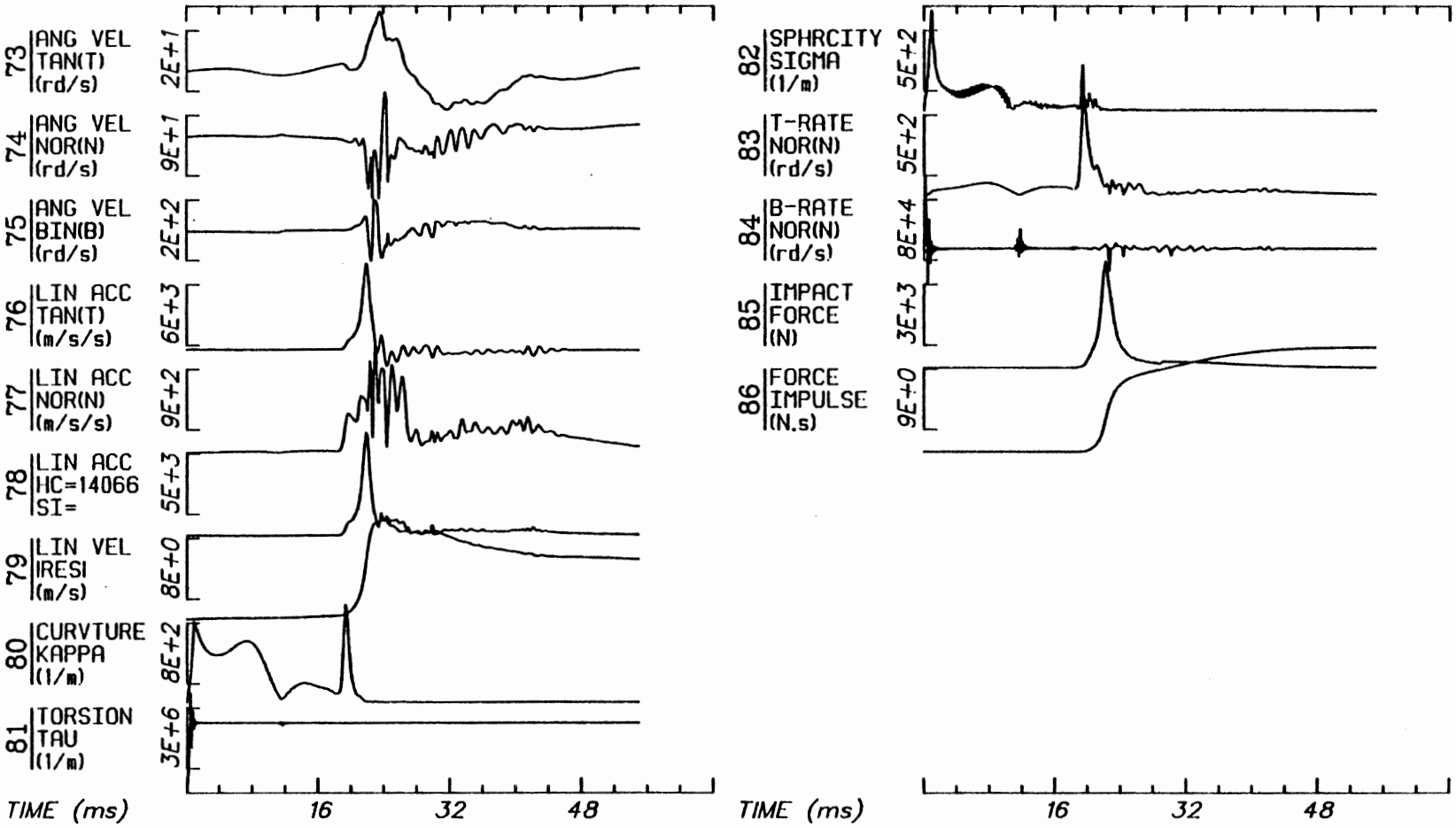

Run ID: 86R013 H7 Disk: R013.3D File: 1 Date: APR 8, 1986 Sheet: 5

No Filtering

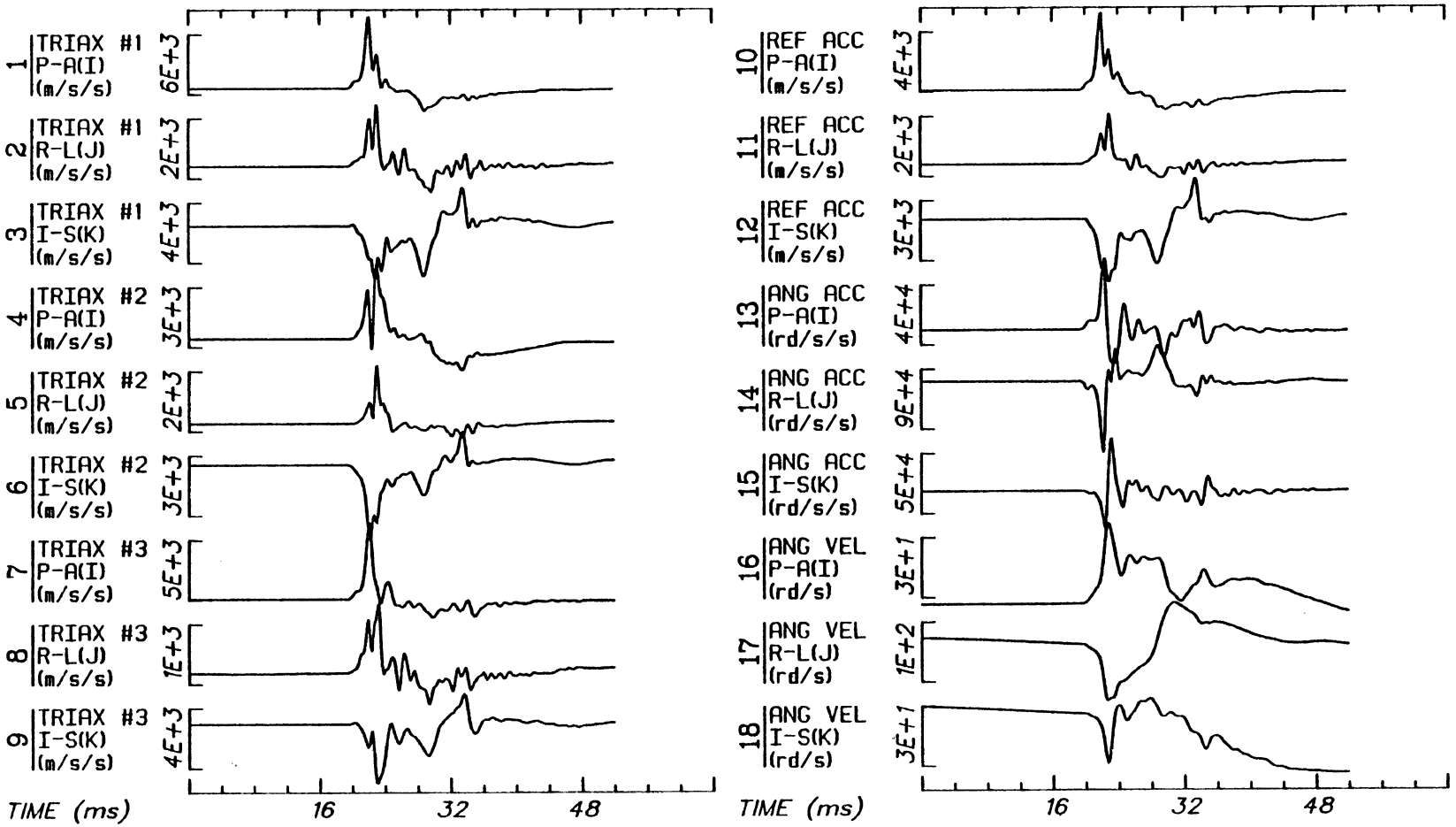

Run ID: 86R014 H7 Disk: R014.3D File: 1 Date: APR 8, 1986 Sheet: 1

No Filtering

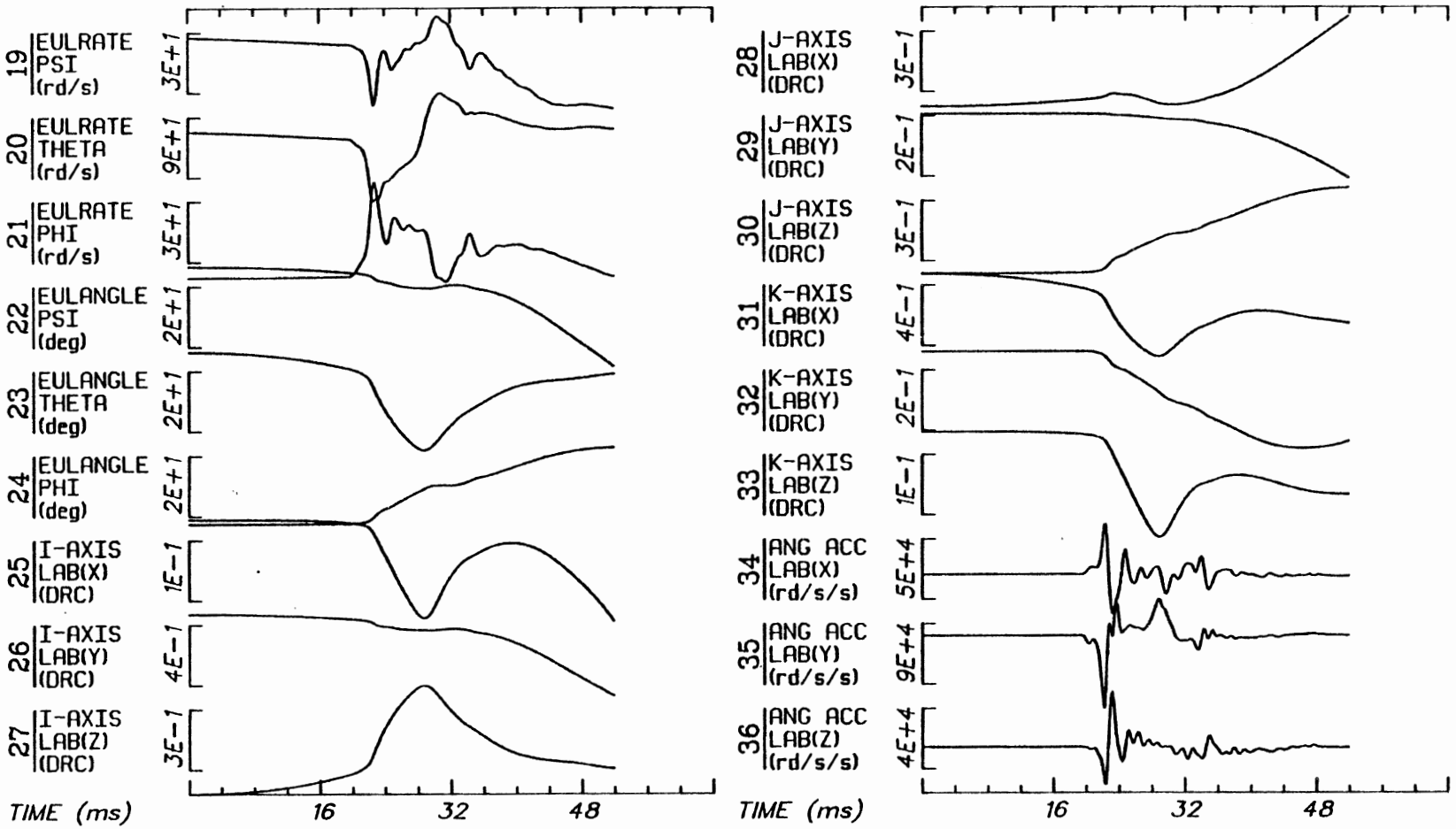

Run ID: 86R014 H7 Disk: R014.3D File: 1 Date: APR 8, 1986 Sheet: 2

No Filtering

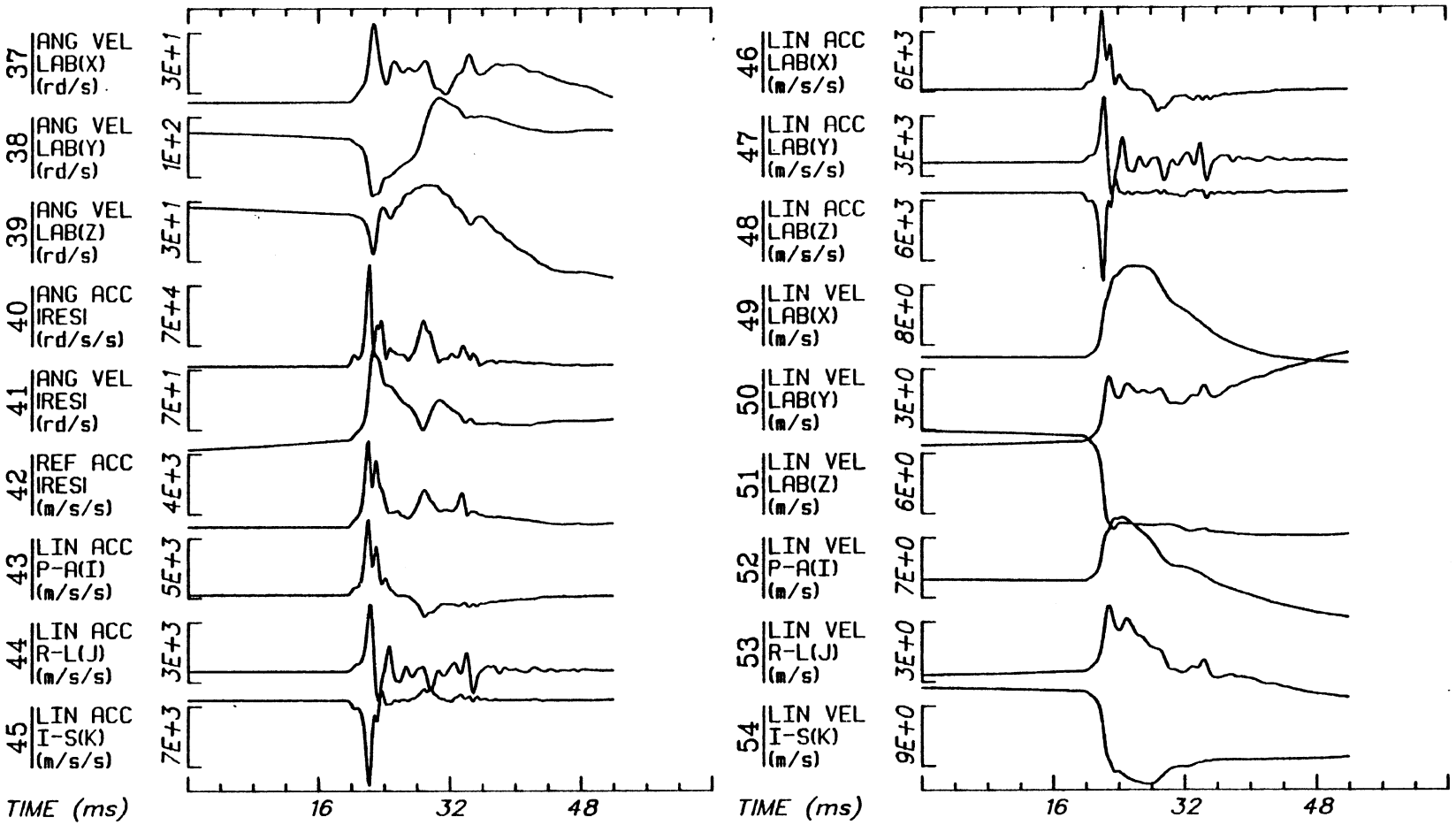

Run ID: 86R014 H7 Disk: R014.3D File: 1 Date: APR 8, 1986 Sheet: 3

No Filtering

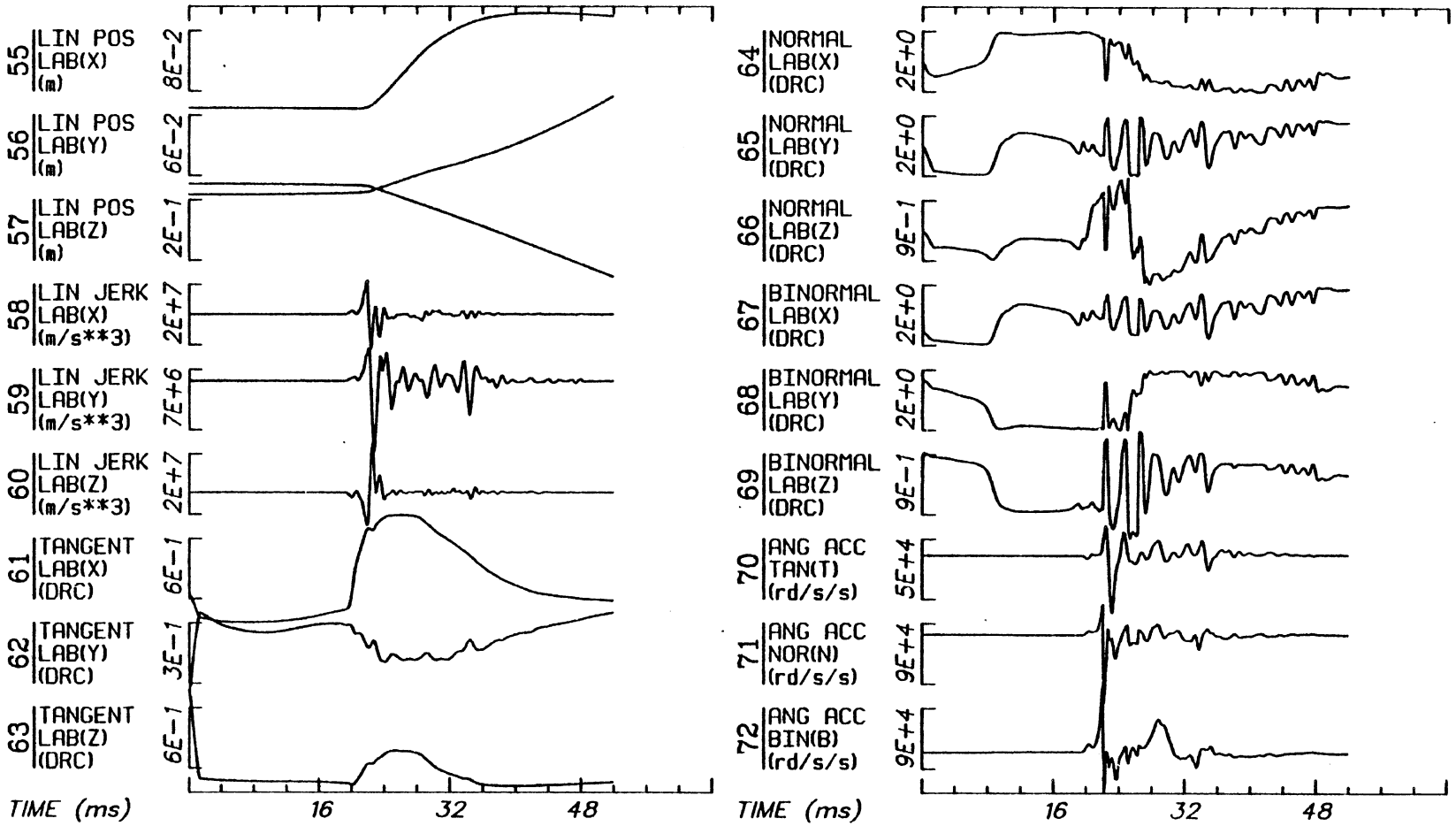

Run ID: 86R014 H7 Disk: R014.3D File: 1 Date: APR 8, 1986 Sheet: 4

No Filtering

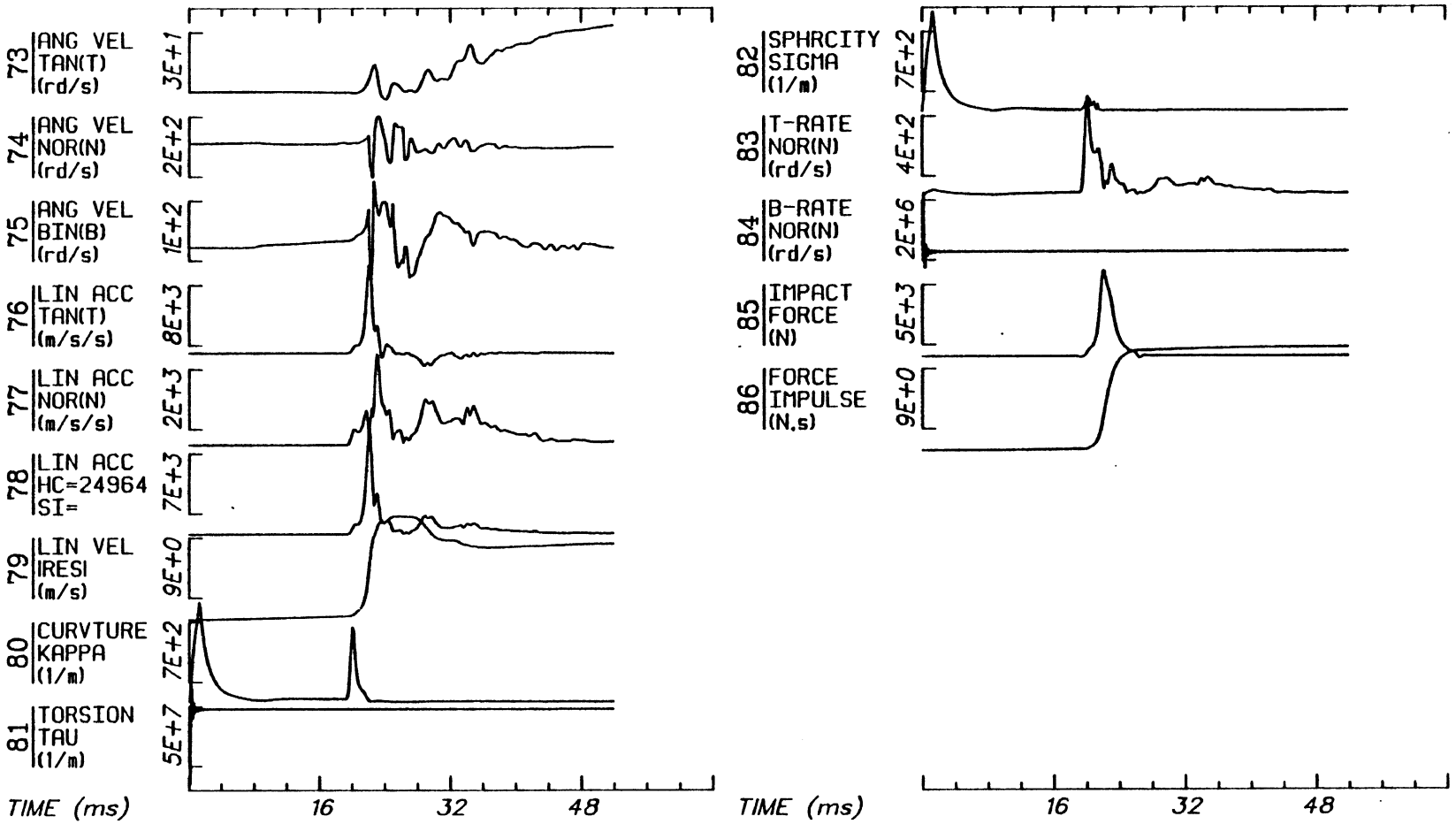

Run ID: 86R014 H7 Disk: R014.3D File: 1 Date: APR 8, 1986 Sheet: 5

No Filtering

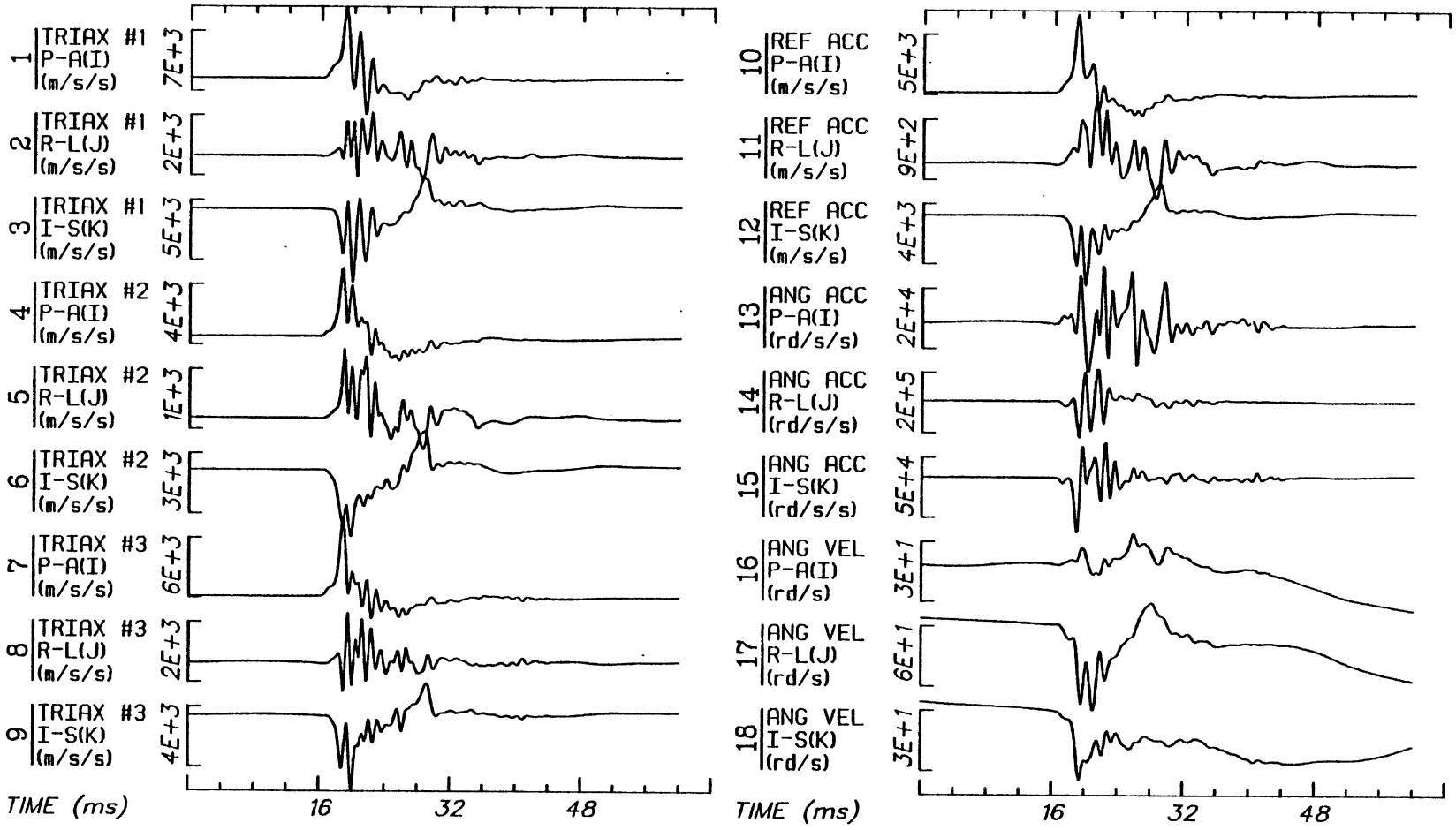

Run ID: 86R015 H7 Disk: R015.3D File: 1 Date: APR 8, 1986 Sheet: 1

No Filtering

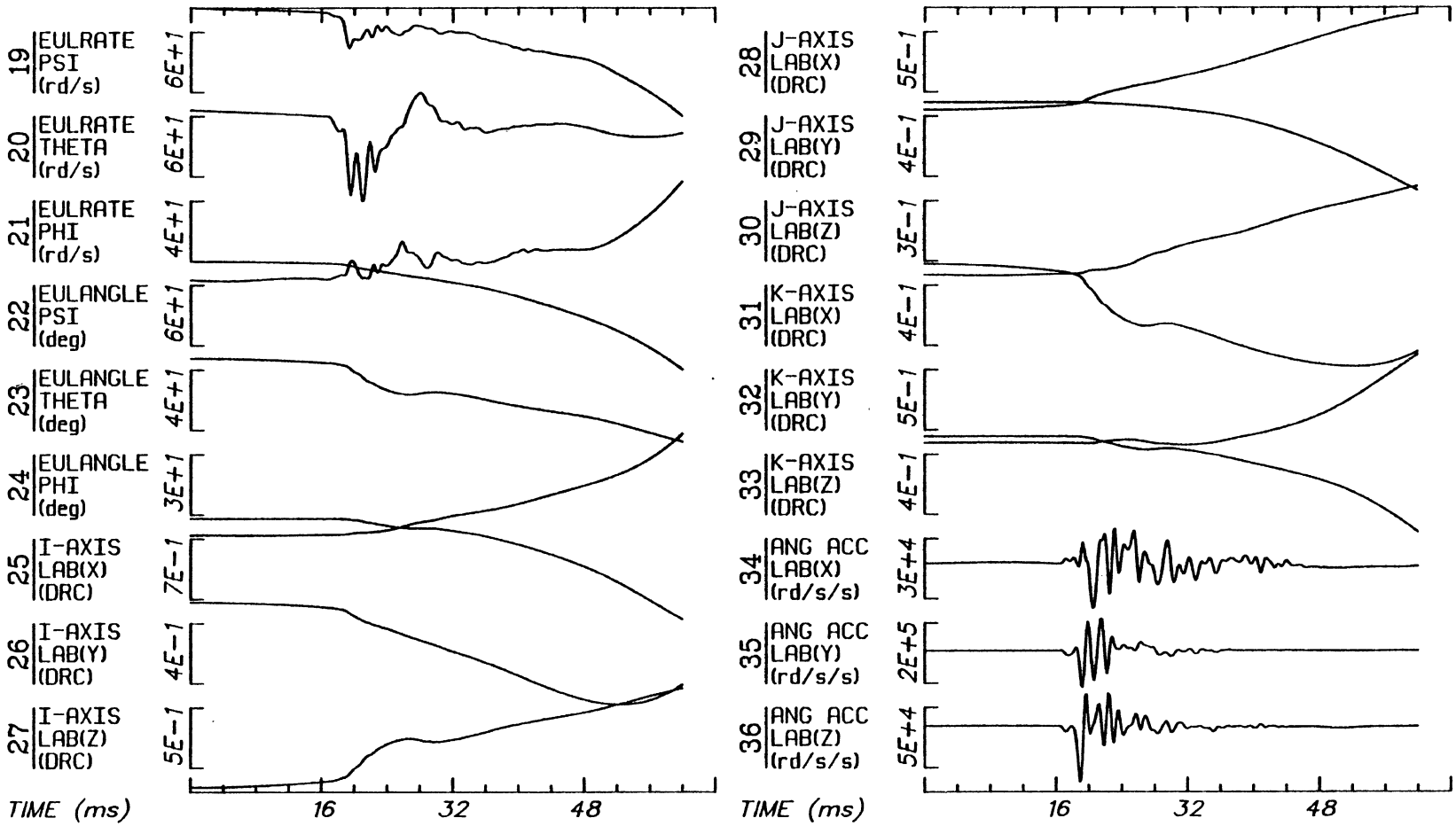

Run ID: 86R015 H7 Disk: R015.3D File: 1 Date: APR 8, 1986 Sheet: 2

No Filtering

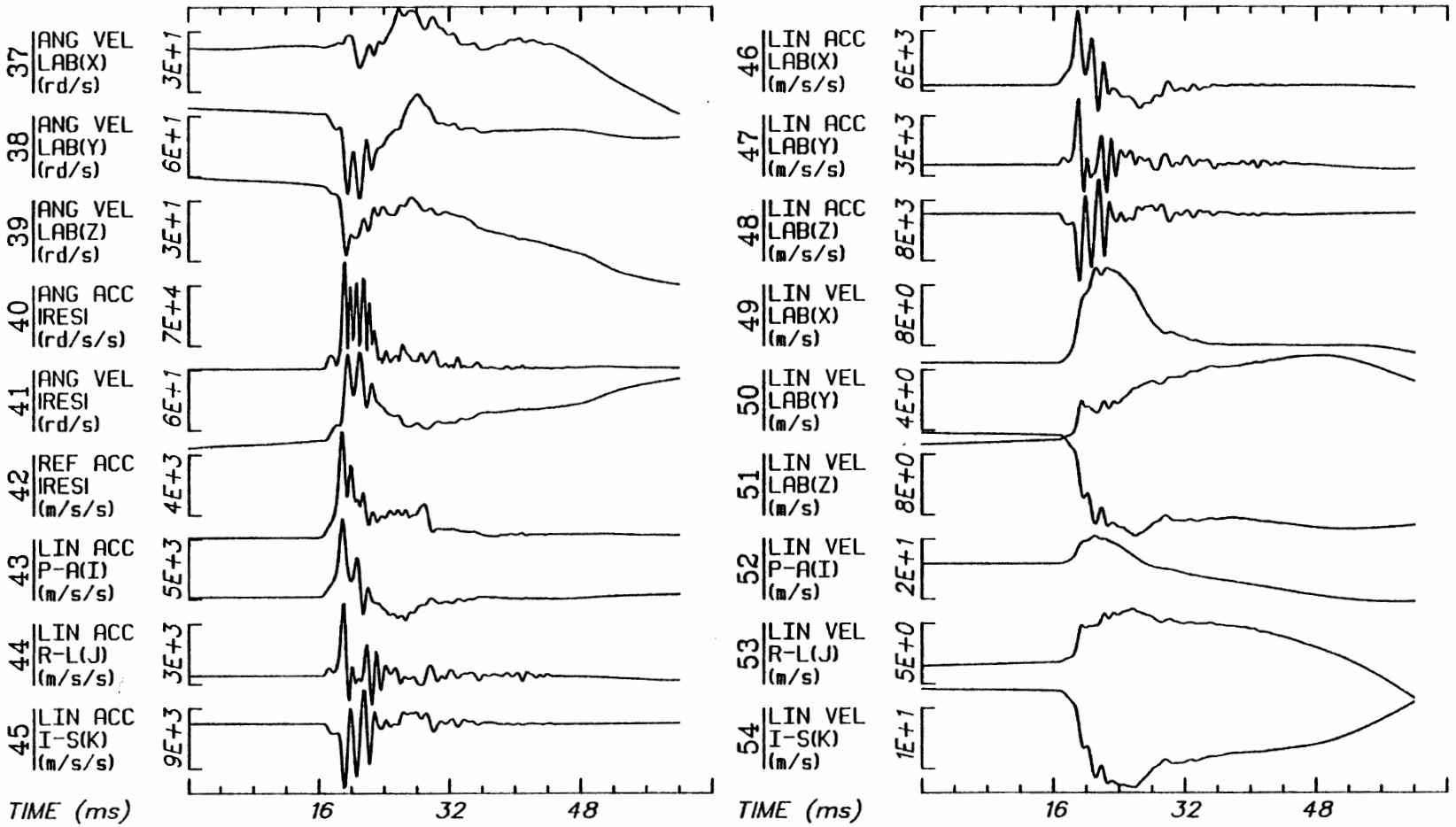

Run ID: 86R015 H7 Disk: R015.3D File: 1 Date: APR 8, 1986 Sheet: 3

No Filtering

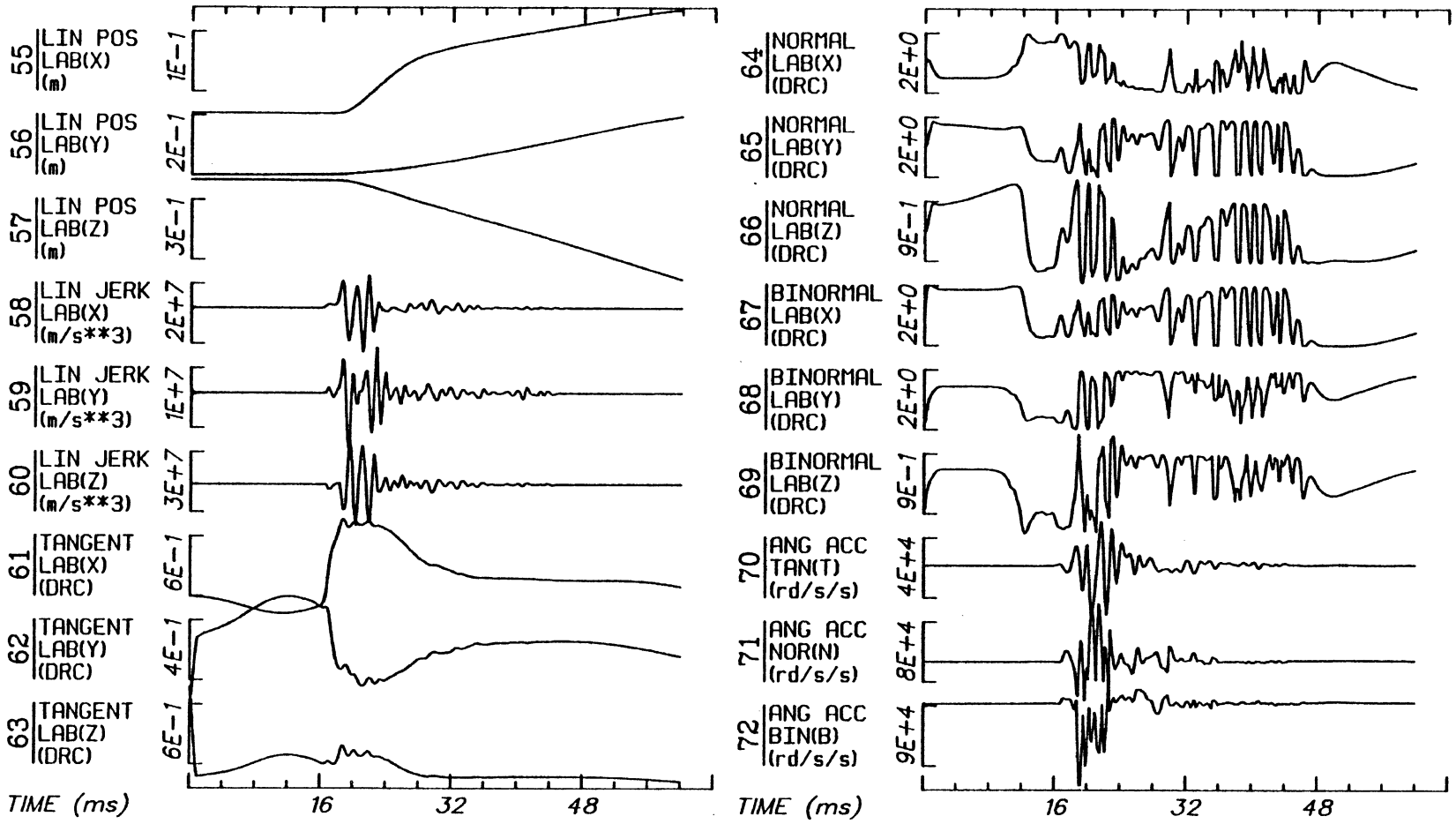

Run ID: 86R015 H7 Disk: R015.3D File: 1 Date: APR 8, 1986 Sheet: 4

No Filtering

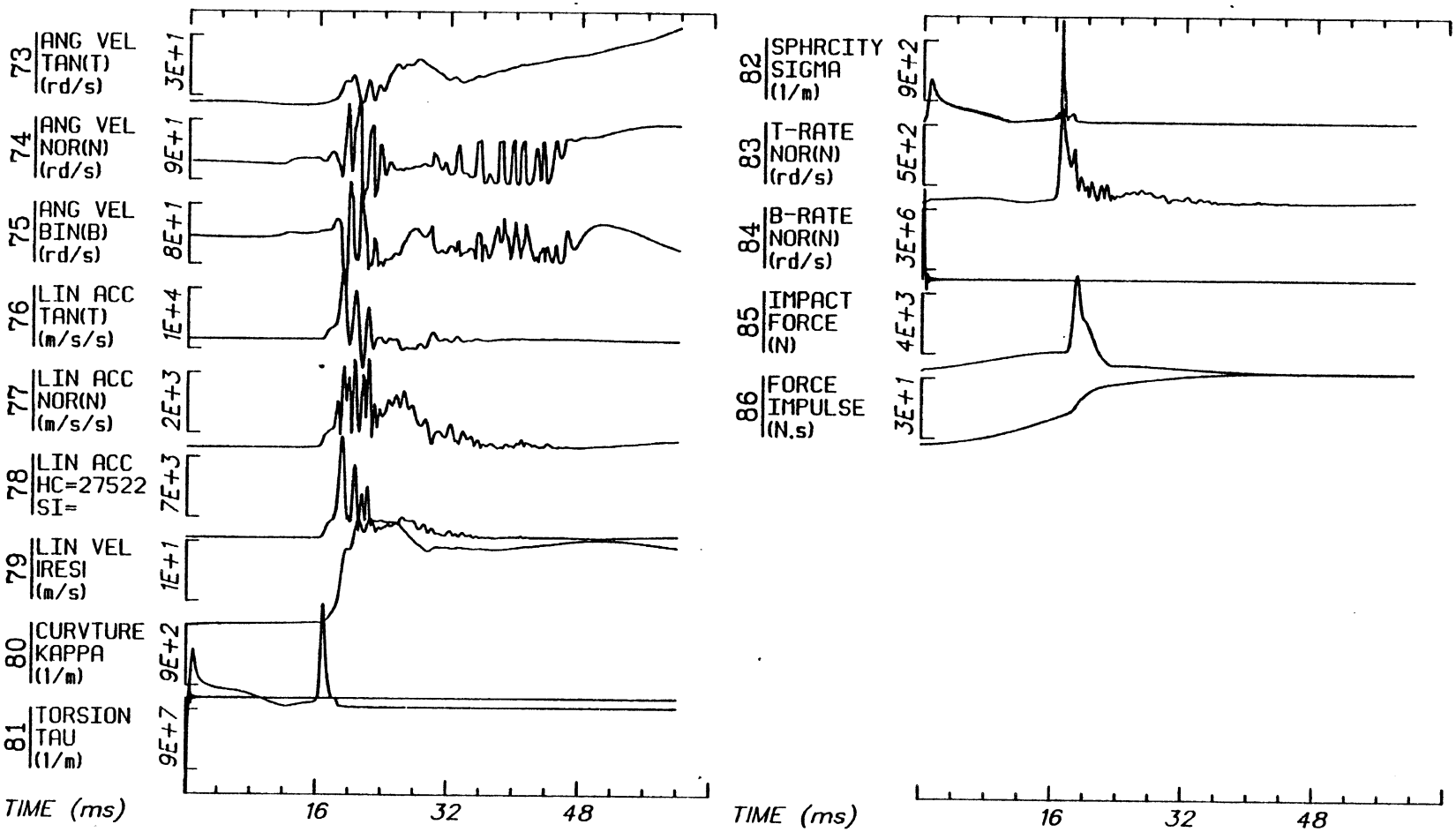

Run ID: 86R015 H7 Disk: R015.3D File: 1 Date: APR 8, 1986 Sheet: 5

No Filtering

Mechanical Impedance for Anesthetized Rhesus - Skull Fracture

Run ID: COMBINED DATA

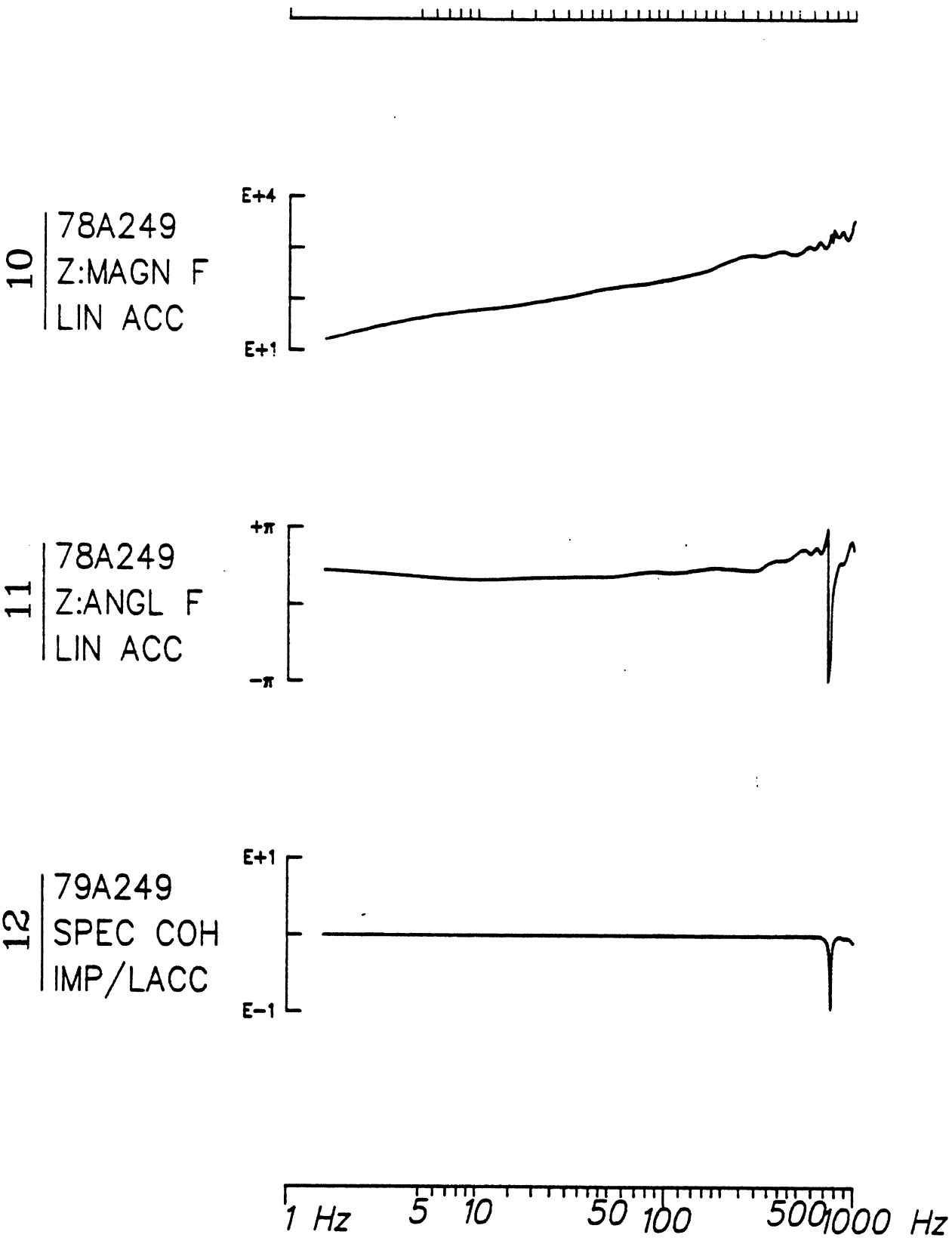

Mechanical Impedance for Anesthetized Rhesus - Skull Fracture

Run ID: COMBINED DATA

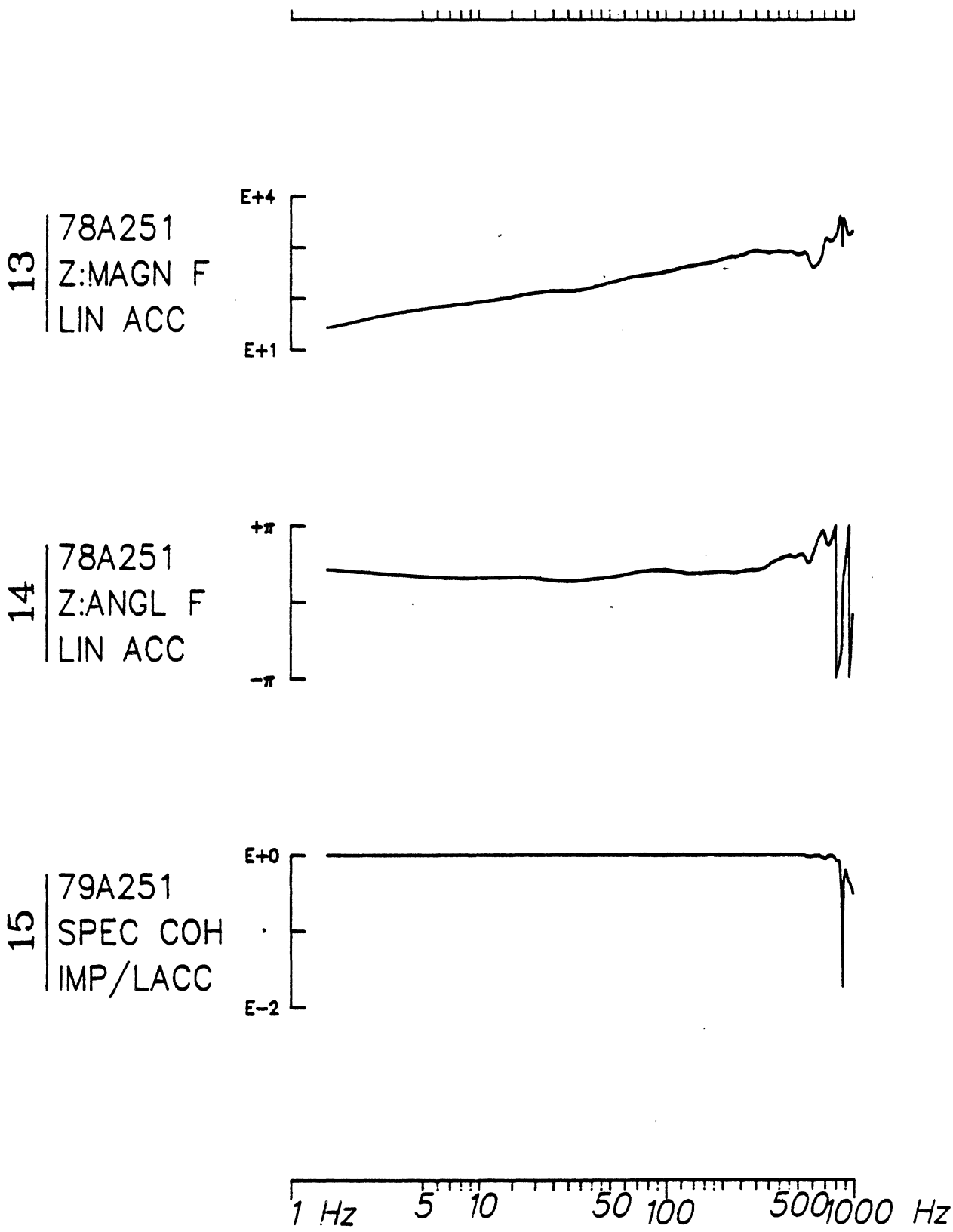

Mechanical Impedance for Unrepressurized Postmortem Rhesus - No Skull Fracture

Run ID: COMBINED DATA

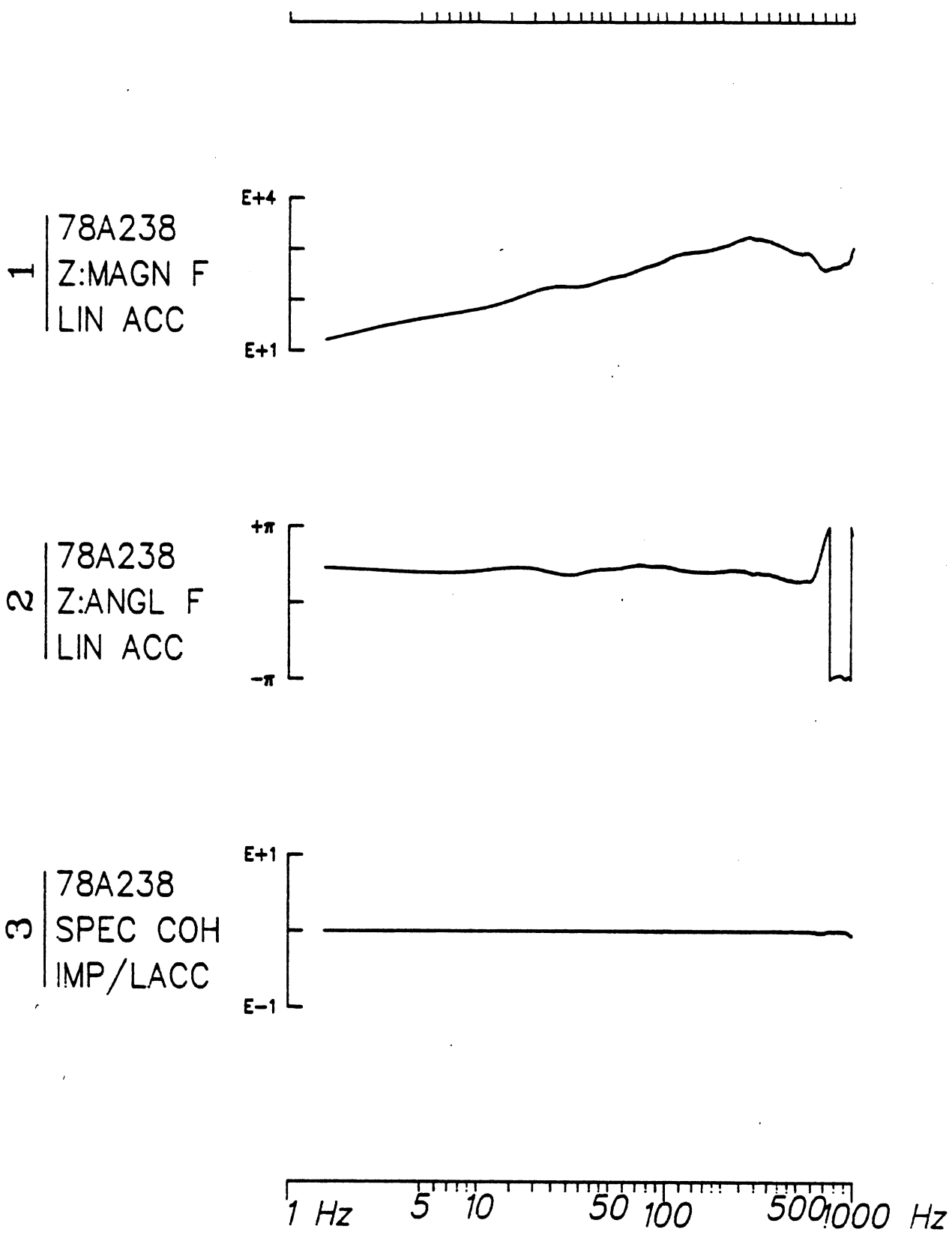

Mechanical Impedance for Anesthetized Rhesus - No Skull Fracture

Run ID: COMBINED DATA

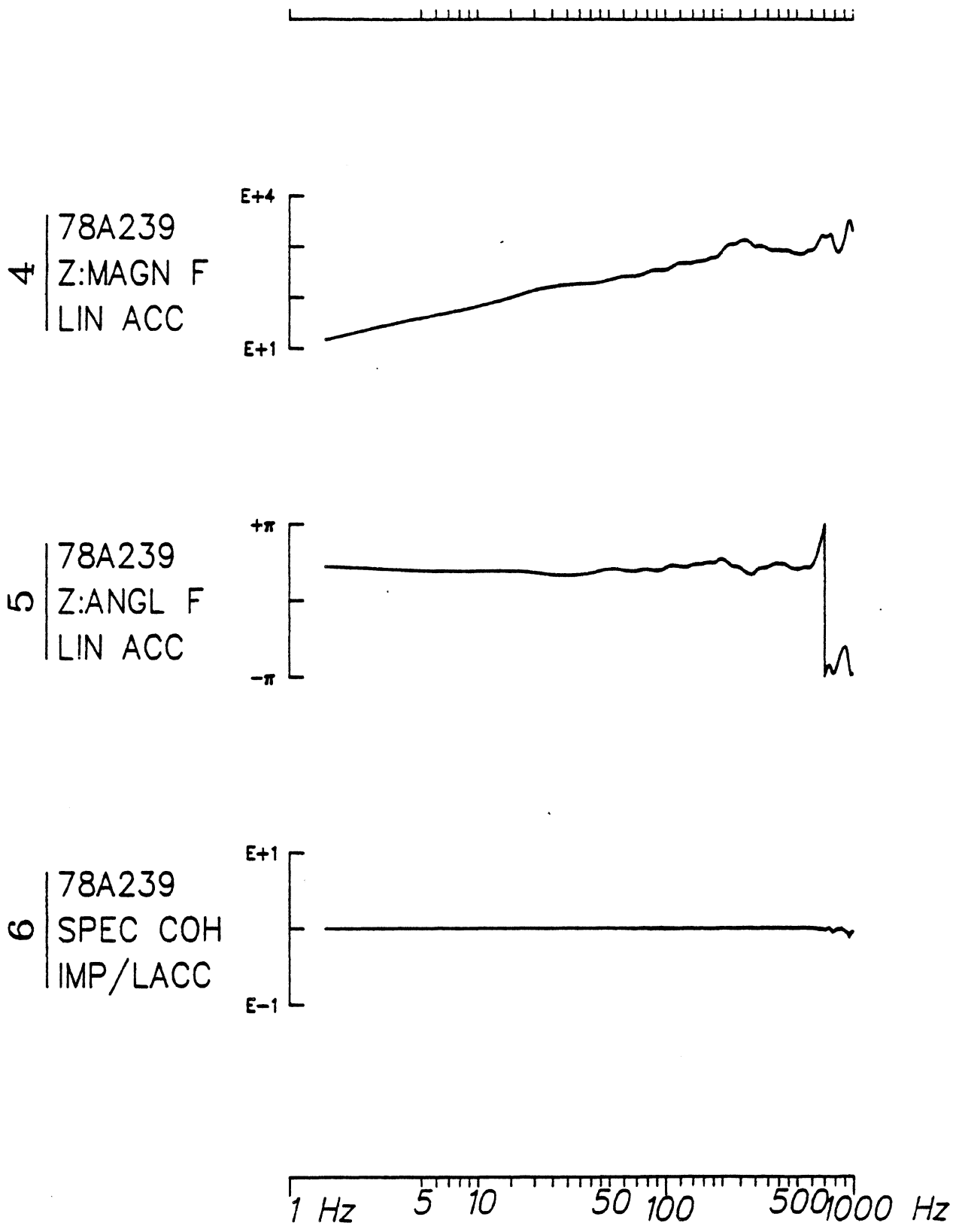

Mechanical Impedance for Anesthetized Rhesus - No Skull Fracture

Run ID: COMBINED DATA

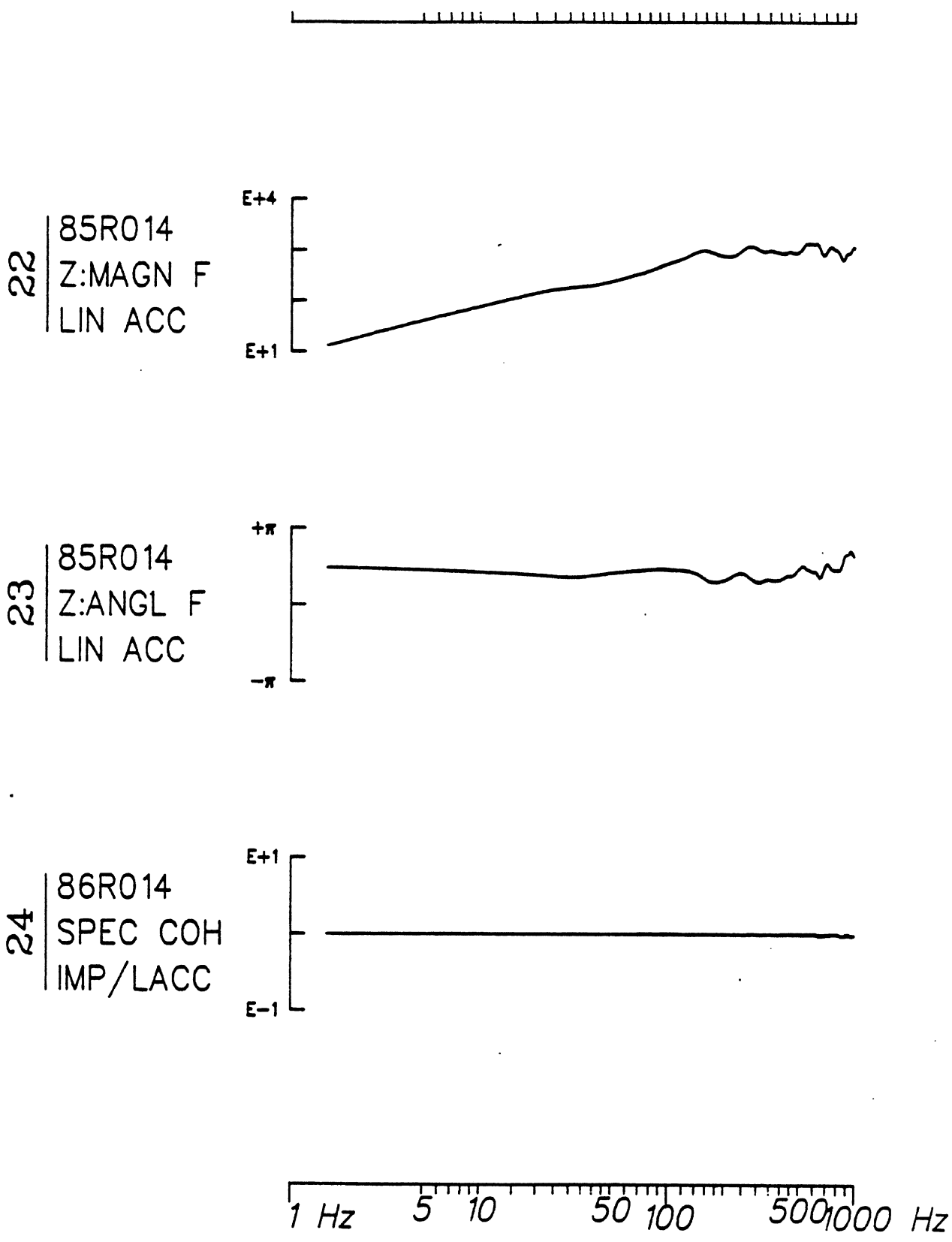

Run ID: 78A236 *Filter: 1600*4C* *Smooth: 3SD*

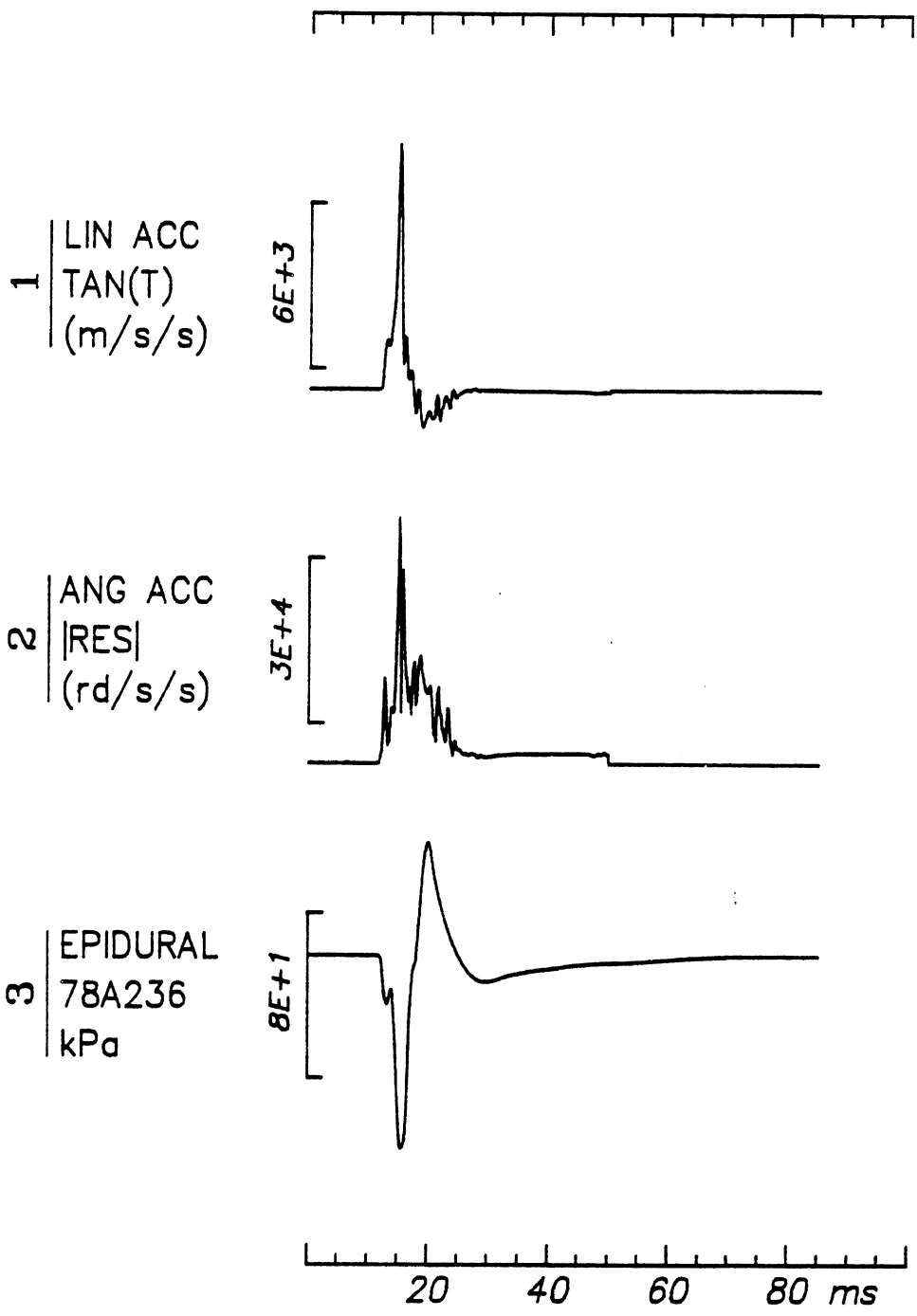

1=Tangential Acceleration
2=Angular Acceleration (Resultant)
3=Epidural Pressure

Run ID: 79A249 *Filter: 1600*4C* *Smooth: 3SD*

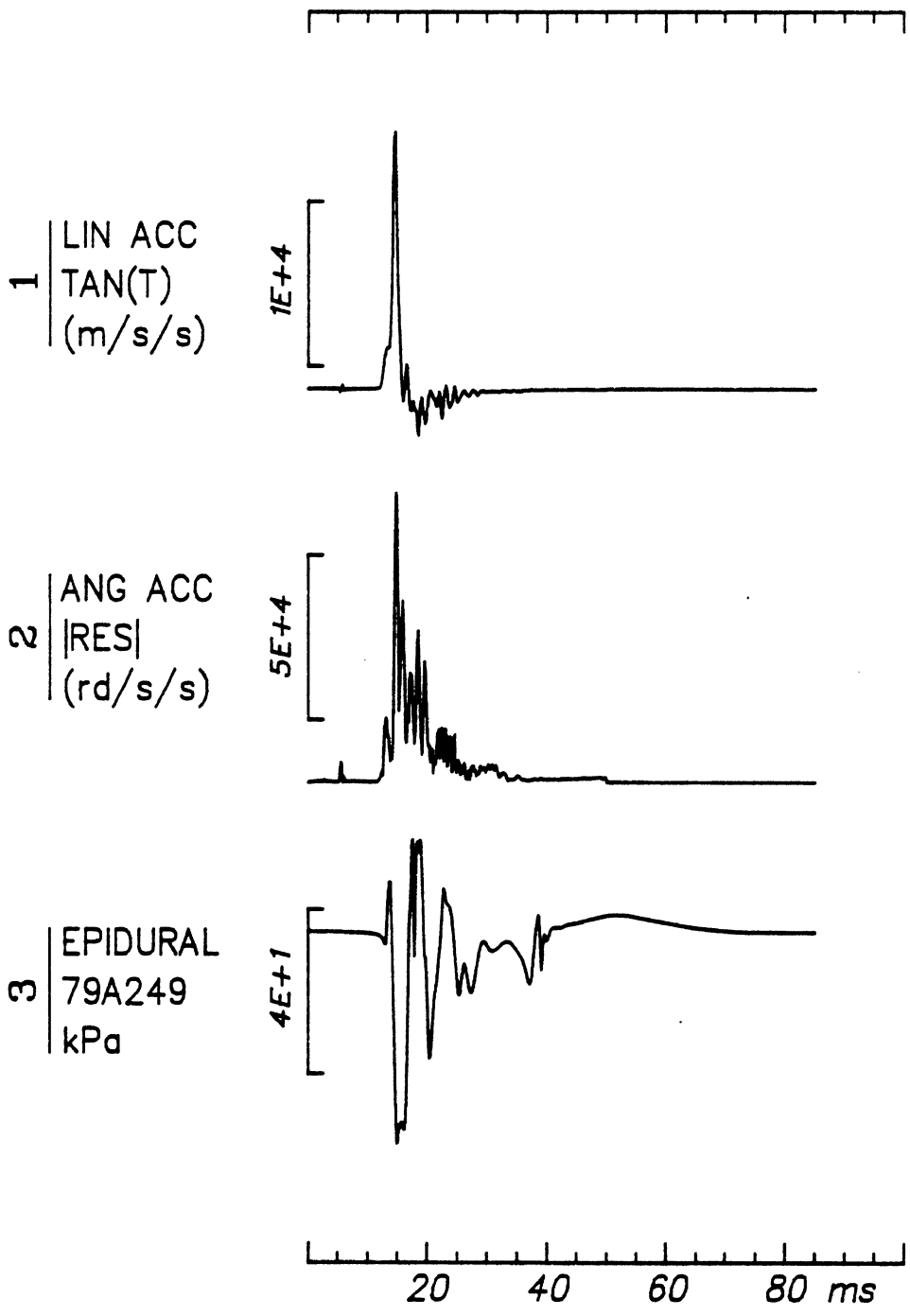

1=Tangential Acceleration
2=Angular Acceleration (Resultant)
3=Epidural Pressure

Run ID: 79A251 *Filter: 1600*4C* *Smooth: 3SD*

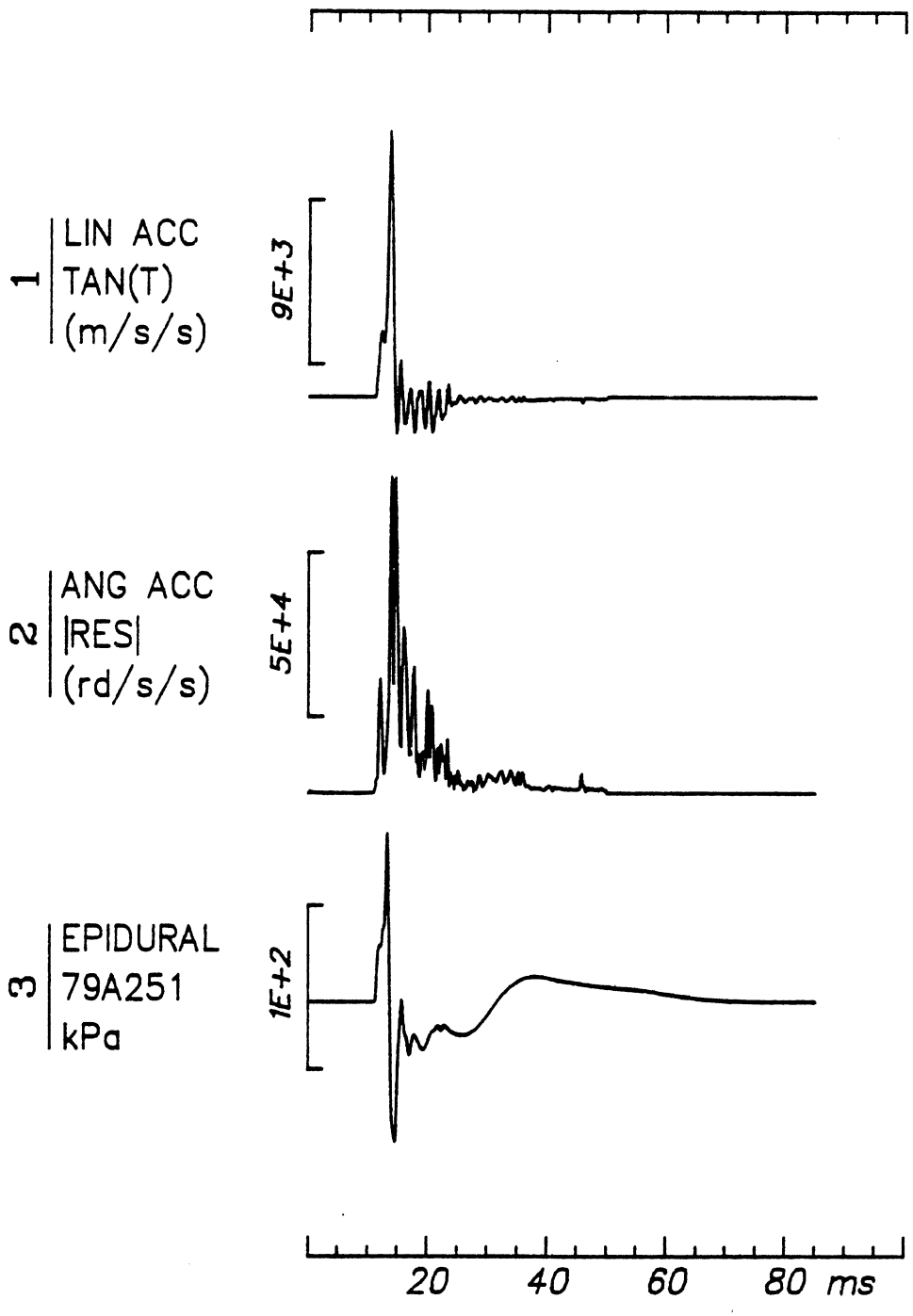

1=Tangential Acceleration
2=Angular Acceleration (Resultant)
3=Epidural Pressure

Run ID: 85R006 H9 *No Filtering*

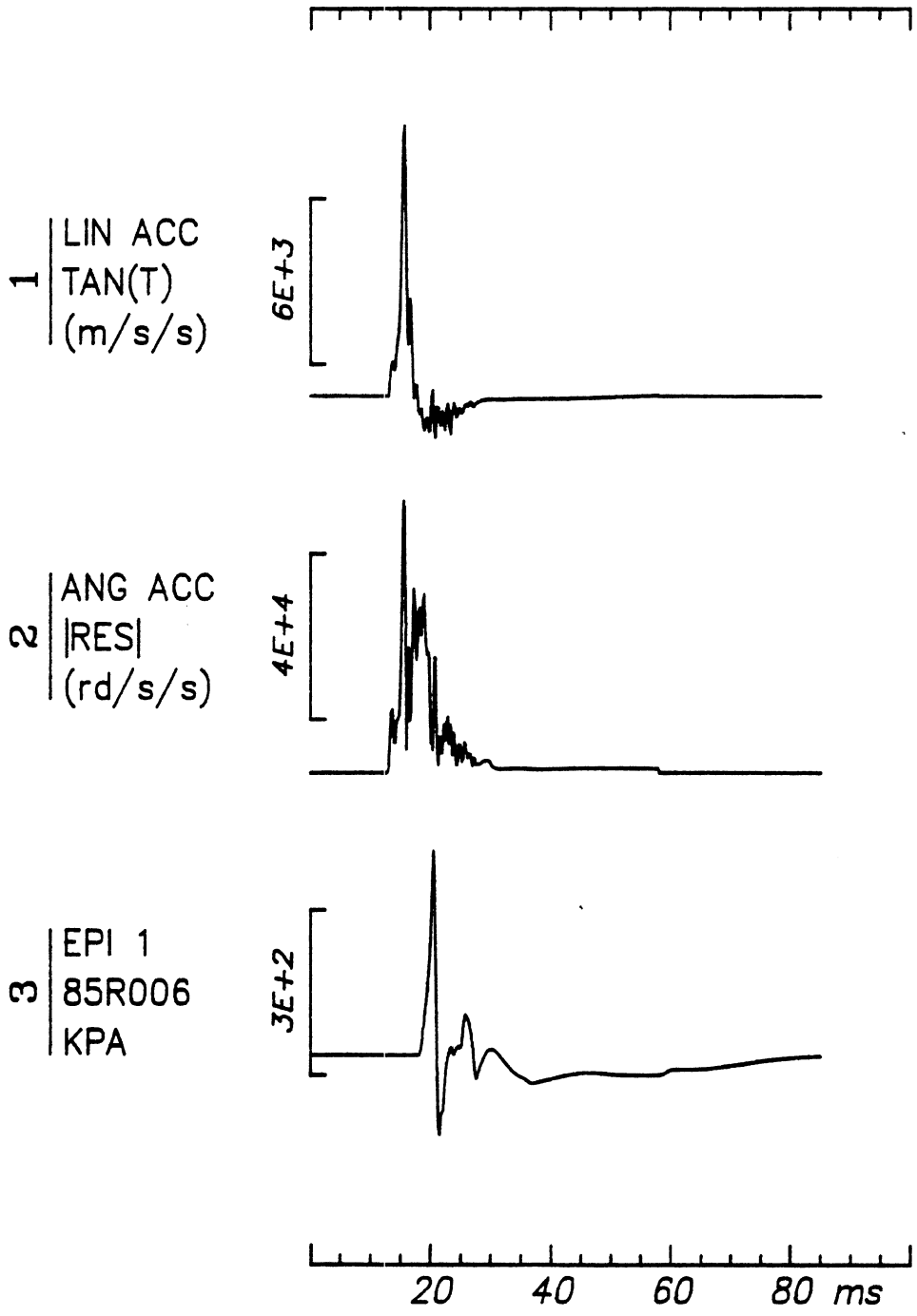

1=Tangential Acceleration
2=Angular Acceleration (Resultant)
3=Epidural Pressure

Run ID: 86R013 H7 *No Filtering*

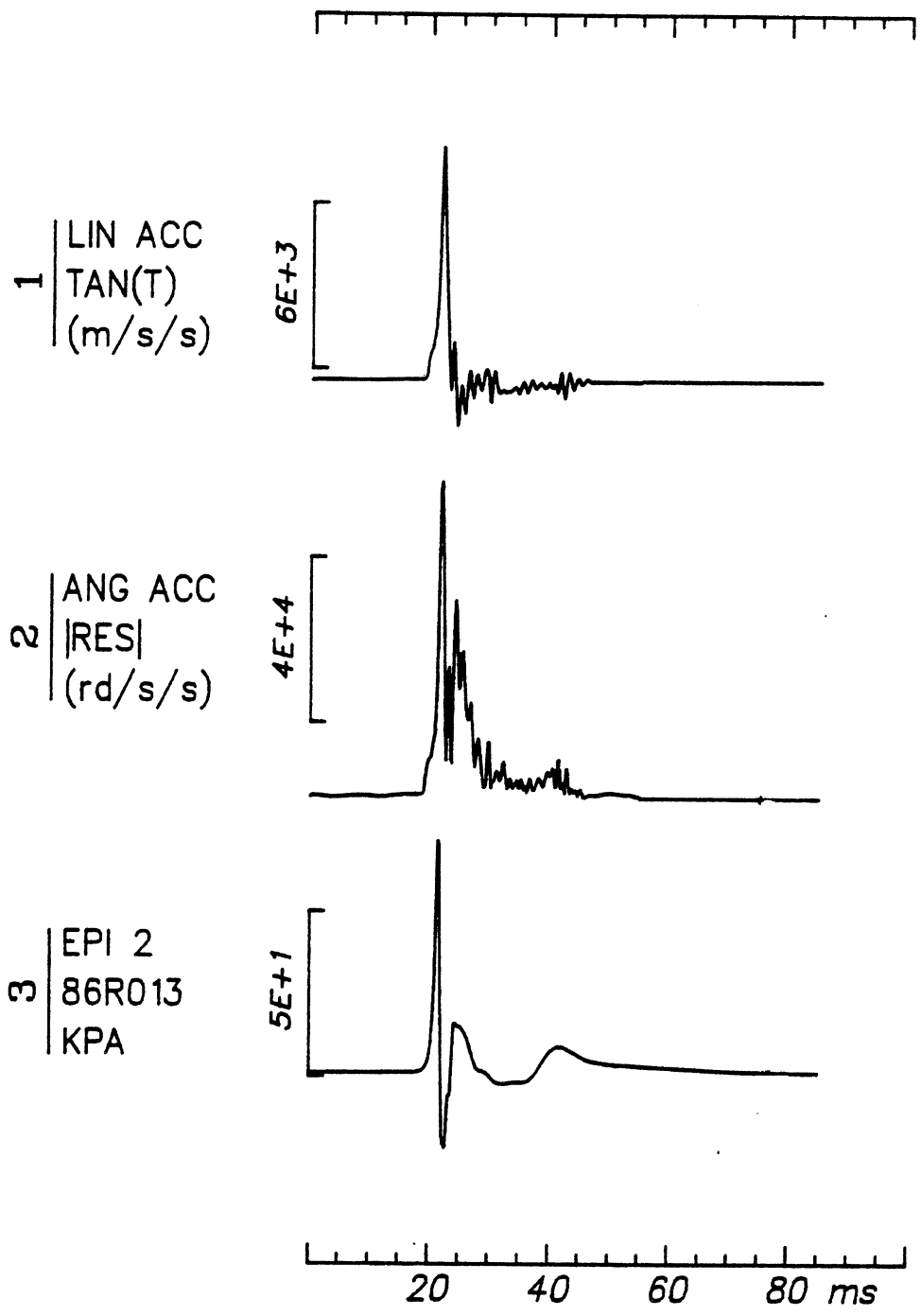

1=Tangential Acceleration
2=Angular Acceleration (Resultant)
3=Epidural Pressure

Run ID: 86R014 H7 *No Filtering*

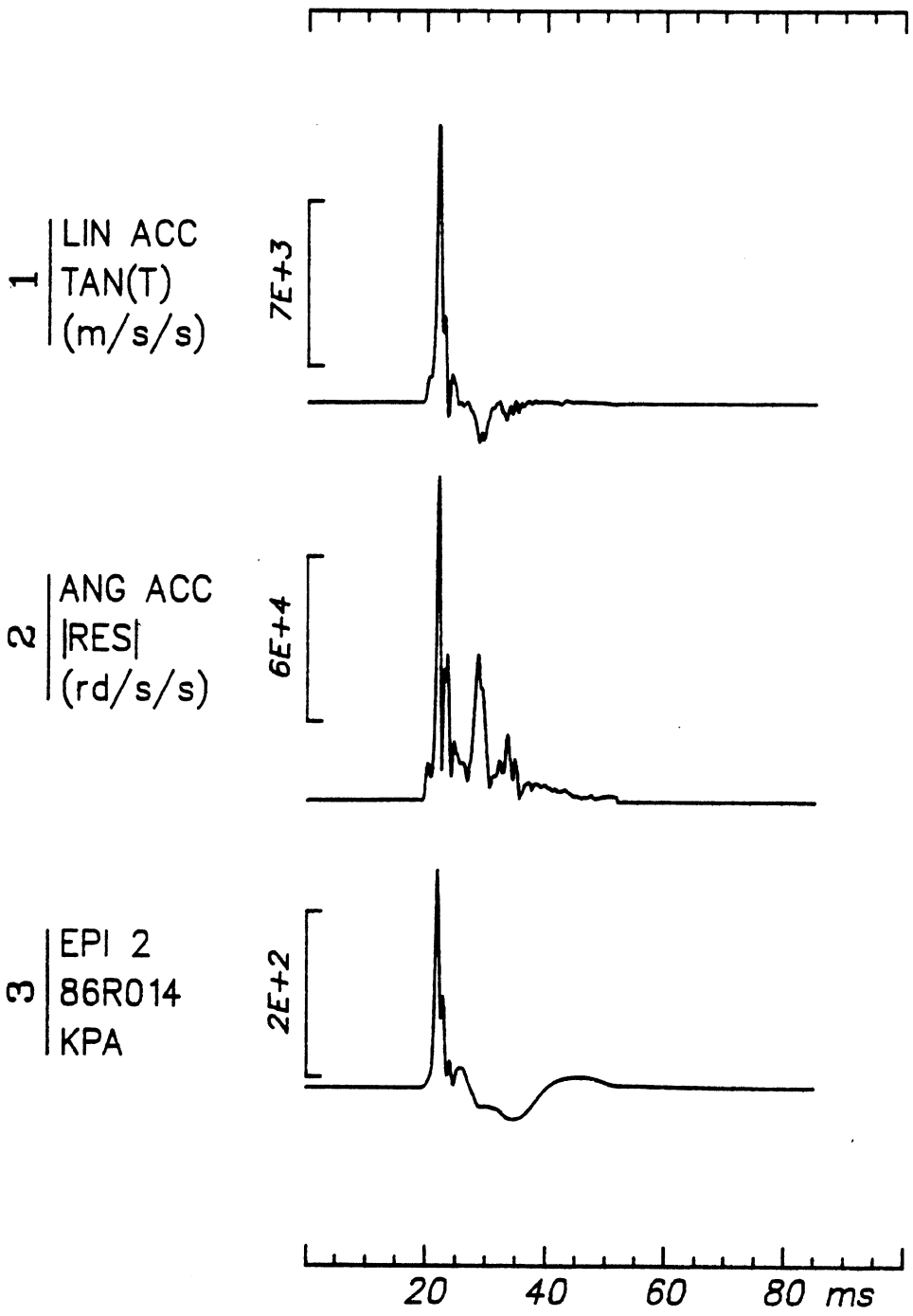

1=Tangential Acceleration
2=Angular Acceleration (Resultant)
3=Epidural Pressure

Run ID: 86R015 H7 *No Filtering*

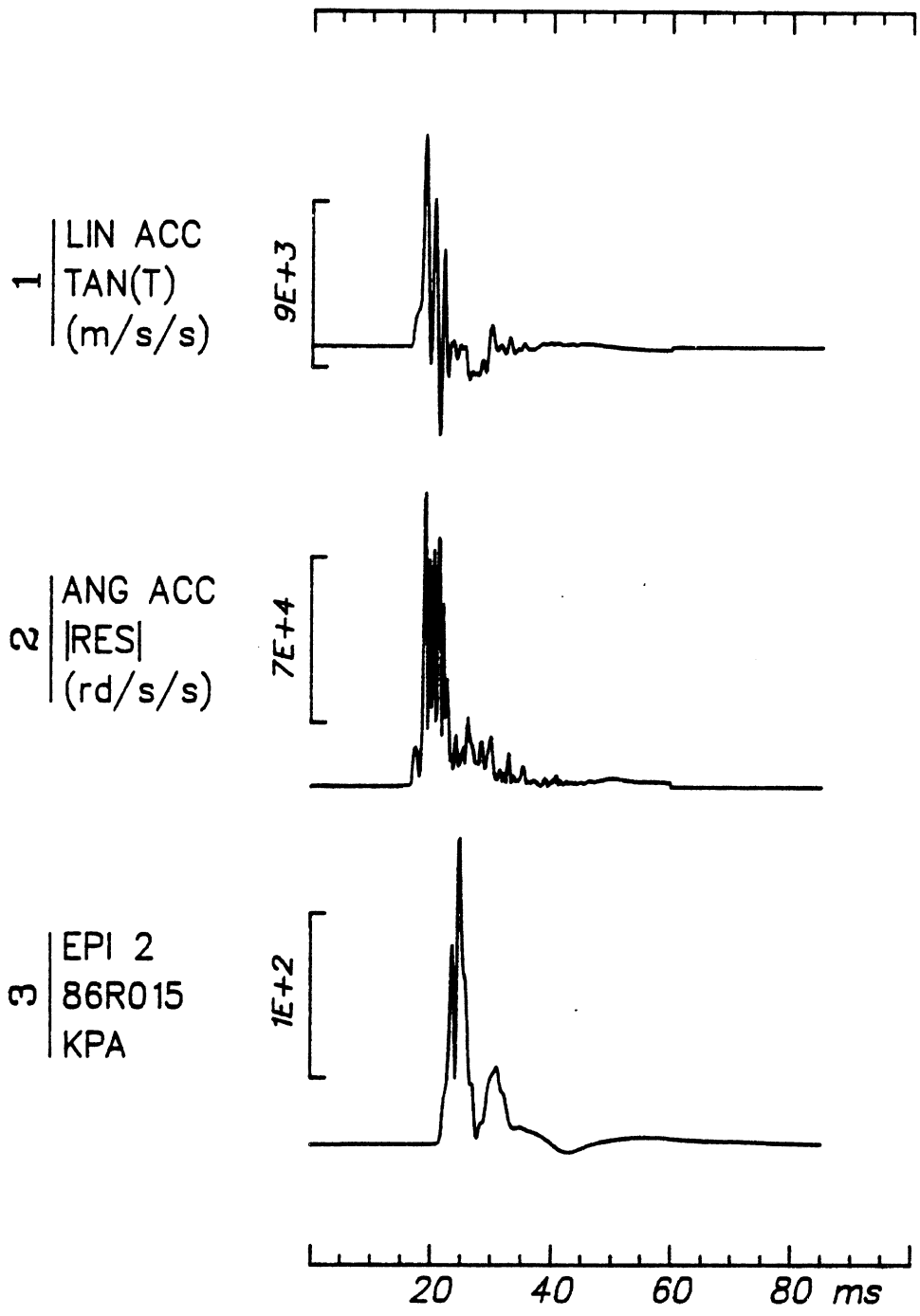

1=Tangential Acceleration
2=Angular Acceleration (Resultant)
3=Epidural Pressure

APPENDIX C: ECG REPORT (30)

Introduction

Experimental impact testing of non-human primates provides basic neurophysiological information related to neuropathology. The cardiovascular system of the Rhesus monkey resembles that of the human in several details - the heart's internal structure, it's placement and attachments in the thoracic cavity, and the coronary distribution gives an advantage to the study of the ECG. However, although the Rhesus geometry is very similar to man's, it is significantly different in anatomic soft tissue distribution and skull morphology (Figure 1). Not only does this present problems when scaling the test results to human levels, ultimately these differences lead to complication in the very complex phenomena of head injury (Thomas, et al., 1974). (See Appendix C for a brief test protocol description.)

ECG System

The UMTRI ECG system is comprised of Honeywell parts no. 790802-001 and 790808-001, the Accudata 108 AC Amplifier and the Accudata 109 DC Amplifier. The ECG is recorded unfiltered on a Honeywell 7600 (78 series) or Honeywell 96 (79 series) tape recorder at 1-7/8 ips. Data is played back through a Brush recorder onto Brush Accuchart paper. The ECG's are recorded from a standard lead II configuration. ECG's are recorded before and after the test for each monkey. (About 5 seconds for 78 series and as indicated in Appendix A for 79 series).

ECG Data

In the experimental laboratory the anesthetized Rhesus is positioned, instrumented and setup photographs are taken. Then the ECG is checked and the experiment begins. After impact, the ECG is monitored for approximately 15 mintues, at which time a 5 ml dose of Uthol (concentrated, unpure sodium pentobarbitol) is injected via the hind leg I.V. catheter to uthanize the monkey.

Next, the transducers are removed and the Rhesus moved to the autopsy room where a bilateral pneumothorax is performed to assure termination.

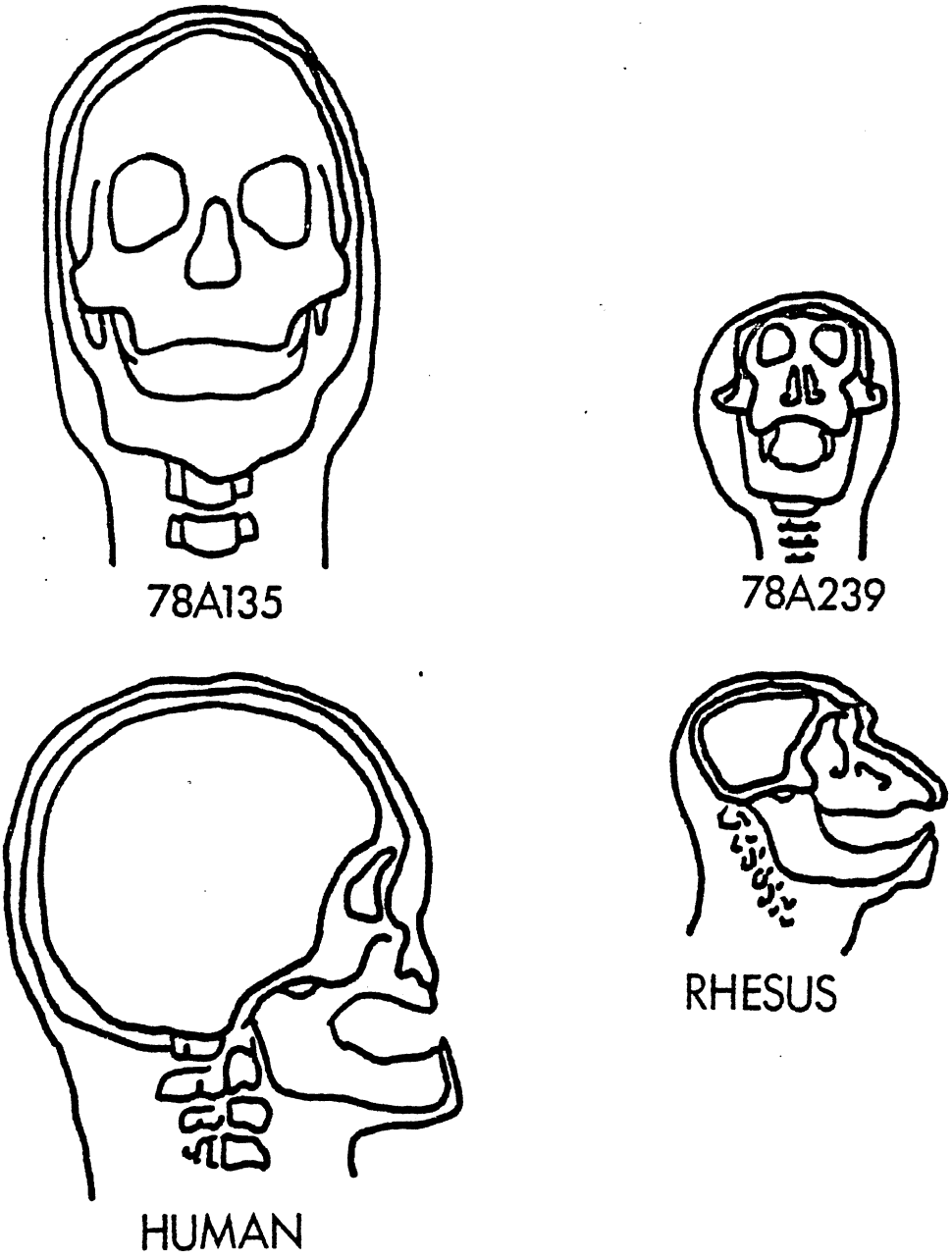

Figure 1

Rhesus-Human Head Anatomy

Pre-test ECGs

Pre-test ECG's of the five Rhesus monkeys were examined, and abnormalities noted, so they would not be attributed to impact. (See Appendix A for complete results.)

ECG Analysis

Heart rates, changes in the wave forms of the ECG (P, QRS complex, T) were noted. P-R and Q-T intervals were measured for determination of the Q-T_c. (Singh, et al., 1970). These results are summarized in Tables I.and II.

TABLE I. IMPACT SUMMARY

Test No.	Wgt. (kg).	Impactor Vel. (ft/sec)	Impactor Force (lb)	Heart Rate (beats/min)		Time After Impact (min)
				Pre-test	Post-test	
78A239	8.2	40	1130	120	150	1.5
78A241	10.6	40	1950	150	150	1.5
79A249	5.8	46	1450	135	84	3.0*
79A251	7.5	42	1650	120	90	1.0
79A253	5.2	48	1100	105	75	2.0
				x=126	y=110	

*A problem with the amplifier elminated the first three minutes of post-impact ECG.

Monkeys 79A249 and 79A253 showed very normal ECG patterns (See Appendix A, for all ECG samples.) In Rhesus 78A239, it was difficult to distinguish P and T waves. QRS was easily measured. Rhesus 78A241 exhibited a rather peculiar ECG pattern. Due to poor skin electrode contact, the pre-test ECG looked somewhat abnormal. However, all parameters measured were identical to the post-test measurements. This impact produced only a minimal concussion (See Table III for autopsy

TABLE II Summary of ECG Changes

Rhesus Test	Heart Rate/min		Per-cent Reduc-tion	P-wave	QRS Pattern	T-wave	$Q\text{-}T_c$ Before	Post*	Per cent Shor-tening	(AIS) Degree of Concussion
	Pre-test	Post-test*								
78A239	120	150	+20	**	**	**	--	--	--	2-3
78A241	150	150	0	peaked no change	qRS-- qRS R decreased amplitude	no change	.36	.36	0	2-3
79A249	135	66	51		QRs-- QRs-- qRS amplitude decreased sinus arrhythmia	flattened	.39	.36	8	6
79A251	120	90	25		inversion to about 1 minute post-impact QRS-- QRs-- qRS	no change	.38	.35	8	5
79A253	105	75	28	**	**	**	.45	.37	18	4

* 1-3 minutes after impact
** waveforms difficult to distinguish

TABLE III. AUTOPSY RESULTS

Monkey	Degree of Concussion (AIS)	Skull	Brain Damage
78A239	2-3	No injury to skull	Epidural hematoma over occiput
78A241	2-3	No injury to skull	Hematoma in muscle covering the occiput
79A249	6	Basilar skull fracture	Hematoma at brain stem between root of cerebellum and spinal cord
79A251	5	Occipital skull fracture	Epidural Hematoma in cerebellum
79A253	4	Basilar skull fracture of occipital and temporal bone	Subdural hematoma between cerebrum and cerebellum and subdural hematoma at base of brain stem

results.) Rhesus 79A251 had a rather normal ECG except for an occasional inversion of the QRS complex (See Figure 2).

The S-T segment (Fernando, et al., 1969) was not examined because of the difficulty in determining the isoelectric axis in most of the ECG's.

Heart Rate

Nothing more than heart rates could be determined in Rhesus 78A239 due to poor quality of the ECG recording. Unlike the other four monkeys, which showed either a decrease or no change in the heart rate, 78A239 underwent an increase.

P-Wave

The P-wave underwent no change with impact in Rhesus 78A241. 79A251 exhibited first a broadening, then a flattening, while 79A253 had

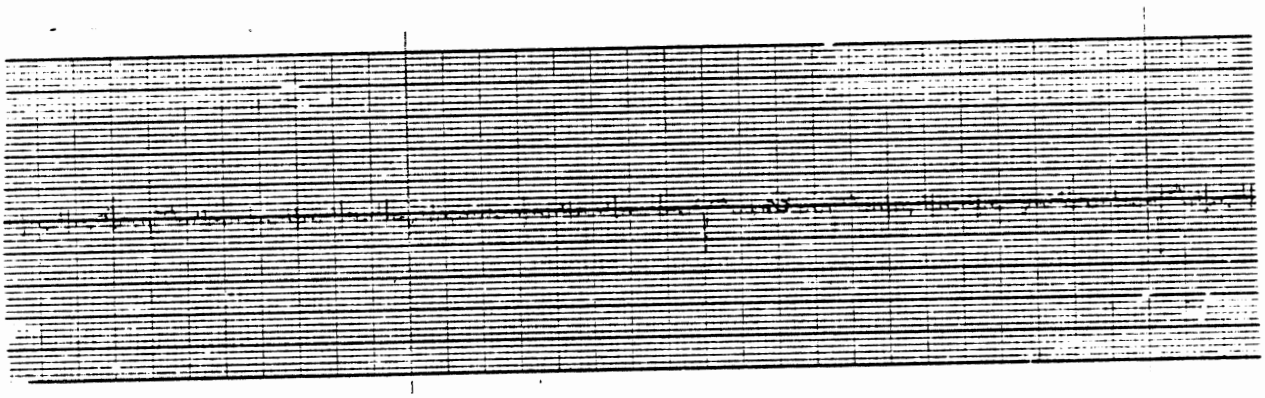

Figure 2

Rhesus 79A251 QRS Complex Inversion

an initial decrease in amplitude, but returned to normal in a few minutes. There were definite changes in the P-wave configuration in the fatal and seriously wounded animals.

QRS Complex

There were some interesting changes in the QRS complex of 79A253, - complete inversion immediately after impact, then reversion at 50 seconds. In 79A249, the QRS underwent changes in amplitude associated with arrhythmia.

T-Wave

Little or no change was seen in the T-wave except in 79A251 where it became flat. Again, the relatively flat nature of the T-wave with respect to the isoelectric line made it difficult to observe in most of the ECG's recorded.

$Q\text{-}T_c$

$Q\text{-}T_c$ is computed as: $Q\text{-}T_c$ = Q-T (sec)/ P-R (sec). The $Q\text{-}T_c$ was shortened in the severely concussed subjects (79A249, 79A251, and 79A253), the percent shortening ranging from 8 - 18 percent.

DISCUSSION

Several problems were encountered in recording the ECG's. The poor quality of the 78 series can be attributed to problems with "ground loops" due to the large amount of instrumentation involved in the experiment. This problem was worked out for the 79 series, however a problem with the amplifier was encountered during Test 79A249, eliminating the first 3-minutes of post-impact ECG.

Heart Rate

Pre-test heart rates were lower than "normal" heart rates of Macaca mulatta found by others (Malinow, 1966; Singh, et al., 1970). This was attributed to the use of sodium pentabarbitol for anesthesia.

In the mildly concussed animals, the heart rate remained the same in one, but increased (with arrhythmia) in the other. The severely concussed animals (See Table II) all underwent a decrease in heart rate. This is in agreement with other studies (Fernando, et al., 1969). Atrepine studies (Jacobson and Danufsky, 1954) and vagotomy studies (Glasser, 1960) indicate that brachycardia is mediated by nerve fibers of the vagus. Miller (Miller, 1942) stated that vagal tone is largely, if not wholly, controlled by the medullary centers (See Figure 3). Changes in rate, rhythm and the wave configurations appeared too rapidly to be produced by the action of acetylcholine released into the blood.

Post-test arrhythmias were produced in the mildly concussed (78A239) and in a severely concussed (79A249) monkey. Arrhythmias of all varieties have been attributed to vagal stimulation in humans (Hersch, 1961).

The shortened $Q\text{-}T_c$ (corrected Q-T interval) found in all the severely concussed monkeys indicates a hastened recovery process (repolarization) of the myocardium following ventricular contraction (depolarization). This shortening may be related to the automaticity of the heart following vagal discharges after impact (Fernando, et al., 1969).,

In one study (Fernando, et al., 1969) a correlation was found bet alween severity of concussion and the percent shortening of the $Q\text{-}T_c$.

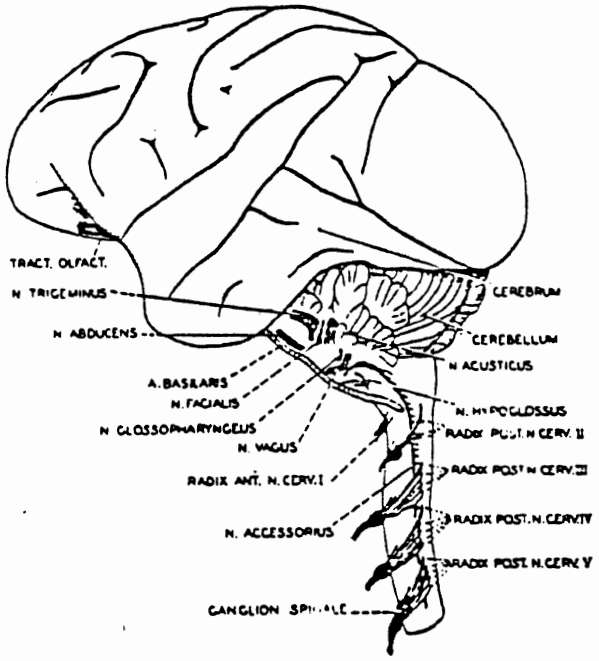

Brain and part of the cervical spinal cord from the left side, to show the origins of some of the cranial nerves.

Figure 3

Vagal Tone Controlled by Medullary Center

Due to the small sample size, no such correlation in this study could be ascertained.

The shortening of the Q-T_c is contrary to the lenthening of the Q-T_c after head injury in humans (Hersch, 1961).

The high voltage, peaked P-wave which was found in the test monkeys is usually indicative of right atrial enlargement or disturbed intraatrial conduction in the human. Since this is seen so often in Macacas, it can be assumed to represent the normal pattern.

P-wave changes could be determined in only two of the monkeys - 79A249 and 79A251. Both underwent a decrease after impact, which returned to the pre-test value within a few minutes in 79A251 and which flattened in 79A249.

T-wave changes were difficult to determine due to a combination of poor quality recording and the relatively "flat" nature of this wave.

The appearance of the S-wave in monkeys 79A249 and 79A251 has the pattern of bundle branch block. When there is something producing a block in one branch, the impulse will first invade the opposite ventricle and must reach the ventricle on the side of the lesion by way of the muscle of the interventricular septum (Ashman and Hull, 1941). The appearance of the post-test ECG of monkey 79A253 also suggests a bundle branch block pattern.

The inversion of the QRS complex in monkey 79A251 may not be significant since the erratic occurrence of QRS inversions was present before the impact. More samples are needed to determine whether this is a general response to head impact injury.

Head impact has been shown to produce definite changes in the ECG pattern of Macaca mulatta in this study. Arrhythmias, reduced heart rates, shortened Q-T_c, and S waves were present in more than one subject after impact.

Analysis of the clinical manifestations of concussion in the cat, dog, and monkey have shown that they are the result of intense excitation of the central nervous system at the moment of the blow to the head (Walker, Kollres, Case, 1944). Mechanical forces produce a

breakdown of the polarized cell membranes of many neurons in the central nervous system, thus discharging them (Walker, Kollres, Case, 1944). The neuronal discharge of the vagus from the medullary center seems to be the causative factor of ECG changes.

Gross autopsy results (shown in Table III) reveal that no damage to the heart muscle itself was found. Hematomas were present in all monkeys, with skull fractures present only in Rhesus 79A249, 79A251, and 79A253. This indicates that changes in the heart beat as manifested by ECG changes are produced by occurrences in the brain and not by direct effect on the heart.

Many more samples need to be gathered in order to understand the relation between head impact and heart function. The size of the sample in this study was much too small to make any statistically valid inferences from the data.

CONCLUSIONS

1. Heart rate can be significantly reduced in severely concussed Rhesus monkeys.

2. A direct occipital head impact can produce arrhythmia of the heart rate in Rhesus monkeys.

3. The appearance of an S-wave is common to the most severely concussed Rhesus monkeys.

4. The Q-T_c is shortened in the severely concussed Rhesus monkey.

Five non-human primate subjects[1], Macaca mulatta, were used in these experiments. These were obtained by HSRI from the University of Michigan Unit for Laboratory Animal Medicine (ULAM). Prior to acquisition, the Rhesus subjects had been used in one or more pharmacological research projects.

On the morning of the experiment, the Rhesus is given an intramuscular injection of ketamine (dL-2-[O-chlorophenyl]-2-[methylamino] cyclohexanone hydrochloride) before being delivered to the

---

[1]Animals cared for and handled according to American Association for Accreditation of Laboratory Animal Care and National Institute of Health guidelines.

UMTRI Biomedical Laboratory by a ULAM technician. A catheter with a three-way valve is inserted into the saphena parva vein in the hind leg, and sodium pentobarbital injected through the valve at a dosage of 25 mg/kg, to effect. An airway is established. The upper body is prepared and the weight and biometrical measurements are taken with a standard anthropometer, a stainless steel tape, a ruler and a Homes Model 51HH beam scale.

The Rhesus is then taken to the impact laboratory and placed in the impact chair. The monkey is positioned in front of the impactor with paper tape. All of the transducer wires are then connected and cabled, and the transducers checked for continuity and function.

A Polaroid photograph is then taken through the cineradiograph to check the position of the monkey and the x-ray settings. Final adjustments are made on the x-ray settings, amplifier settings, and the position of the monkey. At this point, setup photographs are taken. The ECG is checked and the tape recording begins. Holes are then punched into the paper tape supporting the monkey. The Polaroid camera is exchanged for the Photosonics high-speed motion picture camera in the cineradiographic system. After impact, the ECG is monitored for approximately 15 minutes, at which time a 5 ml does of Uthol (concentrated, unpure sodium pentobarbital) is injected via the hind leg I.V. catheter to euthanize the monkey.

Next, the transducers are removed and the Rhesus moved to the autopsy room where a bilateral pneumothorax is performed to assure termination. The autopsy is conducted with all injuries being recorded and photographed. The neck and spinal cord are carefully dissected and the coordinates of the instrumentation on the top of the skull measured and recorded. After removing the top of the skull, its measurements are also taken and recorded.

The brain is then examined <u>in situ</u> for evidence of injuries. The cranial nerves are severed and the brain is extracted with the spinal cord attached. After further examination, the brain is weighed and its volume is measured. It is then preserved in a solution of excess calcium carbonate in 10 percent formalin for later histological studies.

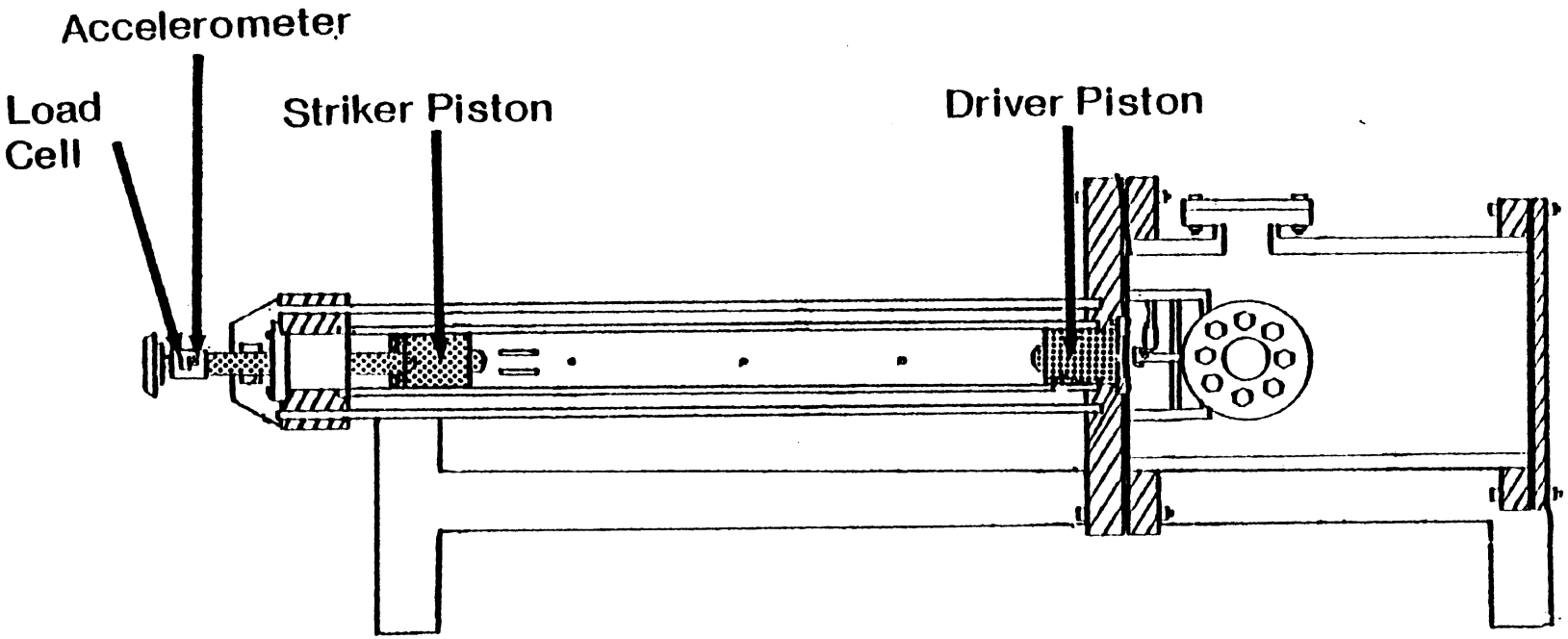

Figure 4

UMTRI Pneumatic Impacting Device

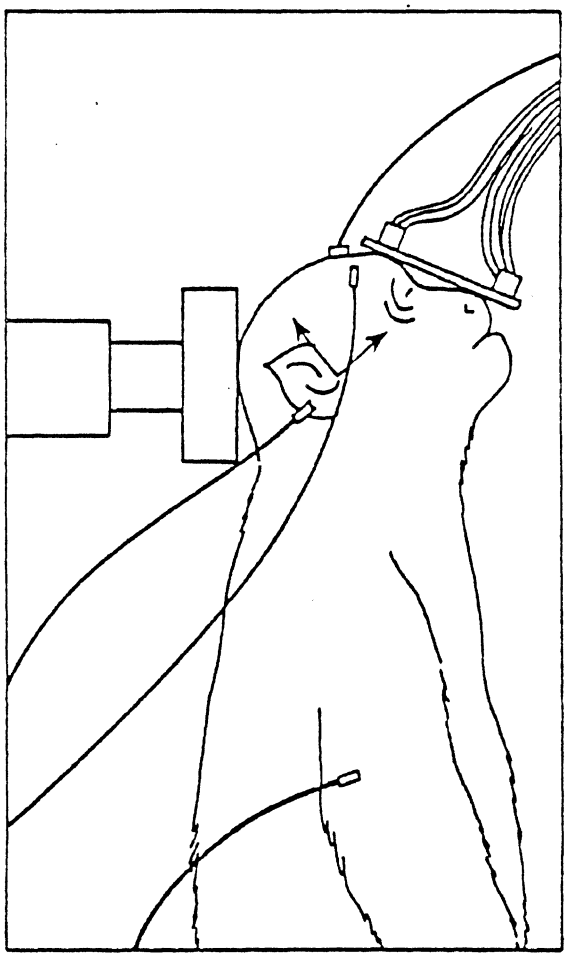

Figure 5

Initial Conditions of Impact Test

ECG References

Ashman, R.; Hull, E. 1941. Essentials of Electrocardiography, N.Y.: The Macmillan Co.

Fernando, O.U., et al., 1969. Electrocardiographic Patterns in Experimental Cerebral Concussion. J. Neurosurg. 31:34-40.

Glasser, R.L. 1960. Brain Stem Augmentation of Cardiovascular Activity. Am. J. Physiol. 198:421-423.

Hersch, C. 1961. Electrocardiographic Changes in Head Injuries. Circulation 23:853-860.

Jacobson, S.A.; Danufsky, P. 1954. Marked Electrocardiographic Changes Produced by Experimental Head Trauma. J. of Neuropath. and Exp. Neurology. 13:462-466.

Malinow, M.R. 1966. An Electrocardiographic Study of Macaca mulatta. Folia Primatol. 4:51-65.

Miller, H. 1942. Central Autonomic Regulations in Health and Disease, N.Y.: Grune and Stratton, p. 188.

Singh, R., et al., 1970. Electrocardiographic Studies in Rhesus Monkeys. J. Applied Physiology 28(3):346-349.

Thomas, D.J.; Robbins, D.H.; Eppinger, R.H.; King, A.I.; Hubbard, R.P. 1974. Guidelines for the Comparison of Human and Human Analogue Biomechanical Data. A report of an ad hoc committee, Ann Arbor, MI, Dec. 6.

Walker, A.E.; Kollres, J.J., Case, T.J. 1944. The Physiological Basis of Concussion. J. Neurosurg. 1:1034.

APPENDICES

Appendix A. ECG Case by Case Summary

Rhesus Test	Pre-test Heart Rate (beats min)	Post-impact Heart Rate (beats min)	Pre-test P-R (sec)	Post-impact P-R (sec)	Post-test Q-T (sec)	Post-impact Q-T (sec)	Pre-test $Q\text{-}T_c$	Post-impact $Q\text{-}T_c$	Comments
78A239	120	150 @1.5 min.	0.32	unreadable		unreadable			Pre-test hard to distinguish P,T waves. Post-impact arrhythmia decreased amplitude of QRS. Pre- and post-impact ECG's are of very poor quality, cannot distinguish any definite waveforms other than R.
78A241	150	150 @1.5 min.	0.38	0.38	0.22	0.22	0.36	0.36	Pre-test peaked P, large S. Entire ECG waveform is inverted due to the reverse polarity switch on amplifier.
79A249	135	84 @3 min. 66 @220 sec. irregular @248 sec.	0.44	0.72 @3 min. 0.84 @220 sec. 0.36-0.96 @248 sec.	0.26	0.34 @3 min. 0.36 @220 sec.	0.39	0.40 @3 min. 0.39 @220 sec.	Pre-test peaked P, Q-wave, no S. At three-minutes post-impact Q-wave and peaked P,Q. At 248 sec. post-impact S wave, varying amplitude of QRS, no Q. Recorded only 9 min. of post-impact ECG. Heart stopped beating immediately after impact, started spontaneously. Stopped recording 4.3 min. post-impact. Subject died 30 min. post-impact.

Appendix A. ECG Case by Case Summary (continued).

Rhesus Test	Pre-test Heart Rate (beats min)	Post-impact Heart Rate (beats min)	Pre-test P-R (sec)	Post-impact P-R (sec)	Post-test Q-T (sec)	Post-impact Q-T (sec)	Pre-test $Q\text{-}T_c$	Post-impact $Q\text{-}T_c$	Comments
79A251	120	90 immediately 75 @20 sec. 90 @50 sec. 80 @320 sec. 85 @4 hrs.	0.48	0.60 immediately 0.80 @20 sec. 0.64 @50 sec. 0.72 @320 sec.	0.26	0.36 immediately 0.40 @20 sec. 0.28+ @50 sec. 0.36+ @320 sec.	0.38	0.46 immediately 0.44 @20 sec. 0.35 @50 sec. 0.42 @320 sec.	Pre-test high peaked P, occasional inversion of QRS ;Q,P waves present. Immediate post-impact inverted QRS, T peaked P, no S. 20 sec. post-impact inverted QRS, T possibly inverted, no S. At 50 sec. post-impact, T, QRS reverted, high, peaked P, no S. At 320 sec. P has smaller amplitude, hard to distinguish Q-S. At 4 hrs. post-impact T-wave is difficult to distinguish +Need to expand scale to obtain more accurate reading.
79A253	105	105 @20 sec. 75 @120 sec. 82.5 @6 min. 90 @3 hrs.	0.56	0.56 @20 sec. 0.72 @120 sec. 0.72 @6 min.	0.34	0.26 @20 sec. 0.32 @120 sec. not measurable @6 min.	0.45	0.34 @20 sec. 0.37 @120 sec.	Pre-test peaked P. At 20 sec. post-impact peaked P. At 120 sec. post-impact hard to distinguish any waveforms except QRS.

Appendix B

SAMPLE ECG WAVEFORMS

78A239

Pre-test ECG

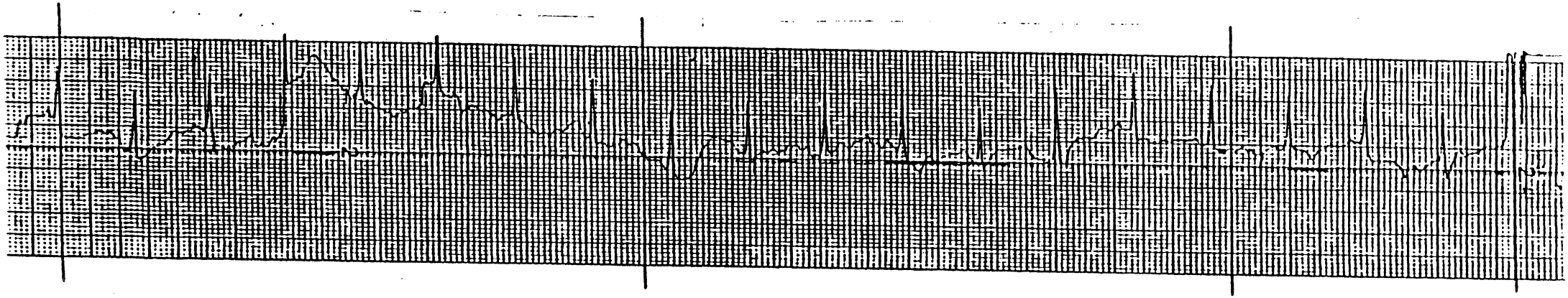

Post-test ECG

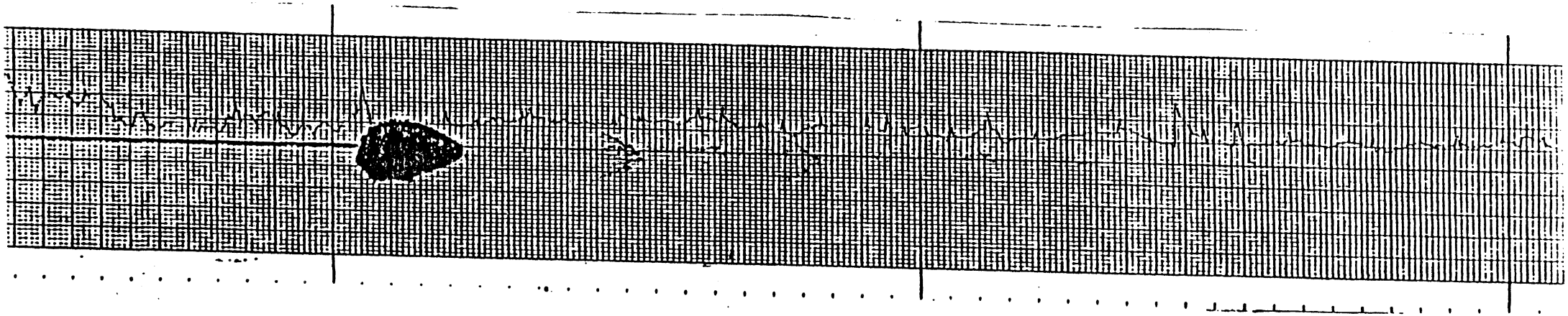

78A241 *

Pre-test ECG

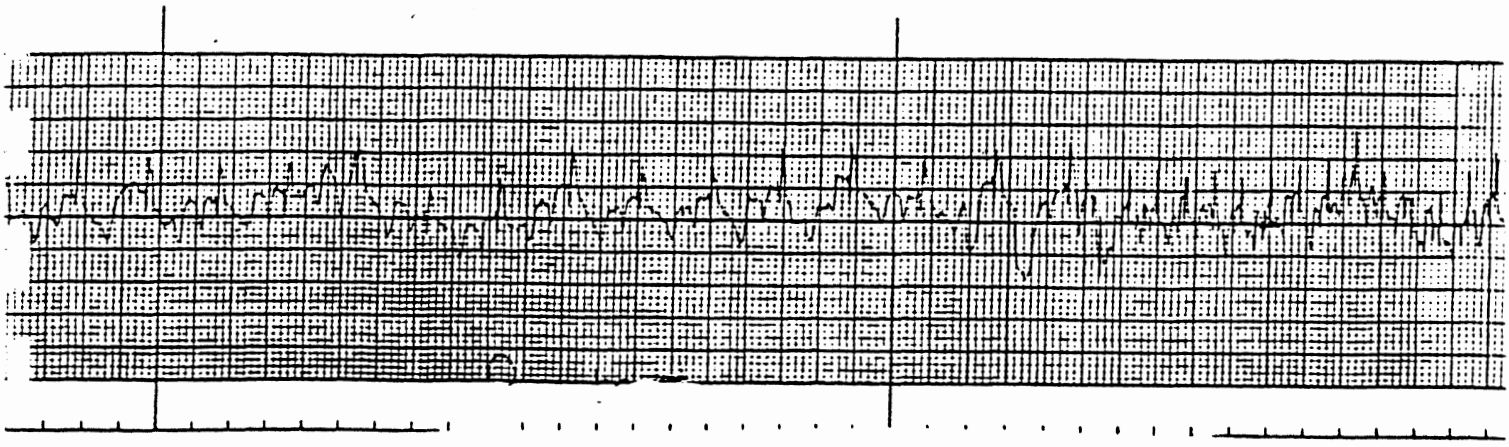

Post-test ECG

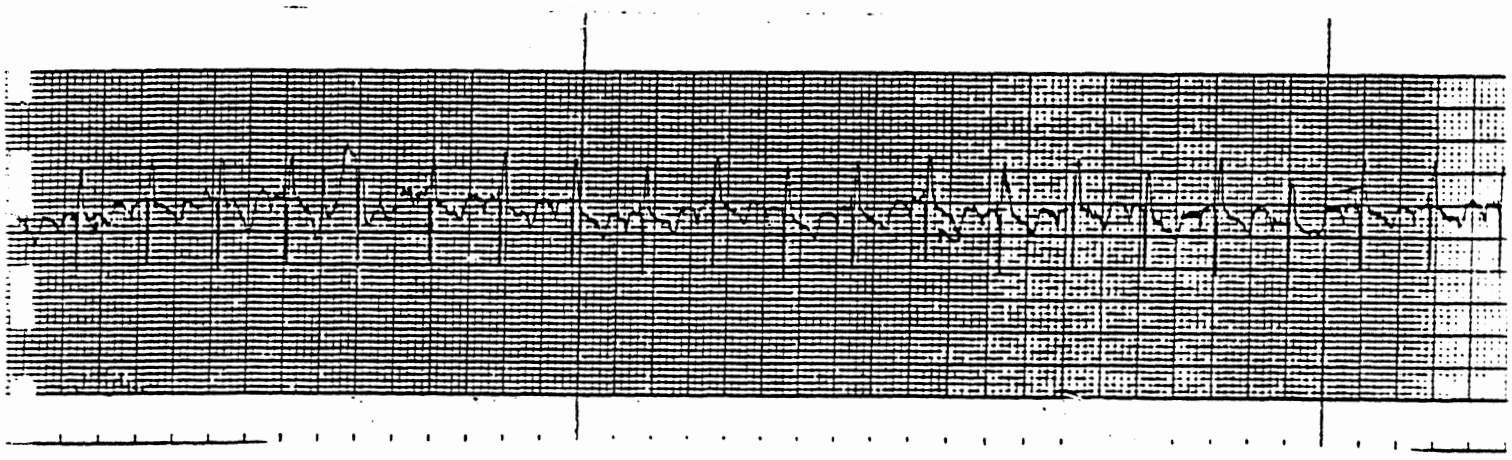

* All ECG waveforms are inverted

79A249 Pre-test ECG

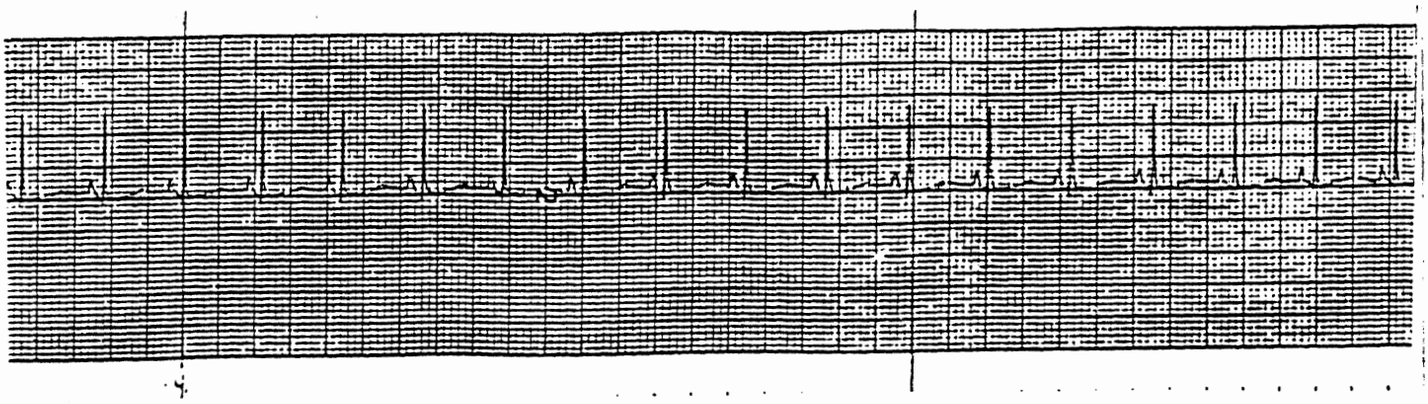

Post-test ECG (3 min)

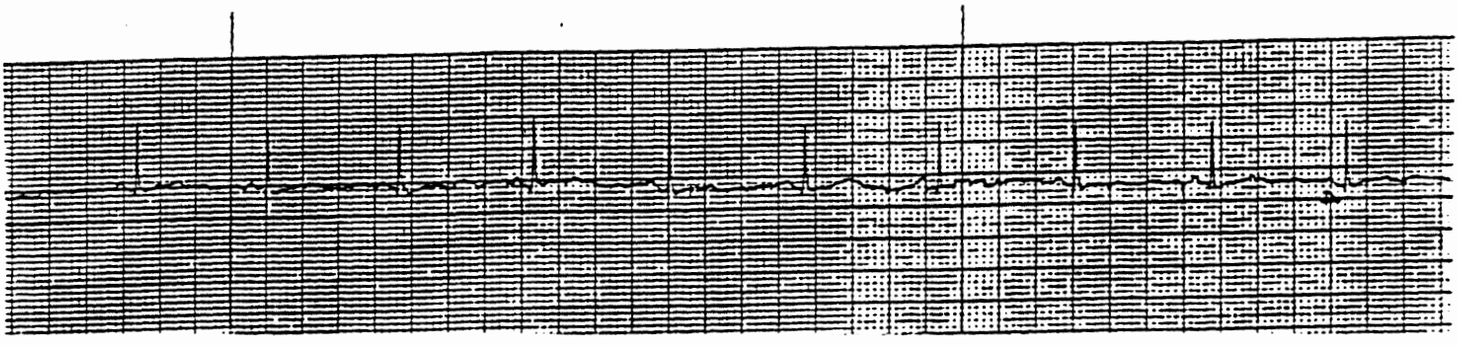

Post-test ECG (9 min)

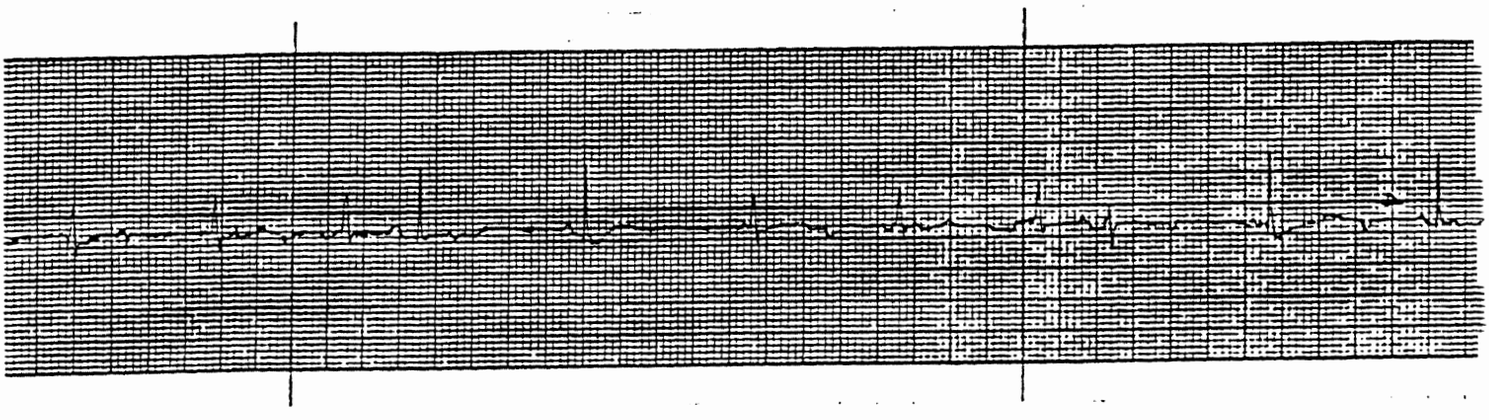

79A251 Pre-test ECG

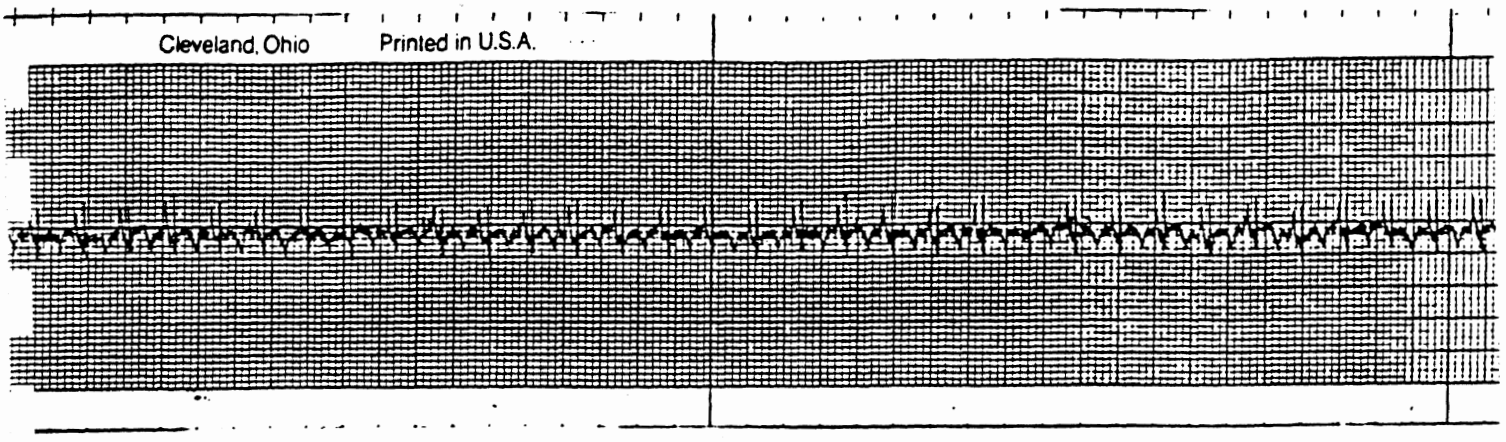

Post-test ECG

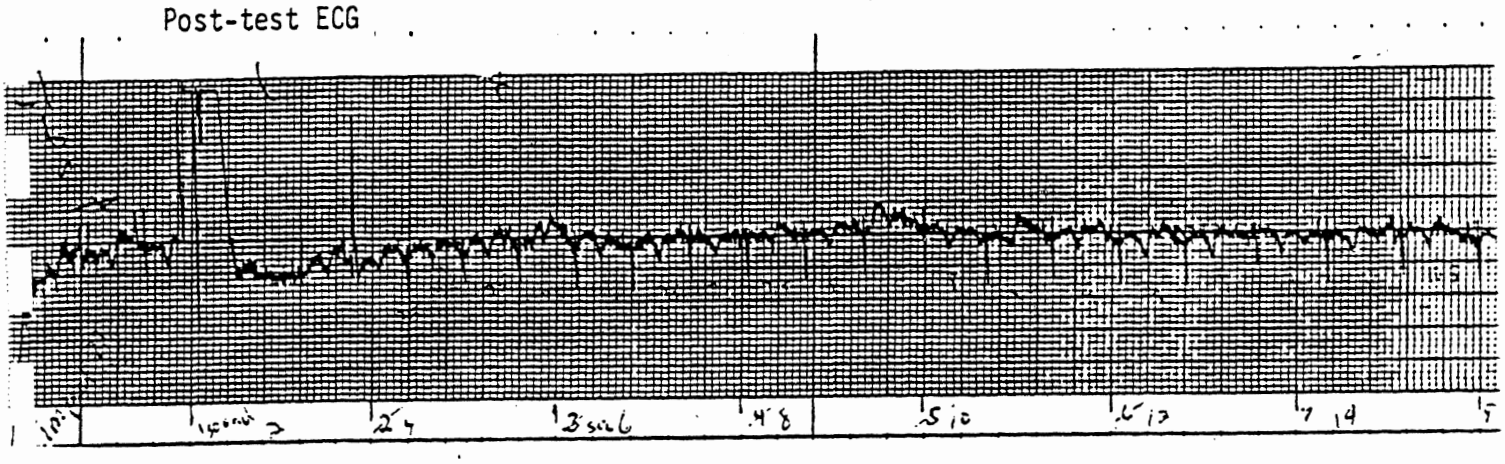

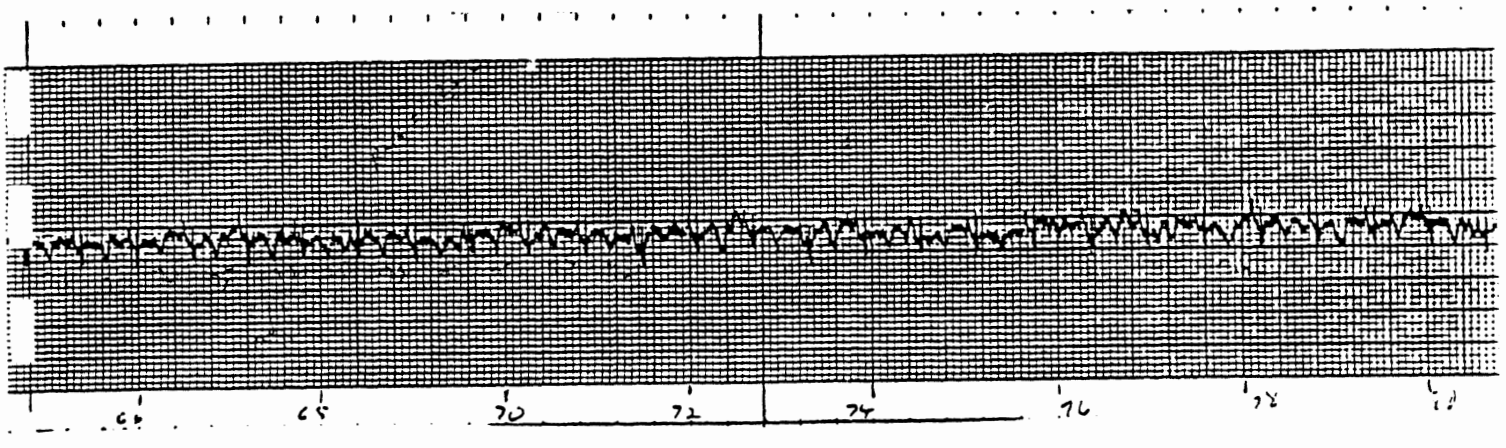

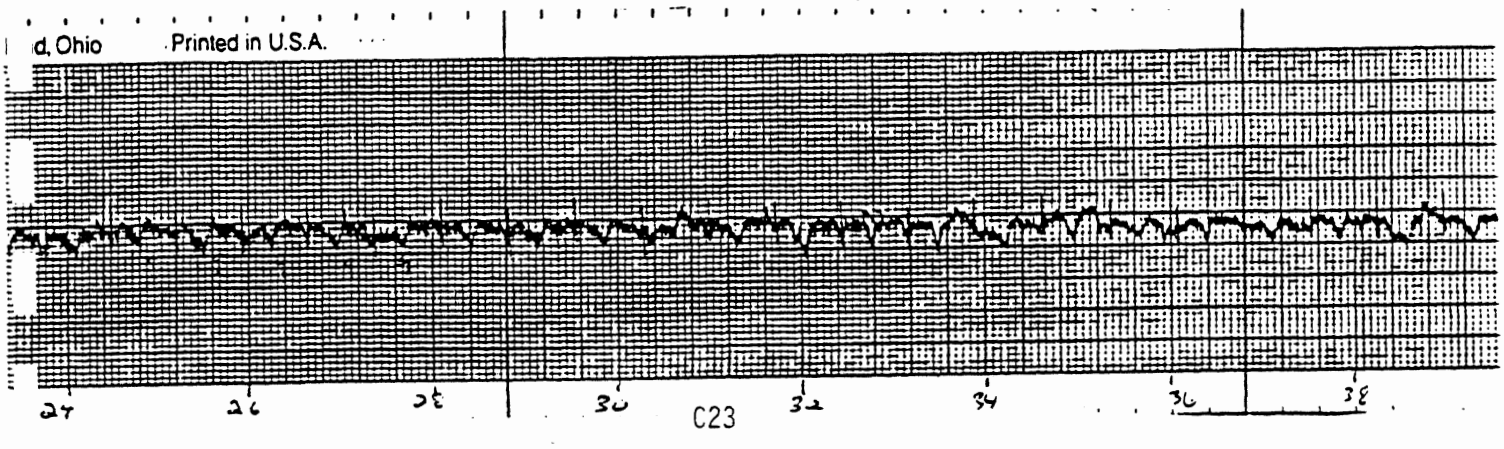

79A253 Pre-test ECG

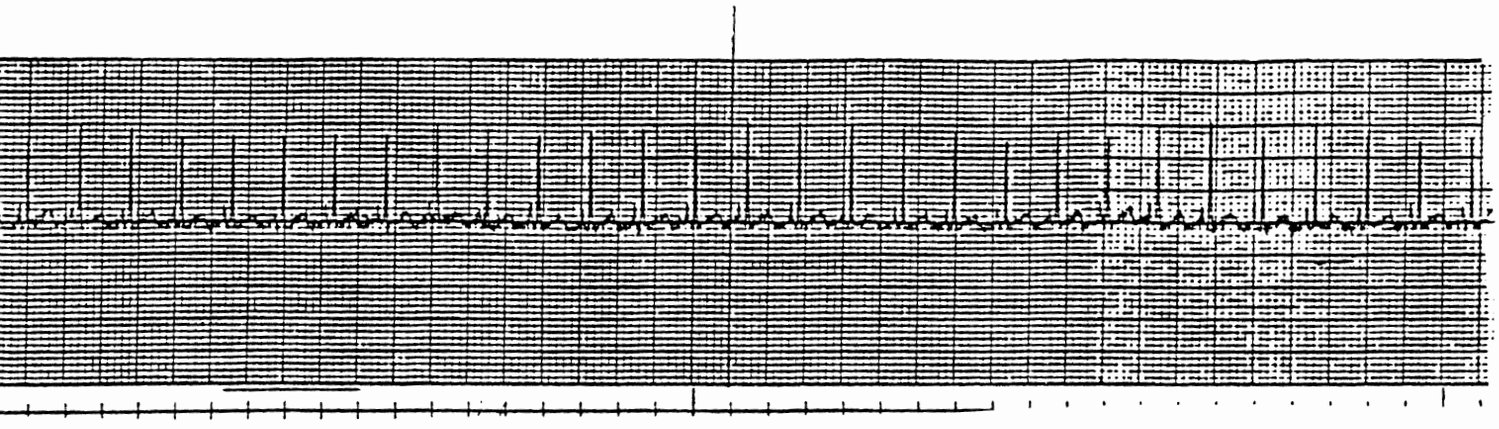

Post-test ECG

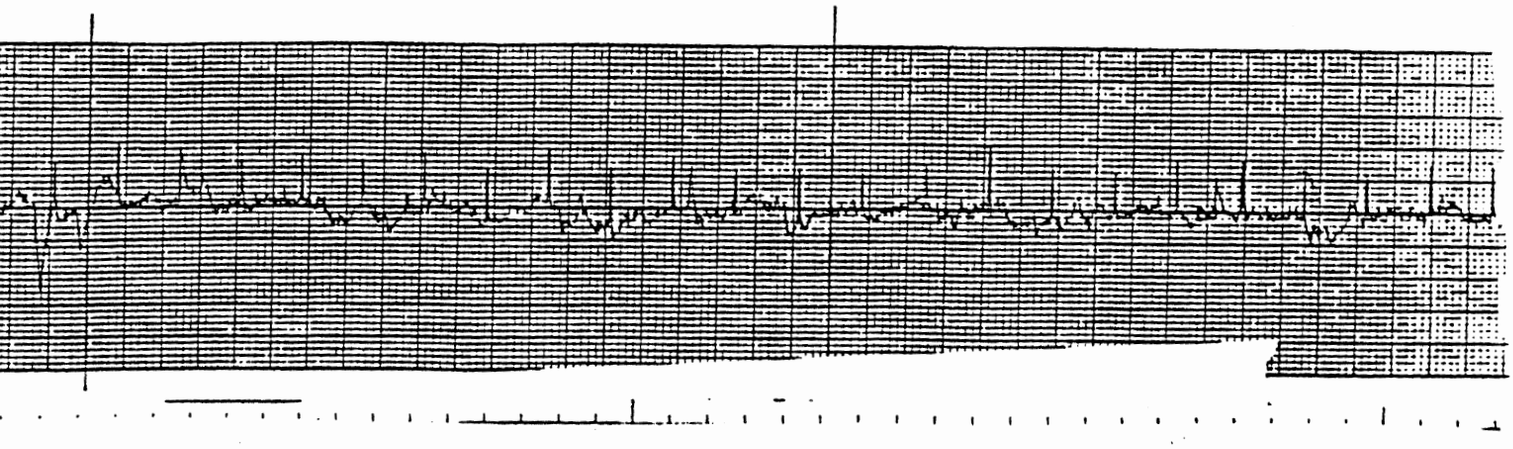

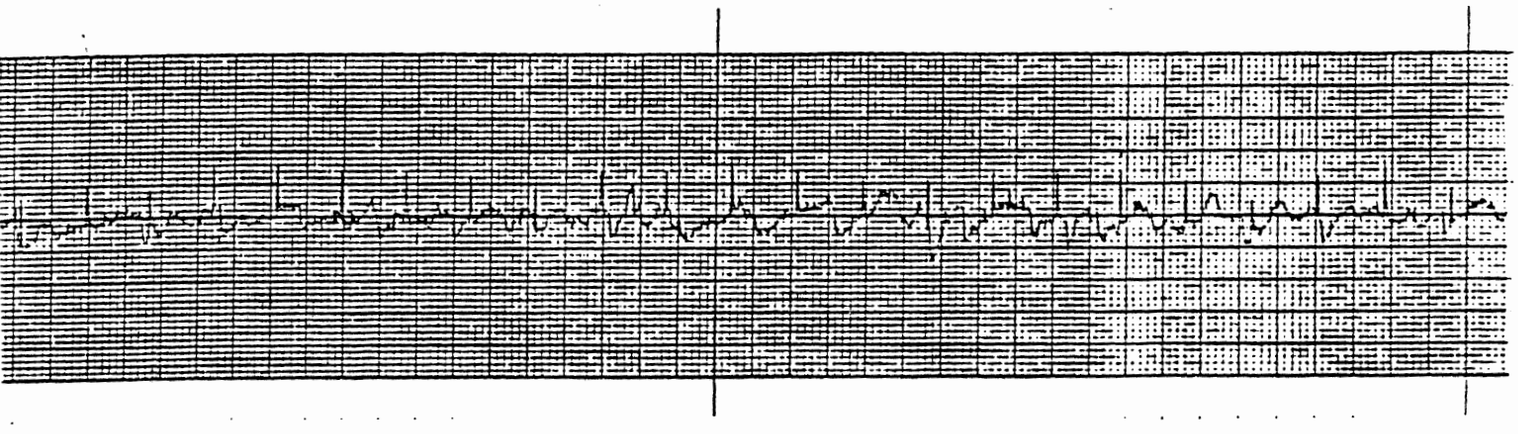

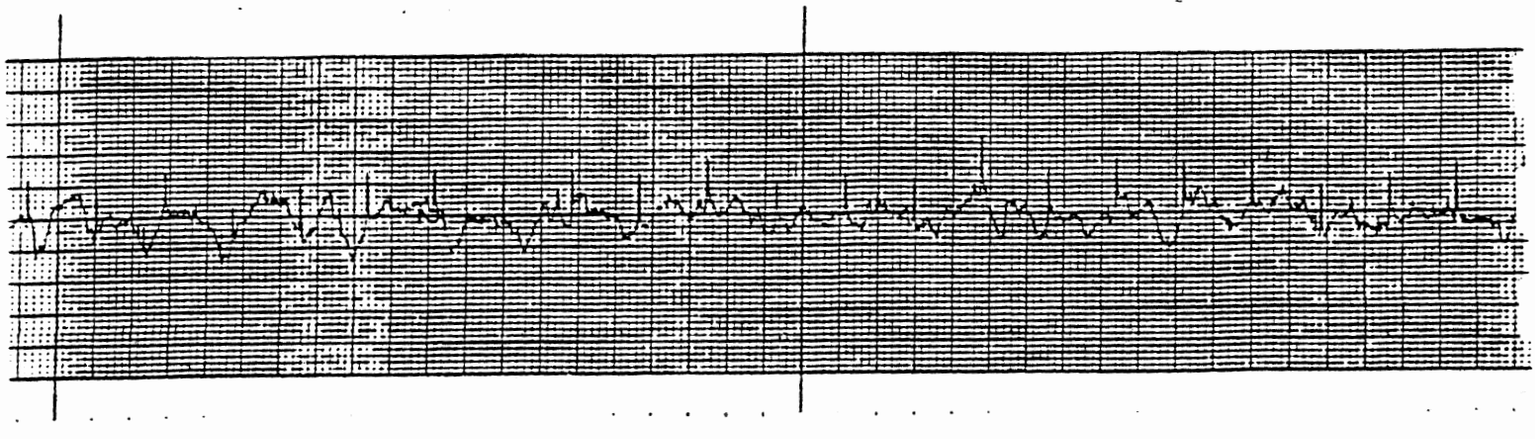

Appendix C

INTIAL CONDITIONS AND IMPACT TESTING

Impact Testing. The impacts were conducted using the UMTRI pneumatic impacting device, which was specifically constructed to give impacts of reproducible velocity. This instrument (Figure 4) is comprised of a 0.43 cubic meter air reservoir attached to a 167 cm long by 10.2 cm diameter honed steel cylinder with two carefully fitted steel pistons.

Compressed air from the building's air compression system is introduced into the reservoir. The pressure is regulated by a series of hand valves and measured with a gauge having an accuracy of 0.25 percent. The driver piston is secured at the reservoir end of the cylinder by an electronically controlled locking mechanism. At the opposite end of the cylinder the striker piston is rigidly connected to the impact force head. Both steel pistons have interchangeable elastic bumpers. When the air reservoir is pressurized and the locking mechanism released, the driver piston is propelled by the compressed air through the cylinder until its bumper impacts the bumper on the striker piston. Momentum is transferred to the striker piston, which is allowed to travel up to 25.1 cm. The excess kinetic energy is absorbed by a 3003 H14 seamless aluminum inversion tube, 6.35 cm in diameter with a 0.165 cm wall thickness.

Impactor velocity is controlled by reservoir pressure and the ratio of the masses of the driver and striker pistons. The desired impactor stroke can be accurately controlled by the initial positioning of the striker piston with respect to the inversion tube. Both driver and striker pistons have a mass of 10 kg for these experiments.

The impactor surface is a 10.2 cm rigid metal plate padded with 2.5 cm Ensolite. The impactor force transducer assembly consists of a Kistler 904A piezoelectric load washer with a Kistler 804A piezoelectric accelerometer mounted internally for inertial compensation.

Positioning. A chair was designed and constructed for positioning of the monkeys for impacting with the pneumatic impacting device which could be adapted to varying non-human primates and test conditions. In addition, a moveable overhead arm facilitated suspension of the monkey.

The Rhesus is placed in an erect sitting position so that impact is to the sagittal plane of the occipital bone in the posterior-anterior direction (See Figure 5). The monkey is held in place with paper tape which grips the body under the armpits, suspending the head and torso from the overhead arm. Immediately before testing, holes are punched into the tape facilitating release upon impact.

In Table I the pertinent impactor data are listed.

791020

Head Impact Response Comparisons of Human Surrogates

Guy S. Nusholtz,
John W. Melvin, and
Nabih M. Alem
Biomechanics Department
Highway Safety Research Institute
University of Michigan

Abstract

The response of the head to impact in the posterior-to-anterior direction was investigated with live anesthetized and post-mortem primates.* The purpose of the project was to relate animal test results to previous head impact tests conducted with cadavers (reported at the 21st Stapp Car Crash Conference (1),** and to study the differences between the living and post-mortem state in terms of mechanical response.

The three-dimensional motion of the head, during and after impact, was derived from experimental measurements and expressed as kinematic quantities in various reference frames. Comparison of kinematic quantities between subjects is normally done by referring the results to a standard anatomical reference frame, or to a predefined laboratory reference frame. This paper uses an additional method for describing the kinematics of head motion through the use of Frenet-Serret frame fields.

The experimental technique used a nine-accelerometer system, mounted rigidly to the head, to measure head motions. Additional measurements included impact force, epidural pressure, and strains in the skull bone. High-speed

*Animals cared for and handled according to AALAC guidelines.
**Numbers in parentheses indicate reference at the end of the paper.

0585-086X/79/1017-1020/$02.50

cineradiography (1000 frames/second) was used during the impact. A total of seven animals were tested in the project, five post-mortem and two live.

The results of the tests are presented to demonstrate the similarities and differences found between animal and human cadaver subjects and between living and post-mortem subjects. The effects of the following factors are discussed:

1. Relative magnitudes of brain mass, skull mass and external soft tissue mass.
2. Head surface geometry at the impact site and mass distribution.
3. Differences in epidural pressures and in head trajectories.

EXPERIMENTAL INVESTIGATIONS IN THE BIOMECHANICS OF HEAD IMPACT RESPONSE have used human cadavers and animals as surrogates of the living human. The parameters commonly used for describing head mechanical response during direct impact have been angular and translational accelerations, velocities, and displacements of the head as a rigid body, skull bone deformations, and internal pressures in the brain. The unembalmed cadaver is often chosen as an experimental model because its geometry and soft-tissue distribution is similar to that of the live human. In addition, soft tissue damage can be directly related to injury patterns observed in clinical studies. The disadvantages of the cadaver include the inability to measure pathophysiological response and the susceptibility of some tissues to post-mortem degradation. Also, it has been reported (1) that, during the contact time of direct impact, the motion of the brain of the unembalmed cadaver can be only partially constrained by the skull; the degree of constraint can depend on the time after death and the preparation of the cadaver. This partial decoupling may have marked effects on kinematic time history of the head during and following an impact.

Experimental impact testing of animals, in particular primates, provides basic neurophysiological information related to neuropathology. However, although the primate geometry is the most similar to man's, it is significantly different in anatomic soft tissue distribution and skull morphology. This can present severe problems when scaling the test results to human levels. Ultimately these differences lead to complications in the very complex phenomena of head injury (2).

Techniques have been developed in the past few years for accurate determination of three-dimensional motion of the human head (3,4,5,6,7,8), preparation of the unembalmed human cadaver (1,9,10), and high speed cineradiography of the body (11). This paper discusses techniques used at the Highway Safety Research Institute (HSRI) for conducting posterior-to-anterior head impacts with primates while

measuring three-dimensional head motion, skull strain, and epidural pressure. In addition, the results of the series of live and post-mortem posterior-to-anterior impacts with primates are compared to previous posterior-to-anterior direct head impacts with unembalmed human cadavers using the same technique.

METHODOLOGY

THREE-DIMENSIONAL MOTION DETERMINATION - The HSRI method used for measuring the three-dimensional motion of the head is based on a technique used to measure the general motion of a vehicle under a simulated crash (12). In the current application, three triaxial clusters of Endevco Series 2264-2000 accelerometers are affixed to a lightweight rigid magnesium plate (Figure 1) which is then solidly attached to the skull. With this method it is possible to take advantage of the physical and geometrical properties of the test subject as well as the site of impact, in the design of a system for measurement of 3-D motion. In the case of small primates, it is more convenient to design a specific system for each species and site of impact. Two systems were designed and constructed at HSRI, each utilizing a lightweight magnesium plate to mount 9-accelerometers, one for each of the two species tested. The prominent orbital ridges and dental plate found in these species were used to install the rigid plate. Using a multipoint attachment scheme, it is secured at a maximum distance from the point of impact. This minimizes the effect of skull deformation on the 3-D motion analysis during impact. The approximate installed weight of the plate and mounts is 50 grams. Typical distances between accelerometer clusters is about 6.5 cm.

The nine acceleration signals obtained from the three triaxial clusters are used for the computation of head motion using a least squares technique, the details of which are described elsewhere (1). The method takes advantage of the redundancy of nine independent acceleration measurements to minimize the effect of experimental error to produce three angular accelerations and three estimates, in the least square sense, of the true solution.

REFERENCE FRAMES - The impact response of the human body and its surrogates may be described as kinematic quantities derived from experimental measurements and expressed as vectors in reference frames which vary from one instrumentation method to another. In general, comparison of mechanical responses between subjects is achieved by referring results to a "standard" anatomical frame which may be easily identified. On the other hand, it is impractical to require that transducers be aligned with this anatomical frame, since this may create unnecessary problems. An alternative is to mount transducers in an arbitrary and convenient reference frame, then describe the transformation

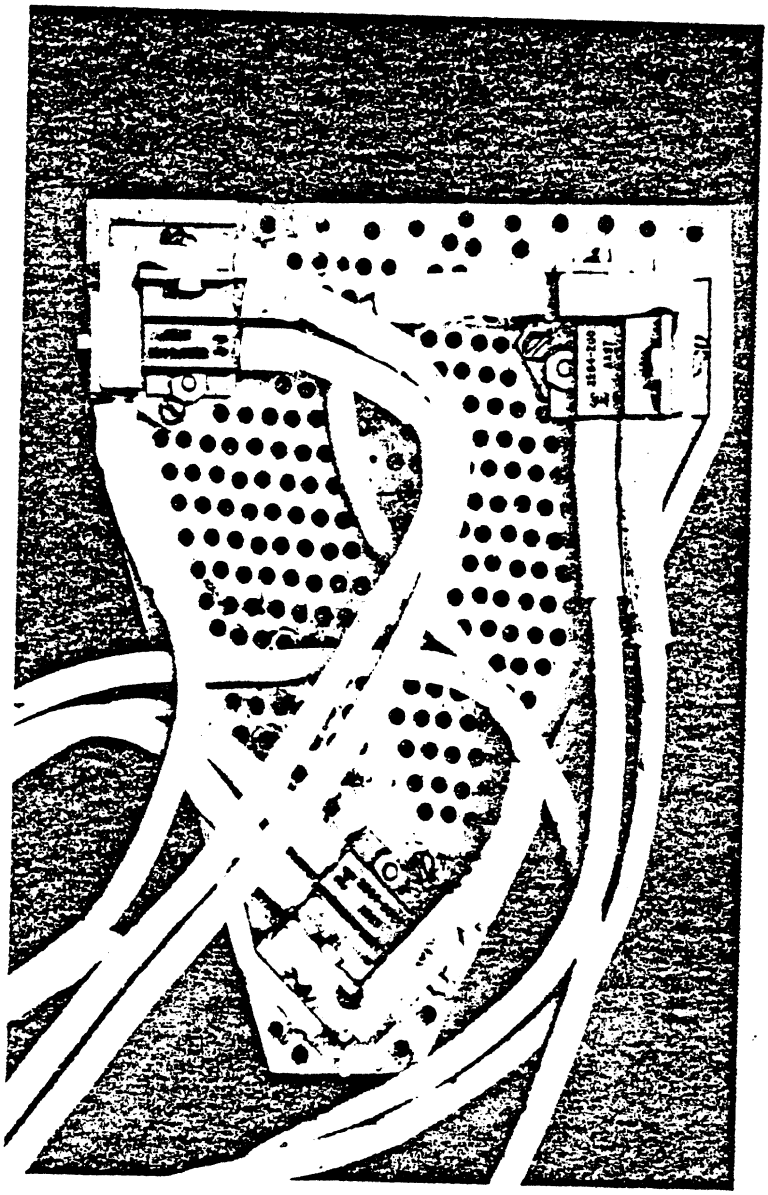

50ths

Fig. 1 - 9-Accelerometer plate

necessary to convert the data from this frame to the desired anatomical frame (13).

The three basic reference frames which are used to describe kinematic quantities are: the instrumentation frame, the anatomical frame and the inertial (or laboratory) frame. An additional method to describe motion in space is to utilize the concepts of vector and frame fields. The definitions of the reference frames used at HSRI are given in the following sections.

Anatomical Reference Frame ($\hat{i},\hat{j},\hat{k}$). The $\hat{i}$-axis and the $\hat{j}$-axis of this reference frame lie in the Frankfort plane. The Frankfort plane is defined as passing through the superior edges of the two auditory meati and the two infraorbital notches. The $\hat{i}$-axis is defined along the intersection of the Frankfort and midsagittal planes in the posterior-to-anterior (P-A) direction. The $\hat{j}$-axis is defined along the line joining the two superior edges of the auditory meati, in the right-to-left (R-L) direction. This $\hat{j}$-axis is perpendicular to the midsagittal plane at the "Anatomical Center" (A.C.), which is taken as the origin of the anatomical frame (Figure 2). Finally, the $\hat{k}$-axis is defined as the cross-product of the unit vectors of $\hat{i}$- and $\hat{j}$-axes, and therefore, will lie in the midsagittal plane perpendicular to the Frankfort plane, and will be in the inferior-to-superior (I-S) direction.

Thus, the anatomical reference frame ($\hat{i}$, $\hat{j}$, $\hat{k}$) can be completely defined once the four anatomical landmarks are specified.

Instrumentation Reference Frame ($\hat{E}1$, $\hat{E}2$, $\hat{E}3$). This orthogonal frame is embedded in the rigid magnesium plate which carries the 9 accelerometers and is defined by its origin and the plane of ($\hat{E}1$, E2) which is parallel to the plate (Figure 2). The E3 axis is defined as the cross-product $\hat{E}1 \times \hat{E}2$. During 3-D radiographic reconstruction, this reference plane is identified by the coordinates of 4 lead pellets permanently installed in the plate to serve as instrumentation landmarks.

The nine accelerometers are arranged in 3 clusters, each forming an orthogonal triad, and are designed to be installed on the plate at precise locations and orientations. Thus, once the instrumentation reference frame ($\hat{E}1$, $\hat{E}2$, E3) has been determined, the location and direction of all nine acceleration readings may be accurately determined. These readings are immediately transformed to the anatomical reference frame before any 3-D motion computations are carried out.

Laboratory Reference Frame ($\hat{I}$, $\hat{J}$, $\hat{K}$). It is desired to describe the instrumentation reference frame ($\hat{E}1$, $\hat{E}2$, $\hat{E}3$) in terms of the anatomical reference frame ($\hat{i}$, $\hat{j}$, $\hat{k}$) unit vectors:

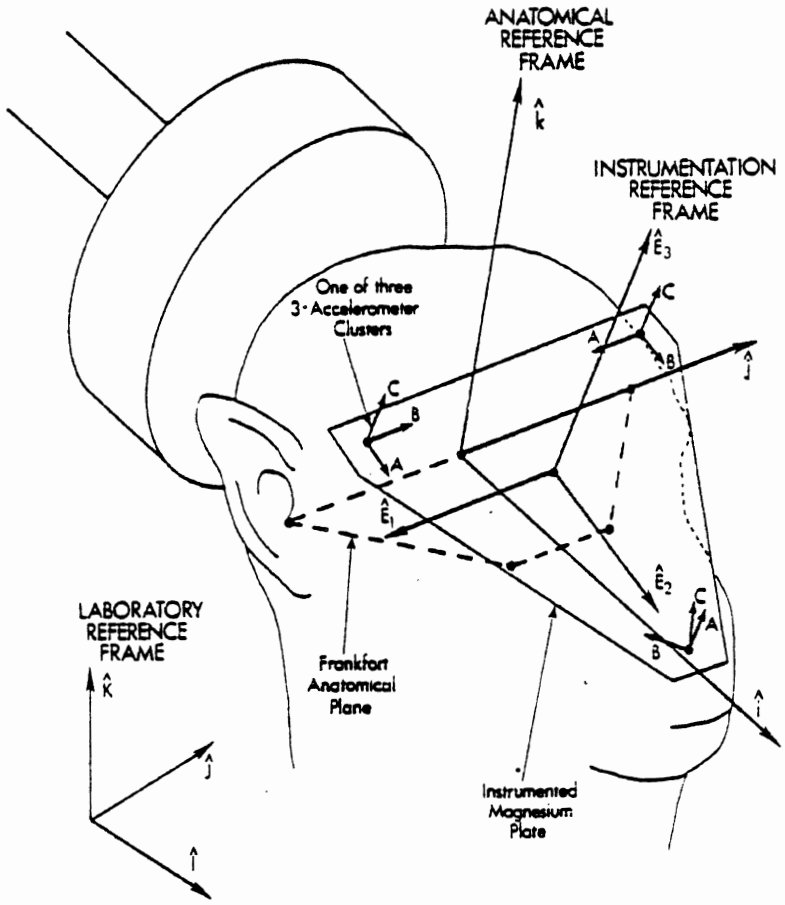

Fig. 2 - Instrumentation reference frame and location of the three triaxial accelerometer

$$\begin{matrix} \hat{E}1 \\ \hat{E}2 \\ \hat{E}3 \end{matrix} = [E] \begin{matrix} \hat{i} \\ \hat{j} \\ \hat{k} \end{matrix}$$

where [E] is an orthogonal transformation matrix consisting of the nine unknown direction cosines. This matrix may be determined by first expressing each of the $\hat{E}1$, $\hat{E}2$, $\hat{E}3$) and ($\hat{i}$, $\hat{j}$, $\hat{k}$) in terms of an arbitrary frame ($\hat{I}$, $\hat{J}$, $\hat{K}$):

$$\begin{matrix} \hat{E}1 \\ \hat{E}2 \\ \hat{E}3 \end{matrix} = [U] \begin{matrix} \hat{I} \\ \hat{J} \\ \hat{K} \end{matrix} \quad \text{and} \quad \begin{matrix} \hat{i} \\ \hat{j} \\ \hat{k} \end{matrix} = (V) \begin{matrix} \hat{I} \\ \hat{J} \\ \hat{K} \end{matrix}$$

then eliminating the ($\hat{I}$, $\hat{J}$, $\hat{K}$) between the two expressions to obtain the matrix [E]:

$$[E] = [U]\ [V]^{-1}$$

Since [U] and [V] are determined from coordinates of several points, the arbitrary frame ($\hat{I}$, $\hat{J}$, $\hat{K}$) will simply be the laboratory frame in which these coordinates are measured. The x-ray method used at HSRI to measure the points automatically defines the laboratory reference frame.

Frame Fields - The description of the motion of the head in response to an impact has always been a central theme in head injury research. With the development of three-dimensional accelerometry techniques for accurate measurement of head motions during impact, it is now possible to produce information on three components of translational acceleration, three components of rotational acceleration and the corresponding components of velocities and displacements. In applying such extensive information to the study of the complex phenomena of head injury it is advantageous to use methods of motion analysis which can simplify and enhance our insight into the events that characterize a particular impact situation. As the head moves through space, any point on the head generates a path in space. In head injury research we are interested in the description of the path of the anatomical center and in events which occur as the head A.C. moves along that path. A very effective method for analyzing the motion of such a point, as it moves along a curved path in space, is to introduce the concept of a frame field. The distance the point travels along the path is a function of time which defines the path and the point of application of any vector on the curve. A vector field is a function which assigns a uniquely defined vector to each point along a path. Similarly, any collection of three mutually orthogonal unit vectors defined on a path is a frame field. Thus, any vector defined on the path (for example, acceleration) may be resolved into three orthogonal components of any well-defined frame field, such as the laboratory or anatomical reference frames. Changes in a frame field with time (for example, angular acceleration

of the frame field) are interpreted as vectors defined on the curve and are also resolved into three components.

A frame field which is particularly useful for describing motion along a curved path in space is the Frenet-Serret frame field (discovered by Frenet in 1847, and independently by Serret in 1851). This orthogonal frame is derived from the three-dimensional space curve traveled by the point of interest (the anatomical center, in our case) and the velocity of travel of the point. A complete discussion of this method can be found elsewhere (14) and will only be summarized here.

The curvilinear distance traveled along the path is a function of time and is denoted by $s(t)$ (see Figure 3). For a point moving along the path, the absolute position vector ($\vec{R}(t)$) can be defined relative to the initial starting position at $t = 0$. The first and second derivatives of the position vector with respect to time yield the velocity and acceleration vectors of the point, respectively. The time derivative of the path distance, denoted $V(t)$, is called the speed of the curve. At any instant of time, a unit vector ($\hat{T}$) which is tangent to the path at that point on the curve can be defined as the derivative ($d\vec{R}/ds$) of the position vector with respect to the curvilinear distance s. Since the velocity vector of the point ($d\vec{R}/dt$) can be written as $d\vec{R}/ds \cdot ds/dt$, it is possible to substitute the tangent unit vector ($\hat{T}$) for $d\vec{R}/ds$ and the speed of the curve ($V(t)$) for ds/dt resulting in the expression $d\vec{R}/dt = \hat{T} \cdot V(t)$ or $\hat{T} = d\vec{R}/dt/V(t)$. Thus, $\hat{T}$ can be considered a normalized velocity vector. A second unit vector which is perpendicular to $\hat{T}$, called the principal normal unit vector, $\hat{N}$, can be defined to be codirectional with the vector $d\hat{T}/ds$ (since the derivative of a vector is normal to the vector). A third unit vector to complete the orthogonal frame can be defined as the cross product of $\hat{T}$ and $\hat{N}$ and is called the binormal unit vector ($\hat{B} = \hat{T} \times \hat{N}$). It can be shown that $\hat{N}$ lies in the plane that contains both the acceleration vector ($\vec{A}$) and the velocity vector ($\vec{V}$) of the moving point. Since $\hat{B}$ is perpendicular to both $\hat{T}$ and $\hat{N}$, it is computed as a normalized cross product $\vec{V} \times \vec{A}$ and then $\hat{N}$ is obtained by forming cross product $\hat{B} \times \hat{T}$.

The three orthogonal unit vectors ($\hat{T}$, $\hat{N}$, $\hat{B}$) shown in Figure 3 form a right-handed triad, called the Frenet triad at each point along the space curve. The collection of these triads along a given curve is known as a Frenet-Serret frame field, which is stationary in three-dimensional space. The turning and twisting of a space curve generated by a moving point can be described in terms of curvature, κ, and torsion, τ. Curvature is defined in terms of the Frenet triad as $\kappa\hat{N} = d\hat{T}/ds$, while the torsion is given by $\tau\hat{N} = -d\hat{B}/ds$. The rates of change of ($\hat{T}$, $\hat{N}$, $\hat{B}$) with respect to time may be obtained from the following relations: ($\hat{T}$-rate) $d\hat{T}/dt = \kappa V\hat{N}$, $d\hat{N}/dt = -\kappa V\hat{T} + \tau V\hat{B}$, and ($\hat{B}$-rate) $d\hat{B}/dt = -\tau V\hat{N}$. Thus,

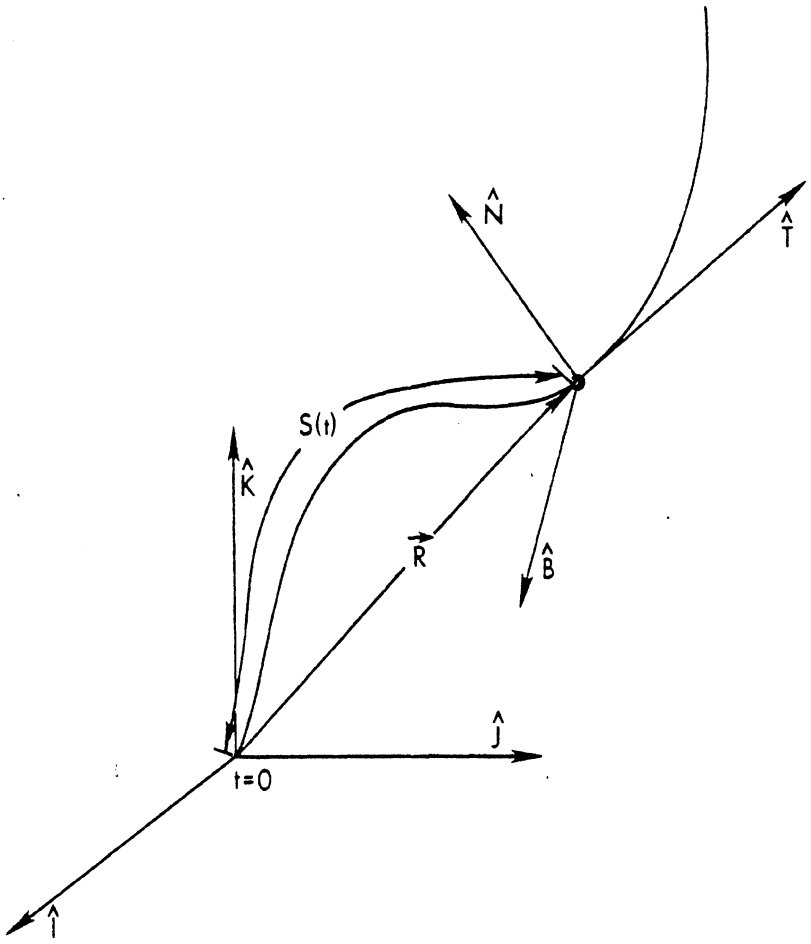

Fig. 3 - Frenet-Serret frame

the turning and twisting of a space curve and the rates of turning and twisting are described by the Frenet triad $(\hat{T}, \hat{N}, \hat{B})$.

In principle, every geometric problem involving motion along a curved path can be solved by means of the Frenet-Serret method. For simple cases, it may be sufficient to record the acceleration data and express it in a convenient form. Examples of such instances are: for zero curvature the motion of a point will be a straight line; for positive curvature ($\kappa > 0$) and zero torsion the motion of a point will be in a plane; and for constant positive curvature with zero torsion, the motion of a point will be in a circle. For more complicated motions, which are common even in simple head impact experiments, it is desirable to be able to classify the types of motions in a convenient manner. The Frenet-Serret frame field approach provides such a method.

In many instances, the motion of a point along a path in space can be usefully reparameterized to describe the motion in terms of distance along the path (s) rather than in time (t). Such a procedure can simplify the formulas associated with the description of the curves and can clarify similarities and differences in events that occur as the curve is traversed.

EXPERIMENTAL TECHNIQUES - The installation of the 9-accelerometer plate is accomplished in the following manner. The scalp is removed from the frontal bone over the orbital ridges. Several metal self-tapping screws are attached firmly to the skull through small pilot holes drilled in the orbital ridges and in the dental plate above the eye teeth. Several magnesium feet are attached to the plate. Quick-setting acrylic plastic is molded around each of the screws and the feet are embedded in the plastic. In fifteen minutes when the acrylic has set, the plate is rigidly attached to the skull. The orientation of the plate in this position is shown in Figure 2.

Since this instrumentation frame does not coincide with the standard anatomical reference frame, it is necessary to determine its exact location and orientation in relation to the anatomical frame. A three-dimensional x-ray technique was developed which requires taking two orthogonal radiographs of the instrumented head. The procedure requires the identification of four anatomical landmarks (two superior edges of the auditory meati and two infraorbital notches) with four distinguishable lead pellets, and the identification of four lead pellets inlaid in the plate to define the instrumentation frame. Lead pellets were located beneath the effective center of gravity of each of the three triaxial accelerometer clusters, and the fourth was placed beneath the effective center of gravity of the three other centroids.

These eight lead pellets are then radiographed twice: once in the x-z plane and once in the y-z plane. On each of

the two radiographs, the optical center and the laboratory vertical z-axis are simultaneously x-rayed, the distances between the x-ray film and each target are recorded for each view.

The computations which follow reconstruct the laboratory coordinates (x, y, z) of each of the eight pellets. The anatomical reference frame is reconstructed from the four anatomical points. The instrumentation frame and its origin are determined from the four plate targets. Finally, the transformation matrix between the instrumentation and the anatomical frame is obtained.

The method used for obtaining epidural pressures employs a Kulite model MCP-055-5F catheter tip pressure transducer. A Stryker bone coring tool is used to make a hole with a special 3 mm circular bit. An adjustable set-screwed collet is used which enables the technicians to core into the skull in small increments, preventing damage to the dura mater. The increment of the bone is then removed using a dental scoop, and the resulting hole is tapped for a coarse thread.

A tubular magnesium coupling device is screwed into the tapped hole in the skull. It is anchored into place using quick-setting acrylic plastic molded around the base. A one cm section of rubber tubing is then clamped onto the top of the device and Dow Corning dielectric gel (silicon fluid) is injected into the tubing to act as a coupling medium. The Kulite pressure transducer is then inserted, and secured at proper depth.

Strain gauges are used on the skull bone to record the vibrations of the skull during impact for the purpose of estimating their effect on the accelerometer signals. A Micro-Measurements Type EA-13-015Y-120 strain gauge rosette is bonded with M-bond 200 cyanoacrylate adhesive to the surface of the frontal bone, anterior to the Bregma over the sagittal sinus. After the leads are soldered, the rosette and leads are covered and sealed by a coat of M-coat D paint.

TEST SUBJECT PREPARATION

Seven primate subjects were used in these experiments: five *Macaca mulatta*, one *Macaca assamensis*, and one *Papio cynocephalus*. These were obtained by HSRI from the University of Michigan Unit for Laboratory Animal Medicine (ULAM). Prior to acquisition, the *Macaca* subjects had been used in one or more pharmacological research projects and the *Papio cynocephalus* had been used in a terminal physiology experiment.

The impacts of the *Papio* and the first four *Macacas* were conducted on post-mortem subjects. Upon termination, they were stored in a cooler at 4°C for 48 hours before testing. Living *Macacas* were used in the two final experiments. The protocol for post-mortem primates was less

complex than for that of the live primates, which is outlined below. Notes, data, and changes in procedures were recorded on a chronological checklist.

On the morning of the experiment the primate is given an intramuscular injection of ketamine (dL-2-[O-chlorophenyl]-2-[methylamino] cyclohexanone hydrochloride) before being delivered to the HSRI Biomedical Laboratory by a ULAM technician. A catheter with a three-way valve was inserted into the saphena parva vein in the hind leg, and sodium pentobarbital injected through the valve at a dosage of 15 mg/kg, to effect. An airway is established. The upper body is prepared and the weight and biometrical measurements are taken with a standard anthropometer, a stainless steel tape, a ruler and a Homes Model 51HH beam scale. Body measurements are illustrated in Figure 4; head measurements in Figure 5. Using a cauterizing scalpel, the scalp and muscle mass are removed from the frontal bone and the screws used to moor the nine-accelerometer plate and the epidural pressure transducer skull fitting are screwed into place. The frontal bone is sanded with 200, then 400 weight wet/dry sandpaper and the strain gauge rosette is then cemented into position. The strain gauge wires are soldered to the leads and the assembly covered with sealant. Quick-setting acrylic is molded around the pressure transducer fitting and nine-accelerometer moorings. When the acrylic is set, the strain gauge wires are strain-relieved by being secured to the nine-accelerometer plate with nylon wire wrap. Figures 2 and 6 show the positioning of the instrumentation on the skull.

Next, eye and ear x-ray targets are positioned. The primate is transported to the x-ray room where two head x-rays (x-z and y-z views) are taken. The distance between each of the eight targets and the surface of the x-ray table is measured and recorded.

The primate is then taken to the impact laboratory and placed in the impact chair. Three triaxial accelerometer clusters are fastened to the nine-accelerometer plate. Silicon fluid is injected into the pressure coupler, thus removing all air, and the pressure transducer is inserted. The primate is positioned in front of the impactor and stabilized with paper tape. All of the transducer wires are then connected and cabled, and the transducers checked for continuity and function.

A Polaroid photograph is then taken through the cineradiograph to check the position of the primate and the x-ray settings. Final adjustments are made on the x-ray settings, amplifier settings, and the position of the primate. The x-ray settings, the distance from the x-ray head to cineradiograph screen, and the distance from the mid-line of the primate to the cineradiograph screen are recorded. At this point setup photographs are taken. Holes are then punched into the paper tape supporting the primate. The

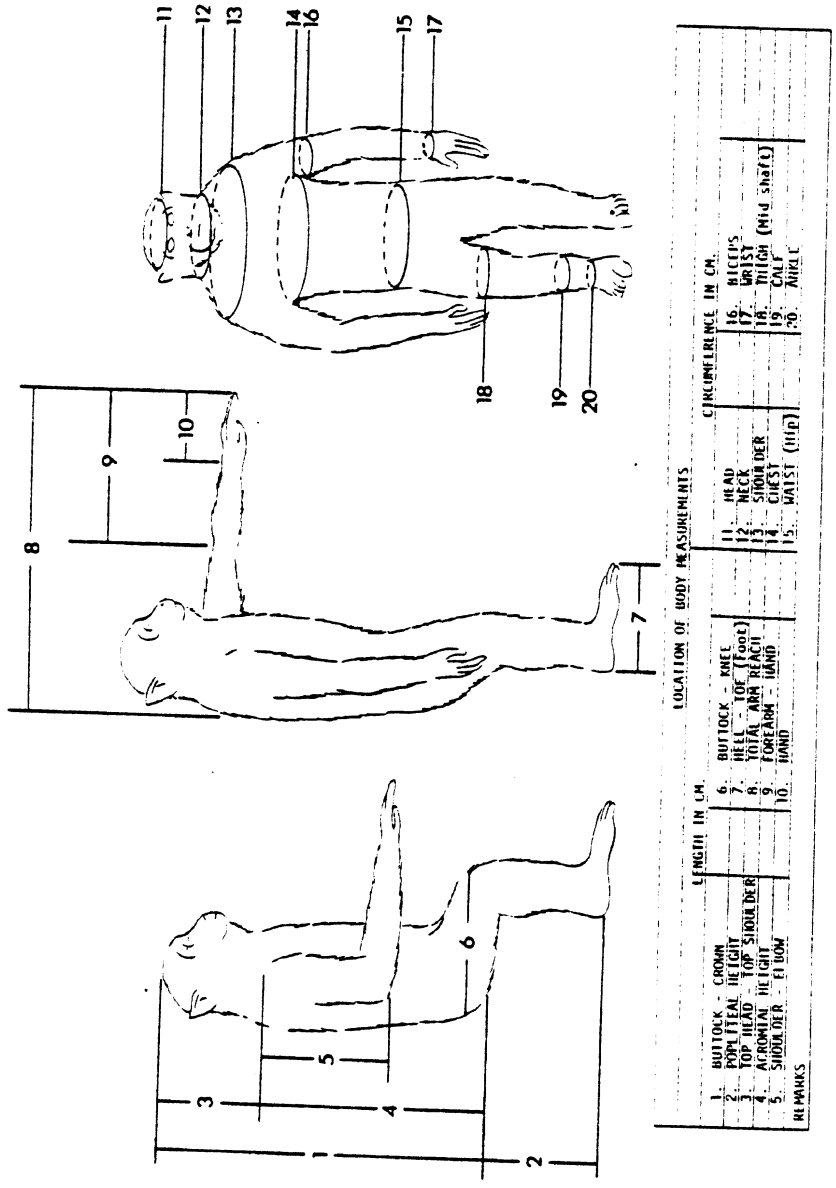

Fig. 4 - Identification of body measurements

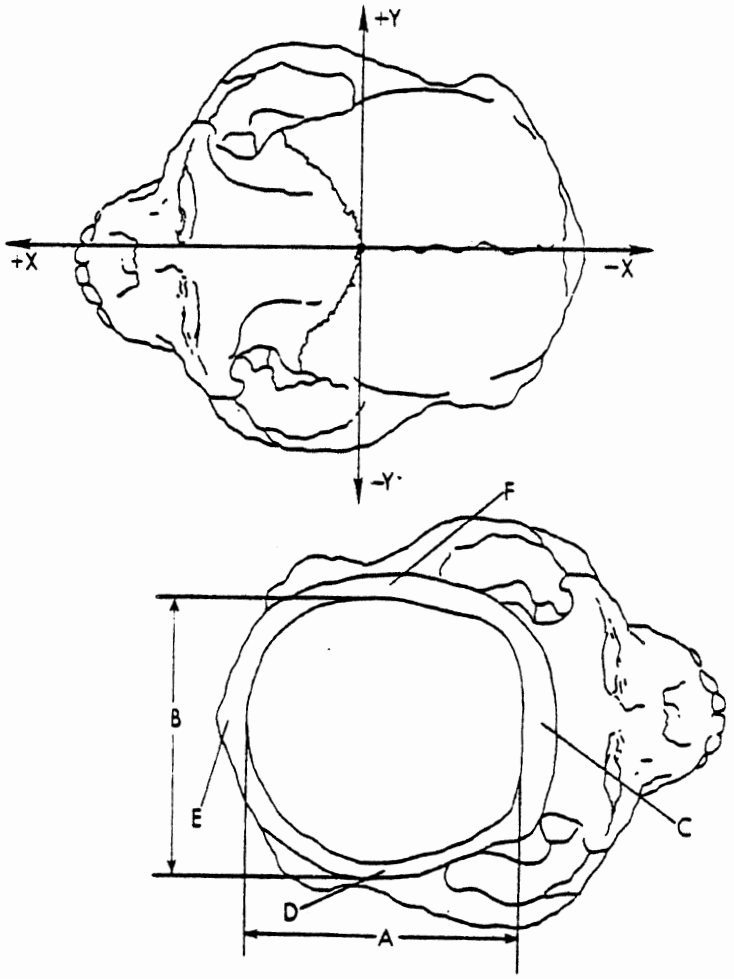

Skull Inside Length A _____ Skull Thickness at Pt. D _____

Skull Inside Width B _____ Skull Thickness at Pt. E _____

Skull Thickness at Pt. C _____ Skull Thickness at Pt. F _____

Fig. 5 - Identification of head measurements

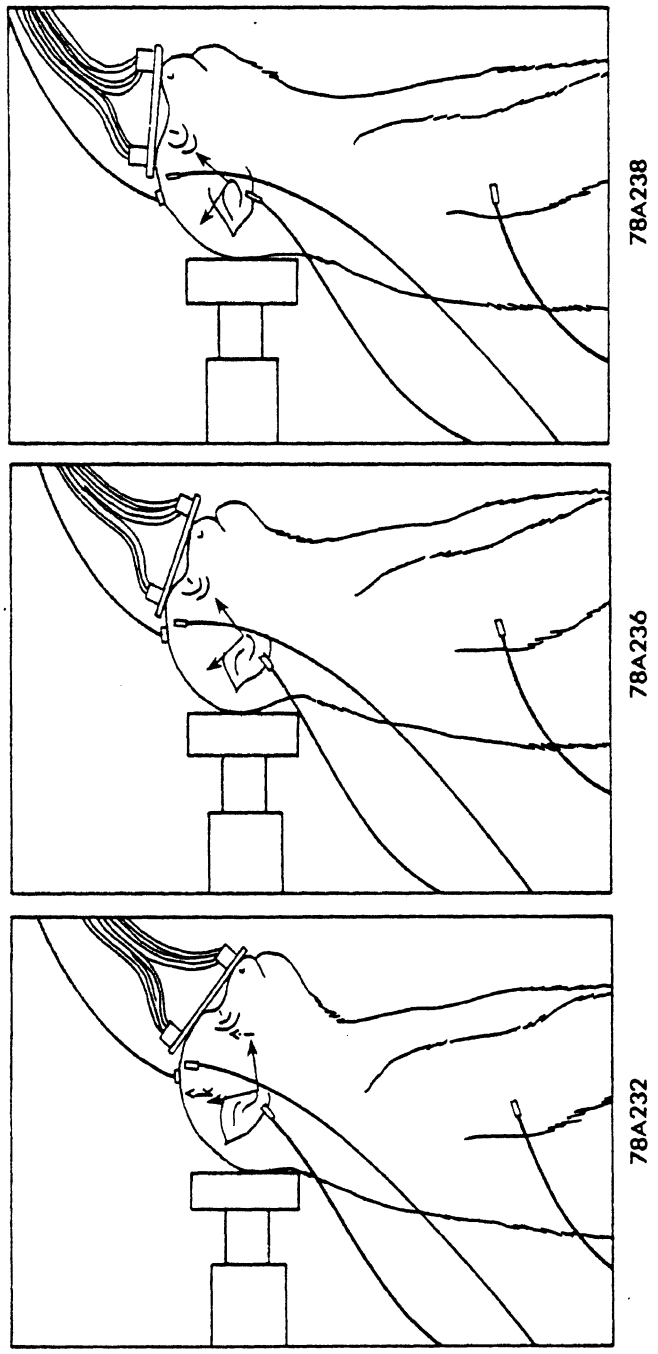

Fig. 6 - Initial conditions of impact test

Polaroid camera is exchanged for the Photosonics high-speed motion picture camera in the cineradiographic system. One hour after impact, a 5 ml dose of Uthol (concentrated, unpure sodium pentobarbital) is injected via the hind leg I.V. catheter to euthanize the primate.

IMPACT TEST CONDITIONS - The impacts were conducted using the HSRI pneumatic impacting device, which was specifically constructed to give impacts of reproducible velocity. This instrument is comprised of a 0.43 cubic meter air reservoir attached to 167 cm long by 10.2 cm diameter honed steel cylinder with two carefully fitted steel pistons.

Compressed air from the buildings's air compression system is introduced into the reservoir. The pressure is regulated by a series of hand valves and measured with a gauge having an accuracy of 0.25%. The driver piston is secured at the reservoir end of the cylinder by an electronically controlled locking mechanism. At the opposite end of the cylinder the striker position is rigidly connected to the impact force head. Both steel pistons have interchangeable elastic bumpers. When the air reservoir is pressurized and the locking mechanism released, the driver piston is propelled by the compressed air through the cylinder until its bumper impacts the bumper on the striker piston. Momentum is transferred to the striker piston, which is allowed to travel up to 25.4 cm. The excess kinetic energy is absorbed by a 3003 H14 seamless aluminum inversion tube, 6.35 cm in diameter with a 0.165 cm wall thickness.

Impactor velocity is controlled by reservoir pressure and the ratio of the masses of the driver and striker pistons. The desired impactor stroke can be accurately controlled by the initial positioning of the striker piston with respect to the inversion tube. Both driver and striker pistons have a mass of 10 Kg for these experiments.

The impactor surface is a 10.2 cm rigid metal plate padded with 2.5 cm Ensolite. The impactor force transducer assembly consists of a Kistler 904A piezoelectric load washer with a Kistler 804A piezoelectric accelerometer mounted internally for inertial compensation.

A chair was designed and constructed for positioning of the primates which could be adapted to the varying primates and test conditions. In addition, a moveable overhead arm facilitated suspension of the primate.

The primate is placed in an erect sitting position with its posterior side towards the impactor, so that the line of impact is in the mid-sagittal plane in the posterior-anterior direction. The primate is held in place with paper tape which grips the body under the armpits, suspending the head and torso from the overhead arm. Immediately before testing, holes are punched into the tape to facilitate release upon impact.

The test subjects were impacted at the occiput. In tests 78A232 and 78A234 the eyes were on a horizontal line through the impact site, thus the estimated center of mass was below the line of impact. In tests 78A236 and 78A239 the eyes were raised to a point slightly above a horizontal line through the impact site, thus the line of impact was through the estimated center of mass. In tests 78A238 and 78A241 the eyes were raised higher than the previous two tests, thus the center of mass was above the line of impact (Figure 6).

CINERADIOGRAPHS - Cineradiographs were taken of the impact events at 1000 frames per second. The HSRI high-speed cineradiographic system (11) consists of a Photosonics 1B high-speed, 16-mm motion-picture camera which views a 2-inch diameter output phosphor of a high-gain , four-stage, magnetically focused image intensifier tube, gated on and off synchronously with shutter pulses from the motion-picture camera. A lens optically couples the input photocathode of the image intensifier tube to x-ray images produced on a fluorescent screen by a smoothed direct-current x-ray generator. Smoothing of the full-wave rectified x-ray output is accomplished by placing a pair of high-voltage capacitors in parallel with the x-ray tube. A 22 cm diameter circular field was viewed in these experiments.

DATA HANDLING - The impact force and acceleration, epidural pressure, and nine head accelerations are recorded unfiltered on a Honeywell 7600 FM Tape Recorder. The impact force, velocity and strain are also recorded unfiltered on a Bell and Howell CEC 3300 FM Tape Recorder. A synchronyzing gate is recorded on both tapes. All data is recorded at 30 ips.

The analog data on the FM tapes is played back for digitizing through proper anti-aliasing analog filters. The A-to-D process for all data, results in a digital signal sampled at a 6400 Hz equivalent sampling rate. Following this step, the power spectrum of the signal is obtained and plotted along with the time history to determine the relevance of the data before being used in the three-dimensional motion analysis computer program.

RESULTS - Full documentation of the experimental results for the primate head impacts discussed in this paper is given in reference 15. The tables and graphs presented here represent the data found to be most pertinent in discussing the test results. A summary of the test conditions are given in Table 1, the primate biometric measurements are given in Table 2, and the time histories are given in the Appendix.

Data obtained from the three-dimensional head motion analysis consisted of translational and angular displacements, velocities, and accelerations resolved into the laboratory, anatomical and Frenet-Serret reference frames. Before impact, the angular velocities of the Frenet-Serret

Table 1 - Primate Head Impact Initial Test Conditions

Test No.	Subject Condition	Subject Positioning C.G. w/r Occipital Impact	Impact Surface	Pressure Transducer Location Relative To Bregma (cm) x	y
78A229	Post-mortem	At	2.5 cm Ensolite		
78A232	Post-mortem	Below	2.5 cm Ensolite	+3.3	+1.3
78A234	Post-mortem	Below	2.5 cm Ensolite	+3.2	-1.1
78A236	Post-mortem	At	2.5 cm Ensolite	+2.8	-0.8
78A238	Post-mortem	Above	2.5 cm Ensolite	+3.0	+0.6
78A239	Live	At	2.5 cm Ensolite	+2.9	-0.8
78A241	Live	Above	2.5 cm Ensolite	+3.6	+0.8

Table 2 - Primate Biometric Measurements

Test No.	Species	Height (Sitting) (cm)	Mass (kg)	Max. Skull Length (cm)	Max. Skull Breadth (cm)	Ave. Skull Thickness (cm)	Head Muscle Mass(g)	Head Mass (g)	Brain Mass (g)	Brain Volume (ml)
78A232	Macaca assamensis	49.1	6.9	6.4	5.1	0.47	125	595	70	
78A234	Macaca mulatta	53.6	9.5	7.4	5.6	0.28	135	625	105	95
78A236	Macaca mulatta	53.4	8.2	6.6	5.6	0.24	140	510	100	90
78A238	Macaca mulatta	53.9	8.2	6.9	5.6	0.23	130	540	115	105
78A239	Macaca mulatta	48.8	8.2	6.4	5.3	0.22	80	510	85	75
78A241	Macaca mulatta	47.0	10.6	8.4	6.4	0.43	190	750	125	115
78A229	Papio cynocephalus		23.0				825	1020	155	

frame are not defined because the path of motion has not been established. However, position, defined as the displacement from the initial condition of the anatomical center, must necessarily be resolved into the laboratory frame.

In order to define the pulse duration, a standard procedure was adopted which determines the beginning and end of the pulse. The procedure is to determine first the peak and the time at which it occurs. Next, the left half of the pulse, defined from the point where the pulse starts to rise to the time of peak, is least-squares fitted with a straight line. This rise line intersects the time-axis at a point which is taken as the formal beginning of the pulse. A similar procedure is followed for the right half of the pulse, i.e., a least squares straight line is fitted to the fall section of the pulse which is defined from the peak to the point where the first pulse minimum occurs. The formal end of the pulse is defined then as the point where the fall line intersects the time axis.

A summary of the test results is given in Table 3 which includes velocity, peak force, force duration, and the greatest positive and negative epidural pressures. The velocity was obtained from a magnetic pickup that produces time pulbes at 1.3 cm intervals on the impacting device. The force duration was determined as described above. The peak positive and negative epidural pressures were obtained by measurement from the zero pressure point on the transducer time histories. Two similar cadaver tests (1) are also listed.

DISCUSSION

The work presented in this paper is part of a continuing program on head injury research. A great deal of data has been generated and a complete presentation of the data is beyond the scope of this paper. The results discussed in this section are based on analysis of the data presented in abbreviated form in the Appendix to this paper. Because of the complexity of the experiments, only a limited number of subjects have been tested. Thus, the features of the data noted in this section represent trends that are felt to be important factors in head impact response. Continued work is necessary to be able to generalize the findings.

HEAD IMPACT RESPONSE DEFINITION - Head impact response may be defined as a continuum of "events" characterized by the path, and all the vectors defined on that path, which are generated by the motion of the anatomical center and by changes of the attached frame fields. Physically this implies that head impact response is interpreted as the response of a material body (the skull) which is in contact with other material bodies (the neck, impactor, soft tissue and brain). The curve and the vectors generated as the anatomical center moves in time are therefore a result of the interactions of the skull with these other material

Table 3 - Impact Test Summary

Test No.	Description	Velocity (m/s)	Force (N)	Force Duration (ms)	Pressure (mm Hg)
78A229	Post-mortem Occipital Impact	14.0	11500	6 msec	-
78A232	Post-mortem Occipital Impact	11.5	5800	3 msec	-
78A234	Post-mortem Occipital Impact	13.5	5700	4 msec	-
78A236	Post-mortem Occipital Impact	12.5	5600	4 msec	-721/+420
78A238	Post-mortem Occipital Impact	12.5	6600	3 msec	+1041/-410
78A239	Live Occipital Impact	12.5	5000	5 msec	+1977
78A241	Live Occipital Impact	12.5	8700	3 msec	+3682/-710
76A135	Post-mortem (cadaver) Occipital Impact	7.0	5000	13 msec	-
76A137	Post-mortem (cadaver) Occipital Impact	8.0	5500	8 msec	-

Table 4 - Reparameterization of Primate and Cadaver Test Data

PRIMATES

Test No.	Arc Length (mm)			Time (ms)		
	Q1	Q2	Q3	Q1	Q2	Q3
78A229	0	6.5	15	0	3.0	4.7
78A232	0	6.7	58	0	2.5	7.5
78A234	0	7.3	50	0	3.0	6.5
78A236	0	7.3	50	0	2.5	7.0
78A238	0	6.8	90*	0	3.0	10.5*
78A239	0	8.0	55	0	3.0	7.0
78A241	0	7.2	56	0	2.5	8.5

*ill-defined due to instrumentation difficulties.

CADAVERS

Test No.	Arc Length (mm)			Time (ms)		
	Q1	Q2	Q3	Q1	Q2	Q3
76A135	0	8.3	56	0	5.0	13.1
76A137	0	8.7	60	0	5.0	8.4

bodies.

Generally, an event that happens in one specific impact will not occur in all other impacts. However, in specific impacts, certain events will always occur. Examples of these events which are important in head impact are: the initiation of head impact response (denoted by Q_1 on the tangential acceleration-time histories in the accompanying data); the positive maximum of the tangential acceleration-time history (denoted Q_2 in the accompanying data); and the negative maximum of the tangential acceleration-time history (denoted by Q_3 on the accompanying data). These events can then be used to define different types of impacts and to compare the response of one type of surrogate to another.

The motion of a rigid body in space is the result of generalized forces: the total force, and the total torque about a suitable axis. The dynamic problem of the motion of the skull can be interpreted in the same way. However, because of the complex interactions of the skull with the other material bodies, serious problems can arise in determining which of the bodies is producing these generalized forces.

EFFECT OF SKULL DEFORMATIONS ON RIGID BODY MOTION ANALYSIS - The condition of small skull deformations in head impacts is generally not of interest from an injury standpoint. However, in the circumstances of rigid body motion, intractable complications can result if precautions are not taken to minimize the effect of skull deformations. The choice of location of the accelerometers is critical in this respect for primate impacts. The orbital ridges proved to be relatively stable during impact, as the strain gage rosettes placed near the point of attachment of the 9 acceleration plates showed that minimal strains ($<200\mu\varepsilon$) occurred in this area. In addition, a filter, applied to the raw data, can be used to minimize the effects of high frequency vibrations. The choice of filter is based on the power spectrum of the raw data. The power spectrum revealed that the highest frequency content, excluding those components attributed to noise, were in the pressures, where the power spectrum dropped effectively to zero at 600 Hz. The reconstructed time histories, filtered at 600 Hz, show no significant difference from the raw time histories except for the elimination of high-frequency noise.

EFFECT OF SKULL GEOMETRY - The time history of the anatomical center during the time interval (Q_1-Q_2) is considered to be primarily a result of the interation of the impactor with the skull. During this period, the angular acceleration found to be principally in the binormal direction (although there were lesser components in the normal and tangential directions) in tests 78A232, 78A234, 78A238 and 78A239. This implies that the skull may be rotating about a point of closest approach of the skull to the impactor (soft tissue prevents actual contact of the skull and

impactor surface). Under this condition the rate of change of the tangent unit vector (T-rate) and the translational acceleration in the normal direction will be a result of the torque produced by this rotation. Calculations of the translational acceleration in the normal direction at this point show significant reductions of this acceleration in comparison to that of the A.C., confirming that this type of rotational motion is taking place.

The implication of this result relates directly to skull geometry. Figure 7 shows reconstruction of the x-rays from test 76A135, an unembalmed human cadaver, test 78A229 and test 78A239. Examination of this figure shows that the shape of the human skull in the posterior section is considerably different from the other primates. This difference has a direct effect on the rotational stability of the skull during impact.

Figure 6 is a reconstruction of the test set-up for three different types of impacts: Test 78A232 is arranged in a manner similar to the unembalmed human cadaver, the eyes being in a frontal direction; Test 78A236 is positioned in an attempt to minimize rotation about the right-left axis during impact; and Test 78A238 is positioned in order to produce such a rotation. These types of set-ups take advantage of the skull geometry of the primate and use the location of the center of gravity relative to the applied impact force axis to adjust the direction of applied torque. This phenomenon is apparent in the evaluation of the angular acceleration for Tests 78A232, 78A2236 and 78A238 during the (Q-Q_2) interval. In test 78A232, the angular acceleration is about the right-left axis, while in Test 78A236, during the (Q_1-Q_2) time interval, the angular acceleration is in the opposite direction. Similarly, the angular acceleration in test 78A238 is like that of 78A236, but greater in magnitude.

The top portion of Figure 8 represents the general directions of the tangent and normal vectors at an instant after the Q_2 event. The direction of the binormal vector is determined by the right plane represented in the illustration. Care must be taken in the interpretation of this figure since motion during the (Q_1-Q_2) interval is usually three-dimensional and will not be restricted to a single convey, schematically, the general idea of the differences in head motion produced by the different initial conditions. The three types of tests are distinguished by the Frenet frame and the angular acceleration defined on the path during the (Q_1-Q_2) interval. The significant feature is that dynamically similar head motions can be produced in cadaver and lower primate impact tests, but the lower primates require different initial conditions than the cadaver due to skull geometry differences.

EFFECT OF SOFT TISSUE - In general, as the impact is increasing, the response, when unopposed by additional

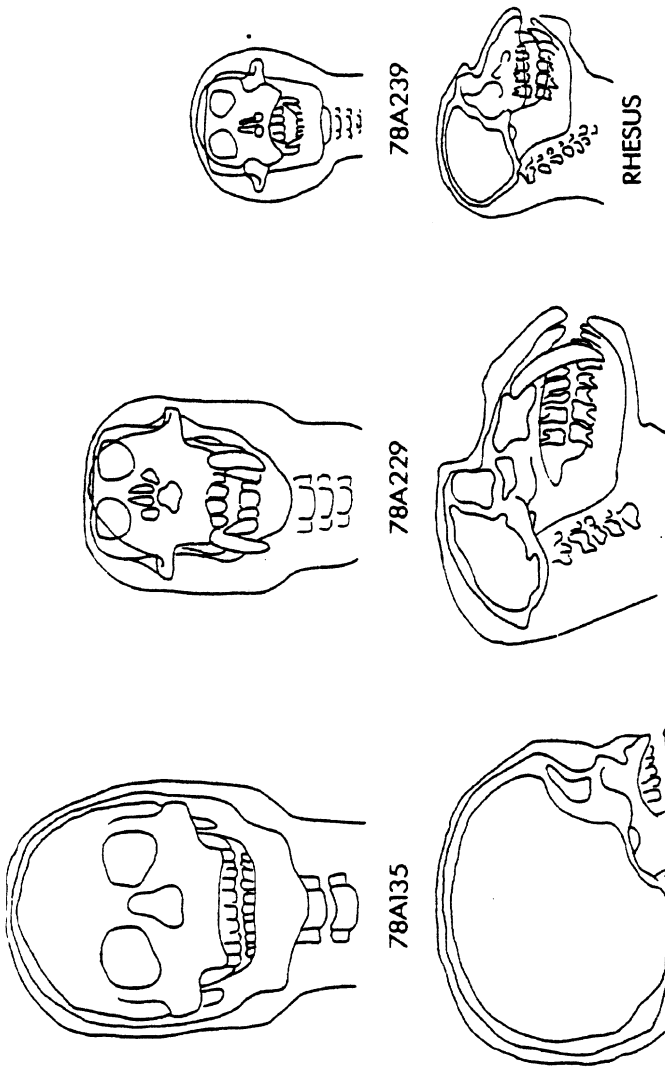

Fig. 7 - Reconstruction of skull x-rays

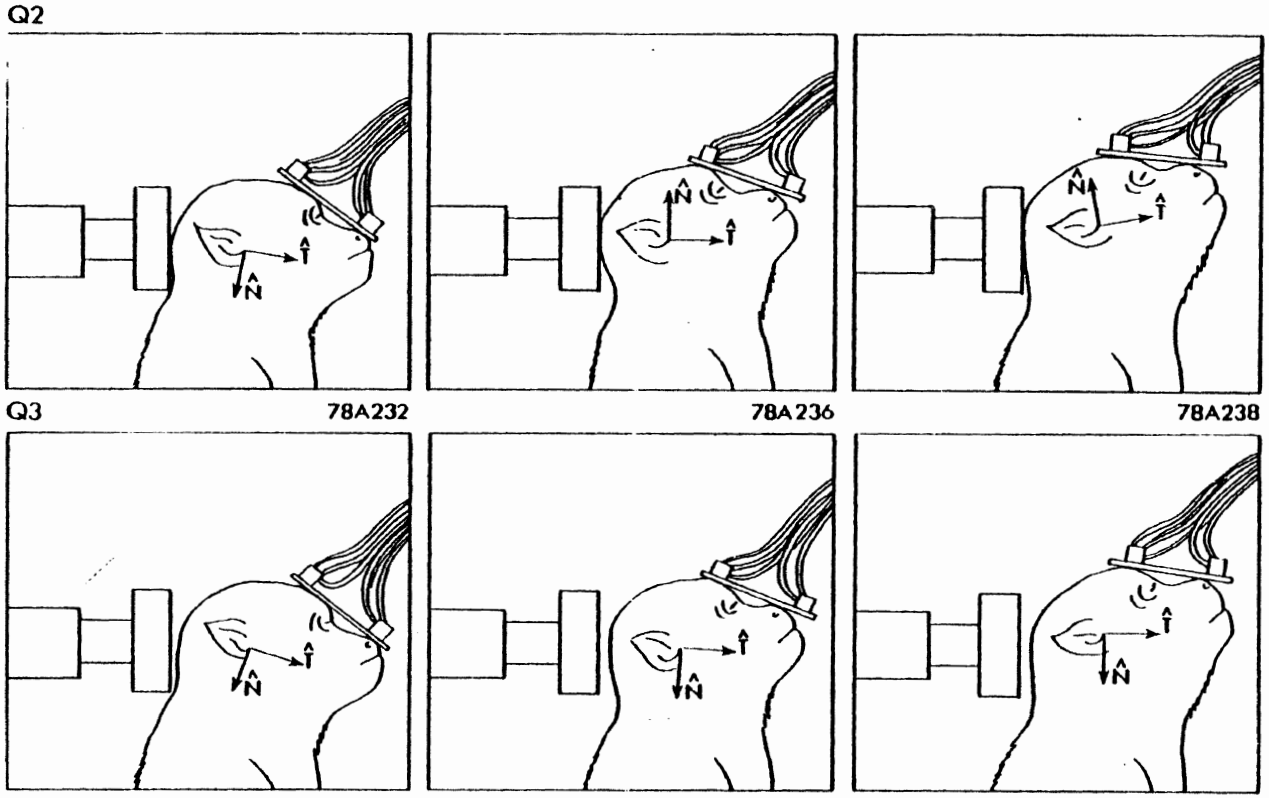

Fig. 8 - Reconstruction of motion from x-ray, cineradiographs, and kinematic time histories for the HSRI 3-D motion measurements

generalized forces, will be increasing. Conversely, when the force on the head is decreasing the response should decrease. During the time interval (Q_2-Q_3) this was generally found not to be the case. In this interval, it can be assumed that the impactor no longer dominates the skull's response and that other material bodies contribute input to the path of the A.C. and its vectors. In addition, the events during the interval (Q_1-Q_2) can affect those during (Q_2-Q_3). This conclusion is based on the following findings. For all the tests, the tangential acceleration decreases more rapidly than the force, from the Q_2 event until the time it crosses the zero axis. In tests 76A135 (cadaver), 78A236, 78A238, 78A239 and 78A241 (all Macaca) the normal acceleration and angular acceleration remain significant after the impact force drops to zero and the binormal vector rotates π radians during the (Q_2-Q_3) interval.

Examination of all the tests reported in the Appendix shows that during the (Q_1-Q_2) interval, unless there are rapid changes in the binormal vector direction (large B-rates), the normal acceleration and the binormal vector direction are induced by the angjlar acceleration of the head. For tests 76A135, 78A238, 78A239, and 78A241 the angular acceleration vector reverses direction around the Q_2 event time with the binormal vector rotating π radians shortly afterwards. This indicates that, in those tests, there are torques being generated that are sufficiently large that they dominate the other factors (such as the impact force) involved in the establishment of the binormal vector direction and the normal acceleration. In addition, the angular acceleration vector is of sufficient duration in its new direction eventually to re-establish it in the binormal vector direction. The rotation of the binormal vector can be very rapid, indicating an inflection point in the path of the A.C. in space. Test 78A239 (see Appendix) shows a large B-rate with the binormal vector rotating π radians almost instantaneously. The fact that in tests 78A232 and 78A234, during the (Q_2-Q_3) interval, there is relatively little rotation of the binormal vector and that the angular acceleration is greatly reduced after the force drops to zero indicates that the torque induced by the impactor is codirectional or much greater than the torque generated by other forces. Therefore the normal and binormal vector directions are basically the same for all tests at the end of the (Q_2-Q_3) interval, as represented for the Macaca subjects by the bottom section of Figure 8.

The fact that torques which result at the beginning and end of the (Q_2-Q_3) interval are opposite in direction is best understood by examining the resultant angular velocity Comparison of tests 78A236 and 78A239 to test 78A232 reveals the basic differences. In tests 78A236 and 78A239 the angular velocity reaches a maximum close to the Q_2 time, with

the minimum occurring around Q_3. Shortly following Q_3, there is a rapid rise in the angular velocity with rotation in the opposite direction. A similar behavior can occur in cadavers (test 76A135) but the first peak is generally significantly smaller than the second. This may be attributed to the differences in skull geometries and soft tissue distributions.

In the unembalmed cadaver, it has been determined (1) that the source of the generalized forces during (Q_2-Q_3) is the soft tissue (i.e., the brain). It is, however, more difficult in primates to separate the effects of the brain from that of the soft issue in the head and neck. In Figure 7, the x-ray reconstruction compares the soft tissue distribution of the various human surrogates. The brain is the primary source of soft tissue in the head of the cadaver while in the primate, it is the external head and neck masses. The effect of muscle mass can become so great that, during Papio Test 78A229, more momentum is transferred to the soft tissue than to the skull. Examination of the data in the Appendix for that test shows that a large positive tangential acceleration occurs after impact, indicating that momentum is being transferred to the skull from an outside source. The amount transferred is, in fact, so great that the maximum velocity is not reached until well after impact. This is consistent with the measured masses of the soft tissue and skull of this subject, given in Table 2.

REPARAMETERIZATION OF EVENT OCCURENCE FROM TIME TO ARC LENGTH - Examination of the primate test data reveals that many of the time histories of the motions are similar in waveform to that of a cadaver (Test 76A135). However, the time intervals between events are necessarily much shorter for primates than for the cadaver, since the inertias of their respective masses are quite different. The events that occur for all tests during the (Q_1-Q_3) interval suggests that, by reparameterization of the data from time (t) to path arc length (s(t)), the geometry of the space curves of the A.C. could be made more congruent. This was done for all the primate tests and for two equivalent cadaver tests, reported in Reference (1), by integrating the resultant velocity of the A.C. to obtain arc length. Table 4 lists the results of the reparameterization for both primates and cadavers in posterior-to-anterior impacts. With two exceptions (78A229 and 78A238) the reparameterization shifts the occurence of the Q_2 and Q_3 events into congruence in terms of arc length. Test 78A238 produced a reasonable shift of the Q_2 event but, due to instrumentation difficulties, Q_3 was poorly defined in time and therefore produced a poor definition in terms of arc length. Test 78A229 was conducted with a Papio test subject and, as noted earlier, the head motion was dominated by soft tissue

effects which produced a different trajectory during the (Q_2-Q_3) interval and thus, is expected to result in a different head impact response.

EFFECTS OF THE POST-MORTEM STATE - Previous work, reported at the 21st Stapp Car Crash Conference (1), has shown that major effects attributable to gross brain motions in head impact with unembalmed human cadavers can be studied using the nine-accelerometer motion analysis technique and with high-speed cineradiography. One of the original purposes of the present study was to investigate such effects in living and post-mortem animal subjects. As discussed in the previous section, there are large soft tissue masses (external muscle masses) in primates whose motions can mask the effects of the motion of the brain on the skull response. Thus, the use of motion analysis of the skull to indicate resulting partially decoupled brain motion is difficult with animal test subjects. Within a particular species comparative effects can be discerned, however. Test 78A236 is a post-mortem test with the same initial conditions as Test 78A239, a live animal test. Examination of the resultant angular velocity traces for both these tests (see Appendix) shows significant differences in the waveform shape and magnitude. For the post-mortem subject the waveform is smoother with less abrupt changes in angular velocity than for the live subject. The initial peak angular velocity for the post-mortem subject was only about one-half that for the live subject while the final levels were similar. Tests 78A238 and 78A241 (traces not shown in this paper) provide a similar comparison for a different initial test condition.

High-speed cineradiography is a technique which can provide a more direct indication of brain motion. In some of the previously reported cadaver head impacts (1) this method has demonstrated the formation of radiotransparent regions in the brain cavity during impact motion. The appearance of these regions was considered to be related to motion of the brain relative to the skull. In the six tests conducted with Macaca subjects, cineradiographs were taken and no such phenomena were noted. This may be due to tangential accelerations which were insufficient to move the skull away from the brain or due to angular accelerations which affected the dynamics of the motion sufficiently to suppress the phenomena. A more severe impact environment than that used in this test series may be necessary to produce conditions in the primates which are analogous to those for cadavers.

Measurement of epidural pressures is another direct measurement of brain response to impact. Figures 9 and 10 present epidural pressure-time histories and their accompanying power spectra for post-mortem and live primate test subjects. The peak pressures for the living state are about two to five times the values for the post-mortem state and,

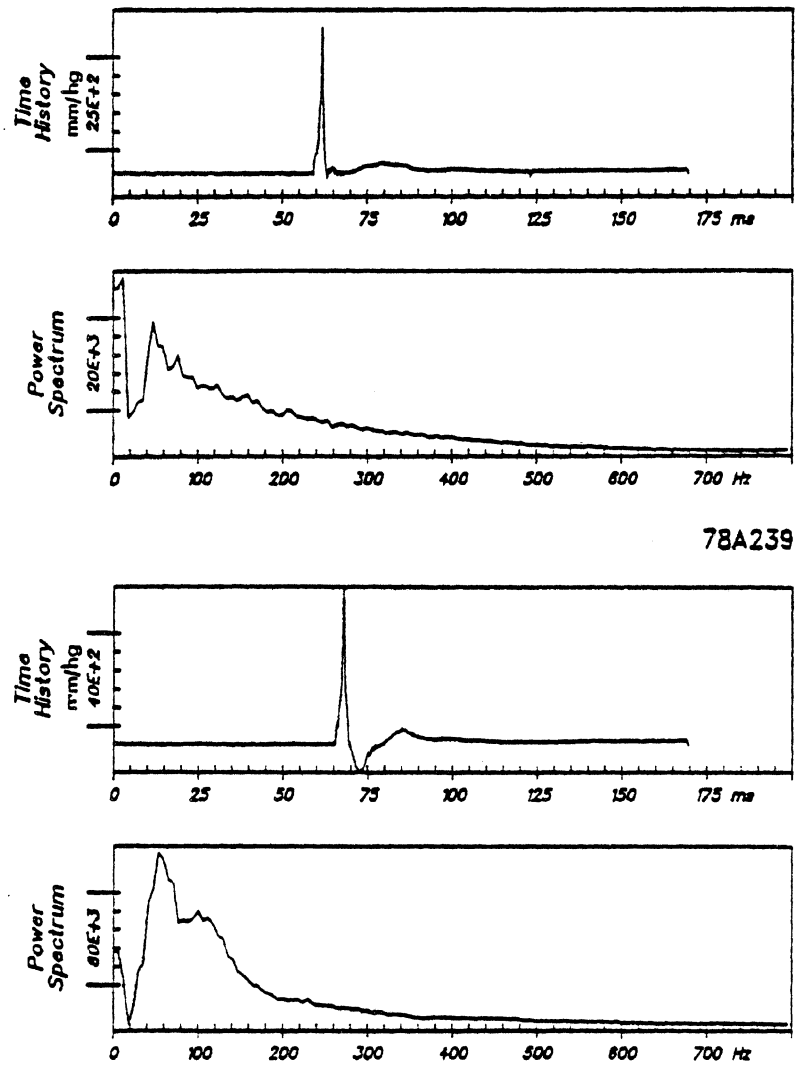

Fig. 9 - Time history and power spectrum of post-mortem primate subjects

in addition, the post-mortem waveforms contain much lower power than those of the living state. This difference suggests that the living brain is stiffer than the unpressurized post-mortem brain.

CONCLUSIONS

Many features of the data presented in this paper are felt to be indicative of important kinematic factors in head impact. More work is necessary before these findings can be generalized. The following specific conclusions can be drawn:

1. Three-dimensional accelerometry techniques can be applied to direct head impacts with lower primate subjects.
2. The Frenet-Serret frame field method for characterizing the motion of a point in space shows promise in describing head impact motion.
3. Reparameterization of head impact motion events may be useful in describing similarities and differences between the head impact responses of human surrogates.
4. The response of the head, during the time of contact, in direct impact is affected by the geometry of the skull in the region of contact.
5. The response of the head, during and after the time of contact, is affected by the soft tissues of the head and neck.
6. Comparison of live and post-mortem (unpressurized) Macaca test subjects shows differences in both head impact response and epidural pressure.

ACKNOWLEDGEMENTS

This work was conducted under the sponsorship of the Motor Vehicle Manufacturers Association. The authors would like to acknowledge the contributions of J. Axelrod, J. Benson, J. Brindamour, M. Dunlap, G. Holstein and D. Kashkashian in the performance of this work.

REFERENCES

1. R. L. Stalnaker, J. W. Melvin, G. S. Nusholtz, N. M. Alem and J. B. Benson, "Head Impact Response." Paper No. 770921, Proceedings of the Twenty-first Stapp Car Crash Conference, Society of Automotive Engineers, Inc., 1977.

2. L. M. Patrick, "Head Impact Protection." Head Injury Conference Proceedings, edited by W. F. Caveness and A. E. Walker, pp. 4:41-48, J. P. Lippincott Co., 1966.

3. A. J. Padgaonkar, K. W. Krieger, A. J. King, "Measurement of Angular Acceleration of a Rigid Body Using Linear Accelerations." ASME Preprint -75-APM3, June 1975.

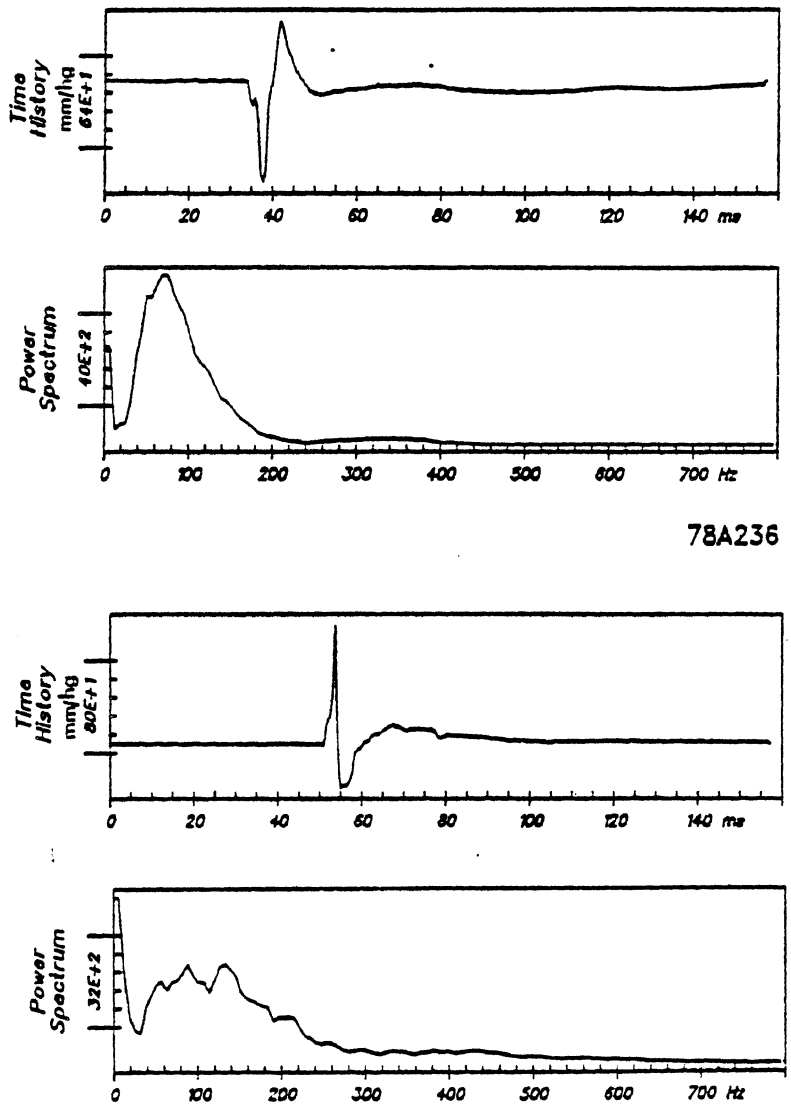

Fig. 10 - Time history and power spectrum of live primate subjects

4. E. Becker, G. Willems, "An Experimentally Validated 3-D Inertial Tracking Package for Application in Biodynamic Research." Paper No. 751173, Proceedings of the Nineteenth Stapp Car Crash Conference, Society of Automotive Engineers, Inc., 1975.

5. C. L. Ewing, et al., "The Effect of the Initial Position of the Head and Neck on the Dynamic Response of the Human Head and Neck to -Gx Impact Acceleration." Paper No. 751157, Proceedings of the 19th Stapp Car Crash Conference, Society of Automotive Engineers, Inc., 1975.

6. C. L. Ewing, D. J. Thomas, "Human Head and Neck Response to Impact Acceleration." Naval Aerospace Medical Research Laboratory Detachment, New Orleans, Monograph 21, August 1972.

7. C. L. Ewing, D. J. Thomas, "Torque versus Angular Displacement Response of Human Head to -Gx Impact Acceleration." Paper No. 730976, Proceedings of the 17th Stapp Car Crash Conference, Society of Automotive Engineers, Inc., 1973.

8. D. J. Thomas, "Specialized Anthropometry Requireemtns for Protective Equipment Evaluation." AGARD Conference Proceedings No. 110, Current Status in Aerospace Medicine, Glasgow, Scotland, September 1972.

9. A. Fayon, et al., "Thorax of 3-Point Belt Wearers During a Crash (Experiments for Cadavers)." Paper No. 751148, Proceedings of the Nineteenth Stapp Car Crash Conference, Society of Automotive Engineers, Inc., 1975.

10. A. M. Nahum, R. W. Smith, "An Experimental Model for Closed Head Injury." Paper No. 760825, Proceedings of the Twentieth Stapp Car Conference, Society of Automotive Engineers, Inc., 1976.

11. M. Bender, J. W. Melvin, R. L. Stalnaker, "A High-Speed Cineradiographic Technique for Biomechanical Impact." Paper No. 760824, Proceedings of the Twentieth Stapp Car Crash Conference, Society of Automotive Engineers, Inc., 1976.

12. J. A. Bartz, F. E. Butler, "Passenger Compartment with Six Degrees of Freedom." Auxiliary Programs to "Three Dimensional Computer Simulation of a Motor Vehicle Crash Victim," Final Technical Report for DOT Contract No. FH-11-7592, 1972.

13. D. J. Thomas, D. H. Robbins, R. H. Eppinger, A. I. King, and R. P. Hubbard, "Guidelines for the Comparison of Human and Human Analogue Biomechanical Data." A report of an ad hoc committee, Ann Arbor, Michigan, December 6, 1974.

14. B. O'Neill. "Elementary Differential Geometry." Academic Press, New York, 1967.

15. G. S. Nusholtz, et al., "Direct Head Impacts of Human Surrogates." Final Report for Motor Vehicle Manufacturers Association of the United States, Inc., In Preparation.

APPENDIX

The following time-histories are included for reference with this paper. Because of space limitations not all the test variables are shown and some of the tests, which were essentially duplicates of the ones presented, are also deleted.

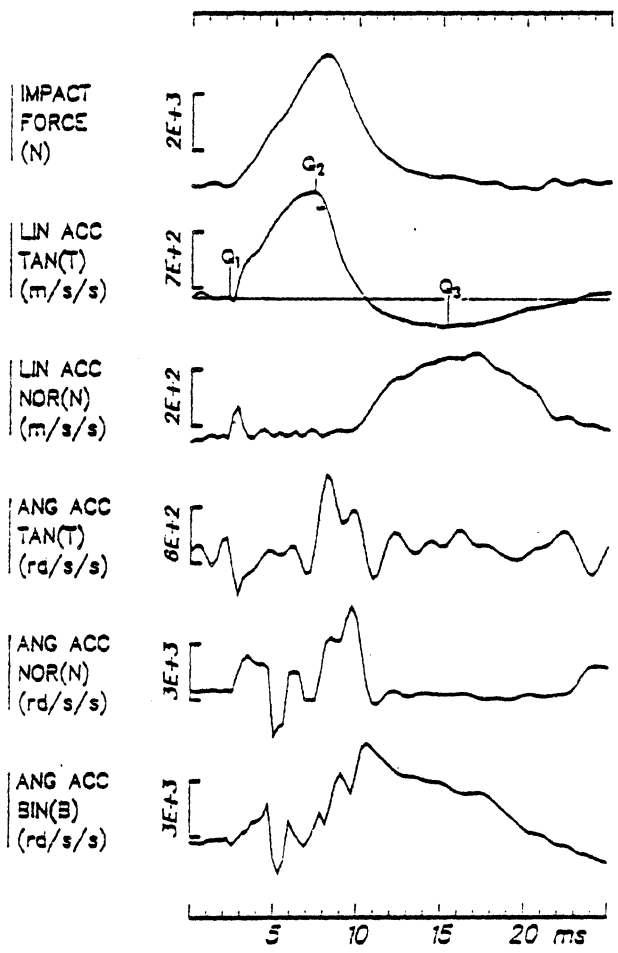

Fig. A-1

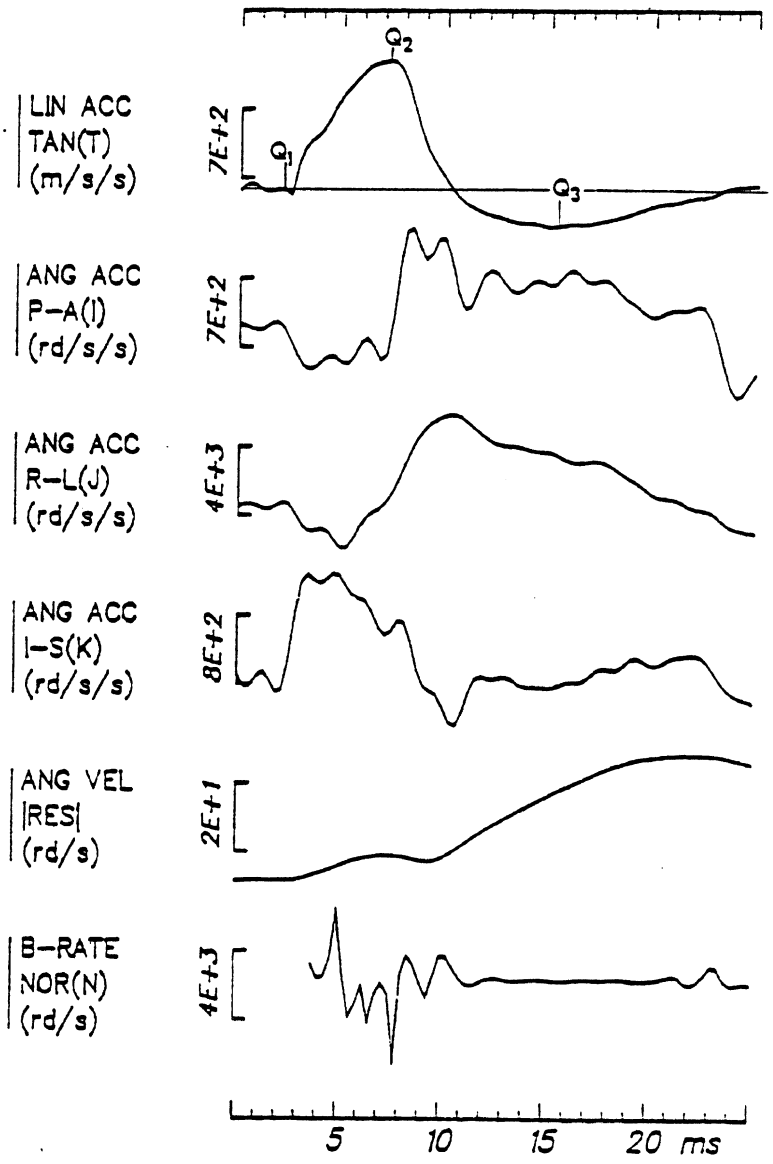
LIN ACC
TAN(T)
(m/s/s)
7E+2
Q1
Q2
Q3
ANG ACC
P-A(I)
(rd/s/s)
7E+2
ANG ACC
R-L(J)
(rd/s/s)
4E+3
ANG ACC
I-S(K)
(rd/s/s)
8E+2
ANG VEL
|RES|
(rd/s)
2E+1
B-RATE
NOR(N)
(rd/s)
4E+3
5
10
15
20 ms

Fig. A-2

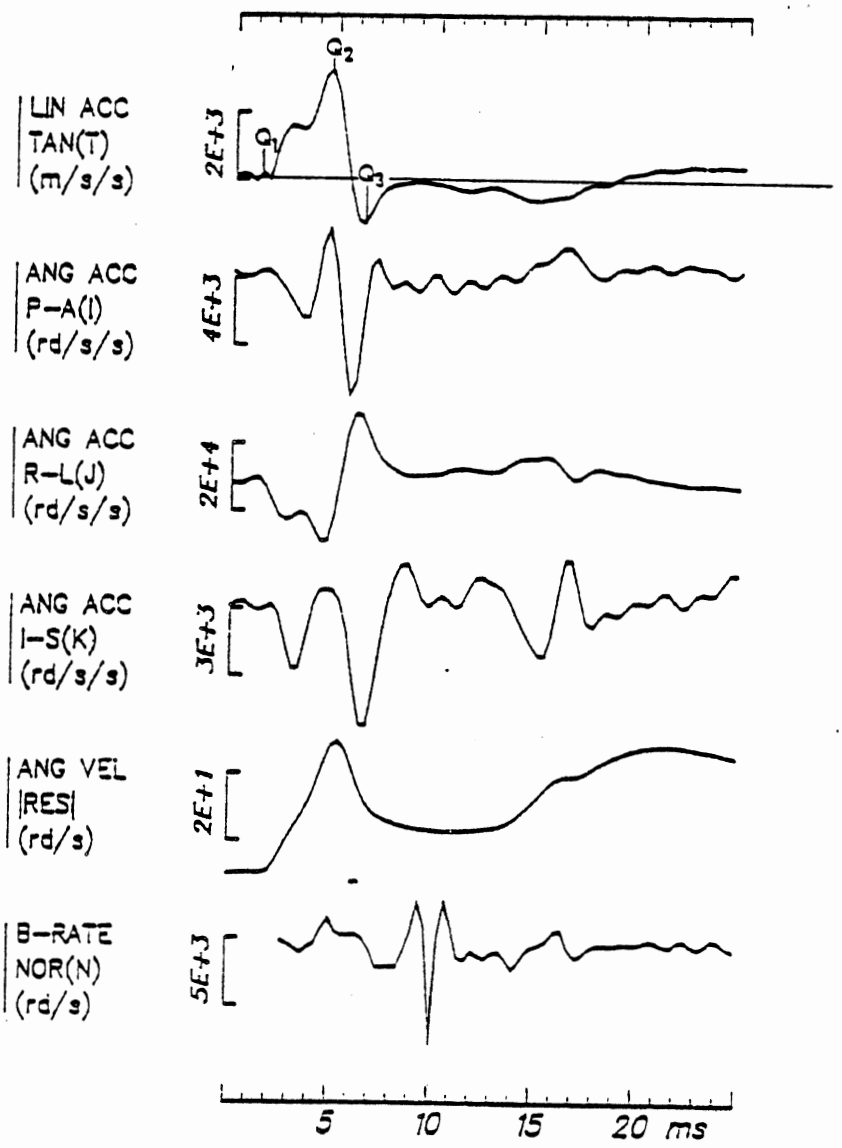
LIN ACC
TAN(T)
(m/s/s)
2E+3
C2
C1
C3
ANG ACC
P–A(I)
(rd/s/s)
4E+3
ANG ACC
R–L(J)
(rd/s/s)
2E+4
ANG ACC
I–S(K)
(rd/s/s)
3E+3
ANG VEL
|RES|
(rd/s)
2E+1
B–RATE
NOR(N)
(rd/s)
5E+3
5
10
15
20 ms

Fig. A-3

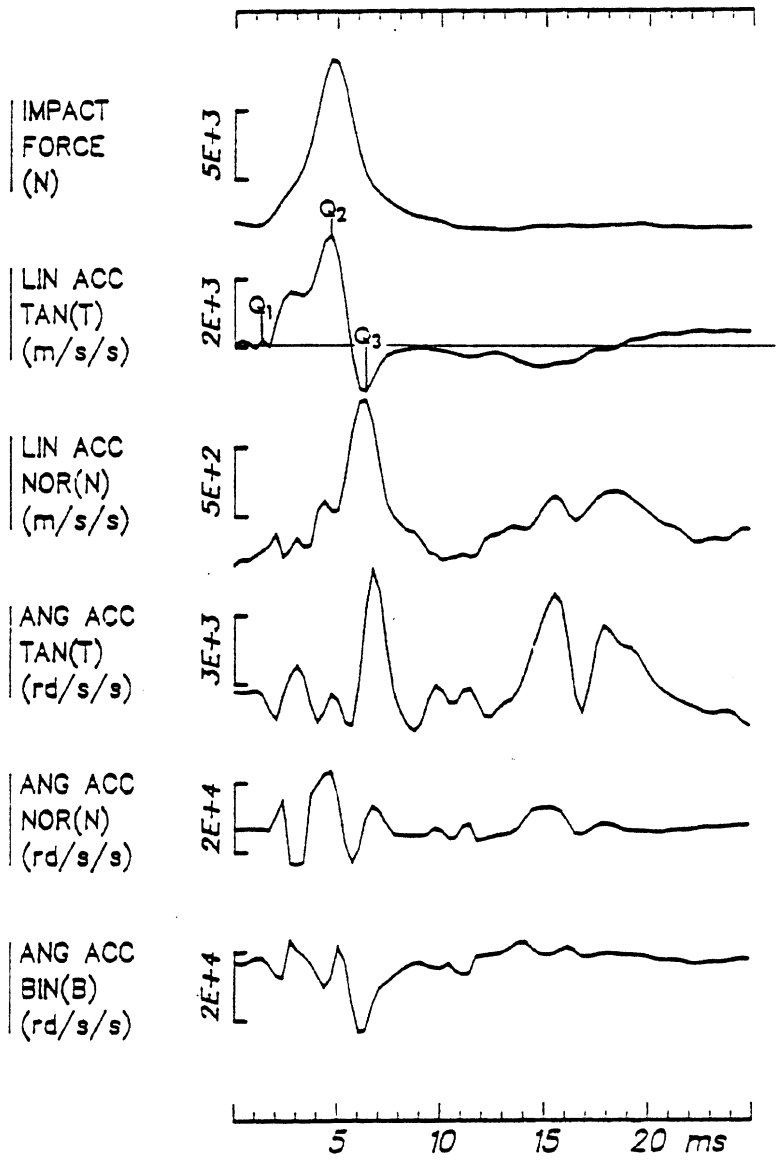
IMPACT
FORCE
(N)
5E+3
LIN ACC
TAN(T)
(m/s/s)
2E+3
Q1
Q2
Q3
LIN ACC
NOR(N)
(m/s/s)
5E+2
ANG ACC
TAN(T)
(rd/s/s)
3E+3
ANG ACC
NOR(N)
(rd/s/s)
2E+4
ANG ACC
BIN(B)
(rd/s/s)
2E+4
5
10
15
20 ms

Fig. A-4

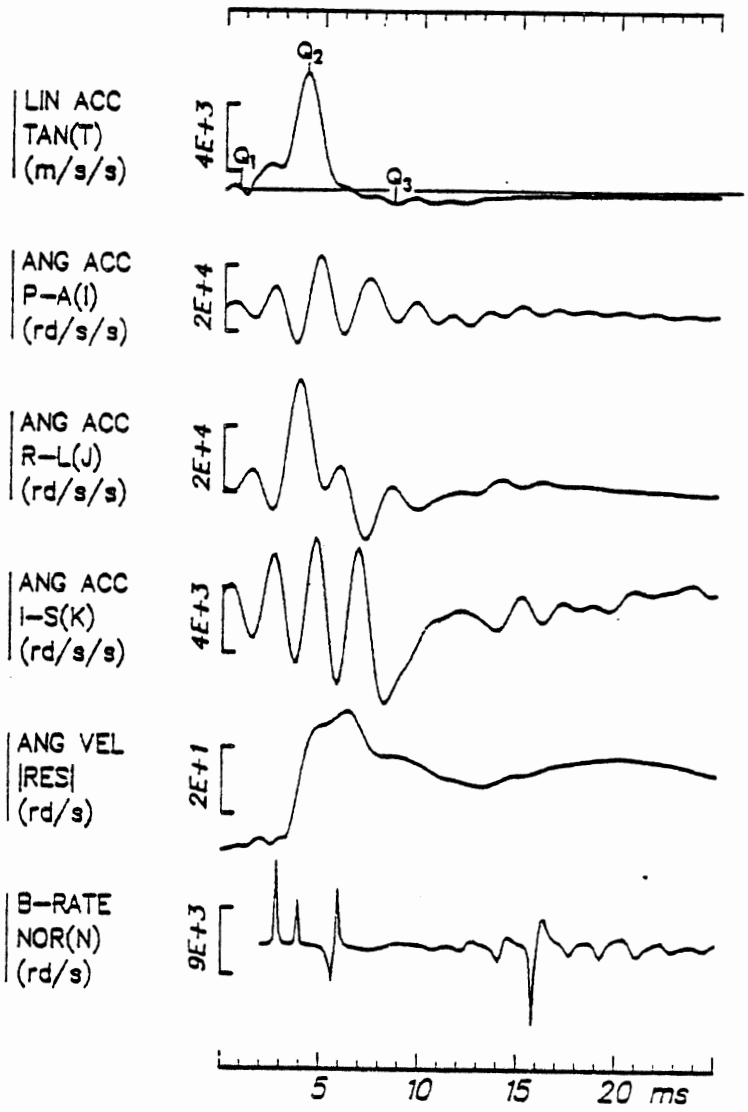
LIN ACC
TAN(T)
(m/s/s)
4E+3
Q1
Q2
Q3
ANG ACC
P–A(I)
(rd/s/s)
2E+4
ANG ACC
R–L(J)
(rd/s/s)
2E+4
ANG ACC
I–S(K)
(rd/s/s)
4E+3
ANG VEL
|RES|
(rd/s)
2E+1
B–RATE
NOR(N)
(rd/s)
9E+3
5
10
15
20 ms

Fig. A-5

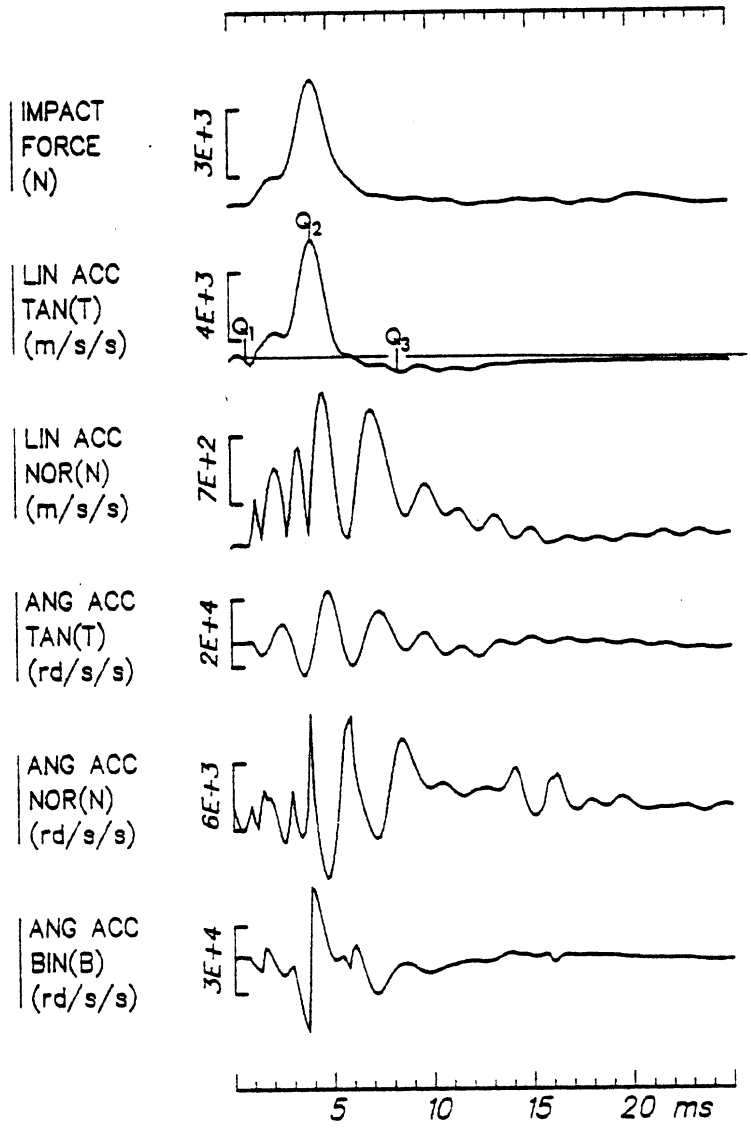
IMPACT
FORCE
(N)
3E+3
LIN ACC
TAN(T)
(m/s/s)
4E+3
Q1
Q2
Q3
LIN ACC
NOR(N)
(m/s/s)
7E+2
ANG ACC
TAN(T)
(rd/s/s)
2E+4
ANG ACC
NOR(N)
(rd/s/s)
6E+3
ANG ACC
BIN(B)
(rd/s/s)
3E+4
5
10
15
20 ms

Fig. A-6

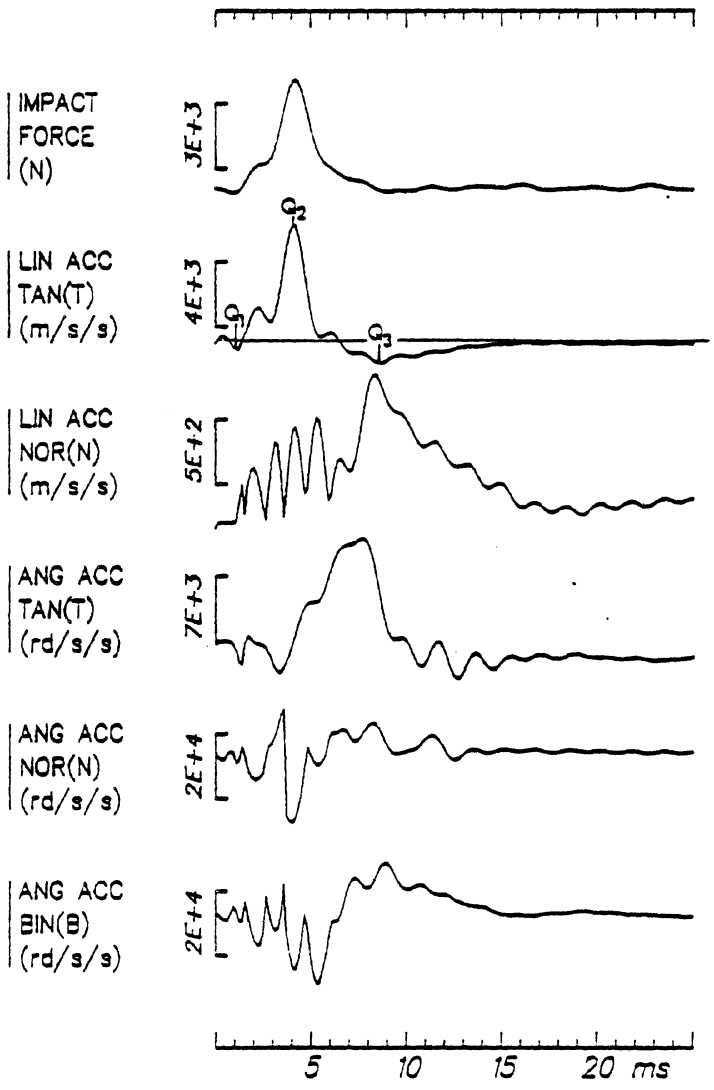
IMPACT
FORCE
(N)
3E+3
LIN ACC
TAN(T)
(m/s/s)
4E+3
C2
C1
C3
LIN ACC
NOR(N)
(m/s/s)
5E+2
ANG ACC
TAN(T)
(rd/s/s)
7E+3
ANG ACC
NOR(N)
(rd/s/s)
2E+4
ANG ACC
BIN(B)
(rd/s/s)
2E+4
5
10
15
20 ms

Fig. A-7

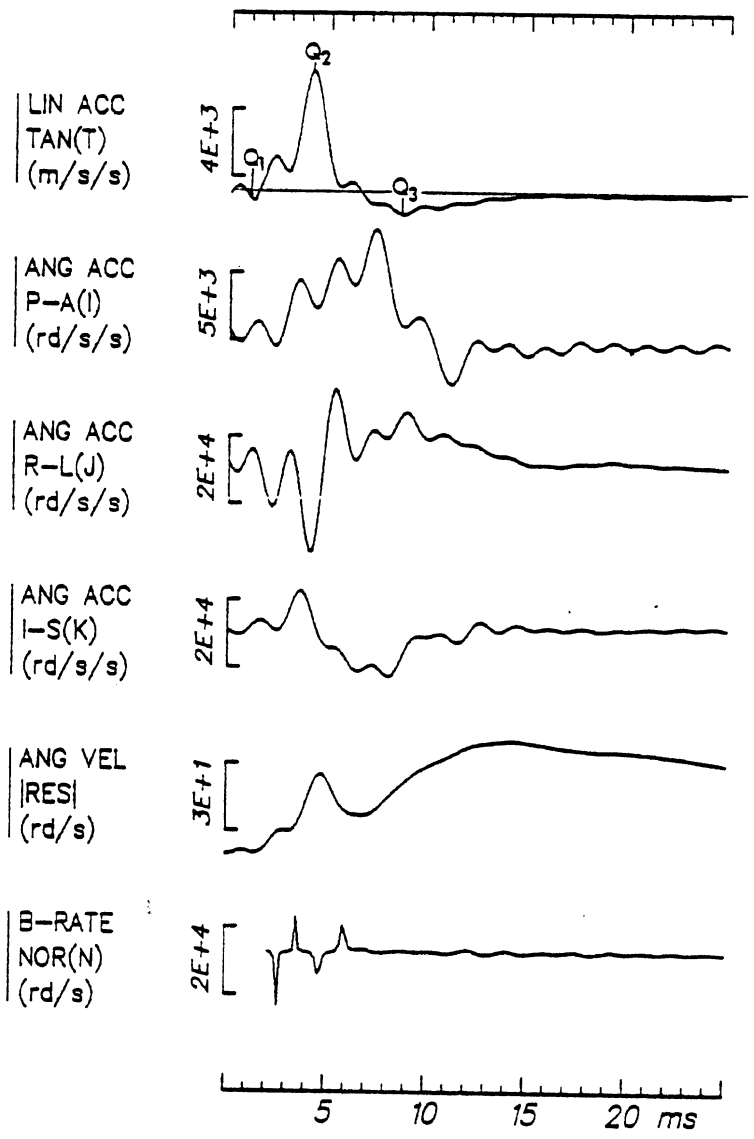
LIN ACC
TAN(T)
(m/s/s)
4E+3
Q1
Q2
Q3
ANG ACC
P–A(I)
(rd/s/s)
5E+3
ANG ACC
R–L(J)
(rd/s/s)
2E+4
ANG ACC
I–S(K)
(rd/s/s)
2E+4
ANG VEL
|RES|
(rd/s)
3E+1
B–RATE
NOR(N)
(rd/s)
2E+4
5
10
15
20 ms

Fig. A-8

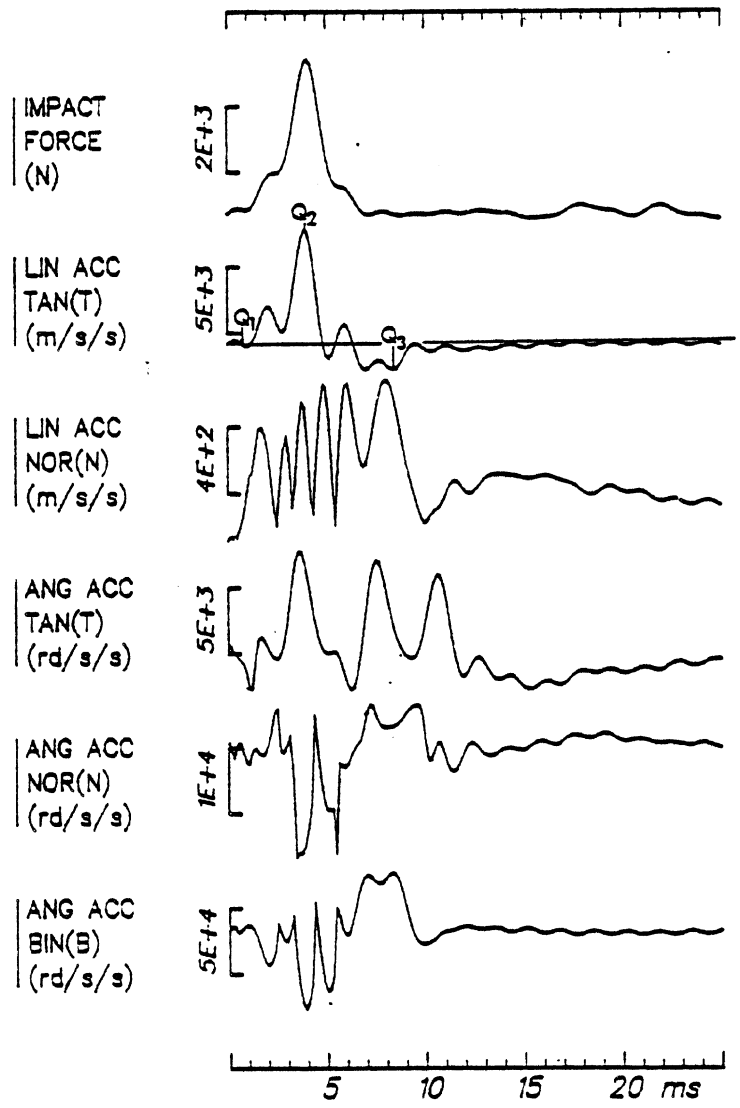
IMPACT
FORCE
(N)
2E+3
LIN ACC
TAN(T)
(m/s/s)
5E+3
O1
O2
O3
LIN ACC
NOR(N)
(m/s/s)
4E+2
ANG ACC
TAN(T)
(rd/s/s)
5E+3
ANG ACC
NOR(N)
(rd/s/s)
1E+4
ANG ACC
BIN(B)
(rd/s/s)
5E+4
5
10
15
20 ms

Fig. A-9

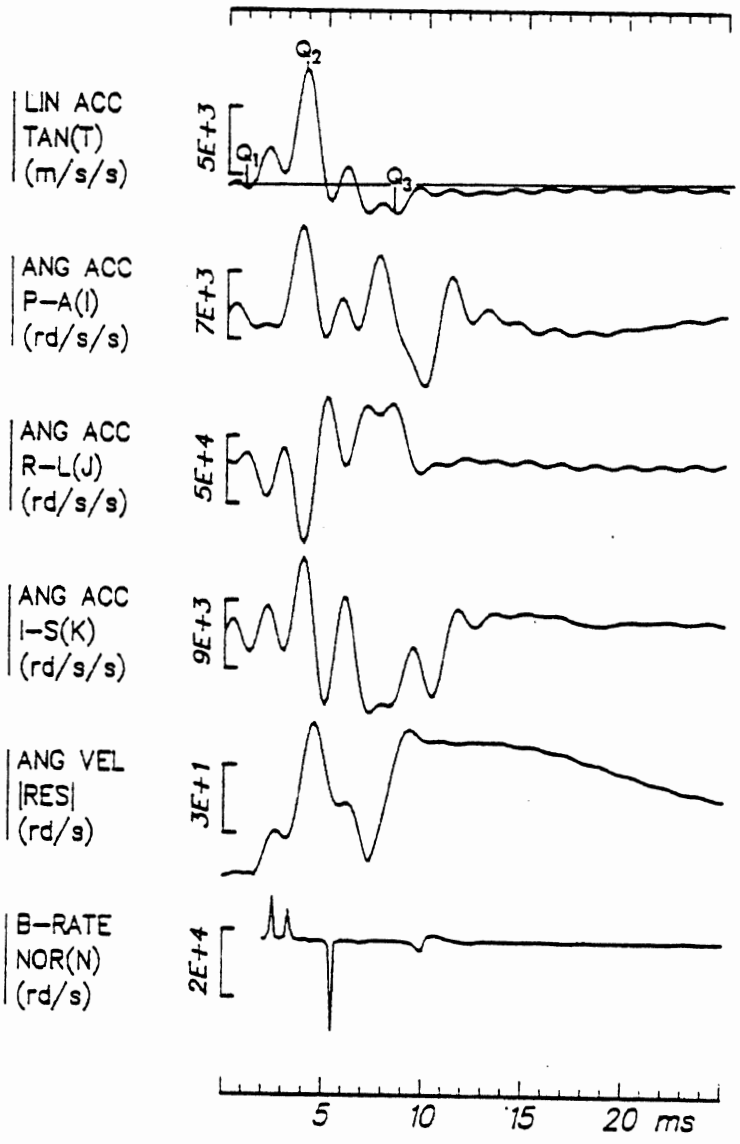
LIN ACC
TAN(T)
(m/s/s)
5E+3
Q1
Q2
Q3
ANG ACC
P–A(I)
(rd/s/s)
7E+3
ANG ACC
R–L(J)
(rd/s/s)
5E+4
ANG ACC
I–S(K)
(rd/s/s)
9E+3
ANG VEL
|RES|
(rd/s)
3E+1
B–RATE
NOR(N)
(rd/s)
2E+4
5
10
15
20 ms

Fig. A-10

APPENDIX E: "HEAD IMPACT RESPONSE--SKULL DEFORMATION AND ANGULAR ACCELERATIONS"

841657

Head Impact Response—Skull Deformation and Angular Accelerations

Guy S. Nusholtz, Paula Lux, Patricia Kaiker, and Miles A. Janicki
University of Michigan
Transportation Research Institute

SAE The Engineering Resource For Advancing Mobility

REPRINT

Reprinted from:
P-152-Twenty-Eighth Stapp Car Crash Conference Proceedings

SAE 400 Commonwealth Drive Warrendale, PA 15096

ISSN 0148-7191

Persons wishing to submit papers to be considered for presentation or publication through SAE should send the manuscript or a 300 word abstract of a proposed manuscript to: Secretary, Engineering Activity Board, SAE.

36 page booklet. Printed in U.S.A.

841657

Head Impact Response—Skull Deformation and Angular Accelerations

Guy S. Nusholtz, Paula Lux, Patricia Kaiker, and Miles A. Janicki
University of Michigan
Transportation Research Institute

ABSTRACT

The response of the head to impact was investigated using live anesthetized and post-mortem Rhesus monkeys and repressurized cadavers. The stationary test subject was struck by a guided moving impactor of 10 kg for monkeys; 25 or 65 kg for cadavers. The impactor striking surface was fitted with padding to vary the contact force-time characteristics. The experimental technique used a nine-accelerometer system rigidly mounted on the head to measure head motion, transducers placed at specific points below the skull to record epidural pressure, repressurization of both the vascular and cerebral spinal systems of the cadaver model, and high-speed cineradiography (at 400 or 1000 frames per second) of selected test subjects. The results of the tests demonstrate the potential importance of skull deformation and angular acceleration on the injury produced in the live Rhesus and the damage produced in both the post-mortem Rhesus and the cadaver as a result of impact.

IN THE UNITED STATES roughly 49 percent of head injuries can be attributed to motor vehicle accidents(1-3)*. Investigation of trauma to the head and of mechanisms of injury becomes invaluable for allocating resources and for formulating policy to reduce its incidence, morbidity, and mortality.

Because motor vehicle field accident data do not provide the level of detail necessary to ascertain mechanisms of injury resulting from the interactions of the passenger with the vehicle interior during an accident, bioengineers use trauma experiments with human surrogates (cadavers or animals) to document kinematic parameters so that mechanisms of injury can be better simulated, modeled and verified.

*Numbers in parenthesis designate references at end of paper.

The repressurized cadaver is often chosen as an experimental model because its geometry and soft tissue distribution is similar to that of a live human. Damages to repressurized cadavers which correlate well with clinically observed injuries are those that can be documented by gross autopsy. They include scalp lacerations (linear, flap, stellate), fractures of the cranial vault or base (linear, depressed, comminuted), lesions which are visible to the naked eye and hemorrhage (petechia; contusion; epidural, subdural, subarachnoid and intracerebral hematomas). Mild concussion, cerebral concussion and diffuse brain injury disrupt the functioning of the brain without gross overt structural evidence. Because diagnosis of concussion requires the observation of behavioral responses, animal subjects are necessary in experimental contexts. As a result, subtle distinctions are lost, making scaling of the results to the human level approximate (4).

The bioengineering literature on mechanisms of injury is a rich one (5-43). However, despite conscientious speculation as to the mechanics which produce head trauma and theoretical and experimental scrutiny of various hypotheses about it, considerable controversy still exists. The hypotheses usually cannot wholly fit clinical or pathological observations, assessment of biomaterial properties, or may not agree with predictions of mathematical models.

Several such controversies involve angular and linear acceleration and skull deformation (5-8,12,16-17,21-22,34,38,40). These debates are complicated by the complex mechanical structure of the head and brain. A number of biomechanical analyses (finite element analyses, in particular) have attempted to model the brain with reasonable geometric precision. However, these calculations involve over-simplified modeling of materials and behavior, assuming simple elasticity or homogeneous materials (12-13,23-24,38,41-44). A number of other investigators have attempted to define the

pressure-volume relationship of the skull to impact (19,25-26,28-30,32,36,43-44). However, the skull-brain interface as well as the effects of skull deformation on the impact response of the brain is not well understood.

A major difficulty in the investigation of head trauma is designing kinematic experiments which interfere minimally with the biological and and physical systems being observed, yet produce results that correspond well with clinically observed trauma. Some understanding of head injury mechanisms as a result of blunt impact has resulted from relating kinematic parameters to injury modes. However, with the possibility of several injury mechanisms correlations of this type do not always imply causation. The parameters commonly used for describing head mechanical response during direct impact have been angular and translational accelerations, velocities, displacements of the head as a rigid body, skull bone deformations, and internal pressures in the brain. Many investigators have chosen to investigate a single parameter, such as resultant head acceleration for Head Injury Criterion (HIC) calculation, and later use it as an index of severity or tolerance threshold.

This paper discusses techniques developed and used by the Biomechanics Group at the University of Michigan Transportation Research Institute (UMTRI) for measuring three-dimensional head motion, epidural pressure, and internal brain motion of repressurized cadavers and Rhesus monkeys during head impact. The results will be compared to those previously presented (30,40) and a possible injury mechanism will be suggested.

METHODOLOGY

Three live anesthetized and three post-mortem Rhesus monkeys* and nine repressurized cadavers** were tested. Five cadavers were each subjected to a series of up to three head impacts using the UMTRI pneumatic impacting device with a 25 or 65 kg impactor. The remaining four cadavers were subjected to two head impacts each with the UMTRI pendulum impacting device with a 25 kg impactor. The cadavers were instrumented with a nine-accelerometer array located on the head to measure three-dimensional motion. Epidural pressure transducers were used to monitor pressure changes during impact of the brain-skull interface. Both cerebrospinal and vascular systems of the cadaver head-brain complex were repressurized. In addition, high-speed photokinemetrics were obtained using normal photographic or cineradiographic techniques.

Using the pneumatic impacting device with a 10 kg impactor, three live and three post-mortem non-human primates (Macaca mulatta) were each subjected to a single head impact to the occipital region. The six Rhesus subjects used in these experiments were obtained by UMTRI from the University of Michigan Unit for Laboratory Animal Medicine (ULAM). The six Rhesus subjects were instrumented similarly to the cadavers with nine-accelerometer arrays on the head and with epidural pressure transducers to document transient pressures. For post-mortem Rhesus subjects, neither cerebrospinal nor vascular systems of the head-brain complex were repressurized.

IMPACT TESTING - The methods and procedures used in this research are outlined below. Additional information can be found in (30-32,45-46).

Linear Pendulum Impact Device - The UMTRI linear pendulum impact device, using a free-falling pendulum as an energy source, strikes either a 25 kg or 56 kg impact piston. The piston is guided by a set of Thomson linear ball bushings. Axial loads were calculated from data recorded using a Setra Model 111 accelerometer.

Impact conditions between tests were controlled by varying impact velocity and the type and depth of padding on the impactor surface. Piston velocity was measured by timing the pulses from a magnetic probe which senses the motion of the targets in the piston.

A specially designed timer box was used to control and synchronize the impact events during a particular test, such as the release of the pendulum and activation and deactivation of the lights and high-speed cameras.

Ballistic Impact Device - The UMTRI ballistic impact device (Figure 1), consists of an air reservoir, a ground and honed cylinder, and a carefully fitted piston mechanically coupled to a ballistic pendulum. The piston, propelled by compressed air through the cylinder from the air reservoir chamber, accelerates the ballistic pendulum. The mass of the ballistic pendulum can be varied from 10 to 150 kg. The piston is arrested at the end of its travel allowing the ballistic pendulum to become a free-traveling impactor. The ballistic pendulum is fitted with an inertia-compensated load cell.

Nine-Accelerometer Head Plate - For Rhesus subjects, the installation of the nine-accelerometer plate is accomplished as follows.

---

*Animals were handled according to the American Association for Accreditation of Laboratory Animal Care and National Institutes of Health guidelines.

**The protocol for the use of cadavers in this study was approved by the Committee to Review Grants for Clinical Research of the University of Michigan Medical Center and follows guidelines established by the U.S. Public Health Service and recommended by the National Academy of Sciences/National Research Council.

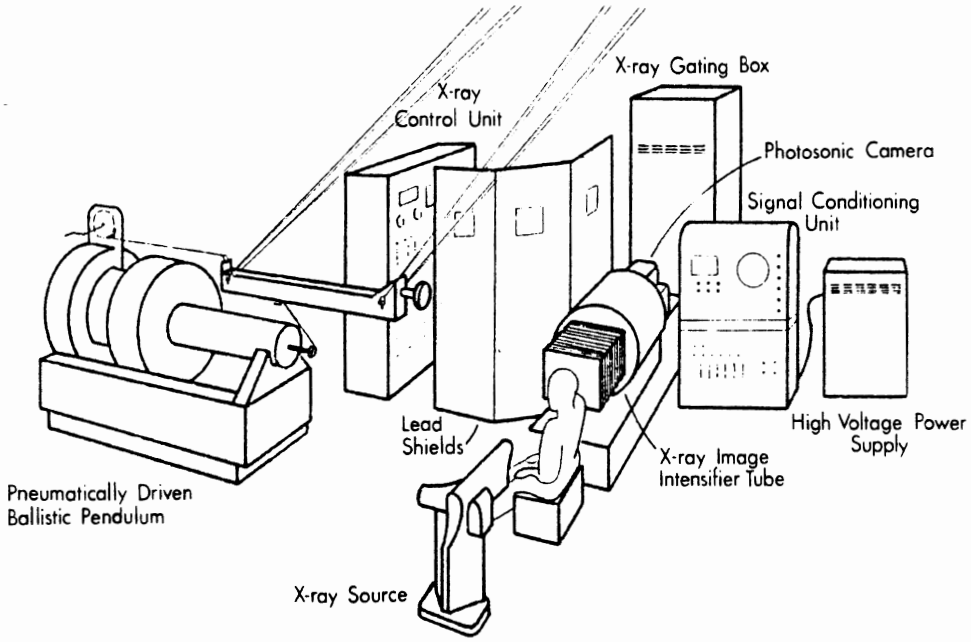

Fig. 1. Pneumatic Ballistic Pendulum and Test Setup for Cadaver Impacts.

The scalp is removed from the frontal bone over the orbital ridges. Several metal self-tapping screws are attached firmly to the skull through small pilot holes drilled into the orbital ridges and into the dental plate above the canine teeth. Quick-setting acrylic plastic is molded around each of the screws and the base of the plate mount embedding it in the plastic. The orientation of the plate in this position is shown in Figure 2.

For cadavers, the nine-accelerometer plate is installed in the following manner. A two-by-two inch patch of scalp is removed from the right occipital-parietal area. Four small screws are then placed in a trapezoidal pattern in the skull within the dimensions of the accelerometer plate mount. Quick setting acrylic plastic is molded around the screws forming a base. The plate mount is then placed in the acrylic base. See Figure 3A for the location of the plate mount.

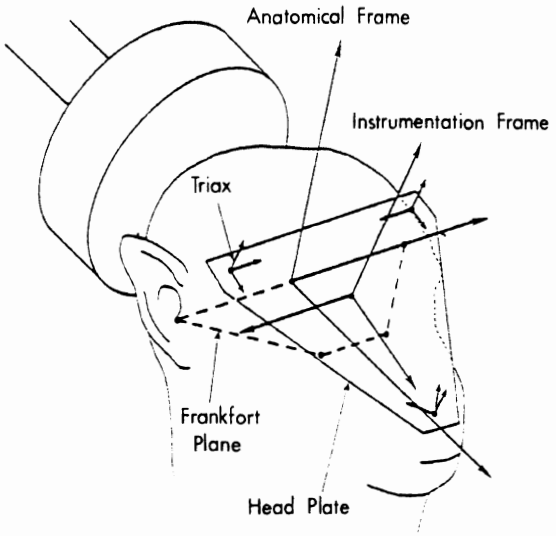

Fig. 2. Nine-Accelerometer Plate Position for Rhesus Monkey Impacts.

It is necessary to determine the instrumentation frame's exact location and orientation in relation to the anatomical frame. A three-dimensional x-ray technique was developed which requires taking two orthogonal radiographs of the instrumented head. The procedure requires the identification of four anatomical landmarks (two superior edges of the auditory meati and two infraorbital notches) with four distinguishable lead pellets, plus the identification of four lead pellets inlaid in the plate to define the instrumentation frame. A similar radiographic technique was used with Rhesus monkeys to determine the orientation and location of the instrumentation frame with respect to the anatomical frame.

Epidural Pressure Measurements - Epidural pressures of Rhesus subjects are obtained with a Kulite model MCP-55-5F catheter tip pressure transducer. For cadavers, Endevco series 8510 piezoresistive pressure transducers are used.

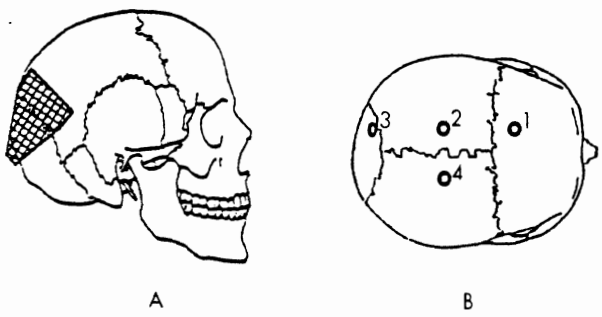

Fig. 3A. Nine-Accelerometer Plate Position for Cadaver Impacts.

3B. Location of Transducers for Epidural Pressures 1, 2, 3, and 4.

For Rhesus subjects a small circle of scalp is removed and a Stryker bone coring tool is used to make a hole in the skull with a circular bit. An adjustable set-screwed collet is used to core into the skull in small increments, preventing damage to the dura mater. The increment of bone is then removed using a dental scoop, and the hole is tapped for a coarse thread. A tabular magnesium coupling device is screwed into the tapped hole in the skull (Figure 4A). It is anchored into place using quick-setting acrylic plastic molded around the base. Dow Corning dielectric gel (silicon fluid) is injected into the tubing to act as a coupling medium. The Kulite pressure transducer is then inserted and secured at proper depth.

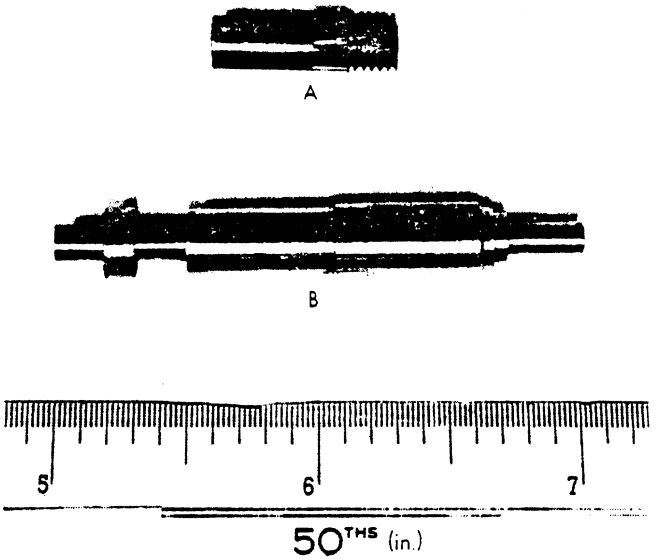

Fig. 4A. Magnesium Coupling Device.
4B. Skull Bone Coring Device.

For cadaver subjects four 1 cm diameter circles of scalp are removed over the frontal, parietal and occipital bones and a Stryker bone coring tool is used to make four holes in the skull with a circular bit (Figure 4B). Holes are placed out of the contact area of the impacting surface and are not drilled into sutures (Figure 3B). The dura mater under these holes is perforated without cutting the brain. The holes are tapped. The brass transducer couplings are inserted into the tapped holes. Two pinhead screws are attached 2 cm from each transducer. Quick-setting acrylic plastic is molded around the pinhead screws and the mouth of each transducer coupling as a mooring device. After checking fluid flow, the Endevco series 8510 piezoresistive pressure transducers are attached to the fittings.

Radiopaque Target Gel - A neutral density radiopaque gel is used to determine motion of the brain during impact. The gel is injected into the brain through the holes used for insertion of the pressure transducers. The injection technique produces lines of radio-contrast in the brain that show up in high-speed cineradiographic movies. See Figure 5.

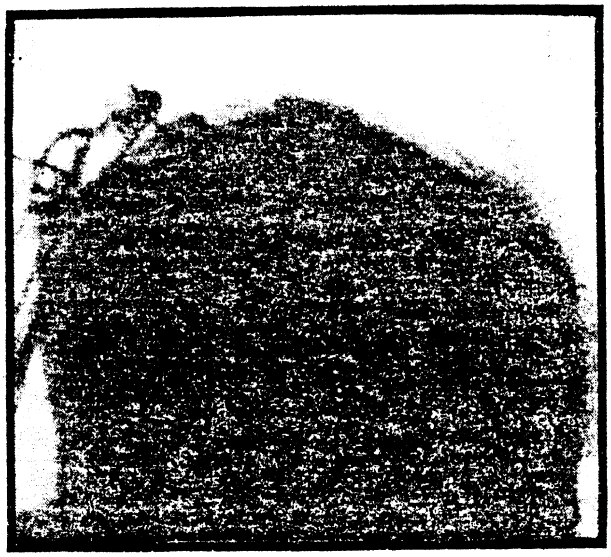

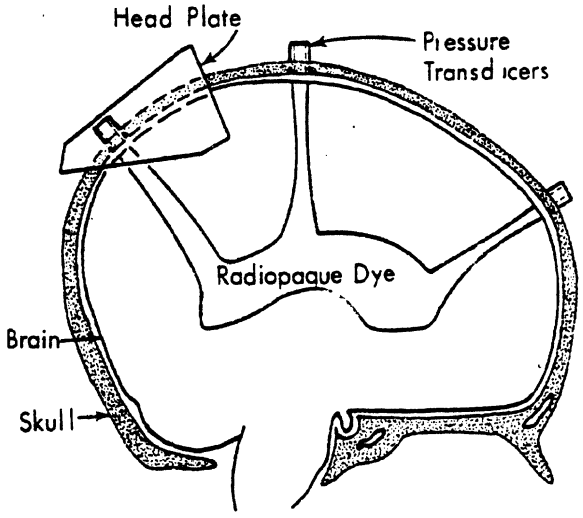

Fig. 5. Radiograph and Reconstruction of Radiograph With Radio-contrast Dye in situ.

X-Ray Motion Descriptors - The procedures used for defining x-ray motion descriptors are explained in (45) and briefly outlined below. The cineradiograph system allows non-invasive viewing of internal anatomical structure in vivo. In the case of a rigid structure such as bone, the radiopaque targets can be placed on or near anatomical landmarks and motion can be described similarly to that of standard photometric techniques. Problems arise when soft tissue is to be analyzed and rigid body dynamics no longer offer a good approximation.

Several methods could be suggested to produce analytical information describing the soft tissue of the brain. In this paper the motion discriptors chosen are based upon the shadows of objects in a two-dimensional image space produced by a point source of x-rays which are associated with the anatomical structures or the radiopaque dye injected into the brain. The descriptors are at most two-dimensional and do not take into account rotations and translations which move objects in and out of the plane of gross whole body motion. In addition, changes in the x-ray cross-section of objects can lead to changes in the descriptors which do not have a direct relation to rigid body motion. In the impact tests presented in this paper radiopaque gel was injected into the head producing four curved lines in the brain and outlining the ventricles in some tests. Differential motion between the brain and the skull was obtained by comparing the motion of points on the curve closest to the center of the epidural pressure transducer. General characteristics of the motion of the brain were obtained through the changes in shape of the curved lines and ventricles.

Cadaver Vascular Repressurization - To pressurize the cadaver vascular system of the head, the common carotid artery is located at a point in the neck and an incision is made. (See Figure 6.) A balloon catheter is inserted and positioned such that the balloon is in the internal carotid artery just above the point where the external carotid artery branches. A narrow polyethylene tube is inserted at the same point and runs into the internal carotid artery just past the balloon. A Kulite pressure transducer is then fed through this tube so that vascular pressure may be monitored. Finally, the vertebral arteries are tied off above the clavicle such that fluid pressure in the head may be maintained. Just prior to testing, a solution of India ink and saline is released from a tank into the vascular system of the head. A pressure transducer monitors the flow so that the system is brought to normal physiological pressure just prior to impact.

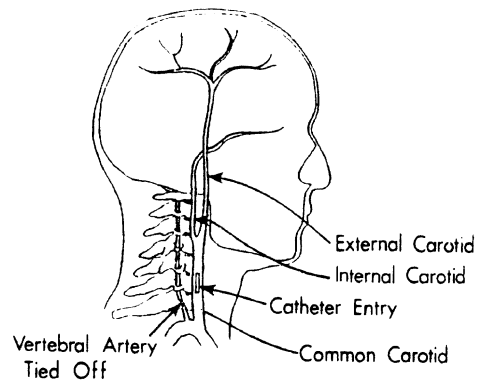

Fig. 6. Vascular Pressurization Procedure and Placement.

Cadaver Cerebrospinal Repressurization - For the cadaver head impacts, the subdural region surrounding the brain and spinal cord is repressurized by coring a small hole into the second lumbar vertebra and inserting a Foley catheter under the dura of the spinal cord such that the balloon of the catheter reaches mid-thorax level. To check fluid flow through the ventricles, saline is injected through the Foley catheter until fluid rises to the top of the piezoresistive pressure transducer couplings. The couplings are capped until the radiopaque sodium iodide gel target has been slowly injected through the couplings into the brain cortex and a setup radiograph has been made of the head. The point at which the catheter passes through the lamina of the second lumbar vertebra is sealed with plastic acrylic. (Figure 7)

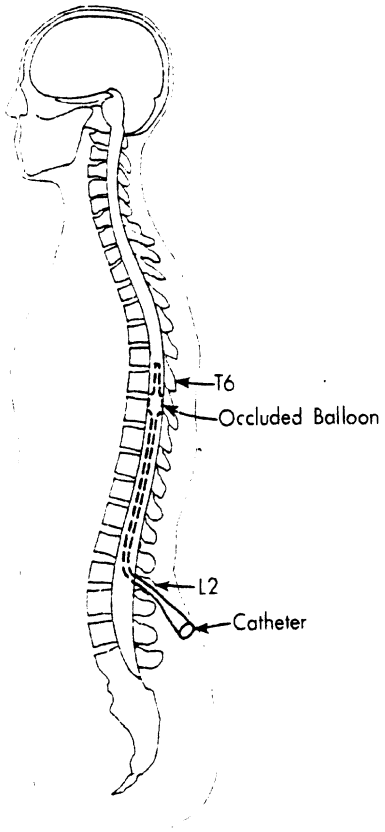

Fig. 7. Cerebrospinal Pressurization Procedure and Placement.

Test Subject Preparation - The unembalmed cadavers were stored at 4 degrees centigrade prior to testing. The cadaver is x-rayed as part of the structural damage evaluation and anthropomorphic measurements are recorded. Next, the cadaver is instrumented, sanitarily, dressed and transported to the testing room where the accelerometers and pressure transducers are attached. The subject is positioned. Next, the radiopaque gel target is inserted, and pretest x-rays and photographs are taken. Pressurization is checked. Then the subject is impacted. Each cadaver received either two duplicate head impacts or one low-

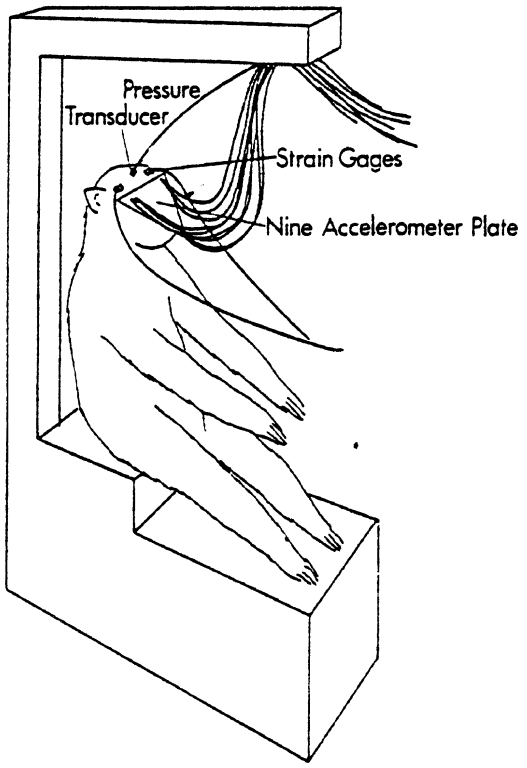

Fig. 8. Test Setup for Posterior-Anterior Rhesus Head Impact.

energy heavy-padded frontal impact and one medium energy slightly-padded frontal impact.

Three Rhesus impacts were conducted on post-mortem subjects. Upon termination, they were stored in a cooler at 4 degrees centigrade for 48 hours before testing. Living Macacas were used in the other three experiments. The protocol for post-mortem animals was less complex than that for the live animals, which was presented earlier (32), outlined below.

The subject is first anesthetized with ketamine and then maintained with ketamine and sodium pentobarbital. An airway is established. The upper body is prepared and the weight and biometric measurements are taken. Using a cauterizing scalpel, the scalp and muscle mass are removed from the frontal bone and the screws used to affix the nine-accelerometer plate and the epidural pressure transducer skull fitting are screwed into place. Figure 8 shows the positioning of the instrumentation on the Rhesus skull.

The Rhesus is placed in an erect sitting position with its posterior side towards the impactor, so that the line of impact is in the mid-sagittal plane in the posterior-anterior direction. The Rhesus is stabilized with paper tape. A polaroid photograph is then taken through the cineradiograph to check the position of the animal and the x-ray settings. Figure 8 also shows the basic test setup. Eight hours after impact, a 5 ml dose of Uthol (concentrated, unpure sodium pentobarbital) is injected via the hind leg I.V. catheter to euthanize the animal.

Rhesus Initial Test Conditions - The tests being reported here are a continuation of Rhesus tests reported earlier (30). Conditions for this set of tests were similar except higher impact energy levels were used and the subjects were positioned so that impact occurred through the estimated center of mass. The impactor was the UMTRI 10 kg pneumatic impacting device and the impacting surface was 10 cm in diameter and padded with 2.5 cm Ensolite.

Cadaver Initial Test Conditions - Tests 82E001 thru 82E062 used the UMTRI 25 kg linear pendulum impacting device with a 15 cm diameter impacting surface padded with 2.5 cm Ensolite. Tests 82E081 thru 84E141D used the UMTRI 25 kg ballistic impacting device fitted with a 15 cm diameter impacting surface padded with 2.5 cm Ensolite, or a sandwich of 2.5 cm styrofoam, 5 cm Dow Ethafoam plus 2.5 cm Ensolite, or one of 0.5 cm Ensolite, 5 cm seating foam plus 0.5 cm Ensolite. Tests 84E151A through 84E161C used the UMTRI 65 kg ballistic impacting device fitted with a 15 cm diameter impacting surface padded with either 0.5 cm Ensolite or a sandwich of 0.5 Ensolite, 5 cm seating foam, and 0.5 cm Ensolite. The target area for all of these impacts was the center of the forehead above the orbits (frontal). Impact occurred in the anterior to posterior direction. All cadavers were seated and positioned with paper tape so that the subject and the impact target were stable (Figure 9).

Cineradiographs - In selected subjects high-speed cineradiographs were taken (some cadavers and all Rhesus). The cineradiographs were taken of the impact events at 1000 or 400 frames per second. The UMTRI high-speed cineradiographic system (47-48) consists of either a Photosonics 1B or Miliken high-speed 16 mm motion-picture camera which views a 5 cm diameter output phosphor of a high-gain, four-stage, magnetically focused image intensifier tube, gated on and off synchronously with shutter pulses from the motion-picture camera. A lens optically couples the input photocathode of the image intensifier tube to x-ray images produced on a fluorescent screen by a smoothed direct-current x-ray generator. Smoothing of the full-wave rectified x-ray output is accomplished by placing a pair of high-voltage capacitors in parallel with the x-ray tube. The viewing field for these experiments was between 20 and 40 cm.

Photokinemetrics - The motion of the subject was determined from the high-speed (1000 frames per second) film by following the motion of single-point phototargets on the head and on the impactor piston. For selected cadaver frontal impacts, a Hycam camera operating at 3000 frames per second provided a close-up

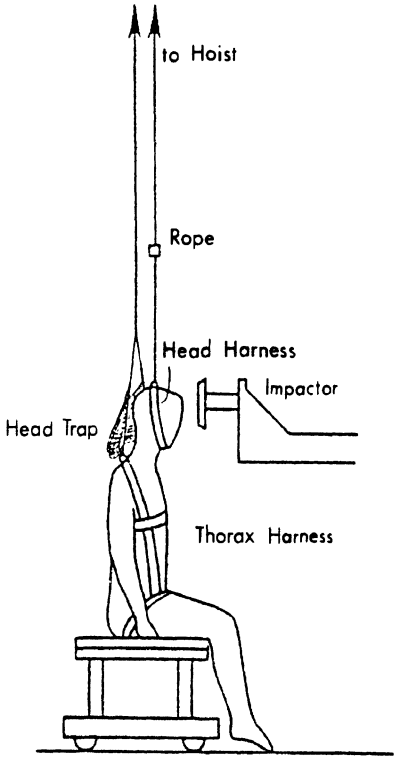

Fig. 9. Initial Conditions for Cadaver Frontal Head Impact.

lateral view of the impact. For selected cadaver frontal impacts the Photosonics provided a lateral 1000 frames per second overall view.

Data Handling - All transducer time histories (impact force, impact acceleration, epidural pressures, nine head-accelerations) were recorded unfiltered on either a Honeywell 7600 FM Tape Recorder or a Bell and Howell CEC 3300/CEC 3400 FM Tape Recorder. A synchronizing gate was recorded on all tapes. All data was recorded at 30 ips. The analog data on the FM tapes was played back for digitizing through proper anti-aliasing analog filters. The analog-to-digital process for all data, results in a digitial signal sampled at 6400 Hz equivalent sampling rate. It has been reported that skull vibrations above 1300 Hz could cause very local motion in the accelerometer mountings (40). To reduce this effect, the raw transducer time histories were filtered, digitally, with a Butterworth filter at 1000 Hz, 6th order.

METHOD OF ANALYSIS - The techniques used to analyze the results are outlined below. Additional information can be found in (30-32,41-42).

Frame Fields - As the head moves through space, any point on the head generates a path in space. In head injury research we are interested in the description of the path of the anatomical center and in events which occur as it moves. A very effective tool for analyzing the motion of such a point (the anatomical center), as it moves along a curved path in space, is the concept of a moving frame (49-52). The path generated as the point travels through space is a function of time and velocity. A vector field is a function which assigns a uniquely defined vector to each point along a path. Thus, any collection of three mutually orthogonal unit vectors defined on a path is a frame field. Therefore, any vector defined on the path (for example, acceleration) may be resolved into three orthogonal components of any well-defined frame field, such as the laboratory or anatomical reference frames. Changes in a frame field with time (for example, angular acceleration of the frame field) are interpreted as vectors defined on the curve and are also resolved into three components.

In biomechanics research, frame fields are defined based on anatomical reference frames. Other frame fields such as the Frenet-Serret frame or the Principal Direction Triad (32,46), which contain information about the motion embedded in the frame field, have also been used to describe motion resulting from impact.

The Frenet-Serret frame (51-52) consists of three mutually orthogonal vectors T, N, B. At any point in time a unit vector can be constructed that is co-directional with the velocity vector. This normalized velocity vector defines the tangent direction T. A second unit vector N is constructed by forming a unit vector co-directional with the time derivative of the tangent vector T (the derivative of a unit vector is normal to the vector). To complete the orthogonal frame, a third unit vector B (the unit binormal) can be defined as the cross product T x N. This procedure defines a frame at each point along the path of the anatomical center. Within the frame field, the linear acceleration is resolved into two distinct types. The tangent acceleration [Tan(T)] is always the rate of change of speed (absolute velocity) and the normal acceleration [Nor(N)] gives information about the change in direction of the velocity vector. The binormal direction contains no acceleration information.

Transfer Function Analysis - With blunt impacts, the relationship between a transducer time history at a given point and the transducer time history of another given point of a system can be expressed in the frequency domain through the use of a transfer function. A Fast Fourier Transformation of simultaneously monitored transducer time histories can be used to obtain the frequency response functions of impact force and accelerations of remote points. Once obtained, a transfer function of the form:

$$(Z)(iw) = (w) \quad F[F(t)]/\ F[A(t)]$$

can be calculated from the transformed quantities where w is the given frequency, and F[F(t)] and F[A(t)] are the Fourier transforms of the impact forces and acceleration of the

point of interest, at the given frequency. This particular transfer function is closely related to a mechanical transfer impedance (53) which is defined as the ratio between simple harmonic driving force and corresponding velocity of the point of interest. Mechanical transfer impedance is a complex valued function which for the purpose of presentation will be described by its magnitude and its phase angle. In addition to a transfer function relating force to velocity, a transfer function can be generated which relates the response of one point in the system to another point in the system, the response being expressed in the frequency domain. Analogous to mechanical impedance, a Fast Fourier Transformation of simultaneously monitored transducer time histories from any two points in the system can be used to obtain the frequency response functions relating those two points. In the case of a force and a pressure, such as impact force and epidural pressure, a transformation of the form:

$$(X)(iw) = F[F(t)]/\ F[p(t)]$$

can be calculated from the transformed quantities, where w is the given frequency, $F[F(t)]$ and $F[p(t)]$ are the Fourier transforms of the impact force time history and the pressure time history.

Correlation Functions - To describe some of the fundamental properties of a time history, such as acceleration or force, two types of statistical measures may be used:

1. Auto-correlation Function. This measure is the correlation between two points on a time history and is a measure of the dependence of the amplitude at time t_1 on the amplitude at t_2.

2. Cross-correlation Function. This is a measure of how predictable, on the average, a signal (transducer time history) at any particular moment in time is from a second signal at any other particular moment in time.

The auto-correlation function is formally defined as the average over the ensemble of the product of two amplitudes:

$$R_x(t_1,T_2) = \int_{-\infty}^{+\infty}\int_{-\infty}^{+\infty} X_1,X_2,P(x_1,x_2,T_1,T_2)dx_1,dx_2$$

where x_1, x_2 are the amplitudes of the time history and $p(x_1,x_2,t_1,t_2)$ is the joint probability density. Normally the above definition cannot be used to generate an auto-correlation function directly. However, it can be shown that for a discrete time history of a finite duration, a close approximation of the auto-correlation function can be obtained through the use of a Fourier transform. (53)

In addition to auto-correlation, cross-correlation can be used to obtain useful information about the relationship between two different time histories. For example, the cross-correlation between acceleration measurements at two different points of a material body may be determined for the purpose of studying the propagation of differential motion through the material body. Cross-correlation functions are not restricted to correlation of parameters with the same physical units; for example, one might determine the cross-correlation between the applied force and the acceleration response to that force. Similar to the auto-correlation function, the calculation of the cross-correlation of two signals begins by taking the Fourier transform of both time histories (Y_1,Y_2). The cross-spectral density is the complex-valued function $(Y_1 \cdot Y_2^*)$. The cross correlation is then the Fourier transform of the cross-spectral density. (53)

Pressure Time Duration Determination - Two different types of pressure-time histories were observed, unimodal and bimodal. The unimodal waveform was characterized by one maximum and the bimodal waveform by two local maxima. In order to define the pressure duration, a standard procedure was adopted which determined the beginning and end of a pulse. This procedure began by determining the peak, or the first peak in the case of a bimodal waveform. Next, the left half of the pulse, defined from the point where the pulse starts to rise to the time of peak, was least-squares fitted with a straight line. This rise line intersected the time axis at a point which was taken as the formal beginning of the pulse. A similar procedure was followed for the right half of this pulse, i.e., a least-squares straight line was fitted to the fall section of the pulse, which was defined from the peak to the point where the pulse minimum occurred. The point where this line intersected the time axis was the formal end of the pulse in the unimodal case, and the formal end of the first peak in the bimodal case. The pressure duration for a unimodal waveform was defined by these points. For a bimodal waveform, these two points were used to determine the first pressure duration. Another least-squares straight line was fitted to the fall section of the second pulse. The point at which this line intersected the time axis was the formal end of the waveform, and the total pressure duration was then defined from this point and the beginning point.

Force Time History Determination - In general the force-time histories were unimodal with a single maximum, smoothly rising, peaking and then falling. Paddings on the striker

surface effected different force-time history durations. Force duration was determined using the same techniques for determining pressure duration, that is the same boundary defining and least-squares straight-line fitting techniques were used.

RESULTS

Table 1 lists the initial test conditions for the Rhesus subjects while Table 2 lists those for cadaver subjects. Table 3 summarizes the Rhesus impacts and Table 4 summarizes the cadaver impacts. Table 5 characterizes impact pressures for cadavers. Table 6 reports the injuries/damages for the Rhesus subjects for which kinematic response was reported earlier (30) and Table 7 reports on injuries/damages for Rhesus subjects for which the kinematic response is being reported here. Table 8 reports the damage observed in cadaver subjects. A gross inspection was carried out for each test subject. In addition, representative microscopic sections were examined histologically for each Rhesus brain and included samples from the following areas: frontal cortex, anterior commisure level, mammilary body level, hoppocampus at lateral geniculate level, occipital cortex, cerebellum, midbrain, pons, medulla, and spinal cord. Selected time histories in the appendix are examples of important kinematic factors associated with the research performed in this project. The variables these examples illustrate are tangential and normal acceleration, resultant acceleration, rate of change of the tangential vector (T-rate) and rate of change of the binormal vector (B-rate). In addition, impact force, resultant angular acceleration and velocity, linear velocity, and pressures for both live Rhesus and repressurized cadavers are shown.

Table 1. Rhesus Head Impact
Initial Test Conditions

Test No.	Subject Condition	Subject Positioning Center of Gravity With Respect to Occipital Impact	Impact Surface Padding Thickness+	Pressure Transducer Location Relative to Bregma (cm)		Velocity (m/s)
				X	Y	
78A232	post-mortem	below	2.5 cm Ensolite++	3.2	-1.1	11.5
78A234	post-mortem	below	2.5 cm Ensolite++	2.8	-0.8	13.5
78A236	post-mortem	at	2.5 cm Ensolite++	3.0	0.6	12.5
78A238	post-mortem	above	2.5 cm Ensolite++	2.9	-0.8	12.5
78A239	live	at	2.5 cm Ensolite++	3.6	0.8	12.5
78A241	live	above	2.5 cm Ensolite++	1.4	0.3	12.5
79A249	live	at	2.5 cm Ensolite++	0.0	-2.0	15.4
79A251	live	at	2.5 cm Ensolite++	-2.5	-2.0	13.0
79A253	live	at	2.5 cm Ensolite++	-2.0	2.0	14.8
79A256	post-mortem	at	2.5 cm Ensolite++	-1.0	-2.0	15.4
79A258	post-mortem	at	2.5 cm Ensolite++	-1.5	.5	14.5
79A260	post-mortem	at	2.5 cm Ensolite++	-2.5	2.5	16.0

+10 cm diameter

++10kg striker

Table 2. Cadaver Initial Test Conditions

Test No.	Subject Condition	Impact Surface Padding Thickness+	Velocity m/s
82E001++	repressurized	2.5 cm Ensolite	5
82E021++ 82E022++	repressurized repressurized	2.5 cm Ensolite 2.5 cm Ensolite	5.2 5.7
82E041++ 82E042++	repressurized repressurized	2.5 cm Ensolite 2.5 cm Ensolite	5.5 5.5
82E061++ 82E062++	repressurized repressurized	2.5 cm Ensolite 2.5 cm Ensolite	5.5 5.5
82E081+++ 82E082+++	repressurized repressurized	2.5 cm Ensolite 2.5 cm Ensolite	3.8 3.8
83E102+++	repressurized	2.5 cm styrofoam 5.0 cm Dow Ethafoam 2.5 cm Ensolite	4.5
84E141A+++	repressurized	0.5 cm Ensolite 5.0 cm seating foam 0.5 cm Ensolite	4.5
84E141B+++	repressurized	0.5 cm Ensolite 5.0 cm seating foam 0.5 cm Ensolite	4.5
84E141C+++	repressurized	0.5 cm Ensolite	4.5
84E141D+++	repressurized	0.5 cm Ensolite	3.8
84E151A++++	repressurized	0.5 cm Ensolite 5.0 cm seating foam 0.5 cm Ensolite	3.6
84E151B++++	repressurized	0.5 cm Ensolite	3.8
84E161A++++	repressurized	0.5 cm Ensolite 5.0 cm seating foam 0.5 cm Ensolite	3.8
84E161B++++	repressurized	0.5 cm Ensolite	5.0

+15 cm diameter
++25 kg pendulum
+++25 kg cannon
++++65 kg cannon

Table 3. Rhesus Impact Test Summary

Test No.	Linear Acceleration Tangent m/s/s	Resultant Acceleration m/s/s	Resultant Angular Acceleration r/s/s	Resultant Angular Velocity r/s	Linear Velocity m/s	Kulite Pressure Kpa	Force N	Force Duration ms
78A232	7000	7000	22000	40	12	117	5800	3
78A234	7500	6400	37500	40	14	--	5700	4
78A236	7000	7000	28000	30	13	-9	5600	4
78A238	7100	7500	40000	60	13	100,-55	6600	4
78A239	7500	7500	41200	60	13	260	5000	5
78A241	8400	8000	54000	70	13	490	8700	3
79A249	14000	15200	70000	63	16	-70	7200	4
79A251	13000	13600	63600	75	13	200,-110	7500	4
79A253	9500	9800	40000	75	15	-101	5400	5
79A256	10500	10500	66000	84	16	--	6000	10
79A258	10000	11900	70000	75	15	-35,40	5700	5
79A260	12600	12600	60000	80	16	140,-100	7100	5

Table 4. Cadaver Impact Test Summary

Test No.	Linear Acceleration Tangent m/s/s	Resultant Acceleration m/s/s	Resultant Angular Acceleration r/s/s	Resultant Angular Velocity r/s	Linear Velocity m/s	Force N	Force Duration ms
82E001	3600	4500	42000	52	5	9100	10
82E021	1400	1440	7500	20	5.2	8400	11
82E022	1900	1900	7250	28	7.0	9600	10
82E041	1800	1800	7000	19	6.4	9600	12
82E042	1600	1800	8000	20	7.5	10200	12
82E061	1600	1700	6000	25	6.5	9000	10
82E062	1500	1600	7500	30	6.5	9600	12
83E081	1350	1350	7500	22	3.8	9600	12
83E082	1250	1000	7000	24	3.5	4100	8
83E102	—	—	—	—	—	1800	64
84E14,1A	500	560	5600	37.5	4.5	3200	30
84E141B	375	420	3900	30	4.5	2400	25
84E141C	1500	1575	20000	45	4.5	7500	10
84E141D	980	1200	16000	45	3.8	7500	8
84E151A	350	350	9000	50	2.6	2600	25
84E151B	2200	2200	25000	44	2	8000	10
84E161A	240	250	840	18	3.8	840	50+
84E161B	780	840	3750	25	5	4800	15

Table 5. Cadaver Test Summary Pressures

Test No.	Location	Type	Maximum Kpa	Time at Maximum ms	Duration ms
82E001	Epidural 1	Unimodal	75	5	10
	Epidural 2	Bimodal	11,3	5/25	10/120+
	Epidural 3	Unimodal	-36	5	15
	Epidural 4	Unimodal	11	5	5
82E021	Epidural 1	Unimodal	161	5	12
	Epidural 2	Bimodal	48,7	5/40	5/80
	Epidural 3	Bimodal	-61,8	5/45	10/80
	Epidural 4	Bimodal	34,6	5/25	5/70
82E022	Epidural 1	Unimodal	180	5	10
	Epidural 2	Bimodal	47,6	5/35	10/80
	Epidural 3	Bimodal	-43,6	5/50	15/100
	Epidural 4	Bimodal	12,51	5/13	5/5
82E041	Epidural 1	Bimodal	22,2	5/40	15/20
	Epidural 2	Bimodal	-20,11	5/45	10/15
	Epidural 3	Bimodal	-55,28	5/50	10/40
	Epidural 4	Bimodal	39,31	5/50	10/70
82E042	Epidural 1	Unimodal	58	5	140+
	Epidural 2	Bimodal	-20,9	5/45	5/20
	Epidural 3	Bimodal	-53,13	5/45	10/40
	Epidural 4	Bimodal	38,42	5/60	5/25
82E061	Epidural 1	Unimodal	97	5	8
	Epidural 2	Unimodal	24	5	5
	Epidural 3	Unimodal	-31	5	8
	Epidural 4	Bimodal	15,7	5/40	10/150
82E062	Epidural 1	Unimodal	55	5	12
	Epidural 2	Bimodal	27,12	5/40	10/35
	Epidural 3	Bimodal	31,14	5/42	10/40
	Epidural 4	Bimodal	37,12	5/45	10/40
83E081	Epidural 1	Unimodal	52	5	150+
	Epidural 2	Bimodal	20,14	5/20	10/135+
	Epidural 3	Bimodal	-18,14	5/20	7/125+
	Epidural 4	Unimodal	25	5	75
83E082	Epidural 1	Unimodal	46	5	15
	Epidural 2	Bimodal	10,5	5/20	10/125+
	Epidural 3	Bimodal	-13,3	5/50	10/100+
	Epidural 4	Bimodal	7,4	5/25	5/50
83E102	Epidural 1	Unimodal	-6	5	—
	Epidural 2	Unimodal	-4	5	—
	Epidural 3	Unimodal	6	5	—
	Epidural 4	Unimodal	3	5	—
84E141B	Epidural 1	Bimodal	30,7	5/65	30/210
	Epidural 2	Bimodal	10,6	5/65	30/200
	Epidural 3	Bimodal	-8,12	5/85	30/250+
	Epidural 4	Bimodal	11,12	5/75	20/250+
84E141D	Epidural 1	Bimodal	46,28	5/50	10/250+
	Epidural 2	Bimodal	21,11	5/55	5/250+
	Epidural 3	Bimodal	-62,28	5/65	5/250+
	Epidural 4	Bimodal	28,13	5/65	5/250+
84E151A	Epidural 1	Bimodal	40,8	5/105	20/200+
	Epidural 2	Bimodal	10,8	5/140	40/200+
	Epidural 3	Unimodal	15	5	30
	Epidural 4	Bimodal	4,12	5/75	50/250
84E151B	Epidural 1	Unimodal	41	5	5
	Epidural 2	Unimodal	30	5	5
	Epidural 3	Unimodal	8	5	10
	Epidural 4	Bimodal	33,17	5/80	20/180
84E161A	Epidural 1	Unimodal	6	80	200+
	Epidural 2	Unimodal	20	70	130
	Epidural 3	Unimodal	2	80	200+
	Epidural 4	Unimodal	15	70	200+
84E161B	Epidural 1	Unimodal	19	140	250+
	Epidural 2	Unimodal	32	15	250+
	Epidural 3	Bimodal	10	135	250+
	Epidural 4	Bimodal	14	140	200+

+Extends beyond the end of sampling.

Table 6. Rhesus Injuries/Damages+

Test No.	Gross Skull	Gross Brain	Micro Brain	Micro Spinal Cord	Gross Other
78A232	No abnormality or injury	No abnormality or injury	No abnormality or injury	No abnormality or injury	Epidural hematoma at C1, dura lacerated at C1
78A234	No abnormality or injury	No abnormality or injury	No abnormality or injury	No abnormality or injury	Epidural hematoma at C1, torn muscle at base of occiput
78A236	No abnormality or injury	No abnormality or injury	No abnormality or injury	No abnormality or injury	No abnormality or injury
78A238	No abnormality or injury	No abnormality or injury	No abnormality or injury	No abnormality or injury	Epidural hematoma at C1 disk
78A239	No abnormality or injury	Nc abnormality or injury	No abnormality or injury	No abnormality or injury	1/4 cc blood in occiput from epidural hematoma at C1
78A241	No abnormality or injury	No abnormality or injury	No abnormality or injury	No abnormality or injury	Epidural hematoma at C1
78A249	No abnormality. Basilar fracture (ring)	No abnormality. 3/4cc subdural hematoma right frontal lobe (cerebrum) subarachnoid hemorrhage base of cerebellum, pons and medulla	Foci of acute hemorrhage frontal cortex and cerebellum. Subarachnoid hemorrhage base of midbrain, cerebellum, and pons	Subarachnoid hemorrhage around spinal cord	Epidural hematoma at C1, occipital muscles damaged

+The kinetic impact response for these tests is presented in Reference 38.

Table 7 Rhesus Injuries/Damages

Test No.	Gross Skull	Gross Brain	Micro Brain	Micro Spinal Cord	Gross Other
79A251	No abnormality. Linear basilar fracture from foramen magnum to occipital contact point	No abnormality or injury	No abnormality or injury	No abnormality or injury	Epidural hematoma at C1 and C2
79A253	No abnormality. Basilar fracture (quasi-ring), temporal fracture	No abnormality. Petechial lesion left frontal lobe (cerebrum) subarachnoid hemorrhage base, pons, medulla and vermis of cerebellum	Focal hemorrhage frontal cortex, focal hemorrhage cerebellum associated with focal necrosis of purkinje cells, sarachnoid hemorrhage cerebellum and base of midbrain plus blood in aqueduct of sylvius, hemorrhage base of midbrain	Subarachnoid hemorrhage over spinal cord and blood in its central canal at C1-C2 level	Damaged neck ligaments
79A256	Abnormality. Very thin skull. Basilar fracture (petrous to petrous). Connected linear fractures to to frontal, temporal, parietal bones	No abnormality. Dura torn along sagittal sinus, emaciated tissue cerebellum, medulla	No abnormality or injury	No abnormality	Lacerated spinal cord
79A258	No abnormality. Basilar fracture (quasi-ring)	No abnormality. Lacerated medulla	No abnormality or injury	No abnormality	Epidural hematoma at C1
79A260	No abnormality. Basilar fracture (right petrous)	No abnormality. Subdural hematoma along sagittal sinus	No abnormality or injury	No abnormality	Epidural hematoma at C1

Table 8. Cadaver Damages

Test No.	Gross Skull	Gross Brain	Gross Other
82E001	No abnormality. Parietal fracture. Basilar fracture.	No abnormality. Subarachnoid hematoma frontal lobes (cerebrum) and on base of occipital lobe (cerebrum)	No abnormality or injury
82E021 82E022	No abnormality or injury	No abnormality. Subarachnoid hematoma right frontal lobe (cerebrum), hemorrhage central area left frontal lobe (cerebrum)	No abnormality or injury
82E041 82E042	No abnormality or injury	No abnormality. Subarachnoid hematoma frontal lobes (cerebrum) and subarachnoid hemorrhage parietal lobe (cerebrum)	No abnormality or injury
82E061 82E062	No abnormality or injury	No abnormality or injury	No abnormality or injury
82E081 82E082	No abnormality or injury	No abnormality or injury	No abnormality or injury
83E101 83E102	No abnormality or injury	No abnormality or or injury Mechanical abnormality of incomplete repressurization	No abnormality or or injury
84E141A 84E141B 84E141C 84E141D	No abnormality or injury	No abnormality. Subarachnoid hemorrhage frontal lobes (cerebrum) and subarachnoid hemorrhage right parietal lobe (cerebrum)	7 cm longitudinal laceration between eyes on forehead
84E151A 84E151B	No abnormality. 2 cm linear fracture of frontal bone continues as left orbital fracture	No abnormality. Subarachnoid hemorrhage left frontal lobe (cerebrum), subarachnoid hematoma right frontal lobe (cerebrum)	Hemorrhage to occipital belly muscle small laceration to side of skull fracture
84E161A 84E161B	Abnormality of very thick skull	Abnormality of massive tumor on the right frontal lobe (cerebrum). Coded "no injury"	No other abnormality

DISCUSSION

The results of a series of head impact research programs conducted during the past five years at UMTRI are presented. The tests entail different initial conditions, human surrogates, impact directions, and locations for the recording instruments. Therefore, in order to compare tests, frame-independent variables and Frenet-Serret vectors are used for examination and analysis. Frame-independent variables include resultant angular and linear velocities and accelerations. Vectors expressed in the Frenet-Serret frame field include tangential acceleration, normal acceleration, T-rate and B-rate. The features of the data discussed in this section in abbreviated form represent trends that may be important factors in head impact response. In particular, the potential effect of skull deformation on head angular acceleration as well as on impact and injury response appears significant.

FORCE TIME HISTORIES - Force time histories of repressurized cadaver tests are divided into two types which correlate well with fracture and non-fracture cases. In non-fracture cases, the force rises smoothly to a maximum and drops smoothly to zero. In fracture cases, although the force rises smoothly to a maximum, the drop to zero has a greater number of inflections or local maxima and is of longer duration. Fracture cases include Tests 82E001 and 84E151B. Test 82E001 is illustrated in the appendix.

Non-fracture impacts of repressurized cadavers can be broken into two groups consisting of long and short-duration impacts. Short-duration impacts are those lasting less than 15 ms; long-duration impacts are defined as 15 ms or longer. In some cases, such as Test 83E102, durations as long as 60 ms were recorded. In the appendix Test 82E041 illustrates a short duration impact and Test 84E161A illustrates a long duration impact.

Force time histories of Rhesus impacts can also be divided into two types which correlate well with non-fracture (or simple linear fracture) and basilar fracture. In the non-fracture/simple linear fracture group (Test 79A251 in the appendix), the force time history smoothly rises to a maximum and drops smoothly to zero. However, as with the repressurized cadaver, in cases with complex basilar fractures (Test 79A253 in the appendix), the force smoothly rose to a maximum, but fell with a greater number of inflections and/or local maxima of longer durations. The energy released from the skull appears to affect the force time history of repressurized cadaver subjects, but not Rhesus subjects, in non-fracture/simple linear fracture cases. Possibly, the Rhesus neck-head soft tissue muscle mass buffers the effect of fracture until "significant fracture" (complex basilar fracture) has occurred.

TANGENTIAL ACCELERATION TIME HISTORIES - The tangential acceleration time histories of repressurized cadavers divide into two groups that correlate well with subarachnoid hemorrhage or the absence of it. For those tests in which no subarachnoid hemorrhage was observed, the tangential acceleration had a single local maximum in the area of maximum acceleration. However, for those tests in which subarachnoid hemorrhage was observed, there were several local maxima in the area of maximum acceleration.

For both live and post-mortem Rhesus, the multimodal tangential acceleration occurred when complex skull fracture (basilar skull fracture) was observed. When there was an absence of complex fracture, the tangential acceleration was unimodal and smooth in the area of the maximum acceleration for both live and post-mortem Rhesus.

COMPARISON OF IMPACTS: CADAVER VARIABILITY - To examine variability within cadaver subjects, some subjects received two similar impacts (Tests 82E001 thru 82E082). Figure 10 is an example of cross-and auto-correlations for Tests 82E021 X 82E022 and 82E061 X 82E062 and 82E021 X 82E061. The figure represents the general trend observed in relating similar tests with different subjects to similar tests with the same subject in terms of force time histories. In general, it seems that force-time history as well as acceleration-time history vary more between subjects than between tests on the same subject. An analogous comparison for epidural pressures (not illustrated) shows equivalent variance between different subjects having similar impacts or between the same subject having similar impacts. This implies that experimental techniques associated with repressurization or with the effects of the post-mortem state may produce as much variance in the pressure time history response as do variations due to the population of test subjects.

IMPACT RESPONSE - The motion of a rigid body in space is the result of generalized forces: the total force and the total torque about a suitable axis. The dynamic problem of the motion of the area of the skull local to the nine-accelerometer array can be interpreted in the same way. However, because of the complex interactions of the area of the skull local to the nine-accelerometer array with the other material bodies, (for example, the muscle soft tissues of the neck, the rest of the skull, the brain, or the impactor), serious problems can arise in determining which of the bodies is producing these generalized forces.

For example, when the head receives an impact, several events occur: 1) stress waves are propagated from the impact site, 2) the skull starts to deform, and 3) the skull begins to move due to the impact, transmitting energy

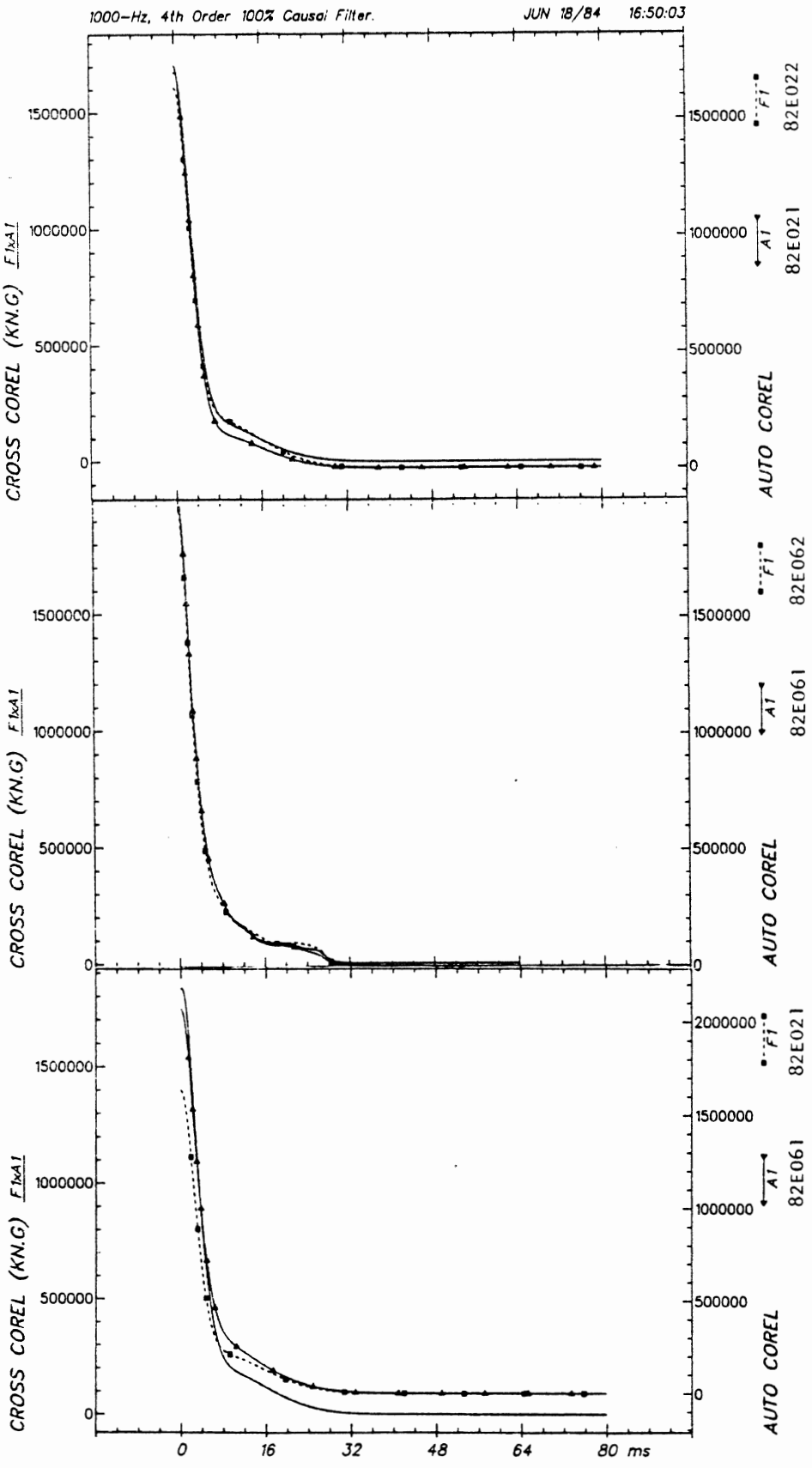

Fig. 10. Auto- and Cross-Correlation for Force Time History.

to the brain via the dura mater. Eventually, the waves are dissipated, the deformation of the skull recovers partially or fully on removal of the impact loads, and the acceleration of the skull comes primarily from forces generated from the brain and neck. If differential skull motion is severe, essentially due to either sufficient energy in the high frequency components of the force time history or sufficient peak force, the stresses at some point in the skull may exceed the failure strength of the bone, thereby producing fracture. The loads producing this type of impact are generally of shorter duration or contain a rise time sufficient to generate the necessary high frequency components to fracture the skull. The motion of the entire skull as a rigid body as estimated by the nine-accelerometer array depends on the degree of skull deformation as well as on the degree of precision being used in the investigation. If the skull deformations are small during and after impact, and the accelerometers are sufficiently far from the impact contact point, then valid rigid body motion can be assumed. However, if skull deformations are significant, then three-dimensional motion of the nine-accelerometer array and of the skull local to its instrumentation mount can only be used to estimate the motion of the rest of the skull through the use of an "estimated anatomical center." Interpretation of the results from the nine-accelerometer array must, therefore, take into account the non-rigid body motion taking place during "significant skull deformation" impacts. Using translations obtained from x-rays, three-dimensional approximate motion of an "estimated anatomical center" can be determined.

Impact Response Definition-With the use of the UMTRI nine-accelerometer array it is possible to record three-dimensional six-degrees-of-freedom motion of an area of the the skull in which the accelerometers are located. Therefore, head impact response can be defined as a continuum of "events" characterized by the path traced by the motion of the "estimated anatomical center," all the vectors defined on that path, and by changes of the associated frame fields. Physically this implies that head impact response is interpreted as the response of a material body (the nine-accelerometer array and area of the skull local to it) in contact with other material bodies. The curve and the vectors generated as the "estimated anatomical center" moves in time are, therefore, a result of the interactions of the skull-mount area with other material bodies.

Examples of events which are used to characterize head impact are: the initiation of head impact response (denoted by Q_1 on the tangential acceleration time histories in the appendix); the positive maximum of the tangential acceleration time history (denoted by Q_2 in the accompanying data); and the negative maximum of the tangential acceleration time history (denoted by Q_3 in the accompanying data). In research reported earlier in which similar Q_1, Q_2 and Q_3 events were defined (38), the tangential acceleration rose smoothly to a single maximum and fell smoothly until crossing zero. In some of the tests being reported here the time interval near Q_2 contains several local maxima, therefore direct comparison is complex. Nevertheless, these defined events can be used to compare different types of impacts for the same human surrogate and to compare the response of one type of human surrogate to another.

THE EFFECTS OF SKULL DEFORMATION ON LINEAR AND ANGULAR ACCELERATION - Inspection of the three-dimensional motion of the skull local to the accelerometers, epidural pressure transducer response, and contact forces showed that skull deformation may have important implications for injury produced in blunt head impact.

For repressurized cadaver tests with time histories having unimodal peaks of the tangential acceleration of the "estimated anatomical center," the time interval between the events Q_1-Q_2 is probably primarily a result of the interaction of the impactor with the skull. During the Q_1-Q_2 interval, the "estimated anatomical center" does not move more than 1 cm and the motion is to some extent three-dimensional. This is indicated by the rate of change of the tangent vector (T-rate) and binormal vector (B-rate). (A positive T-rate implies a curvature of the path or two-dimensional motion; significant T and B rate imply a torsion of the path or three-dimensional motion.) However, the angular acceleration is small or non-existent, and when present lies principally in the binormal direction. The normal acceleration of a point on the skull of closest approach to the impactor was found to be less than that of the "estimated anatomical center." (Reduced normal acceleration implies a "straighter" path of that point.) These measurements of angular and normal acceleration imply that the skull may be rotating about a point of closest approach to the impactor. For those tests with time histories displaying multimodal peaks of the tangential acceleration of the "estimated anatomical center" in the neighborhood of the Q_2 event, the time interval between the events Q_1-Q_2 is also probably primarily a result of the interaction of the impactor and skull. However, in these these tests skull deformations seem to have significant effect on the angular, tangential, and normal acceleration responses. Comparison of this multimodal impact response (Test 82E041 in the appendix) to the unimodal tangential acceleration response (Test 82E061 in the appendix), shows that the following variables are greater during the Q_1-Q_2 interval: angular acceleration, normal acceleration, T-rate and B-

rate. This implies that for the multimodal type of impact, the path of the "estimated anatomical center" is, to a greater degree than for the unimodal pattern impacts, moving in a three-dimensional manner and that this increased three-dimensional motion correlates well with the angular acceleration.

Comparison of the ratios of peak angular acceleration and velocity during the Q_1-Q_2 interval to those of peak angular acceleration and velocity during the Q_2-Q_3 interval indicates that for a given test subject there is respectively more angular acceleration during the Q_1-Q_2 interval for the multimodal impacts. In addition, the local maxima of the angular velocities in the multimodal impact as well as the rapid rotation of the binormal and normal vectors of between $\pi/2$ and π radians indicates that the path of the "estimated anatomical center" has passed an inflection point near the Q_2 event. This is most evident when the skull fractures. In a skull fracture test, the head is loaded very rapidly (e.g., Test 82E001, the force drops while the tangential acceleration drops below zero). This is accompanied by a short-lived rotation of the skull which produces a local maximum in the angular velocity. Subsequent to fracture, the skull is in more complete contact with the impactor. The tangential acceleration increases, the angular velocity decreases, and the angular acceleration reverses direction.

In general, the head is modeled as a rigid body when interpreting angular acceleration from nine accelerometers. However, the complex nature of the skull (4,24,54-55) causes asymmetric loading during blunt impact, which leads to an interpretation of an angular acceleration by the nine-accelerometer array that is not directly related to rigid body motion. Therefore, in addition to local skull bending in the area of the nine-accelerometer array, a second mechanism of skull deformation which causes the accelerometers to interpret angular acceleration can be hypothesized.

A schematic display of this type of response is presented in Figure 11 to illustrate the effect of skull deformation on angular acceleration (a rotation is produced). The figure demonstrates the type of motion that might occur and is not necessarily representative of motion actually observed. Also, motion of the skull is not necessarily in the anterior-posterior, inferior-superior plane. Because angular displacement is small, movements are best detected through evaluation of angular acceleration.

Because angular acceleration is an acceleration gradient over displacement at a given instant in time, the results of the linear acceleration are influenced by the angular acceleration. Thus, the differences in the neighborhood of the Q_2 event between the multimodal aspect and the unimodal aspect of the tangential acceleration of the "estimated anatomical center" are a result of the acceleration gradient caused by the angular acceleration.

Figure 12 represents the mechanical impedance corridor of force and tangential acceleration for repressurized cadaver tests in which skull deformation was observed and no skull fracture occurred (81E021, 82E022, 82E041, 82E042, and 84E141). The impedance values for these impacts are similar to driving point impedance tests reported by other researchers (19-20,27,33,39-40,56). This implies that the skull deformation observed could be related to the same type of skull deformation obtained from the driving point impedance tests mentioned above. The results from Tests 84E161A and 84E161B support this conclusion. This test subject had the thickest skull of any of the subjects tested. Both Tests 84E161A and 84E161B were at low severity HIC values of 70 and 400, respectively. If the results of the impedance are primarily a result of skull deformation, then it would be expected that the tests would look more like those of a rigid body. In the frequency range between 10 and 1000 Hz this is,

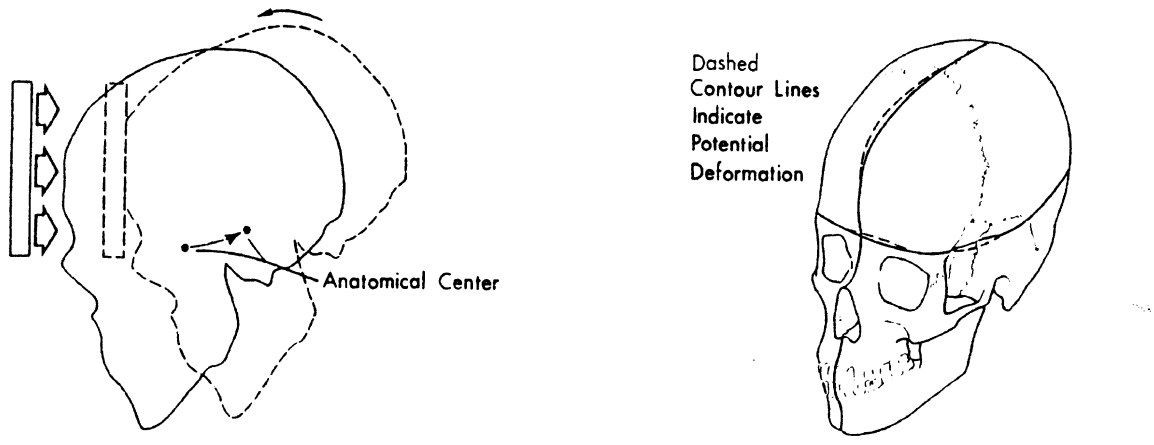

Fig. 11. Schematic Representations of Skull Deformation and Potential Effect on Angular Accelerations.

indeed, the case for Test 84E161A (Figure 13). However, for Test 84E161B there is a slight difference between its response and that of a rigid body at the low frequency. This is, perhaps, the result of the differential movement of soft tissue.

The results reported here extend the studies of the kinematic response of non-human primates (30) and cadavers (40) to blunt impacts. The earlier reports showed some of the differences in kinematic response between non-human primates and cadavers to be attributable to two factors: soft tissue distribution and skull geometry.

In the present study, skull fracture and non-skull fracture tests were analyzed for both Rhesus and cadavers. The difference between fracture and non-fracture impact response was found to be greater for cadavers. This is illustrated by the following tests presented in the appendix: non-fracture Rhesus, 78A241; fracture Rhesus, 79A249 and 79A251; non-fracture cadavers, 82E061; fracture cadavers, 82E001. Differences may be attributed to: 1) the nine-accelerometer array in Rhesus tests are mounted in an area that is to some degree more removed from the calvarium (the accelerometers are mounted on the orbital ridges of the face of the Rhesus), 2) the mounting site in the Rhesus is more massive with respect to the rest of the skull than that of the mounting site for cadavers (the instrumentation is the same size, but the Rhesus head is much smaller than the cadaver head), 3) the skull geometry is significantly different between the Rhesus and cadaver at the impact site, and 4) the differences in the external muscle mass at the impact site affect the interaction of the skull with the load cell.

KINEMATIC RESPONSE AFTER IMPACT: EFFECT OF SOFT TISSUE - Transmission of energy during intervals Q_1-Q_2 and Q_2-Q_3 was analyzed by comparing the acceleration response of the skull to the force-time history of the impactor. The following observations were made. During the Q_1-Q_2 interval, energy was transferred from the impactor to the skull and from the skull to the brain and neck. During the Q_2-Q_3 interval, significant energy was transferred from the brain and neck to the skull. Examination of all the tests shows that during the Q_2-Q_3 interval, unless there were rapid changes in the binormal vector direction (large torsion and large B-rate), the normal acceleration is established by angular acceleration. In addition, the normal and binormal vectors are established first by the angular acceleration during the Q_2-Q_3 interval and then by the angular acceleration and angular velocity after the Q_3 event. In general, for those tests with multimodal/unimodal peaks, the angular acceleration direction changes near the Q_2 event. The extent and amount of rotation changes from test to test. This is probably a result of complex three-dimensional motion of the head during the Q_1-Q_2 interval as well as of the geometry of the head and skull. The rotation tends to be between $\pi/2$ and π radians. The motion past the Q_3 event for multimodal tangential acceleration tests is similar to the unimodal tangential acceleration tests. In other words, the trajectory traced by the "estimated

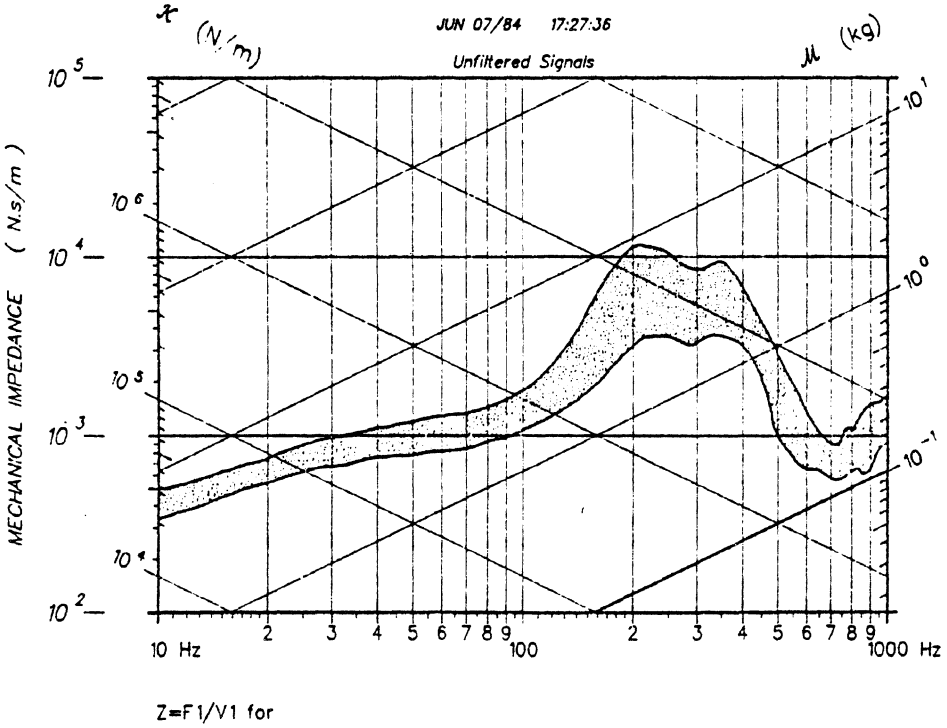

Fig. 12. Mechanical Impedance Corridor of Impact Force and Tangential Accelerations for Tests 82E021, 82E022, 82E041, 82E042, and 84E141.

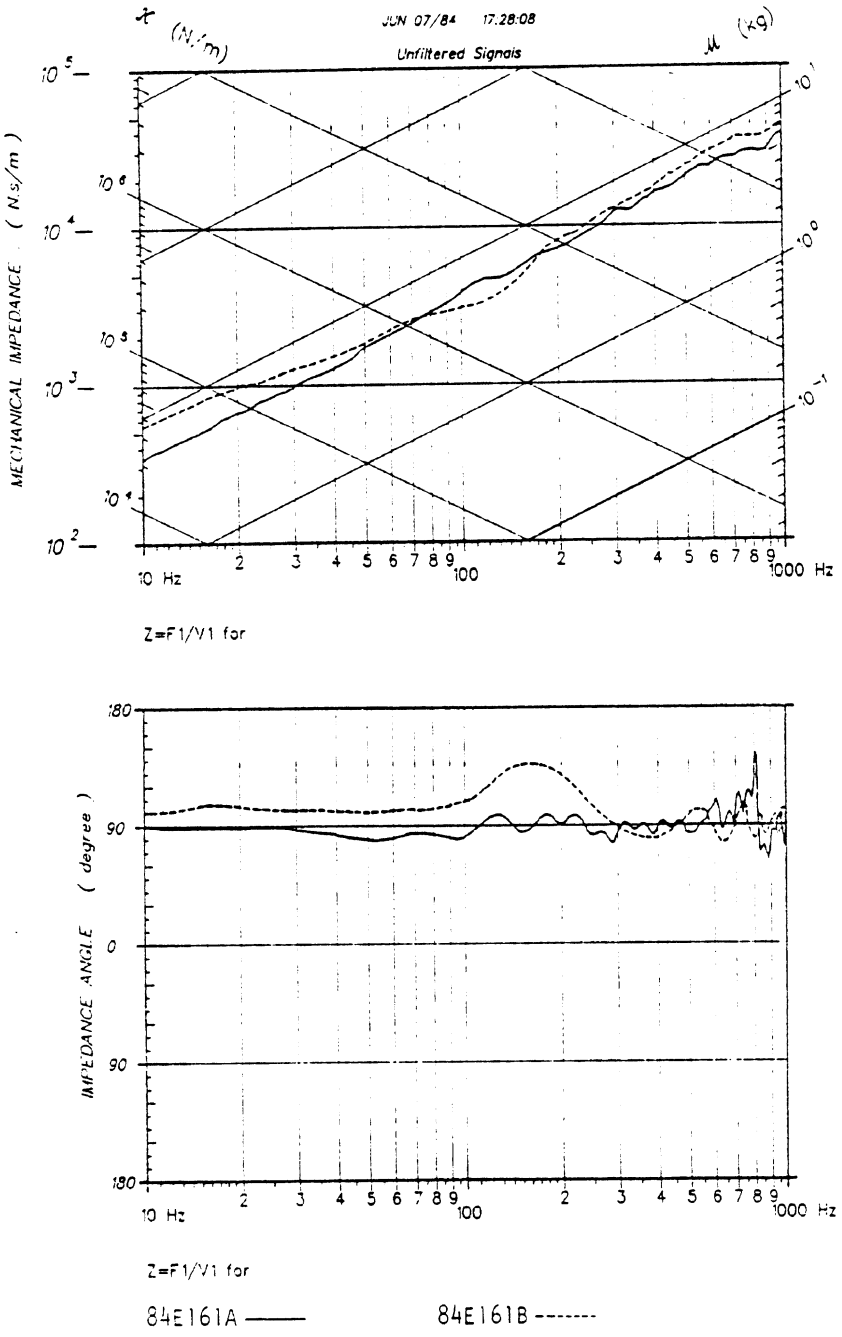

Fig. 13. Mechanical Impedances of Impact Force and Tangential Acceleration for Tests 84E161A and 84E161B.

anatomical center" and its attached frame field during multimodal tangential acceleration impacts is different from that traced during unimodal tangential acceleration impacts. However, the motion after impact is similar and the driving force is obviously other than the impactor. In past research (40) it has been determined that in the unpressurized or partially repressurized cadaver the response of the skull after impact is influenced by differential motion of the brain. In a similar manner, in the data presented here it seems that the brain is driving the skull and that this is manifested in both a linear and rotational manner. Potentially, energy has been transferred from the skull to the brain during impact, was stored as energy and then was released as the impact force dropped below a given level.

PRESSURE TIME HISTORY RESPONSE - The pressure time histories for repressurized cadavers were separated into two significant types, unimodal and bimodal. The unimodal pressure pulses correlate well with short-duration (less than 15 ms) large-valued (1500 m/s/s) tangential accelerations. Bimodal pressure pulses were more commonly observed in longer

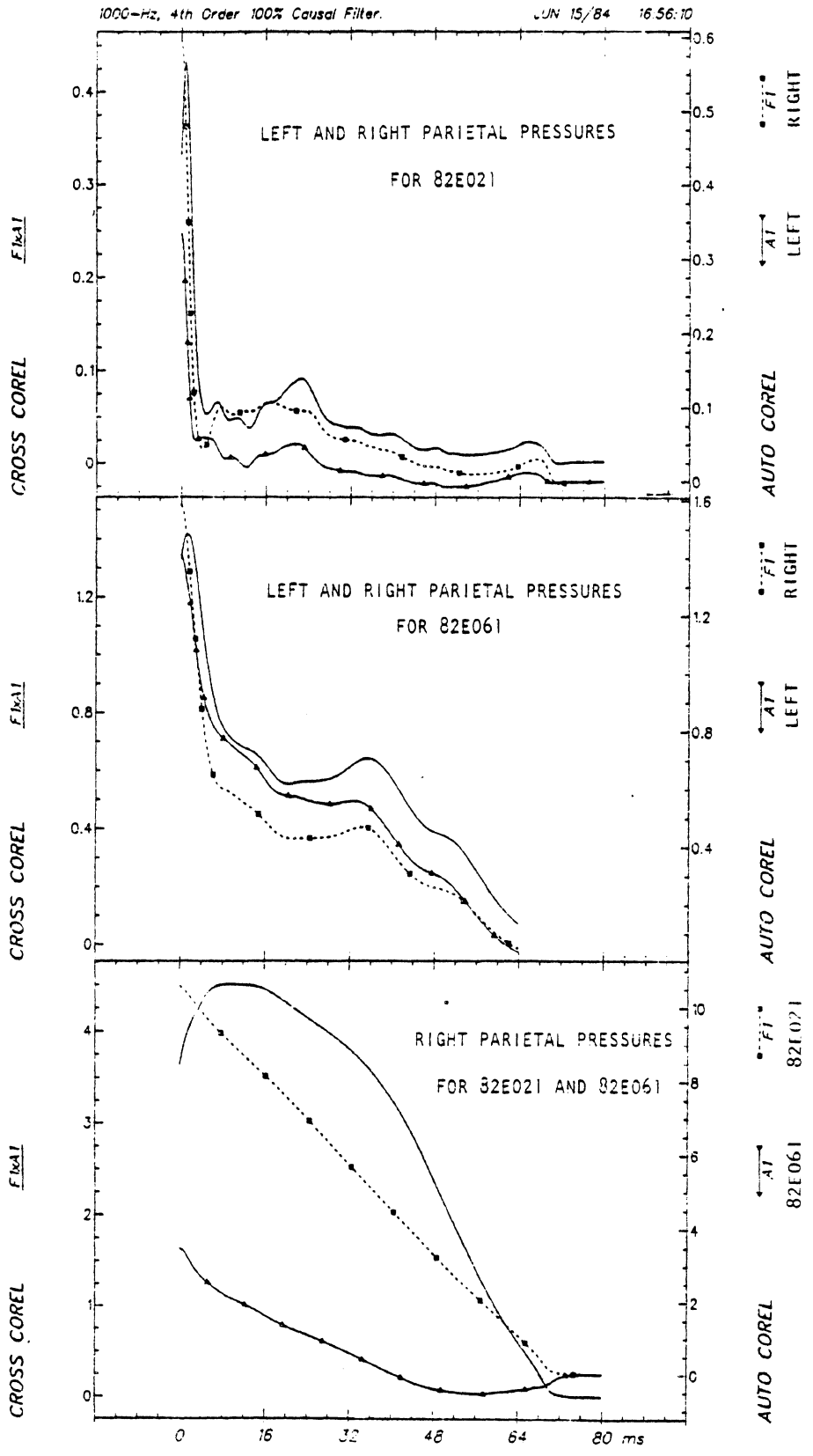

Fig. 14. Comparison of Right and Left Parietal Pressures and Comparison of Right Parietal Pressures for Different Impacts.

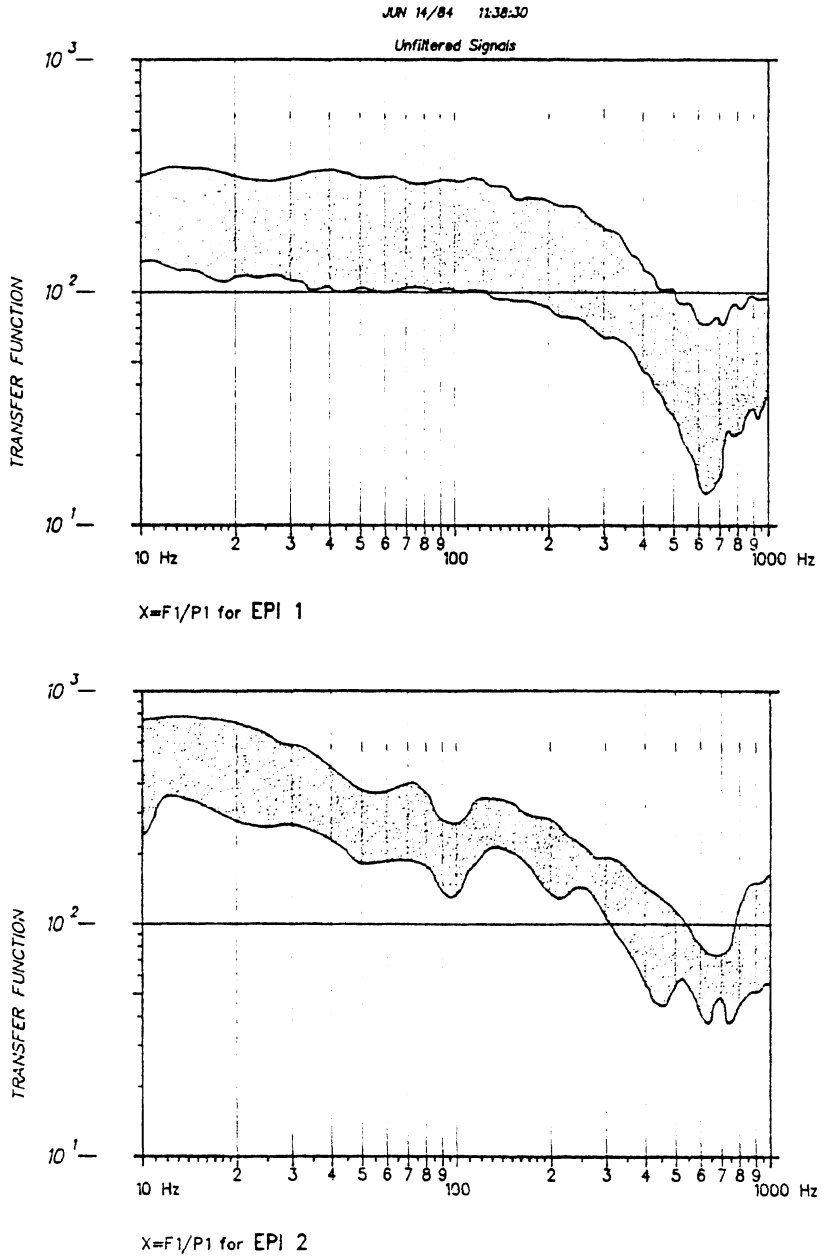

Fig. 15. Transfer Function Corridor of Frontal and Right Parietal Epidural Pressures for Tests 82E021, 82E022, 82E041, 82E042, and 84E141.

duration and lower acceleration impacts. This result seems to be a consequence of the superposition of two different types of mechanisms for producing pressure changes in the head during and after blunt impact.

The first pressure mechanism is associated with impact force time histories which contain sufficient high-frequency components to excite a short-duration loading of the skull on the brain, and probably is primarily a result of inertial loading. When a blunt impact blow is delivered to the head, the skull is initially accelerated. Shortly afterwards the brain compresses on the side closest to impact and is in tension on the side polarly distal to impact. The result is a pressure gradient in the brain going from point of impact to an area opposite from impact. Test 82E021 in the appendix illustrates such pressures for selected impacts and shows that highest magnitudes and positive pressures occur in the frontal lobe (epidural 1) and that negative pressures develop in the occipital lobe (epidural 3). Pressures in the parietal areas (epidural 2, epidural 4) are between the coup and counter coup areas. The pressures in epidural 2 and epidural 4, for most, of these repressurized cadaver tests, correlated well indicating that the pressure gradients were, in general, symmetric. However, some differences do exist which may be the result of three-dimensional motion of the head or of some asymmetry associated with the test subject. Figure 14 illustrates a cross- and auto-correlation between epidural 2 and epidural 4 for Tests 82E021 and 82E061 and shows that the auto-correlation for each pressure is similar to the cross-correlation. This is similar to results reported by others (42-43).

Figure 15 represents transfer functions between the force and the epidural 1 and 2 pressures for Tests 82E021, 82E022, 82E041 and 82E042 in which skull deformation occurred in the absence of skull fracture. These transfer functions have a possible resonance in the area

for which a resonance was predicted from the impedance transfer function for force and acceleration. This indicates that although the exact amount of the effect of skull deformation on the pressure response is not completely determined, it has some effect which is observable in the pressure time history. Therefore, a reasonable correlation might be found between pressure and acceleration. However, such a correlation would depend on where the accelerometers are placed on the skull.

The second pressure mechanism is associated with impact force time histories which contain low-frequency components or motion of the head after blunt impact. Unlike the first pressure mechanism which rarely produces pressure pulses longer than 15 ms, the second pressure mechanism produces pressure pulses that can last as long as 200 ms. Possibly, the second pressure mechanism is a result of the brain driving the skull as discussed earlier. Since the pressure is positive in all transducers regardless of position, the brain is possibly transferring energy to the skull, thus, accelerating it. This is consistent with the results discussed earlier where the brain stores energy and releases it shortly afterwards in a way that is manifested by skull angular acceleration. The results obtained from the high-speed cineradiograph support this hypothesis. Figure 16 is two frames from 16 mm high-speed cineradiograph movies of Test 84E161 showing the outline of the radio-opaque gel target injected into the brain tissue and ventricles. Inspection of the curves traced out by the gel from the pressure transducers to the ventricles, shows that although no motion could be detected between the skull and the brain, differential motion of parts of the brain was occurring.

All the pressure time histories for Rhesus subjects were unimodal and of short duration. This may be the result of the greater tangential acceleration which was associated with Rhesus impacts as compared to cadaver ones, or it may be the result of the differences between the response of the repressurized cadaver and that of the live unpressurized post-mortem Rhesus. Although there are a limited number of tests in this study, comparisons with pressure time histories from tests reported earlier not having skull fracture (30) indicate that there is a difference in response between those tests and the ones being reported here. Possibly, this is a result of the pressure-volume changes which accompany skull deformation that become acute during basilar skull fracture. The feature of the data that seems to indicate that this is true, is that near the Q_2 event the pressure becomes negative faster and obtains a greater negative maximum. Test 79A249, for example, reaches a negative maximum of about one atmosphere and maintains this for approximately 2 ms. In the appendix, Test 78A241 (non-skull fracture) and Tests 79A249 and 79A251 (skull fracture) illustrate this contrast. In addition, the high-speed cineradiographic film recorded a radio-transparent region forming at the top of the skull for Test 79A253 (Figure 17) indicating that the skull in the area of the pressure transducer had moved completely away from the brain. In previous work (40), there

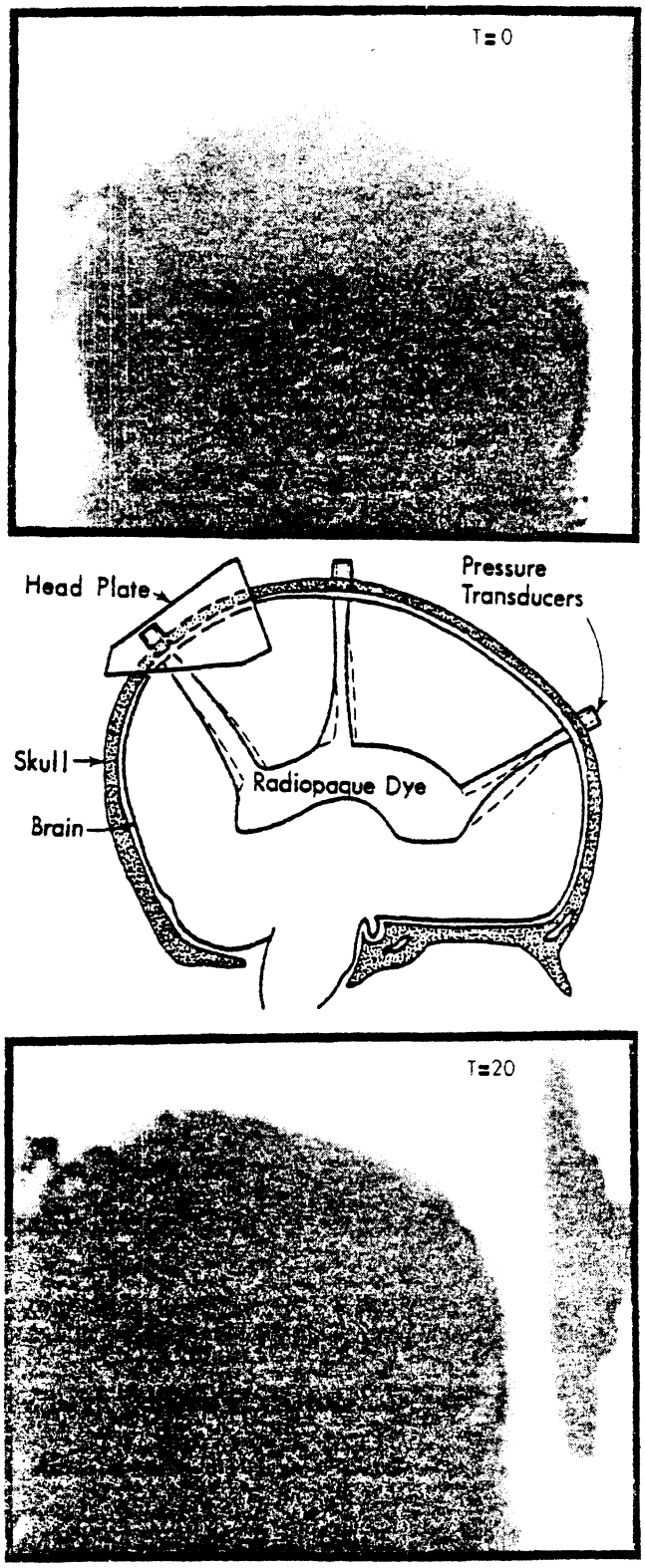

Fig. 16. Radiographs and Reconstruction of Radiographs with Radio-contrast Dye Injection Showing Differential Motion of the Brain at T=0 and T=20 ms.

was a significant difference in response between live and unpressurized post-mortem Rhesus; however, in this study when complex skull fracture occurred, it seems that skull deformation obscurred determination of whether there was such a difference between live, unpressurized post-mortem Rhesus.

INJURY/DAMAGE RESPONSE - The results presented in Tables 6,7 and 8 show that the most common brain injury/damage in the Rhesus and

Fig. 17. Radiograph of Test 79A253.

repressurized cadaver is subarachnoid hemorrhage. In the live Rhesus, the injury tends to be in the area at the base of the brain near the cerebellum, pons and midbrain. In the post-mortem Rhesus, no brain damage was observed except damage associated with the skull impinging upon the soft tissue of the brain during skull fracture. In particular, Test 79A256 was the only Rhesus test with this type of damage to the brain: the skull was thin enough so that fracture resulted to a much greater degree than for any other test. Damage occurs for repressurized cadavers in the frontal or parietal lobes of the cerebrum.

Despite the different types of surrogates for humans in these series, the different initial test conditions, and the different injury locations, subarachnoid hemorrhage did not occur unless "significant skull deformation" was present. Except for Test 79A251, no subarachnoid hemorrhage was observed in the absence of skull deformation.

Identifying mechanisms of head injury poses a formidable problem. In head impact response a number of potential injury mechanisms have been proposed (5-43). It is believed that different mechanisms occur for direct head impact than for non-impact (inertial conditions). It is also possible that several mechanisms could be responsible for producing the same injury/damage. The complex nature of the head/skull system under loading implies that under any given impact several mechanisms could be occurring and that they may complement each other to produce injury/damage.

One possible mechanism for production of subarachnoid hemorrhage in both the repressurized cadaver and the live Rhesus human surrogates is induced differential motion between the skull-brain interface. Potentially, there are two types of differential motion of the skull with respect to the brain. One is associated with "local" movement of the skull differentially with respect to the brain. The second requires rotational differential motion of a "significantly large" section of the skull with respect to the brain. In Tests 84E161A and 84E161B the high-speed cineradiograph films show changes in the radiopaque target area that formed curves extending from the pressure transducers to the lateral ventricle, which clearly indicate internal movement of the brain. However, no movement of the skull with respect to the brain was concurrently observed. Yet, in Test 84E151 both skull fracture and differential movement of the brain with the skull of up to 6 mm was observed. This potentially indicates that a "stick-slip" condition occurs, and that a "significant local acceleration" of any part of the skull can initiate differential motion of the brain surface with respect to the skull. However, because only a limited number of tests have been performed using techniques which make such observations possible, more work needs to be done before this hypothesis can be verified.

In repressurized cadaver tests, comparatively large pressure peaks were observed. It is possible that in those tests, high stress in the brain as well as skull deformations and angular accelerations were needed to produce the observed damage.

In several tests, duplicate impacts were made to each subject. It is possible that this enhanced the damage response; and therefore the results presented here should not be used to set tolerance levels. However, it is believed that this did not affect the general trend of damage and/or injury response observed.

CONCLUSIONS

This was a limited study of some important kinematic factors and injury/damage modes associated with direct blunt head impact. Because of the complex nature of the skull-brain interaction during an impact event, more work is necessary before these kinematic factors can be generalized to describe head impact response. However, the following conclusions can be made:

1. "Severe impacts" to the heads of repressurized cadavers can cause local motions in the skull with or without skull fracture. The motions are interpreted as angular acceleration by nine accelerometers mounted in a single array used to determine three-dimensional motion.
2. In repressurized cadavers and live Rhesus subjects skull deformation may cause direct and/or indirect subarachnoid hemorrhage.
3. For live Rhesus subjects, negative pressure peaks during an impact event equal to or greater than one atmosphere do not appear to produce injury.
4. Three-dimensional rigid body motion is not well defined in a "severe head impact" when using accelerometers located on the skull. The acceleration time histories, including the resultant acceleration used to calculate the Head Injury Criterion (HIC), of the anatomical center, depends not only on where the accelerometers have been placed on the skull but also on the biovariability of the test subject's skull.
5. Short duration impacts (less than 15 ms) in the anterior to posterior direction appear to involve two skull-brain interactions. One occurs during impact and is characterized by a transfer of energy from the skull to the brain and a pressure gradient in the brain positive at the frontal bone and negative at the occipital bone. The second interaction occurs during and after impact and is characterized by energy transmission from the brain to the skull and positive pressure in the brain at the frontal, parietal, and occipital bones.

ACKNOWLEDGEMENTS

The results presented in this paper were obtained through series of independently funded research programs conducted during the past five years. The funding agencies were: The Motor Vehicle Manufacturers Association and the United States Department of Transportation, National Highway Traffic Safety Administration, Contract No. DOT-HS-7-01636.

The authors acknowledge the assistance in injury evaluation provided by C.J. D'Amato, P.W. Gikas, Don Huelke and Julian Hoff as well as the encouragement of John C. Scowcroft. The authors also acknowledge the technical assistance of Nabih Alem, John Melvin, Jeff Axelrod, Gary Blair, Gary Holstein, Jeff Lehman, Gail Muscott, Jeff Pinsky, Carol Sobecki, and Bryan Suggitt. A special thanks is given to Jeff Marcus without whom this project could not have been completed.

REFERENCES

1. Anderson, D.W.; Miller, J.D.; and Kalsbeek, W.D. 1983. Findings from a Major Survey of Persons Hospitalized with Head Injuries. Public Health Reports 98(5):475-478.

2. Insurance Institute for Highway Safety, 1982. The Year's Work 1981-1982. Washington, D.C.

3. Kraus, J.F., et al. 1984. The Incidence of Acute Brain Injury and Serious Impairment in a Defined Population. American Journal of Epidemiology. 19(2):186-201.

4. Thomas, D.J.; Robbins, D.H.; Eppinger, R.H.; King, A.I., and Hubbard, R.P. 1974. Guidelines for the Comparison of Human and Human Analogue Biomechanical Data. A report of an ad hoc committee, Ann Arbor, Michigan, December 6.

5. Abel, J.M.; Gennarelli, T.A.; and Segawa, H. 1978. Incidence and Severity of Cerebral Concussion in the Rhesus Monkey Following Sagittal Plane Angular Acceleration. In: 22nd Stapp Car Crash Conference Proceedings, 24-26 October 1978, Ann Arbor, MI, Warrendale, PA: SAE Paper No. 780886, pp. 35-53.

6. Adams, J.H.; Graham, D.I.; and Gennarelli, T.A. 1981. Acceleration Induced Head Injury in the Monkey. II Neuropathology. In: K. Jellinger, F. Gullotta, M. Mossakowski, eds., Experimental Clinical Neuropathology. Acta Neuropathol. (Berl.) Suppl. vii, pp. 26-28.

7. Aldman, B.; Thorngren, L.; and Ljung, C. 1981. Patterns of Deformation in Brain Models Under Rotational Motion. In: DOT, NHTSA, Head and Neck Injury Criteria, Washington, D.C.

8. Alem, N.M. 1974. Simulation of Head Injury Due to Combined Rotation and Translation of the Brain. In: 18th Stapp Car Crash Conference Proceedings, pp. 579.

9. Chan, M. and Ward, C. 1981. Relative Importance of Skull Deformation. Proceedings ASME. Biomechanics Symposium, June 22-24.

10. Engin, A.E. 1969. Axisymmetric Response of a Fluid-filled Spherical Shell to a Local Radial Impulse--A Model for Head Injury. Journal of Biomechanics 2(3):395-341.

11. Engin, A.E. and Akkas, N. 1978. Application of a Fluid-Filled Spherical Sandwich Shell as a Biodynamic Head Injury Model for Primates. Aviation, Space and Environmental Medicine, pp. 120-124.

12. Evans, F.G.; Lissner, H.R.; and Lebow, M. 1958. The Relation of Energy, Velocity and Acceleration to Skull Deformation and Fracture. Surgery, Gynecology and Obstetrics 107:593-601.

13. Ewing, C.L. and Thomas, D.J. 1972. Human Head and Neck Response to Impact Acceleration. Naval Aerospace Medical Research Laboratory Detachment, New Orleans, Monograph 21, August.

14. Ewing, C.L. and Thomas, D.J. 1973. Torque Versus Angular Displacement Response of Human Head to -Gx Impact Acceleration. In: 17th Stapp Car Crash Conference Proceedings, Paper No. 730976.

15. Ewing, C.L., et al. 1975. The Effect of the Initial Position of the Head and Neck on the Dynamic Response of the Human Head and Neck to -Gx Impact Acceleration. In: 19th Stapp Car Crash Conference Proceedings, Paper No. 751157.

16. Gennarelli, T.A., et al. 1979. Differential Tolerance of Frontal and Temporal Lobes to Contusion Induced by Angular Acceleration. In: 23rd Stapp Car Crash Conference Proceedings, 17-19 October, San Diego, pp. 563-586. SAE Paper No. 791022.

17. Gennarelli, T.A.; Adams, J.H.; and Graham, D.I. 1981. Acceleration Induced Head Injury in the Monkey. 1. The Model Its Mechanical and Physiological Correlates. In: K. Jellinger, F. Gullotta, M. Mossakowski, eds, Experimental Clinical Neuropathology. Acta Neuropathol. (Berl.) Suppl. VII, pp. 23-25.

18. Gennarelli, T.A., et al. 1982. Diffuse Axonal Injury and Traumatic Coma in the Primate. Ann. Neurol. 12:564-74.

19. Gurdjian, E.S., et al. 1961. Intracranial Pressure and Acceleration Accompanying Head Impacts in Human Cadavers. Surgery, Gynecology and Obstetrics 113:185-190.

20. Gurdjian, E.S., et al. 1968. Significance of Relative Movements of Scalp, Skull and Intracranial Contents During Impact Injury of the Head. Journal of Neurosurgery 29(1):70-72.

21. Higgins, L.S. and Schmall, R.A. 1967. A Device for the Investigation of Head Injury Effected by Non-Deforming Head Accelerations. In: 11th Stapp Car Crash Conference Proceedings, pp. 35-46.

22. Hodgson, V.R. and Thomas, L.M. 1979. Acceleration Induced Shear Strains on a Monkey Brain Hemisection. In: 23rd Stapp Car Crash Conference Proceedings, 17-19 October, San Diego, Calif, pp. 589-611. SAE Paper No. 791023.

23. Hosey, R.R. and Liu, Y.K. 1982. A Homeomorphic Finite Element Model of the Human Head and Neck. In: R. H. Gallagher, et al., Finite Elements in Biomechanics, NY: John Wiley and Sons, Ltd., pp. 379-401.

24. Khalil, T.B. and Hubbard, R.P. 1977. Parametric Study of Head Response by Finite Element Modeling. Journal of Biomechanics 10(2):119-132.

25. Lissner, H.R.; Lebow, M.; and Evans, F.G. 1960. Experimental Studies on the Relation between Acceleration and Intracranial Pressure Changes in Man. Surgery, Gynecology, and Obstetrics 111:329-338.

26. Lowenhielm, P. 1974. Strain Tolerance of the W. Cerebri Sup. (bridging veins) Calculated from Head-on Collision Tests with Cadavers. Z. Rechtsmedizin 75:131-144.

27. McElhaney, J.H.; Stalnaker, R.L.; and Roberts, V.L. 1972. Biomechanical Aspects of Head Injury. In: W.F. King and H.J. Mertz, eds., Human Impact Response: Measurement and Simulation, N.Y.: Plenum Press.

28. Nahum, A.M. and Smith, R.W. 1976. An Experimental Model for Closed Head Injury. In: 20th Stapp Car Crash Conference Proceedings, Paper No. 760825.

29. Nahum, A.; Smith, R.W.; and Ward, C.C. 1977. Intracranial Pressure Dynamics During Head Impact. In: 21st Stapp Car Crash Conference Proceedings, pp. 337-366.

30. Nusholtz, G.S.; Melvin, J.W.; and Alem, N.M. 1979. Head Impact Response Comparisons of Human Surrogates. In: 23rd Stapp Car Crash Conference Proceedings, 17-19 October, San Diego, Calif., pp. 499-541. SAE Paper No. 791020.

31. Nusholtz, G.S.; Melvin, J.W.; and Lux, P. 1983. The Influence of Impact Energy and Direction on Thoracic Response. In: 27th Stapp Car Crash Conference Proceedings, pp. 69-94.

32. Nusholtz, G.S., et al. 1979. Comparison of Epidural Pressure in Live Anesthetized and Post-Mortem Primates. In: 7th International Workshop on Human Subjects for Biomechanical Research Proceedings, 16 October 1979, Coronado, Calif., pp. 175-200. Washington, D.C.: Distributed by National Highway Traffic Safety Administration.

33. Ommaya, A.K.; Hirsch, A.E.; Flamim, E.S.; and Mahone, R.H. 1966. Cerebral Concussion in the Monkey: An Experimental Model. Science, 153:211-212.

34. Ono, K.; Kikuchi, K.; and Nakamura, M. 1980. Human Head Tolerance to Sagittal Impact Reliable Estimation Deduced from Experimenetal Head Injury Using Subhuman Primates and Human Cadaver Skulls. In: 24th Stapp Car Crash Proceedings, 15-17 October, Troy, MI, pp. 104-160. SAE Paper No. 801300.

35. Padgaonkar, A.J.; Krieger, K.W.; and King, A.J. 1975. Measurement of Angular Acceleration of a Rigid Body Using Linear Accelerations. ASME Preprint-75-APM3, June.

36. Roberts, V.L.; Hodgson, V.R.; and Thomas, L.M. 1967. Fluid Pressure Gradients Caused by Impact to the Human Skull. In: Biomechanics Monograph, pp. 223-235. New York: American Society of Mechanical Engineers.

37. Sances, A., et al. 1984. Biodynamics of Vehicular Injuries. In: G. A. Peters and B. J. Peters, Eds., Automotive Engineering and Litigation, New York: Garland Law Publishing, pp. 449-550.

38. Shugar, T.A. 1975. Transient Structural Response of the Linear Skull-Brain System. In: 19th Stapp Car Crash Conference Proceedings, pp. 581-614.

39. Stalnaker, R.L., et al. Door Crashworthiness Criteria. Final Report. 1971. Contract No. FH-11-7288, U.S. Dept. of Transportation, National Highway Traffic Safety Administration, Washington, D.C.

40. Stalnaker, R.L., et al. 1977. Head Impact Response. In: 21st Stapp Car Crash Conference Proceedings, 19-21 October, New Orleans, pp. 303-335. SAE Paper No. 770921.

41. Thomas, L.M., et al. 1968. Static Deformation and Volume Changes in the Human Skull. In: 12th Stapp Car Crash Conference Proceedings, pp. 260-270.

42. Unterharnscheidt, F. 1983. Neuropathology of Rhesus Monkeys Undergoing -Gx impact acceleration. In: C.L. Ewing, et al., eds., Impact Injury of the Head and Spine, Springfield, IL: Thomas, pp. 94-176.

43. Ward, C.C.; Chan, M.; and Nahum, A. 1980. Intracranial Pressure - A Brain Injury Criterion. In: 24th Stapp Car Crash Conference Proceedings. SAE Paper No. 801304.

44. Ward, C.C.; Nikravesch, P.E.; and Thompson, R.B. 1978. Biodynamic Finite Element Models Used in Brain Injury Research. Journal of Aviation Space and Environmental Medicine, 49(1).

45. Nusholtz, G.S., et al. 1980. Thoraco-Abdominal Response and Injury. In: 24th Stapp Car Crash Conference Proceedings, pp. 187-228.

46. Nusholtz, G.S., et al. 1983. Cervical Spine Injury Mechanisms. In: 27th Stapp Car Crash Conference Proceedings, pp. 179-188.

47. Alem, N.M.; Melvin, J.W.; and Holstein, G.L. 1978. Biomechanics Applications of Direct Linear Transformation in Close-Range Photogrammetry. Proceedings of the Sixth New England Bioengineering Conference, New York: Pergamon Press.

48. Bender, M.; Melvin, J.W.; and Stalnaker, R.L. 1976. A High-Speed Cineradiograph Technique for Biomechanical Impact. In: 20th Stapp Car Crash Conference Proceedings, Paper No. 760824.

49. Bishop, R.L. and Goldberg, S.I. 1968. Tensor Analysis on Manifolds, New York, MacMillan.

50. Cartan, E. 1946. Lecons sur la Geometrie des Espaces de Rieman, Second Edition, Paris, Gautheir Villars.

51. O'Neill, B. 1967. Elementary Differential Geometry, New York Academic Press.

52. Stoker, J.J. 1969. Differential Geometry, New York, Wiley Intersciences.

53. Harris, C.M., and Crede, C.E. 1976. Shock and Vibration Handbook. New York, McGraw-Hill Book Company.

54. Hartman, C.G. and Straus, Jr., W.L., eds. The Anatomy of the Rhesus Monkey (Macaca mulatta), New York: Hafner Publishing Co., 1965 edition.

55. Heimer, L. 1983. The Human Brain and Spinal Cord Functional Neuroanatomy and Dissection Guide, New York: Springer-Verlag.

56. Ommaya, A.K. 1973. Head Injury Mechanisms. Final Report Contract No. DOT-HS-081-1-106IA, U.S. Dept. of Transportation, National Highway Traffic Safety Administration, Washington,D.C.

APPENDICES

Three-Dimensional Motion Time History

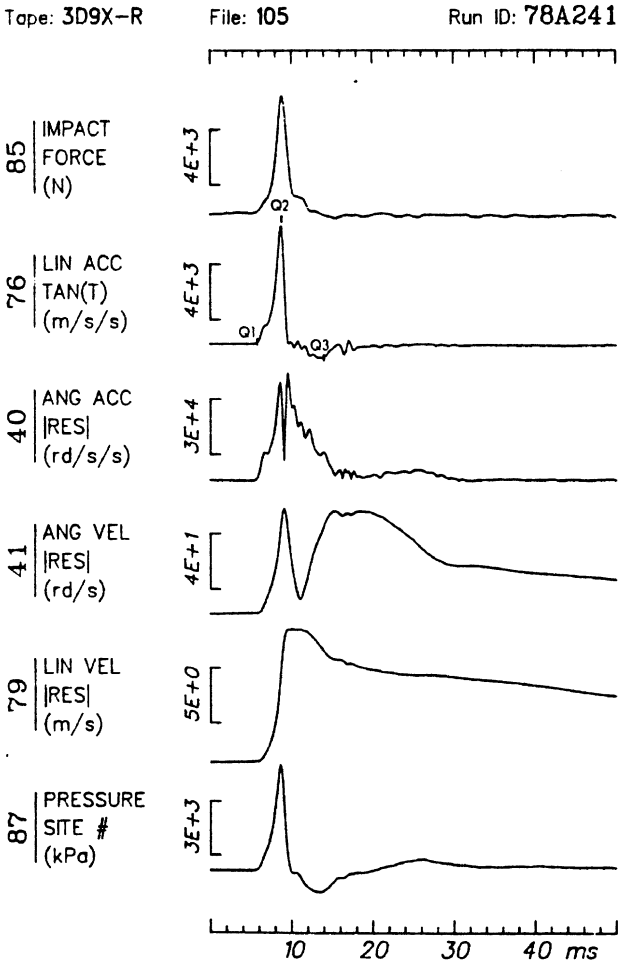

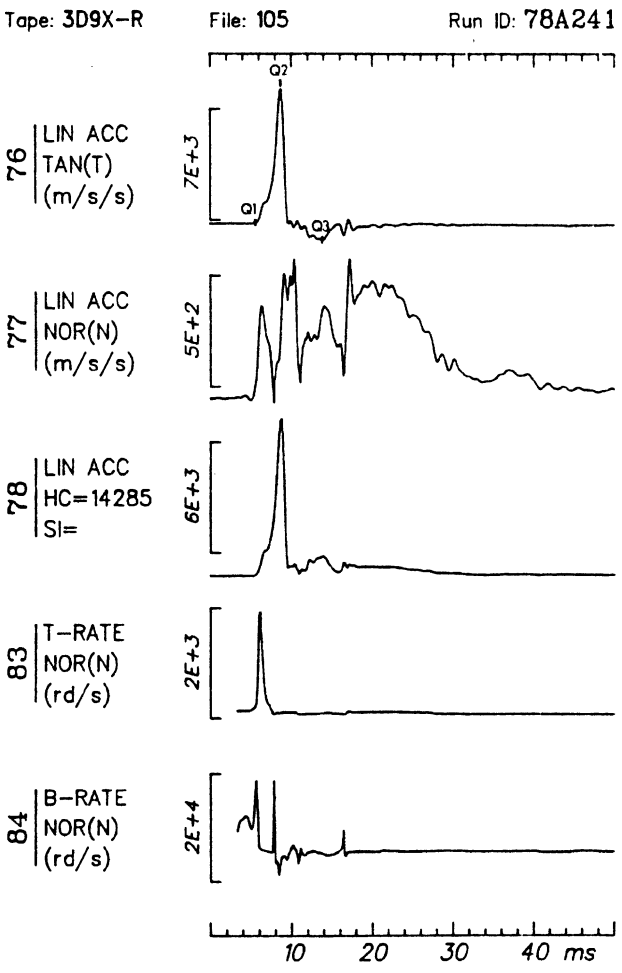

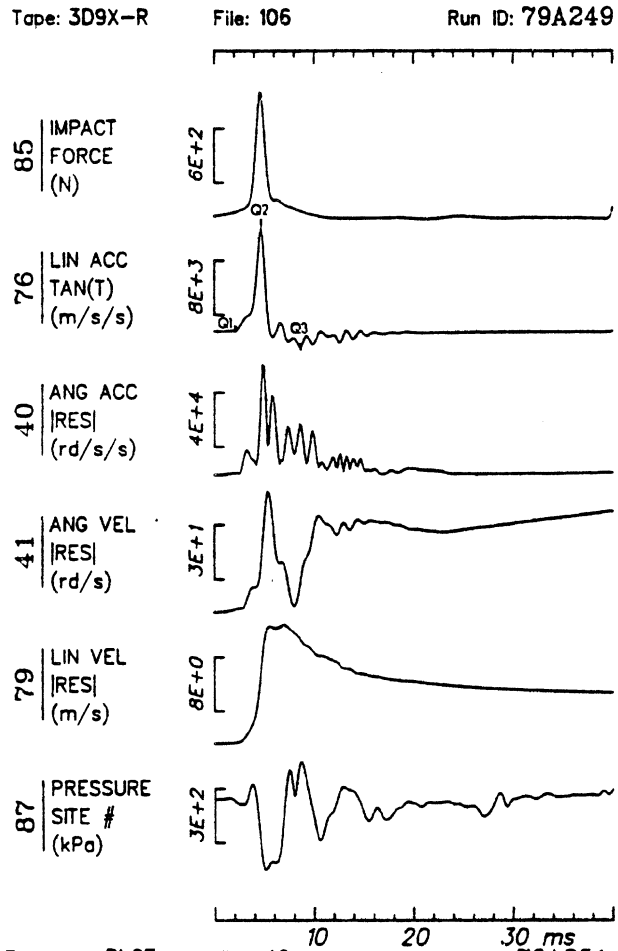
Tape: 3D9X-R
File: 106
Run ID: 79A249
85 IMPACT FORCE (N)
6E+2
Q2
76 LIN ACC TAN(T) (m/s/s)
8E+3
Q1
Q3
40 ANG ACC |RES| (rd/s/s)
4E+4
41 ANG VEL |RES| (rd/s)
3E+1
79 LIN VEL |RES| (m/s)
8E+0
87 PRESSURE SITE # (kPa)
3E+2
10
20
30 ms

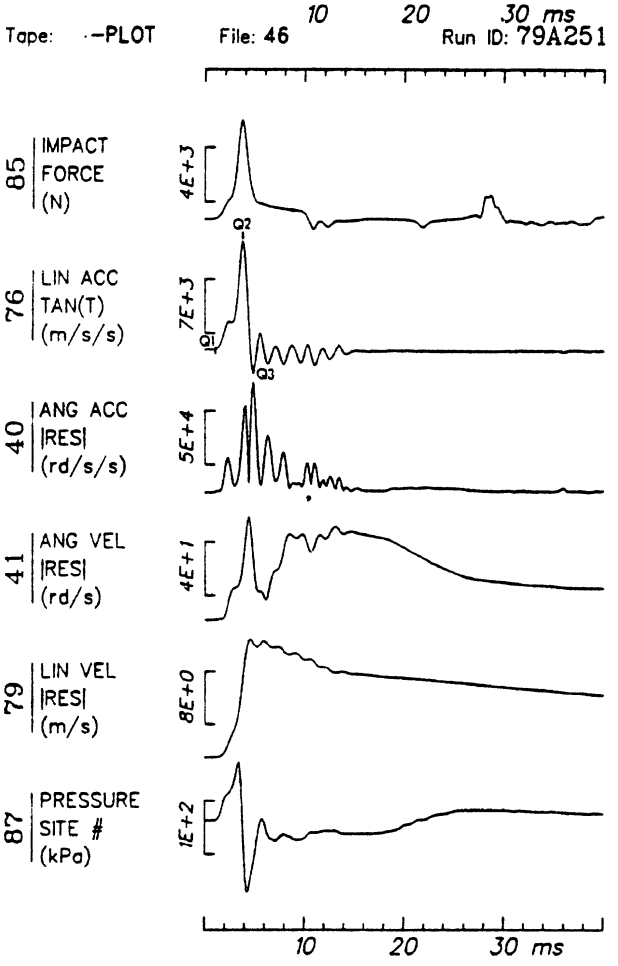
Tape: -PLOT
File: 46
Run ID: 79A251
85 IMPACT FORCE (N)
4E+3
Q2
76 LIN ACC TAN(T) (m/s/s)
7E+3
Q1
Q3
40 ANG ACC |RES| (rd/s/s)
5E+4
41 ANG VEL |RES| (rd/s)
4E+1
79 LIN VEL |RES| (m/s)
8E+0
87 PRESSURE SITE # (kPa)
1E+2
10
20
30 ms

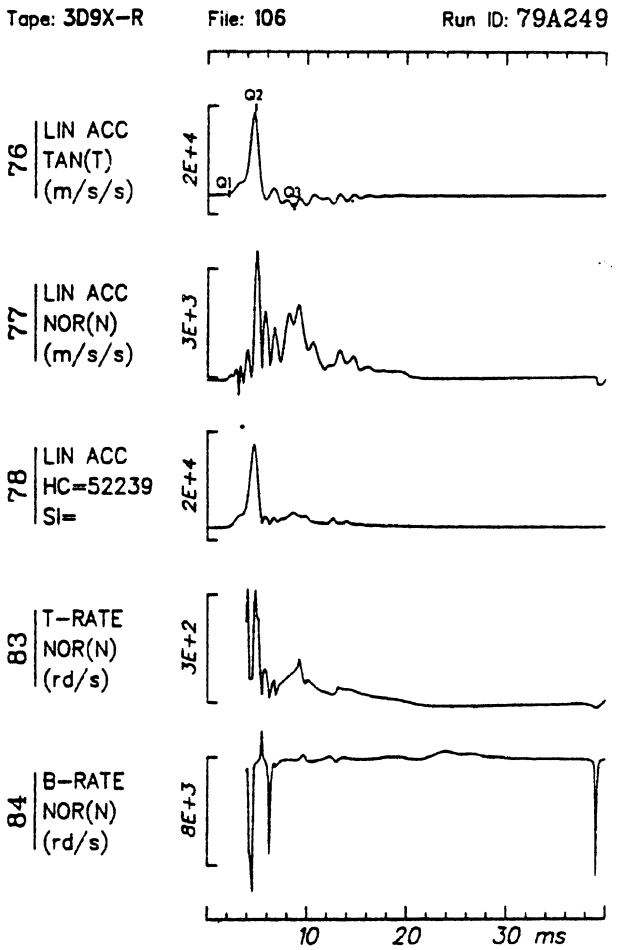
Tape: 3D9X-R
File: 106
Run ID: 79A249
76 LIN ACC TAN(T) (m/s/s)
2E+4
Q2
Q1
Q3
77 LIN ACC NOR(N) (m/s/s)
3E+3
78 LIN ACC HC=52239 SI=
2E+4
83 T-RATE NOR(N) (rd/s)
3E+2
84 B-RATE NOR(N) (rd/s)
8E+3
10
20
30 ms

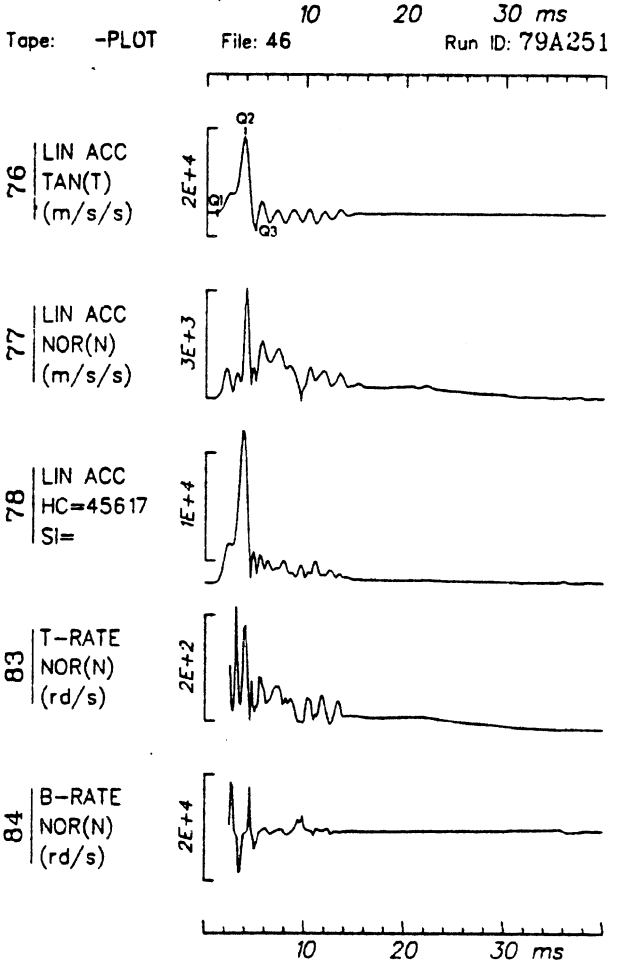
Tape: -PLOT
File: 46
Run ID: 79A251
76 LIN ACC TAN(T) (m/s/s)
2E+4
Q2
Q1
Q3
77 LIN ACC NOR(N) (m/s/s)
3E+3
78 LIN ACC HC=45617 SI=
1E+4
83 T-RATE NOR(N) (rd/s)
2E+2
84 B-RATE NOR(N) (rd/s)
2E+4
10
20
30 ms

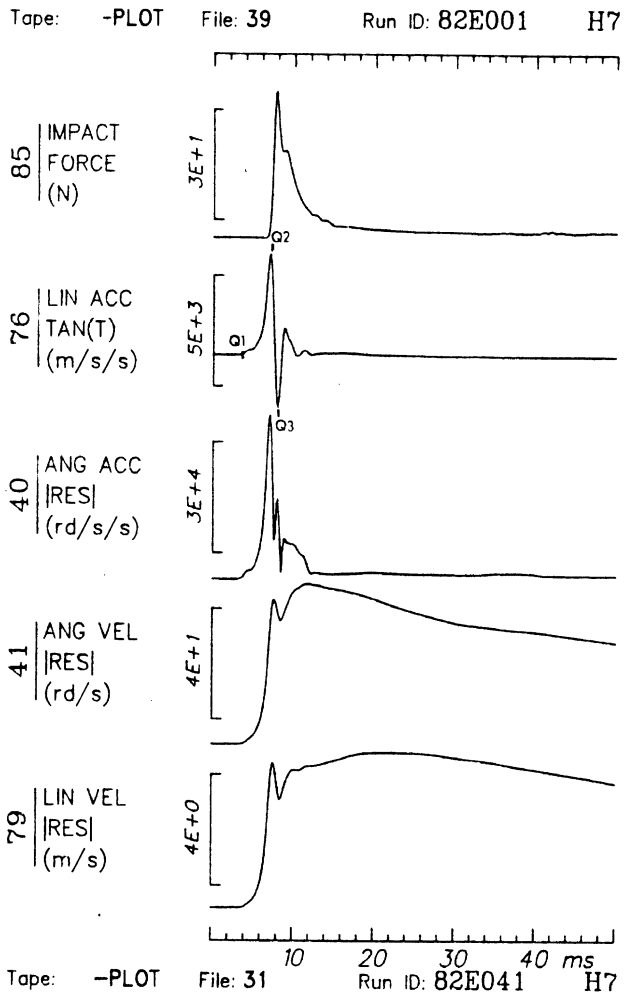
Tape: -PLOT File: 39 Run ID: 82E001 H7
85 IMPACT FORCE (N)
3E+1
76 LIN ACC TAN(T) (m/s/s)
5E+3
Q1
Q2
40 ANG ACC |RES| (rd/s/s)
3E+4
Q3
41 ANG VEL |RES| (rd/s)
4E+1
79 LIN VEL |RES| (m/s)
4E+0
10 20 30 40 ms

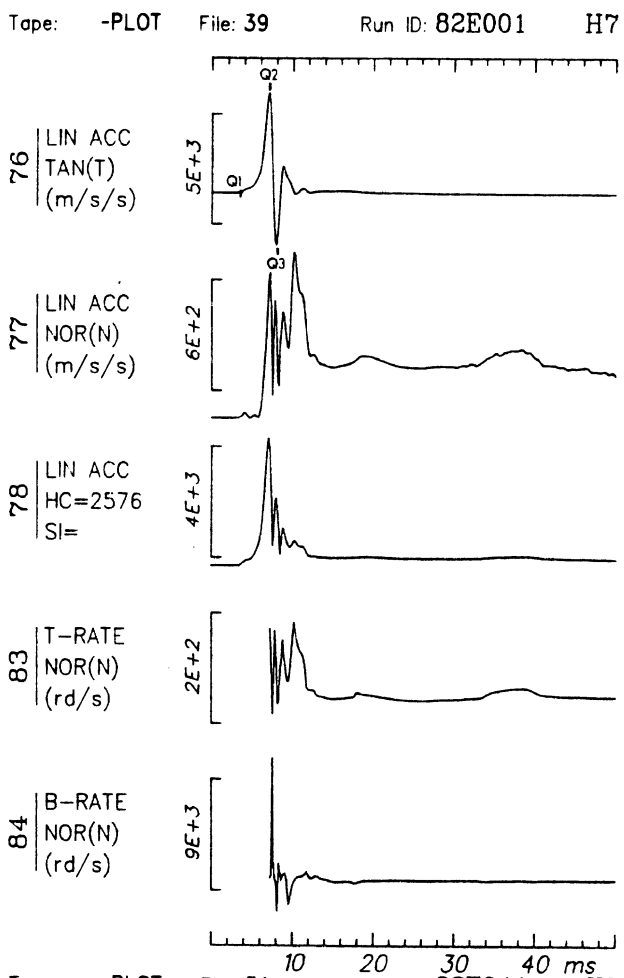
Tape: -PLOT File: 39 Run ID: 82E001 H7
76 LIN ACC TAN(T) (m/s/s)
5E+3
Q1
Q2
77 LIN ACC NOR(N) (m/s/s)
6E+2
Q3
78 LIN ACC HC=2576 SI=
4E+3
83 T-RATE NOR(N) (rd/s)
2E+2
84 B-RATE NOR(N) (rd/s)
9E+3
10 20 30 40 ms

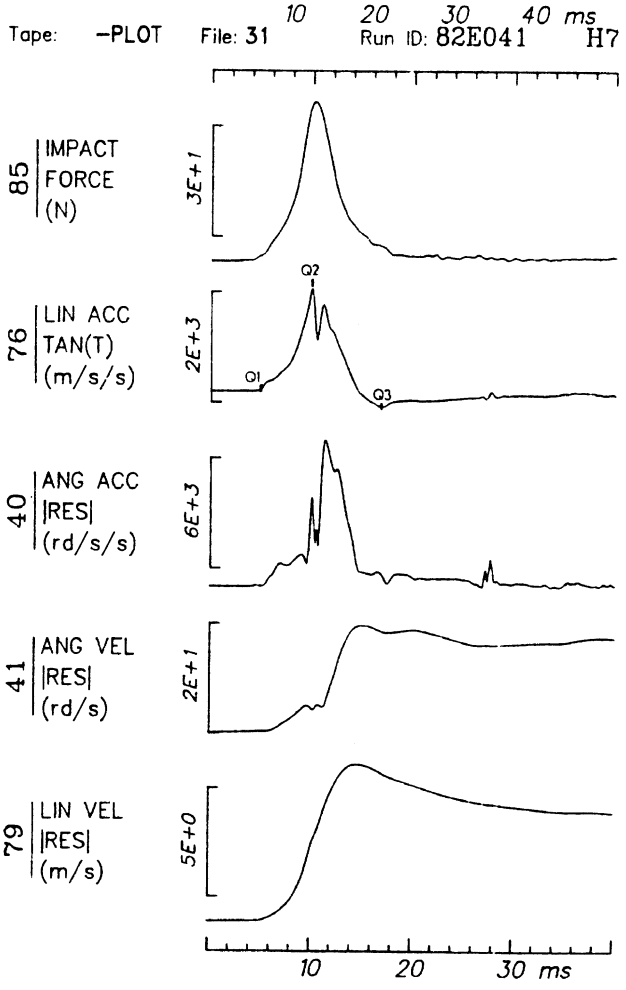
Tape: -PLOT File: 31 Run ID: 82E041 H7
85 IMPACT FORCE (N)
3E+1
76 LIN ACC TAN(T) (m/s/s)
2E+3
Q1
Q2
Q3
40 ANG ACC |RES| (rd/s/s)
6E+3
41 ANG VEL |RES| (rd/s)
2E+1
79 LIN VEL |RES| (m/s)
5E+0
10 20 30 ms

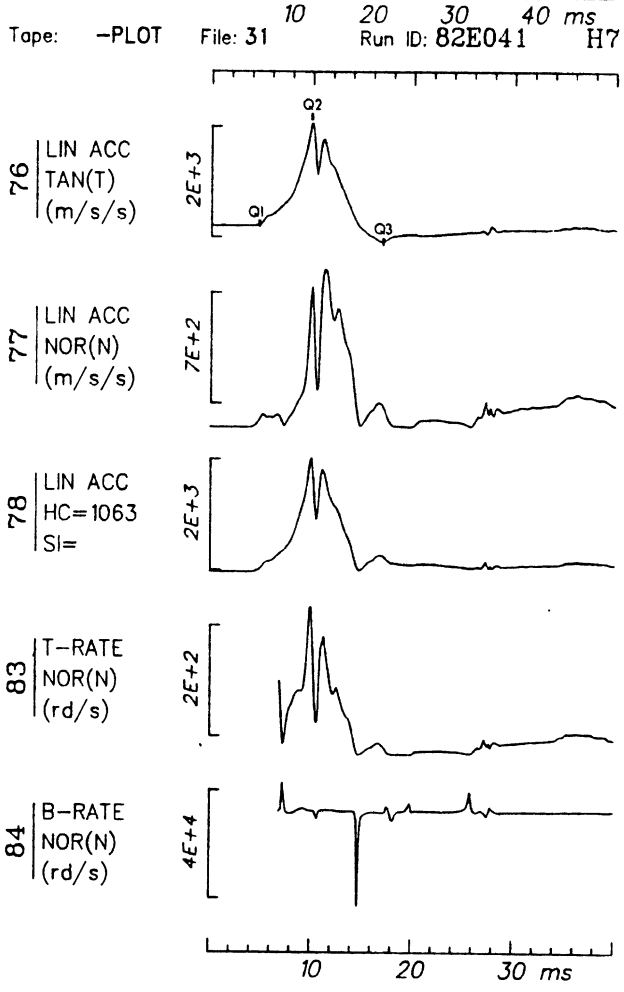
Tape: -PLOT File: 31 Run ID: 82E041 H7
76 LIN ACC TAN(T) (m/s/s)
2E+3
Q1
Q2
Q3
77 LIN ACC NOR(N) (m/s/s)
7E+2
78 LIN ACC HC=1063 SI=
2E+3
83 T-RATE NOR(N) (rd/s)
2E+2
84 B-RATE NOR(N) (rd/s)
4E+4
10 20 30 ms

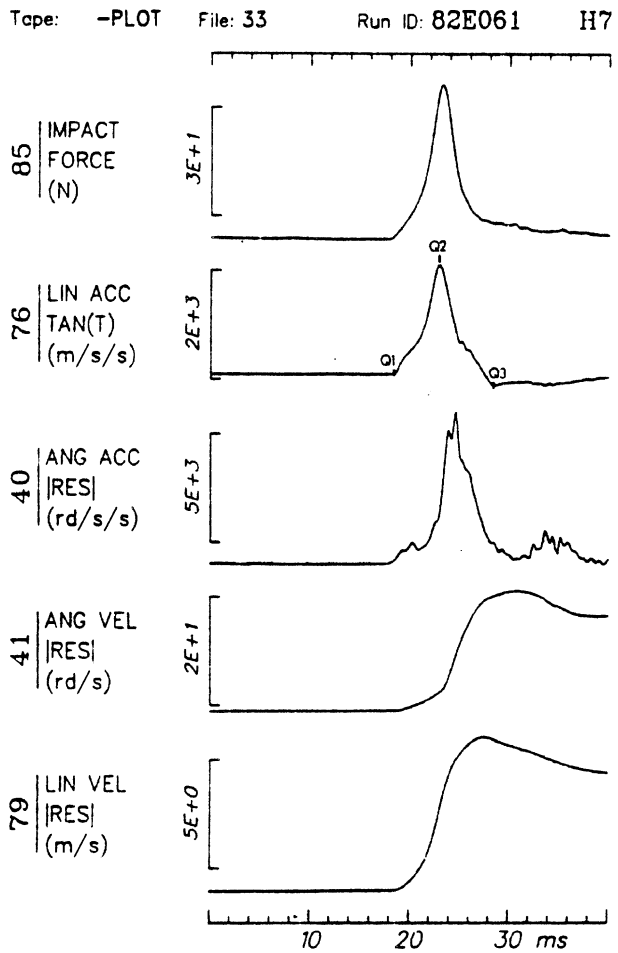
Tape: -PLOT File: 33 Run ID: 82E061 H7
85 IMPACT FORCE (N)
3E+1
76 LIN ACC TAN(T) (m/s/s)
2E+3
Q1
Q2
Q3
40 ANG ACC |RES| (rd/s/s)
5E+3
41 ANG VEL |RES| (rd/s)
2E+1
79 LIN VEL |RES| (m/s)
5E+0
10 20 30 ms

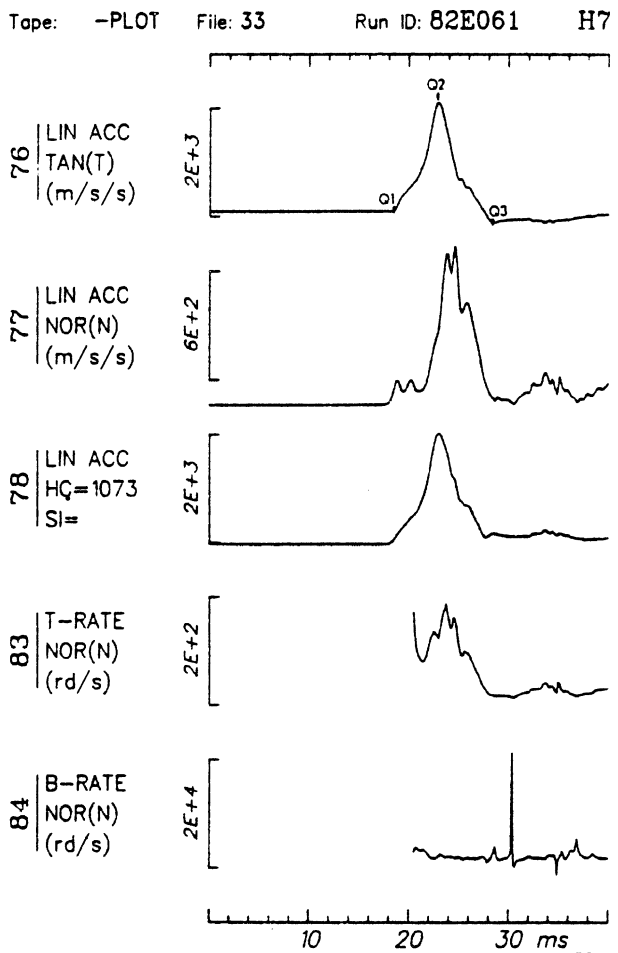
Tape: -PLOT File: 33 Run ID: 82E061 H7
76 LIN ACC TAN(T) (m/s/s)
2E+3
Q1
Q2
Q3
77 LIN ACC NOR(N) (m/s/s)
6E+2
78 LIN ACC HC=1073 SI=
2E+3
83 T-RATE NOR(N) (rd/s)
2E+2
84 B-RATE NOR(N) (rd/s)
2E+4
10 20 30 ms

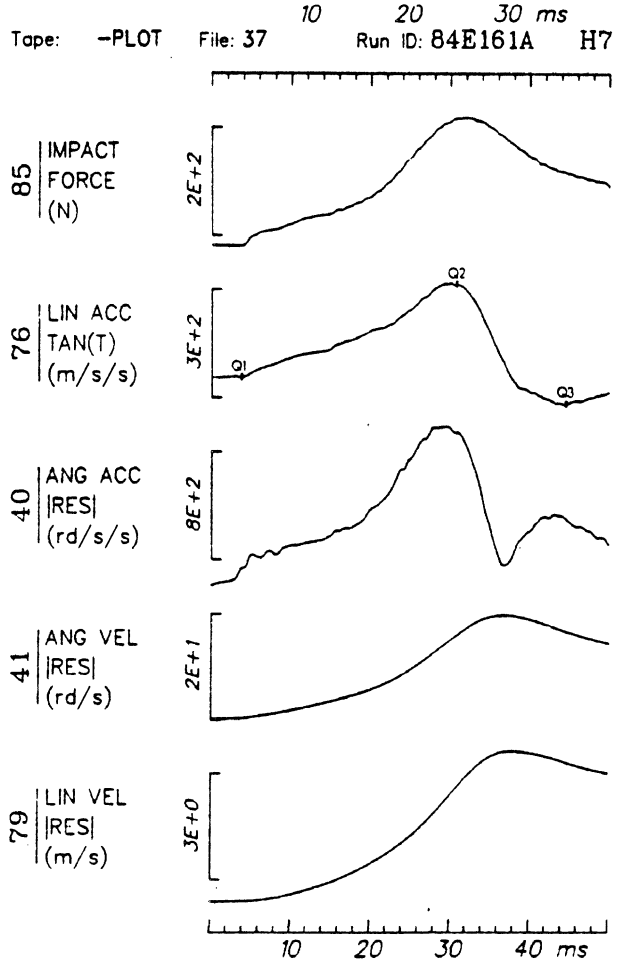
Tape: -PLOT File: 37 Run ID: 84E161A H7
85 IMPACT FORCE (N)
2E+2
76 LIN ACC TAN(T) (m/s/s)
3E+2
Q1
Q2
Q3
40 ANG ACC |RES| (rd/s/s)
8E+2
41 ANG VEL |RES| (rd/s)
2E+1
79 LIN VEL |RES| (m/s)
3E+0
10 20 30 40 ms

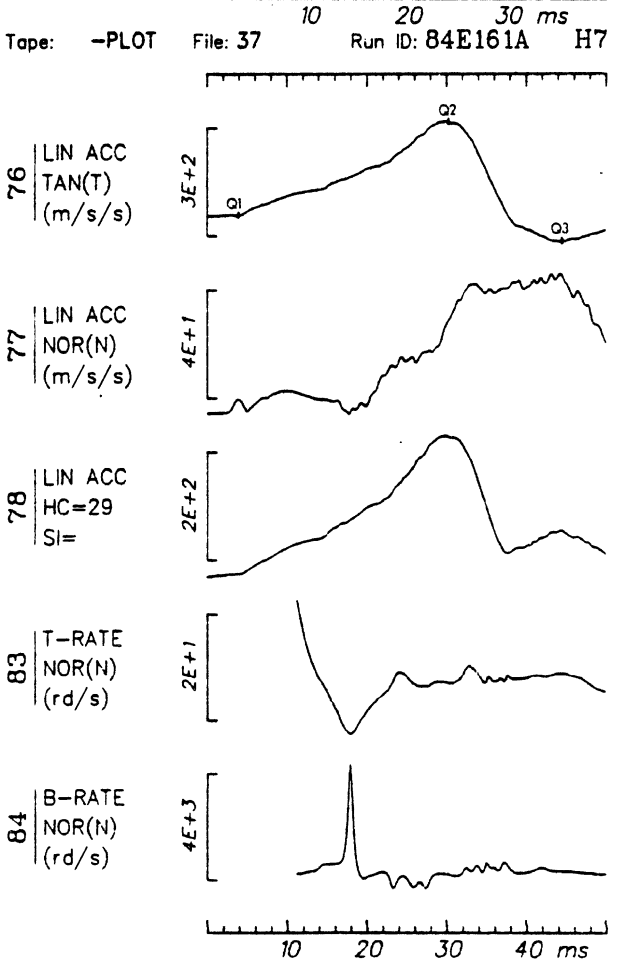
Tape: -PLOT File: 37 Run ID: 84E161A H7
76 LIN ACC TAN(T) (m/s/s)
3E+2
Q1
Q2
Q3
77 LIN ACC NOR(N) (m/s/s)
4E+1
78 LIN ACC HC=29 SI=
2E+2
83 T-RATE NOR(N) (rd/s)
2E+1
84 B-RATE NOR(N) (rd/s)
4E+3
10 20 30 40 ms

Force and Pressure Time History

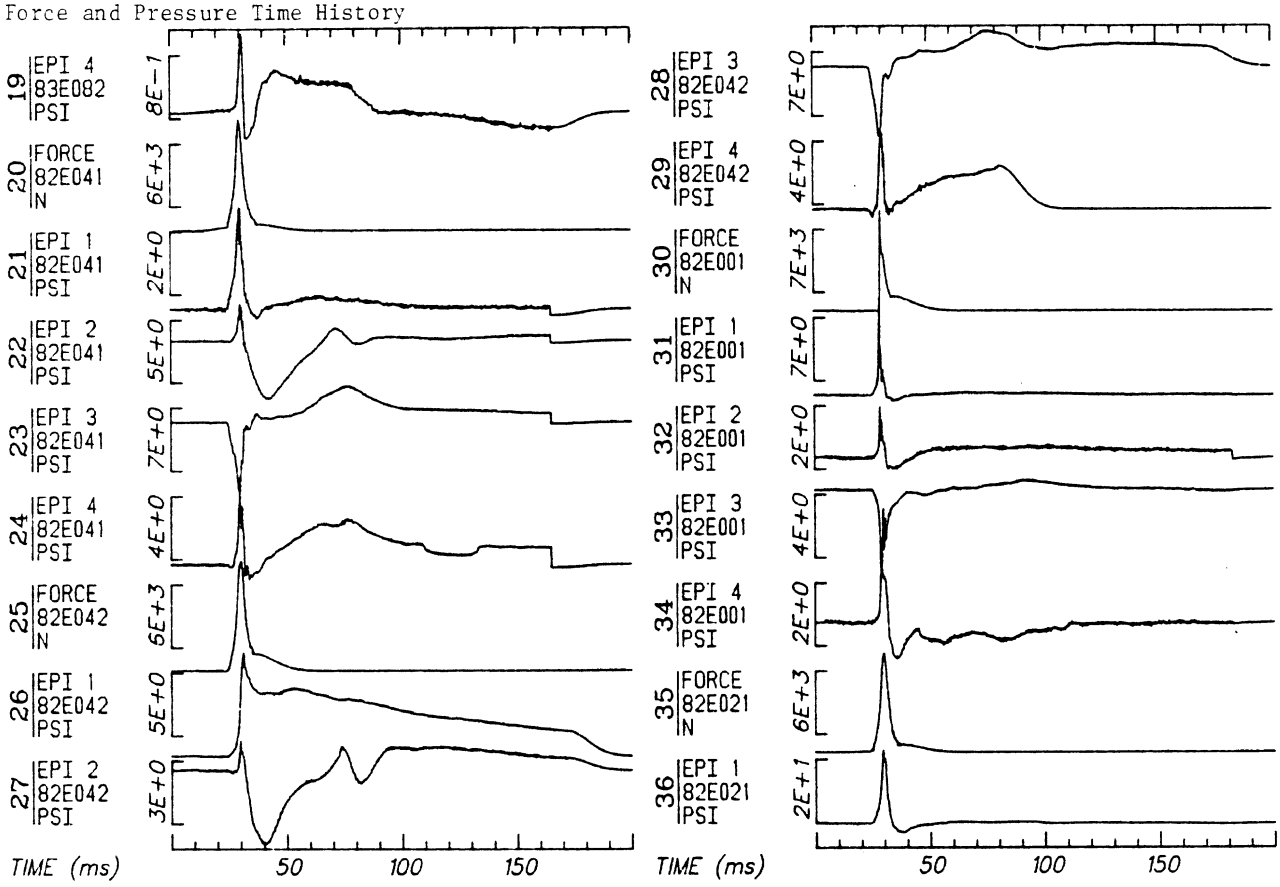

Run ID: 82E021 C3 Disk: SQ2F:PRE File: 1 Date: JUN 12, 1984

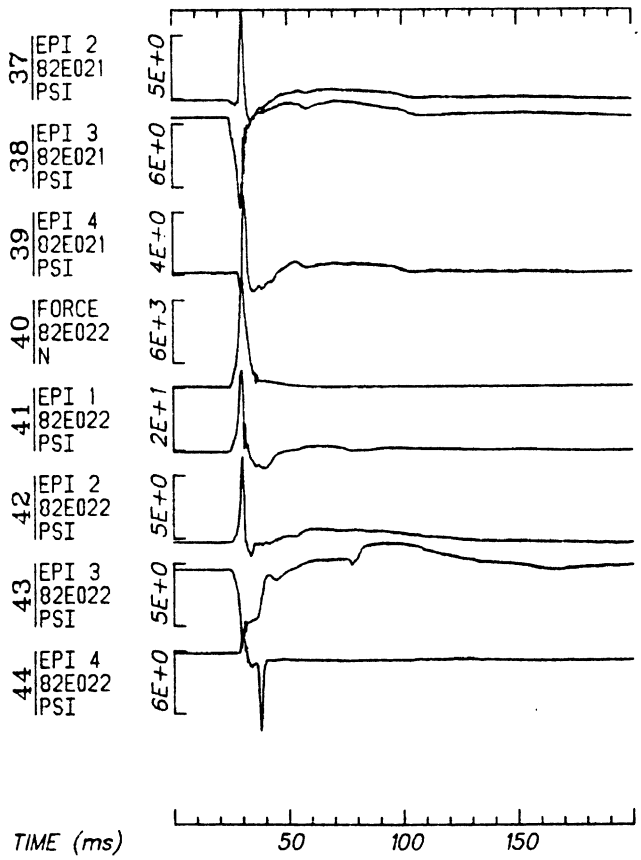

Run ID: 82E022 C3 Disk: SQ2F:PRE File: 1 Date: JUN 12, 1984

FORCE AND PRESSURE TIME HISTORIES

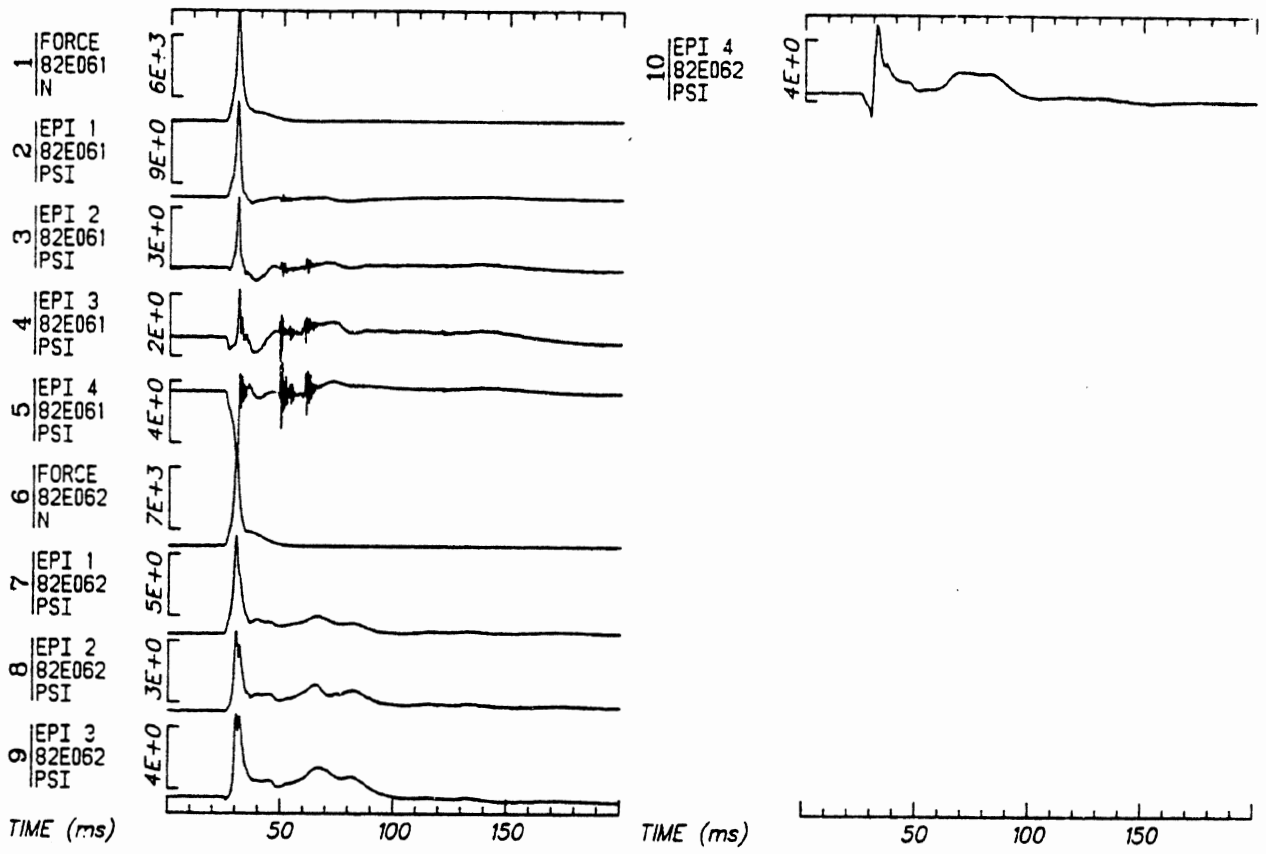

Run ID: 82E062 C3 Disk: SQ2F:PRE File: 1 Date: JUN 12, 1984

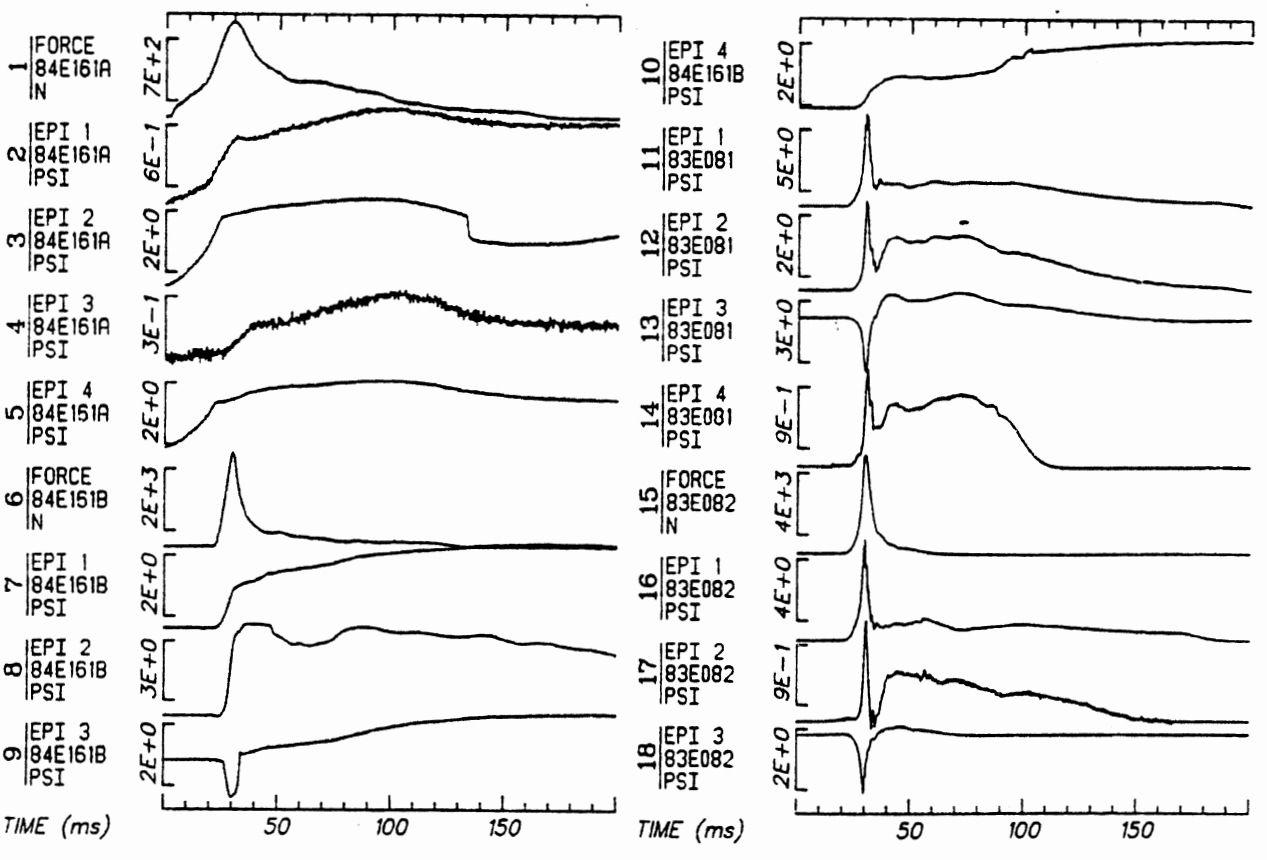

Run ID: 83E082 C3 Disk: SQ2F:PRE File: 1 Date: JUN 12, 1984

FORCE AND PRESSURE TIME HISTORIES

APPENDIX F: "COMPARISON OF EPIDURAL PRESSURES IN LIVE ANESTHETIZED AND POSTMORTEM PRIMATES"

TITLE PAGE

TITLE: COMPARISON OF EPIDURAL PRESSURE IN LIVE ANESTHETIZED AND POST-MORTEM PRIMATES

Running Head: Epidural Pressures in Live vs. Post-Mortem

Authors: Guy S. Nusholtz, B.S., M.S.
Biomechanics Division, Transportation Research Institute,
University of Michigan, Ann Arbor, Michigan 48109
Title: Assistant Research Scientist

Carley Ward, M.S., Ph.D.
Biodynamics Engineering, Inc.
705 Hampden Place
Pacific Palisades, California 90272

Correspondence Address: Guy S. Nusholtz
University of Michigan
Transportation Research Institute
2901 Baxter Road
Ann Arbor, Michigan 48109

Telephone Number: 313-763-3462

In Press: Journal of Space, Aviation and Environmental Medicine

Abstract

The response of the head to impact in the posterior to anterior direction was investigated with live anesthetized and post-mortem primates. The study was conducted at the University of Michigan Transportation Research Institute (UMTRI)* under the sponsorship of the Motor Vehicle Manufacturers Association. 3-D motion and epidural pressures were experimentally measured. Interpretation of the results by simulating the tests using a 3-D mathematical model of the primate brain was done by Carley Ward. The results of the tests and the simulation are presented to demonstrate the differences found between live and post-mortem primate brains.

---

*At the time this study was conducted, the University of Michigan Transportation Research Institute was known as the Highway Safety Research Institute.

Index words: brain injury, finite method, impact biomechanics

INTRODUCTION

Experimental investigations in the biomechanics of head impact response have used human cadavers and animals as surrogates of the living human. The parameters commonly used for measuring mechanical response during direct impact have been: angular and translational accelerations, angular and translational velocity, displacements, deformation, and pressures. These parameters, once obtained, can then be used in developing and validating mathematical models of the head.

The unembalmed cadaver is chosen as an experimental model because its geometry and soft tissue distribution is similar to that of the live human. In addition, soft tissue damage can be directly related to injury patterns observed in clinical studies. The disadvantages of the cadaver include the inability to measure pathophysiological response and the susceptibility of some tissues to post-mortem degradation. Also, it has been reported (10) that during the contact of direct impact, the motion of the brain of the unembalmed cadaver is only partially constrained by the skull. The degree of constraint can depend on the time after death and preparation of the cadaver. This partial decoupling can have a marked effect on kinematic time histories of the head during and following impact.

Experimental impact testing of animals, in particular primates, provides basic neurophysiological information related to neuropathology. However, although the primate geometry is the most similar to man's, it is significantly different in anatomic soft tissue distribution and skull morphology. This can present severe problems when scaling test results to human levels. Ultimately these differences lead to complications in the very complex phenomena of head injury (9).

Mathematical models can be used to interpret the results from impact tests and they can also provide information at locations in the brain where measurements are impossible, giving a more complete picture of the response. Despite the difficulties in scaling from primates to humans, mathematical modelling is also helpful in extrapolating the animal findings to the human and allows for a minimum use of live animal subjects.

Techniques have been developed in the past few years for accurate determination of three-dimensional motion of the head (2,4,5,8,11), preparation of the unembalmed cadaver (6,7,10), and creation of biodynamic finite element models (13), for use in brain injury research. This article discusses the techniques used for conducting posterior to anterior head impacts with primates, while measuring three-dimensional motion and epidural pressure. In addition, the basic features of the mathematical model of the primate brain are given and the results of the simulation are used in interpreting the test results.

METHODOLOGY

Three-Dimensional Motion Determination

The UMTRI method used for measuring the three-dimensional motion of the head is based on a technique used to measure the general motion of a vehicle under a simulated crash (1). In the current application, three triaxial accelerometer clusters are affixed to a light-weight rigid magnesium plate (Figure 1) which is then solidly attached to the skull. The nine acceleration signals are used for the computation of the three-dimensional head motion.

With this method, it is possible to take advantage of the physical and geometrical properties, as well as the site of impact, in the design

of a system for measurement of 3-D motion. In the case of small primates, it is more convenient to design a specific system for each species and site of impact. A system was designed and constructed at UMTRI utilizing a light-weight magnesium plate to mount 9-accelerometers used for the Macaca primates. The prominent orbital ridges and dental plate found in this genus were used to install the rigid plate. Using a multi-point attachment scheme, it was secured at a maximum distance from the point of impact.

Epidural Pressure Measurement

UMTRI has developed a method for obtaining epidural pressures which employs a fluid-filled catheter tip Kulite model MCP-55-5F pressure transducer with an accuracy of .6 psi. A small circle of scalp is removed and a Stryker bone-coring tool is used to make a hole in the skull with a 3 mm circular bit. This circular bit (Figure 2) with an adjustable set-screwed collect, was especially machined to enable the technicians to core into the skull in small increments, thus preventing a dura damaging breakthrough.

A magnesium coupling device (Figure 2) is screwed into the cored and tapped hole. It is anchored into place using a quick-setting acrylic molded around the base. A 5 cm section of rubber tubing is then clamped onto the top of the device and Dow Corning dielectric gel (silicon fluid) is injected into the tubing to act as a coupling media between the dura and pressure sensitive tip of the pressure transducer. A pressure transducer is then inserted, and secured at proper depth (14).

Finite Element Models

The tests are simulated using three-dimensional mathematical models of the monkey brain. Small primate models of this type were first described in Ward et al., 1978 and are shown in Figures 3 and 4. The soft brain tissue and fluids are modeled using isoparametric brick elements. The internal membranes, the falx and tentorium, are modeled using membrane elements. The input to the model is linear acceleration, angular velocity computed from the 9-accelerometers. In other words, the models are mathematically forced to move just as the head moved in the test. Computational improvements reported in Ward et al., 1979 were incorporated into the models. In addition to these changes, simulation of this test series required two new modifications. A 20 cm cervical cord was added for some simulations and the Poission's ratio was varied from .499 to .4999, varying the effective compressibility of the brain. In each simulation, the model was scaled to approximate the size and weight of the actual brain.

TEST SUBJECT PREPARATION

Five primate subjects were used in these experiments: four Macaca Mulatta and one Macaca Assamensis (Table 1). Prior to acquisition, the Macaca subjects had been used in one or more pharmacological research projects. Each subject was impacted only once. Both kinematic and injury response were evaluated. The impacts of three Macacas were conducted on post-mortem subjects. Upon termination, they were stored in a cooler at 4° for 48 hours before testing. Living Macacas were used in the two final experiments. The protocol for post-mortem primates was less complex than for that of the live anesthetized primates, which is outlined below.

On the morning of the experiment, the primate was given an intramuscular injection of ketamine and sodium pentobarbital was injected through the saphena parva vein at a dosage of 25 mg/kg to effect. The upper body was prepared and weight and biometrical measurements were taken with a standard anthropometer, a stainless steel tape, a ruler and a Homes Model 51 HH beam scale. Body measurements are illustrated in Figure 5; head measurements in Figure 6. Using a cauterizing scalpel, the scalp and muscle mass were removed from the frontal bone. The screws used to moor the nine-accelerometer plates and the epidural pressure transducer skull fitting are screwed into place. Quick-setting acrylic was molded around the pressure transducer fitting and 9-accelerometer moorings of this acute implant. Figures 7 and 8 show the positioning of the instrumentation on the skull. Eye and ear x-ray targets were positioned and two orthogonal head x-rays (x-z and y-z views) were taken.

The primate was then taken to the impact laboratory and positioned. Three triaxial units were fastened to the nine-accelerometer plate. Silicon fluid was injected into the pressure coupler, thus removing all air and allowing a fluid connection with the pressure transducer which was then inserted. The test was run with all data recorded on analogue tape.

RESULTS

Two live animal and three post-mortem animal tests were conducted. There were no significant injuries observed in the central nervous system. Stress (or pressure) and displacements were computed versus time throughout the brain. Stresses at the transducer locations were plotted in Figure 9-15: (stress is equal to pressure but opposite in

sign). When two computed traces are shown on one curve, the transducer location was between two elements. In Figures 9-15 the measured pressures were converted to stress and plotted for comparison with the computed values. The results show the following: To simulate the live animal response (Figures 9 and 10) the model must have a Poisson's ratio of .4999 and a 20 cm cervical cord. To simulate the post-mortem animal response (Figures 11-13), the model must have a lower Poisson's ratio (ν=.499) and no cervical cord. When a cervical cord was added in this post-mortem animal simulation, higher negative stresses resulted, and the correlation degrades as shown in Figure 14. When a value of .4999 is used for ν (value for live animal) in the post-mortem animal simulations, the measured response tends to lag the computed values. Even when .499 is used, the measured value lags the computed value, Figures 12 and 13. When .499 (value for the post-mortem animal) is used for ν in the live animal simulation, the computed response lags the measured response as shown in Figure 15. If the cord is removed in the live simulations, the computed stresses are much too low (Figure 16). The maximum computed stress in Figure 16 is -110 kPa and the measured stress is -390 kPa (Figure 9). There is a factor of 4 differences between the measured and computed values when the cord is eliminated. Even when the cord is included, the computed results lag the measured stresses (Figures 9 and 10). This delay is a limitation of the existing model. The model does not simulate neck compression, it only simulates the inertial motion of the cord. If neck compression were included in the model, the stress initiated by the cord should be shifted in time.

DISCUSSION

The response of the post-mortem brain is slower and more damped than that of the live brain. The post-mortem brain is in effect more compressible than that of the live brain and as a result, pressure (stress) in the post-mortem brain is lower than what would occur in the live brain under similar impact conditions. This is possibly due to post-mortem degradation and the fact that fluid is easily expelled out of the brain into the unpressurized arteries and into the CSF space surrounding the cervical cord. The unpressurized cervical canal and flaccid neck in the post-mortem animal may uncouple the cervical cord from the brain response. The results show that the cord can increase the pressures in the brain by a factor of 4. The difference is greatest when the head undergoes S-I acceleration because the effect of the cervical cord is lacking in the post-mortem animal.

To investigate the effects of fluid in the arteries and CSF system, a third type of test is needed. Similar tests on pressurized (CSF and arterial pressurization) post-mortem animals should be simulated, and compared to the results in this report.

SUMMARY

The dynamic response of live and post-mortem brains in situ varies considerably. Response time was faster in the live brain than in the post-mortem. Damping and effective compressibility were more noticeable in the post-mortem brain. Response magnitude for some head acceleration was higher in the live animal brain. Cervical cord and brain response seemed to be coupled in the live brain, while uncoupled in the post-mortem brain. Lastly, the model implies that one effect of the spinal cord is to increase the intracranial pressure in the impact response.

ACKNOWLEDGEMENTS

The authors gratefully acknowledge the contributions of Nabih M. Alem, Joseph Benson, Jean Brindamour, Marvin Dunlap, Garry Holstein, Dikran Kashkashian, and Valerie A. Moses. Thanks is also due to Drs. Daniel H. Ringler and Bennett J. Cohen from the University of Michigan Unit for Laboratory Animal Medicine for their veterinary assistance.

In conducting the research described in this report, the investigators adhered to the "Guide for the Care and Use of Laboratory Animals," as prepared by the committee on Care and Use of Laboratory Animals of the Institute of Laboratory Animal Resources, National Research Council.

REFERENCES

1. Bartz, J A, Butler, F E. Passenger Compartment with Six Degrees of Freedom. Auxiliary Programs to "Three-Dimensional Computer Simulation of a Motor Vehicle Crash Victim," Final Technical Report for DOT Contract No. FH-11-7592. 1972
2. Becker, E, Willems, G. An Experimentally Validated 0-D Inertial Tracking Package for Application in Biodynamic Research. Proc. 19th Stapp Conf., 1975.
3. Ewing C L, Thomas D J, Lustick L, Becker E, Willems G, and Muzzy III W H. The Effect of the Initial Position of the Head and Neck on the Dynamic Response of the Human Head and Neck to -Gx Impact Acceleration. Paper 751157. Proc. 19th Stapp Conf., 1975.
4. Ewing, C L, Thomas, D J. Torque versus Angular Displacement Response of Human Head to -Gx Impact Acceleration. Paper 700976. Proc. 17th Stapp Conf., 1973.
5. Ewing, C L, Thomas, D J. Human Head and Neck Response to Impact Acceleration. Naval Aerospace Medical Research Laboratory Detachment, New Orleans, Monograph 21, 1972.
6. Fayon A, Tarriere C, Walfisch G, Got C, and Patel A. Fayon A. Thorax of 3-Point Belt Wearers During a Crash (Experiments with Cadavers). Proc. 19th Stapp Conf., 1975.
7. Nahum A M, Smith R W. An Experimental Model for Closed Head Injury. Proc. 20th Stapp Conf., 1976.
8. Padgaonkar A J, Krieger K W, King A J. Measurements of Angular Acceleration of a Rigid Body Using Linear Accelerations. ASME Preprint-75-APMO., 1975.

9. Patrick L M. Head Impact Protection. Head Injury Conference Proceedings. (Edited by Caveness, W.F. and Walker, A.E.) 1966; 4:41-48-48.

10. Stalnaker R L, Melvin J W, Nusholtz, G S, Alem, N M, Benson J B. Head Impact Response. Proc. 21st Stapp Conf., 1977.

11. Thomas D J. Specialized Anthropometry Requirements for Protective Equipment Evaluation. AGARD Conference Proceedings No. 110, Current Status in Aerospace Medicine, Glasgow, Scotland, 1972.

12. Ward C C, and Nahum A. Correlation Between Brain Injury and Intracranial Pressures in Experimental Head Impact. Presented at the International Conference on Impact Trauma, Gotenburg, Sweden. 1979. Navy Report TM No. 51-79-15.

13. Ward C C, Nikravesh, P E, Thompson, R B. Biodynamic Finite Element Models Used in Brain Injury Research. Journal of Aviation, Space and Environmental Medicine, 1978, Vol. 49, No. 1.

14. Nusholtz G S, Melvin J W, and Alem N M. Head Impact Response Comparisons of Human Surrogates. Proc. 23rd Stapp Conf., 1979.

FIGURE CAPTIONS

1. 9-Accelerometer Plate
2. Coring Tool and Epidural Coupling Device
3. Finite Element Monkey Brain Model
4. Monkey Brain Mid-Sagittal Plane Model
5. Identification of Body Measurements
6. Identification of Head Measurements
7. Instrumentation Reference Frame and Location of the Three Triaxial Accelerometer
8. Pressure Transducer Instrumentation
9. Test 78A209 (cervical cord present)
10. Test 78A241 (cervical cord present)
11. Test 78A202 (cervical cord not present)
12. Test 78A208 (cervical cord not present)
10. Test 78A206 (cervical cord not present)
14. Test 78A208 (cervical cord present)
15. Test 78A209 (cervical cord present)
16. Test 78A209 (cervical cord not present)

Table 1. Primate Biometrics

Test No.	Age (years)	Weight (Kg)	Sex
78A232	15-20*	6.9	Male
78A236		8.2	Male
78A238		8.2	Male
78A239		8.2	Male
78A241		10.6	Male

*The exact age of the subjects is unknown. However, they were all all adult specimens ranging in age from 15 to 20 years.

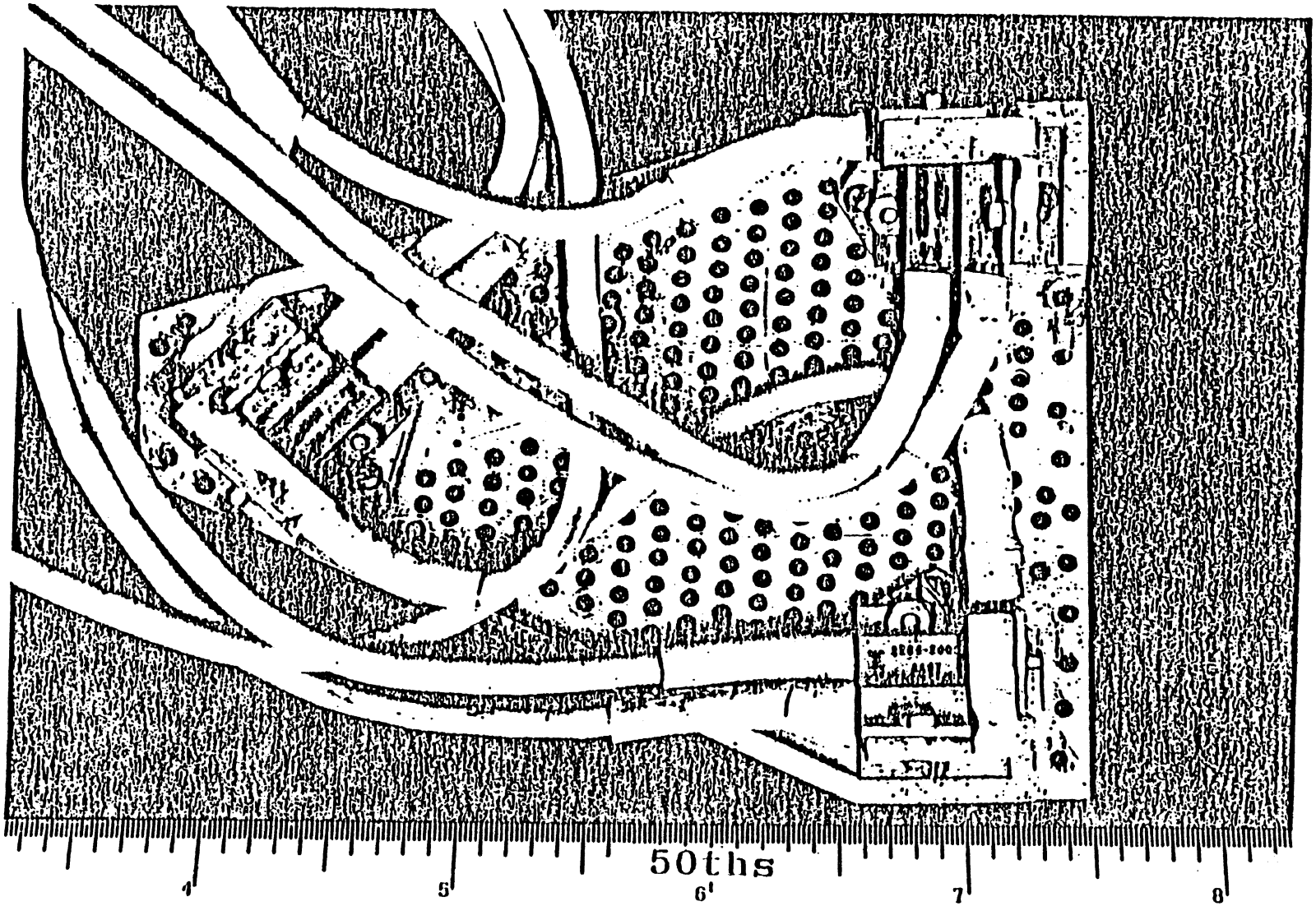

FIGURE 1. 9-Accelerometer Plate

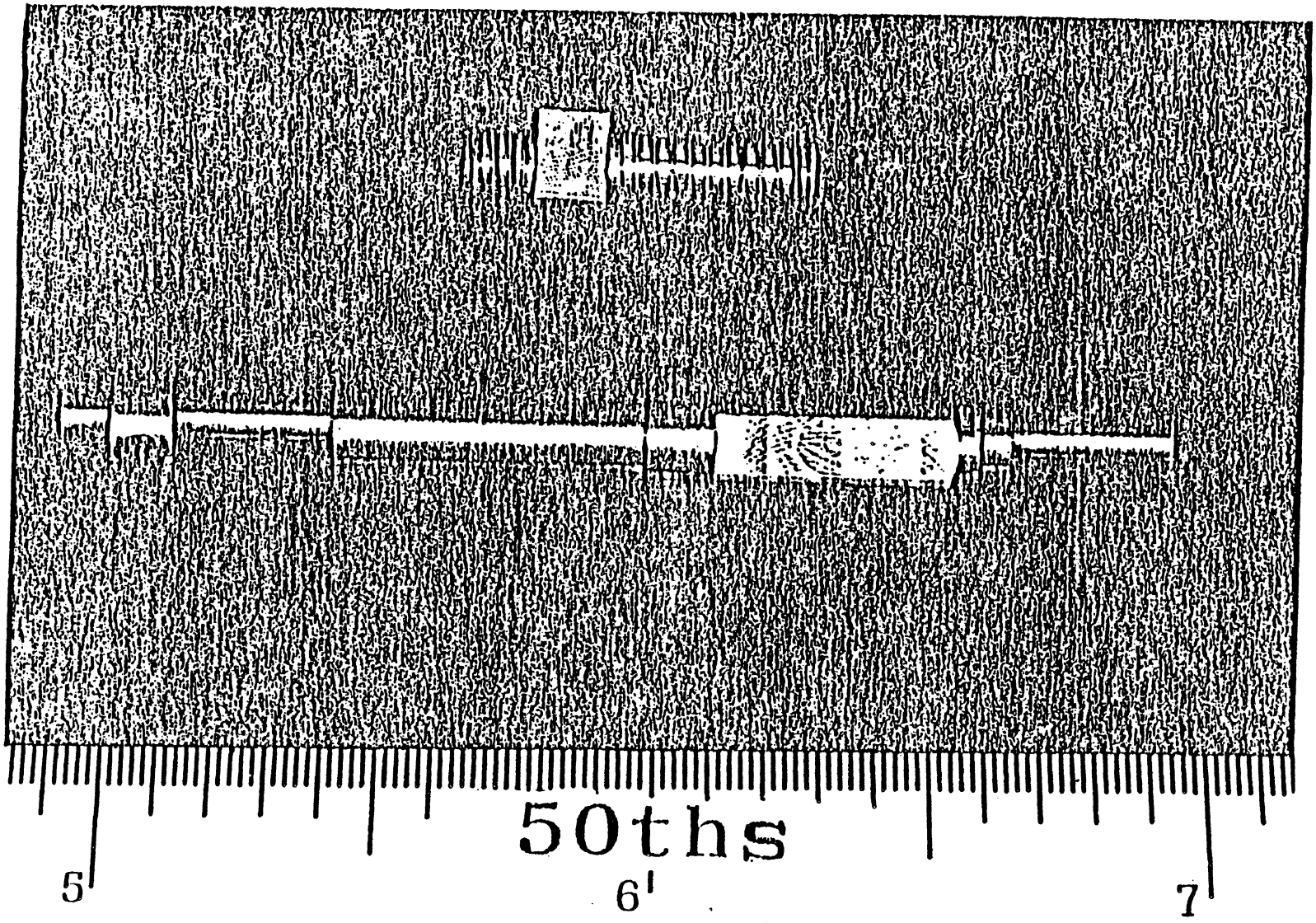

FIGURE 2. Coring Tool and Epidural Coupling Device

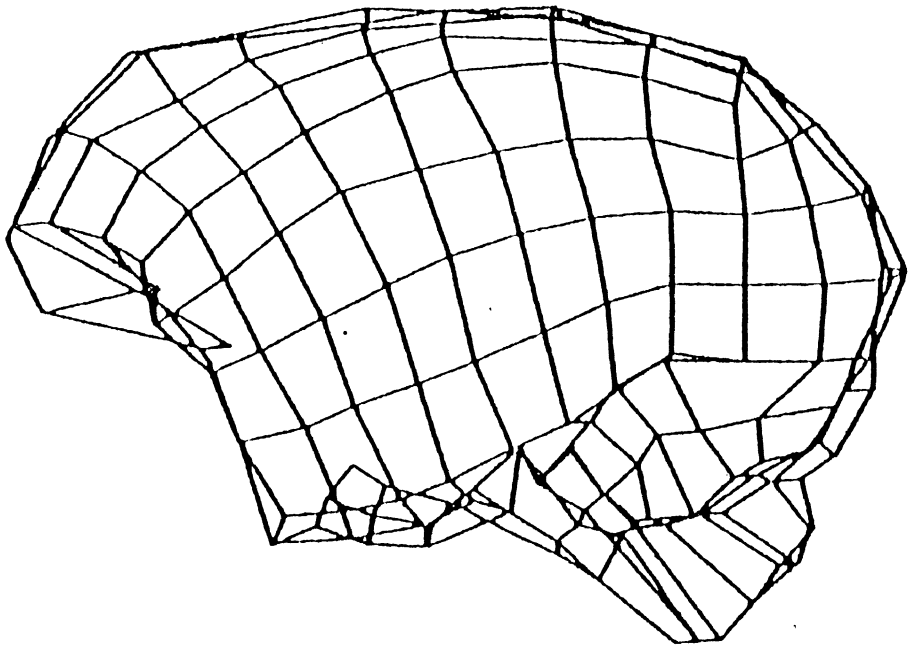

FINITE ELEMENT MONKEY BRAIN MODEL

FIGURE 3

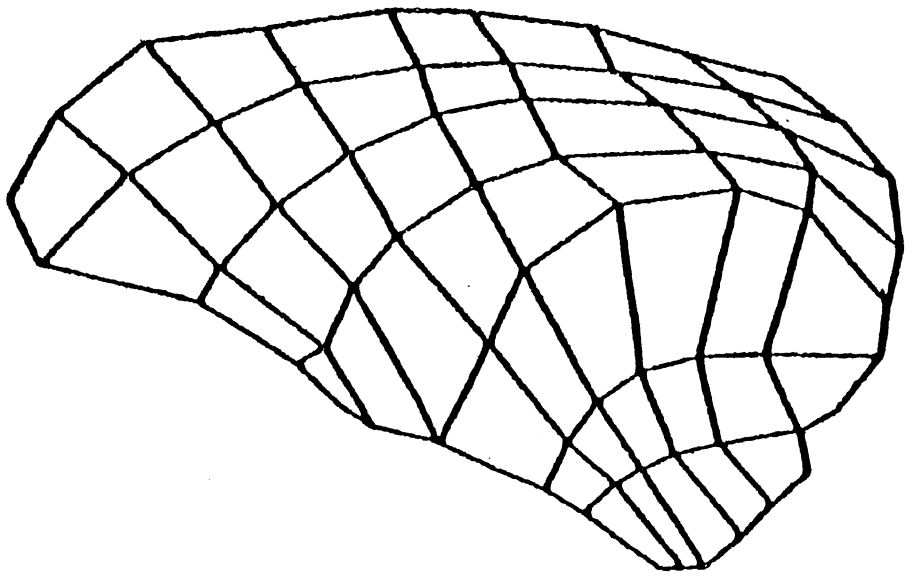

Figure 4. Monkey Brain Mid-Sagittal Brain Model

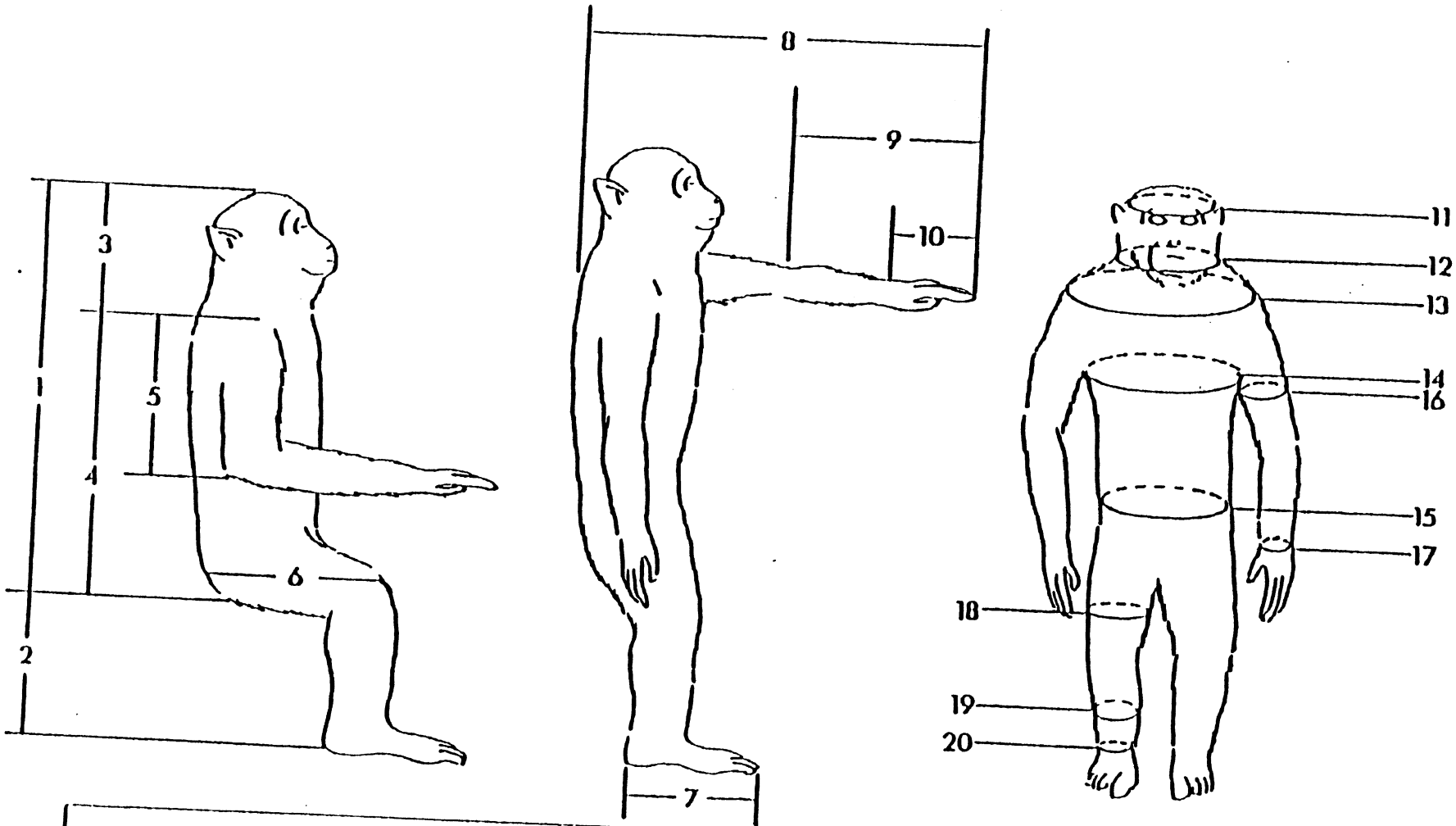

LOCATION OF BODY MEASUREMENTS

LENGTH IN CM.				CIRCUMFERENCE IN CM.			
1. BUTTOCK - CROWN		6. BUTTOCK - KNEE		11. HEAD		16. BICEPS	
2. POPLITEAL HEIGHT		7. HEEL - TOE (Foot)		12. NECK		17. WAIST	
3. TOP HEAD - TOP SHOULDER		8. TOTAL ARM REACH		13. SHOULDER		18. THIGH (Mid shaft)	
4. ACROMIAL HEIGHT		9. FOREARM - HAND		14. CHEST		19. CALF	
5. SHOULDER - ELBOW		10. HAND		15. WAIST (HIP)		20. ANKLE	

REMARKS

FIGURE 5. Identification of Body Measurements

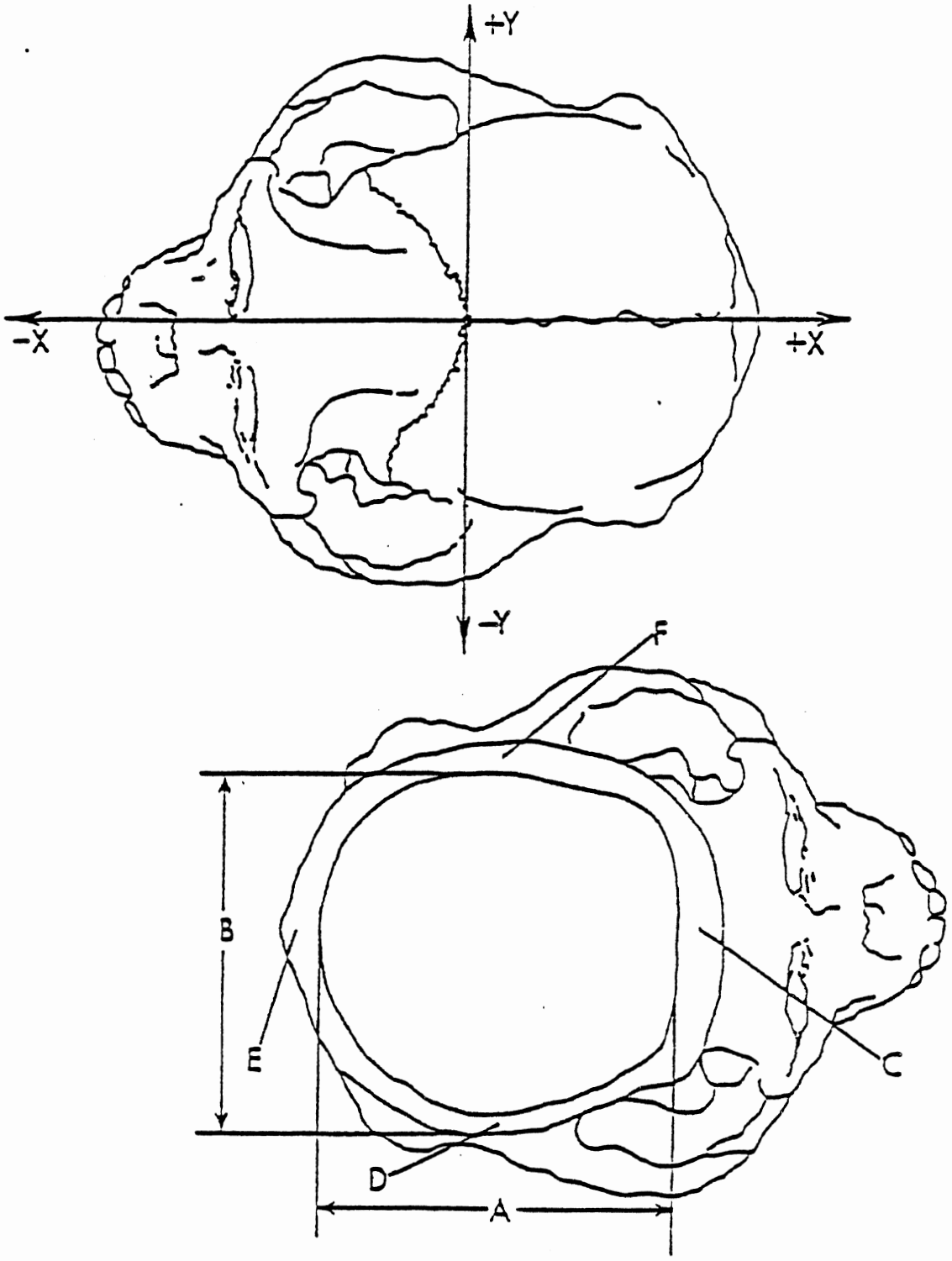

Skull Inside Length A _____ Skull Thickness at Pt. D _____

Skull Inside Width B _____ Skull Thickness at Pt. E _____

Skull Thickness at Pt. C _____ Skull Thickness at Pt. F _____

FIGURE 6. Identification of Head Measurements

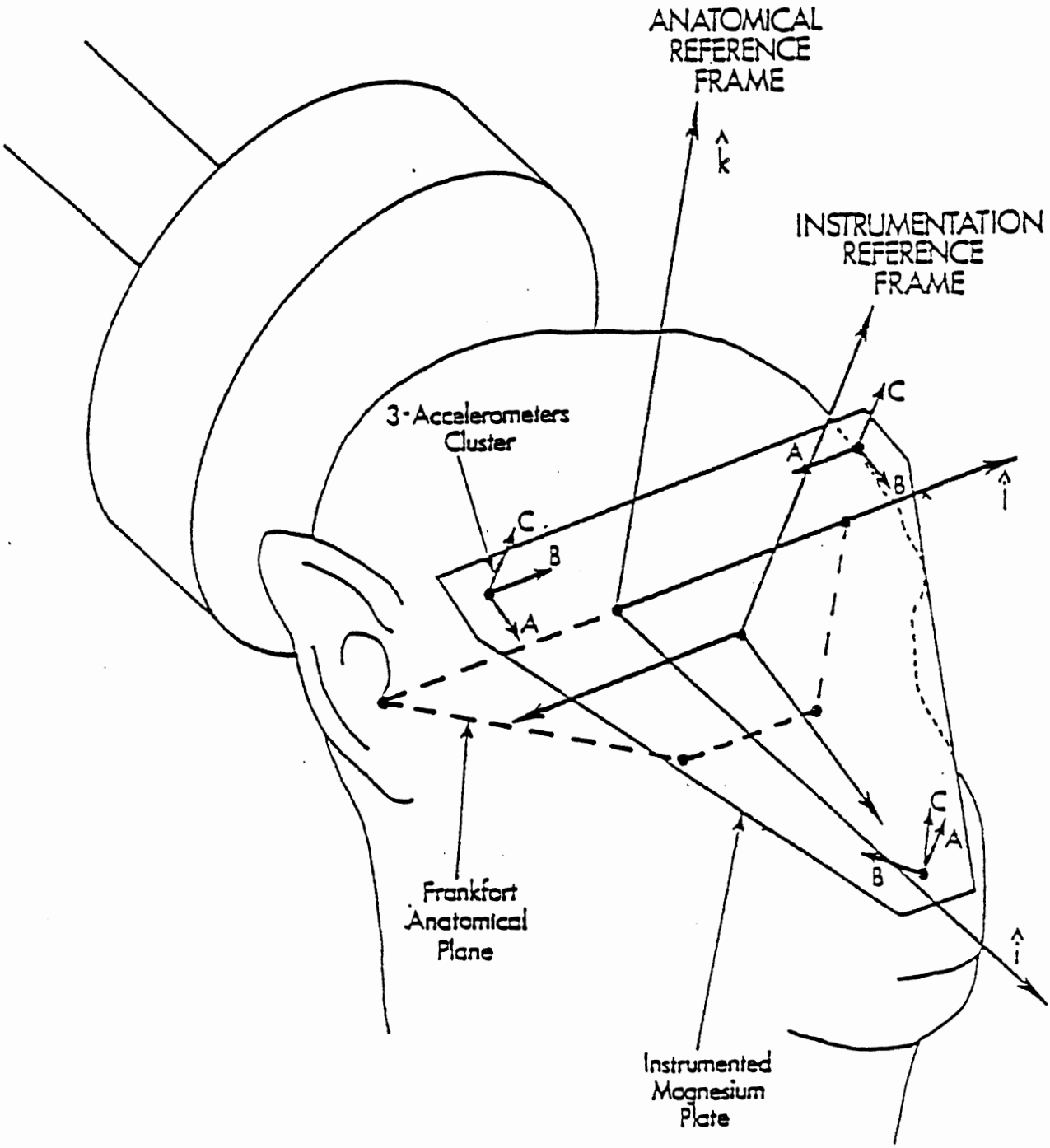

FIGURE 7. Instrumentation Reference Frame and Location of the Three Triaxial Accelerometer

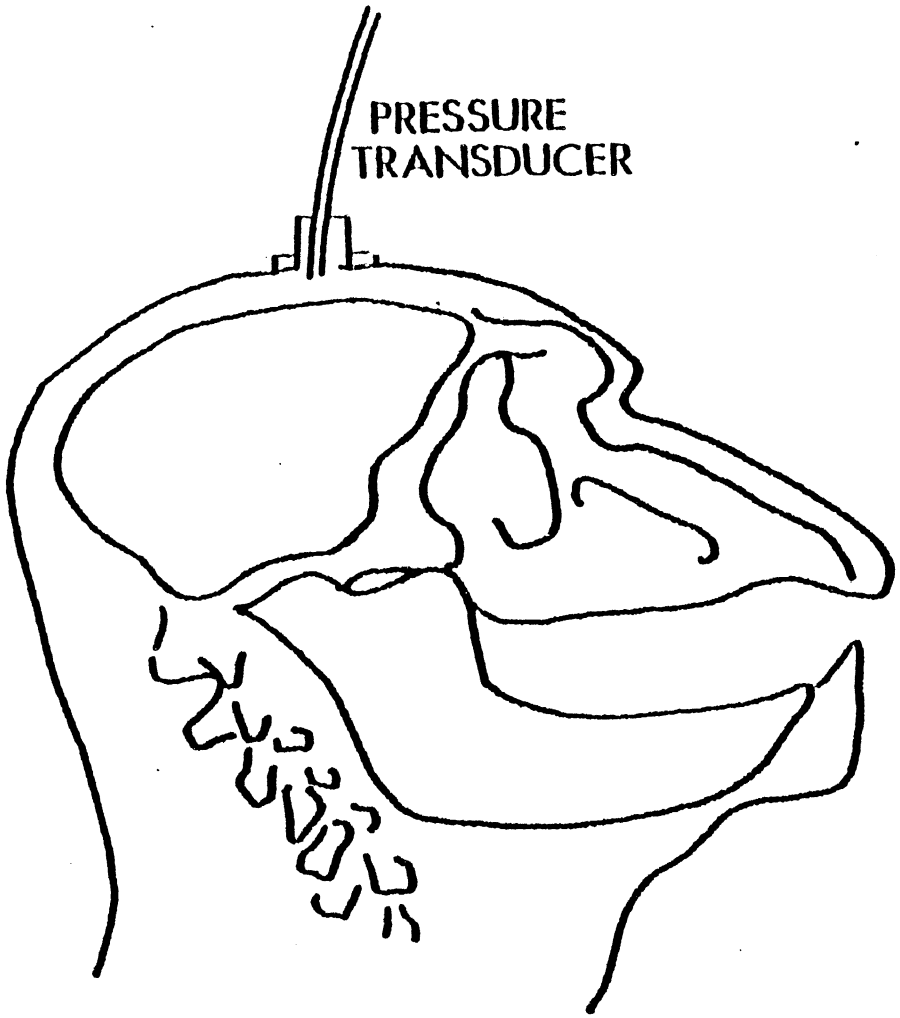

Figure 8. Pressure Transducer Instrumentation

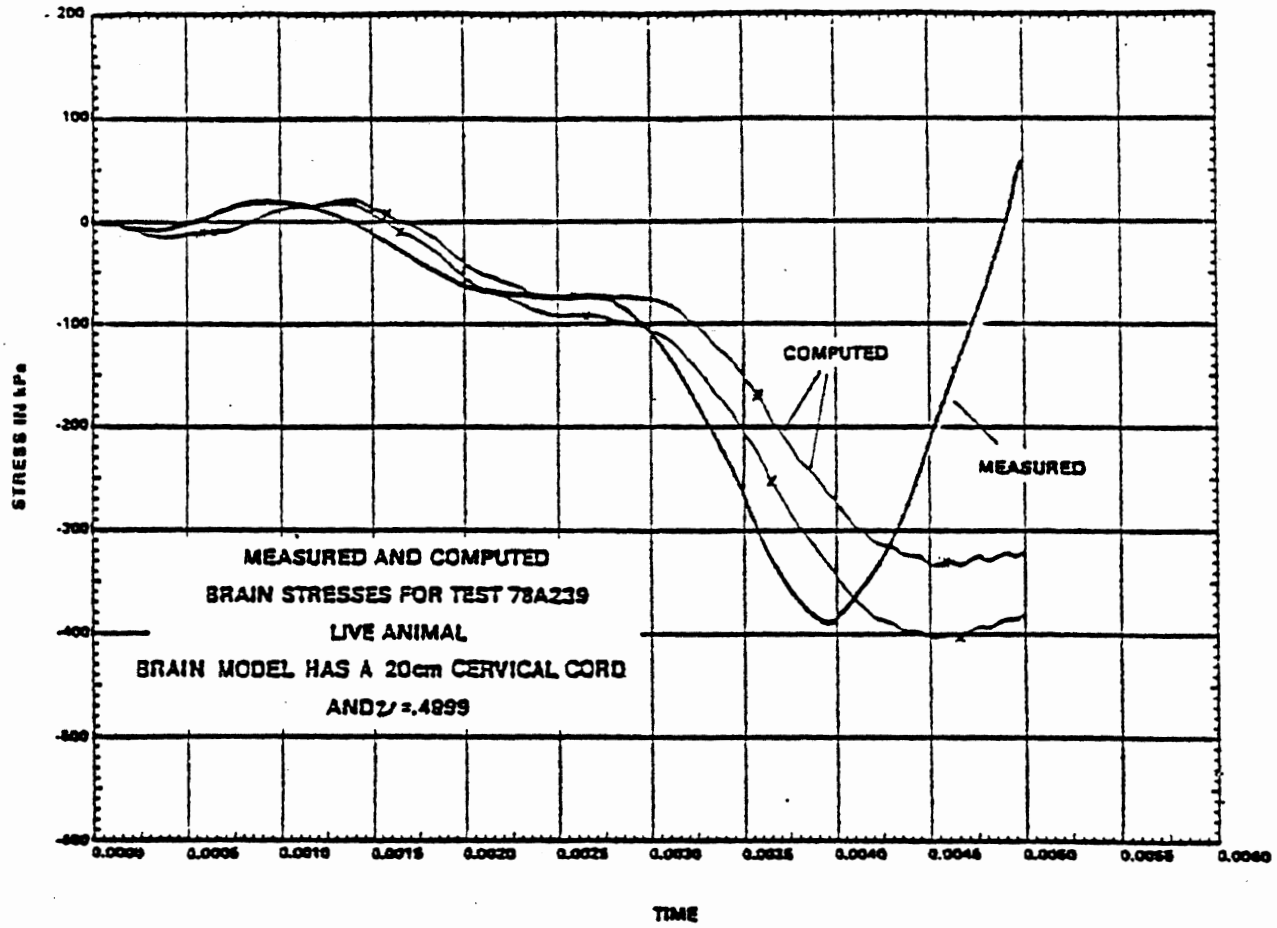

FIGURE 9 - Test 78A239 (cervical cord present)

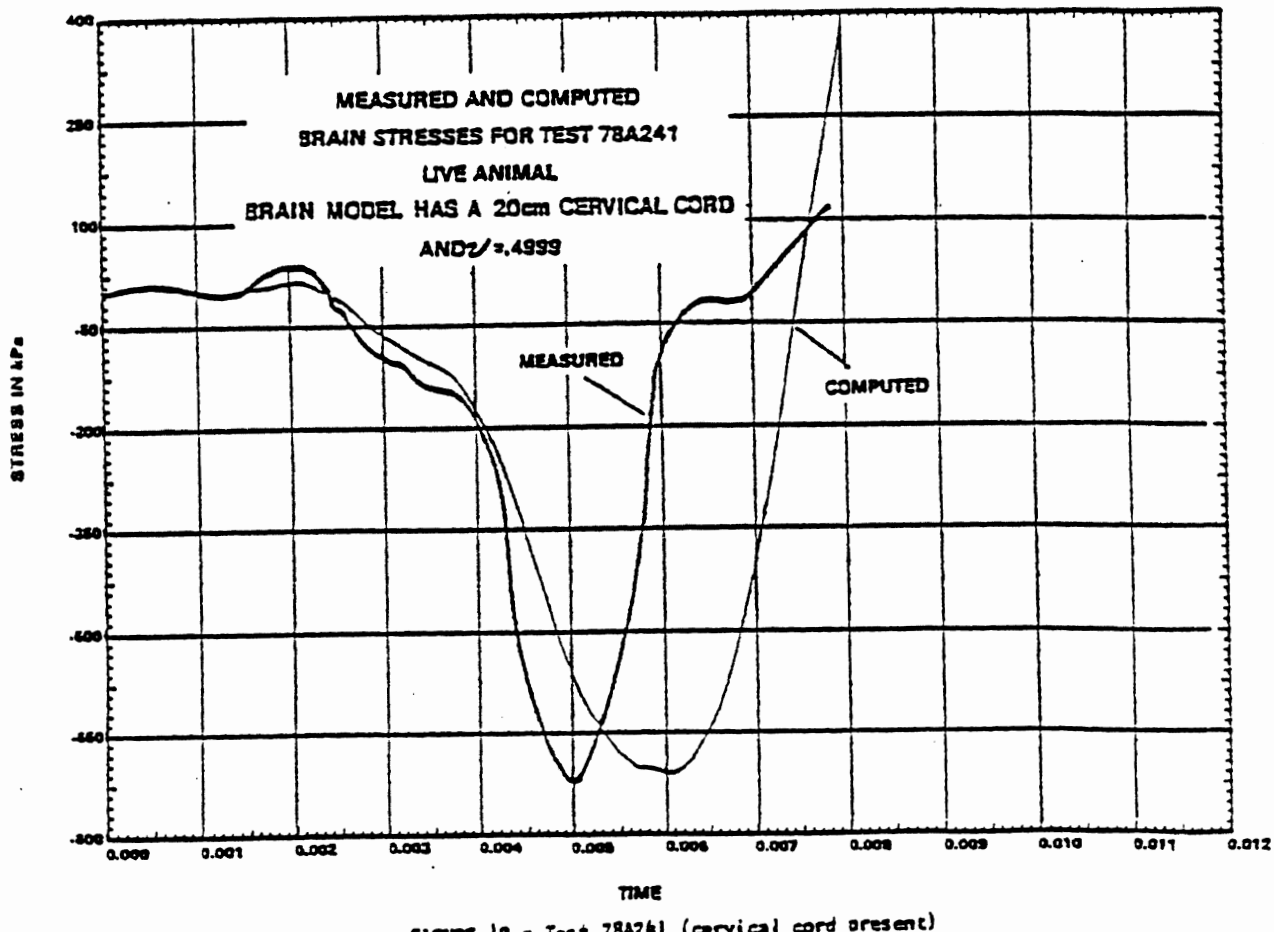

FIGURE 10 - Test 78A241 (cervical cord present)

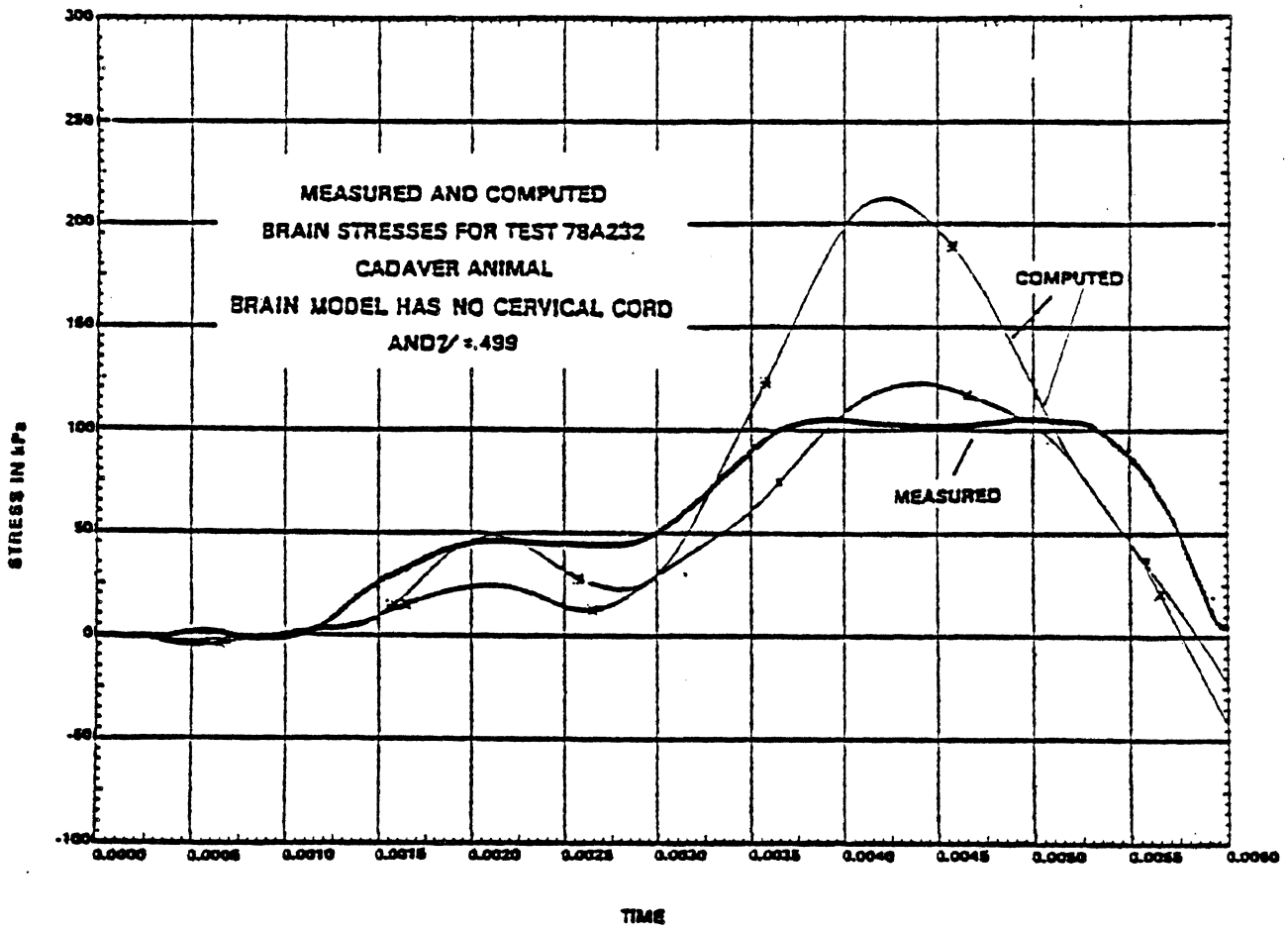

FIGURE 11 - Test 78A232 (cervical cord not present)

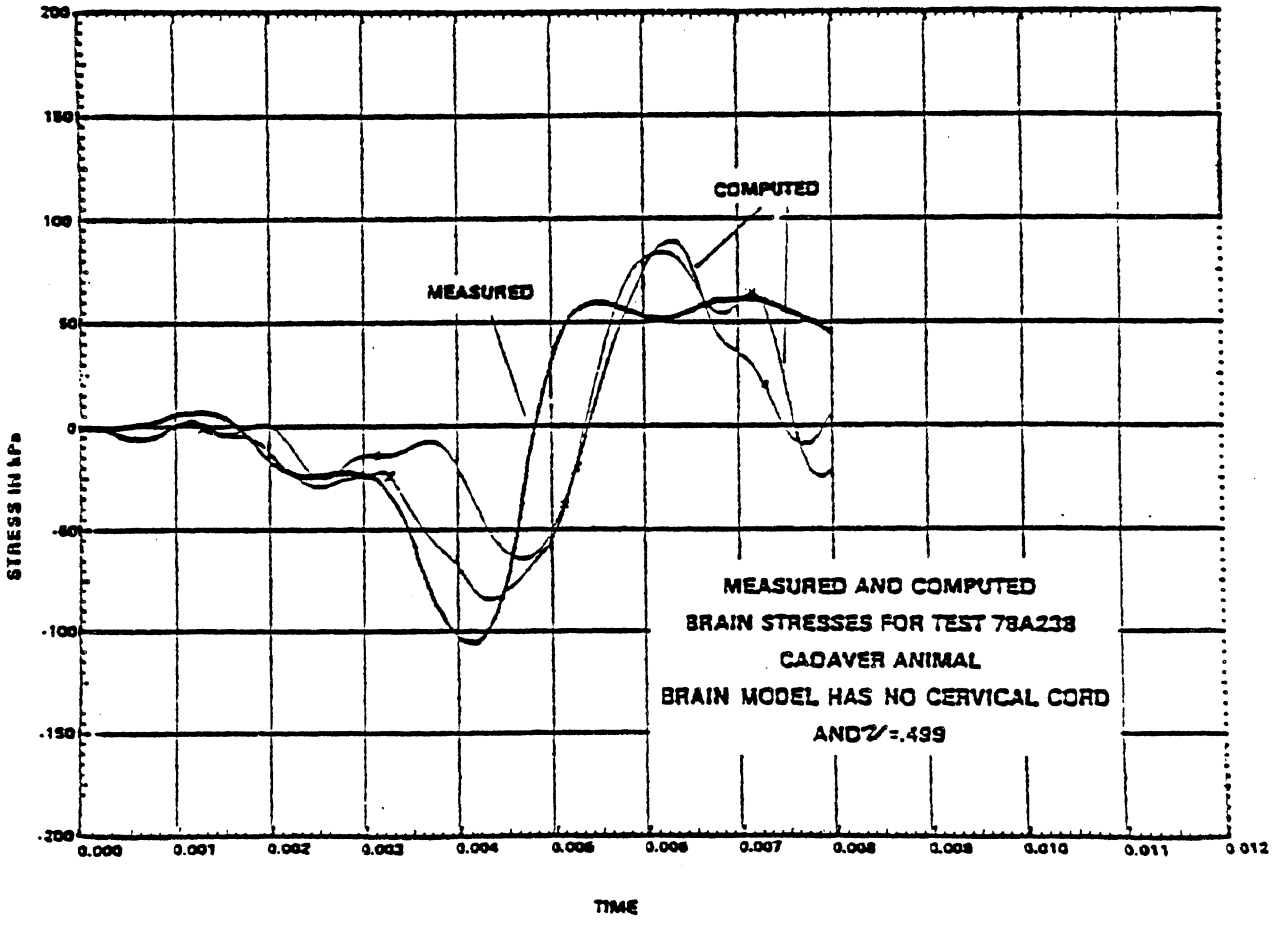

FIGURE 12 - Test 78A238 (cervical cord not present)

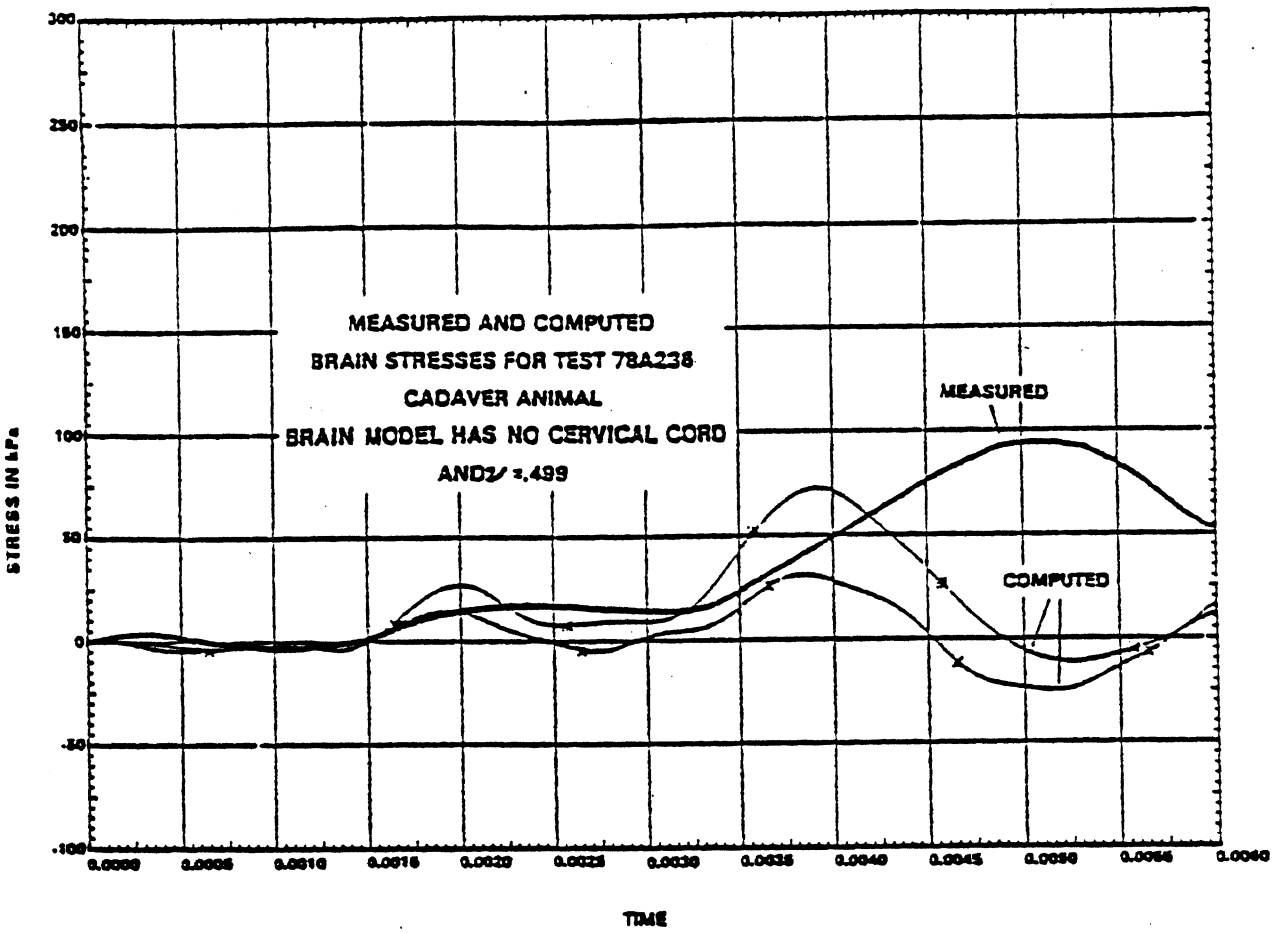

FIGURE 13 - Test 78A236 (cervical cord not present)

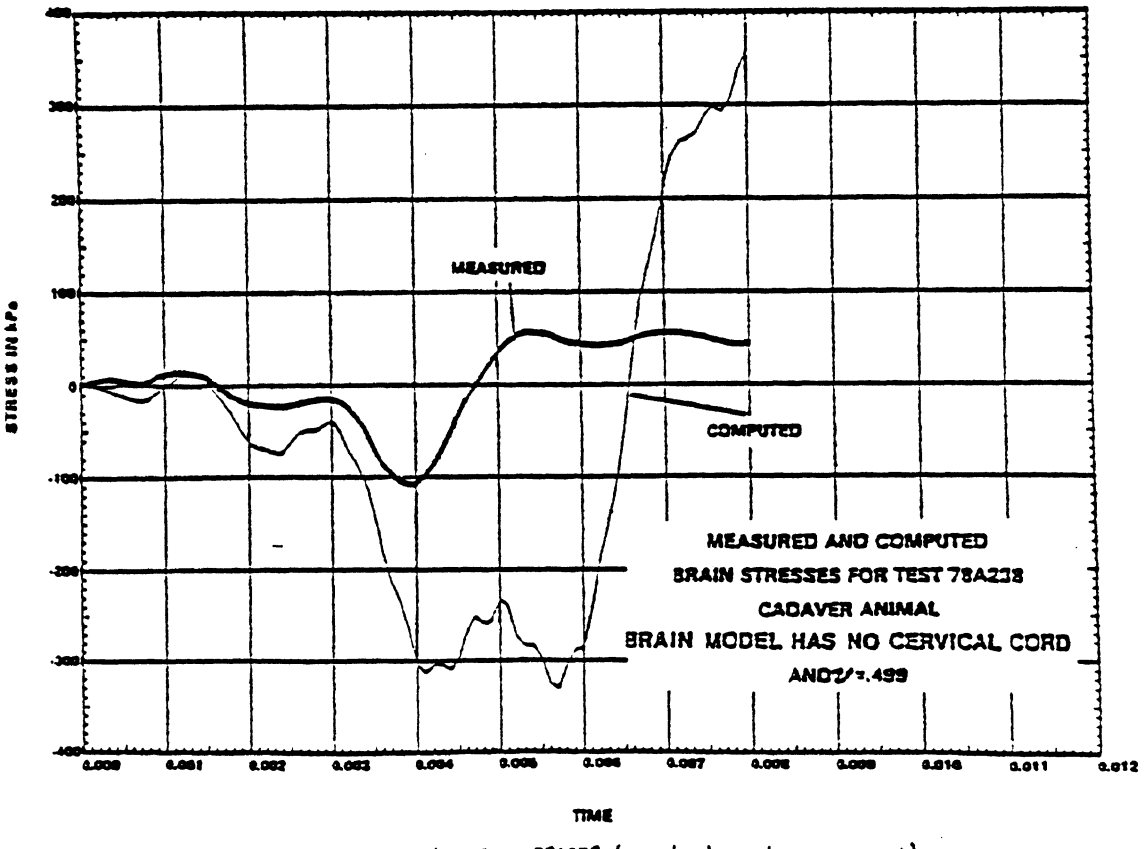

FIGURE 14 - Test 78A238 (cervical cord present)

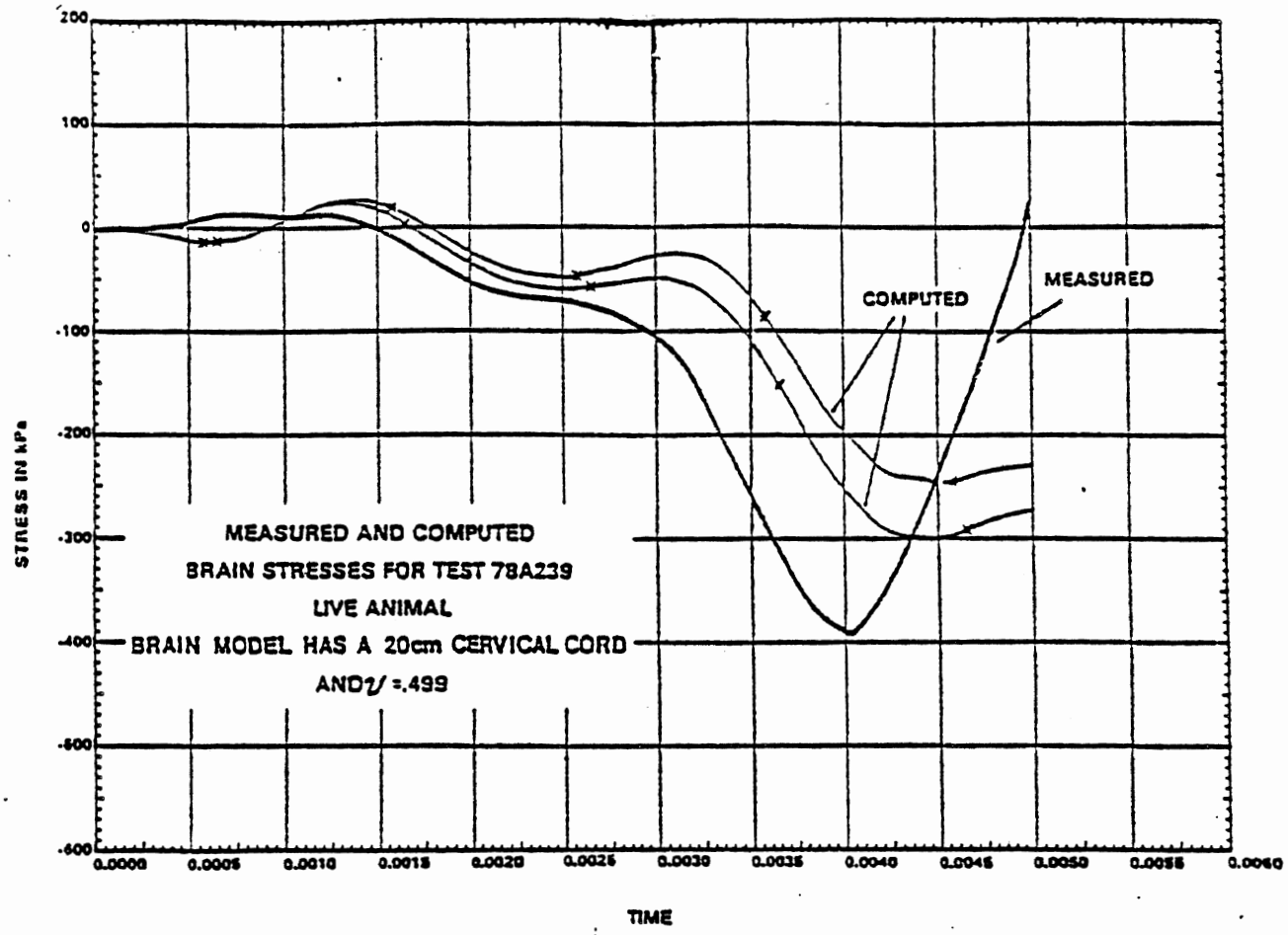

FIGURE 15 - Test 78A239 (cervical cord present)

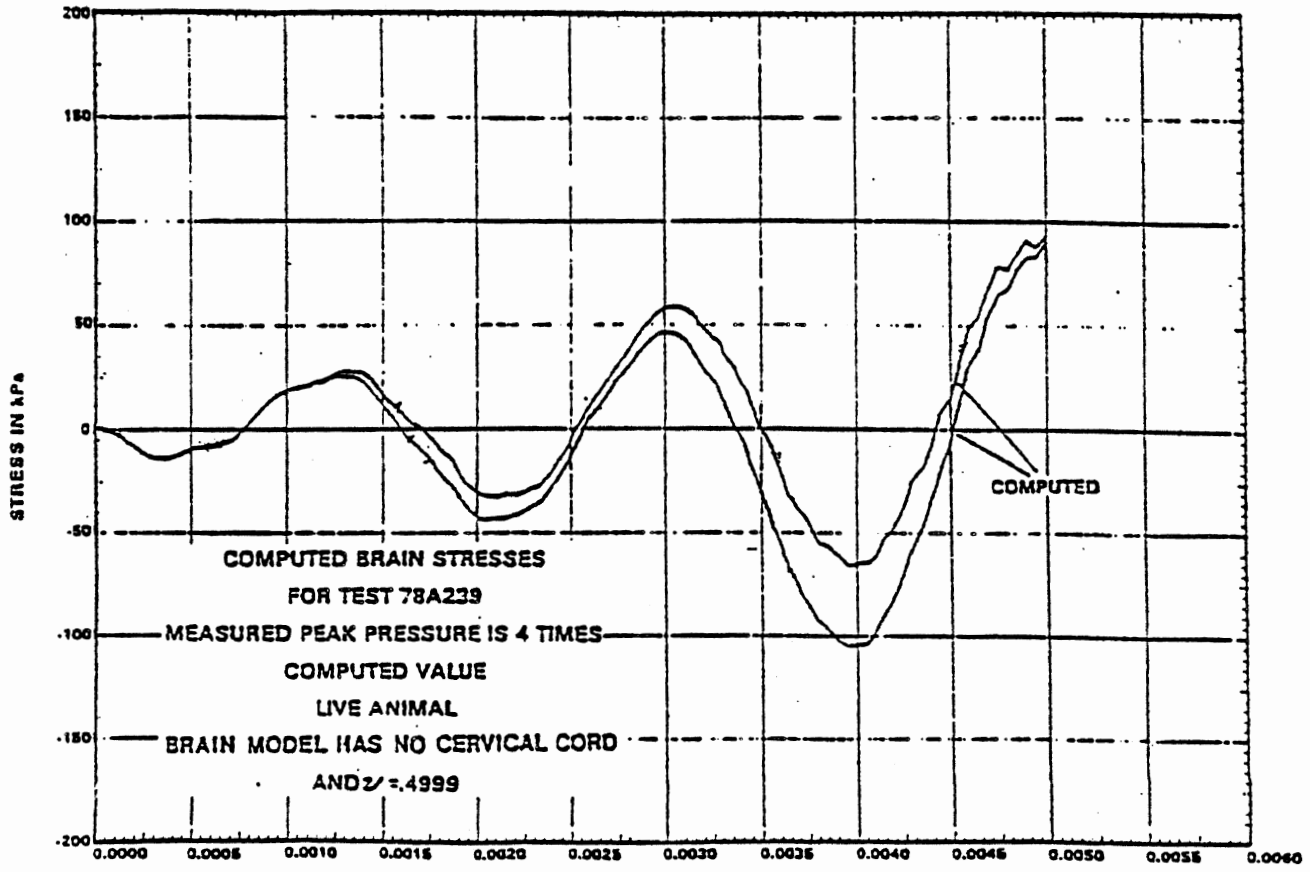

APPENDIX G: "Critical Limitations on Significant Factors in Head Injury Research"

Title: Critical Factors in Head Injury Research

Authors: Guy S. Nusholtz, Patricia S. Kaiker, and Richard J. Lehman

Correspondence Address: Guy S. Nusholtz
Biosciences Division
Transportation Research Institute
University of Michigan
2901 Baxter Road, Room 406
Ann Arbor, MI 48109

Submitted to: 30th Stapp Car Crash Conference Proceedings

ABSTRACT

The response of the head to blunt impact was investigated using anesthetized live and repressurized- and unrepressurized-postmortem Rhesus. The stationary test subject was struck on the occipital by a 10 kg guided moving impactor. The impactor striking surface was fitted with padding to vary the contact force-time characteristics. A nine-accelerometer system, rigidly affixed to the skull, measured head motion. Transducers placed at specific points below the skull recorded epidural pressure. The repressurization of postmortem subjects included repressurization of both the vascular and cerebrospinal systems. The results of the tests demonstrate that: 1) Head impact and injury response are complex phenomena and require careful attention to the experimental techniques used to obtain the impact data as well as the interpretation of the results; 2) A set of initial conditions has been found such that the repressurized-postmortem Rhesus was more similar in head impact response to the anesthetized Rhesus than was the unrepressurized-postmortem Rhesus (in terms of the transfer function relationships between tangential acceleration and epidural pressure; 3) In terms of subarachnoid hemorrhage in the *medulla-pons* area associated with skull fracture, the repressurized-postmortem and anesthetized Rhesus were similar in injury response; 4) The initial position of the head-neck system was a critical factor associated with the brain-cerebrospinal fluid system's response to head impact; 5) The thermodynamic response (fluid vaporization) of the head-brain system was an important consideration when the impact produced significant tension; and 6) No relationships could be found between injury and negative pressures equal to one atmosphere.

INTRODUCTION

EXPERIMENTAL IMPACT TESTING of human surrogates provides useful information about biomechanics data-gathering techniques, the general nature of human injury mechanisms, kinematic and injury response parameters, and injury tolerance values. One body region that has been investigated through the use of the human surrogate is the head (1,5,6,9,11-21,23,25-28)[1]. In an attempt to reduce the injuries that can occur as a result of blunt impact to the head, researchers have used a number of procedures to deliver a calibrated amount of energy to the head of a human surrogate. The resulting kinematic motion and injury, then, potentially, can be used to obtain information to address head injury mechanisms, providing that the experimental techniques (including the choice and preparation of a surrogate) are appropriate.

A major difficulty in the investigation of head trauma is designing kinematic experiments which minimally interfere with the biological and physical systems being studied, yet produce results that are accurate and can be used effectively to describe the physical phenomena which occur as a result of impact. The goal of such research is a paradigm of injury mechanisms which corresponds well with clinically observed trauma. Some understanding of head injury mechanisms as a result of dynamic biomechanics blunt impact experiments has resulted from relating kinematic parameters to injury modes. Correlations of this type do not always imply causation, however, because of 1) the possibility of several injury mechanisms; 2) experimental inaccuracy associated with the choice of human surrogate; and 3) misinterpretation of the results as a consequence of faulty assumptions often compounded by errors which occur because of experimental techniques that do not (or do not or accurately) measure the needed parameters. In this regard it is critical to understand the problems and limitations associated with the experimental techniques used in head injury research.

For example, the Head Injury Criterion (HIC) is derived from an acceleration response. One method of obtaining the acceleration information required to generate the HIC for human surrogates, such as the cadaver, is to mount

[1]Numbers in parentheses refer to references found at the end of the text.

accelerometers on the skull and assume that rigid body motion will occur during impact. In a previous study in which a nine-accelerometer array was rigidly affixed to the human cadaver skull, it was concluded that three-dimensional rigid body motion of the head is not well defined during a "severe" head impact when motion is measured by accelerometers affixed to the skull (14). In such impacts, skull deformation was interpreted by the nine-accelerometer array as an angular and linear acceleration not directly related to rigid body motion. Therefore, when the skull deformations (with or without skull fracture) were significant in severe impacts, the three-dimensional motion derived from the nine-accelerometer array could only be used to estimate the motion of the rest of the skull. This result implies that even when three-dimensional motion (consisting of both linear and angular motion) is obtained using a nine-accelerometer array in one lab, the results may not be closely comparable to those obtained in other labs, and may not truly represent the desired three-dimensional motion. Different experimental techniques (e.g. transducer, mount type, and location) employed for obtaining the three-dimensional motion may produce uncomparable data. Therefore, the HIC may not be well-defined for "severe" head impacts.

A second example of the problems that can be associated with experimental techniques comes from human cadaver blunt crown head impact observations (13). The experimental testing showed that peak forces are not a good indicator of cervical spine injury. Forces as high as 3000 lbs did not produce cervical spine injury in some tests, while those as low as 500 lbs produced spinal cord transection in others. The faulty assumption that the kinematic parameter of peak force correlates with injury to the cervical spine allowed an experimental design in which a negative correlation between peak force and trauma to the cervical spine was obtained.

A third example comes from the earlier observations made on some of the Rhesus being presented in this report (12,16). A particular set of initial conditions produced a very significant difference in blunt head impact response between the unrepressurized-postmortem and anesthetized Rhesus. However, we realize that other sets of initial conditions may produce a very small difference between these two models. It should be possible to conduct two series of impact experiments having two slightly different sets of initial conditions in which one set would produce no difference in response between the unrepressurized-postmortem and anesthetized Rhesus, while the other would produce a significant difference. Therefore, it would be possible for two different labs using seemingly similar procedures to produce contradictory conclusions. Such variations in conclusions seem to stem from a lack of knowledge of the subtle aspects of head impact.

The purpose of the dynamic biomechanics blunt head impact study being reported here was to qualify, in a limited sense, a few of the critical factors associated with head trauma research. In particular, the effects of fluid vaporization, the effects of material flow through the foramen magnum, the potential effects of the postmortem state, the effects of vascular and cerebrospinal repressurization on the postmortem state, the effect of the initial positioning of the head and neck on kinematic/injury response, and the effect of constraints on results produced by experimental techniques (i.e. measurement and analytical procedures) will be discussed. The techniques developed and used by the University of Michigan Transportation Research Institute (UMTRI) for measuring three-dimensional head motion and epidural pressure will be presented. Anesthetized live Rheus and repressurized- and unrepressurized-postmortem Rhesus were subjected to a posterior-to-anterior direction occipital head impact. The results presented here are in addition to, build upon, and are compared with those previously presented (See 12,14,16) so that they cover the data from related research programs conducted over the last nine years.

METHODOLOGY

The methods and procedures that were used in this dynamic biomechanics trauma research are outlined below. Additional information about the methods and procedures can be found elsewhere (2,3,8,12,14,16).

Impact Testing - The twenty-two laboratory animal subjects used in these experiments were obtained by UMTRI from the University of Michigan Unit for Laboratory Animal Medicine. The Rhesus were instrumented using procedures similar to those used to instrument human cadaver subjects. A nine-accelerometer array was rigidly affixed to the skull and epidural pressure transducers were used to document pressure changes. The cerebrospinal and vascular systems of five of the postmortem Rhesus were repressurized.

Using the pneumatic impacting device with a 10 kg impactor (12), ten anesthetized and twelve postmortem Rhesus were each subjected to a single head impact to the occipital region. Preliminary findings on five of the anesthetized Rhesus and seven of the postmortem Rhesus have been presented earlier elsewhere (12,14,16).

The impactor surface was a 10.2 cm rigid metal plate padded with 2.5 cm Ensolite. The impactor force transducer assembly consisted of a Kistler 904A piezoelectric load washer with a Kistler 804A piezoelectric accelerometer mounted internally for inertial compensation.

A specially designed timing unit was used to synchronize the impact events during each test, such as the release of the striker and activation and de-activation of the high-speed photographic equipment. The impact conditions between tests were controlled by varying the impact velocity and the initial positioning of the test subject. The piston velocity was measured by timing the pulses from a magnetic probe which sensed the motion of targets in the piston.

Triaxial Acceleration Measurement - An interrelated set of three triaxial accelerometers (the nine-accelerometer array) recorded head accelerations. The accelerometers were either Endevco 2264-2000 piezoresistive ones or Kistler Model 8694 piezoelectric ones.

Epidural Pressure Measurements - Epidural pressures were measured with piezoelectric Kulite model MCP-055-5F catheter tip pressure transducers or with Endevco 8507-50 pressure transducers.

Cineradiographs - High-speed cineradiographs were taken of the impact events at 400 or 1000 frames per second. The UMTRI high-speed cineradiographic system (24) consists of either a Photosonics 1B or Milliken high-speed 16 mm motion-picture camera which views a 5 cm diameter output phosphor of a high-gain, four-stage, magnetically focused image intensifier tube, gated on and off synchronously with shutter pulses from the motion-picture camera. A lens optically couples the input photocathode of the image intensifier tube to x-ray images produced on a fluorescent screen by a smoothed direct-current x-ray generator. Smoothing of the full-wave rectified x-ray output is accomplished by placing a pair of high-voltage capacitors in parallel with the x-ray tube. The viewing field for these experiments was between 20-by-40 cm (See Figure 1).

Data Handling - All transducer time-histories (i.e. impact force, impact acceleration, epidural pressures, nine head accelerations) were recorded unfiltered on a Honeywell 9600 FM Tape Recorder with an EMI multiplex unit or a Honeywell 7600 FM Tape Recorder. A synchronizing gate was recorded on all tapes. The analog data on the FM tapes were played back for digitizing through proper anti-aliasing analog filters. The analog-to-digital process for all data resulted in a digitial signal sampled at 6400 Hz equivalent sampling rate.

Test Synopsis

Twelve head impacts were conducted on postmortem Rhesus. Upon termination, they were stored in a cooler at 4°C for 72 hours (78A232-79A260)/5 days (85R005-86R015)/3 weeks (85R002) prior to testing. Anesthetized Rhesus were used in the other ten experiments. The protocol for postmortem animals, presented in detail elsewhere (12), was less complex than that for the anesthetized laboratory animals, which is outlined below.

Test Subject Preparation - The animal was first anesthetized with an injection of ketamine and then maintained with ketamine and sodium pentobarbital by means of a catheter with a three-way valve which had been inserted into the *long saphenous* vein of the leg. An airway was established to aid breathing when necessary. Then the subject was weighed and measured. Next, using a cauterizing scalpel, the scalp and muscle mass were removed from the frontal bone and the screws used to secure the epidural pressure transducer coupling devices were screwed into place. Then the nine-accelerometer plate was installed. Next, a strain gauge was attached to the skull bone to record the vibrations of the skull during impact for the purpose of estimating their effect on the accelerometer signals.

Eye and ear x-ray targets were positioned and the Rhesus was transported to the x-ray room where two head x-rays (x-z and y-z views) were taken, or were taken later as part of the necropsy examination (85R002-86R015). The subject was then taken to the impact laboratory and placed in an erect sitting position with its posterior side towards the impactor, so that the line of impact was in the mid-sagittal plane in the posterior-anterior direction.

Subject Positioning - The subject was held in place with paper tape which secured the body under the armpits, suspending the head and torso from an overhead hoist. The test subjects were impacted at the occiput. In tests 78A232 and 78A234 the eyes were on a horizontal line through the impact site, thus the estimated center of mass was below the line of impact. In tests 78A236 and 78A239 the eyes were raised to a point slightly above a horizontal line through the impact site, thus the line of impact was through the estimated center of mass. In tests 78A238 and 78A241 the eyes were raised higher than the previous two tests, thus the center of mass was above the line of impact (See Figure 2). Tests 79A249-79A260 were similar to those just de-

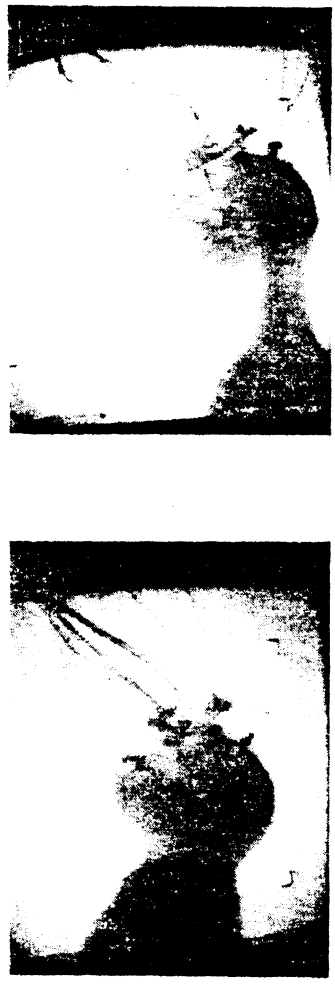

FIGURE 1:
CINERADIOGRAPH PHOTOS OF INITIAL POSITIONING OF THE HEAD-NECK: NECK-STRETCHED (TOP) AND NECK-RELAXED (BOTTOM)

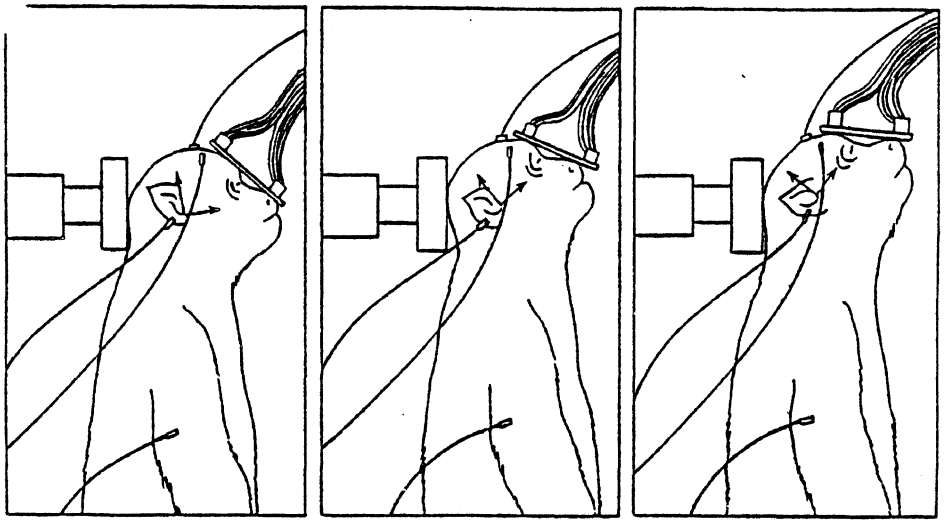

FIGURE 2: SUBJECT POSITIONING - CENTER OF HEAD MASS RELATED TO LINE OF IMPACT

scribed except that higher impact energy levels were used and the subjects were positioned so that impact occurred through the estimated center of mass. For Tests 85R002-86R015, the eyes were raised, positioning the subjects similar to those in Tests 79A238 and 78A241.

The initial positioning of the subject also included placing the subject in either the neck-stretched (86R011-86R013) or neck-unstretched position (78A232-79A260, 85R002-8, and 86R014-15). See Figure 1 for illustration of the initial positioning of the head-neck. To achieve the neck-stretched configuration, strings were placed through the ears and the subject was suspended by an overhead hoist so that approximately one-half of its entire body weight was supported by the neck. To achieve the neck-unstretched configuration, paper tape was used to support the head via the overhead hoist so that only one-half the weight of the head and none of the remaining body weight was supported by the neck.

After the positioning, three triaxial accelerometer clusters were fastened to the nine-accelerometer plate. Silicon fluid was injected into the pressure couplings, thus removing all air, and the pressure transducers were inserted. The subject was positioned in front of the impactor and stabilized with paper tape. All of the transducers were then connected, cabled, and checked for continuity and function.

Figure 3 shows the basic dynamic biomechanics impact test setup. One and a half-hours after impact for Tests

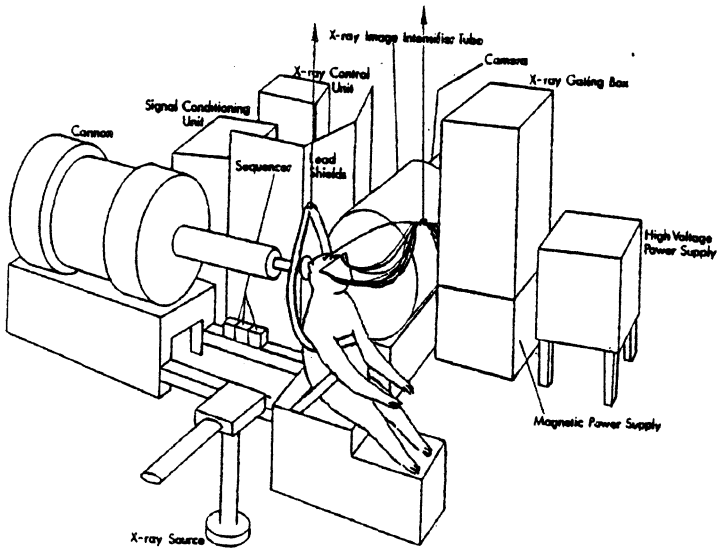

FIGURE 3: TEST SET-UP FOR DYNAMIC BIOMECHANIC IMPACT TESTING

85R002-86R015, one hour after impact for tests 78A232-78A249, and eight hours after impact for tests 79A251-79A260, a 5 ml dose of Uthol (concentrated, unpure sodium pentobarbital) was injected via the hind leg intravenous catheter to euthanize the anesthetized laboratory animal subjects. A bilateral pneumothorax was performed to insure termination.

Surgical Instrumentation

Nine-Accelerometer Head Plate - To install the nine-accelerometer plate the scalp was removed from the frontal bone over the orbital ridges. Five metal self-tapping screws were attached firmly to the skull through small pilot holes drilled into the orbital ridges and into the dental plate above the canine teeth. Quick-setting acrylic plastic was molded around each of the screws and the nine-accelerometer plate mount, embedding the mount in the plastic. After the acrylic set, the plate was rigidly attached to the skull. The orientation of the plate in this position is shown in Figure 4.

Since it was necessary to determine the instrumentation frame's exact location and orientation in relation to the anatomical frame, a three-dimensional x-ray technique was developed. Two orthogonal radiographs of the instrumented head were taken. The procedure required the identification of four anatomical landmarks (i.e. two superior edges of the auditory meati and two infraorbital notches) with four distinguishable lead pellets, plus the identification of four lead pellets inlaid in the plate which defined the instrumentation frame. The targets were digitized and related using a mathematical algorithm which resolved the instrumentation center of gravity into the translations and rotations of the anatomical center of gravity.

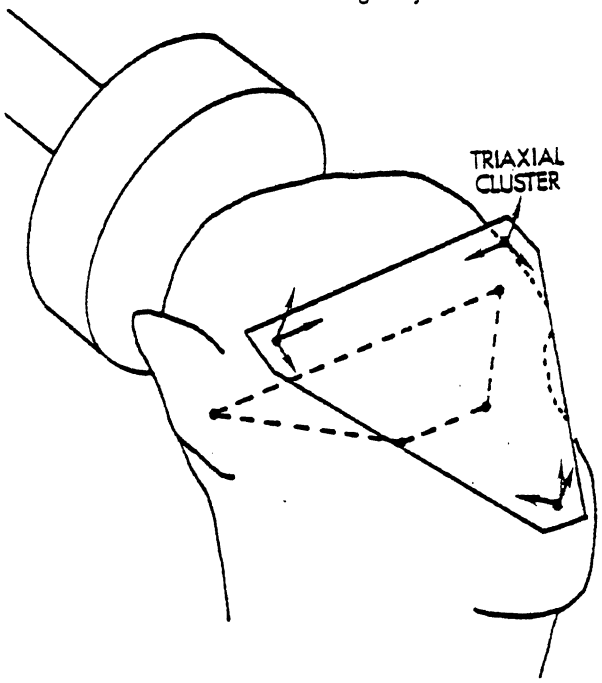

FIGURE 4: ORIENTATION OF NINE-ACCELEROMETER PLATE

Epidural Pressure Couplings - After the scalp was removed from a small area over the right and left sides of the frontal bone, the surface was sanded. Next, two 0.3 cm diameter holes were drilled using a Stryker bone coring tool, the bone was tapped, and the *dura mater* was punctured under each hole. Aluminum couplings for the pressure transducers were screwed into the tapped holes (See Figure 5). Dental acrylic was applied around the base of the couplings to secure them.

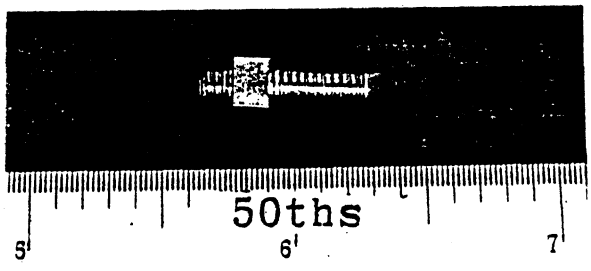

FIGURE 5:

EPIDURAL PRESSURE COUPLER

Strain Gauge - A Micro-Measurement Type EA-13-015Y-120 strain gauge rosette was bonded with M-bond 200 cyanoacrylate adhesive to the surface of the frontal bone, anterior to the bregma over the sagittal sinus. After the leads were soldered, the rosette and leads were covered and sealed with M-coat D paint.

Cerebrospinal Repressurization - A small hole was cored in the L6 lumbar vertebra and a Foley catheter was inserted under the dura of the spinal cord such that the balloon of the catheter reached mid-thorax level (See Figure 6). The point at which the catheter passed through the lamina of the sixth lumbar vertebra was sealed with plastic acrylic. To check fluid flow through the ventricles, saline was injected through the Foley catheter until it rose to the top of the couplings. The couplings were capped until the pressure transducers were attached in the impact laboratory. Dow Corning dielectric gel (silicon fluid) was injected into each coupling device to act as a securing medium. The pressure transducer was then inserted and secured at the proper depth. Then a setup radiograph was made of the head.

Vascular Repressurization - The common carotid artery was located at a point in the neck and an incision was made. String was looped around the common carotid and it was cut lengthwise. A polyethylene tube was inserted into the ascending common carotid, and the descending common carotid was ligated. The opposite common carotid was located and similarly cut. Vascular flow was checked. Then a Millar catheter tip pressure transducer was inserted into the ascending common carotid to the point of its branching with the external carotid, secured with tape and sewn in place (See Figure 7).

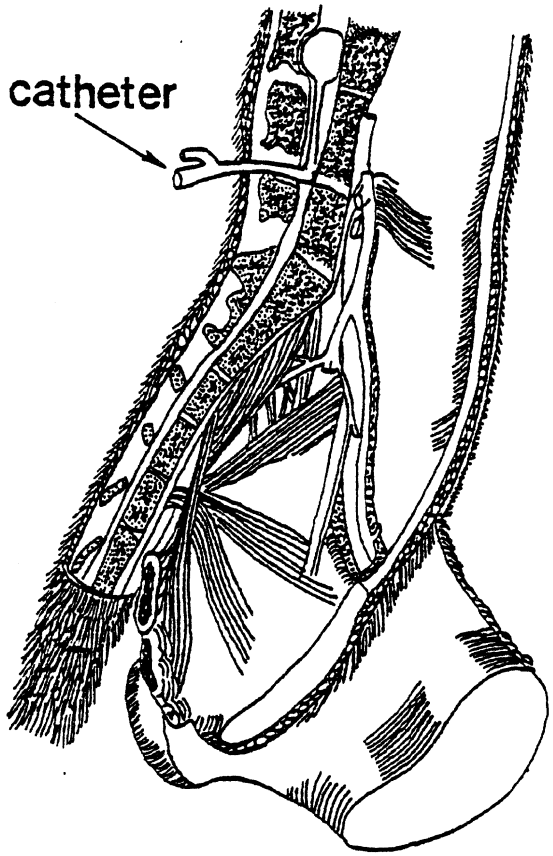

FIGURE 6:
RHESUS CEREBROSPINAL
REPRESSURIZATION CATHETER

METHOD OF ANALYSIS - The techniques used to analyze the results are outlined below. Additional information can be found elsewhere (2,3,8,12,14,16,24).

Tangential Acceleration - As the head moves through space, any point on the head generates a path in space. In head injury research interest is in the description of the path of the anatomical center and in events which occur as it moves. A very effective tool for analyzing the motion of the anatomical center as it moves along a curved path (a one-dimensional manifold) in space is the concept of a moving frame (2,3,19,24). The Frenet-Serret frame (3), which contains information about the motion embedded in the frame field, is one such moving frame. The tangential acceleration is a quantity which can be derived from the Frenet-Serret frame. The tangential acceleration is the rate of change of the absolute value of the velocity of a given moving point. It is co-directional with the velocity. The tangential acceleration is a very useful tool when working with one-dimensional transfer functions. A short summary of this method is included elsewhere (14).

Transfer Function Analysis - With blunt impacts, the relationship between a transducer time-history at a given point and the transducer time-history of another given point of a system can be expressed in the frequency domain through the use of a transfer function. A Fast Fourier Transformation of simultaneously monitored transducer time-histories can be used to obtain the frequency response functions of the impact force and accelerations of remote points. Once obtained, a transfer function of the form:

$$(Z)(i\omega) = (\omega)\ \mathbf{F}[F(t)]/\mathbf{F}[A_t(t)]$$

can be calculated from the transformed quantities where ω is the given frequency, and $\mathbf{F}[F(t)]$ and $\mathbf{F}[A_t(t)]$ are the Fourier transforms of the impact force and tangential acceleration of the point of interest, at the given frequency. This particular transfer function is closely related to a mechanical transfer impedance (8). Mechanical transfer impedance is defined as the ratio between the harmonic driving force and the corresponding velocity of the point of interest, and is a complex-valued function which can be described simply by its magnitude and phase angle. In addition to a transfer function relating force to velocity, a transfer function can be generated which relates the response of one point in the system to another point in the system, the relationship being expressed in the frequency domain. Analogous to mechanical impedance, a Fast Fourier Transformation of simultaneously monitored transducer time-histories from any two points in the system can be used to obtain the frequency response functions relating those two points. In the case of an acceleration and a pressure, such as tangential acceleration and epidural pressure, a transformation of the form:

$$(X)(i\omega) = \mathbf{F}[A_t(t)]/\mathbf{F}[p(t)]$$

can be calculated from the transformed quantities, where ω is the given frequency, and $\mathbf{F}[A_t(t)]$ and $\mathbf{F}[p(t)]$ are the Fourier transforms of the tangential acceleration time-history and the epidural pressure time-history, respectively. The data will be presented in terms of a transfer function generated for tangential acceleration divided by epidural pressure.

Transfer Function Spectral Coherence - The coherence function $Cxy^2(\omega)$ is not strictly speaking a transfer function, but instead is a measure of the quality of a given transfer function at a given frequency.

$$Cxy^2(\omega) = |Gxy(\omega)|^2 / (Gxx(\omega)Gyy(\omega))$$

where $Gxx(\omega)$ and $Gyy(\omega)$ are the power spectral densities of the two signals, respectively. Power Spectral Density is a Fourier Transform of each signal's auto-correlation. $|Gxy(\omega)|^2$ is the Cross-Spectral Density function squared. Cross-Spectral Density is the Fourier Transform of the cross-correlation of the two signals and ω at the given frequency. By definition, $0 \leq Cxy^2(\omega) \leq 1$. Values of $Cxy^2(\omega)$ near 1 indicate that the two signals may be considered causally connected at that frequency. Values sig-

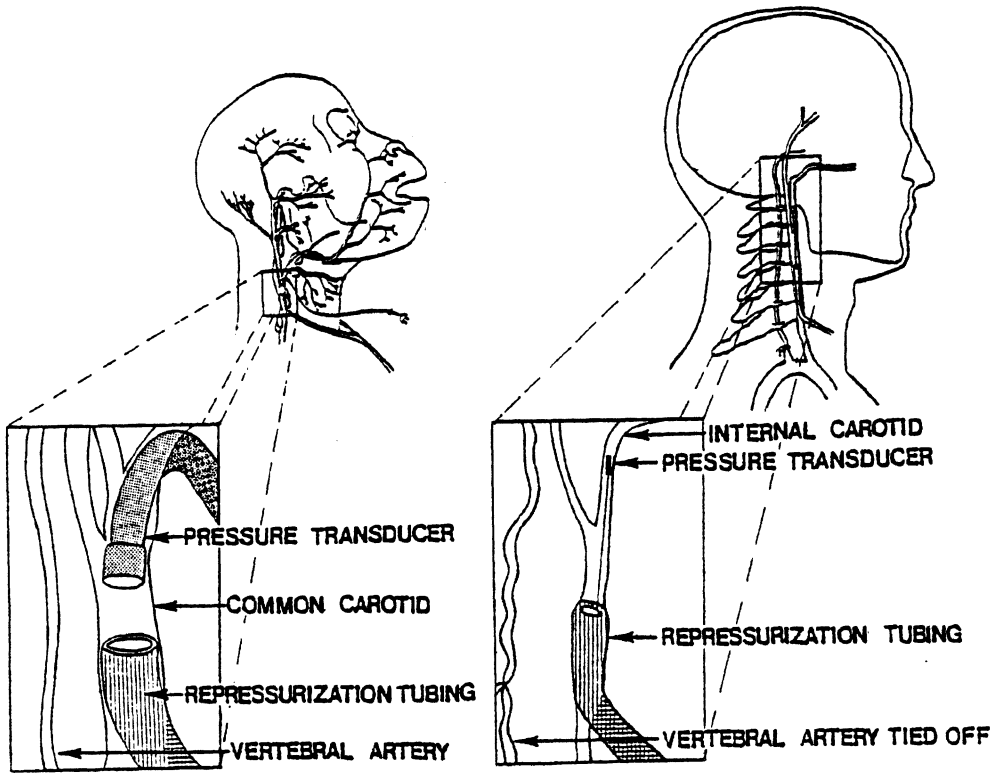

FIGURE 7: LOCATION OF VASCULAR PRESSURE TRANSDUCER IN RHESUS AND CADAVER MODELS

nificantly below 1 at a given frequency indicate that the transfer function at that frequency cannot accurately be determined. In the case of an input-output relationship, values of $Cxy^2(\omega)$ less than 1 indicate that the output is not attributable to the input and is perhaps due to extraneous noise. The coherence function in the frequency domain is analogous to the correlation coefficient in the time domain. The coherence function can be used to determine the useful range of the data in the frequency domain.

Correlation Functions - Correlation function statistical measures (8) were also used in the analysis of the data to describe some of the fundamental properties of a time-history, such as linear acceleration or epidural pressure as shown in the appendix.

Auto-correlation Function. This measure is the correlation between two points on a time-history and is a measure of the dependence of the amplitude at time t_1 on the amplitude at t_2 and is defined as:

$$R_{xx}(t_1,t_2)=\int\int x_1 \cdot x_2 \cdot p(x_1,x_2,t_1,t_2)dx_1 \cdot dx_2$$

where x_1,x_2 are the amplitudes of the time-history and $p(x_1,x_2,t_1,t_2)$ is the joint probability density.

Cross-correlation Function. This is a measure of how predictable, on the average, a signal (transducer time-history) at any particular moment in time is from a second signal at any other particular moment in time and is defined as:

$$R_{xy}(t_x,t_y)=\int\int x \cdot y \cdot p(x,y,t_x,t_y)dx \cdot dy$$

where x,y are the amplitudes of the two time-histories, respectively, and $p(x,y,t_x,t_y)$ is the cross probability density. Cross-correlation can be used to obtain useful information about the relationship between two different time-histories. For example, the cross-correlation between the acceleration measurements at two different points of a material body may be determined for the purpose of studying the propagation of differential motion through the material body. Cross-correlation functions are not restricted to correlation of parameters with the same physical units; for example, we determined the cross-correlation between the linear acceleration and the epidural pressure for the three Rhesus models. Cross-correlations, in general, do not commute, i.e. tangential acceleration cross epidural pressure does not equal epidural pressure cross tangential acceleration.

RESULTS

Table 1 lists the initial test conditions. Table 2 lists the Rhesus biometric measurements. Table 3 summarizes the head impacts. Table 4 reports the injuries/damages for which the preliminary analysis of the kinematic response was reported earlier (12) and Table 5 reports on the injuries/damages for which the kinematic response is being reported here. A gross pathological inspection was carried

Table 1. Rhesus Head Impact
Initial Test Conditions

Test No.	Subject Condition	Repressurization Condition	Subject Positioning Center of Gravity With Respect to Occipital Impact	Neck Condition	Velocity (m/s)
78A232	postmortem	unrepressurized	below	unstretched	11.5
78A234	postmortem	unrepressurized	below	unstretched	13.5
78A236	postmortem	unrepressurized	at	unstretched	12.5
78A238	postmortem	unrepressurized	above	unstretched	12.5
78A239	anesthetized	--	at	unstretched	12.5
78A241	anesthetized	--	above	unstretched	12.5
79A249	anesthetized	--	at	unstretched	15.4
79A251	anesthetized	--	at	unstretched	13.0
79A253	anesthetized	--	at	unstretched	14.8
79A256	postmortem	unrepressurized	at	unstretched	15.4
79A258	postmortem	unrepressurized	at	unstretched	14.5
79A260	postmortem	unrepressurized	at	unstretched	16.0
85R002	postmortem	repressurized	above	unstretched	11.0
85R005	postmortem	repressurized	above	unstretched	12.2
85R006	postmortem	repressurized	above	unstretched	11.9
85R008	postmortem	repressurized	above	unstretched	11.0
86R010	postmortem	unrepressurized	above	unstretched	11.0
86R011	anesthetized	--	above	stretched	10.0
86R012	anesthetized	--	above	stretched	12.2
86R013	anesthetized	--	above	stretched	11.9
86R014	anesthetized	--	above	unstretched	11.9
86R015	anesthetized	--	above	unstretched	12.1

Table 2. Rhesus Biometric Measurements*

Test No.	Height (Sitting) (cm)	Mass (kg)	Max. Skull Length (cm)	Max. Skull Breadth (cm)	Ave. Skull Thickness (cm)	Head+ Muscle Mass (g)	Head Mass (g)	Brain Mass (g)	Brain Volume (ml)
78A232	49.1	6.9	7.4	6.1	0.47	94	276	70	N/A
78A234	53.6	9.5	7.4	5.6	0.28	135	907	105	95
78A236	53.4	8.2	6.6	5.6	0.24	149	510	100	100
78A238	53.9	8.2	6.9	5.6	0.23	130	540	115	90
78A239	48.8	8.2	6.4	5.3	0.22	80	510	85	75
78A241	47.0	10.6	8.4	6.4	0.43	190	750	125	115
79A249	55.0	5.8	6.5	5.5	0.40	128	454	85	80
79A251	66.1	7.7	8.0	6.0	0.45	113	726	113	105
79A253	58.5	5.0	6.8	5.5	0.25	99	610	92	85
79A256	51.3	6.9	7.0	6.0	0.10	106	823	99	80
79A258	62.0	7.6	7.0	5.5	0.26	85	595	110	90
79A260	61.8	7.1	7.3	6.0	0.41	113	957	85	90
85R002	71.0	5.0	6.2	5.8	0.38	116	475	71	75
85R005	72.3	9.1	7.5	6.0	0.38	287	N/A	99	100
85R006	67.3	8.4	7.2	6.0	0.31	191	481	99	90
85R008	65.0	6.8	N/A	N/A	0.25	156	511	N/A	70
86R010	70.0	7.3	7.2	5.5	0.25	198	595	99	80
86R011	66.0	4.9	6.5	5.0	0.41	142	425	99	80
86R012	68.5	6.9	6.5	5.5	0.35	170	479	99	70
86R013	86.5	8.7	6.8	5.6	0.30	225	709	113	100
86R014	71.0	8.6	6.5	5.5	0.35	298	759	113	95
86R015	69.0	8.0	7.0	6.0	0.25	255	730	113	90

*All test subjects were Macaca mulatta except 78A232 which was Macaca assamenis.

Table 3. Rhesus Impact Test Summary

Test No.	Linear Acceleration Tangent m/s/s/	Resultant Acceleration m/s/s/	Resultant Angular Acceleration r/s/s	Resultant Angular Velocity r/s	Linear Velocity m/s	Epidural Pressure Kpa	Force N	Force Duration ms
78A232	7000	7000	22000	40	12	117	5800	3
78A234	8000	6400	38000	40	14	N/A	5700	4
78A236	7000	7000	28000	30	13	-9	5600	4
78A238	7100	8000	40000	60	13	-100,55	6600	4
78A239	8000	8000	41000	60	13	260	5000	5
78A241	8400	8000	54000	70	13	490	8700	3
79A249	14000	15000	70000	63	16	-70	7200	4
79A251	13000	14000	64000	75	13	200,-110	7500	4
79A253	10000	10000	40000	75	15	-101	5400	5
79A256	11000	11000	70000	84	16	N/A	6000	10
79A258	10000	12000	70000	75	15	-35,40	5700	5
79A260	13000	13000	60000	80	16	140,-100	7100	4
85R002	5300	5300	7900	30	12	270	4000	4
85R005	20000	18000	28000	45	15	-100,-105	N/A	N/A
85R006	11000	10000	65000	75	13	375	7500	5
85R008	11000	11000	60000	70	16	-98,-100	5800	5
86R010	7900	7900	16000	33	11	-375	7000	4
86R011	6000	5300	33000	24	13	11	N/A	N/A
86R012	18000	18000	110000	130	16	45	7000	4
86R013	9000	8800	80000	105	13	75	4900	5
86R014	12000	11000	120000	105	15	250	7000	4
86R015	13000	11000	120000	90	16	140,190	6500	4

Table 4. Rhesus Injuries/Damage Summary

Test No.	Gross Skull	Gross Brain	Gross Other
78A232	No injury	No injury	Epidural hematoma at C1, dura lacerated at C1
78A234	No injury	No injury	Epidural hematoma at C1, torn muscle at base of occiput
78A236	No injury	No injury	No abnormality or injury
78A238	No injury	No injury	Epidural hematoma at C1 disk
78A239	No injury	No injury	1/4 cc blood in occiput from epidural hematoma at C1
78A241	No injury	No injury	Epidural hematoma at C1
79A249	Basilar fracture (ring)	3/4 cc subdural hematoma right frontal lobe (cerebrum) subarachnoid hemorrhage base of cerebellum, pons, and medulla	Epidural hematoma at C1, occipital muscles damaged
79251	Linear basilar fracture from foramen magnum to occipital contact point	No injury	Epidural hematoma at C1 and C2
79A253	Basilar fracture (quasi-ring), temporal fracture	Petechial lesion left frontal lobe (cerebrum) subarachnoid hemorrhage base, pons, medulla and vermis of cerebellum	Damaged neck ligaments
79A256	Basilar fracture (petrous to petrous). Connected linear fracture to parietal bone*	Dura torn along sagittal sinus, emaciated tissue cerebellum, medulla	Lacerated spinal cord
79A258	Basilar fracture (quasi-ring)	Lacerated medulla	Epidural hematoma at C1
79A260	Basilar fracture (right petrous)	Subdural hematoma along sagittal sinus	Epidural hematoma at C1

*Abnormality - Test subject had very thin skull.

Table 5. Rhesus Injuries/Damage Summary

Test No.	Gross Skull	Gross Brain	Gross Other
85R002	No injury	No injury	No injury
85R005	Basilar skull fracture	Subarachnoid hemorrhage at medulla and brain stem	No injury
85R006	No injury	No injury	No injury
85R008	Basilar ring fracture*	Subarachnoid hemorrhage at medulla and brain stem	No injury
86R010	Basilar ring fracture	No injury	No injury
86R011	No injury	No injury	Subdural hemorrhage of spinal cord at base of brain
86R012	No injury	Subdural hemorrhage ,left frontal lobe	No injury
86R013	No injury	Subdural hemorrhage left frontal lobe	No injury
86R014	No injury	No injury	Subdural hemorrhage of spinal cord at base of brain
86R015	Linear fracture of superior right petrous Linear fracture of left occipital, Linear fracture of right temporal	No injury	Bilateral hemorrhage to side of spinal cord at base of medulla

*Abnormality - Test subject had a thin skull

out for each test subject. Selected time-histories in the appendix are examples of important kinematic factors associated with the observed head impact response.

DISCUSSION

The results of a series of head impact experiments conducted over the past nine years at UMTRI using anesthetized and postmortem Rhesus are presented. The tests entail different initial conditions and are compared to tests of another human surrogate (i.e. the repressurized human cadaver) reported in previous Stapp Conferences (12,14 and 16). Frame-independent variables and vectors were used to compare these different tests. The significant frame-independent vector tangential acceleration will be presented in detail throughout this discussion.

It would be preferable to run a limited set of experiments and generalize the results. However, because of the geometry of the skull-brain-spinal cord, the possible different initial conditions, the complex interaction of the skull with the brain, and of the different injury modes that can result from blunt head impact, *the results presented here apply only to the test conditions in which the experiments were run and may not apply to all situations*. The features of the data, discussed in this section in abbreviated form, represent trends that are felt to be important factors in head injury research.

The experiments can be broken into three significant classes: repressurized-postmortem subjects, unrepressurized-postmortem subjects, and anesthetized live subjects. Each class can be divided into two groups, skull fracture and no skull fracture. In addition, the anesthetized test subjects can be divided into two groups, neck-stretched and neck-unstretched. Although most of the subjects were positioned so that the estimated center of mass of the head was above the contact point of the head with a line running horizontally through the center of the impactor, a few were positioned "at" or "below." This means that, in general, there were two-four subjects in each grouping. Therefore, when comparing between groupings it is necessary to use only the most robust aspects of the data.

In head impact experiments it is common to find variations in the input force time-histories as well as variations in the acceleration (both linear and angular) responses. The differences and similarities in the force time-histories as well as in the linear and angular accelerations for the impact conditions used in these tests have been described elsewhere (12,16). The two initial test conditions (neck-stretched positioning and repressurization), absent in the tests reported earlier (12,16) and part of the entire sample being reported here did not affect significantly the response in terms of force and angular/linear acceleration. for other similar initial conditions, the repressurized-postmortem and the neck-stretched anesthetized Rhesus subjects were not distinguishable in response from the class, anesthetized Rhesus. For a given set of initial conditions, these variations can be addressed when the sample size is large for each class and group and the statistics are appropriate. However, for the small sample size that each of the different classes of this study entail, it is helpful to normalize the data through the use of transfer functions and to address only the most robust aspects of the differences.

In general, the force time-histories were similar in terms of wave shape and magnitude for the no-skull-fracture case. A general idea of the range of peak forces and durations can be obtained by referring to Table 3 which shows an average peak force of 6300 N with a standard deviation of 1100 N and a duration of 4.5 ms with a standard deviation of 1.5 ms. Because of the small sample size and the variations among the tests, there was no significant difference in response in terms of peak values for linear/angular velocity or linear/angular acceleration between the different group of tests for the no-skull-fracture case.

Impact Response Definition - Using the UMTRI nine-accelerometer array, it is possible to record three-dimensional six-degrees-of-freedom motion of an area of the skull in which the accelerometers are located. Since the nine-accelerometer motion analysis assumes rigid body motion and the skull and brain deform during impact, the output from this three-dimensional motion experimental technique can only be used to estimate the motion of the head. Thus, head impact response can be defined as a continuum of "events" characterized by the path traced by the motion of the "estimated anatomical center," by all the vectors defined on that path, and by the changes of the accelerated frame fields. Physically, head impact response is interpreted as the response of a material body (i.e. the nine-accelerometer array) in contact with other material bodies. The curve and the vectors generated as the "estimated anatomical center" moves in time are, therefore, a result of the interactions of the skull-mount area with other material bodies.

Three-Dimensional Motion Technique - When the head receives an impact, several events occur: 1) stress waves are propagated from the impact site, 2) the skull starts to deform, and 3) the skull begins to move due to the impact, transmitting energy to the brain via the *dura mater*. Eventually, the stress waves are dissipated, the deformation of the skull recovers partially or fully on removal of the impact loads, and the acceleration of the skull continues primarily from forces generated by the brain and neck. If the differential skull motion is "severe," due to either sufficient energy in the high frequency components of the force time-history or to sufficient peak force, the stresses at some point in the skull may exceed the failure strength of the bone, thereby producing fracture. Dynamic human cadaver impact experiments have shown that the motion of the entire skull as a rigid body as estimated by the nine-accelerometer array depends on the degree of skull deformation (14). The previous study showed that cadaver skull deformation, with or without skull fracture, correlated well with injury. In addition, whenever skull deformation was present, it significantly affected the linear and angular acceleration response. For the Rhesus model, however, the accelerometers are located on the orbital ridges and dental palate, sufficiently far from the impact site so that the local perturbations are small even when the skull fractures (12,14). If the skull near the nine-accelerometer array had been significantly perturbed by skull fracture, then the mechanical impedance of the skull-fracture tests should have been different from that of the no-skull-fracture tests. This, in general, was not the case. The mechanical impedance

transfer functions in the appendix show that the mechanical impedance for both the skull-fracture and the no-skull-fracture tests were the same. Based upon human cadaver data, that result is different from what would be expected for the live human. It is believed that the mechanical impedance observed for the Rhesus tests was a result of the different skull geometry and soft-tissue distribution between the Rhesus and human cadaver models. The observation implies that the effect of skull deformation on the nine-accelerometer recording is different for the Rhesus as compared to the human cadaver models. Because skull deformation can be an important aspect of mechanisms of focal injury and kinematic response (14), and because the experimental techniques used to simulate the three-dimensional motion of the head of the human cadaver and lower primate models produce significantly different results with regard to skull deformation, this difference implies that the scaling of impact and injury response between human cadaver and Rhesus models for some types of impacts may not be possible. As stated for the no-skull-fracture case, there was no significant difference in terms of peak values for linear/angular velocity and linear/angular acceleration; the no-skull-fracture and skull-fracture cases had the same mechanical impedance which further supports that finding significant difference in terms of force and linear acceleration was difficult for this sample.

Vascular Repressurization Technique - The results presented here regarding the repressurized-postmortem Rhesus are potentially a function of the repressurization technique used. Different repressurization techniques may give different results. The repressurization techniques developed for Rhesus subjects are similar to those used for repressurized human cadavers (12,14,16). However, because of the smaller size of the vessels in the vascular system of the Rhesus as compared to that of the human cadaver, somewhat different procedures had to be used (See Figure 7). The Rhesus vertebral artery was not ligated. In the Rhesus model the pressure transducer in the external carotid artery restricts the flow of the internal carotid artery at the measurement site. The pressure transducer used to monitor the carotid pressures, and, therefore, used to determine the vascular pressure in the brain, was placed in different locations in the two species. In the cadaver model the transducer was in the internal carotid close to the entrance of the carotid into the brain. In the Rhesus model the transducer was in the external carotid distal to the brain. The precise difference this makes between the results is unknown. The initial repressurization levels may not be comparable. In addition, it was more difficult to remove the air in the Rhesus skull-brain area than in the cadaver model; thus, a greater proportion of the Rhesus brain cavity may have contained air than that of the cadaver brain cavity.

The No Skull Fracture Impacts - Comparisons of the three classes of no-fracture head impacts for experiments, in which the initial conditions were impact velocity of 11.5-12.5 m/s, neck-unstretched positioning, impact below the head center of mass, 2.5 cm Ensolite padding, and the pressure transducer located at the front of the skull, imply that:

1. The unrepressurized-postmortem Rhesus is significantly different than the anesthetized Rhesus as shown by the transfer function relationships of tangential acceleration divided by epidural pressure.

2. In terms of peak pressure (largest absolute value), the repressurized-postmortem Rhesus' response is more similar to the anesthetized Rhesus' than the unrepressurized-postmortem Rhesus'.

3. The impact responses of the anesthetized, unrepressurized-postmortem and repressurized-postmortem Rhesus are all different as shown by the transfer function relationships of tangential acceleration divided by epidural pressure.

Inspection of the peak pressures presented in Table 3 shows that the peak pressures of the unrepressurized-postmortem Rhesus were between 95 and 150 kPa, and those for the anesthetized and repressurized-postmortem Rhesus were between 250 and 500 kPa. Although there were a limited number of tests in each category, the results were consistent enough to show that, in terms of peak pressures, the anesthetized and the repressurized-postmortem subjects were similar. In addition, for some of the tests, the peak pressures for the unrepressurized-postmortem Rhesus were opposite in sign to those of the anesthetized Rhesus and the repressurized-postmortem Rhesus (see Test 78A236 in the appendix). Figure 8 represents the transfer function corridors for the tangential acceleration divided by epidural pressure for the no-fracture class of Rhesus subjects. The key defines the corridors for the anesthetized, the unrepressurized-postmortem, and the repressurized-postmortem Rhesus subjects.

Successful understanding of the performance of a given system depends on being able to predict accurately the output response for a given input. In the case of a time invariant linear system, a transfer function can be generated that characterizes the system and is independent of the input to the system, i.e. it is an invariant of the system. Comparisons of outputs for different inputs will show some variations, but transfer functions that characterize the system will not. In general, systems in the real world are inherently non-linear and that is probably also true for the head when struck by a blunt impactor. We can, however, assert that a linear system is a valid approximation of a non-linear one over a limited range such as the range seen in these experiments. For example, if a transfer function generated for tangential acceleration divided by epidural pressure for an impact to an unrepressurized Rhesus subject is compared to another transfer function of the same parameters for an anesthetized Rhesus subject and is found to be similar, then the transfer functions correlated well and represent the same biological system; when they are found to be different, then the transfer functions do not correlate well and are said to be representing different biological systems. For the tests being reported here the force time-histories are similar enough so that a valid linear range can be assumed.

For the unrepressurized-postmortem versus the anesthetized Rhesus, the magnitude differed by at least a

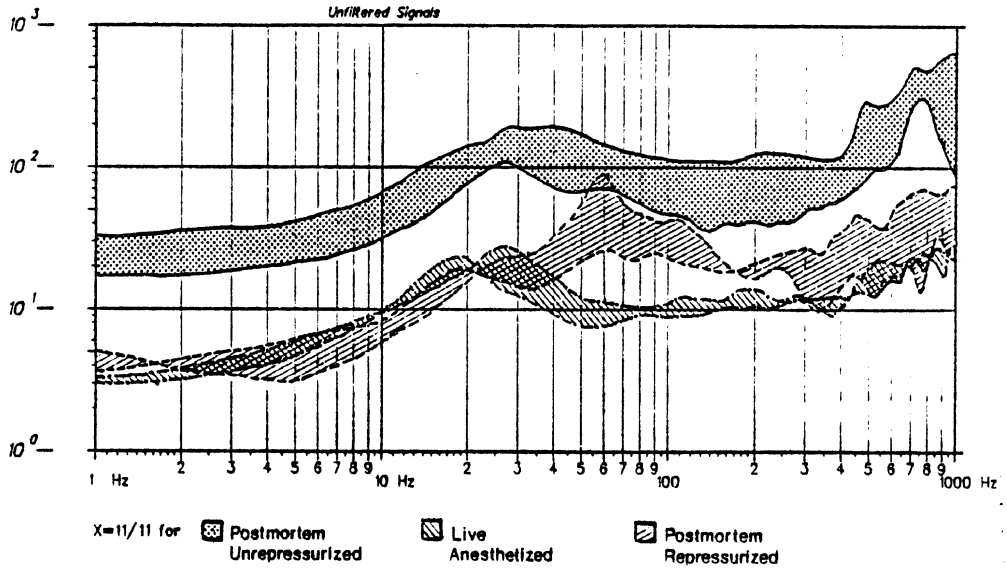

FIGURE 8: TRANSFER FUNCTION CORRIDORS TANGENTIAL ACCELERATION/EPIDURAL PRESSURE NO-FRACTURE RHESUS

factor of 3 at all frequencies, indicating that there is more energy at any given frequency in the output (pressure) for a given input (tangential acceleration) for the anesthetized subject than for the unrepressurized-postmortem subject. However, it is also evident that when comparing the transfer function corridors between the repressurized-postmortem Rhesus and the anesthetized Rhesus, the differences suggested by the comparison of peak pressure are not entirely substantiated. For example, although the magnitude of the transfer function of the repressurized-postmortem Rhesus is similar to that of the anesthetized Rhesus up to about 35 Hz, above that frequency the transfer function magnitude indicates that the repressurized-postmortem, the unrepressurized-postmortem, and the anesthetized Rhesus all differ to some degree. In Figure 8 the greatest energy in the pressure for a given acceleration is in the anesthetized Rhesus, while that for the repressurized-postmortem Rhesus has its magnitude between those of the anesthetized and the unrepressurized-postmortem subjects.

It can be concluded that even though the repressurized-postmortem Rhesus was more similar than the unrepressurized-postmortem Rhesus to the anesthetized Rhesus in response as shown by the transfer function relationships, there were still detectable differences between them. **Note:** It was also realized that this difference only applied to experiments of those initial conditions and would not apply in a general sense. Potentially it would be possible to choose a different set of initial conditions and run a series of blunt head impact experiments to the unrepressurized-postmortem and anesthetized Rhesus and show that there is no difference in the pressure response for similar force and acceleration time-histories between the two models. In general it cannot be stated that there is a difference in pressure response between the unrepressurized-postmortem and anesthetized Rhesus for similar force and acceleration responses, but there exists an initial condition in which such a difference will manifest itself. By comparing blunt head impact experiments conducted (12) on both unrepressurized-postmortem and anesthetized Rhesus plus the additional subjects being reported here, and by carefully choosing the initial position of the head and neck as well as the impact velocity and padding on the impactor surface, it can be shown that in terms of epidural pressure there is a significant difference in the pressure response of the two types of surrogates for similar force and acceleration time-histories.

Transfer functions are complex-valued, including both magnitude and phase. The phase relationship was evaluated with the cross-correlation function. The analysis obtained from the cross-correlation function between the tangential acceleration and the epidural pressure shows that: 1) Effectively there was no phase lag between the tangential acceleration and the epidural pressure for the anesthetized Rhesus (See Figure 9 which illustrates the maximum positive cross-correlation at zero lag and the appendix for other tests); 2) An effective phase lag between the tangential acceleration and the epidural pressure of one or two milliseconds for repressurized-postmortem Rhesus was observed (See Figure 10 which illustrates the maximum positive cross-correlation at one to two milliseconds and the appendix for other tests); and 3) The greatest phase lags between tangential acceleration and the epidural pressure were observed for unrepressurized Rhesus (See Figure 11 which illustrates the maximum negative cross-correlation for these tests and the appendix for other tests). The anesthetized and the repressurized-postmortem Rhesus had more similar phase lags between tangential acceleration and epidural pressure than the unrepressurized- and repressurized-postmortem Rhesus. Therefore, repressurization seemed to make the postmortem subject a better model of the anesthetized subject. However, it seems that the

FIGURE 9: ANESTHETIZED RHESUS, NO SKULL FRACTURE, NECK UNSTRETCHED

Cross- and Auto- Correlations

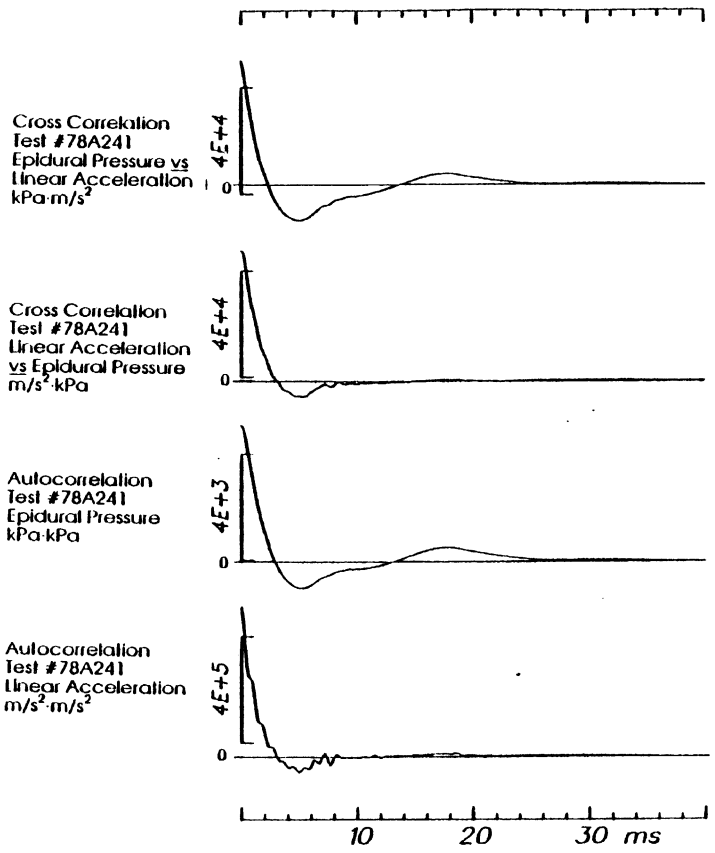

HEAD CENTER OF GRAVITY WITH RESPECT TO LINE OF IMPACT = ABOVE

FIGURE 10: REPRESSURIZED POSTMORTEM RHESUS, NO SKULL FRACTURE, NECK UNSTRETCHED

Auto- and Cross- Correlations

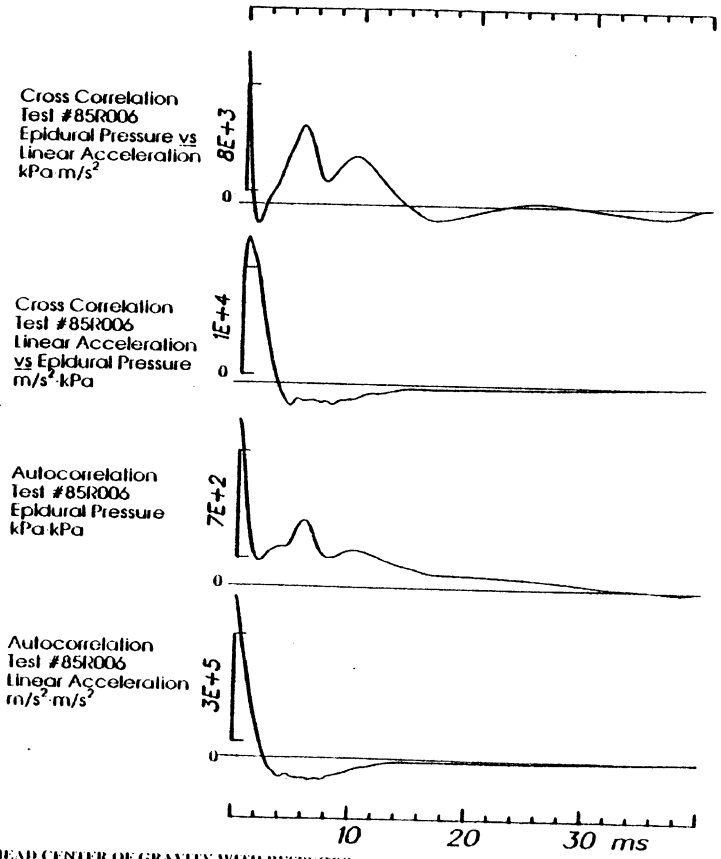

HEAD CENTER OF GRAVITY WITH RESPECT TO LINE OF IMPACT = ABOVE

FIGURE 11: UNREPRESSURIZED POSTMORTEM RHESUS, NO SKULL FRACTURE, NECK UNSTRETCHED

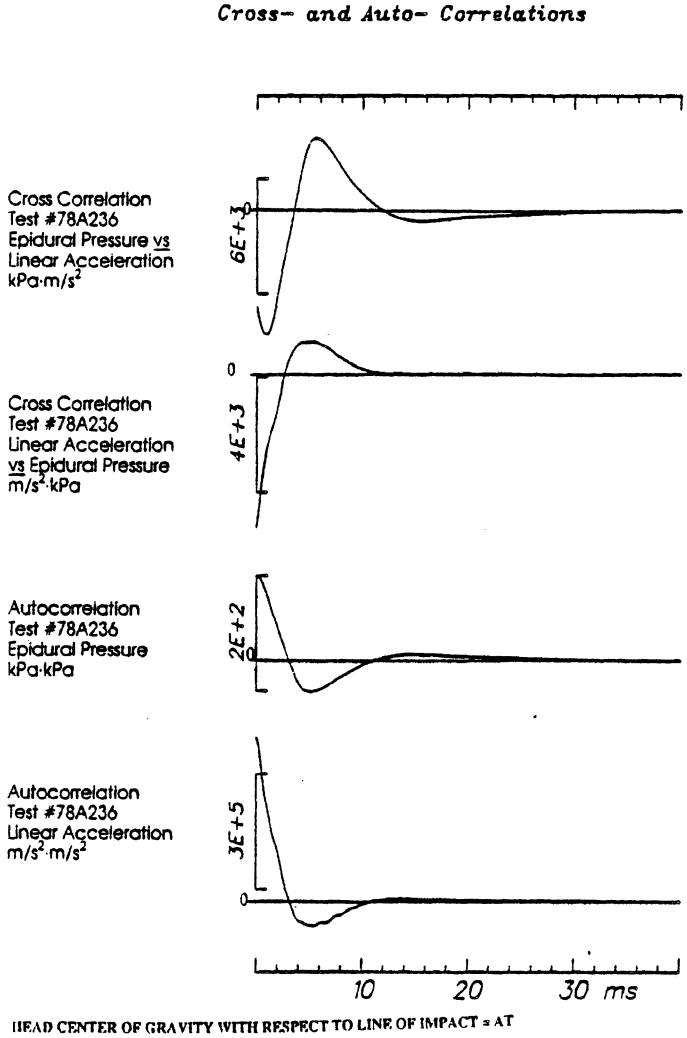

postmortem Rhesus brain, whether repressurized or unrepressurized, was not as "stiff" as that of an anesthetized subject. This may have been due to the postmortem degradation of the brain tissues, incomplete repressurization, or the repressurization process not removing all of the air from the skull-brain area.

The results reported elsewhere (14) indicated that when basal skull fracture occurred in Rhesus subjects, subarachnoid hemorrhaging was common in the *medulla-pons* area. In addition, this injury did not occur in the unrepressurized-postmortem Rhesus. For the repressurized-postmortem Rhesus, focal injuries similar to those of the anesthetized subject were observed. The implications were that in terms of injury response *for this type of injury mode*, the repressurized-postmortem subject was similar to the anesthetized subject. Caution must be exercised in interpreting these results because one injury mode for a very particular type of impact was involved and the sample size was small. *The results may not occur for other injury modes or impact conditions.*

Head-Neck Positioning Parameter - The results reported elsewhere (16) indicated that the interaction of the spinal cord and the *foramen magnum* with the rest of the brain - cerebrospinal fluid system was a critical factor in certain types of head impact response. In an attempt to determine the effect of the interaction of the head with the cervical spine, a series of impacts were run with the neck stretched. Figure 3 is an x-ray of the two types of initial neck conditions. One shows the neck-stretched configuration, and the other the neck-unstretched configuration. Although the impedance values between force and tangential acceleration as well as the time-histories of the linear and angular accelerations for the two neck conditions were similar (See appendix), the transfer functions for the tangential acceleration divided by epidural pressures were not (Figure 12). This implies that the flow of material through the *foramen magnum* as well as the inertial

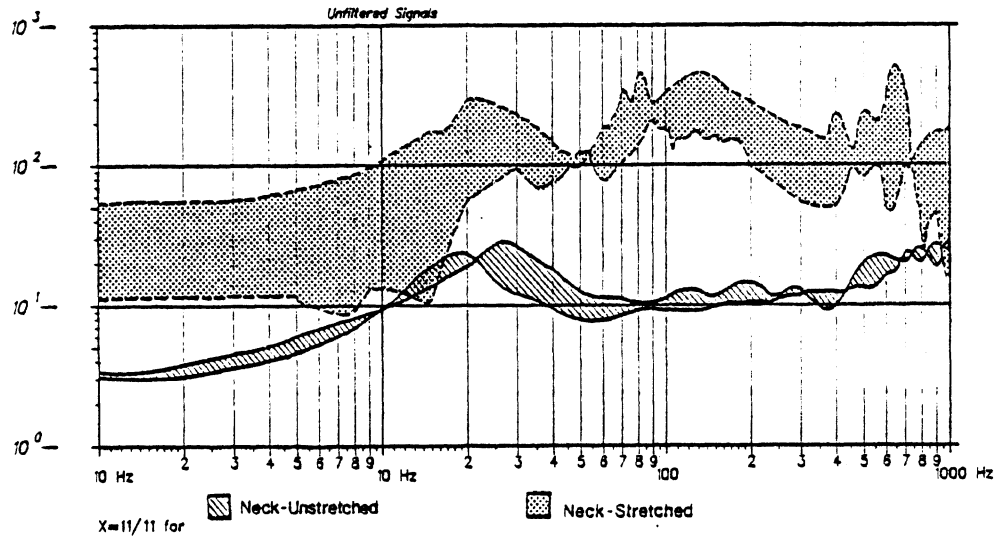

FIGURE 12: TRANSFER FUNCTION CORRIDORS TANGENTIAL ACCELERATION/EPIDURAL PRESSURE NECK-STRETCHED VS. NECK UNSTRETCHED RHESUS

properties of the cord may have been critical factors in determining the type of pressure and stress that developed in the brain during impact. In addition, the neck-stretched tests were the only ones in which subdural hemorrhaging was observed in the frontal lobes of the brain. Therefore, not only was the impact response different, in terms of transfer functions for tangential acceleration and epidural pressure, but the injury response also changed. The difference in initial positioning may have changed the hydrodynamic lubrication and the mechanical restriction associated with the skull-brain interface. In addition, the large pressures that developed during impact in the neck-unstretched anesthetized Rhesus subject and the inertial properties of the restricted flow of the spinal cord-cerebrospinal fluid through the *foramen magnum* may have helped to reduce the differential motion between the brain and the skull during impact. The observed injuries (subdural hematomas in the frontal lobes) in the neck-stretched case with angular acceleration similar to the neck-unstretched case imply that the interaction of the cervical cord and the *foramen magnum* may be critical for these types of injury, and perhaps is more important than the angular or linear velocity/acceleration parameters for determining head-impact tolerance levels.

The Skull-Deformation Impacts - To understand the effects of skull deformation on pressure it is first instructive to look at small deformation experiments, i.e. no skull fracture ones. In a manner similar to that of the repressurized human cadaver, skull deformation played a small part in the pressure response of the anesthetized Rhesus brain up to the level where the skull fractured (see also 14,16). The features of the data that indicated this for anesthetized subjects are:

1) The auto-correlations of the tangential acceleration and epidural pressures were similar to those of the cross-correlation between the two signals for the anesthetized no-skull fracture Rhesus. (See Figure 9 and the appendix for other tests. When the auto-correlation of two given signals have the same magnitude, lag, and wave shape as the cross-correlation of those two signals, then statistically the two signals correlate well. Therefore, it is reasonable to assume that when the correlations follow this pattern as the tangential acceleration ones shown in Figure 8, the pressure response is most likely due to the inertial loading of the brain.); and
2) The greatest *absolute* maximum value for severe skull-fracture subjects was generally a negative quantity (i.e. a negative cross-correlation near zero lag as shown in Figure 13. Other examples are given in the appendix), whereas for simple skull fracture subjects the tangential acceleration correlated better with epidural pressure than for severe skull fracture subjects. The negative correlation implies the pressure did not follow the inertial loading of the skull. It is reasonable to assume that because of the geometry of the skull, deformation of the skull as a result of impact to the occiput would increase the volume and decrease the pressure. The negative pressure and the negative cross-correlation seen in the severe skull fracture case indicates the pressure followed the increase in volume associated with skull deformation.

The result that skull deformation played a small part in the epidural pressure response of the Rhesus brain up to the level where the skull fractured has important implications in terms of head trauma modeling. If the head is viewed as a closed shell and the brain and its surrounding tissues and fluids as an incompressible, or nearly incompressible, vis-

FIGURE 13: ANESTHETIZED RHESUS, SKULL FRACTURE, NECK UNSTRETCHED

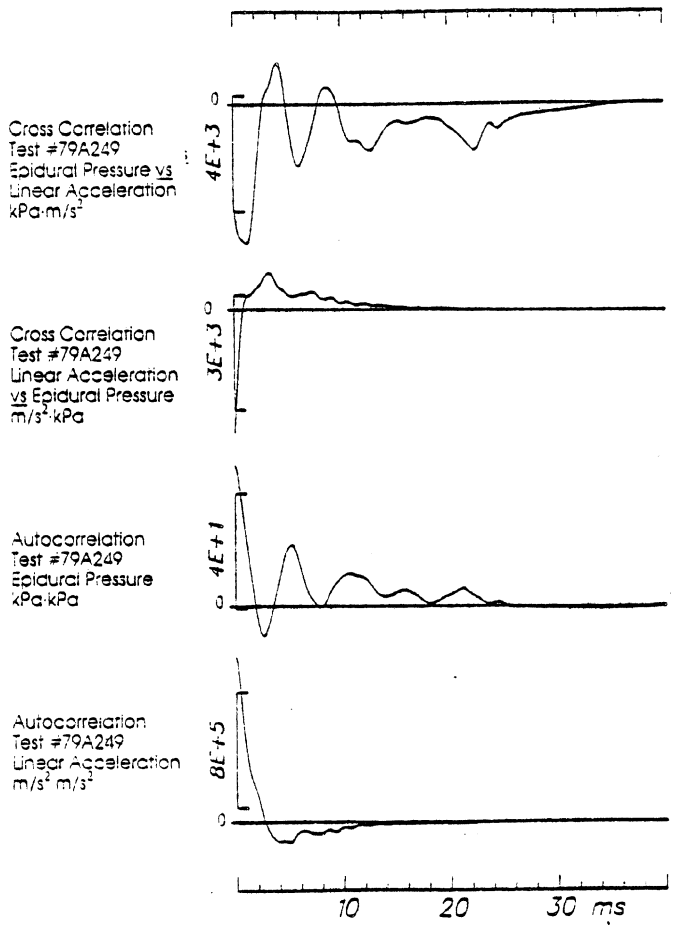

HEAD CENTER OF GRAVITY WITH RESPECT TO LINE OF IMPACT = ABOVE

coelastic material (i.e. as having a bulk modulus near that of water), then small changes in volume would be expected to produce larger pressure changes than those observed in the response of the anesthetized test subjects. In addition, one would expect negative pressures and a negative cross-correlation between tangential acceleration and epidural pressure for the no-skull fracture subjects, because the pressure volume change mechanism would dominate any of the inertial phenomena. The results imply three possibilities for head trauma modelers: 1) The *foramen magnum* was significantly large enough so that it needs to be included in modeling of head blunt impact response; 2) The *effective bulk modulus* may need to be viewed as significantly less than that of water or an equivalent system should be used (Rather than attempting to model all of the foramina and canals of the skull, an equivalent system model might be useful which can reproduce the same kinematics occurring in blunt head impacts by incorporating a "skull" having an evenly distributed set of holes.); and 3) or both.

Although the bulk modulus of the brain may be very close to water, the concept of an effective bulk modulus may be useful in describing the blunt impact response of the brain. The need for an effective bulk modulus concept results from the fact that although the foramen magnum is the largest entrance and exit port of the skull, other holes may have some small effect on the pressure response of the brain. Therefore, to estimate this effect as well as the effect of small amounts of dissolved gas in the brain-cerebrospinal fluid system, an effective bulk modulus may be needed for successful modeling. An alternative approach might be to leave the bulk modulus similar to that of water and use an equivalent system in which the skull is idealized as a structure with small openings.

Fluid Vaporization - Cavitation - In any situation where fluid is involved (e.g. water) and the tensile stress is reduced below the vapor pressure, vaporization occurs almost instantaneously (7,29,30). Therefore, in any blunt head impact test in which the epidural pressures are less than 0.13 kPa *absolute* fluid vaporization occurs.

During skull-fracture Rhesus tests, pressures slightly below one negative atmosphere gauge were observed

(See 14 and appendix). These were the only tests in which negative pressures of that magnitude were produced. Therefore, it seems that vaporization of the fluid near the pressure transducer was rapid enough to effectively act as a tension[2] (negative pressure) limiting function. This thermodynamic phenomenon would have affected significantly the stresses and strains (8) that were being produced in other parts of the brain during the severe impacts. The earlier observations indicated that when negative pressures were equal to or slightly less than one negative atmosphere for anesthetized Rhesus, no injuries were observed in the brain near the pressure transducer measuring sites (14). The same observation was made for all the anesthetized Rhesus in this study in which skull fractures produced epidural pressures of negative one atmosphere. Therefore, it seems that cavitation[3] was not a mechanism of injury for these experiments. Cavitation as a potential mechanism of injury for these tests would require the non-repetitive formation of bubbles or cavities within the fluid surrounding and within the brain tissue, displacing the tissue. We believe that cavities did not form within the fluid within the brain tissue, but rather occurred within the cerebrospinal fluid located at the dura-cerebrospinal fluid interface because no focal injuries or evidence of cavities were observed within the brain tissue.

Injury prediction based on stress or the differential motion between the skull and the brain should address the phenomenon of fluid vaporization at the dura-cerebrospinal fluid interface. It, therefore, may be essential to include this phenomenon in any modeling effort of head impact response.

CONCLUSIONS

This has been a limited study, using anesthetized, unrepressurized-postmortem, and repressurized-postmortem Rhesus, of a few important kinematic factors and injury modes associated with blunt impact to the head. Because of the complex nature of the head during impact, more work is necessary before these kinematic factors can be generalized to describe the responses of the skull, brain, cerebrospinal fluid, and the neck to blunt head impact. However, the following conclusions are drawn.

1. A set of initial conditions can be found such that in terms of peak pressure, the repressurized-postmortem and the anesthetized Rhesus responses are significantly different from that of the unrepressurized-postmortem Rhesus.

2. A set of initial conditions exists in which the repressurized-postmortem Rhesus, when compared to the unrepressurized-postmortem Rhesus, will be more similar in response to that of the anesthetized Rhesus (as shown by transfer function relationships for tangential acceleration divided by epidural pressure). The differences detected between the repressurized-postmortem and the anesthetized Rhesus may be important in terms of kinematic response.

3. The repressurized-postmortem Rhesus and the anesthetized Rhesus produce similar subarachnoid hemorrhaging in the *medulla-pons* area associated with skull fracture.

4. The initial position of the head-neck system is a critical factor associated with the brain-cerebrospinal system's response to head impact. For given linear and angular acceleration-time histories, the initial position of the head-neck system was, in general, successful in predicting the pressure and injury response. Unless the initial position of the head-neck system is included in the head tolerance criteria function (unlike those functions solely based on linear and angular accelerations, intracranial pressure, and skull strain), the function may not prove useful.

5. The thermodynamic response (fluid vaporization) of the head-brain system is an important consideration when the impact produced significant tension.

6. For the anesthetized Rhesus presented here and in the results presented elsewhere (12,16), no relationships could be found between injury and negative pressures equal to one atmosphere. This implies that cavitation does not seem to be a mechanism of injury in head impact response.

7. The above conclusions are important for both the mathematical modeling and the determination of the injury tolerance of the head. The following factors significantly affect the stress and possibly the strain in the brain as well as the interaction of the brain with the skull.

- The tension in the brain, limited by vaporiztion in "severe" impacts;
- The inertial properties of the cervical cord as well as the flow of material through the foramen magnum;
- The initial position of the head-neck system; and
- The repressurization of postmortem surrogates.

ACKNOWLEDGEMENTS

The results presented in this paper were obtained through a series of independently funded research programs conducted during the past nine years. The funding agencies were: The Motor Vehicle Manufacturers Association and the United States Department of Transportation, National Highway Traffic Safety Administration. The assistance in injury evaluation provided by C. J. D'Amato, P. W. Gikas, D. F. Huelke, and J. Hoff is gratefully acknowledged. The authors are indebted to Nabih Alem.

[2]Tensile Stress or Tension is the internal force that resists the action of external forces tending to increase the length of the body. Compression is the internal force that resists the actions of external forces tending to decrease the length of a body (4).

[3]When fluid pressure is reduced to the vapor pressure at the particular temperature, then the liquid will vaporize and a cavity forms. As the fluid flows into a region of higher pressure, the bubbles of vapor suddenly condense. This may produce very high dynamic pressure upon adjacent structures. When this action is continuous and has a high frequency, the material of the adjacent structure may be damaged (7. See also 22,30).

Joseph Benson, Miles Janicki, John Melvin, Richard Stalnaker, Paula Lux, Wendy Gould, Valerie Karime, Lilly Kim, and Shawn Cowper for their technical assistance. A special thanks is given to Jeff Marcus for his support.

In conducting the research on the laboratory Rhesus subjects described in this study, the investigators adhered to the "Guide for the Care and Use of Laboratory Animals," as prepared by the Committee on the Care and Use of Laboratory Animals of the Institute of Laboratory Animal Resources, National Research Council.

REFERENCES

1. Atluri, S., Kobayashi, A.S., and Cheng, J.S. 1975. Brain Tissue Fragility - A Finite Strain Analysis by Hybrid Finite-Element Method. Journal of Applied Mechanics 42:269-273. June.

2. Bishop, R.L. and Goldberg, S.I. 1968. Tensor Analysis on Manifolds, New York: MacMillan.

3. Cartan, E. 1946. Lecons sur la Geometrie des Espaces de Rieman, Second Edition, Paris: Gautheir Villars.

4. Esbach, O.W. and Souders, M., editors, 1975 ed. Handbook of Engineering Fundamentals. NY: John Wiley and Sons, especially p. 488.

5. Ewing, C.L., et al. 1975. The Effect of the Initial Position of the Head and Neck on the Dynamic Response of the Human Head and Neck to -Gx Impact Acceleration. 19th Stapp Car Crash Conf. Proc., Paper No. 751157.

6. Flexner, L.B. and Weed, L.H. 1983. Note on Cerebrospinal Elasticity in a Chimpanzee. Am. J. Physiol. 105:571-573.

7. Granger, R.A. 1985. Fluid Mechanics. NY: Holt, Rinehart and Winston, p. 231.

8. Harris, C.M. and Crede, C.E. 1976. Shock and Vibration Handbook. New York: McGraw- Hill Book Company.

9. Hashizume, K. 1972. A Study of the Experimental Brain Injury. Brain and Nerve, 14:991-1002.

10. Nusholtz, G.S. 1985. Critical Factors in Head Injury Research. Head Injury Prevention - Past and Present. Publisher: Harbo. In press.

11. Nusholtz, G.S., Bender, M. and Kaiker, P.S. 1986. Photogrammetric Techniques Using High-Speed Cineradiography. Optical Engineering, 25(6):791-798.

12. Nusholtz, G.S., Melvin, J.W., and Alem, N.M. 1979. Head Impact Response Comparisons of Human Surrogates. 23rd Stapp Car Crash Conf. Proc., 17-19 October, San Diego, Calif., pp. 499-541. SAE Paper No. 791020.

13. Nusholtz, G.S., et al. 1981. Response of the Cervical Spine to Superior-Inferior Head Impact. 25th Stapp Car Crash Conference Proc., pp. 197-237.

14. Nusholtz, G.S., et al. 1984. Head Impact Response-Skull Deformation and Angular Accelerations. 28th Stapp Car Crash Conf. Proc., pp. 41-74.

15. Nusholtz, G.S., et al. 1986. Evaluation of Experimental Techniques in Head Injury Research. Final Report, UMTRI-86-30. DOT-NHTSA Contract No. DTNH22-83-C-07095.

16. Nusholtz, G.S. and Ward, C.C. 1986. Comparison of Epidural Pressure in Live Anesthetized and Postmortem Primates. Journal of Aviation, Space and Environmental Medicine. In press.

17. Ommaya, A.K., et al. 1967. Scaling of Experimental Data on Cerebral Concussion in Sub-Human Primates to Concussion Threshold for Man. 11th Stapp Car Crash Conf. Proc., pp. 45-52.

18. Ommaya, A.K. 1973. Head Injury Mechanisms. Final Report Contract No. DOT-HS-081-1-1061A, U. S. Dept. of Transportation, National Highway Traffic Safety Administration, Washington, D.C.

19. O'Neill, B. 1967. Elementary Differential Geometry, New York: Academic Press.

20. Portnoy, H.D., et al. 1970. Intracranial Pressure and Head Acceleration During Whiplash. 14th Stapp Car Crash Conf. Proc., pp. 152-168. SAE Paper No. 700900.

21. Saczalski, K.J. 1976. A Critical Assessment of the Use of Non-Human Surrogates for Safety System Evaluation. 20th Stapp Car Crash Conf. Proc., pp. 159-187.

22. Schweitzer, D.H. and Szebehely, V.G. 1950. Gas Evolution in Liquids and Cavitation. J. of Applied Physics 21:1218-1224 (Dec.).

23. Smith, R.W. 1979. The Response of Unembalmed Cadaveric and Living Cerebral Vessels to Graded Injury - A Pilot Study. 23rd Stapp Car Crash Conf. Proc., pp. 543-560. SAE Paper No. 791021.

24. Stoker, J.J. 1969. Differential Geometry, New York: Wiley Intersciences.

25. Symon, L. 1967. A Comparative Study of Middle Cerebral Pressure in Dogs and Macaques. Journal of Physiol. 191:449-465.

26. Thomas, D.J., Robbins, D.H., Eppinger, R.H., King, A.I., and Hubbard, R.P. 1974. Guidelines for the Comparison of Human and Human Analogue Biomechanical Data. A report of an ad hoc committee, Ann Arbor, Michigan, December 6.

27. Unterharnscheidt, F. and Higgins, L.S. 1969. Traumatic Lesions of Brain and Spinal Cord Due to Nondeforming Angular Accelerations of the Head. Texas Report on Biol. and Med. 27:127-166.

28. Weed, L.H. and Flexner, L.B. 1932. Cerebrospinal Elasticity in the Cat and Macaques. American Journal of Physiol. 101:668-667.

29. Wiggert, D.C. and Sundquist, M.J. 1979. The Effect of Gaseous Cavitation on Fluid Transients. J. of Fluid Engineering 101:79-88 (March).

30. Wylie, E.B. and Streeter, V.L. 1985 edition, Fluid Transients. Ann Arbor, MI: FEB Press, especially pp. 12-13 and 136-155.

MECHANICAL IMPEDANCE

TYPE: UNREPRESSURIZED POSTMORTEM RHESUS, NO SKULL FRACTURE, NECK UNSTRETCHED

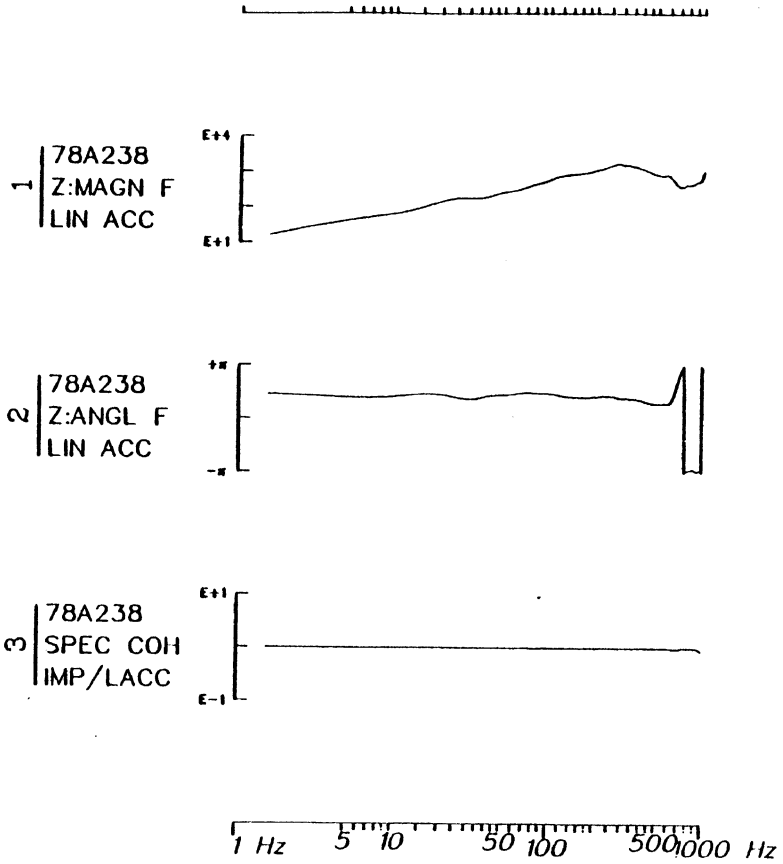

HEAD CENTER OF GRAVITY WITH RESPECT TO LINE OF IMPACT = ABOVE

MECHANICAL IMPEDANCE

TYPE: ANESTHETIZED RHESUS, NO SKULL FRACTURE, NECK UNSTRETCHED

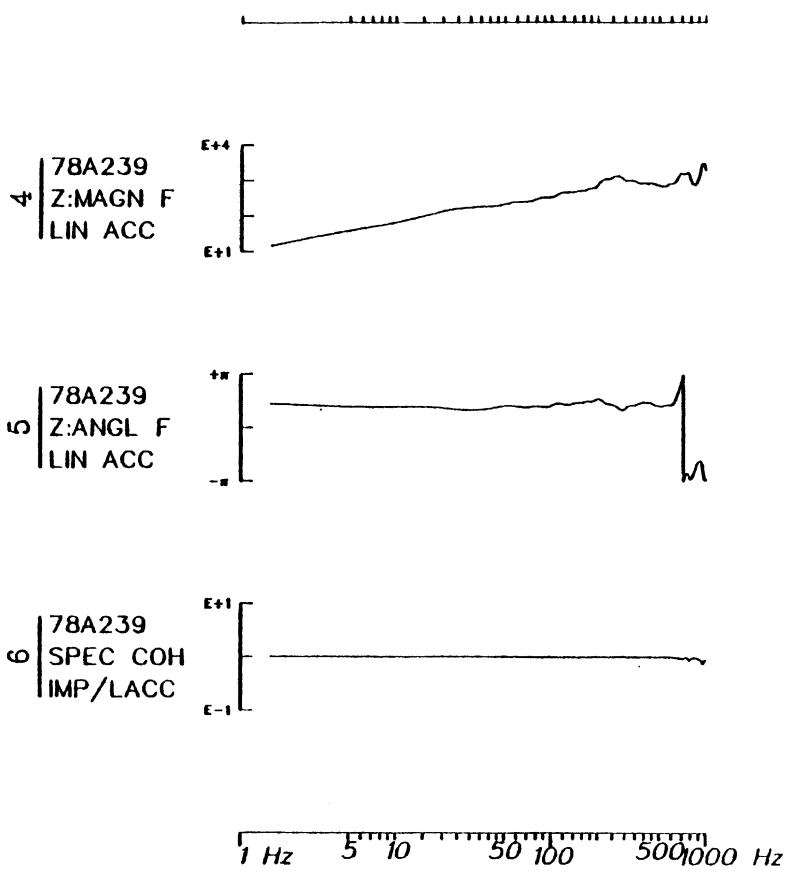

HEAD CENTER OF GRAVITY WITH RESPECT TO LINE OF IMPACT = AT

MECHANICAL IMPEDANCE

TYPE: ANESTHETIZED RHESUS, SKULL FRACTURE, NECK UNSTRETCHED

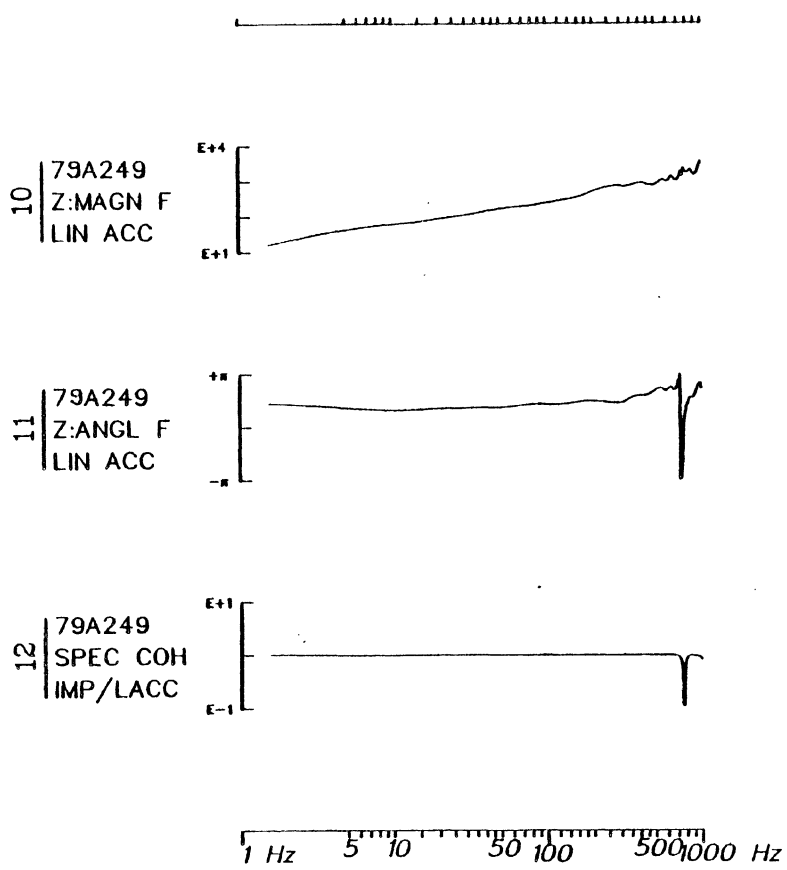

HEAD CENTER OF GRAVITY WITH RESPECT TO LINE OF IMPACT = ABOVE

MECHANCIAL IMPEDANCE

TYPE: ANESTHETIZED RHESUS, SKULL FRACTURE, NECK UNSTRETCHED

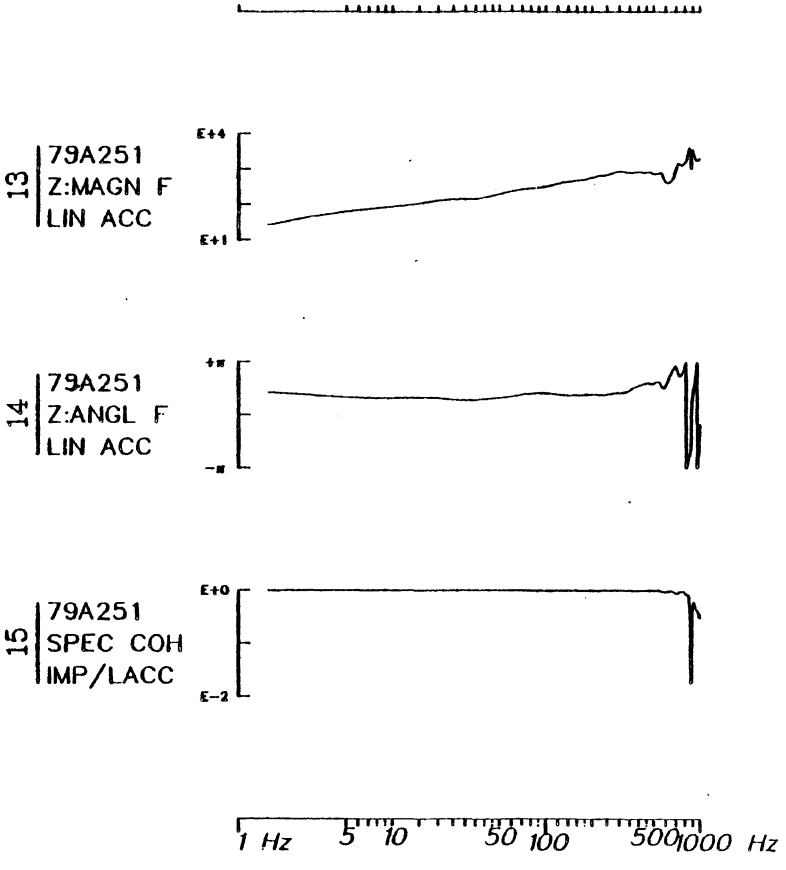

HEAD CENTER OF GRAVITY WITH RESPECT TO LINE OF IMPACT = AT

MECHANICAL IMPEDANCE

TYPE: ANESTHETIZED RHESUS, NO SKULL FRACTURE, NECK UNSTRETCHED

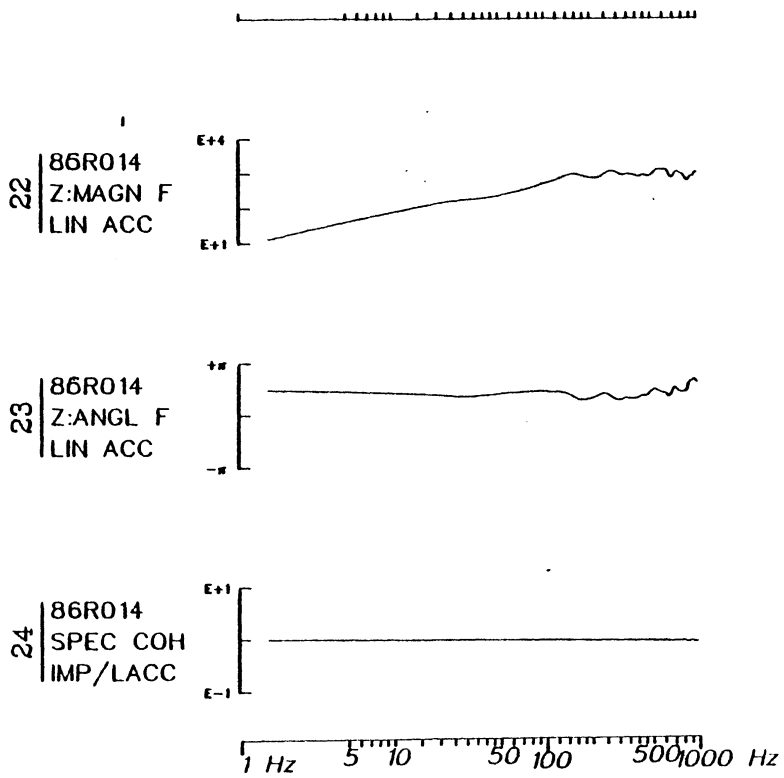

HEAD CENTER OF GRAVITY WITH RESPECT TO LINE OF IMPACT = ABOVE

Auto- and Cross- Correlations

TYPE: UNREPRESSURIZED POSTMORTEM, NO SKULL FRACTURE, NECK UNSTRETCHED

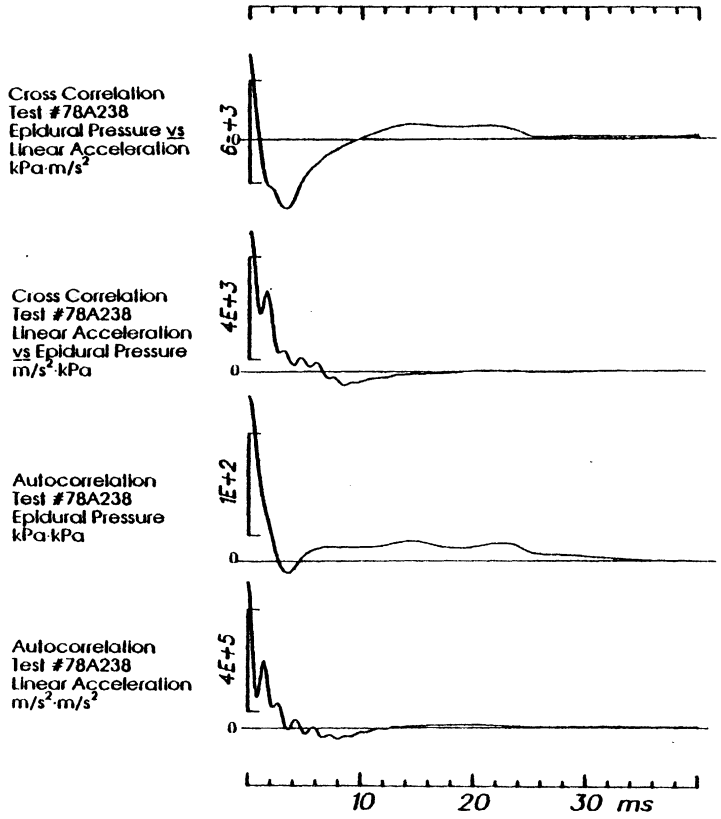

HEAD CENTER OF GRAVITY WITH RESPECT TO LINE OF IMPACT = ABOVE

Cross- and Auto- Correlations

TYPE: ANESTHETIZED, NO SKULL FRACTURE, NECK UNSTRETCHED

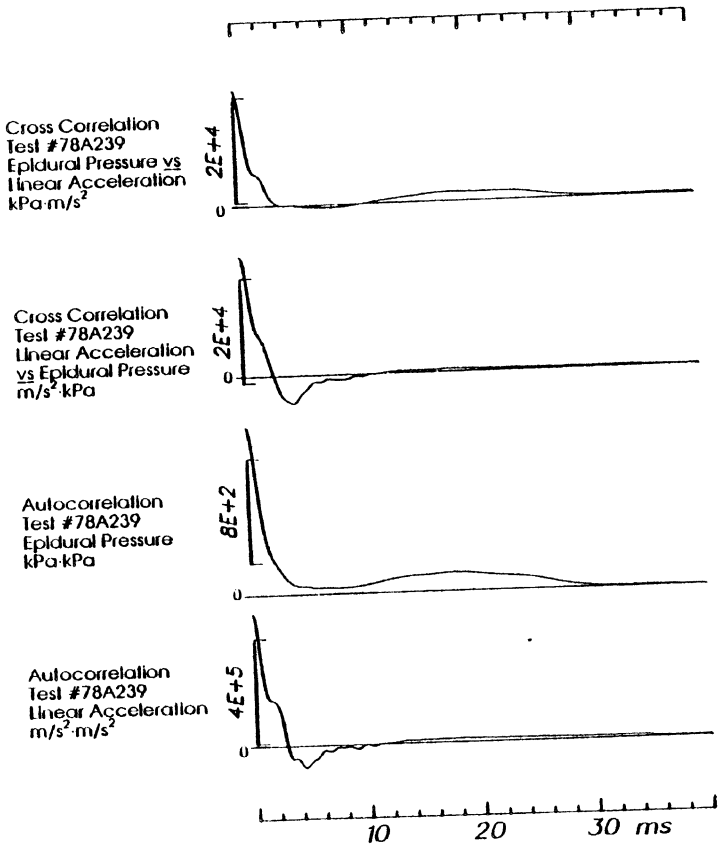

HEAD CENTER OF GRAVITY WITH RESPECT TO LINE OF IMPACT = AT

Cross- and Auto- Correlations

TYPE: ANESTHETIZED, SKULL FRACTURE, NECK UNSTRETCHED

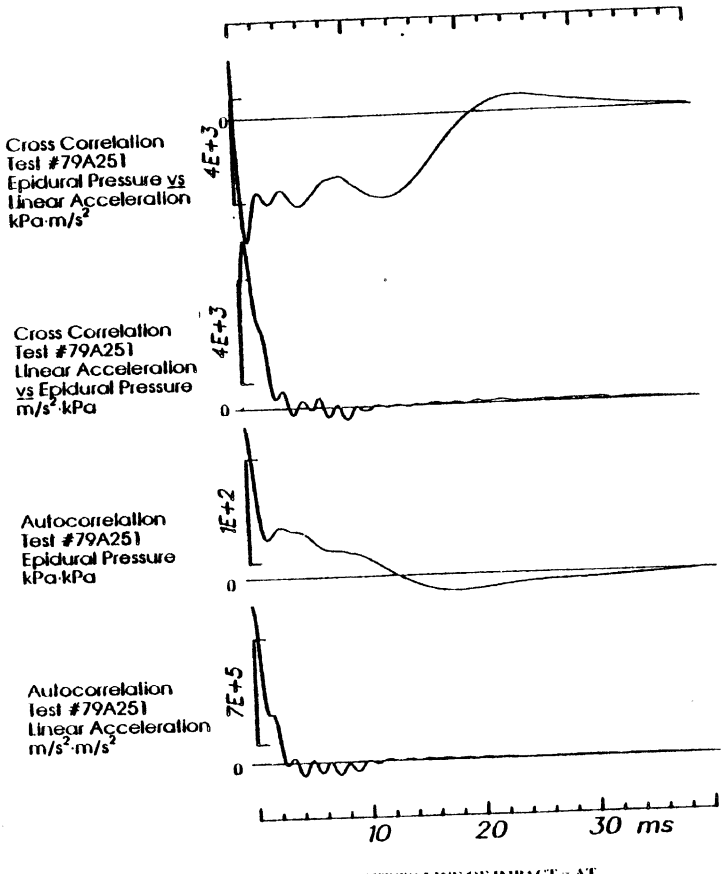

HEAD CENTER OF GRAVITY WITH RESPECT TO LINE OF IMPACT = AT

Cross- and Auto- Correlations

TYPE: UNREPRESSURIZED POSTMORTEM, SKULL FRACTURE, NECK UNSTRETCHED

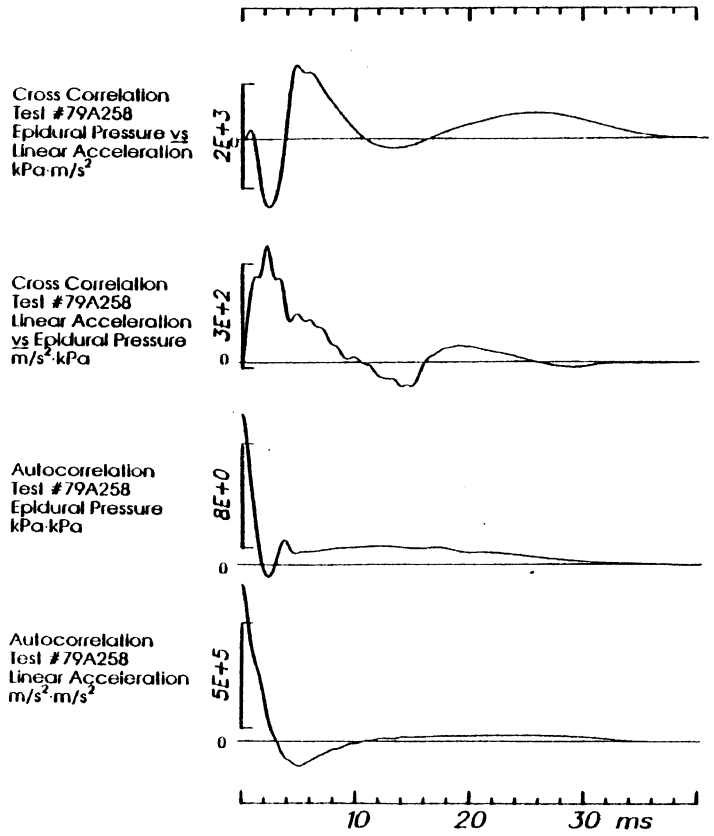

HEAD CENTER OF GRAVITY WITH RESPECT TO LINE OF IMPACT = AT

Cross- and Auto- Correlations

TYPE: UNREPRESSURIZED POSTMORTEM, SKULL FRACTURE, NECK UNSTRETCHED

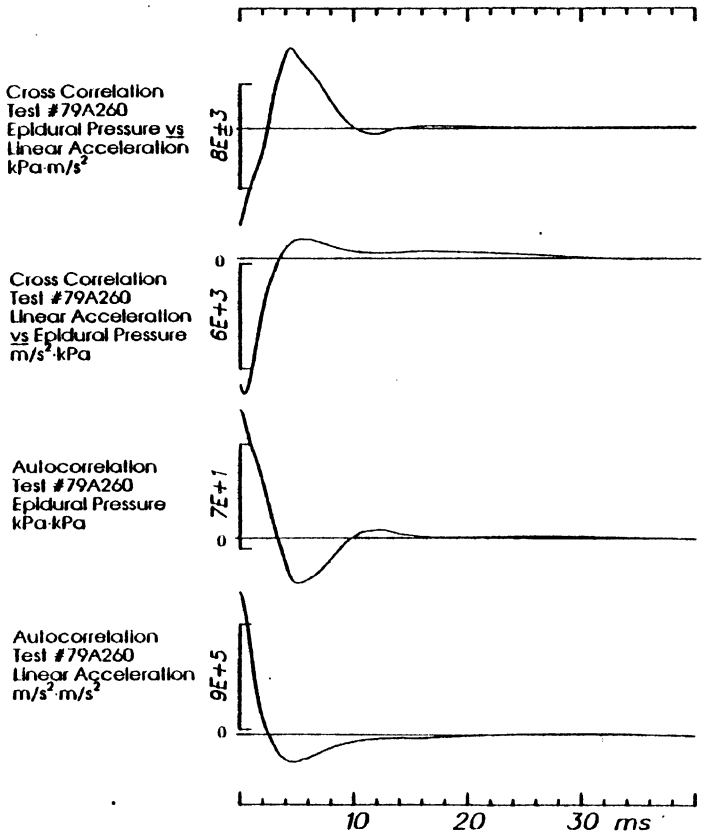

HEAD CENTER OF GRAVITY WITH RESPECT TO LINE OF IMPACT = AT

Auto- and Cross- Correlations

TYPE: REPRESSURIZED POSTMORTEM, SKULL FRACTURE, NECK UNSTRETCHED

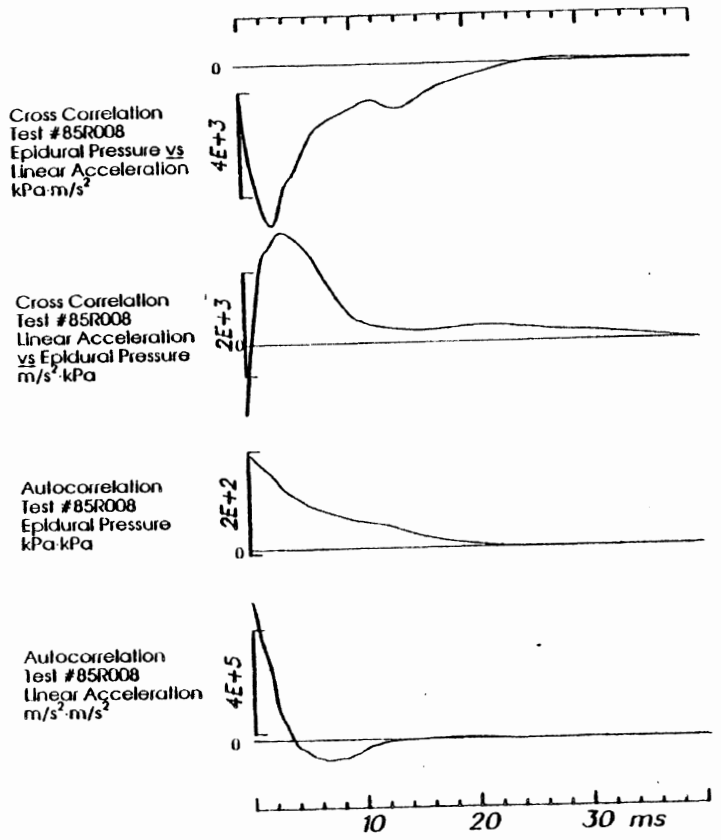

HEAD CENTER OF GRAVITY WITH RESPECT TO LINE OF IMPACT = ABOVE

Cross- and Auto- Correlations

TYPE: ANESTHETIZED, NO SKULL FRACTURE, NECK STRETCHED

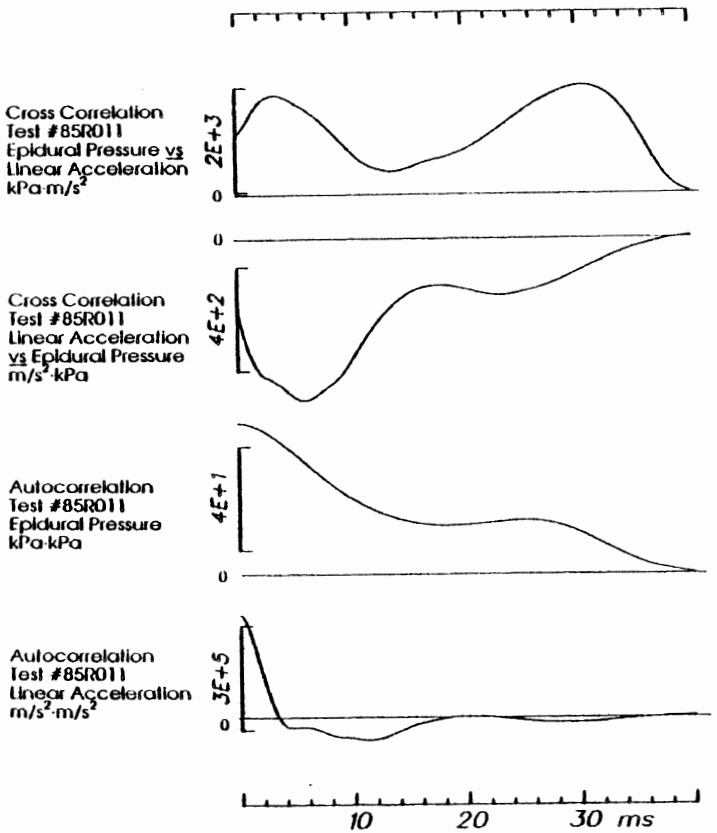

HEAD CENTER OF GRAVITY WITH RESPECT TO LINE OF IMPACT = ABOVE

Cross- and Auto- Correlations

TYPE: ANESTHETIZED, NO SKULL FRACTURE, NECK STRETCHED

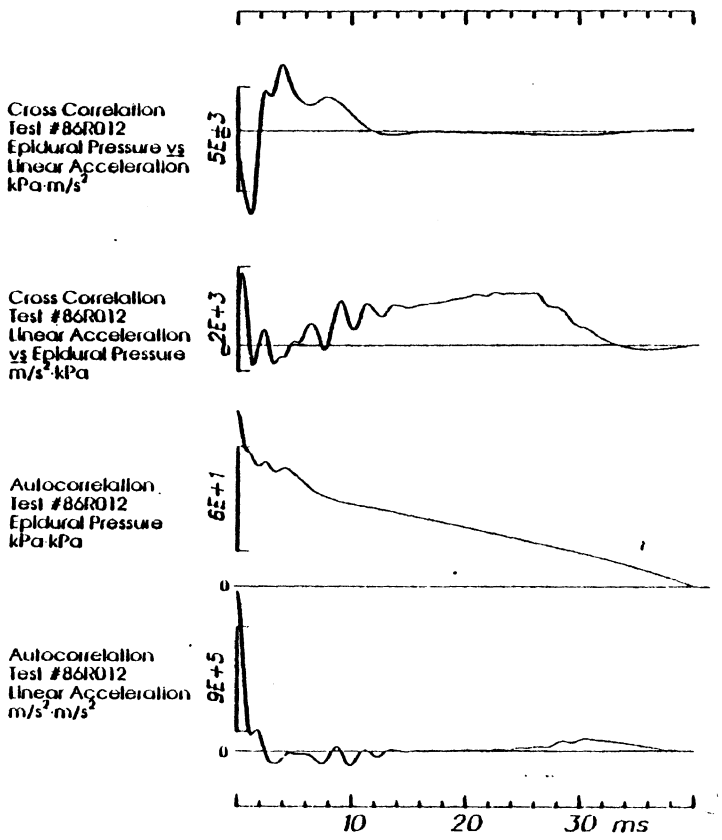

HEAD CENTER OF GRAVITY WITH RESPECT TO LINE OF IMPACT = ABOVE

Cross- and Auto- Correlations

TYPE: ANESTHETIZED, NO SKULL FRACTURE, NECK STRETCHED

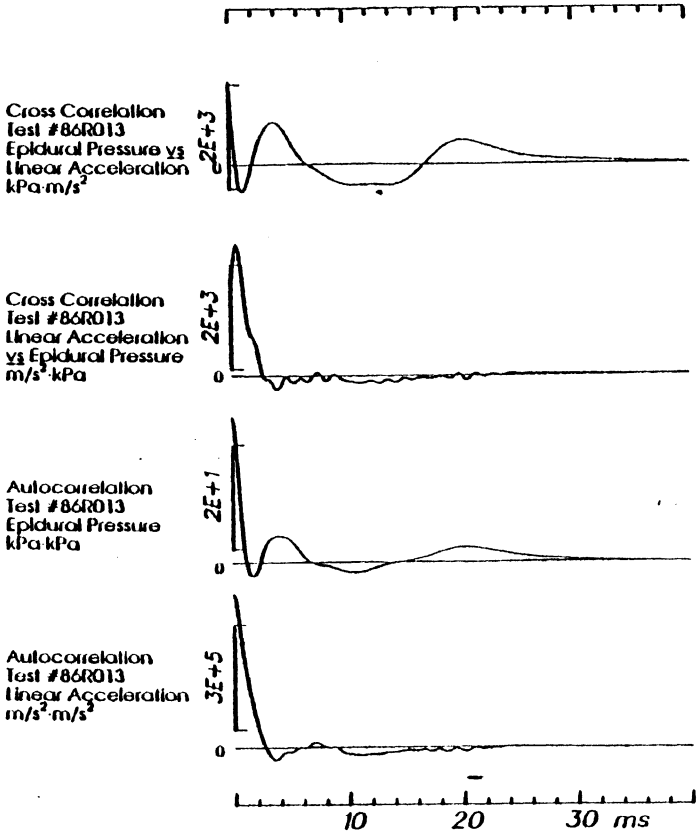

HEAD CENTER OF GRAVITY WITH RESPECT TO LINE OF IMPACT = ABOVE

Cross- and Auto- Correlations

TYPE: ANESTHETIZED, NO SKULL FRACTURE, NECK UNSTRETCHED

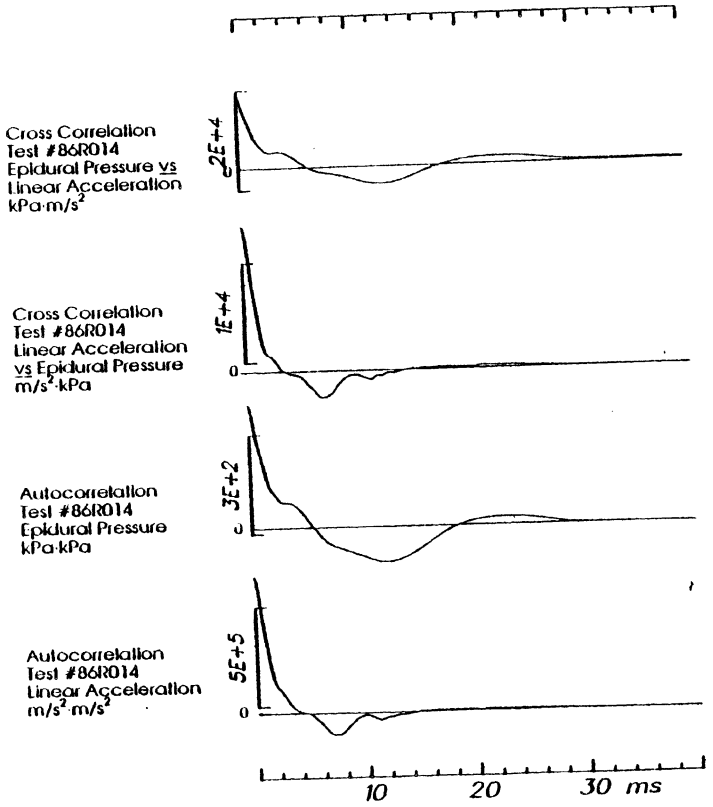

HEAD CENTER OF GRAVITY WITH RESPECT TO LINE OF IMPACT = ABOVE

KINEMATIC TIME-HISTORIES

TYPE: UNREPRESSURIZED POSTMORTEM, NO SKULL FRACTURE, NECK UNSTRETCHED

Run ID: 78A236 *Filter: 1600*4C* *Smooth: 3SD*

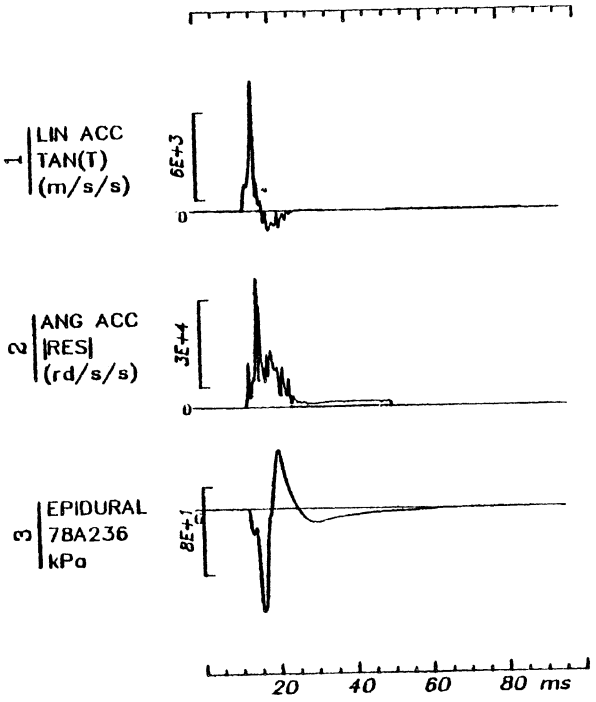

1=Tangential Acceleration
2=Angular Acceleration (Resultant)
3=Epidural Pressure

HEAD CENTER OF GRAVITY WITH RESPECT TO LINE OF IMPACT = AT

KINEMATIC TIME-HISTORIES

TYPE: ANESTHETIZED, SKULL FRACTURE, NECK UNSTRETCHED

Run ID: 79A249 *Filter: 1600*4C* *Smooth: 3SD*

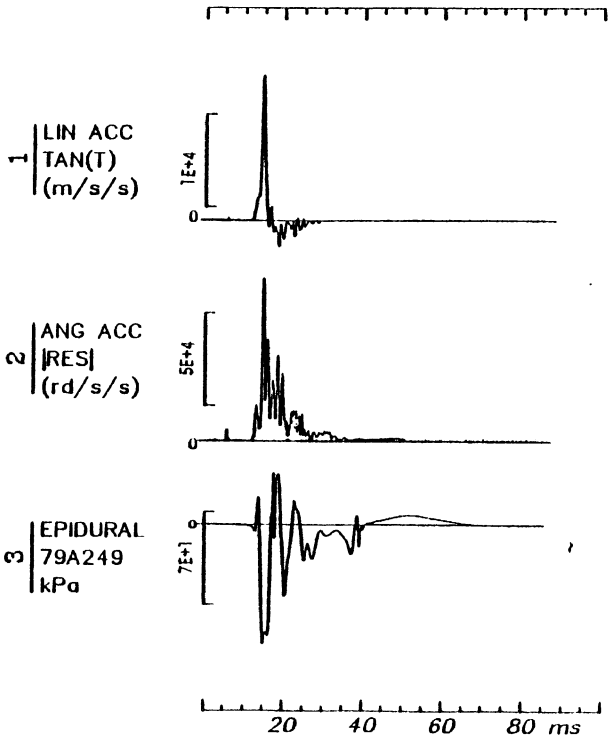

1=Tangential Acceleration
2=Angular Acceleration (Resultant)
3=Epidural Pressure

HEAD CENTER OF GRAVITY WITH RESPECT TO LINE OF IMPACT = ABOVE

KINEMATIC TIME-HISTORIES

TYPE: ANESTHETIZED, SKULL FRACTURE, NECK UNSTRETCHED

Run ID: 79A251 *Filter: 1600*4C* *Smooth: 3SD*

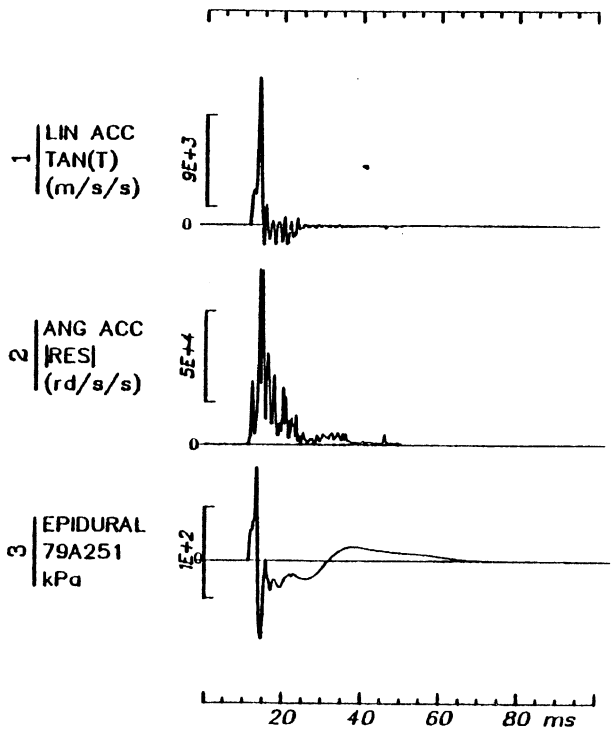

1=Tangential Acceleration
2=Angular Acceleration (Resultant)
3=Epidural Pressure

HEAD CENTER OF GRAVITY WITH RESPECT TO LINE OF IMPACT = AT

KINEMATIC TIME-HISTORIES

TYPE: REPRESSURIZED POSTMORTEM, NO SKULL FRACTURE, NECK UNSTRETCHED

Run ID: 85R006 H9 *No Filtering*

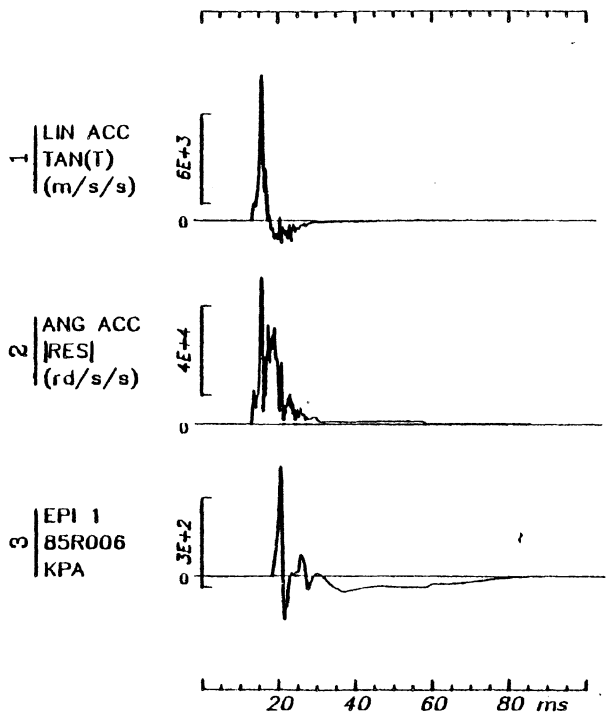

1=Tangential Acceleration
2=Angular Acceleration (Resultant)
3=Epidural Pressure

HEAD CENTER OF GRAVITY WITH RESPECT TO LINE OF IMPACT = ABOVE

KINEMATIC TIME-HISTORIES

TYPE: ANESTHETIZED, NO SKULL FRACTURE, NECK STRETCHED

Run ID: 86R013 H7 *No Filtering*

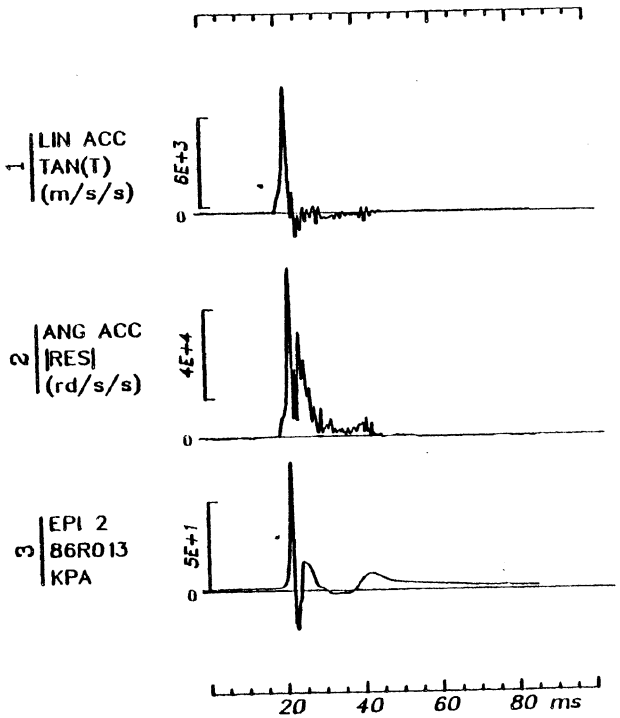

1=Tangential Acceleration
2=Angular Acceleration (Resultant)
3=Epidural Pressure

HEAD CENTER OF GRAVITY WITH RESPECT TO LINE OF IMPACT = ABOVE

KINEMATIC TIME-HISTORIES

TYPE: ANESTHETIZED, NO SKULL FRACTURE, NECK UNSTRETCHED

Run ID: 86R014 H7 *No Filtering*

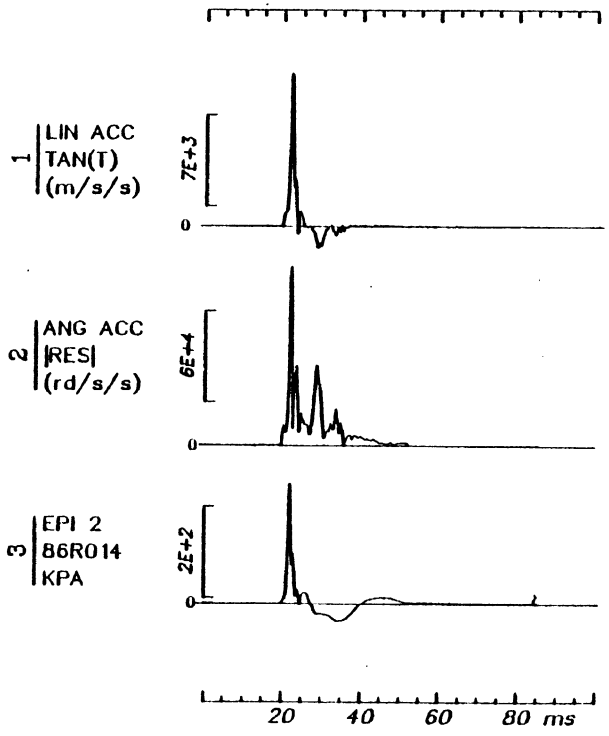

1=Tangential Acceleration
2=Angular Acceleration (Resultant)
3=Epidural Pressure
HEAD CENTER OF GRAVITY WITH RESPECT TO LINE OF IMPACT = ABOVE

KINEMATIC TIME-HISTORIES

TYPE: ANESTHETIZED, SKULL FRACTURE, NECK UNSTRETCHED

Run ID: 86R015 H7 *No Filtering*

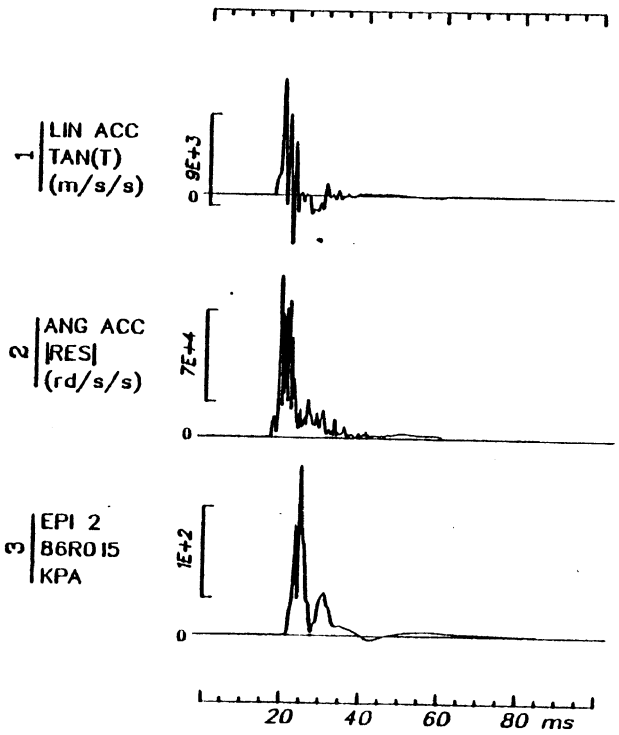

1=Tangential Acceleration
2=Angular Acceleration (Resultant)
3=Epidural Pressure
HEAD CENTER OF GRAVITY WITH RESPECT TO LINE OF IMPACT = ABOVE

APPENDIX H: Test Protocol

EXPERIMENTAL TECHNIQUES IN HEAD INJURY RESEARCH

DOT Contract No. DTNH22-83-C-07095

DEPARTMENT OF TRANSPORTATION

RHESUS HEAD IMPACT TESTS

[LIVE OR POSTMORTEM SUBJECT]

_____ Through _____

as performed by

the Biomechanics Department of

the Transportation Research Institute

Ann Arbor, Michigan

1985 A Series

This protocol for the use of rhesus monkeys in this test series follows guidelines established by the National Institutes of Health and provides that the animals are handled according to the practices of the American Association of Laboratory Animal Care.

START TEST PROTOCOL

TASK	TIME	COMMENTS
Start film hyping.		
Begin filling out test forms.		
Set up and check equipment in Impact Lab.		
ELECTRONICS CHECK and Pre-Test Trial Run.		
Set up Anatomy Lab, X-Ray, X-Ray developing, and Physiology Lab.		
Set up Vivarium Prep Room.		
Set up Impact Lab Cart.		
Animal arrives from ULAM.		
Transport animal to Vivarium Prep Room.		
Log animal information.		

HYPING PROCESS FOR 16MM HIGH-SPEED FILM

In order to obtain better image clarity of processed high-speed 16mm film, it is prepared by gas hyping in an oven at 30-35 degrees Centigrade for 24 hours. (Although the test samples at 50 degrees Centigrade did not break and the clarity was enhanced, the film was very brittle and potentially breakable during filming.) This treatment permits ASA variability in a range between ASA 50 and ASA 2000 with good resolution. Also the film can be developed commercially without unusual processing requests. The hyping agent is forming gas (10%H, 90%N) which removes the oxygen layer that has formed on the film emulsion and replaces it with hydrogen. A spacer (a piece of ribbon the width of 16mm film) is fed simultaneously (in the darkroom) onto a metal film wheel with the film so that the film to be hyped is separated from itself and the spacer. This permits even gas flow across the film surface and uniform replacement of the oxygen with the hydrogen. In the hyping oven the lid of the light-tight film cannister is removed without exposing the film to light (the oven is draped with a light-tight cloth). After hyping, the film is rewound onto its wheel and is ready for use in any 16mm camera. Currently, we use this technique for hyping film for a 16mm Milliken high-speed camera which operates at 400 frames/ second.

INSTRUMENTATION GUIDE

Anatomical Site	Head Impacts		COMMENTS	
	Accs.*	Targets**	Accs.	Targets
Head				
Head				
Head				
Head				
Head				
Head				
Sternum				
Sternum				
Rib				
Rib				
Thoracic vertebra				
Thoracic vertebra				
Thoracic vertebra				

*Indicate AX, 3AX, 9AX, strain gauge as SG1/SG2, and EPI1/EPI2
**Indicate paper target, ball target, or 5-pt. target.

ELECTRONICS CHECK AND PRE-TEST TRIAL RUN

___ Inspect triaxes and uniaxes for signs of wear

___ Complete wiring

___ Establish and record gains settings

___ Calibrate tape recorder

___ Check pendulum and load cell, velocity transducer, gate, ropecutter

___ Set timerbox

___ Check excitation and balances

___ Gate signal amplifier on

___ Suspend rubber tube five inches from ballistic impactor with fiber tape

___ Tape all accelerometers to tube with paper tape

___ Wire in and tape Miletus contact circuit to tube with paper tape

___ RUN TRIAL TEST

___ Examine signals, check wiring if necessary

___ Verify operation of cameras, ropecutter,

cineradiograph, pressure transducers, ECG, and EEG.

___ Load high-speed film

HEAD IMPACT TIMER BOX SETUP

TEST NO._____

EQUIPMENT		TIMER VALUES		
Control	Signals	Delay		Run
			1	
			2	
			3	
			4	
			5	
			6	
			7	
			8	

DRUG RECORD

DRUG	DOSAGE	TIME

HEAD IMPACT TEST DESCRIPTION

Animal No._____ Sex:_____ Height:_____ Weight:_____

Test No._____

Test description:_____

_____

_____

_____

_____

Type of Impactor:_____

Striking Surface:_____

Pressure:_____

Padding:_____

Pre-Impact Travel:_____

Post-Impact Travel:_____

35mm stills:

___ Black and White

___ Color

CAMERAS	FRAME RATE	POSITION
Photosonics 1B:	_____	_____
HyCam:	_____	_____
Milliken:	_____	_____

Polaroid _____

Notes:_____

_____

_____

LIVE, ANESTHETIZED HEAD IMPACT TEST DIAGRAM

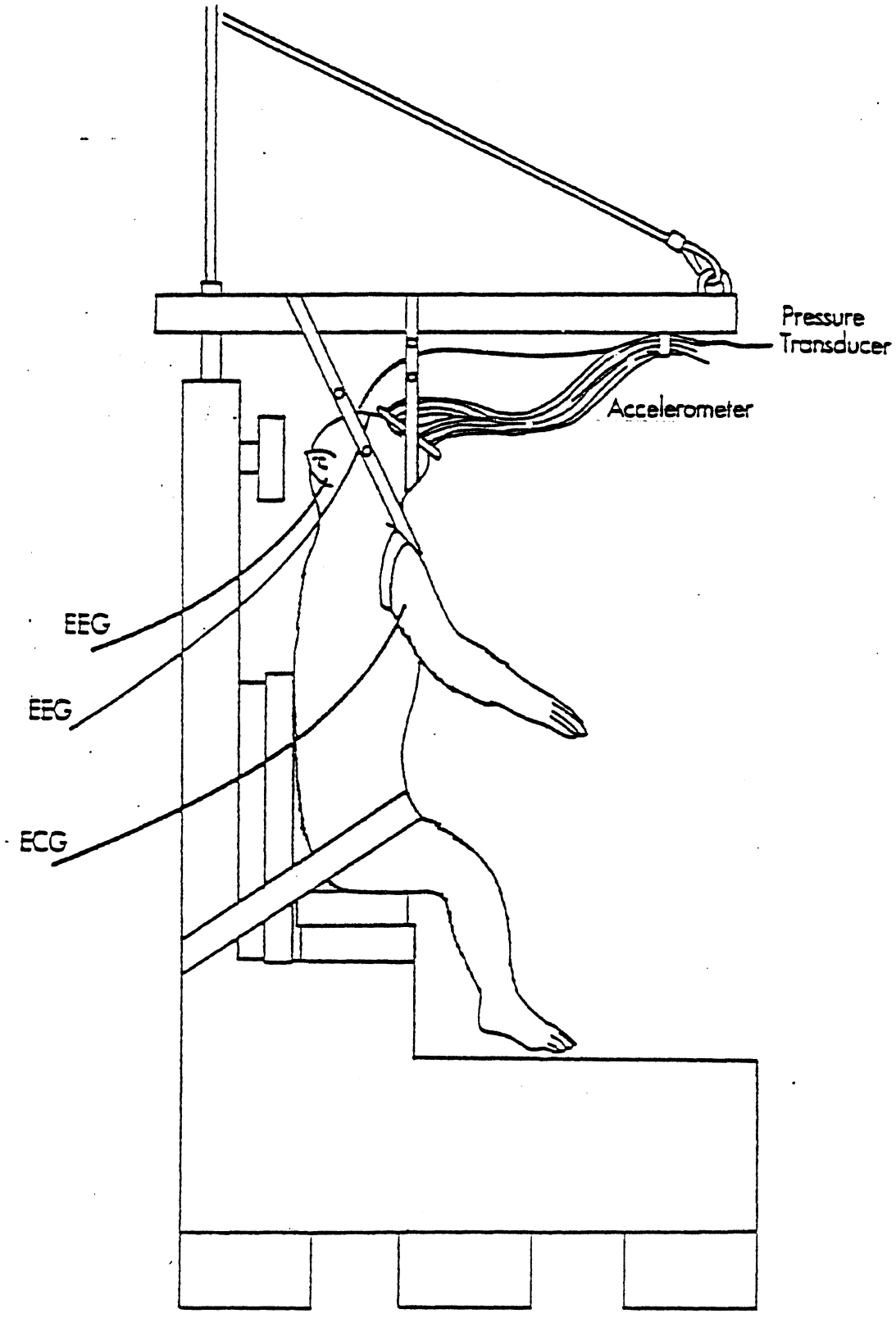

POSTMORTEM HEAD IMPACT TEST DIAGRAM

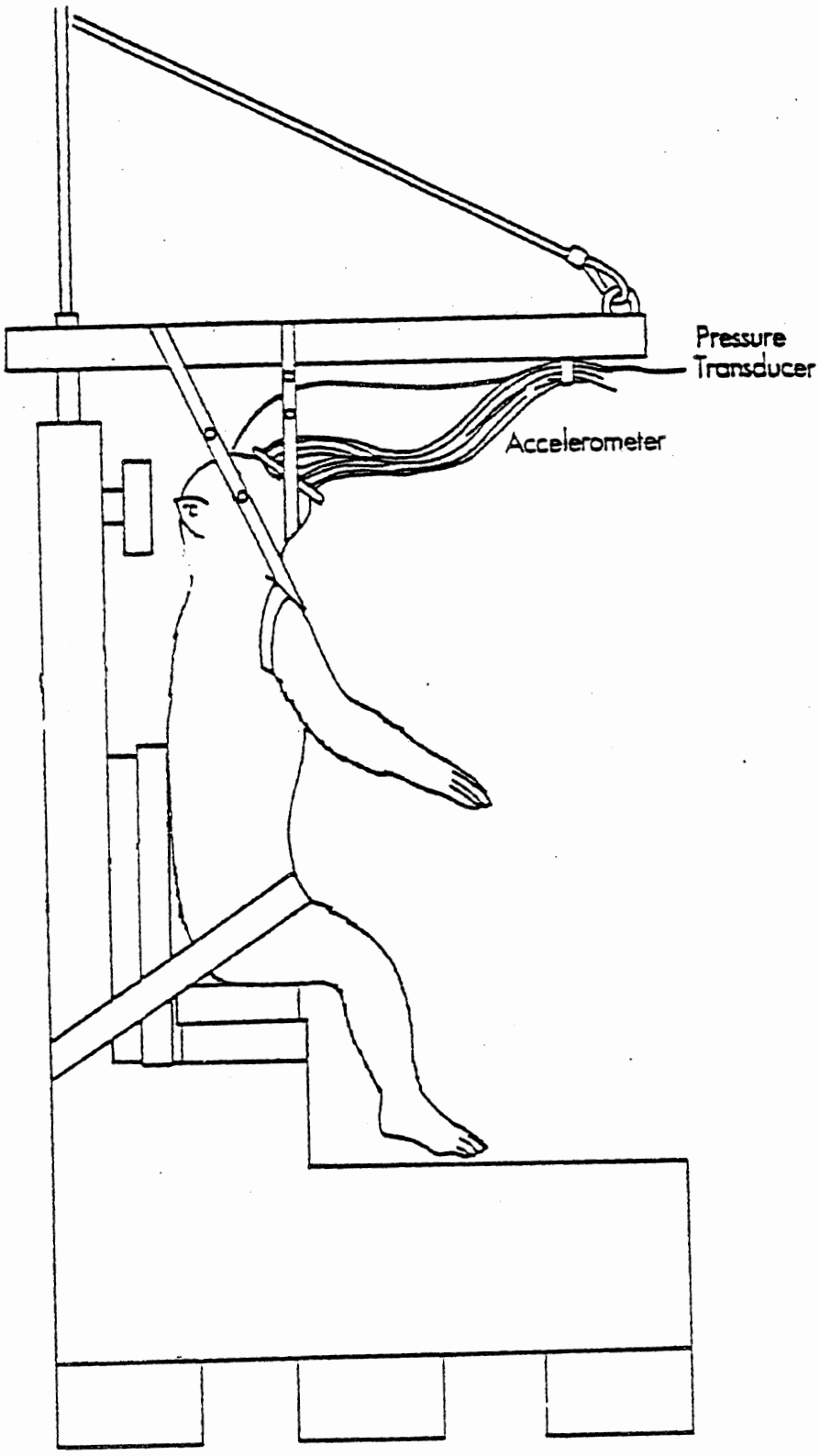

VIVARIUM PREP AND ANESTHESIA MAINTENANCE

TASK	TIME	COMMENTS
Inject animal with ketamine if necessary.		
Shave lower part of both hind legs.		
Place I.V. catheter in hind leg vein for drug administration.		
Insert stopcock into catheter, and tape it securely to the leg.		
Inject Na pentobarbitol via lower leg catheter.		
Establish an airway if necesary.		
Shave back, chest, all of head, neck, and upper arms.		

BLOOD SAMPLE CATHETER

TASK	TIME	COMMENTS
Tie off and diaper animal.		
Establish I.V. Abbocath in the *Saphena parva* vein of the left leg for drawing blood samples.		
Suture incisions.		

ANTHROPOMETRY

TASK	TIME	COMMENTS
Weigh animal.		
Transport to Anatomy Lab.		
Anthropometry.		
Position animal for instrumentation surgery on table.		

ANTHROPOMETRY

Height (sitting) cm_____ Weight kg_____

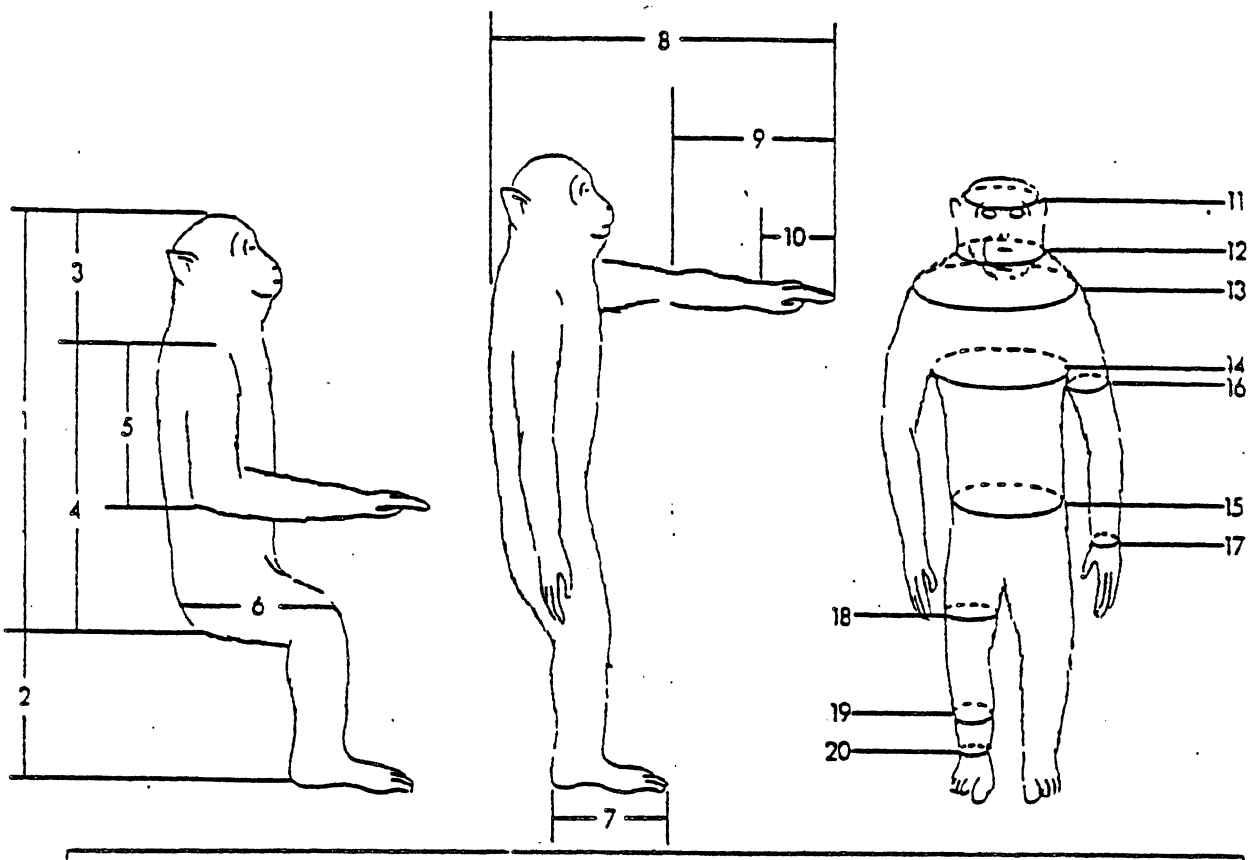

LOCATION OF BODY MEASUREMENTS							
LENGTH IN CM.				CIRCUMFERENCE IN CM.			
1. BUTTOCK - CROWN		6. BUTTOCK - KNEE		11. HEAD		16. BICEPS	
2. POPLITEAL HEIGHT		7. HEEL - TOE (Foot)		12. NECK		17. WRIST	
3. TOP HEAD - TOP SHOULDER		8. TOTAL ARM REACH		13. SHOULDER		18. THIGH (Mid shaft)	
4. ACROMIAL HEIGHT		9. FOREARM - HAND		14. CHEST		19. CALF	
5. SHOULDER - ELBOW		10. HAND		15. WAIST (Hip)		20. ANKLE	
REMARKS							

ANATOMICAL ANOMALIES/CLINICAL OBSERVATIONS

1. Skull

2. Neck

3. Other Structures

Observations

1. Thoracic Skeleton

2. Heart

3. Lungs

9-AX MOUNT

TASK	TIME	COMMENTS
Cauterize scalp to clear area for mount.		
Core two 0.128" holes into the right and left sides of frontal bone over orbital ridge (avoiding sagittal sinus). Record postion of holes. Remove bone core with dental scoop. Tap holes with 8-32 tap. Screw metal epidural pressure transducer fittings into the 0.128" holes in the skull. Apply dental acrylic around fittings.		
Drill and tap three holes in frontal ridge for self-tapping screws to hold 9-axial accelerometer mount. Insert screws.		
Drill holes for 1/4x6 pan type A sheet metal screws in dental plate, to hold 9-Ax accelerometer mount. Screw them in.		
Affix the 9-Ax plate to the skull with dental acrylic.		

CEREBROSPINAL PRESSURIZATION FOR POSTMORTEM HEAD IMPACT

TASK	TIME	COMMENTS
Locate L2 by palpation and counting from T12.		
Core a small hole in the lamina.		
Insert Foley catheter (#10) such that balloon is in mid-thorax.		
Insert small screws in lamina and process.		
Seal off hole with acrylic.		
Check for structural integrity of vertebra.		
Cerebral-spinal flow check.		
Check pressurization.		

VASCULAR PRESSURIZATION FOR POSTMORTEM HEAD IMPACT

TASK	TIME	COMMENTS
Locate right carotid and cut lengthwise.		
Loop six pieces of string around carotid arteries.		
Insert pressure transducer into carotid artery.		
Using syringe, squirt acrylic into artery. Tie and sew.		
Locate left carotid, cut, loop strings.		
Insert arterial pressurization catheters (#10) into carotid artery.		
Acrylic, tie and sew.		
Vascular flow check.		

LIVE HEAD IMPACT SUBJECT POSTIONING

TASK	TIME	COMMENTS
Place head and body harnesses on animal.		
Transport animal to test area for Live Head Impact being careful not to damage mounts.		
Place the animal in the impact chair in front of the cannon.		
Attach head accelerometer mounts to plate with 1-72 screws.		
Initial positioning (lap belts). Use paper tape only.		

LIVE HEAD IMPACT SET-UP

Test No._____

psi:_____ Velocity:_____

TASK	TIME	COMMENTS
Plug in strain gauge cables. Align notch on cable to angle corner.		
Connect EEG, ECG.		
Turn on blower of cineradiograph. Throughout the procedure, be careful not to "suffocate" it by blocking its air intake.		
Place padding on impactor head surface. Attach ball targets and phototargets.		
Continuity check of strain gauges, accelerometers, etc.		
Strain gauge balance.		
Turn on cineradiograph focussing magnet. Check to see that it limits.		
Position cineradiograph.		
Position X-ray head approximately 40 inches from the screen of the cineradiograph.		
Lock the wheels on the X-ray head and cineradiograph.		
Check filters.		
Set polaroid camera at f 16.		

LIVE HEAD IMPACT SET-UP (CONT.)

TASK	TIME	COMMENTS
CLEAR LAB OF ALL INDIVIDUALS NOT WEARING X-RAY BADGES.		
Polaroid checklist. Take polaroid photo.		
If it is necessary to do so, adjust the KVP and the distance from the X-ray head to the cineradiograph screen; retake the polaroid photo. Check the second photo to see if further adjustment is necessary. Record the number of polaroids taken. Save and label the good ones.		
Exchange the high speed movie camera for the polaroid camera in the cineradiograph camera mount.		
Check alignment of movie camera with photocathode.		
Focus the movie camera.		
Set the lens opening of the movie camera at its greatest aperture.		
Take setup photos. Make sure test number and necessary targets are visible.		
High-speed X-Ray checklist. 16 mm checklist.		

LIVE HEAD IMPACT SET-UP (CONT.)

TASK	TIME	COMMENTS
Check the pulse width on the gating circuit. It should be at 225 microseconds.		
Set X-ray head to cine-radiograph screen distance. Record.		
Measure and record the subject midline to cineradiographic screen distance.		
Punch holes in paper tape which is supporting animal.		
Check the power console for proper gains on all channels.		
MAKE SURE LAB IS CLEAR OF ALL INDIVIDUALS NOT WEARING X-RAY FILM BADGES.		
Turn off all lights.		
Set KV on X-ray. Record.		
Set milleamps on X-ray. Record.		
Set time on X-ray. Record. Turn on gating circuit. (To External).		

LIVE HEAD IMPACT SET-UP (CONT.)

TASK	TIME	COMMENTS
Turn on high voltage. Set it at 35 KVP.		
Turn gating circuit to 4 KV.		
Arm Cannon.		
Final positioning		
Cerebrospinal pressure check.		
Measure and record head and neck angles Head:___ Neck:___		
Take in-place X-rays.		
Setup photos.		
HiSpeed X-ray checklist 16 mm checklist		
Final checklist.		
RUN LIVE HEAD IMPACT TEST.		

LIVE HEAD IMPACT POST-TEST PROCEDURE

TASK	TIME	COMMENTS
Remove all targets and accelerometers.		
Disconnect EEG and ECG.		
Remove animal from impact chair		
Transport animal to anatomy lab.		
Reconnect EEG and ECG and moniter them.		
Take blood chemistry and/or cerebrospinal chemistry.		
Terminate. Bilateral pneumothorax to guarantee termination.		
Remove the millars.		
Store animal if necessary.		
Remove screws and epidural pressure transducer fittings from the skull.		
Do not remove 9AX head plate.		

POSTMORTEM HEAD IMPACT SUBJECT POSITIONING

TASK	TIME	COMMENTS
Place head and body harnesses on animal.		
Transport animal to test area, being careful not to damage mounts.		
Set up pressurization equipment (pulmonary, cerebro-spinal, vascular head and vascular thorax).		

POSTMORTEM HEAD IMPACT SET-UP

Test No._____

psi:_____ Velocity:_____

TASK	TIME	COMMENTS
Place the animal in the impact chair in front of the cannon.		
Attach Head accelerometer mounts to plate with 1-72 screws.		
Initial positioning (lap belts). Use paper tape only.		
Couple both Kulite or Endevco to epidural pressure transducer fittings using a No.12 French Foley catheter tubing section, silicon fluid, and flat waxed string.		
Plug in strain gauge cables. Align notch on cable to angle corner.		
Turn on blower of cineradiograph. Throughout the procedure, be careful not to "suffocate" it by blocking its air intake.		
Place padding on impactor head surface. Attach ball targets and phototargets.		
Continuity check of strain gauges, accelerometers, etc.		

POSTMORTEM HEAD IMPACT SET-UP (CONT.)

TASK	TIME	COMMENTS
Strain gauge balance.		
Turn on cineradiograph focusing magnet. Check to see that it limits.		
Position cineradiograph.		
Position X-ray head approximately 50 inches from the screen of the cineradiograph.		
Lock the wheels on the X-ray head and cineradiograph.		
Check filters.		
Set polaroid camera at f 16. CLEAR LAB OF ALL INDIVIDUALS NOT WEARING X-ray BADGES.		
Polaroid checklist. Take polaroid photo.		

POSTMORTEM HEAD IMPACT SET-UP (CONT.)

TASK	TIME	COMMENTS
If it is necessary to do so, adjust the KVP and the distance from the X-ray head to the cineradiograph screen; retake the polaroid photo. Check the second photo to see if further adjustment is necessary. Record the number of polaroids taken. Save and label the good ones.		
Exchange the high speed movie camera for the polaroid camera in the cineradiograph camera mount.		
Check alignment of movie camera with photocathode.		
Focus the movie camera.		
Set the lens opening of the movie camera at its greatest aperture.		
Take setup photos. Make sure test number and necessary targets are visible.		
High-speed X-Ray checklist. 16 mm checklist.		
Check the pulse width on the gating circuit. It should be at 225 microseconds.		

POSTMORTEM HEAD IMPACT SET-UP (CONT.)

TASK	TIME	COMMENTS
Set X-ray head to cine-radiograph screen distance. Record.		
Measure and record the subject midline to cineradiographic screen distance.		
Punch holes in paper tape which is supporting animal.		
Check the power console for proper gains on all channels.		
MAKE SURE LAB IS CLEAR OF ALL INDIVIDUALS NOT WEARING X-ray FILM BADGES.		
Begin pressurization of vascular and cerebrospinal systems for check.		
Turn off all lights.		
Set KV on X-ray. Record.		
Set milleamps on X-ray. Record.		
Set time on X-ray. Record. Turn on gating circuit. (To External).		
Turn on high voltage. Set it at 35 KVP.-		
Turn gating circuit to 4 KV.		
Arm Cannon.		

POSTMORTEM HEAD IMPACT SET-UP (CONT.)

TASK	TIME	COMMENTS
Prepare radiopaque target jell.		
Place padding on impactor head surface. Attach ball targets and phototargets.		
Final positioning		
Cerebrospinal pressure check.		
Inject jell into brain.		
Screw epidural pressure transducers into head.		
Measure and record head and neck angles Head:___ Neck:___		
Take in-place X-rays.		
Setup photos.		
HiSpeed X-ray checklist 16 mm checklist		
Pressurize vascular and cerebrospinal systems.		
Final checklist.		
RUN POSTMORTEM HEAD IMPACT TEST.		

POSTMORTEM HEAD IMPACT POST-TEST PROCEDURE

TASK	TIME	COMMENTS
Remove all targets and accelerometers.		
Cut strain guage wires leaving 1/4" of each on skull to preserve the color.		
Remove animal from impact chair		
Store animal if necessary.		
Transport animal to anatomy lab.		
Remove screws and epidural pressure transducer fittings from the skull.		
Do not remove 9-AX head plate.		
Place X-ray targets on the animal: 2 eye targets, 2 ear targets.		
Remove head and transport it to X-ray room for post test radiographs.		
Remove the Kulite and the 9-Ax plate from animal.		

NECROPSY

TASK	TIME	COMMENTS
Place X-ray targets on the animal: 2 eye targets, 2 ear targets.		
Remove head and transport it to X-ray room for post test radiographs.		
Take 2 X-rays: AP (Y-Z) and RL (X-Z).		
After completion of radiographs, transport head to Anatomy Room for necropsy.		
Necropsy begins.		
Thorax and abdominal dissection.		
Head and neck dissection.		
Take head measurements and record.		
Autopsy completed.		
Store at 4 degrees C if necessary.		
Return to ULAM for disposal.		

X-RAYS (X-RAY ROOM)

Reference Point	Z-X Distance from Table	Z-Y Distance from Table
R. Eye		
L. Eye		
R. Ear		
L. Ear		
Q1		
Q2		
Q3		
CG		

KVP MA SEC LABEL

Z-X _____/_____/_____/_____ (80/10/1)

Z-Y _____/_____/_____/_____ (80/10/1)

NECROPSY HEAD MEASUREMENTS

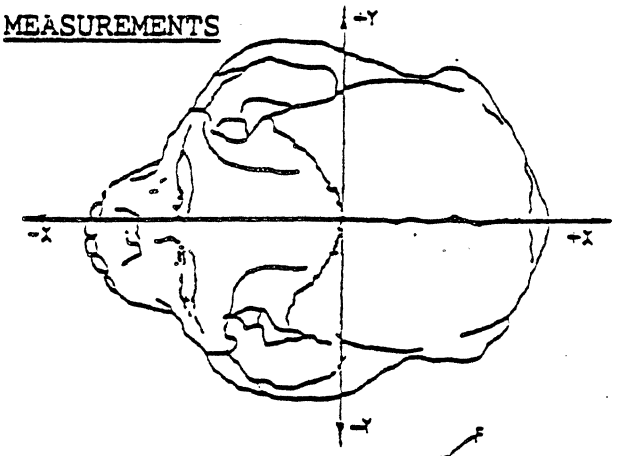

Head Muscle Weight _____

Head Weight _____

Brain Weight _____

Brain Volume _____

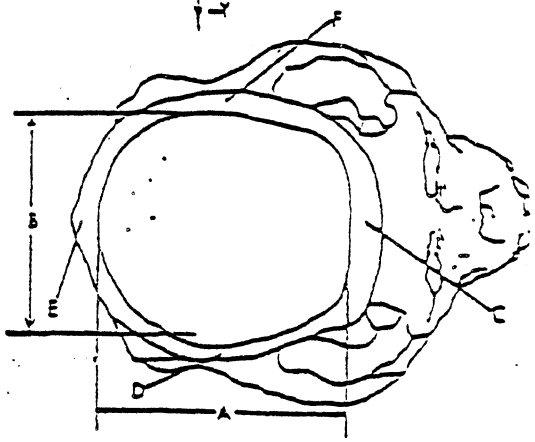

Skull Inside Length A _____

Skull Inside Width B _____

Skull Thickness at Pt. C _____

Skull Thickness at Pt. D _____

Skull Thickness at Pt. E _____

Skull Thickness at Pt. F _____

Skull Thickness at location of strain gauge 1 (SG1)_____

Skull Thickness at location of strain gauge 2 (SG2)_____

Skull Thickness at pressure transducer location EPI1 _____

Skull Thickness at pressure transducer location EPI2 _____

Comments on Injuries Observed

Head Impact

1. Neck

2. Skull

3. Brain

4. Others

SETUP CHECKLISTS

Vivarium Setup
Anatomy Setup
Testing Area Setup
Impact Cart Setup
Timer Box Setup
Autopsy Setup

Vivarium Prep Room Setup

ALWAYS WEAR LAB COAT.

ALWAYS WEAR FACE MASK.

___ Blue absorbent pads taped to counter.

Number of items on this list apply
for a run of 2 animals:

___ leather handling gloves
___ scale to weigh animal
___ needle and syringe wastebasket

___ wastebasket

___ green gloves

___ electric hair clippers

Drugs: ___ Ketamine
___ Na pentobarbitol

Calculate how much will
be needed according to species
and approximate weight of the subject;
add extra for total amount which should
be available for use during the
experiment.

e.g. ketamine for cynomolgus (Rhesus)
50mg/kg x 6kg = 300 mg.

___ Stethoscope

___ 6 20-6 Abbocath-T catheters

___ 3 white plastic stopcocks which
fit catheter

___ 2 5-c.c. syringes

___ 2 3-c.c. syringes

___ 2 1-c.c. syringes

___ Adhesive tape

___ 5 sterile needles

___ Gauze

___ 2 plain forceps

___ Medium surgical scissors

___ 2 hemostats

___ Small scalpel handle

___ Large scalpel handle

___ 2 no. 15 scapel blades

___ 2 no.22 scapel blades

___ Flat waxed string

___ Airway tubing of various diameters

___ Tongue depressor

Anatomy Instrumentation Setup

BROUGHT FROM VIVARIUM WITH ANIMAL

___ Drugs
___ Syringes and needles
___ ETOH
___ UTHOL (concentrated Sodium pentobarbitol)

MEASUREMENT

___ Anthropometer
___ Metric measuring tape

PAPER AND PLASTICS

___ Visqueen on autopsy table
___ Blue pads on table
___ Gauze
_____ heavy duty trash bags
_____ diapers and 3 safety pins

TAPES AND STRINGS

___ Silver tape
___ Masking tape
___ Adhesive tape
___ Fiber tape
___ Flat waxed string
___ tie wraps
___ cellophane tape

SCALPELS

___ 1 large (#8) handle
___ 1 small (#3) handle
___ 2 #22 blades
___ 2 #15 blades
___ 2 #12 blades

FORCEPS

___ 2 hooked
___ 2 large plain
___ 2 small plain

HEMOSTATS

___ needle
___ small straight
___ small curved
___ large straight
___ large curved

SCISSORS

___ 2 small
___ 2 medium
___ 2 large

SPREADERS

___ 2 large
___ 2 medium

NEEDLES

___ 2 double curved
___ Trocar with stainless stell lockwire
___ 2 5cc sringes

PRESSURIZATION

___ Modified Foley (#10) balloon catheters
___ Kulite shield
___ Tracheal tube
___ Right and left carotid pressurization catheters (Foley #10)
___ Cerebral spinal French Foley #10 catheter
___ Respiratory pressure tank
___ Manometer
___ Fluid pressure tank
___ 7% saline solution with India ink

BOLTS AND SCREWS

___ 6 self-tapping lag bolts 1/4 x 6 pan head type A sheet metal screws
___ 3 lengths of wood screws (No.2 self tapping)
___ 1-72 screws
___ 2-56 tap ___ Tap "T" holder
___ Strain relief bolt
___ Wood and metal self-tapping screw boxes

MISCELLANEOUS

___ OMIT PLUS (canned pressurized air for cleaning cauterizing scalpel)
___ animal holding chair
___ tongue depressor

___ Wet/dry sand paper: 200, 400, 600 grit

MOUNTS/INSTRUMENTS/FITTINGS

___ Strain Gauge rosette
___ M-Bond glue
___ M-Bond,catalyst

___ Nine-accelerometer plates (small and 8 feet)
___ M-Coat D air drying acrylic coating, powder and liquid
___ Silicon

___ X-ray targets (2 square; one with tail) (2 round; one with tail, both in end of 2" long I.D. polyethylene tube).
___ Two 18" (0.085" I.D.) and two 18" (0.066" I.D.) lengths of polyethylene tubing, each with one beveled end.
___ Various lenths of airway tubing

___ Dental acrylic

___ Bone wax
___ 2 epidural pressure transducer fittings

TOOLS

___ Stryker bone coring drill, coring tool, and allen head wrench to fit its screw.
___ Dental scoop
___ Wire cutters and fastening wire

___ Electric hair clippers

___ Electric drill

___ Drill bits (6/32 1/16", etc.)
___ large and small screwdrivers (2-56 and No.2)
___ nut driver (for lag bolts)
___ wire twisters
___ bone shears
___ 2-56 drill bit with adhesive tape on its shaft

___ Soldering iron with hooked tip

___ Transformer

___ Solder and flux
___ Wet gauze in film cannister for cleaning soldering iron tip.

TESTING AREA SETUP

___ masking tape

___ silver tape

___ fiber tape

___ large surgical scissors

___ 1 pr. large hemostat

___ bone wax

___ small screwdrivers for mounting accelerometers

___ styrofoam

___ balsa wood for impact chair

___ foam padding for impact chair

___ small tie wraps

___ extra tubing (various I.D.)

___ 50 ml. syringe for dye injector

___ plastic garbage bag taped onto cart ring

___ adhesive tape

___ blue pads

___ green gloves, 4 pr.

___ gauze

___ large scalpel handle

___ small scalpel handle

___ scalpel blades, 1 each: no. 15
no. 12
no. 22

___ 2 hemostats

___ 2 forceps

___ large surgical scissors

___ 2 trocar needles

___ black thread

___ waxed string

___ 5 ml syringe with adapter tubing attached, filled with silicone coupling fluid

___ polyethylene tubing, 18" each: I.D. .066", I.D. .085"

BROUGHT FROM ANATOMY WITH ANIMAL

___ soldering iron with hooked tip

___ solder

___ flux

___ transformer

___ moist gauze in film cannister for cleaning soldering iron tip

___ Radiopaque dye 40 c.c.

___ Anesthetic drugs, Uthol, syringes, and needles

MATERIALS

___ balsa wood

___ rags

___ foam (at least 6 sheets of 3x4 ft 6")

___ Ensolite (.5 cm thickness)

___ Styrofoam

___ Dow Ethafoam

___ APR pads

ROPE CUTTERS

___ head, 1/8"

___ nylon strings (10 24" 3/16"; 10 18" 1/8")

PHOTOMETRICS (X-RAYS)

____ X-RAY GE dental head and power supply

____ X-ray labels prepared.

____ Developer checked and changed, if necessary.

____ Cassettes loaded with film

____ Filters --Ta, Maglens, Ag

____ Polaroid Cable

____ Power supply and cable

____ Black cloth

____ Flashlight

____ Calibration target

MISCELLANEOUS

___ calculator

___ bone wax

___ Pressurization equipment (thoracic arterial, head arterial, cerebral spinal)

___ Timer box

___ Strobes

TAPES

___ adhesive

___ fiber

___ silver

___ masking

___ black

___ double stick

IMPACT LAB CART SETUP

PAPER AND PLASTIC

___ blue pads

___ gauze

___ gloves

___ plastic garbage bags

SCALPELS

___ 1 medium (#4) handle

___ 1 small (#3) handle

___ 2 #22 blades

___ 2 #15 blades

___ 1 #12 blade

SURGICAL TOOLS

___ 2 forceps

___ 2 hemostats

___ large scissors

___ 2 double curved needles

STRING

___ flat waxed string

___ black thread

TOOLS

___ small (1-72) screwdriver

___ large screwdriver

___ nut driver

___ ball driver (6-32, 0-80)

___ 1-72 screws

___ 2-56 screws

___ 0-80 screws

___ wiretwisters

MISCELLANEOUS

___ ball targets

___ paper targets

___ bone wax

___ vaseline

___ Q-tips

___ tubing connectors

___ tie wraps

___ lockwire

___ 50cc syringe

___ pulmonary pressurization relief valves

___ rubber cement

NECROPSY SETUP

ALWAYS WEAR LAB COAT.

___ plastic taped to and covering metal table

___ heavy duty trash bags from Vivarium prep room

___ zip lock plastic bags for saving parts

___ 10 blue pads

___ gauze

___ silver tape

___ masking tape

___ Stryker saw

___ large and small scalpel hjandles

___ 2 no.60 scalpel blades

___ 2 no.22 scalpel blades

___ 2 no.15 scalpel blades

___ 3 hemostats

___ forceps - 1 hooked and 1 plain

___ small surgical scissors

___ medium surgical scissors

___ medium spreaders

___ squeeze bottle, filled with water

___ 10% Formalin and calcium carbonate

___ Fixation bottle

___ skull wedges, one with "T" and one without

PRELIMINARY IMPACT LAB CHECKLISTS

CAMERAS

___ light banks positioned, 480-V power ON
___ cameras in position and set
___ camera fps correct
___ TEST ID and phototargets visible
___ DO POLAROID CHECKLIST

POLAROID CHECKLIST

___ magnet ON
___ external OFF
___ HV at 35 kV
___ check filters
___ set polaroid camera at f16
___ set objective lens at 2 for 4x, 2.8 for 2x, 4 for 1x
___ X-ray centered
___ CLEAR LAB OF ALL INDIVIDUALS NOT WEARING X-RAY BADGES!

HIGH-SPEED CINERADIOGRAPH CAMERA CHECKLIST

___ external ON
___ power supply read lilght ON and BRIGHT
THIS MUST BE DONE BEFORE HV IS TURNED ON!
___ HV at 35 k
___ gating HV at 4 kV
___ HV ON
___ camera power supply light ON and BRIGHT
___ image intensifier objective lens at 0.6 m
___ Newtonian reference
___ calibration completed
___ cables clear of field of view
___ DO HIGH-SPEED X-RAY OPERATION CHECKLIST

HIGH-SPEED X-RAY OPERATION CHECKLIST

___ Position Cineradiograph
___ Position X-Ray head approximately 40 inches from the screen of the cineradiograph
___ Lock wheels on the X-Ray head and cineradiograph table
___ Record X-Ray head to Cineradiograph screen distance_____
___ Record subject mid-line to cineradiograph screen distance_____
___ Turn on cineradiograph focusing magnet. Check to see that it limits.
___ check filters
___ take polaroid photo [in-place X-Ray photos]
___ If necessary adjust the KVP and distance from the X-Ray head to the cineradiograph screen. Retake polaroid photos until no further adjustment is necessary. Label all polaroids.
___ Exchange the polaroid for the high-speed movie camera

in the cineradiograph mount.
___ Check alignment of the movie camera with the output screen
___ Focus the high-speed movie camera
___ Set the lens opening of the high-speed movie camera at the correct aperture
___ Check the pulse width on the gating circuit. Set the pulse width at 350 microseconds.
___ Set objective lens at 1.2
___ TAKE 35 mm STILL SET-UP PHOTOS.

SUBJECT CHECKLIST

___ Labels and phototargets visible
___ Hoist in correct position and locked
___ Ropecutter threaded and cable clear
___ Measure and record angles_____
___ Strobe check
___ Pressurization equipment check
___ Door locked
___ GO TO FINAL CANNON ROOM OPERATION CHECKLISTS

FINAL CHECKLIST

FINAL CANNON OPERATION CHECKLIST

___ padding correct?
___ Solenoid switches set to synchronize timerbox?
___ Timerbox times correct?
___ Timerbox firing channels correct?
___ Strobe set?
___ Cock Cannon-Impactor
___ Piston status GREEN, GREEN, GREEN?
___ Record launch rope angle_____
___ Head noose and ropecutter checked?
___ All cables clear and strain relieved?
___ Calibration sequences completed?
___ Gate established and reset?
___ Pressurize cannon
___ Pulse pressurize subject
___ BEGIN INSTRUMENTATION ROOM COUNTDOWN

INSTRUMENTATION ROOM COUNTDOWN

___ Earphone contact?
___ necessary re-wiring accomplished?
___ amplifier gains set?
___ amplifier excitation set?
___ amplifiers zeroed [balanced?]?
___ Tape Recorders set at 30 ips?
___ Volume of tape recorders off?
___ Tapes positioned?
___ Subject pressure at 70 mm Hg?
___ Ratchet and turn handle off brake winch?
___ Timerbox armed?
___ TEST NUMBER verified?
___ RUN TEST